

REPORT DOCUMENTATION PAGE

Form Approved OMB No. 0704-0188

Public reporting burden for this collection of information is estimated to average 1 hour per response, including the time for reviewing instructions, searching existing data sources, gathering and maintaining the data needed, and completing and reviewing the collection of information. Send comments regarding this burden estimate or any other aspect of this collection of information, including suggestions for reducing this burden to Washington Headquarters Services, Directorate for Information Operations and Reports, 1215 Jefferson Davis Highway, Suite 1204, Arlington, VA 22202-4302, and to the Office of Management and Budget, Paperwork Reduction Project (0704-0188), Washington, DC 20503.

1. AGENCY USE ONLY (Leave blank)		2. REPORT DATE 15 July 2005	3. REPORT TYPE AND DATES COVERED Final Report, Project 1 July 2003 to 30 June 2005	
4. TITLE AND SUBTITLE Micro-mechanics of fiber reinforced bounded and unbounded solids: effective local and non-local thermo-elastic properties, stress concentration factors, and edge effect			5. FUNDING NUMBERS FA8655-05-1-5008	
6. AUTHOR(S)				
7. PERFORMING ORGANIZATION NAME(S) AND ADDRESS(ES) S.P. Timoshenko Institute of Mechanics			8. Performing Organization Report Number	
9. SPONSORING/MONITORING AGENCY NAME(S) AND ADDRESS(ES) EOARD Unit 802 Box 14 FPO 09499-0014			10. SPONSORING/MONITORING AGENCY REPORT NUMBER STCU-00-8010	
11. SUPPLEMENTARY NOTES				
12a. DISTRIBUTION/AVAILABILITY STATEMENT Approved for public release: distribution is unlimited. (approval given by local Public Affairs Office)			12b. DISTRIBUTION CODE Distribution A	
<p>ABSTRACT (Maximum 200 words)</p> <p>Initiation of failure in a composite specimen can be related to the non-linear elastic stress field presents in constituents. More often one examines the distribution of extreme values for the stress in the elastic inclusion's coatings. Inclusion-reinforced materials are the objects of the investigations of the P-1 10 project. The early analysis work on the damage of the composites has used linear elastic mechanics so it has been less successful in applications than those to metals. So the new approaches ~have been created recently in composite micro-mechanics. One of these is mathematical model of multi-particle effective field method (MEFM) that has reached a level for which many of practical significant problems can be solved. Four scientific groups worked on implementation of its idea in some branches of composite material mechanics to investigate a stress distribution caused by external loading and interaction of structural in-homogeneities. The project has been done in two years and consists of the four parts in accordance to scientific groups involved in.</p>				
14. SUBJECT TERMS EOARD, Micro-mechanics, Bounded solids, unbounded solids, Thermo-elastic properties, Stress concentration factors, edge effect, Non-linear elastic stress, Inclusion-reinforced materials, Composites,, Linear elastic mechanics, Multi-particle effective field method (MEFM), Composite media			15. NUMBER OF PAGES	
			16. PRICE CODE	
17. SECURITY CLASSIFICATION OF REPORT UNCLASSIFIED	18. SECURITY CLASSIFICATION OF THIS PAGE UNCLASSIFIED	19. SECURITY CLASSIFICATION OF ABSTRACT UNCLASSIFIED	20. LIMITATION OF ABSTRACT UL	

Micro-mechanics of fiber reinforced bounded and unbounded solids: effective local and non-local thermo-elastic properties, stress concentration factors, and edge effect

Project manager: Maslov Borys Petrovich, Dr. Sc. in Physics and Mathematics
Phone: +380-44-454-7764, Fax: –, E-mail: maslov@inmech.kiev.ua
Institutions: S.P. Timoshenko Institute of Mechanics
Financing parties: USA, European Office of Aerospace Research and Development (EOARD)
Operative commencement date: 01.07.2003
Project duration: 2 years
Project technical area: mechanics
Reported : 01.07.2003 – 30.06.2005
Date of submission: 15.07.2005

Executive summary

Initiation of failure in a composite specimen can be related to the non-linear elastic stress field presents in constituents. More often one examines the distribution of extreme values for the stress in the elastic inclusion's coatings. Inclusion-reinforced materials are the objects of the investigations of the P-110 project. The early analysis work on the damage of the composites has used linear elastic mechanics so it has been less successful in applications than those to metals. So the new approaches have been created recently in composite micro-mechanics. One of these is mathematical model of multi-particle effective field method (MEFM) that has reached a level for which many of practical significant problems can be solved. Four scientific groups worked on implementation of its idea in some branches of composite material mechanics to investigate a stress distribution caused by external loading and interaction of structural in-homogeneities. The project has been done in two years and consists of the four parts in accordance to scientific groups involved in.

Composite media is assumed consisting of a homogeneous matrix containing a random set of inclusions of ellipsoidal shape. A realistic model of the problem cannot be solved by analytical methods in the general case of inclusion shape and its coating structures. The hybrid boundary integral equation and volume integral equation method considered in this project enables one to restrict discretisation to the inclusions only and an inhomogeneous structure of inclusions presents no problem in the framework of the same numerical scheme, compared to the standard BIE method. Additional fundamental difficulties appear in the analysis of micro-macro problems when micro-inclusions and their spacing have a length-scale that is a few orders of magnitude smaller than the length-scales of the macroscopic problem. An edge effect yields to the redistribution of local stresses in a boundary layer region. In so doing, the eventual abandonment of so-called hypothesis of statistically homogeneous field would leads to a non-local coupling between statistical averages of stresses and the strains tensors. As a result the non-local effective elastic properties take place. So new numerical tool is developed for solution of singular integral equations involving the hybrid BIE and VIE method. Consideration of random structure composites is performed using the MEFM. Within this method one constructs a hierarchy of statistical moment equations for conditional averages of stresses in the inclusions; the interaction of different inclusions is taken into account. The influence of the ellipsoidal shape, coating structure and orientation on inclusions on the effective local and non-local properties as well as stress concentrator factors were estimated. The advanced version of this method without effective field hypothesis is proposed. A proper approximation is provided by solving the multi-particle model problem by means of the multipole expansion technique. Based on theoretical analysis, the efficient numerical algorithms and relevant computer codes have been developed providing a detailed analysis of stress fields and macroscopic thermoelastic behavior of a wide class of modern composites.

An accurate solutions have been obtained of the 2D and 3D elastostatics problem for a piece-homogeneous half-space containing a finite array of non-overlapping ellipsoidal inclusions of arbitrary size, aspect ratio, location and elastic properties. The method combines the multipole expansion solution in terms of partial vector solutions of Navier equation for unbounded space with the expansion formulas and integral transforms to obtain a complete solution of the composite half-space problem. By exact satisfaction of all the matrix-inclusion interfaces and flat boundary conditions, a primary boundary-value problem stated on a complicated heterogeneous domain has been

reduced to an ordinary well-posed set of linear algebraic equations. Properly chosen structure of general solution provides remarkably simple form of resolving equations and thus an efficient computational algorithm. The advanced structure model of composite half-plane involving a number ellipsoidal inclusions, cavities and/or cracks with an accurate account for the microstructure statistics and interaction effects can be considered in this way. The statistical moments of stress concentration factors in the random structure fibrous composite have been evaluated from the numerical experiments on the generalized periodic structure model being a periodicity unit cell with a number of inclusions. The relevant numerical code has been developed and a wide series of numerical experiments has been performed with 50 to 100 randomly placed inclusions per cell and statistically meaningful results were obtained for the statistical moments of stress concentration factors in phases and interfaces of a random structure fibrous composite. They include, in particular, the second moment of stress playing a fundamental role in a wide class of non-linear elasticity problems, damage initiation, etc. The developed method finds a variety of applications in the composite mechanics: so, combined with the MEFM, a micro mechanical model has been built to predict the thermoelastic behavior of random structure nanocomposites reinforced by the aligned silicate nanoplate clusters of deterministic structure. Numerical (finite element) solution has been obtained of the “solid with a coated high-aspect ratio inclusion” anisotropic elastostatics problem in 2D and 3D. The developed solution has been applied to evaluate the stress concentrator factors and other relevant local and averaged tensors entering the general theory of the MEFM. The special emphasis was made on the problem of the continuum estimation of effective thermoelastic properties of nanocomposites.

The powerful numerical tool was developed involving the hybrid BIE and VIE methods, combined with the analytical multipole expansion and finite element methods. The hybrid micro-macro formulation allows decomposition of a complete multi-scale problem into two associated sub-problems, one receding entirely at the micro-level. The latter was evaluated by the macro-scale BIE technique capable of handling complex geometry and general boundary conditions. Within this method one constructs a hierarchy of statistical moment equations for conditional averages of stresses in the inclusions; the interaction of different inclusions is taken into account. The influence of the shape, coating structure and orientation on inclusions on the effective local and non-local properties as well as stress concentrator factors were estimated.

Cooperation with foreign collaborators

Scientific materials are being exchanged both as among members of four work groups in Ukraine as with experts and consultants from AFRL, so that the research is carried out jointly with foreign collaborators. Contribution was made to the 21st International Congress of Theoretical and Applied Mechanics, ICTAM04 taking place in August 15-20, 2004 in Warsaw, which is definitely relevant within the scope of the P110-Project. The participation in the most important international meetings to deal with scientific in the field of solid and fluid mechanics was aimed at discussing the achievements made in the framework of the P-110 project in the scientific society. Close collaboration with personnel in the Materials and Manufacturing Directorate of the AFRL at Wright-Patterson AFB, OH is realized. AFRL’s scientists Drs V. Bechel and V. Buryachenko are the persons who ensured a close connection of the project with the current practical interests of AFRL as well as an incorporation of the developed approaches and software into the MEFM for design of random structure advanced types of composites.

Publications

1. Maslov B.P. Nonlinear overall visco-elastic properties of the random multi-component media. – in: Proceeding of the 21st International Congress of Theoretical and Applied Mechanics, ICTAM04.-Warsaw.-2004.
2. Maslov B.P., Shatylo L.V. The equation of fatigue crack growth in damaged material with strengthening // Kyiv University Visnyk.-2005.-N1.-pp.32-39.
3. Maslov B.P., Shatylo L.V. Fatigue crack growth in non-linear material with damage // Archives of Mechanics - submitted
4. Buryachenko, V.A., Maslov B.P. Stress concentration in non-linear random composites with n -coated inclusions // (in final preparation)
5. Kushch, V.I., Shmegeera, S.V. and Buryachenko, V.A. (2005). Interacting elliptic inclusions by the method of complex potentials. International Journal of Solids and Structures, 42(20), 5491–5512.
6. Kushch, V.I., Shmegeera, S.V. and Buryachenko, V.A. (2005). Elastic equilibrium of a half plane containing a finite array of elliptic inclusions. International Journal of Solids and Structures, 42(22).
7. Buryachenko, V.A., Kushch, V.I. (2005) Effective transverse elastic moduli of composites at non-dilute concentration of a random field of aligned fibers. ZAMP, in press.
8. Buryachenko V.A., V.I.Kushch, A.Roy (2005) Effective thermoelastic properties of random structure composites reinforced by the clusters of deterministic structure (application to clay nanocomposites) Journal of the Mechanics and Physics of Solids - submitted.

9. Buryachenko, V.A., Kushch, V.I. (2005) Effective elastic and failure properties and stress distributions in fiber aligned composites. International Journal of Solids and Structures (in final preparation)
10. Buryachenko V.A., V.I. Kushch, Dutka V.A. (2005) Finite element analysis in the continuum estimation of effective thermoelastic properties of nanocomposites" (in final preparation)
11. Mykhas'kiv V.V., Kunets Ya.I. and Mishchenko V.O. Stresses in a three-dimensional body with thin compliant inclusion behind the front of pulsed waves // Materials Science.- 2003.- **39**, No. 3.- P. 377-384.
12. Mykhas'kiv V.V. Transient response of a plane rigid inclusion to an incident wave in an elastic solid // Wave Motion. – 2005.- **41**, No 2.- P. 133-144.
13. Mykhas'kiv V.V. and Kalyniak O.I. Nonstationary disturbances of a 3-D elastic matrix with a rigid disk inclusion // Physicochemical Mechanics of Materials.- 2005.- **41**, No. 2.- P. 7-15 (in Ukrainian).
14. Mykhas'kiv V.V. and Stepanyuk O.I. BIE method for 3D static problems of rigid disc-inclusion and crack interaction in elastic matrix // Computer Modeling in Engineering & Sciences (CMES) (accepted).
15. Mykhas'kiv V.V. and Stasyuk B.M. Solution of 3D elastostatic problems on the loading transfer in a solid with inclusion of nonclassical shape by boundary element method // Int. Applied Mechanics (in Russian, accepted).
16. Buryachenko V.A. and Mykhas'kiv V.V. 3D boundary element analysis in the continuum estimation of effective thermoelastic properties of nanocomposites // (in preparation).

Prospects of future development.

The completed P-110 project provides a firm background for developing a unique technique for the numerical modeling of the thermoelastic multifunctional nanocomposites with random structures, enhances our understanding of the damage processes in these structures. This technique based computer programs will have wide-ranging applications in the aerospace industry, material science, and in mechanical, civil, polymer, and electric engineering.

The very important and potentially fruitful application area of the developed method is *nanocomposites*, and the highly promising preliminary results have been obtained in the framework of a given Project. However, in order to develop the realistic models of composites reinforced by the nanoelements of noncanonical shape, say, cylindrical and waved fibers with smooth ends embedded into the thick coatings, with random location, orientation, and arrangement (statistically homogeneous clustered, and functionally graded structure), a considerable additional effort must be applied. It includes generalization of the multipole expansion technique on the composites with anisotropic constituents, development of more sophisticated finite element models combined with the molecular dynamics simulations, etc. Incorporation into the MEFM of the estimations of the local stress and strain concentrator factors given by these methods can be considered as a fundamentally new bridging mechanism between nano- and micromechanics.

A hybrid method based on a combination of the FEA, BEM, and multipole expansion method incorporated into the MEFM may be proposed for the micro-macro solution of elastostatic 2-D and 3-D problems in bounded and unbounded solids containing the interacting multiple inclusions of different scales. The hybrid nano-micro-macro formulation allows decomposition of the complete problem into two associated subproblems, one residing entirely at the nano-level and the other at the micro- and macro-level. At the micromechanical level the known approach of the MEFM would be generalized to the analyses of both the clustered effects for nanosilicate composites (taking into account such key factors as: shape of the nanoelements, interlayer distance, and the number of nanoelements in the stack of deterministic structure) and the prescribed random orientation of anisotropic nanofibers of noncanonical shape (cylindrical and waved fibers with smooth ends embedded into the thick coatings with elastic properties continuously varying in both the radial and circumferential direction). A fundamental role of an edge effect yielding to the redistribution of local stresses in a boundary layer region compared to the stress estimations in remote points being considered is detected. Both deterministic (periodic and nonperiodic) and random (statistically homogeneous and inhomogeneous) structures would be considered. The effective local and nonlocal properties as well as stress concentrator factors are estimated. The most challenging issue of nanotechnology is how mechanics can contribute to our understanding of the bridging mechanism between the coupled scales, which is described by the nonlocal constitutive equations. The results of the MD simulation should be incorporated in a hierarchical model of estimation of effective properties of nanocomposites by the Multiparticle Effective Field Method, which is a milestone in the progress of mathematical materials science. The MEFM is based on the theory of functions of random variables and Green's functions, taking into account the interaction of different inclusions, and will be taken directly in the framework of the hypothesis of the effective field. A realistic model of problems cannot be solved by analytical methods in the general case of inclusion shape, its coating structures, and arrangement such as, e.g., random orientation, location, and clustered. Additional fundamental difficulties appear in the analysis of nano-micro-macro problems when microinclusions and their spacing have a problem (geometric, loading, and boundary conditions). So it is known a fundamental role of an edge effect yielding to the redistribution of local stresses in a boundary layer region. In so doing, the eventual abandonment of so-called hypothesis of statistically homogeneous fields leads to a

nonlocal coupling between statistical averages of stresses and the strain tensors when the statistical average stress is given by an integral of the field quantity weighted by some tensorial function, i.e. the nonlocal effective elastic properties hold.

The most challenging issue of nanotechnology is how mechanics can contribute to our understanding of the bridging mechanism between the coupled scales, which is described by the nonlocal constitutive equations. The results of the MD simulation should be incorporated in a hierarchical model of estimation of effective properties of nanocomposites. The MEFM is based on the theory of functions of random variables and Green's functions, taking into account the interaction of different inclusions, and will be taken directly in the framework of the hypothesis of the effective field. Additional fundamental features may be investigated by the analysis of nano-micro-macro problems when microinclusions and their spacing have a specific mismatches. It is known a fundamental role of an edge effect yielding to the redistribution of local stresses in a boundary layer region. In so doing, the eventual abandonment of so-called hypothesis of statistically homogeneous fields leads to a nonlocal coupling between statistical averages of stresses and the strain tensors when the statistical average stress is given by an integral of the field quantity weighted by some tensorial function, i.e. the nonlocal effective elastic properties hold.

Project manager
Dr. B. Maslov

For the Coordinating Institution
Approved

V.D. Kubenko
Deputy Director,
academician NAS Ukraine

	Short form	File/page
	Executive summary	SF.doc PAGE 1
	Cooperation with foreign collaborators	SF.doc PAGE 2
	Publications	SF.doc PAGE 2
	Prospects of future development (for final report only)	SF.doc PAGE 3
	Full form	
	Project main idea	FF.doc PAGE 2
	Technical approach	FF.doc PAGE 2
	Technical progress overview	FF.doc PAGE 4
	Current status of the project	FF.doc PAGE 156
	Summary of personnel commitment	FF.doc PAGE 156
	Description of travels	FF.doc PAGE 156
	Information about major equipment and materials acquired, other direct costs, related to the project	FF.doc PAGE 157
1.	Mesomechanics of bounded and unbounded composites: effective local and nonlocal elastic properties, stress concentration factors, and edge effect	T08.doc PAGE 1
	1. Effective properties, local stresses and edge effects in multi-component materials with n-coated inclusions	T08.doc PAGE 2
	2 The statistical moments of stress concentration factors in continuum estimation	T08.doc PAGE 3

Project main idea

Composite materials are used in a lot of structural applications due to their well-known advanced properties. Prediction of the behavior of these materials is the important step in the process of its implementation in structural design. Inclusion-reinforced materials are the subject of the investigations of the P-110 project. Many of works have been devoted to determination of the effective linear elastic properties, singularity fields of stress and deformation near the tip of cracks etc. It was assumed usually that the inclusions are imbedded in a linear defect free continuum. As a result three obstacles have not been investigated till now. Macroscopic interacting cracks and multi-component inclusions, then distributed microscopic damage and third the non-linear properties of constituents. The early analysis work on the damage of the composites has used linear elastic fracture mechanics so it has been less successful in applications than those to metals. The new approaches has been created recently would be a fruitful tool in composite micro-mechanics. One of these developed last years is the mathematical model of multi-particle effective field method that has reached a level for which many of practical significant problems can be solved. The P-110 project is carrying out right on the model mentioned. Four scientific groups are working on implementation of its idea in some branches of composite material mechanics to investigate a stress distribution caused by external loading and interaction of structural in-homogeneities. Eight points of the work plan were done.

1. Development of an iteration hybrid volume integral equation (VIE) and boundary integral equation (BIE) method for analysis of a finite number of inclusions in a half space.
2. Development of software for solutions of multi-scale problems with a finite number of inclusions in a half space.
3. The examination of accuracy and efficiency of the method proposed through comparison with results obtained from finite element analysis and some analytical results.
4. Development of general integral equations governing the stress state of homogeneous half space with a random field of residual stress inclusions appropriate for the subsequent numerical solution.
5. Development of general integral equations governing the stress state of micro-inhomogeneous half space appropriate for the subsequent numerical solution.
6. An approximate estimation of local effective properties.
7. An approximate estimation of non-local effective properties as well as stress concentrator factors in random structure half space.
8. An approximate estimation of statistical moments of stress concentrator factors in random structure half space.

Technical approach

The fundamental problem being investigated is an elastic equilibrium of a fibrous composite half-space. Provided the surface load and far stress field do not vary in fiber direction, the problem can be thought as two-dimensional (2D), namely, an elastic half plane with a finite number of circular inclusions. And, likewise the majority of 2D linear elasticity problems, the powerful method of complex potentials is applied here to obtain an accurate analytical solution. This problem continues for a long years to be relevant and attracts attention of investigators. Although only well separated and distant from the flat boundary inclusions were considered, discrepancy in the numerical data generated by the different methods compared has been observed. The complete analytical solution has been obtained here for a half plane containing a finite or infinite quasi-periodic array of arbitrarily placed non-overlapping circular inclusions. The stress and strain state of inhomogeneous half plane is governed by the uniform far stress field and arbitrary load applied at the flat boundary. To get an accurate solution of the problem, the Kolosov-Muskhelishvili method of complex potentials has been combined with the Fourier-integral transform technique. By exact satisfaction of all the boundary conditions, the primary boundary-value problem is reduced to an ordinary well-posed set of linear algebraic equations and this provides high computation efficiency and accuracy of the method developed. The results of numerical study are presented and possible ways to improve computational efficiency of the method are discussed. In the case of short fiber reinforcing, the problem is essentially three-dimensional (3D) and requires more sophisticated math to analyze it. The multi-pole expansion method has been combined with a newly developed numerical technique to solve for a finite array of spheroid inhomogeneities in an unbounded solid. Likewise the above 2D problem, this model is a first step in development the large-scale model of a near-to-surface volume of fibrous composite. Composite media is assumed consisting of a homogeneous matrix containing a random set of inclusions of ellipsoidal shape (2-D and 3-D cases). A considerable number of methods are known in the linear theory of such composites yielding the effective elastic constants and stress field averages in the components. A

realistic model of the problem cannot be solved by analytical methods in the general case of inclusion shape and its coating structures. The hybrid boundary integral equation and volume integral equation method considered in this project enables one to restrict discretization to the inclusions only and an inhomogeneous structure of inclusions presents no problem in the framework of the same numerical scheme, compared to the standard BIE method. Additional fundamental difficulties appear in the analysis of micro-macro problems when micro-inclusions and their spacing have a length-scale that is a few orders of magnitude smaller than the length-scales of the macroscopic problem. An edge effect yields to the redistribution of local stress in a boundary layer region. In so doing, the eventual abandonment of so-called hypothesis of statistically homogeneous field leads to a non-local coupling between statistical averages of stresses and the strains tensors when the statistical average stress is given by an integral of the field quantity weighted by some tensor function, i.e. the non-local effective elastic properties take place. So new numerical tool is developed for solution of singular integral equations involving the hybrid BIE and VIE method with evaluation of the appropriate integrals with a Gauss formulae in a spirit of a subtraction technique together with the iteration method. Judicious choice of the initial approximation for interacting inclusions in an unbounded medium subjected to inhomogeneous loading is made. The hybrid micro-macro formulation allows decomposition of a complete multi-scale problem into two associated sub-problems, one receding entirely at the micro-level. The latter is evaluated by the macro-scale BIE technique capable of handling complex geometry and general boundary conditions. Consideration of random structure composites with non-linear matrix is performed using the Multi-particle Effective Field Method (MEFM) based on the theory of functions of random variables and Green's functions and refined approach of conditional-moment method (CMM) with hypothesis of MEFM. Within this method one constructs a hierarchy of statistical moment equations for conditional averages of stresses in the inclusions; the interaction of different inclusions is taken into account. The influence of the ellipsoidal shape, coating structure and orientation on inclusions on the effective local and non-local properties as well as stress concentrator factors will be estimated. For a finite number of interacting inclusions in a half space the iteration hybrid BIE and VIE method combined with judicious choice of initial approximation of interacting inclusions with random distribution of size, shape, orientation and properties in a half space, the advanced version of Multi-particle Effective Field Method without effective field hypothesis is used.

The part one of this project is devoted to working out the methods of prediction the elastic and strength properties of the multi-component unidirectional composites with linear and physically non-linear matrix, polymer or metallic. Random structure of material is adopted. The feature new is that the matrix is assumed be weakened by microscopic damage so the effective properties are the function not only of the volume concentrations of the constituents but of the new material parameter reflecting the damage evolution mechanisms. The part two deals with the stress concentration in the composite laminates containing macroscopic risers of holes, cutouts and bolted joints type. An edge effects and adhesive bonded joints are going to be investigated. The boundary element method, the advanced version of multi-particle effective field method model are involved to obtain the solution of the theory elasticity's problems of the first and second type. The part three is connected with the modeling of singularities at the fiber-matrix interfaces and at the free edge of composite specimen. The four part is devoted to investigation the stress concentration near macroscopic stress risers in the composites with initial residual stress in components and prediction the life-time and fatigue resistance parameters for materials with micro-structural damage. The general integral equations governing the stress state of micro-inhomogeneous half space appropriate for the subsequent numerical solution is developed in part five. An approximate estimation of local effective properties and an approximate estimation were done of non-local effective properties as well as stress concentrator factors in random structure half space is determined. An approximate estimation of statistical moments of stress concentrator factors in random structure half space is the problem solved in eight, final part of the project.

Rather powerful numerical tool is developed for solution of singular integral equations involving the hybrid BEM and FEM methods. The hybrid micro-macro formulation allows decomposition of a complete multi-scale problem into two associated sub-problems, one receding entirely at the micro-level. The latter has been evaluated by the macro-scale BEM technique capable of handling complex geometry and general boundary conditions. Consideration of random structure composites is performed using the Multi-particle Effective Field Method based on the theory of functions of random variables and Green's functions. Within this method one constructs a hierarchy of statistical moment equations for conditional averages of stresses in the inclusions; the interaction of different inclusions is taken into account. The influence of the ellipsoidal shape, coating structure and orientation on inclusions on the effective local and non-local properties as well as stress concentrator factors is estimated.

Composite media is assumed consisting of a homogeneous matrix containing a random set of inclusions of ellipsoidal shape (2-D and 3-D cases). A considerable number of methods are known in the linear theory of such composites yielding the effective elastic constants and stress field averages in the components. A realistic model of the problem cannot be solved by analytical methods in the general case of inclusion shape and its coating structures. The hybrid BIE and VIE method considered in this project enables one to restrict discretisation to the inclusions only (in contrast to the Finite Element Method), and an inhomogeneous structure of inclusions presents no problem in the framework of the same numerical scheme (compared to the standard BIE method). Additional fundamental difficulties appear in the analysis of micro-macro problems when micro-inclusions and their spacing have a length-scale that is a few orders of magnitude smaller than the length-scales of the macroscopic problem (geometric, loading, and boundary conditions). So it is known a fundamental role of an edge effect yielding to the redistribution of local stresses in a boundary layer region. In so doing, the eventual abandonment of so-called hypothesis of statistically homogeneous fields leads to a non-local coupling between statistical averages of stresses and the strains tensors when the statistical average stress is given by an integral of the field quantity weighted by some tensor function, i.e. the non-local effective elastic properties take place.

An accurate analytical method has been developed to solve for stress in a layer containing an infinite quasi random array of circular inclusions, the last being a "cell model" of near-to-surface domain of fibrous composite. The method combines technique of periodic complex potentials with the Fourier series expansion to reduce a primary boundary-value elasticity problem for a complicated multiple-connected domain to an ordinary well-posed set of linear algebraic equations. It provides high numerical efficiency of the method, accuracy of which is controlled entirely by a number of harmonics in the truncated series retained for practical calculations. Up to several hundred of interacting inclusions can be considered in this way which makes the model sufficiently realistic and flexible to provide numerical simulation of random microstructures of composites and their local stress concentrations and effective elastic moduli. A highly accurate numerical-analytical variation of boundary element method has been used to solve the problem of defining stress of plane with multicoated inclusion of elliptical shape. Due to two-dimensional approximation of unknown densities of potential on the boundary of considered discretized body it is possible to obtain simultaneously all the components of stress-strain state. Even use of linear approximation gives very good correlation with solution of known particular cases of considered problem, namely plane with hole (Kirsh problem), plane with elastic inclusion, plane with set of two holes and, at last the set of two interacting inclusions in plane. It was ascertained that there are three quite predictable factors influencing the level of stress concentration on the contour of coated inclusion, The code provides fast and accurate analysis of stress field in any point of the matrix, inclusions and interfaces. Testing has shown rapid convergence of solution excluding the case of nearly touching inclusions. In this extreme case, to achieve accuracy prescribed, a number of harmonics is to be increased. For the moderate size of the reduced linear system, the standard LU decomposition solver is utilized which gives $O(N^3)$ or $O(N^2)$ rise of computational time with number N of equations increased depending on whether direct or iterative procedure is chosen in the above mentioned method. To improve efficiency of code for large N , application of an alternate GMRES conjugate gradient iterative solver is reserved. The algorithm developed can be readily incorporated in the general scheme of the numerical BIEM method.

Technical progress overview

1. Effective properties, local stresses and edge effects in multi-component materials with n -coated inclusions

The first part of the P-110 project final report is devoted to working out the methods of prediction the elastic and strength properties of the multi-component unidirectional or more complex structure composites with linear and non-linear matrix and n -coated inclusions.

1.1 Nonlinear meso-mechanics of multi-component materials

To increase the strength and reliability of constructions built up with composite materials is largely a multi-parametrical problem [5,8,15], one of its solutions being the evaluation of stress concentration in microstructure elements and the formulation of required criteria of durability which correspond to classical methods of strength theory. The service life of units made up of composite materials is dependent on average or maximum cyclic stresses both in matrix, inclusions and coatings. The number of load cycles is very important, amplitude etc. [11,14] Moreover, many behavior singularities of non-homogenous material as it was mentioned in P-110 First Annual

Report can be given only in terms of nonlinear mechanics [5,8,15,16]. More detailed considerations of the mechanical behavior of composite materials require the analysis of the interface between the reinforcement and the matrix. These interfaces may represent: weak interfacial layer due to imperfect bonding between the two phases; inter-diffusion or chemical interaction zones (with properties varying through the thickness and/or along the surface) at the interface between the two phases. It is well known that the overall effective properties of composite materials are significantly influenced by the properties of the interfaces between the constituents. First, the interface controls the in situ reinforcement's (particles or fibers) strength and hence the strength of the composite. Secondly, defects and damage are likely to occur at the interface (for example debonding, sliding and interface cracks, etc.) and these interfacial defects control the degradation of the composite. Therefore, to evaluate more accurately the effective properties of a composite non-linear especially, the behavior and structures of interfaces must be taken into consideration [1,6,13].

Therefore, to develop algorithms of designing new multi-constituent composites with given properties requires an in-depth study of stress in microstructure elements and calculation of effective elastic constants in the scope of nonlinear elasticity theory. The results extracted from the references [3-12] involve effective elastic modules of nonlinear compressible and incompressible composites of stochastic structure containing two components: matrix and non-coated inclusions. The problem addressed in reference [8,15,16] is concerned with defining the microstructure stress in nonlinear non-compressible multi-constituent composites. The present result sets forth the previous investigations [8,12] and gives a summary for the compressible material problems. The multi particle effective field method (MEFM) [1,2] and refined approach of conditional-moment method (CMM) is implemented [11], the solution of first iteration for small concentration of inclusions being based on the results obtained earlier in [8,15].

First, a representative volume v_R of the composite body \mathbf{B} taken in the reference configuration κ_R is considered,

$v_R = v_m \cup v_a$, $v_a = \bigcup_{i=1}^n v_i$. It is assumed that composite specimen subjected to some non random system of loading.

The stress and strain fields vary from point to point. If every detail of the geometry of a composite were known, overall properties can be calculated exactly and local stress concentrators as a result too. In practice, however, except in cases such as those displaying periodicity etc. a complete solution could not even be computed. So random media may be used as a model useful for engineer problems solution. A random medium we understand as one of a family, any member of which may be characterized by a label α that belongs to a sample space A . For an n -phase composite material it is convenient to introduce the indicator function $f_r(\mathbf{x})$, that takes the value 1 if \mathbf{x} lies in phase r , $\mathbf{x} \in v_r$ and zero otherwise. It depends on α that denote individual members of a sample space A , defined by $p(\alpha)$. the probability density of α in A . The mean value or ensemble average of $f_r(\mathbf{x})$ defines the probability $P_r(\mathbf{x})$ of finding phase r at $\mathbf{x} \in \mathbf{B}$. Thus

$$P_r(\mathbf{x}) = \langle f_r(\mathbf{x}) \rangle = \int_A f_r(\mathbf{x}, \alpha) p(\alpha) d\alpha.$$

Likewise the probability $P_{rs}(\mathbf{x}, \mathbf{y})$ of finding simultaneously phase r at \mathbf{x} and phase s at \mathbf{y} is

$$P_{rs}(\mathbf{x}, \mathbf{y}) = \langle f_r(\mathbf{x}) f_s(\mathbf{y}) \rangle = \int_A f_r(\mathbf{x}, \alpha) f_s(\mathbf{y}, \alpha) p(\alpha) d\alpha$$

We assume that functions $f_r(\mathbf{x}, \alpha)$ are known [16] and there is in each of volumes v_r , $r \in [1, n+1]$, an elastic material with the properties governed by the third order potential of type [17]

$$\hat{W}(\mathbf{F}) = \mu \left[\left(1 + \frac{1}{2} \alpha \right) I_1^2 - 2I_2 + \beta_1 I_1^3 + \beta_3 I_1 I_2 + \beta_3 I_3 + \mathcal{O}(|\mathbf{E}|^4) \right], \quad (1.1)$$

where I_i - are the main invariants of Lagrange finite strain tensor \mathbf{E} , $\lambda, \mu, \beta_1, \beta_2, \beta_3$ - constants of non linear material, tr - is an operator of tensor convolution, \mathbf{F} - is a deformation gradient. \mathbf{H} - is a gradient of displacement vector $\mathbf{u}(\mathbf{x})$ in the coordinates \mathbf{x} of reference system, \mathbf{x}^A - coordinates of an actual configuration κ_A , $\mathbf{1}$ - a unit symmetric tensor of the second rank [15,18]. After being averaged over non-deformed representative volume v_R of the composite body \mathbf{B} , the first asymmetric stress tensor of Piola-Kirchhoff $\boldsymbol{\sigma}(\mathbf{x})$ and the deformation gradient $\mathbf{F}(\mathbf{x})$ can be used as conjugate variables [3,8] of the nonlinear deformation theory. It follows, the state equations of the hyper-elastic medium can be written as

$$\sigma_{ka} = \partial W(\mathbf{F}) / \partial F_{ka}, \quad (1.2)$$

Then, for the first and second approximation by displacement values

$$\begin{aligned} \sigma_{ij(1)}(\mathbf{e}) &= \lambda_{ijkl} e_{kl(1)}; \\ \sigma_{ij(2)}(\mathbf{e}, \mathbf{F}) &= \lambda_{ijkl} E_{kl(2)} + H_{im(1)} \lambda_{mjkl} e_{kl(1)} + v_{ijklmn} (e_{kl} e_{mn})_{(1)}. \end{aligned} \quad (1.3)$$

Here

$$\begin{aligned} e_{ij} &= \frac{1}{2} (H_{ij} + H_{ji}); & H_{ij} &= F_{ij} - \delta_{ij} = \nabla_j u_i = u_{i,j}; \\ E_{ij(2)} &= e_{ij(2)} + f_{ij(2)}; & f_{ij(2)} &= \frac{1}{2} (H_{mi} H_{mj})_{(1)}; \\ \lambda_{ijkl} &= \mu (\alpha \delta_{ij} \delta_{kl} + 2I_{ijkl}); \\ v_{ijklmn} &= \frac{1}{2} v_1 \delta_{ij} \delta_{kl} \delta_{mn} + v_2 (\delta_{ij} I_{klmn} + \delta_{kl} I_{ijmn} + \delta_{mn} I_{ijkl}) + 4v_3 I_{ijklmn}; \\ I_{ijkl} &+ \frac{1}{2} (\delta_{ik} \delta_{jl} + \delta_{il} \delta_{jk}); & I_{ijklmn} &= \frac{1}{2} (I_{ipkl} I_{jpmn} + I_{jpkl} I_{ipmn}), \\ v_1 &= 2\mu (6\beta_1 - 3\beta_2 - 5\beta_3); \\ v_2 &= -\mu (\beta_2 + \beta_3); & v_3 &= \mu \beta_3 / 4; \quad \alpha = \lambda / \mu, \end{aligned} \quad (1.4)$$

the subscript in parenthesis stays for the order of approximation of nonlinear displacement, δ_{ij} - is the Kronecker delta, λ, μ - are Lamé elastic modules in the linear strain theory (the constants of second order), v_1, v_2, v_3 are the Lamé constants of the third order [17]. When matrix response is nonlinear but rather in elasto-visco-plastic sense than simply elastic it's more convenient to use the deformation potential in form [5]

$$W(\mathbf{F}) = \mu \left[\left(1 + \frac{1}{2} \alpha_1 \right) I_1^2 - 2I_2 + \beta (I_1^2 - 3I_2)^{\frac{1+n}{2n}} \right].$$

Here μ, α_1, β, n - material constants. So stress strain relation will be

$$\begin{aligned} \sigma_{ij} &= \lambda_{ijab} e_{ab} + v_3 (I_1^2 - 3I_2)^{\frac{1-n}{2n}} K_{ijab} e_{ab}; \\ K_{ijab} &= I_{ijab} - J_{ijab}; & J_{ijab} &= \frac{1}{3} \delta_{ij} \delta_{ab}. \end{aligned} \quad (1.5)$$

Included in this family (1.4), (1.5) of materials is a linear elastic solid with $n=1$ and a rigid-perfectly plastic solid with $n \rightarrow \infty$. These constitutive relations are being particularly appropriated for the investigation of a wide range of material behaviors [7].

1.2. Two-phase linear elastic material

The stochastic equilibrium equations and the boundary conditions of the first linear approximation can be written in the form [2,8,15]

$$\begin{aligned}
 \mathbf{A}^0 \mathbf{u}_{(1)}(\mathbf{x}) &= \mathbf{b}_{(1)}(\mathbf{x}); & \mathbf{x} &\in \mathbf{B}; \\
 \mathbf{u}_{(1)}(\mathbf{x}) &= 0, & \mathbf{x} &\in \partial \mathbf{B}; \\
 \mathbf{b}_{(1)}(\mathbf{x}) &= -\mathbf{f}(\mathbf{x}) e_{(1)}(\mathbf{x}); & \mathbf{f}(\mathbf{x}) &= \boldsymbol{\lambda}(\mathbf{x}) - \boldsymbol{\lambda}^0; \\
 \mathbf{u}_{(1)}(\mathbf{x}) &= \mathbf{u}^R_{(1)}(\mathbf{x}) - \bar{\mathbf{u}}_{(1)}, & &
 \end{aligned} \tag{2.1}$$

$\partial \mathbf{B}$ - is a boundary of compressible composite body \mathbf{B} , the dash above indicates the results of statistical averaging in the sample with random elasticity $\boldsymbol{\lambda}(\mathbf{x})$, $\mathbf{u}^R(\mathbf{x})$ - is a random displacement vector. Fourier transform $\mathbf{A}(\mathbf{k})$ of $\mathbf{A}(\nabla)$ operator is defined in [2,8,17]

$$\left[\mathbf{A}^0(\mathbf{k}) \right]_{im} = \lambda_{ijmn}^0 k_j k_m; \quad \underline{\boldsymbol{\lambda}}^0 = \mu_0 (\alpha_0 \underline{\mathbf{I}} \otimes \underline{\mathbf{I}} + 2\underline{\mathbf{I}}), \tag{2.2}$$

$\boldsymbol{\lambda}^0$ - is a tensor of elastic moduli of the homogenous comparison body, that is the parameters μ_0, α_0 are the constants within the volume $v_R \in \mathbf{B}$, $\underline{\mathbf{I}}$ is a unit symmetric tensor of the fourth rank, $\boldsymbol{\tau}(\mathbf{x})$ is a stress polarization tensor [17]. The Green's function \mathbf{G} of the equation (2.1) can be defined from the following conditions

$$\mathbf{A}^0(\nabla) \mathbf{G}(\mathbf{x}) + \mathbf{I} \boldsymbol{\delta}(\mathbf{x}) = \mathbf{0}; \tag{2.3}$$

$\boldsymbol{\delta}(\mathbf{x})$ - 3D space Dirac function here, so that

$$G_{im}(\mathbf{k}) = \left[\mathbf{A}^0(\mathbf{k}) \right]_{im}^{-1}.$$

Using the technique described in the previous works [1- 4,8,15], the solution can be written as the integral of the convolution type over \mathbf{B} location

$$\mathbf{e}_{(1)}(\mathbf{x}_1) = \boldsymbol{\Gamma}(\mathbf{x}_1, \mathbf{x}_2) * \boldsymbol{\tau}_{(1)}(\mathbf{x}_2), \tag{2.4}$$

$\boldsymbol{\Gamma}(\mathbf{x}_1, \mathbf{x}_2)$ - is an operator with the kernel expressed through derivatives of the Green's function $\mathbf{G}(\mathbf{x}_1, \mathbf{x}_2)$. Now, take two-constituent isotropic material with the matrix being reinforced by randomly oriented in space inclusions of ellipsoid form. The result of $\boldsymbol{\Gamma}(\mathbf{x}, \mathbf{y})$ convolution with any two rank tensor function $\mathbf{b}(\mathbf{y})$ may be obtained by integrals [8]

$$\boldsymbol{\Gamma}_{ijab} * \mathbf{b} = \int_{\mathbf{B}} G_{a(i,j)b}(\mathbf{x} - \mathbf{y}) \mathbf{b}(\mathbf{y}) d\mathbf{y} + \oint_{\partial \mathbf{B}} G_{a(i,j)b}(\mathbf{x} - \mathbf{y}) \mathbf{n}_y d\mathbf{y},$$

With boundary condition

$$\mathbf{b}(\mathbf{y}) = \mathbf{b}^0, \quad \forall \mathbf{y} \in \partial \mathbf{B},$$

it transformed to more simpler relation [2,15]

$$\boldsymbol{\Gamma}_{ijab} * \mathbf{b} = \int_{\mathbf{B}} G_{a(i,j)b}(\mathbf{x} - \mathbf{y}) [\mathbf{b}(\mathbf{y}) - \mathbf{b}^0] d\mathbf{y}.$$

The non-linear elastic properties of inclusions are defined by the $W_i(\boldsymbol{\epsilon})$ potential, and that of the matrix are defined by the $W_m(\boldsymbol{\epsilon})$ potential, i.e. $i = 1, m = 2$. Averaging of the equation (2.4) requires the argument coordinate of the

left-hand part to be placed in the v_a volume containing inclusions oriented in the \mathbf{n}_a – direction, $a \in [1, n]$, which results in

$$\mathbf{e}^a(\mathbf{x}_1) = \mathbf{F}(\mathbf{x}_1, \mathbf{x}_2) * [\mathbf{f}^i \sum_{b=1}^n \mathbf{e}^{ba}(\mathbf{x}_2, \mathbf{x}_1) p_{b|a}(\mathbf{x}_2, \mathbf{x}_1) + \mathbf{f}^m \mathbf{e}^{ma}(\mathbf{x}_2, \mathbf{x}_1) p_{m|a}(\mathbf{x}_2, \mathbf{x}_1)]. \quad (2.5)$$

Here we take the following notations for the statistical moment function \mathbf{m}^{ba} [8]

$$\begin{aligned} \mathbf{m}^{ba}(\mathbf{x}_1, \mathbf{x}_2) &= \langle \mathbf{m}(\mathbf{x}_1) : \{ \mathbf{x}_1 \in v_b, \mathbf{x}_2 \in v_a \} \rangle; \\ p_{b|a}(\mathbf{x}_1, \mathbf{x}_2) &= p(\mathbf{x}_1 \in v_b | \mathbf{x}_2 \in v_a), \end{aligned} \quad (2.6)$$

i.e. the operation of statistical averaging is denoted by angular brackets which embrace the condition of what set a point belongs to. The probability densities of distribution when transiting from the state of $\mathbf{x}_1 \in v_a$, that is from an inclusion of \mathbf{n}_a – direction, into the state of $\mathbf{x}_2 \in v_b$, that is into inclusion of \mathbf{n}_b – direction, and into the state of $\mathbf{x}_2 \in v_m$, where v_m is the volume containing the matrix, are written as follows [8,11]

$$\begin{aligned} p_{b|a}(\mathbf{x}_1, \mathbf{x}_2) &= p(\mathbf{x}_1, \mathbf{x}_2) \delta_{ba} + c_b p^*(\mathbf{x}_1, \mathbf{x}_2) (1 - \delta_{ba}); & p(\mathbf{x}_1, \mathbf{x}_2) &= c_a + c_a^* \varphi(\mathbf{x}_1, \mathbf{x}_2); \\ p_{m|a}(\mathbf{x}_1, \mathbf{x}_2) &= c_m \varphi^*(\mathbf{x}_1, \mathbf{x}_2); & p^*(\mathbf{x}_1, \mathbf{x}_2) &= 1 - p(\mathbf{x}_1, \mathbf{x}_2); \\ \varphi^*(\mathbf{x}_1, \mathbf{x}_2) &= 1 - \varphi(\mathbf{x}_1, \mathbf{x}_2); & c_a^* &= 1 - c_a, \end{aligned} \quad (2.7)$$

$\varphi(\mathbf{x}_1, \mathbf{x}_2)$ - is two-point correlation function of the elastic field, c_a - is volume concentration of set X_a of inclusions oriented in the \mathbf{n}_a – direction, c_m - is volume concentration of the matrix.

Integrating equations (2.5) is derived by the technique proposed in the previous works [2,8,15], the algebraic matrix of \mathbf{g} operator obtained from the integral \mathbf{F} being composed of

$$\begin{aligned} k_g &= g_1(j_1 + r_3)/2; & l_g &= -g_1 r_3; \\ l_g^T &= l_g; & n_g &= 2g_1(j_1 + r_3); \\ m_g^T &= g_0 j_2 + k_g; & m_g &= g_0(1 + j_1) + 2l_g; \\ g_0 &= -(2m_0)^{-1}; & g_1 &= -(2n_0)^{-1}; & r_3 &= k_0 \mu_0^{-1} j_3. \end{aligned} \quad (2.8)$$

Here the common notations are used [17] to define the elements of the algebraic matrix \mathbf{g} :

$$\begin{aligned} k_g &= (g_{11} + g_{12})/2; & l_g &= g_{13}; \\ l_g^T &= g_{31}; & n_g &= g_{33}; \\ m_g^T &= 2g_{66}; & m_g &= 2g_{44} \end{aligned} \quad (2.9)$$

Parameters j_1, j_2, j_3 are defined by formula

$$\begin{aligned} j_2 &= 1 - j_1; & j_3 &= [(1 + 2w^2)j_1 - 1]/(2r); \\ r &= w^2 - 1; & j &= \text{arch}(w), \end{aligned} \quad (2.10)$$

w - stays here for the aspect ratio of longitude and transverse sizes of spheroid inclusion.

Statistical fluctuations of \mathbf{e}^a strains of inclusions of X_a -set are expressed through the average deformations of the matrix \mathbf{e}^m in the representative volume v_R of the composite body \mathbf{B}

$$\mathbf{e}^a = c_m \mathbf{a} \mathbf{e}^m, \quad \mathbf{a} = \mathbf{z} \mathbf{L}, \quad (2.11)$$

c_m - is the volume concentration of the matrix, $\mathbf{L}^i = \boldsymbol{\lambda}^i - \boldsymbol{\lambda}^m$, transversally isotropic tensor \mathbf{z} is given by relation

$$\mathbf{z} = (\mathbf{g}^{-1} - \mathbf{f})^{-1}. \quad (2.12)$$

After averaging the equation (2.11) over the set X_i of inclusions of all possible orientations we define the statistical average strains of inclusions \mathbf{e}^i and that of the matrix \mathbf{e}^m through macro-strains \mathbf{e} of the representative volume v_R

$$\begin{aligned} \mathbf{e}^i &= \mathbf{A}^i \mathbf{e}; & \mathbf{e}^m &= \mathbf{A}^m \mathbf{e}; \\ \mathbf{A}^i &= \mathbf{A}^m (\mathbf{I} + \mathbf{a}); & \mathbf{A}^m &= (\mathbf{I} + c_1 \mathbf{a})^{-1}; \quad \mathbf{a} = \langle \mathbf{a} \rangle_\omega, \end{aligned} \quad (2.13)$$

angular brackets with subscript ω denote the operation of statistical averaging over the set of possible inclusion orientations. Using the expressions (2.13), the Lamé effective linear elastic modules λ and μ for two-constituent material of random structure take the following form

$$\begin{aligned} \lambda &= 3 \sum_{r=1}^2 c_r \kappa_r \kappa_{Ar} - 2\mu/3; & \mu &= 2 \sum_{r=1}^2 c_r \mu_r \mu_{Ar}; \\ \mu_{A1} &= \mu_{A2} (1 + 4\mu_z \mu_L); & \mu_{A2} &= \frac{1}{2} (1 + 4c_1 \mu_z \mu_L)^{-1}; \\ \kappa_{A1} &= \kappa_{A2} (1 + 9\kappa_z \kappa_L); & \kappa_{A2} &= \frac{1}{3} (1 + 9c_1 \kappa_z \kappa_L)^{-1}; \\ \mu_z &= \frac{1}{15} (k + n - l + 3m + 3p)_{za}; & \kappa_r &= (3\lambda_r + 2\mu_r)/3; \\ \kappa_z &= \frac{1}{9} (4k + 2l + 2l^T + n)_{za}. \end{aligned} \quad (2.14)$$

Here we use the conditions $c_1 = c_i$; and the elements of algebraic matrix \mathbf{z} are calculated by the formula (2.12).

1.3. Multi-constituent compressible linear composites with n -coated inclusions

In the case of multi-constituent materials we apply the technique of multi-particle effective field [1, 2], refined approach of conditional-moment method (CMM) and the Mori-Tanaka scheme [11]. Thus, consider the set of operators for the deformation fields of components and the appropriate micro-values. The exact solution is assumed to exist

$$\mathbf{e}^a = \mathbf{G}^i \mathbf{e}^m \quad (3.1)$$

Then, tensors $\mathbf{A}^i, \mathbf{A}^m$, where i is the number of inclusions with the elastic potential $\hat{W}_i(\mathbf{E})$, $i \in [1, n]$ and m is the subscript of the matrix with an elastic potential $\hat{W}_m(\mathbf{F})$, ($m = n + 1$) are defined through expressions

$$\mathbf{A}^i = \mathbf{G}^i \mathbf{A}^m; \quad \mathbf{A}^m = (c_m \mathbf{I} + \sum_{i=1}^n c_i \mathbf{G}^i)^{-1}. \quad (3.2)$$

The approximate solution can be derived by replacing in the general case the unknown operator \mathbf{G}^i by the approximated operator \mathbf{T}^i (by operator of deformation concentration) for the average deformations of inclusions denoted by i , $i \in [1, n]$ number and the average strains of the representative volume v_R , that is

$$\mathbf{e}^i = \mathbf{T}^i \mathbf{e}. \quad (3.3)$$

Next, to define tensors $\mathbf{A}^i, \mathbf{A}^m$ we obtain the formulas

$$\begin{aligned} \mathbf{A}^i &= \mathbf{T}^i \mathbf{A}^m; & i &\in [1, n]; \\ \mathbf{A}^i &= \left(c_m \mathbf{I} + \sum_{i=1}^n c_i \mathbf{T}^i \right)^{-1}; \end{aligned} \quad (3.4)$$

In the present investigation we define the \mathbf{G}^i operator from the solution based on one-point approximation of multi-particle effective field or conditional statistical functions of moments for two-constituent media [8] i.e.

$$\mathbf{G}^i = \mathbf{T}^i = \mathbf{I} + \mathbf{a}^i; \quad \mathbf{a}^i = \langle \mathbf{a}^i \rangle_{\omega}; \quad (3.5)$$

Here the algebraic matrix \mathbf{a}^i is resulted from analyzing the stress-strain state in set X_i of inclusions with i number. Thereby, to define tensors $\mathbf{A}^i, \mathbf{A}^m$ the following expressions are derived:

$$\begin{aligned} \mathbf{A}^i &= \mathbf{A}^m (\mathbf{I} + \mathbf{a}^i)^i; & i &\in [1, n]; \\ \mathbf{A}^m &= (\mathbf{I} + c_f \langle \mathbf{a} \rangle)^{-1}; & c_f &= \sum_{i=1}^n c_i. \end{aligned} \quad (3.6)$$

As in the case of incompressible materials [11] we can immediately demonstrate that the presentation of two-constituent material (3.6) is identical to formula (2.13). In particular, it means that the accuracy of results (3.6) is in agreement with the accuracy level of solutions [1,8,15] derived by the technique of multi-particle effective field or MEFM [1,2], conditional statistical moment functions for multi-constituent media [13].

1.4. The second order nonlinear solutions. The equilibrium equations of representative volume v_R for statistical fluctuations of second order displacement $\mathbf{u}_{(2)}(\mathbf{x})$ in the coordinate reference configuration κ are written in the form

$$\begin{aligned} \mathbf{A}^0 (\nabla) \mathbf{u}_{(2)}(\mathbf{x}) &= -\nabla \boldsymbol{\tau}_{(2)}(\mathbf{x}); & \mathbf{x} &\in \mathbf{B}; \\ \mathbf{u}_{(2)}(\mathbf{x}) &= 0, & \mathbf{x} &\in \partial \mathbf{B}; \\ \boldsymbol{\tau}_{(2)}(\mathbf{x}) &= \mathbf{f}(\mathbf{x}) \mathbf{e}_{(2)}(\mathbf{x}) + \mathbf{t}(\mathbf{x}, \mathbf{e}, \mathbf{H}); \\ \mathbf{t}(\mathbf{x}, \mathbf{e}, \mathbf{H}) &= \frac{1}{2} \boldsymbol{\lambda} (\mathbf{H}^T \mathbf{H})_{(1)} + \mathbf{H}_{(1)} (\boldsymbol{\lambda} \mathbf{e}_{(1)}) + \mathbf{v} (\mathbf{e} \otimes \mathbf{e})_{(1)}. \end{aligned} \quad (4.1)$$

The differential operator of equation (4.1) agrees in form with corresponding operator from (2.3). This enables us to make use of Green's function of linear problem and derive the integral equation defining the displacement gradient of second approximation

$$\mathbf{H}_{(2)}(\mathbf{x}_1) = \boldsymbol{\Gamma}(\mathbf{x}_1, \mathbf{x}_2) * \boldsymbol{\tau}_{(2)}(\mathbf{x}_2). \quad (4.2)$$

Statistical averaging of expression (4.2) is performed when provided that left-hand part argument is placed in the volume containing ellipsoid inclusion of \hat{W}_i properties and oriented in \mathbf{n}_a -direction. Then, to define the average over this direction of inclusion deformation we obtain the following equation

$$\mathbf{e}_{(2)}^a(\mathbf{x}_1) = \boldsymbol{\Gamma}(\mathbf{x}_1, \mathbf{x}_2) * \left[\sum_{b=1}^n \tau^{ba}(\mathbf{x}_2, \mathbf{x}_1) \mathbf{p}_{b|a}(\mathbf{x}_2, \mathbf{x}_1) + \tau^{ma}(\mathbf{x}_2, \mathbf{x}_1) \mathbf{p}_{m|a}(\mathbf{x}_2, \mathbf{x}_1) \right]_{(1)}. \quad (4.3)$$

According to the calculation scheme proposed we find the solution of this equation after integrating by probability density functions of (2.7) type. Herewith, nonlinear members in right-hand part are expressed through macro-deformations $\mathbf{e}_{(1)}$ of the representative volume of composite that are already known in first approximation.

$$\begin{aligned} \mathbf{H}_{(1)}^r &= \mathbf{A}^r \mathbf{e}_{(1)} + \mathbf{R}_{(1)}; & r \in [1, n+1]; \\ \mathbf{R} &= \text{skew}(\mathbf{H}) = \frac{1}{2}(\mathbf{H} - \mathbf{H}^T); \end{aligned} \quad (4.4)$$

After some elementary analysis we obtain

$$\begin{aligned} \mathbf{e}_{(2)}^r &= \mathbf{A}^r \mathbf{e}_{(2)} + \mathbf{e}^{ar}(\mathbf{e}_{(1)}); & r \in [i \cup m]; & i \in [1, n]; \\ \mathbf{A}^m &= (\underline{\mathbf{I}} + \mathbf{a})^{-1}; & \mathbf{a} &= \sum_{i=1}^n c_i \mathbf{a}^i; \\ \mathbf{A}^i &= (\underline{\mathbf{I}} + \mathbf{a}^i) \mathbf{A}^m; & \mathbf{a} &= \mathbf{zL}; \\ \mathbf{e}^{am} &= -\mathbf{A}^m \left(\sum_{i=1}^n c_i \mathbf{z}^i \mathbf{r}^i \right) = -\sum_{i=1}^n c_i \mathbf{q}^i \mathbf{r}^i; \\ \mathbf{r}^i &= \mathbf{t}^i(\mathbf{e}_{(1)}, \mathbf{H}_{(1)}) - \mathbf{t}^m(\mathbf{e}_{(1)}, \mathbf{H}_{(1)}); \\ \mathbf{q}^i &= \mathbf{A}^i \mathbf{z}^i; & \mathbf{e}^{ai} &= (\underline{\mathbf{I}} + \mathbf{a}_i) \mathbf{e}^{am} + \mathbf{z}^i \mathbf{r}^i; \end{aligned} \quad (4.5)$$

Here, the condition of $\mathbf{A}^r, \mathbf{e}^{ar}$ operator normalization is satisfied, i.e.

$$\sum_{r=1}^{n+1} c_r \mathbf{A}^r = \underline{\mathbf{I}}; \quad \sum_{r=1}^{n+1} c_r \mathbf{e}^{ar} = \mathbf{0}. \quad (4.6)$$

From substituting the solution (4.5) into averaged physical relations of second order taken from (1.8), we benefit the application of the \mathbf{T} Cauchy macro-stress tensor and the deformation gradient \mathbf{F} to the multi-constituent compressible isotropic composite

$$\begin{aligned} \mathbf{T}(\mathbf{F}) &= \mathbf{J}^{-1} \mathbf{F} \mathbf{S}(\mathbf{F}) \mathbf{F}^T; & J &= \det(\mathbf{F}); \\ \mathbf{S}(\mathbf{F}) &= \mu \left[\alpha_1 \mathbf{I} + 2\mathbf{E} + 3\beta_1 \mathbf{I}_1^2 \mathbf{I} + \beta_2 \mathbf{I}_2 \mathbf{I} + \beta_2 \mathbf{I}_1 (\mathbf{I}_1 \mathbf{I} - \mathbf{E}) + \beta_3 (\mathbf{I}_2 \mathbf{I} - \mathbf{I}_1 \mathbf{E}) + \mathbf{E}^2 \right]; \\ \alpha_1 &= \lambda / \mu; & \beta_1 &= (\nu_1 + 6\nu_2 + 8\nu_3) / (6\mu); \\ \beta_2 &= -2(\nu_2 + 2\nu_3) / \mu; & \beta_3 &= 4\nu_3 / \mu; \end{aligned} \quad (4.7)$$

The overall Lamé constants of second and third order are defined by formula

$$\begin{aligned} \lambda &= 3 \sum_{r=1}^{n+1} c_r \kappa_r \kappa_{Ar} - 2\mu / 3; & \mu &= 2 \sum_{r=1}^{n+1} c_r \mu_r \mu_{Ar}; \\ \nu_1 &= \sum_{r=1}^{n+1} 3c_r \left[l_A \left[2\lambda \kappa_A (3\kappa + \mu)_A + n_A f_A \right] + 9\nu_1 \kappa_A^3 + \right. \\ & \quad \left. 6\nu_2 l_A \kappa_A (3\kappa + 2\mu)_A + 8\nu_3 l_A^2 n_A \right]_r; \\ \nu_2 &= \sum_{r=1}^{n+1} c_r \left[4\mu_A^2 \left(\frac{1}{2} f_A + 3\nu_2 \kappa_A + 4\nu_3 l_A \right) - \frac{1}{2} (3\lambda \kappa_A + 2\mu_A) \right]_r; \\ \nu_3 &= \sum_{r=1}^{n+1} c_r \left[\frac{3}{2} \mu \mu_A (4\mu_A^2 - 1) + 8\nu_3 \mu_A^3 \right]_r. \end{aligned} \quad (4.8)$$

Here we denote $f_{Ar} = (3\lambda\kappa_A + 6\mu l_A)_r$, the coefficients κ_{Ar} , μ_{Ar} , l_{Ar} are defined by formula (3.6), $\mu_r, \kappa_r, \nu_{1r}, \nu_{2r}, \nu_{3r}$ are the elastic constants of second and third order of r -component, c_r is volumetric concentration of r , $r \in [1, n+1]$ -component. Taking into account the members of second order only, the equation (4.7) takes the form of

$$\begin{aligned} \mathbf{T} &= \mu \left[\alpha I_1 \mathbf{I} + 2\mathbf{e} + (\alpha f_0 + \alpha_3 I_1^2 + \alpha_4 I_2) \mathbf{I} + \alpha_5 I_1 \mathbf{e} + \mathbf{H}\mathbf{H}^T + \alpha_6 \mathbf{e}^2 + O(|\mathbf{H}|^3) \right]; \\ \alpha_3 &= (3\beta_1 + \beta_2 - \alpha_1) / \mu; & \alpha_4 &= (\beta_2 + \beta_3) / \mu; \\ \alpha_5 &= (2\alpha_1 - 2 - \beta_2 - \beta_3) / \mu; & \alpha_6 &= (4 + \beta_3) / \mu. \end{aligned} \quad (4.9)$$

Following the technique [12,13], the expressions for tensor coefficients of stress concentration in elements of multi-constituent material and in the matrix

$$\begin{aligned} \boldsymbol{\sigma}^i(\mathbf{x}) &= \mathbf{K}_c^i(\mathbf{x}, \mathbf{H}) \boldsymbol{\sigma}^0 & \boldsymbol{\sigma}^m(\mathbf{x}) &= \mathbf{K}_c^m(\mathbf{x}, \mathbf{H}) \boldsymbol{\sigma}^0; \\ \mathbf{K}_c^i(\mathbf{H}) &= \mathbf{B}^i + \mathbf{b}^i(\mathbf{H}); & \mathbf{b}^i(\boldsymbol{\sigma}^0) &= \boldsymbol{\lambda}^i \mathbf{e}^{ai} / \boldsymbol{\sigma}^0; \\ \mathbf{B}^i &= \boldsymbol{\lambda}^i \mathbf{A}^i \tilde{\boldsymbol{\mu}}; & \mathbf{K}_c^m(\mathbf{H}) &= \mathbf{B}^m + \mathbf{b}^m(\mathbf{H}); \\ \mathbf{K}_c^m(\mathbf{H}) &= \mathbf{B}^m + \mathbf{b}^m(\mathbf{H}); & \mathbf{b}^m(\boldsymbol{\sigma}^0) &= \boldsymbol{\lambda}^m \mathbf{e}^{am} / \boldsymbol{\sigma}^0, \end{aligned} \quad (4.10)$$

where $\tilde{\boldsymbol{\mu}} = \tilde{\boldsymbol{\lambda}}^{-1}$ is overall compliance.

Stress concentration tensors $\mathbf{B}^r(\mathbf{x})$ may be written in more simple way [8,11]

$$\begin{aligned} \mathbf{B}^i &= \mathbf{B}^m (\underline{\mathbf{I}} + \mathbf{b}), & \mathbf{B}^m &= (\underline{\mathbf{I}} + \langle \mathbf{b} \rangle)^{-1}, \\ \mathbf{b} &= \mathbf{q} \mathbf{M}, & \mathbf{q} &= (\mathbf{p}^{-1} - \mathbf{y})^{-1}, \\ \mathbf{p} &= -\boldsymbol{\lambda}^0 (\underline{\mathbf{I}} + \mathbf{g} \boldsymbol{\lambda}^0), & \mathbf{y} &= \boldsymbol{\mu}(\mathbf{x}) - \boldsymbol{\mu}^0, \\ \mathbf{M}(\mathbf{x}) &= \boldsymbol{\mu}(\mathbf{x}) - \boldsymbol{\mu}^0, & \boldsymbol{\mu}^0 &= (\boldsymbol{\lambda}^0)^{-1}. \end{aligned} \quad (4.11)$$

Then for single inclusion $v_i \in \mathbf{B}$ we will get presentation

$$\mathbf{B}^i(\mathbf{x}) = (\underline{\mathbf{I}} + \mathbf{b}), \quad \mathbf{b} = \mathbf{q} (\boldsymbol{\lambda}^0) \mathbf{M}. \quad (4.12)$$

When elasticity tensor of comparison body is defined by $\boldsymbol{\lambda}^0 = \boldsymbol{\lambda}^m$ [2,16] the well known Eshelby's solution for stress in a single inclusion is immediately followed

$$\mathbf{B}^{IE} = (\underline{\mathbf{I}} - \mathbf{p} \mathbf{M})^{-1}, \quad \mathbf{p} = -\boldsymbol{\lambda}^m (\underline{\mathbf{I}} + \mathbf{g} \boldsymbol{\lambda}^m) \quad (4.13)$$

As a result an effective stress field hypothesis of MEFM [1] may be naturally used to determine stresses in any inclusion v_i loaded by equivalent or effective field $\tilde{\boldsymbol{\sigma}}^i(\mathbf{x})$ in non-linear elastic matrix.

1.5 Local stress fields in cores and coatings in non-linear composites

The refined approach of conditional-moment method (CMM) [8,11-15] with hypothesis of multi-particle effective field method (MFFM) [1,2] proposed here to investigate local stress fields in inclusions with n -layered coatings. We consider here a non linear elastic composite medium [3,5,8] with stress free strains $\mathbf{h}(\mathbf{x})$, which consists of a homogeneous matrix containing a homogeneous and statistically uniform random set X_i of coated ellipsoidal or

spheroidal inclusions having all the same form, orientation and mechanical properties. We are using the refined approach of CMM [8,11] with the main hypothesis of many micro-mechanical methods, according to which each inclusion is located inside a homogeneous so-called effective or equivalent field. It is shown, in the framework of the effective field hypothesis [2], that from a solution of the classical linear elastic problem with zero stress free strains for the composite the relations for effective non linear, stored energy and average elastic strains inside the components can be found. This way one obtains the generalization of the known formulae by Rosen and Hashin [6,15], which are exact for two-component composites. The proposed theory is applied to the example of composites reinforced with particles with thin inhomogeneous (along inclusion surface) coatings. For a single coated inclusion the micro-mechanical approach is based on the Green function technique as well as on the interfacial Hill operators [7,12,13].

As a generalization of the results [8,12,13] consider here a certain representative meso-domain \mathbf{B} with a characteristic function $f_{\mathbf{B}}(\mathbf{x}, \alpha)$ containing a set X_i of inclusions v_i with characteristic functions $f_i(\mathbf{x}, \alpha)$ ($i = 1, 2, \dots$). No restrictions are imposed on the elastic symmetry of the phases or on the geometry of the inclusions. The inclusions $\cup v_i = v_i$ are determined as the i -component having identical mechanical and geometrical properties. It is useful to define the effective or equivalent field $\tilde{\sigma}^I(\mathbf{x})$ as a stress field in which the chosen fixed inclusions v_1, v_2, \dots, v_N are embedded. This effective field is a random function of all the other positions of the surrounding inhomogeneities and the average of $\tilde{\sigma}(\mathbf{x})^I$ over a random realization $\alpha \in A$ of these inclusions is equal to the right-hand-side of the n -th line of the integro-differential system of equation for non-homogeneous domain \mathbf{B} [2,15,16]. More detailed considerations of the mechanical behavior of nonlinear composite materials requires the analysis of the interface between the reinforcement and the matrix [4,7,13]. The inhomogeneity of mismatch properties in the coating is a typical situation due to both the production of the coated inclusions and thermo-plastic deformation of the matrix near the inclusion. The micro-mechanical approach is based on the Green function technique [1,15,18] as well as on the interfacial Hill operators. The thin-layer hypothesis and the assumption [1] of a homogeneous stress state in the core are used. The exactness of the accepted assumptions is checked for particular examples by comparisons with finite element analysis results represented in next parts of the report. At first we consider the problem of a single coated inclusion inside an infinite non-linear elastic matrix .

Stresses and strains are related to each other via the constitutive equation [5,8,18]

$$\boldsymbol{\sigma}(\mathbf{x}) = \partial W(\mathbf{x}) / \partial \mathbf{F} \quad (5.1)$$

or

$$\begin{aligned} \boldsymbol{\sigma}(\mathbf{x}) &= \boldsymbol{\lambda}(\mathbf{x})\mathbf{e}(\mathbf{x}) + \mathbf{t}(\mathbf{x}, \mathbf{F}) \\ \mathbf{e}(\mathbf{x}) &= \boldsymbol{\mu}(\mathbf{x})\boldsymbol{\sigma}(\mathbf{x}) + \mathbf{h}(\mathbf{x}, \mathbf{F}) \end{aligned} \quad (5.2)$$

where $\boldsymbol{\lambda}(\mathbf{x})$ and $\boldsymbol{\mu}(\mathbf{x}) = \boldsymbol{\lambda}^{-1}(\mathbf{x})$ are the given phase linear elasticity and compliance fourth-order tensors, respectively, and the common notation for tensor products has been employed [8,17]. Non-linear part of constitutive relations represented by $\mathbf{t}(\mathbf{x}, \mathbf{F})$ and $\mathbf{h}(\mathbf{x}) = -\boldsymbol{\lambda}(\mathbf{x})\mathbf{t}(\mathbf{x}, \mathbf{F})$, second order tensors of local eigenstresses and eigenstrains (transformation fields) which may arise by thermal expansion, plastic deformation, phase transformation, twinning and other changes of shape or volume of the material. We assume that the phases are perfectly bonded, so that the displacements and the traction components of the stresses are continuous across the inter-phase boundaries. We take here uniform external traction boundary conditions

$$\mathbf{T}(\mathbf{x}) = \boldsymbol{\sigma}^0(\mathbf{x})\mathbf{n}(\mathbf{x}), \quad \forall \mathbf{x} \in \partial \mathbf{B} \quad (5.3)$$

where $\mathbf{T}(\mathbf{x})$ is the traction vector at the external boundary $\partial \mathbf{B}$ of the meso-domain \mathbf{B} , $\mathbf{n}(\mathbf{x})$ is its unit outward normal vector, and $\boldsymbol{\sigma}^0$ is a given constant stress tensor.

The original conditional-moment method presented in detail in [15] was worthy of critical notice of course as many of others too. The concrete numerical results were obtained there by truncation of the infinite system of integral equations by taking into account only two-point conditional probabilities, and by neglecting fluctuations of stresses

within the limits of the components. These are equivalent to acceptance of assumption of homogeneous elastic fields and consideration of homogeneous inclusions. For analytical estimation of integrals involved one proposes the analytical representation of the two-point density conforming with the shape of the inclusion v_I that of necessity leads to the acceptance of the hypothesis

$$\varphi(v_I, \mathbf{x}_I / v_K, \mathbf{x}_K) = \varphi(\rho), \quad \rho = |(\mathbf{a}_I^0)^{-1}(\mathbf{x}_J - \mathbf{x}_I)|,$$

where $(\mathbf{a}_I^0)^{-1}$ identifies a matrix of affine transformation which transfers the ellipsoid v_{II}^0 being the included volume or “correlation hole” into a unit sphere. In so doing, the shape of “correlation hole” v_{II}^0 does not depend on the inclusion v_I .

We introduce here a comparison body [8,10,18], whose mechanical properties denoted by the upper index 0. So λ^0 , μ^0 will usually be taken as uniform over B , as a result the corresponding boundary value problem is easier to solve than that for the original body with random elasticity $\lambda(\mathbf{x})$. All tensors \mathbf{t} ($\mathbf{t} = \lambda, \mu, \nu$) of material properties are decomposed as

$$\mathbf{t} = \mathbf{t}^0 + \delta\mathbf{t} = \mathbf{t}^0 + \mathbf{t}' \quad (5.4)$$

The Hill condition [7] for elastic energy representation holds for any compatible strain field \mathbf{e}^0 from (2.1) and equilibrium stress field $\boldsymbol{\sigma}^0$ (5.3) not necessarily related to each other by a specific stress-strain relation. Here and in the following the upper lower case index i indicates the components and the lower upper case index I indicates the individual inclusions ($i = 1, n; I = 1, 2, 3, \dots$).

Let us consider some conditional statistical averages of the general integral equation (2.4) leading to an infinite system [8] of integral equations (2.5). The concrete numerical results may be obtained for aligned or disordered homogeneous ellipsoidal inclusions under different choices of comparison media either the $\lambda^0 = \langle \lambda(\mathbf{x}) \rangle$ or $\lambda^0 = \langle \mu(\mathbf{x}) \rangle^{-1}$ estimation. Of course, there was no a priori justification for the specific choice of λ^0 , not counting the condition that the quadratic form, employed in the proof of the Hashin and Shtrikman variational principle, have a constant sign. The only justification up to recent publication of Talbot and Willis [16] for choosing for λ^0 the Voigt or Reuss estimation [8,15,18] was the fact that specific experimental data agree with the computing curves. Although the final explicit general representation for effective moduli was not presented in the conditional-moment method, the equivalence of assumptions admitted leads to the conclusion that the conditional-moment method can be considered as a particular case of the one particle approximation of MEFM. In addition, in the conditional-moment method the shape of the inclusions is taken into account via prescribed anisotropy of the conditional probability density. For equally probable orientation of ellipsoidal inclusions it is possible to obtain an isotropic function and the estimation of the effective compliance $\tilde{\mu}$ will be invariant with respect to the shape of the inclusion. This result can be avoided easily by taking into account directly the shape of the inclusions via the tensor, as done by Willis [16,18] on the basis of a variational principle. We use here refined conditional method approach that for randomly oriented ellipsoidal inclusions the estimations of effective moduli represented in [11,15] and [16] as are equivalent. The last publication of for a non-linear composite a bound on its effective energy density does not induce a corresponding bound on its constitutive relation. Recently Talbot and Willis [16] proposed the refined method for bounding directly the constitutive relation by employing a linear comparison material. It seems very perspective in sense of approach proposed here that bounds produced [16] are closely related to bounds of Hashin-Strikman type and comparison elasticity of Voigt and Reuss type is used. So determination of comparison elasticity from some kind of experiments [15] is confirmed now by effective energy of a non-linear composite evaluation.

The thin-layer hypothesis appeared in [1] is being a principal step in the investigation of coated inclusions, because it allows the use of the well-developed Eshelby theory and Hill interface operators for the general case of anisotropy of the materials being in contact. It is assumed usually that the stress and strain components inside the inclusion coincide with those already determined before the coating was introduced. Afterwards this assumption was replaced by the hypothesis of homogeneity of the stress state inside the core of inclusion, and elastic problems were considered [1,2]. However, the case of inhomogeneity of elastic and mismatch properties in the coating is a typical situation due to the production of the coated inclusions and due to plastic deformations of the matrix near the

inclusion. Even in situations in which for a specific reference system connected to the unit normal and tangential vectors of the surface of the inclusion homogeneous stress and strain fields may be assumed, the introduction of a global coordinate system requires the consideration of inhomogeneous fields in the coating. Buryachenko and Rammerstorfer analyzed [1] this problem in the framework of the approximate assumption of a homogeneous stress state in the core and the thin-layer hypothesis, which means that the characteristic function of the coating can be replaced by a surface $\rho(y)$ function. According to Eshelby's equivalence principle, the perturbed strain field $e'(x)$ induced by inhomogeneities (inclusions with properties different from those of the homogeneous matrix) can be related to specified eigenstrain $e^*(x)$ by replacing the inhomogeneities with the matrix material. That is, for the domain of r -phase inhomogeneities with the elasticity tensor λ^r , we have

$$\lambda^r [e^0 + e'(x)] = \lambda^m [e^0 + e'(x) - e^*(x)] \quad (5.5)$$

where λ^m is the stiffness tensor of the matrix and e^0 is the uniform strain field by far field loads for a homogeneous matrix material only. λ^r and λ^m could be isotropic or anisotropic if the eigenstrain field $e^*(x)$ is uniform in v_l . So the strain at any point within an RVE is decomposed into two parts: (a) the uniform strain e^0 (without inhomogeneities), and (b) the perturbed strain $e'(x)$ due to distributed eigenstrains $e^*(x)$. It is emphasized that the eigenstrain $e^*(x)$ is nonzero in the inclusion domain and zero in the matrix domain, respectively. In particular, the perturbed strain field induced by distributed eigenstrains $e^*(x)$ can be expressed as

$$e'(x) = \int_B G(x-y)e^*(y)dy \quad (5.6)$$

where B is the volume of an RVE and $x, y \in B$. In addition, G is the second derivative of the Green's function in a linear elastic homogeneous matrix. For example, for a linear, elastic isotropic matrix, we have

$$G_{ijab} = \frac{1}{8\pi(1-\nu_0)r^3} [-15n_{ijab} + 3\nu_0(\delta_{ia}n_{jb} + \delta_{ib}n_{ja} + \delta_{ja}n_{ib} + \delta_{jb}n_{ia}) + 3\delta_{ij}n_{ab} + 3(1-2\nu_0)\delta_{ab}n_{ij} - (1-2\nu_0)\delta_{ij}\delta_{ab} + 2(1-2\nu_0)I_{ijab}] \quad (5.7)$$

where $r = x - y$, $r = |x - y|$ and $n = r/r$. Further, summation convention applied, δ_{ij} denotes the Kronecker delta and ν_0 is Poisson's ratio of the homogeneous matrix. Eshelby used a fourth rank tensor S , which is traditionally called Eshelby's tensor, to describe the strain and stress fields in the inclusion domain. The Eshelby's tensor is defined as

$$S(x) = \int_{B_l} G(x-y)dy \quad (5.8)$$

in which x is the local point inside the inclusion domain B_l . Total strain $e(x)$ at any point $x \in B_m$ in the matrix is given by superposition of uniform strain e^0 and the perturbed strain $e'(x)$ induced by inclusions (inhomogeneities)

$$e(x) = e^0 + e'(x) = e^0 + \int_B G(x-y)e^*(y)dy \quad (5.9)$$

Therefore, the volume-averaged strain tensor is given by

$$\bar{e}(x) = e^0 + \frac{1}{v_B} \int_B \int_{B_l} G(x-y)e^*(y)dydx = e^0 + \frac{1}{v_B} \int_B [\int_B G(x-y)dx] e^*(y)dy \quad (5.10)$$

When considering the strain and stress fields at a local point \mathbf{x} that is outside inclusion, we define a fourth rank tensor $\tilde{\mathbf{G}}(\mathbf{x})$, which is called the exterior-point Eshelby's tensor as

$$\tilde{\mathbf{G}}(\mathbf{x}) = \int_{B_m} \mathbf{G}(\mathbf{x} - \mathbf{y}) d\mathbf{y}, \quad \mathbf{x} \in \mathbf{B} / \mathbf{B}_i \quad (5.11)$$

The essential assumption in the Mori-Tanaka approach states that the each inclusion v_i behaves as isolated one in the infinite matrix $\lambda^0 = \lambda^m$ and subjected to some equivalent effective stress field $\tilde{\sigma}(\mathbf{x}_i) = \sigma^m$ coinciding with the average stress in the matrix. This assumption allows uniquely define the effective non-linear elastic properties of multi-component composite materials. On the other hand this hypothesis is more restrictive than the hypothesis **H1** of MEFM [1]. It gives an opportunity to use the known solution [2,8,15] for each inclusion v_i and to find the average stress in the matrix by the use of a representation of the average stresses in the separate phases as the average stress in the whole composite. It makes possible to represent the statistical average of both the stresses in the matrix and the strain polarization tensor in the inclusions as well as to the estimation of effective properties.

Let the every coated inclusion v_i consist of an ellipsoidal kernel $v_{iK} \in v_i$ with a characteristic function $f_{iK}(\mathbf{x})$ and homogeneous elastic parameters λ^j, ν^j of the second and third order and n -layered thin coatings v_{iJ} with a characteristic functions

$$f_{iJ}(\mathbf{x}) = f_i(\mathbf{x}) - f_{iK}(\mathbf{x}) - \sum_N f_{iN}(\mathbf{x}), \quad J \neq N, \quad J \in [1, CN]. \quad (5.12)$$

There are an inhomogeneous transformation fields $\mathbf{h}^{CJ}(\mathbf{x}) \neq const$, and homogeneous linear compliances $\mu^{CJ} = const$. Such n -coated inclusions are located in an infinite homogeneous matrix with materials properties λ^m, ν^m . We define the jumps of the materials properties on the inter-phase surfaces

$$\mathbf{M}^{JJ} = \mu^j - \mu^j, \quad \mathbf{M}^J = \mu^j - \mu^m. \quad (5.13)$$

Using the standard Green function technique, we transform the equations (2.1) into an integral equation. This way we obtain an estimation of the stress distribution inside the coated inclusion σ^i and $\sigma^c(s)$ in accordance with (4.10). Therefore, the stress concentration tensors $\mathbf{B}(\mathbf{x}), \sigma^{Bi}(\mathbf{x})$ in eqn (4.8)-(4.10) are found to be

$$\mathbf{B}(\mathbf{x}), \quad \sigma^{Bi}(\mathbf{x}) = const, \quad \forall \mathbf{x} \in \mathbf{B}_i$$

and

$$\mathbf{B}(\mathbf{x}), \quad \sigma^K(\mathbf{x}) \neq const, \quad \forall \mathbf{x} \in \mathbf{B}_K \quad (5.14)$$

After that the tensors $\mathbf{R}(\mathbf{x})$ and $\mathbf{e}^{Ri}(\mathbf{x})$ are defined by eqn (4.10) and the non-linear elastic properties of the fictitious homogeneous inclusions $\mathbf{M}(\mathbf{x})$ are evaluated by the relations (5.13). Hence, the non-linear elastic problem for the single n -coated inclusion is completely solved and we can come to the estimation of the overall non-linear elastic properties $\tilde{\lambda}, \tilde{\nu}$ from (4.8) and average stresses (4.9), inside the components by the use of different tensors $\mathbf{B}(\mathbf{x}), \sigma^B(\mathbf{x})$. Some particular methods of such tensor approaches are represented in [13-15].

Different versions of closure assumptions in terms of conditional stress fields analogous to the hypothesis **H2** of the MEFM for the effective stress fields are known [2,15]. The first order approximations of these similar approaches and the principal difference between them is beyond the scope of direct substitution of the stress field for the effective field. Even for statistically homogeneous composites it may be shown that the use of the different known and useful assumption can lead to a variation of effective elastic moduli by a factor of two or more. This fact has been confirmed by experimental data [2,15]. So any model simplification maght to be very evaluated. Let us consider now a simplification of the elastic solution for different particular cases of coated inclusions. For a homogeneous

coating, i.e. $M^c(\mathbf{x}) = \text{const}$, $\forall \mathbf{x} \in \mathbf{B}_C$ are constant for any \mathbf{x} , we get from (5.1) $M(\mathbf{x}) = \boldsymbol{\mu}(\mathbf{x}) - \boldsymbol{\mu}^m$, is the jump of the compliance $\boldsymbol{\mu} = \boldsymbol{\lambda}^{-1}$ of any component with respect to the matrix, By this function the variation of the material properties within coated inclusions is taken into account. The integral operator kernel

$$\begin{aligned} \boldsymbol{\Pi}(\mathbf{x} - \mathbf{y}) &= -\boldsymbol{\lambda}^0 [\underline{\mathbf{I}}\boldsymbol{\delta}(\mathbf{x} - \mathbf{y}) + \underline{\mathbf{G}}(\mathbf{x} - \mathbf{y})\boldsymbol{\lambda}^0] \\ \underline{\mathbf{G}}(\mathbf{x} - \mathbf{y}) &= \nabla\nabla\underline{\mathbf{G}}(\mathbf{x} - \mathbf{y}) \end{aligned} \quad (5.15)$$

is defined by the two rank Green tensor $\underline{\mathbf{G}}$ of the Lamé equation of a homogeneous medium with an elastic modulus tensor $\boldsymbol{\lambda}^0$

$$\nabla\{\boldsymbol{\lambda}^0[\nabla \otimes \underline{\mathbf{G}}(\mathbf{x}) + (\nabla \otimes \underline{\mathbf{G}}(\mathbf{x}))^T]/2\} = -\underline{\mathbf{I}}\boldsymbol{\delta}(\mathbf{x}) \quad (5.16)$$

$\boldsymbol{\delta}(\mathbf{x})$ is the 3D Dirac delta function, $\underline{\mathbf{I}}$ and $\underline{\mathbf{I}}$ are the unit second-order and fourth-order tensors, respectively.

So we may define strain polarization tensors $\boldsymbol{\eta}(\mathbf{x})$ and $\boldsymbol{\eta}^0$

$$\boldsymbol{\eta}(\mathbf{x}) = \mathbf{R}\bar{\boldsymbol{\sigma}} + \boldsymbol{\eta}^R, \quad \boldsymbol{\eta}^0 = \mathbf{R}\boldsymbol{\sigma}^0 + \boldsymbol{\eta}^R \quad \forall \mathbf{x} \in \mathbf{B}_I. \quad (5.17)$$

Let us consider some conditional statistical averages of the general integral equation (4.1) leading to an infinite system of integral equations [2,8,15]. In order to simplify originally the exact system (4.1) we now apply the main hypothesis of many micromechanical methods [1,16], the so-called effective field hypothesis [2].

HI: Each inclusion in domain \mathbf{B}_I with measure v_I has an ellipsoidal shape and is embedded in the field $\tilde{\boldsymbol{\sigma}}^I$ which is homogeneous over the I -inclusion. The perturbation introduced by the inclusion v_I in the point $\mathbf{y} \notin \mathbf{B}_I$ is defined by the relation

$$\int_B f_I(\mathbf{x})\boldsymbol{\Pi}(\mathbf{x} - \mathbf{y})[\mathbf{M}(\mathbf{x})\boldsymbol{\sigma}(\mathbf{x}) + \mathbf{h}_1(\mathbf{x})]d\mathbf{x} = c_I \mathbf{T}^I(\mathbf{y} - \mathbf{x}) \langle \mathbf{M}(\mathbf{x})\boldsymbol{\sigma}(\mathbf{x}) + \mathbf{h}_1(\mathbf{x}) \rangle^I \quad (5.18)$$

where $\langle f \rangle^I$ is an average over the volume of the inclusion v_I and

$$c_I \mathbf{T}^I(\mathbf{y} - \mathbf{x}') = \int_B f_I(\mathbf{x})\boldsymbol{\Pi}(\mathbf{y} - \mathbf{x}')d\mathbf{x}, \quad \mathbf{y} \notin \mathbf{B}_I \quad (5.19)$$

In analogy to [2,15] and in view of linearity of the problem there exist constant fourth- and second-rank tensors $\mathbf{B}(\mathbf{x})$ and $\boldsymbol{\sigma}^B(\mathbf{x})$, respectively, such that

$$\begin{aligned} \boldsymbol{\sigma}^I(\mathbf{x}) &= \mathbf{B}^I(\mathbf{x})\tilde{\boldsymbol{\sigma}}^I(\mathbf{x}) + \boldsymbol{\sigma}^{BI}(\mathbf{x}), \quad \mathbf{x} \in \mathbf{B}_I, \\ c_I[\mathbf{M}(\mathbf{x})\boldsymbol{\sigma}(\mathbf{x}) + \mathbf{h}_1(\mathbf{x})]^I &= \mathbf{R}(\mathbf{x})\tilde{\boldsymbol{\sigma}}^I(\mathbf{x}) + \mathbf{e}^{RI}(\mathbf{x}) \end{aligned} \quad (5.20)$$

where the tensors $\mathbf{R}(\mathbf{x})$ and $\mathbf{e}^{RI}(\mathbf{x})$ are found by the use of the Eshelby theorem [18]

$$\mathbf{R} = -c_I \mathbf{p}^{-1}(\underline{\mathbf{I}} - \mathbf{B}), \quad \mathbf{e}^{RI}(\mathbf{x}) = c_I \mathbf{p}^{-1} \boldsymbol{\sigma}^{BI}(\mathbf{x}). \quad (5.21)$$

The tensor \mathbf{p} is associated with the Eshelby tensor \mathbf{S} by

$$\mathbf{S} = \underline{\mathbf{I}} + \boldsymbol{\mu}^0 \mathbf{p}, \quad \mathbf{p} = \langle \boldsymbol{\Pi}(\mathbf{x} - \mathbf{y}) \rangle^I = \text{const}, \quad \forall \mathbf{x}, \mathbf{y} \in \mathbf{B}_I \quad (5.22)$$

In practice the tensors \mathbf{B} and σ^{BI} are found [13,15,18] from the elastic problem of a single inclusion v_l in the infinite matrix \mathbf{B}_m , when

$$c_l = 0, \quad \tilde{\sigma}^l(\mathbf{x}) = \sigma^0 = const. \quad (5.23)$$

This problem is connected with the calculation of the inhomogeneous four- $\mathbf{B}(\mathbf{x})$ and two-rank $\sigma^{BI}(\mathbf{x})$ tensors by either analytical or numerical methods, such that for $\mathbf{x} \in \mathbf{B}_l$ the following holds:

$$\begin{aligned} \sigma(\mathbf{x}) &= \mathbf{B}(\mathbf{x})\sigma^0 + \sigma^{BI}(\mathbf{x}). \\ \mathbf{B}^l &= \langle \mathbf{B}(\mathbf{x}) \rangle^l, & \sigma^{BI} &= \langle \sigma^{BI}(\mathbf{x}) \rangle^l. \\ \mathbf{R} &= c_l \langle \mathbf{M}(\mathbf{x})\mathbf{B}(\mathbf{x}) \rangle^l, & \mathbf{e}^{RI} &= c_l \langle \mathbf{M}(\mathbf{x})\sigma^{BI}(\mathbf{x}) + \mathbf{h}_1(\mathbf{x}) \rangle^l \end{aligned} \quad (5.24)$$

We consider here an analytical method for the calculation of the tensors $\mathbf{B}(\mathbf{x})$ and $\sigma^{BI}(\mathbf{x})$ for spheroidal inclusions with a thin coatings in a sense of non-linear fields (4.10). Other analytical methods for the analysis of coated ellipsoidal inclusions are mentioned in [1,6]. In the general case the estimation of the tensors $\mathbf{B}(\mathbf{x})$, σ^{BI} is a particular problem of the transformation field $\mathbf{e}^T(\mathbf{y})$ analysis method [10,15]. For the particular case of the homogeneous ellipsoidal domain \mathbf{B}_l with non-coated inclusions $\mathbf{M}^l = \boldsymbol{\mu}^i - \boldsymbol{\mu}^m = const$, we have

$$\begin{aligned} \mathbf{B}^l &= (\underline{\mathbf{1}} + \mathbf{p}\mathbf{M})^{-1}, & \sigma^{BI} &= \mathbf{B}^l \mathbf{p}\mathbf{h}_1^l, \\ \mathbf{R} &= c_l \mathbf{M}\mathbf{B}^l, & \mathbf{e}^{RI} &= c_l (\underline{\mathbf{1}} + \mathbf{M}\mathbf{p})^{-1} \mathbf{h}_1^l \end{aligned} \quad (5.25)$$

By comparison of relation (5.25) with (4.10) one can see that the average non-linear elastic response (i.e. the tensors \mathbf{B} , σ^{BI} , \mathbf{R} , \mathbf{e}^{RI}) of any n -coated inclusion is the same as that of some fictitious ellipsoidal homogeneous, i.e. non-coated. Inclusion with non linear elastic parameters which also can be expressed in terms of the tensors \mathbf{R} and \mathbf{e}^{RI} . No restrictions are imposed on the microtopology of the coated inclusions as well as on the inhomogeneity of the stress state in the n -coated inclusions.

In a case when a single spheroid inclusion of the radiuses a^i with n homothetic spheroidal coatings of the radiuses a^{ic} with $\mathbf{p}^i = \mathbf{p}^m$ and according to (5.12), $\rho = a^{ic} - a^i$ is embedded in an infinite matrix the problem may be investigated rather strictly. The elastic properties of the coatings coincide with the elastic properties of the isotropic matrix, i.e.

$$\begin{aligned} \lambda^m(3\kappa_m, 2\mu_m) &\equiv 3\kappa_m \mathbf{J} + 2\mu_m \mathbf{K}, \\ J_{ijab} &= \frac{1}{3} \delta_{ij} \delta_{ab}, & K_{ijab} &= (\delta_{ia} \delta_{jb} + \delta_{ib} \delta_{ja}) / 2 - J_{ijab}, \\ \lambda^i(3\kappa_i, 2\mu_i), & & \lambda^{cn}(3\kappa_{cn}, 2\mu_{cn}) & \end{aligned} \quad (5.26)$$

Tensors

$$\mathbf{t}^m = \mathbf{v}^m (\mathbf{e} \otimes \mathbf{e})^m, \quad \mathbf{t}^i = \mathbf{v}^i (\mathbf{e} \otimes \mathbf{e})^i, \quad \mathbf{t}^{cn} = 0$$

have a special form with physical meaning represented by constitutive equations (1.1), (1.2). According to R. Hill [7] we define the projective operators $\underline{\mathbf{n}}$, $\underline{\mathbf{v}}$ and $\underline{\mathbf{E}}$, $\underline{\mathbf{F}}$ of the second- and fourth-order, respectively, as follows:

$$n_{ij} = n_i n_j, \quad v_{ij} = \delta_{ij} - n_{ij},$$

$$\underline{E} = \underline{I} - \underline{F}, \quad \underline{F} = [\underline{\nu} \otimes \underline{\nu} + (\underline{\nu} \otimes \underline{\nu})^T] / 2. \quad (5.27)$$

Furthermore, the surface tensors are defined by

$$\begin{aligned} \lambda(n)^\pm &= \lambda^\pm \underline{n}, & \underline{G}(n)^\pm &= [\lambda(n)^\pm]^{-1}, \\ \mathbf{B}^H(n)^\pm &= \lambda^\pm [\underline{I} - \mathbf{A}^H(n)^\pm \lambda^\pm], \\ \mathbf{A}^H(n)^\pm_{ijab} &= [n_i \mathbf{G}(n)^\pm_{ja} n_b]_{(ij)(ab)}. \end{aligned} \quad (5.28)$$

Here and below the symbols + and - relate to the different boundary sides. By testing we immediately obtain orthogonal properties of the operators defined in [7]

$$\begin{aligned} \underline{n}\underline{n} &= \underline{n}, & \underline{\nu}\underline{\nu} &= \underline{\nu}, & \underline{n}\underline{\nu} &= 0, \\ \mathbf{F}\mathbf{F} &= \mathbf{F}, & \mathbf{E}\mathbf{E} &= \mathbf{E}, \\ \mathbf{E}\underline{\nu} &= 0, & \mathbf{F}\underline{n} &= 0, & \mathbf{E}\mathbf{F} &= 0. \end{aligned} \quad (5.29)$$

Hence the tensors $\mathbf{A}^H(n)$, $\mathbf{B}^H(n)$ in (5.28) can be expressed in terms of the projective operators

$$\mathbf{A}^H(n) = [\mathbf{E}\lambda\mathbf{E}]^{-1}, \quad \mathbf{B}^H(n) = [\mathbf{F}\mu\mathbf{F}]^{-1}. \quad (5.30)$$

Perfect contact between two materials means

$$\mathbf{E}\sigma^+ = \mathbf{E}\sigma^-, \quad \mathbf{F}e^+ = \mathbf{F}e^-. \quad (5.31)$$

So the following relations between the stress tensors near the interface may be involved here [1,12,13,15]

$$\begin{aligned} \sigma^- &= \sigma^+ + \mathbf{B}^H(n)^- [(\mu^+ - \mu^-)\sigma^+ + (\mathbf{h}^+ - \mathbf{h}^-)], \\ \sigma^+ &= \sigma^- + \mathbf{B}^H(n)^+ [(\mu^- - \mu^+)\sigma^- + (\mathbf{h}^- - \mathbf{h}^+)]. \end{aligned} \quad (5.32)$$

Substitution of (5.32) into the right-hand-side of (2.5) leads to

$$\mathbf{B}^H(n)^- - \mathbf{B}^H(n)^+ = \mathbf{B}^H(n)^+ (\mu^+ - \mu^-) \mathbf{B}^H(n)^+. \quad (5.33)$$

Let an ellipsoidal inclusion v_l with the homogeneous compliance μ^+ be located in an infinite homogeneous matrix with compliance μ^- and loaded by the homogeneous stress σ^0 on remote boundary Γ_B . Then, according to Eshelby's theorem (with $\mathbf{h} = 0$), we have

$$\begin{aligned} \sigma^+ &= \sigma^0 + \mathbf{p}^l (\mu^+ - \mu^-) \sigma^+, \\ \sigma^- &= \sigma^0 + c_l \mathbf{T}^l(x_l - \mathbf{x}^-) (\mu^+ - \mu^-) \sigma^+, \end{aligned} \quad (5.34)$$

where the tensor \mathbf{p}^l of the inclusion v_l is associated with the Eshelby tensor \mathbf{S}^E by

$$\mathbf{S}^E = \underline{I} + \mu^- \mathbf{p}^l \quad (5.35)$$

and the tensor $\mathbf{T}^l(x_l - \mathbf{x}^-)$ is defined by the relation (5.19) for the point $\mathbf{x}^- \in v_l$ near the ellipsoidal surface $\Gamma_i = \partial v_l$. Substituting the relations (5.34) and (5.35) into (5.18) we obtain

$$c_l \mathbf{T}^l(x_l - \mathbf{x}^-) = \mathbf{B}^H(n)^- + \mathbf{p}^l. \quad (5.36)$$

Let us consider a coated inclusion $v_i = v_{IK} \cup v_{IC}$ with a characteristic function $f_i = f_{IK} + f_{IC}$. According to (5.12) the tensor $\mathbf{B}^H(\mathbf{n})$ in (5.33) is integrated over the coating v_{IC}

$$\int f_{IC}(\mathbf{y}) \mathbf{B}^H(\mathbf{n})^- d\mathbf{y} = -c_{IC} \mathbf{p}^I + \int [f_I(\mathbf{y}) - f_{IK}(\mathbf{y})] \int f_{IK}(\mathbf{x}) \mathbf{\Pi}(\mathbf{x} - \mathbf{y}) d\mathbf{x} d\mathbf{y}. \quad (5.37)$$

Changing the integration sequence and applying Eshelby's theorem, we get from (5.33)

$$\int f_{NC}(\mathbf{y}) \mathbf{B}(\mathbf{n})^- d\mathbf{y} = -[c_{NC} \mathbf{p}^I + c_I (\mathbf{p}^I - \mathbf{p}^N)]. \quad (5.38)$$

In particular for an isotropic medium with the elastic moduli λ the inversion of the matrix $\lambda(\mathbf{n})$ may be simplified

$$\begin{aligned} \lambda(\mathbf{n})_{ij} &= \mu \delta_{ij} + (\kappa + \mu/3) n_{ij}, \\ G_{ij} &= \frac{1}{\mu} \left(\delta_{ij} - \frac{2\kappa + \mu}{3\kappa + 4\mu} n_{ij} \right) \\ \mathbf{A}^H(\mathbf{n})_{ijab} &= \frac{1}{m} \left(E_{ijab} - \frac{3\kappa - 2\mu}{3\kappa + 4\mu} n_{ij} n_{ab} \right), & m = 2\mu, \\ \mathbf{B}^H(\mathbf{n})_{ijab} &= m \left(F_{ijab} + \frac{3\kappa - 2\mu}{3\kappa + 4\mu} v_{ij} v_{ab} \right) \end{aligned} \quad (5.39)$$

The matrix stresses in the immediate vicinity of the inclusions v_i denoted by $\sigma_i^-(\mathbf{n})$, are given by the formula

$$\sigma_i^-(\mathbf{n}) = \sigma_i^+(\mathbf{n}) + \mathbf{B}^H(\mathbf{n}) [\mathbf{M}(\mathbf{x}) \sigma_i^+ + \mathbf{h}_i(\mathbf{x})], \quad (5.40)$$

where $\sigma_i^-(\mathbf{n})$ and $\sigma_i^+(\mathbf{x})$ are the limiting stresses outside and inside, respectively, near the inclusion boundary $\Gamma_i = \partial B_i$

$$\begin{aligned} \sigma_i^-(\mathbf{n}) &= \lim_{\mathbf{y} \rightarrow \mathbf{x}} \sigma(\mathbf{y}); & \mathbf{y} &\rightarrow \mathbf{x}, & \mathbf{y} &\in v_m, \\ \sigma_i^+(\mathbf{x}) &= \lim_{\mathbf{z} \rightarrow \mathbf{x}} \sigma(\mathbf{z}), & \mathbf{z} &\rightarrow \mathbf{x}, & \mathbf{z} &\in v_i, & \mathbf{x} &\in \Gamma_i, \end{aligned}$$

\mathbf{n} – is the unit outward normal vector on Γ_i . The relation (5.31) is correct for any shape of the inclusion v_i . The tensor $\mathbf{B}^H(\mathbf{n})$ depends only on the elastic properties of the matrix material λ^m and on the direction of the normal \mathbf{n} . The expression for $\mathbf{B}^H(\mathbf{n})$ is presented as follows

$$\mathbf{B}^H(\mathbf{n})_{ijab} = m \left(F_{ijab} + \frac{3\kappa - 2\mu}{3\kappa + 4\mu} v_{ij} v_{ab} \right) \quad (5.41)$$

The equations (4.5) and (4.6) allow the estimation of the ensemble average of the matrix stresses in the vicinity of the inclusions near a point \mathbf{x} . By rearranging the latter equation into an integral one and transforming it by a method developed earlier, we obtain

$$\begin{aligned} \sigma(\mathbf{x}) - \mathbf{\Pi}(\mathbf{x} - \mathbf{y}) * \eta &= \sigma^0; \\ \mathbf{\Pi} &= -\lambda^0 (\mathbf{I} + \mathbf{g} \lambda^0); & \eta &= \mathbf{h} + \gamma \\ \gamma &= \mathbf{y} \sigma; & \mathbf{y} &= \mu - \mu^0; \end{aligned} \quad (5.42)$$

The jump of the compliance $\mathbf{M}(\mathbf{x})$ of the component v_i with respect to the matrix v_m

$$\mathbf{M}(\mathbf{x}) = \boldsymbol{\mu}(\mathbf{x}) - \boldsymbol{\mu}^m$$

By the function $\mathbf{M}(\mathbf{x})$ the variation of the material properties within coated inclusions is taken into account. The integral operator kernel is defined by the Green tensor $\mathbf{G}(\mathbf{x})$ of the Lamé equation of a homogeneous comparison medium with elasticity $\boldsymbol{\lambda}^0$. Eqn (2.14) means that the average stress $\langle \boldsymbol{\sigma} \rangle = \boldsymbol{\sigma}^0$ is precisely and that the average strain $\langle \mathbf{e} \rangle = \mathbf{e}^0$ can be measured in terms of the boundary displacements. As a special case, if two of the three semi-axes of the ellipsoid are the same, then the ellipsoid will become a spheroid. Let us assume that $a^1 = a^2$, where the spheroid aspect ratio w is defined as $w = a_3 / a_1$. Following [12,13,15], if all fibers are spheroid and the matrix is linear elastic, then for the particular case of the homogeneous ellipsoidal domain \mathbf{B}_i , $v_i = \text{mes} \mathbf{B}_i$ (uncoated inclusions) with

$$\mathbf{M} = \boldsymbol{\mu}^i - \boldsymbol{\mu}^m = \text{const}$$

we have

$$\mathbf{B} = (\mathbf{I} - \mathbf{pM})^{-1};$$

The tensor \mathbf{p} is associated with the tensor \mathbf{S} by

$$\mathbf{S} = \mathbf{I} - \mathbf{pM}; \quad \mathbf{p} = -\boldsymbol{\lambda}^0 (\mathbf{I} + \mathbf{g}\boldsymbol{\lambda}^0)$$

In this section a possible application of the above general relations is presented. An analytical method for estimating the tensors $\mathbf{B}(\mathbf{x})$ and $\boldsymbol{\sigma}^B(\mathbf{x})$, see (3.13), is carried out for the example of a single spheroidal inclusion with a thin coating in an infinite matrix loaded by a constant macroscopic stress $\boldsymbol{\sigma}^0$. Let the coated inclusion v_i consist of an ellipsoidal core v_i with a characteristic function $f_i(\mathbf{x})$ and elastic parameters $\mathbf{M}^i = \text{const}$ and a thin coating v_{ic} with a characteristic function $f_{ic}(\mathbf{x})$ and elastic inhomogeneous properties $\mathbf{M}^{ic}(\mathbf{x})$. In the considered case of a single inclusion the origin of the coordinate system is chosen to be the center of the inclusion $\mathbf{x}^i = 0$ and the coordinate axes coincide with the axes of the inclusions. In addition to (2.4) we define the jump of the material properties $[\mathbf{f}] = \mathbf{f}^+ - \mathbf{f}^-$ across the boundary Γ_C between the core and the coating as

$$\mathbf{M}^{cm} = \boldsymbol{\mu}^c - \boldsymbol{\mu}^m$$

For the single coated inclusion equation (2.4) yields after some rearrangement

$$\boldsymbol{\sigma}(\mathbf{x}) = \boldsymbol{\sigma}^0 + \int_B \boldsymbol{\Pi}(\mathbf{x} - \mathbf{y}) [\mathbf{M}(\mathbf{y}) \boldsymbol{\sigma}(\mathbf{y}) + \mathbf{h}_1(\mathbf{y})] d\mathbf{y} \quad (5.43)$$

In analogy to [1,8] we find here an approximative solution of (5.43) under the approximative assumption of a homogeneous stress state in the core

$$\boldsymbol{\sigma}(\mathbf{x}) = \boldsymbol{\sigma}^i = \text{const}; \quad \mathbf{x} \in \mathbf{B}_i \subset \mathbf{B}_i$$

and the thin-layer hypothesis, which means that the characteristic function $f_{BC}(\mathbf{x})$ can be replaced by a surface δ -function with weighting function ρ at the outer surface Γ_i^- of the boundary Γ_i and the volume integral of the continuous function $\mathbf{g}(\mathbf{x})$, $\mathbf{x} \in \mathbf{B}_i$ is equal to a surface integral over outer surface Γ_i^-

$$\int_{B_{IC}} f_{IC}(y)g(y)dy = \oint_{\Gamma_I} f_I^-(s)g(s)\rho ds \quad (5.44)$$

where the product of the characteristic function $f_I^-(s)$ of the boundary Γ_{IC} and some continuous function $g(s) = \lim g(y)$, ($y \rightarrow s$, $y \in v_{IC}$, $s \in \Gamma_I^-$) is integrated over the surface Γ_I^- . In the particular case considered hereafter, the weighting function $\rho(s)$ for a domain B_{IC} bounded by two ellipsoidal surfaces with the same centre and with identically oriented semi-axes a_j and a_j^c respectively, is as follows

$$\rho(y) = \left(\frac{y_1^2}{a_1^4} + \frac{y_2^2}{a_2^4} + \frac{y_3^2}{a_3^4} \right) \frac{1}{2} \sum_{j=1}^3 \frac{(a_j^c - a_j)}{a_j} \frac{y_j^2}{a_j^2}, \quad y \in \Gamma_I^- \quad (5.45)$$

Under these assumptions the integral eqn (5.43) is, after averaging over the domain B_I , reduced to

$$\sigma^i = \sigma^0 + p^i(M^i \sigma^i + h_1) + \oint_{\Gamma_{IC}} f_{IC}(s)T^i(x^i - s)[M^c(s)\sigma(s) + h_1(s)]\rho ds \quad (5.46)$$

Here and in the following the upper index i for the tensors p^i , B^i , T^i stands for the calculation of these tensors for the core B_I by the use of the formulae (5.46), (5.37) and (5.45), respectively. Obviously, discarding the integral term in (5.36) leads to the Eshelby solution. Taking the properties of the interface operator $B^H(n)$ [7] into account leads to

$$\begin{aligned} \sigma^c(s) &= \sigma(s) = \sigma^i + B^H(n, M^c)[M^{cm}(s)\sigma^i + h_2(s)], \\ c_i T^i(x^i - s) &= B^H(n, \mu^m) + p^i, \\ B^H(n, \mu^m)M^c B^H(n, \mu^c) &= B^H(n, \mu^m) - B^H(n, \mu^c), \end{aligned} \quad (5.47)$$

where n is a unit outward normal vector on Γ_I in the point s . Here both interface operators $B^H(n, \mu^m)$ and $B^H(n, \mu^c)$ are defined by formula applied with the compliances μ^m and μ^c , respectively

$$M^c = \mu^c - \mu^m, \quad h^{cm}(s) = h^c - h^m(s).$$

Now eqn (5.47) reduces to an equation with only one unknown constant tensor σ^i

$$\begin{aligned} \sigma^i &= \sigma^0 + \left[-\frac{c_{ic}}{c_i} p^i + p^{cm} \right] (M^i \sigma^i + h^{im}) + \frac{1}{c_i} p^i \oint_{\Gamma_I} f_I^-(s) [M^c(s)\sigma^i + h^{cm}(s)] \rho ds \\ &- \frac{1}{c_i} \oint_{\Gamma_I} f_I^-(s) [\underline{I} - p^i M^c(s)] [\underline{I} + B^H(n, \mu^m) M^c(s)]^{-1} B^H(n, \mu^m) [M^{cm}(s)\sigma^i + h^{cm}(s)] \rho ds. \end{aligned} \quad (5.48)$$

The tensor $p^i(\lambda^0)$ for the ellipsoidal inclusion v_I is determined by the relation (5.45).

References

1. Buryachenko V.A., Rammerstorfer F.G. On the thermo-elasto-statics of composites with coated randomly distributed inclusions // IJSS.-37.-2000.-p.3177-3200.


```

rm,al,al1,al2,alm,bt,bt1,bt2,btm,kv1,kv2,kvm,nup,kc11i1,kc12i1,kc11i2,&
kc12i2,kc11im,kc12im,mc,dc,mct,dct,pc,lc,tc,cc,kpe,mue,lea,kea,ema21,ema11,&
bg1,bg2,bg3,alg1,alg3,alg4,alg5,alg6,lct,nc,w,w1,w2,y,tt1,tt6

```

```

REAL ::a,b,x,lb,s0,e0,ee0,tt0,muav,rmue,kpav,rkpe,n1av,rn1e,n2av,rn2e,rn3e,n3av
INTEGER :: i,ir,js,ic1,ic2,iw1,imu1,ik1,ik,iaa,ikp1,iaa,ni,ifi,itt

```

```
!>>>>>ARRAYS
```

```

real,dimension (nr)::cr,kv,k,mu,m1,nu1,nu2,nu3,alf,bti, kz,mz, ka,&
      ma,la,na,fa, kkc,mkc, kf,mf, kh,mh, f0,f1,f2, ai,bi,ci,&
      d0,d1,d2, h0,h1,h2, c0,c1,c2, b0,b1,b2, r0,r1,r2,&
      kq,mq,lq

```

```
REAL,DIMENSION (6):: s,e,sc,xg,x6,y6,snr
```

```
REAL,DIMENSION(nr,6):: sBb,sE,sN,t,sB
```

```
REAL,DIMENSION(6,6):: y6d,x6d,brm
```

```
REAL,DIMENSION (2):: lcn,mic
```

```
!>>>>>DATA
```

```
! call input
```

```
pi = 3.1415926535897932385E0
```

```
sgl=56.
```

```
imax=nr-1
```

```
nrr=nr+ncmax
```

```
open (unit=1, file="mn01.d", status="old",&
      action="read", form="formatted", position="rewind")
```

```
i=0
```

```
PRINT *, "read_mn01"
```

```
do
```

```
read (unit=1, fmt="(f8.2)", iostat=ios) &
```

```
kv(i+1),mu(i+1),nu1(i+1),nu2(i+1),nu3(i+1)
```

```
if (nr-i-1 > 0) then; i = i + 1;
```

```
else; exit; endif
```

```
enddo
```

```
PRINT*, 'i=',i
```

```
REWIND(1)
```

```
CLOSE(1)
```

```
write(*,103) kv,mu,nu1,nu2,nu3
```

```
103 FORMAT(/20X,(5 f8.2),/20x,(5 f8.2))
```

```
OPEN(UNIT=2,FILE="mn02.r")
```

```
!READ(1,*)
```

```
!Esm1_plstrl
```

```
!kv(nr) = 4.45; mu(nr) = 1.14
```

```
!nu1(nr) = 13.3; nu2(nr) = 4.09; nu3(nr) = -9.45; alf(nr) = 1.
```

```
! 'E-glass
```

```
!kv(1) = 38.87; mu(1) = 29.2
```

```
!nu1(1) = 268.; nu2(1) = -120.; nu3(1) = 105.; alf(1) = 1.
```

```
! 'Bor
```

```
!kv(2) = 538.; mu(2) = 172.0;
```

```
!nu1(2) = -840.; nu2(2) = -420.; nu3(2) = -390.; alf(2) = 1.
```

```
alf=1.; w2=10. !w2
```

```
! 'k,m,a,b
```

```
k=kv*3.; m=2.*mu; l=(k-m)/3. !T(6)
```

```
bti=k*alf; mh=m-m(nr); kh=k-k(nr) !l
```

```
ai=nu1/2.; bi=nu2; ci=4.*nu3 !Murn
```

```
!>>>>>>>>>>r=2
```

```
do ic2 = 1,1
```

```
cr(2) = (ic2 - 1.) * 2. / 10.
```

```
!>>>>>>>>>>>>>>>>iw
```

```
do iw1 = 1,1 ! w1
```

```
If (iw1== 1) then
```

```
w1 = 15.001; endif
```

```
If (iw1== 2) then
```

```
w1 = 1000.; endif
```



```

ee0 = tt0 * mea ** 2 + s0 ** 2 * lea * (kea + mea)
!ne = l(i) / k(i)
nup = -(ema21 + a0 / s(1)) / (ema11 + a2 * s(1) + a1 + a0 / s(1))
!nup = -(ema21) / (ema11)
!stress_components

do i= 1,nr
f0(i)=e0**2*(ai(i)*ka(i)**2+bi(i)*la(i)*(3.*ka(i)+ma(i))+ci(i)*la(i)**2)&
+ee0*bi(i)*ma(i)**2
f1(i) = e0 * 2 * ma(i) * (bi(i) * ka(i) + ci(i) * la(i))
f2(i) = ci(i) * ma(i) ** 2

!repetition_eT=eps=a(sg)
a0 = -s0**2*mea*(ae*kea**2-(3.*ae+2.*be)*ne*kea**2+((3.*be+ce)*ne-be)*ne*(2.-3.*ne)*mea**2&
+ce*ne**2*mea**2)-tt0*(be-ne*(3.*be+ce))*mea**3
a1 = -2.*(be*kea-ce*ne*mea)*mea**2*s0
a2 = -ce * mea ** 3

!g0-g2
f0(i) = f0(i) + f1(i) * (a0 + lea * s0) + lea ** 2 * f2(i) * s0 ** 2
f1(i) = f1(i) * (mea + a1) + 2 * mea * lea * s0 * f2(i)
f2(i) = a2 * f1(i) + f2(i) * mea ** 2

! 'sEi=ti(e,H)

a0 = f0(i); a1 = f1(i); a2 = f2(i)
do js = 1, 6
if (js <=3) then
sE(i, js) = a0 + a1 * s(js) + a2 * s(js) ** 2
else
sE(i, js) = a1 * s(js) + a2 * s(js) ** 2
endif
! 'sB=s
! 'B=B(a,b)
a = kkc(i); b = mkc(i); lb = (a - b) / 3.
x = lb * s0
if (js <= 3) then
sB(i, js) = x + b * s(js)
else
sB(i, js) = b * s(js)
endif
enddo! Next js
enddo! Next i

! 'sBb
do i = 1,nr
r0(i) = f0(i) - f0(nr); r1(i) = f1(i) - f1(nr); r2(i) = f2(i) - f2(nr)
If (i < nr) Then
kq(i) = (ka(i) - ka(nr)) / (k(i) - k(nr)); Else
kq(i) = 0.
endif
If (i < nr) Then
mq(i) = (ma(i) - ma(nr)) / (m(i) - m(nr)); Else
mq(i) = 0.
endif
lq(i) = (kq(i) - mq(i)) / 3.
h0(i) = kq(i) * r0(i) + lq(i) * r1(i) * s0 + lq(i) * r2(i) * tt0
h1(i) = mq(i) * r1(i)
h2(i) = mq(i) * r2(i)
enddo! Next i

! 'eai
d0(nr) = 0; d1(nr) = 0; d2(nr) = 0
do i = 1,imax
d0(nr) = d0(nr) - cr(i) * h0(i)
d1(nr) = d1(nr) - cr(i) * h1(i)
d2(nr) = d2(nr) - cr(i) * h2(i)
enddo! Next i
do i = 1,imax

```


1.8. User interface “ Micro-mechanics of fiber reinforced bounded and unbounded solids: effective local and non-local thermo-elastic properties, stress concentration factors and edge effect”

The user interface “ Micro-mechanics of fiber reinforced bounded and unbounded solids: effective local and non-local thermo-elastic properties, stress concentration factors and edge effect” is developed, being a part of the entire program complex for numerical solution of multi-scale static problems of material with inclusions. The abbreviation of the program complex is MSSPMI (Multi-Scale Static Problems of Materials with Inclusions).

1. Development of user interface

The complex is developed in Lahey/Fujitsu Fortran 95 LF95 environment by use of user-interface and graphics development tool-set Winterector Starter Kit (WiSK). Separate applied programs are developed by use of programming systems Delphi 6 and Visual Basic for Applications. The environment of a program complex is integrated at a level of a source code with applied programs which are developed in language LF95, initiates start of programs and access to the input and output data of the programs developed with use of other programming languages.

2. The solution of multi-scale static problems of material with inclusions.

The multi-scale problem under study is that of the decay of edge effect in non-homogeneous material with its structure being considered at different levels. The non-homogeneous material is in agreement with semi-limited matrix reinforced by rectangular fiber, taken in a general case with isotropic covering. The problem is considered by modeling a piecewise homogeneous medium (Fig.1, Fig.2) and applying the continuity approach based on the overall properties.

2.1. The symmetrical deformation of material is caused by influence of transverse (perpendicular to the reinforce direction) periodic piecewise constant surface load. The plane boundary problems of theory of elasticity for piecewise homogeneous and transverse isotropic bodies, the ones with the overall properties and quantity criteria of the decay of edge effect are made use of as the calculation scheme.

The calculation area is taken in the Cartesian coordinates $Ox_1x_2x_3$. x_1Ox_2 is the plane of deformation, $x(x_1, x_2)$ is a point of the plane. The geometry of calculation area and the scheme of material load are shown in the Fig.1 and Fig.2 with transverse deformation of reinforced matrix and matrix with covering respectively.

2.2. The problems under consideration include the following research directions:

- the analysis of stress-strain state of non-homogeneous material near the concentration area in the form of rectangular inclusions that are subjected to transverse deformation by modeling piecewise homogeneous bodies;
- the analysis of the decay of edge effect in non-homogeneous material caused by non-uniform surface load, the material being subjected to transverse deformation, by modeling piecewise homogeneous media;
- the analysis of the influence of thin isotropic covering on the decay of edge effect in the case of non-homogeneous material;

2.3. Solving the multi-scale problem of stress-strain state and analyzing the decay of edge effect for the calculation scheme under study require the following procedures:

- The stress-strain state of material for the finite calculation area, which is in good agreement with the structure of the material and satisfies the conditions of stress-strain state in the direction of the damping of the boundary effect, is determined at the level of micro-mechanics.
- The representative element of the material is chosen for the analysis of the damping of boundary effect in non-homogeneous material. This element involves different structure levels of investigating the elastic properties of non-homogeneous material. b_{Π} , H_{Π} are the sizes of the representative element of material that are determined by the values λ_{ρ}/b_{Π} , when the size of the calculation area increases in the direction Ox_1 and Ox_2 , respectively; λ_{ρ} – is the maximum length of the decay of edge effect (maximum extent area of the boundary effect), determined with an accuracy of $\rho\%$. The conditions above can be written down as follows:

$$\lambda_{\rho}(b)/b \Big|_{b \geq b_{\Pi}, H \geq H_{\Pi}} = const_{\rho}, \lambda_{\rho} = \max_{x_1, x_2 \in \Gamma_{\rho}}(x_2), \quad (2.1)$$

where Γ_{ρ} – is the edge of boundary effect zone,

b – is the size of calculation area, on which a self-balanced load function is given, H – is the size of calculation area in the direction of the damping of boundary effect.

The determination of the boundary effect zone for the representative element of material by modeling piecewise homogeneous medium. Herewith, the satisfaction of the following condition is taken as the criterion for the decay of edge effect in the case of transverse matrix deformation (Fig.1): the determined strain state is for normal stresses is reached with the given accuracy in the direction of Ox_2 axis in the area of inclusions and matrix.

3. The description of calculation scheme and the analysis of the results obtained

3.1 The calculation area and the load scheme

The symmetrical transverse deformation of semi-limited matrix reinforced by rectangular fiber is considered. The same problem is considered when the influence of fine isotropic covering is taken into account. The appropriate calculation areas, schemes of loading and fastening are presented in the Fig. 1 and Fig.2

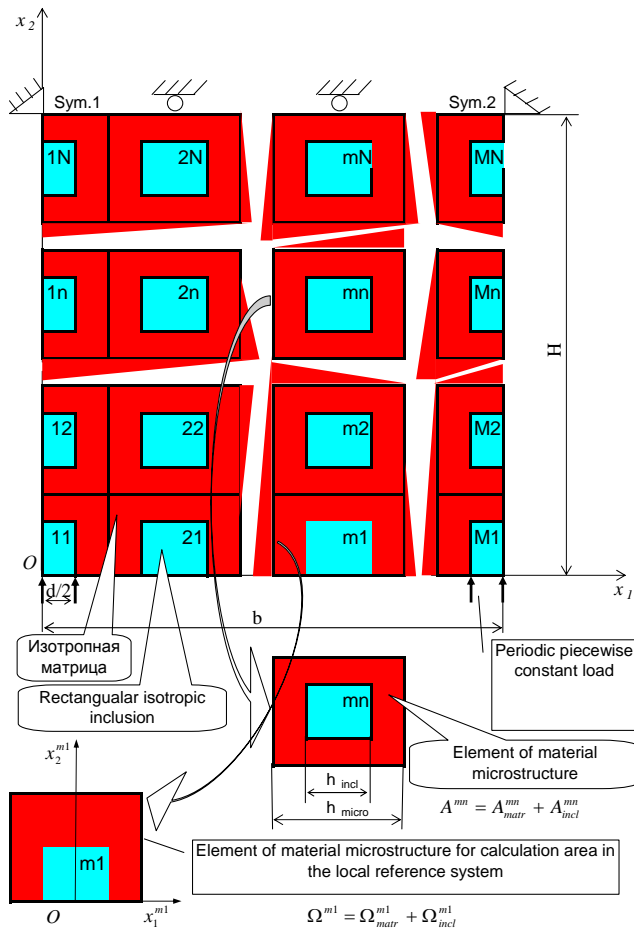


Fig.1 The transverse deformation of semi-limited matrix reinforced by rectangular fibers. Geometry and scheme of loading



Fig. 2 The transverse deformation of semi-limited matrix with covering reinforced by rectangular fibers. Geometry and scheme of loading

The intensity of surface load is assigned by relation $p(x_1) = \sigma_{22}(x_1, 0) = p^0, |x_1| \leq 0.5d + kb, k = 0, 1, \dots$. Here b is a period of load in the direction of the Ox_1 axis. Along the Ox_3 axis the load remains unchangeable. The conditions on infinity meet the terms of joint resistance. The conditions of loading and fastening that are given determine the state of plane deformation (x_1Ox_2 is the deformation plane, $x(x_1, x_2)$ a point of the plane) and the presence of axes of symmetry $x_1 = 0, x_1 = b/2$ which are marked in the Figures as Sym.1 and Sym.2, respectively. The decay of edge effect is considered in the direction of the Ox_2 axis.

The material of the matrix with inclusions is formed with the same element as that of the material microstructure, which is a square, where $A^{mn} = A_{matr}^{mn} + A_{incl}^{mn}, A_{matr}^{mn}, A_{incl}^{mn}$ are areas occupied by the matrix and inclusions, respectively. Thereby, the area occupied by the material can be presented as follows: $A = \sum_{m=1}^M \sum_{n=1}^N A^{mn}$, where M, N are the elements of material microstructure in the direction Ox_1 and Ox_2 . The three-dimensional volumes of the matrix and that of inclusions are defined by relations $c_{matr}^{mn} = A_{matr}^{mn} / A = c_{matr}, c_{incl}^{mn} = A_{incl}^{mn} / A = c_{incl}$.

When the covering is present, the area occupied by the material can be presented as follows: $A' = A + \Omega_{cover}$, where Ω_{cover} is an area occupied by the covering.

According to the calculations schemes illustrated in the Fig.1 ad Fig.2 the element of material microstructure is considered for calculation area. With the same element the calculation area for semi-limited matrix with inclusions loaded along the Ox_1 axis is formed, as shown in the Figure. Thereby, the calculation area, that corresponds to the

calculation scheme, can be presented as follows: $\Omega = \sum_{m=1}^M \sum_{n=1}^N \Omega^{mn}$, where M, N are elements of material microstructure for the calculation area in the direction Ox_1 and Ox_2 .

When the covering is given, the area occupied by the material can be presented as follows: $\Omega' = \Omega + \Omega_{cover}$.

Each element of material microstructure for the calculation area (hereinafter the element of the calculation area) is connected with the local reference system $Ox_1^{mn} Ox_2^{mn}$ ($x^{mn} = (x_1^{mn}, x_2^{mn})$) is a point of the Ω^{mn} area), as it is shown in Fig.1 and Fig.2. Introducing the notion of the element of the calculation area and bounding elements of the calculation area to local reference system allow us to set criteria of the damping of boundary effect in non-homogeneous material, its microstructure and different conditions of loading and fastening for the calculation area being taken into account.

In the present problem the stress distribution σ^{mn} on the element Ω^{mn} of the calculation area in the local reference system $Ox_1^{mn} Ox_2^{mn}$ is compared with the stress distribution $\sigma^{m(N-1)}$ on the element $\Omega^{m(N-1)}$ in local reference system $Ox_1^{m(N-1)} Ox_2^{m(N-1)}$ for equal values of the appropriate coordinates. In such a way the estimation of the damping of boundary effect for inclusions and matrix is properly provided.

3.2. The criterion of the damping of boundary effects

The decay of local and end effects of Saint-Venant is analyzed with functions $\rho(x_1, x_2)$ to estimate the decay of end effects. The condition of the decay of end effect is that the function achieves a certain value $\tilde{\rho}$ on the boundary $\Gamma_\rho(x_1, x_2)$ of the end effect zone. This condition takes the following form

$$\rho(x_1, x_2) \Big|_{x \in \Gamma_\rho} = \tilde{\rho} \quad (3.1)$$

The criterion of the decay of end effect is the condition (3.1) satisfied for the function to estimate the damping of local effect and end effect of Saint-Venant. In general case the criterion can be presented in the global reference system as follows.

1. For normal stresses $\sigma_{22} = \sigma$ the condition is satisfied with a given accuracy $\tilde{\rho}$

$$\sigma(x)/\sigma_{est} = \tilde{\rho}, \quad x = (x_1, x_2) \in \Gamma_\rho, \quad (3.2)$$

where $\sigma_{est} = \sigma(x_1, H)$ are stresses on the edge of the calculation area in the direction of the damping of boundary effect.

2. For normal stresses $\sigma_{22} = \sigma$ the conditions are satisfied with a given accuracy $\tilde{\rho}$

$$(\sigma(x) - \sigma_{est}) / (\sigma_{end} - \sigma_{est}) = \tilde{\rho}, \quad x = (x_1, x_2) \in \Gamma_\rho, \quad (3.3)$$

where $\sigma_{end} = \sigma(x_1, 0) = p(x_1)$.

In the present problem the stresses on the microstructure elements of calculation scheme Ω^{mn} and $\Omega^{m(N-1)}$ are considered. The appropriate comparison takes place in the norm $\|\cdot\|_C$ of the C space like $\|f(x)\|_C = \max_{x \in \Omega} |f(x)|$. The criterion (3.1) can be presented as follows.

1. For normal stresses $\sigma_{22} = \sigma^{mn}$ the condition is satisfied with a given accuracy $\tilde{\rho}$

$$\|\sigma^{mn}(x^{mn}) / \sigma^{m(N-1)}(x^{m(N-1)})\|_C = \tilde{\rho}, \quad x(x^{mn}) \in \Gamma_\rho,$$

$$x^{mn} \in \Omega^{mn}, x^{m(N-1)} \in \Omega^{m(N-1)}, m = \overline{1, M}, n = \overline{1, (N-1)} \text{ for } x^{mn} = x^{m(N-1)}. \quad (3.4)$$

2. For normal stresses $\sigma_{22} = \sigma$ the condition is satisfied with a given accuracy δ

$$\left\| \frac{\sigma^{mn}(x^{mn})}{\sigma^{m(N-1)}(x^{m(N-1)})} \right\|_C = \delta, x(x^{mn}) \in \Gamma_\rho,$$

$$x^{mn} \in \Omega^{mn}, x^{m(N-1)} \in \Omega^{m(N-1)}, m = \overline{1, M}, n = \overline{1, (N-1)} \text{ for } x^{mn} = x^{m(N-1)}. \quad (3.5)$$

The conditions (3.2) and (3.4) determine the decay of local effects. The conditions (3.3), (3.5) correspond to the self-equilibrated load function determine the decay of end effect of Saint-Venant.

The results of calculation shown in the figures are to be interpreted in terms of (3.4), (3.5).

3.3. Statement of the problem

The mixed boundary problem of isotropic theory of elasticity for non-homogeneous bodies is considered in the calculation area $\Omega = \sum_{i=1}^M \sum_{j=1}^N \Omega^{ij}$ and in the $\Omega' = \Omega + \Omega_{cover}$ – in case when the covering is present. The

boundary conditions meet the terms of loading and fastening of material, as shown in Fig.1 and Fig. 2. The conditions on the boundary between inclusions and matrix are taken as that of perfect interface.

3.4. The results of determining the stress-strain state and estimating the damping of boundary effects in the matrix with inclusions in the case of periodic piecewise constant load

The problem is solved by numerical approach based on the net method. The results of calculation are presented as spreadsheets corresponding to the discretisation scheme of calculation area and contain information on stress fields and estimation of the decay of end effects, as stated by (3.4), (3.5). Using the data given in the spreadsheets the results of calculation are presented graphically by Matlab and Excel facilities. The graphics are shown in Fig. 3-20.

The distribution and decay of normal stresses in the direction of Ox_2 axis for fixed coordinate values in the location of inclusions and that in the matrix are researched for different values of period of the surface load.

The sizes of the representative element of material are defined in accordance with the condition (2.1).

The influence of thin isotropic covering on the distribution and nature of the damping of normal stresses are investigated.

Data for estimating the damping of boundary effect are presented according to the conditions (3.4) and (3.5).

The calculations are made for the following geometric and mechanical properties of the calculation area:

$$E_{incl}/E_{matr} = 100, \nu_{incl} = \nu_{matr} = \nu_{cover} = 0,3, E_{cover} = E_{incl}, h_{cover} = 0,25h_{incl}, H = 5b, c_{incl} = 0.25.$$

Here the following notations are used:

$E_{incl}, E_{matr}, E_{cover}$ – the Young moduli of fiber, matrix and that of covering, respectively;

$\nu_{incl}, \nu_{matr}, \nu_{cover}$ – Poisson's coefficients of fiber, matrix and that of covering, respectively;

h_{incl} – transverse fiber of square section;

h_{cover} – thickness of the covering;

c_{incl} – concentration of inclusions;

b, H are sizes of the representative element of material in the direction of Ox_1 and Ox_2 , respectively.

3.4.1 The distribution of normal stresses in the matrix with inclusions

The distribution of normal stresses in the matrix with inclusions for the calculation areas with different number of elements of the calculation area $\Omega^{mn}, m = \overline{1, M}, n = \overline{1, N}: M = 2, N = 6; M = 3, N = 11; M = 4, N = 16; M = 5, N = 21; M = 6, N = 26$ is presented graphically in the Fig.3-7. The number of elements in the direction of Ox_1 axis is defined by a period of the surface load. The number of elements in the direction of Ox_2 axis is determined based on the condition of stress state for value n increasing.

There is a stress concentration on the interface between inclusions and matrix in the direction of Ox_2 for elements Ω^{1n} and Ω^{Mn} (the load is applied to inclusions of elements Ω^{11} and Ω^{M1}). The number of elements of the calculation area $n_{\hat{e}\hat{e}i > 1}$, for which the coefficient of stress intensity $KUH = \sigma/p$ exceeds 1, depends on the period of load (that is on the value M). Assuming such elements to form a stress concentration area, the results of calculation can be written as follows:

Table 1

M	$n_{KUH > 1}$	$n_{\text{кин est}}$	$KUH_{\text{max}} (n = 1)$	$KUH_{\text{max est}}$
2	6	3	2.6	2.2
3	11	6	2.7	1.1
4	2	9	2.7	0.75
5	2	11	2.7	0.55
6	2	12	2.7	0.4

In the Table 1 $n_{\text{кин est}}$ is the number of elements of the calculation area, within which is the value $\hat{e}\hat{e}i$ is determined, $\hat{e}\hat{e}i_{\text{max}}$ is the maximum value of KUH , which is reached on the elements Ω^{11} and Ω^{M1} , $KUH_{\text{max est}}$ is the maximum value on the element of the calculation area with determined stress state.

As it follows from the results presented, the stress concentration decreases with removing from the line of applying the load and gains a determined nature. The stress concentration area, for which the coefficient of stress intensity exceeds 1, depends on the period of load.

3.4.2 The estimation of the damping of normal stresses in matrix with inclusions according to the conditions (3.4), (3.5)

Fig. 8-12 show the distribution of estimation function of the decay of stresses $\rho(x_1, x_2) = \sigma^{mn}(x^{mn}) / \sigma^{m(N-1)}(x^{m(N-1)})$, $x^{mn} \in \Omega^{mn}$, $x^{m(N-1)} \in \Omega^{m(N-1)}$, $m = \overline{1, M}$, $n = \overline{1, (N-1)}$ for $x^{mn} = x^{m(N-1)}$.

In Fig. 13-18 are presented the distribution of estimation function of the decay of stresses $\rho(x_1, x_2) = [\sigma^{mn}(x^{mn}) - \sigma^{m(N-1)}(x^{m(N-1)})] / [\sigma^{m1}(x_1^{m1}, 0) - \sigma^{m(N-1)}(x^{m(N-1)})]$, $x^{mn} \in \Omega^{mn}$, $x^{m(N-1)} \in \Omega^{m(N-1)}$, $m = \overline{1, M}$, $n = \overline{1, (N-1)}$ for $x^{mn} = x^{m(N-1)}$.

As it follows from the results obtained, the extent $\lambda_{\rho}^{\text{max}}$ of the end effect zone, determined with accuracy of $\rho = 1\%$, is found within $1.1 \div 1.6b$ in the location of inclusions and within $1 \div 1.5b$ in the matrix. With increasing the period of the surface load b (i. e. increasing value M) the value of $\lambda_{\rho}^{\text{max}} / b$ changes non-monotonously going through the maximum at $M = 3$, and then receives the determined value at $M = 6$. The value of M determines the size of the representative element of the material in the direction of the Ox_1 axis.

Using the condition (3.5) for estimation of the decay of end effect zone, which corresponds to a self-equilibrated load function, results in higher values of the extent of end effect zone, than in case of the condition (3.4).

3.4.3. The distribution of normal stresses in matrix with inclusions when the covering is present

In. Fig. 18-20 are presented the graphs of distribution of normal stresses in matrix with inclusions for the calculation areas with different number of elements of the calculation area Ω^{mn} , $m = \overline{1, M}$, $n = \overline{1, N}$: $M = 2, N = 6$; $M = 4, N = 16$; $M = 6, N = 26$. The number of elements in the direction of the Ox_1 axis is determined by the period of surface load. The number of elements in the direction of the Ox_2 axis is determined after calculation procedure based on the condition of determined stress state when n is increasing.

There is a stress concentration on the interface between inclusions and matrix in the direction of Ox_2 axis for elements Ω^{1n} and Ω^{Mn} (the load is applied to inclusions of the elements Ω^{11} and Ω^{M1}), as well as at the angular points of the interface between inclusions and covering. The number of elements $n_{\hat{\epsilon}\hat{\epsilon}i > 1}$ of the calculation area, for which the coefficient of stress intensity $\hat{\epsilon}\hat{\epsilon}i = \sigma/p$ exceeds 1, depends on the period of load (that is on the value M). Assuming such elements to form a stress concentration area, the results of calculation can be written as follows.

Table 2

M	$n_{\kappa u H > 1}$	$n_{\kappa u H \text{ est}}$	$\kappa u H_{\max} (n = 1)$	$\kappa u H_{\max \text{ cover}} (n = 1)$	$\kappa u H_{\max \text{ est}}$
2	6	2	2.45	-	2.2
4	2	8	1.9	5	0.75
6	1-2	12	2.0	5.5	0.4

In the Table 2 $\kappa u H_{\max \text{ cover}}$ – the maximum value of $\kappa u H$, which is reached on the elements Ω^{11} and Ω^{M1} , and on the interface between inclusions and covering.

As it follows from the results obtained, the stress concentration decreases with removing from the line of load application and gains determined nature. The stress concentration area, for which the coefficient of stress intensity $\kappa u H = \sigma/p$ exceeds 1, depends on the period of load.

The presence of covering results in the following differences when compared with matrix without covering:

- the stress concentration area decreases, i.e. so does the number of elements of the calculation area in the direction of Ox_2 axis, for which the coefficient of stress intensity $\kappa u H = \sigma/p$ exceeds 1;
- the number of elements of the calculation area $n_{\kappa u H \text{ est}}$, within which there is a determined value of $\kappa u H$, decreases;
- the value of $\kappa u H_{\max}$ decreases, which is reached on the elements Ω^{11} and Ω^{M1} ;
- the presence of covering results in a new stress concentration area on the interface between inclusions and covering;
- the stress concentration on the interface between inclusions and covering reveals itself when there are unloaded inclusions along the Ox_1 axis ($M \geq 3$) (at $M = 2$ such area is absent).

Conclusions:

1. The maximum extent λ_{ρ}^{\max} of the end effect zone in the calculation area considered is defined with the accuracy $\rho = 1\%$ and takes the value of $1.7b$ in the location of inclusions and that of $1.6b$ in the matrix.
2. When the covering is present, the maximum extent λ_{ρ}^{\max} of end effect zone in the calculation area considered is defined with the accuracy of $\rho = 1\%$ and takes the value of $1.65b$ in the location of inclusions and that of $1.5b$ in the matrix.
3. With the period of surface load b being increased (that is the number of inclusions M in the direction of Ox_2 axis is increased), λ_{ρ}^{\max}/b is non-monotonously reaching its determined value when $M = 5$, which corresponds to the volume of representative element in the direction of Ox_1 axis. The volume of representative element in the direction of Ox_2 axis is $3b$, which corresponds to $N = 15$.
4. The non-monotonous changing of value λ_{ρ}^{\max}/b points out that the structure anisotropy of the material reveals itself to the whole extent when $M = 3$. For higher values of M non-homogeneous material can be dealt

with as microscopically isotropic one. The extent $\lambda_{1\%}^{\max}$ of end effect zone for this material is $1.4b$. When the covering is present, this value is that of $1.3b$.

5. There is stress concentration on the interface between inclusions and matrix in the direction of Ox_2 axis when $m = 1$ and $m = M$. The highest values of $\hat{e}\hat{e}i$ are found on the elements Ω^{11} and Ω^{M1} (corresponding to the appropriate loaded inclusions).

6. The presence of thin isotropic covering sets a "blocking" to local and end effects:

- it shrinks the area of inclusion concentrations, for which $\hat{e}\hat{e}i = \sigma/p$ exceeds 1 and the value of KUH on the interface between inclusion and matrix in the direction of the Ox_2 axis.

- it shrinks the maximum extent of edge effect zone.

7. When the covering is present, there is stress concentration located on the interface between inclusion and covering, that reveals itself in case there are unloaded inclusions ($M \geq 3$) along the Ox_1 axis in the calculation area.

8. The non-monotonous nature of the correlations revealed and newly found properties in distributing stress fields can be particularly connected with unloaded inclusions ($M \geq 3$) along the Ox_1 axis in the calculation area and redistributing surface stresses on these inclusions.

9. The representative element of material obtained in the calculation procedure determines the fact that the further investigation of elastic behavior of non-homogeneous material goes from the micromechanical level into macro-mechanical one.

2. The statistical moments of stress concentration factors in continuum estimation

The statistical moments of stress concentration factors in the random structure fibrous composite (2D) have been evaluated from the numerical experiments on the cell model (referred also sometimes as a quasi-random or

generalized periodic structure model) being a periodicity unit cell with a number of inclusions. The relevant numerical code has been developed and a wide series of numerical experiments has been performed with 50 to 100 randomly placed inclusions per cell and statistically meaningful results were obtained for the statistical moments of stress concentration factors in phases and interfaces of a random structure fibrous composite. They include, in particular, the second moment of stress playing a fundamental role in a wide class of non-linear elasticity problems, damage initiation, etc.

The developed earlier numerical (finite element) solution for a “solid with a coated high-aspect ratio inclusion” model has been applied to evaluate the stress concentrator factors and other relevant local and averaged tensors enetering the general theory of the Multiparticle Effective Field Method. The special emphasis was made on the problem of the continuum estimation of effective thermoelastic properties of nanocomposites.

The Chapter 2 of the Final Report, containing the detailed description of the. approach proposed and implemented in the frame work of the current project and results obtained are given in full in the appropriate annexes attached (v. P-110_Annex2.1.pdf, P-110_Annex2.2.pdf, P-110_Annex2.3.pdf, P-110_Annex2.4.pdf and P-110_Annex2.5.pdf).

3. Boundary 3D element analysis in the continuum estimation of effective thermoelastic properties of nanocomposites

The investigations were elaborated in the complete correspondence with coordinated and authorized Plan of Work, within the framework of following problems and subtasks of the Project:

- boundary integral formulation of 3-D elastostatic multiple inclusion problems;
- elaboration of boundary element algorithms for 3-D elastostatic problems on single inclusion in inhomogeneous field;
- examination of accuracy and efficiency of boundary integral equations (BIEM) – boundary element (BEM) method for 3D single inclusion problems;
- micromechanical BIEM–BEM elastic field analysis of 3D partially-homogeneous solids;
- estimation of 3-D inhomogeneous stress fields inside inclusions of complex shapes;
- determination of averaged stresses inside inclusions of complex shapes in 3D elastic matrix;
- 3D macromechanical homogenization analysis of particulate composite materials;
- effective stress concentration in 3D particulate composite materials.

By using the general reciprocity principles, superposition principles and fundamental solutions, the boundary integral representations of static displacement and stress components in an elastic composite solid consisting of 3-D infinite remotely loaded matrix with multiple inclusions (volumetric, thin-walled and crack-like) of complex geometry and arbitrary rigidity are constructed. To define the densities of involved potentials the systems of boundary integral equations with Newtonian potential kernels are obtained by satisfaction the contact conditions at the interfaces. The subtraction technique is applied to construct the regular analogues of equations. In addition, the treatments of hypersingular, strong and weakly singular integrals are given, also the regularizing integrals are evaluated analytically. The boundary element algorithm for numerical solution of deduced integral equations is developed. It bases on both the introduction of quadrilateral (triangular) isoparametric boundary elements on the solid interface and the approximation of unknown functions by the interpolation polynomials within constructed elements. The collocation technique is proposed for obtaining the discrete analogues as systems of linear algebraic equations relative to the interfacial quantities (both displacements and tractions or their jumps) at the nodal points. The software codes (in FORTRAN) are created for implementation of the above algorithm. Two approaches are used for examination of developed numerical tool on accuracy and efficiency: first of them rests on the comparison of actual quantities calculated by the BIEM–BEM with those available in the literature for specific inclusion configurations and disturbing fields; the second one bases on the posterior estimation of the numerical results after implementation of the alternative treatments of involved singular integrals, approximations of unknown functions and boundary element meshes. Actual 3D elastostatic problems for composite solid formed by infinite elastic matrix and perfectly bonded volumetric elastic inclusion of complex shape are brought to numerical results by BIEM-BEM. As an example, the inclusion of the shape of finite cylinder with smoothed edges is considered. The interfacial quantities (both displacements and tractions) are estimated from the discretized BIE with six types of the right parts, that characterize the displacement main field due to the remote unit tensile and shear loadings in three perpendicular X,Y,Z directions.

Then developed BIEM–BEM methodology is applied to the definition of 3-D inhomogeneous displacement and stress fields inside volumetric inclusions of complex shapes in an infinite elastic matrix in the general case of loading. With this purpose the integral representation formulas connecting the actual quantities with the contact displacements and tractions at interfaces (solutions of the BIE) are exploited. The discrete analogues of these relations are constructed by the implementation of the standard Gaussian quadratures to deal with regular integrals as well as subdivision technique to deal with nearly-singular integrals, which occur when the field point is very close to but still off the surface of integration. As a numerical example, the inclusion with smoothed edges is considered. The displacements and stresses as function of the position vector of inclusion internal point are estimated for the six types of loadings, namely the remote unit tensile and shear loadings in three perpendicular X,Y,Z-directions. Different relations between the elastic modulus of the solid constituents and two shape parameters (first parameter describes the relation between the height and radius of the cylinder cross-section, in other words the inclusion aspect ratio, the second one – the degree of rounding of inclusion's edges) are involved in the analysis. In addition, the well-known situation of spherical inclusion (correlation hole) is taken into account as particular case, which has the solution with the analytical counterpart. The technique of stress averaging includes meshing of inclusion domain by the volumetric

elements and constant approximation of all stress components within the introduced elements (then the stress values in the fixed element are equal to the stresses at the centroid of this element). As an output of the proposed technique, the six-rank tensors with the stress components or corresponding strain components are obtained under different geometric and mechanical parameters of the finite cylinder shape inclusion. Also the analogous tensors for the inclusion of the surrounding sphere shape (correlation hole) are evaluated and compared with the known analytical counterparts.

By the multiparticle effective field method in conjunction with the obtained boundary element solutions of 3D one-particle problem for the uniform tensile and shear loading as well as uniform fictitious eigenstrains conditions, the effective elastic properties of random structure composites for arbitrary inclusion shape are estimated. The influence of the nonspherical shape of inclusions (on the example of finite cylinder with the smooth ends) on the effective elastic moduli of a composite material and statistical averages of the stresses in the inclusions is investigated. As 3D object of continuum analysis, a linearly elastic medium of isotropic constituents, which consists of a homogeneous matrix containing a statistically homogeneous random set of inclusions of any shape, is considered. The ensemble averaging is replaced by volume averaging for the random quantities description in such composite structure. The formulas for the 6×6 effective compliance tensor and 1×6 effective stress tensor are exploited, which take into account the "quasi-crystalline" approximation of the inclusion interactions. The elaborated numerical scheme is implemented for the homogenization analysis of composite with the cylinder shape inclusions with the smoothed ends and aligned orientation. The dependences of the effective elastic moduli versus the concentration of inhomogeneities are constructed and studied from the point of view of the reinforcing effects. The distribution of effective stresses along both the cross-section and axis of inclusion of limit fiber shape is studied for different external loadings of composite, the relations between the elastic moduli of its constituents, the inclusion aspect ratios, as well as the dilute and nondilute concentration of inhomogeneities. The points inside the inclusion with the maximal effective stresses are revealed and interpreted as the stress concentration zones.

The BIEM-BEM strategy is extended on the 3D multiple thin-walled inclusion problem. The effective boundary conditions (the jumps of displacements and interfacial stresses across the inhomogeneities, depending on their rigidity) in the inclusion domains are suggested. The problem is reduced to the boundary integral equations of second kind relative these jumps. The stable numerical solution for a wide spectrum of stiff characteristics of the composite constituents and profiles of thin-walled inhomogeneities is given. The relations for the renewing of the stresses inside the inclusions are deduced. The numerical results for the limiting cases of interacting stiff inclusions and crack-like defects are obtained. The reinforcing properties of dispersed phase are estimated by comparing the peak values of stress intensity factors in the crack vicinity in the cases of presence and absence of neighboring inclusion under the same disturbances of the solid. Also within this Project the attempt to extend BIEM-BEM to the similar dynamic problems is made.

The above investigations open the possibilities for study of both static and dynamic micro-macromechanical properties of 3D particulate composites damaged by the inner and interfacial cracks as well as manifold originated interfacial imperfectnesses (due to the presence of partial separation, interface coated layers, slipping, adhesion etc.) simulated by the spring-like contact conditions between the solid constituents.

Within this Project the following papers are prepared:

1. Mykhas'kiv V.V., Kunets Ya.I. and Mishchenko V.O. Stresses in a three-dimensional body with thin compliant inclusion behind the front of pulsed waves // *Materials Science.*- 2003.- **39**, No. 3.- P. 377-384.
2. Mykhas'kiv V.V. Transient response of a plane rigid inclusion to an incident wave in an elastic solid // *Wave Motion.* – 2005.- **41**, No 2.- P. 133-144.
3. Mykhas'kiv V.V. and Kalyniak O.I. Nonstationary disturbances of a 3-D elastic matrix with a rigid disk inclusion // *Physicochemical Mechanics of Materials.*- 2005.- **41**, No. 2.- P. 7-15 (in Ukrainian).
4. Mykhas'kiv V.V. and Stepanyuk O.I. BIE method for 3D static problems of rigid disc-inclusion and crack interaction in elastic matrix // *Computer Modeling in Engineering & Sciences (CMES)* (accepted).
5. Mykhas'kiv V.V. and Stasyuk B.M. Solution of 3D elastostatic problems on the loading transfer in a solid with inclusion of nonclassical shape by boundary element method // *Int. Applied Mechanics* (in Russian, accepted).

6. Buryachenko V.A. and Mykhas'kiv V.V. 3D boundary element analysis in the continuum estimation of effective thermoelastic properties of nanocomposites // (in preparation).

3.1 Boundary Integral Formulation and Solution of 3D Problems for Volumetric Inclusion in Inhomogeneous Field

The 3-D elastostatic problem for remotely loaded infinite matrix (specified by the domain Ω^M , shear modulus μ^M and Poisson's ratio ν^M) with a perfectly bonded inclusion (specified by the domain Ω^I , shear modulus μ^I and Poisson's ratio ν^I) along the surface S with outward normal $\mathbf{n}(n_1, n_2, n_3)$ (Fig. 1) is solved by BIEM-BEM.

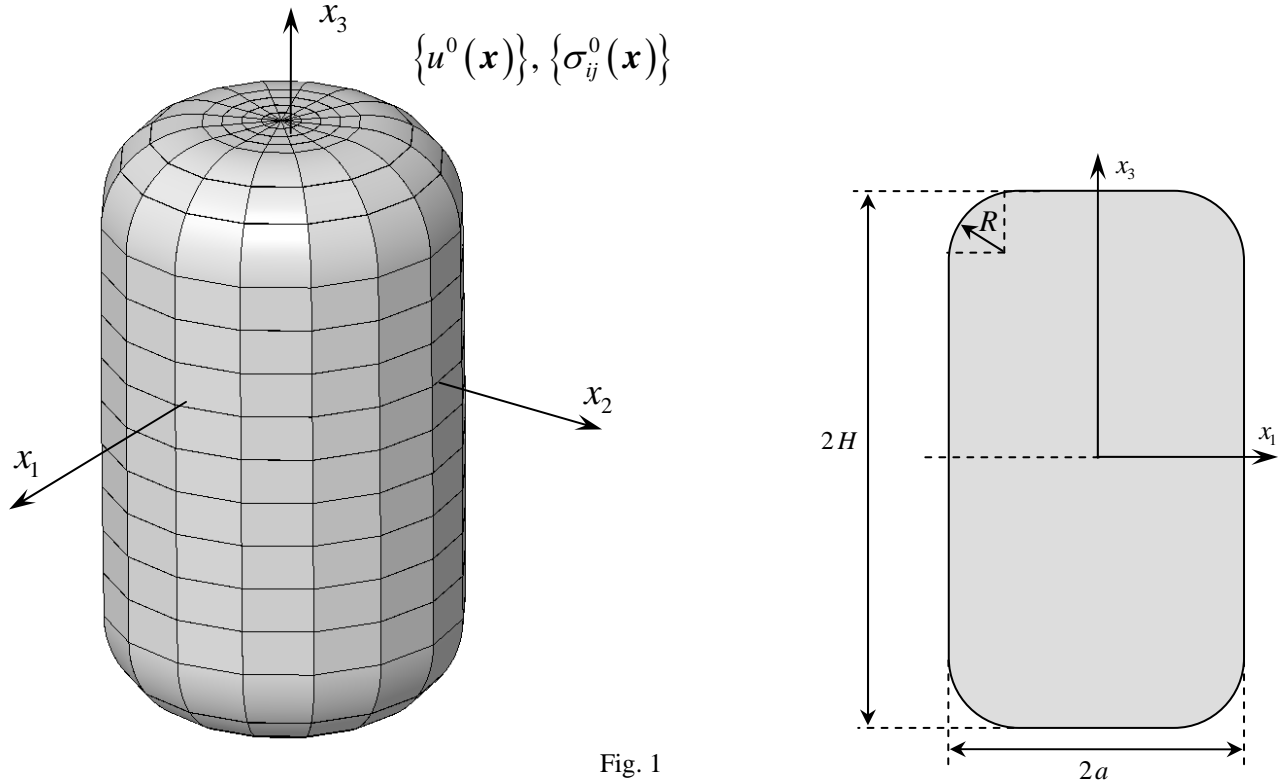


Fig. 1

The inhomogeneous main field due to the outer loading is described by the known distribution of displacement $\mathbf{u}^0(u_1^0, u_2^0, u_3^0)$ and corresponding stress $\sigma_{ij}^0(i, j = 1, 2, 3)$ components. With this purpose the boundary integral representations of displacement components in the matrix (solutions of external problem, with upper index "M") and in the inclusion (solutions of internal problem, with upper index "I") in terms of interfacial quantities are constructed via Betty-Rayleigh formulae as:

$$\begin{aligned}
 u_i^I(\mathbf{x}) &= \iint_S U_{ij}^I(\mathbf{x}, \mathbf{y}) p_j(\mathbf{y}) dS_y - \iint_S T_{ij}^I(\mathbf{x}, \mathbf{y}) u_j(\mathbf{y}) dS_y, \\
 \mathbf{x}(x_1, x_2, x_3) &\in \Omega^I, \quad i = 1, 2, 3, \\
 u_i^M(\mathbf{x}) &= u_i^0(\mathbf{x}) - \iint_S U_{ij}^M(\mathbf{x}, \mathbf{y}) p_j(\mathbf{y}) dS_y + \iint_S T_{ij}^M(\mathbf{x}, \mathbf{y}) u_j(\mathbf{y}) dS_y, \\
 \mathbf{x}(x_1, x_2, x_3) &\in \Omega^M, \quad i = 1, 2, 3,
 \end{aligned}
 \tag{1}$$

where the unknown densities $u_j(\mathbf{y})$, $p_j(\mathbf{y})$ characterize the displacements and tractions at the interface respectively (from the perfect contact conditions they are continuous on S), first $U_{ij}(\mathbf{x}, \mathbf{y})$ and second $T_{ij}(\mathbf{x}, \mathbf{y})$ fundamental elastostatic solutions for the material "I" or "M" can be written in the following form

$$U_{ij}^{\{M\}}(\mathbf{x}, \mathbf{y}) = \frac{1}{16\pi\mu^{\{M\}}(1-\nu^{\{M\}})} \left[\left(3 - 4\nu^{\{M\}} \right) \frac{\delta_{ij}}{|\mathbf{x} - \mathbf{y}|} + \frac{(x_i - y_i)(x_j - y_j)}{|\mathbf{x} - \mathbf{y}|^3} \right],$$

$$i, j = \overline{1, 3},$$

$$T_{ij}^{\{M\}}(\mathbf{x}, \mathbf{y}) = \frac{1}{8\pi(1-\nu^{\{M\}})} \frac{1}{|\mathbf{x} - \mathbf{y}|^2} \left\{ \frac{(x_k - y_k)}{|\mathbf{x} - \mathbf{y}|} n_k(\mathbf{y}) \left[\left(1 - 2\nu^{\{M\}} \right) \delta_{ij} + \right. \right. \quad (2)$$

$$\left. \left. + 3 \frac{(x_i - y_i)(x_j - y_j)}{|\mathbf{x} - \mathbf{y}|^2} \right] - \left(1 - 2\nu^{\{M\}} \right) \left[\frac{(x_i - y_i)}{|\mathbf{x} - \mathbf{y}|} n_j(\mathbf{y}) - \frac{(x_j - y_j)}{|\mathbf{x} - \mathbf{y}|} n_i(\mathbf{y}) \right] \right\}.$$

Satisfying by the integral representations (1) the contact conditions

$$\lim_{\mathbf{x} \rightarrow S} u_i^I(\mathbf{x}) = \lim_{\mathbf{x} \rightarrow S} u_i^M(\mathbf{x}) = u_i(\mathbf{x}), \quad \mathbf{x} \in S \quad (3)$$

and taking into account the boundary properties of involved potentials yield the system of six boundary integral equations relative to the functions $u_j(\mathbf{y})$, $p_j(\mathbf{y})$ ($j = 1, 2, 3$) in the singular form:

$$\frac{1}{2} u_i(\mathbf{x}) + \iint_S T_{ij}^I(\mathbf{x}, \mathbf{y}) u_j(\mathbf{y}) dS_y - \iint_S U_{ij}^I(\mathbf{x}, \mathbf{y}) p_j(\mathbf{y}) dS_y = 0,$$

$$\frac{1}{2} u_i(\mathbf{x}) - \iint_S T_{ij}^M(\mathbf{x}, \mathbf{y}) u_j(\mathbf{y}) dS_y + \iint_S U_{ij}^M(\mathbf{x}, \mathbf{y}) p_j(\mathbf{y}) dS_y = u_i^0(\mathbf{x}), \quad (4)$$

$$\mathbf{x} \in S, \quad i = 1, 2, 3.$$

Then the subtraction technique is applied to construct the regular analogues of integral equations (4). After considering the exact values of Gauss type integrals we obtain the following six boundary integral equations with only polar peculiarities (with the order r^{-1}) in the kernels, which are the most appropriate for the numerical solution:

$$\iint_S \left[u_j(\mathbf{y}) - u_j(\mathbf{x}) \right] T_{ij}^I(\mathbf{x}, \mathbf{y}) dS_y - \iint_S U_{ij}^I(\mathbf{x}, \mathbf{y}) p_j(\mathbf{y}) dS_y = 0,$$

$$u_i(\mathbf{x}) - \iint_S \left[u_j(\mathbf{y}) - u_j(\mathbf{x}) \right] T_{ij}^M(\mathbf{x}, \mathbf{y}) dS_y + \iint_S p_j(\mathbf{y}) U_{ij}^M(\mathbf{x}, \mathbf{y}) dS_y = u_i^0(\mathbf{x}), \quad (5)$$

$$i = 1, 2, 3, \quad \mathbf{x} \in S.$$

Also the boundary integral formulation is extended to the analogous composite solid with the constituents specified by equal Poisson's ratios, but different shear modulus. Then the relations take place $\mu^I U_{ij}^I = \mu^M U_{ij}^M$, $T_{ij}^I = T_{ij}^M = T_{ij}$. This model is interesting because of the division of the system of six equations (4) or (5) into two independent subsystems of equations of second and first kind, namely in regular form:

$$\mu^M u_i(\mathbf{x}) + \left(\mu^B - \mu^M \right) \iint_S T_{ij}(\mathbf{x}, \mathbf{y}) \left[u_j(\mathbf{y}) - u_j(\mathbf{x}) \right] dS_y = \mu^M u_i^0(\mathbf{x}), \quad i = 1, 2, 3, \quad (6)$$

$$\iint_S U_{ij}^I(\mathbf{x}, \mathbf{y}) p_j(\mathbf{y}) dS_y = \iint_S \left[u_j(\mathbf{y}) - u_j(\mathbf{x}) \right] T_{ij}(\mathbf{x}, \mathbf{y}) dS_y, \quad i = 1, 2, 3.$$

Mentioned above circumstance causes the essential economy of computer resources both in terms of CPU time and memory.

Analytical developments are completed by the integral representations for the stresses both inside inclusion and matrix in terms of solutions of the obtained boundary integral equations. They can be written as

$$\sigma_{ij}^I(\mathbf{x}) = \iint_S D_{ijk}^I(\mathbf{x}, \mathbf{y}) p_k(\mathbf{y}) dS_y - \iint_S S_{ijk}^I(\mathbf{x}, \mathbf{y}) u_k(\mathbf{y}) dS_y, \quad \mathbf{x} \in \Omega^I, \quad i, j = 1, 2, 3,$$

$$\sigma_{ij}^M(\mathbf{x}) = \sigma_{ij}^0(\mathbf{x}) - \iint_S D_{ijk}^M(\mathbf{x}, \mathbf{y}) p_k(\mathbf{y}) dS_y + \iint_S S_{ijk}^M(\mathbf{x}, \mathbf{y}) u_k(\mathbf{y}) dS_y, \quad (7)$$

$$\mathbf{x} \in \Omega^M, \quad i, j = 1, 2, 3.$$

Here the kernels are defined from the relations:

$$D_{ijk}^{\{I\}}(\mathbf{x}, \mathbf{y}) = -\frac{1}{8\pi(1-\nu^{\{I\}})} \frac{1}{|\mathbf{x}-\mathbf{y}|^2} \left[(1-2\nu^{\{I\}}) \left(\frac{x_i-y_i}{|\mathbf{x}-\mathbf{y}|} \delta_{jk} + \frac{x_j-y_j}{|\mathbf{x}-\mathbf{y}|} \delta_{ki} - \frac{x_k-y_k}{|\mathbf{x}-\mathbf{y}|} \delta_{ij} \right) + 3 \frac{(x_i-y_i)(x_j-y_j)(x_k-y_k)}{|\mathbf{x}-\mathbf{y}|^3} \right],$$

$$S_{ijk}^{\{I\}}(\mathbf{x}, \mathbf{y}) = \frac{\mu^{\{I\}}}{4\pi(1-\nu^{\{I\}})} \frac{1}{|\mathbf{x}-\mathbf{y}|^3} \left\{ 3 \frac{x_l-y_l}{|\mathbf{x}-\mathbf{y}|} n_l(\mathbf{y}) \left[(1-2\nu^{\{I\}}) \delta_{ij} \frac{x_k-y_k}{|\mathbf{x}-\mathbf{y}|} + \right. \right. \quad (8)$$

$$\begin{aligned}
& +v^{\{I\}} \left(\delta_{jk} \frac{x_i - y_i}{|\mathbf{x} - \mathbf{y}|} + \delta_{ik} \frac{x_j - y_j}{|\mathbf{x} - \mathbf{y}|} \right) - 5 \frac{(x_i - y_i)(x_j - y_j)(x_k - y_k)}{|\mathbf{x} - \mathbf{y}|^3} \Bigg] + \\
& +3 \left[v^{\{I\}} n_i(\mathbf{y}) \frac{(x_j - y_j)(x_k - y_k)}{|\mathbf{x} - \mathbf{y}|^2} + v^{\{I\}} n_j(\mathbf{y}) \frac{(x_i - y_i)(x_k - y_k)}{|\mathbf{x} - \mathbf{y}|^2} + (1 - 2v^{\{I\}}) n_k(\mathbf{y}) \times \right. \\
& \left. \times \frac{(x_i - y_i)(x_j - y_j)}{|\mathbf{x} - \mathbf{y}|^2} \right] + (1 - 2v^{\{I\}}) \left[\delta_{jk} n_i(\mathbf{y}) + \delta_{ik} n_j(\mathbf{y}) \right] - (1 - 4v^{\{I\}}) \delta_{ij} n_k(\mathbf{y}) \Bigg\}
\end{aligned}$$

The boundary element algorithm for numerical solution of obtained integral equations is developed. It bases on both the introduction of eight-node quadrilateral and six-node triangular isoparametric boundary elements S_q ($q = 1, 2, \dots, Q$) on the solid interface. Then the global coordinates for the point $\mathbf{x}_q \in S_q$ are expressed by means of coordinates of nodal points as:

i) for the quadrilateral element

$$\begin{aligned}
x_{iq}|_{S_q} &= \sum_{n=1}^8 x_{iqn} N^n(\xi_1, \xi_2), \quad i = 1, 2, 3, \\
N^1(\xi_1, \xi_2) &= \frac{1}{4}(1 - \xi_1)(1 - \xi_2)(-\xi_1 - \xi_2 - 1); \quad N^2(\xi_1, \xi_2) = \frac{1}{4}(1 + \xi_1)(1 - \xi_2)(\xi_1 - \xi_2 - 1); \\
N^3(\xi_1, \xi_2) &= \frac{1}{4}(1 + \xi_1)(1 + \xi_2)(\xi_1 + \xi_2 - 1); \quad N^4(\xi_1, \xi_2) = \frac{1}{4}(1 - \xi_1)(1 + \xi_2)(-\xi_1 + \xi_2 - 1); \quad (9) \\
N^5(\xi_1, \xi_2) &= \frac{1}{2}(1 - \xi_1^2)(1 - \xi_2); \quad N^6(\xi_1, \xi_2) = \frac{1}{2}(1 - \xi_2^2)(1 + \xi_1); \\
N^7(\xi_1, \xi_2) &= \frac{1}{2}(1 - \xi_1^2)(1 + \xi_2); \quad N^8(\xi_1, \xi_2) = \frac{1}{2}(1 - \xi_2^2)(1 - \xi_1);
\end{aligned}$$

ii) for the triangular element

$$\begin{aligned}
x_{iq}|_{S_q} &= \sum_{n=1}^6 x_{iqn} M^n(\xi_1, \xi_2), \quad i = 1, 2, 3, \\
M^1(\xi_1, \xi_2) &= \frac{1}{6}(\xi_1\sqrt{3} + \xi_2)(\xi_1\sqrt{3} + \xi_2 - \sqrt{3}); \quad M^2(\xi_1, \xi_2) = \frac{1}{6}(\xi_1\sqrt{3} - \xi_2)(\xi_1\sqrt{3} - \xi_2 + \sqrt{3}); \quad (10) \\
M^3(\xi_1, \xi_2) &= \frac{1}{3}\xi_2(2\xi_2 - \sqrt{3}); \quad M^4(\xi_1, \xi_2) = -\frac{1}{3}(\xi_1\sqrt{3} - \xi_2 + \sqrt{3})(\xi_1\sqrt{3} + \xi_2 - \sqrt{3}); \\
M^5(\xi_1, \xi_2) &= \frac{2}{3}\xi_2(\xi_1\sqrt{3} - \xi_2 + \sqrt{3}); \quad M^6(\xi_1, \xi_2) = \frac{2}{3}\xi_2(-\xi_1\sqrt{3} - \xi_2 + \sqrt{3}).
\end{aligned}$$

Following approximation of unknown functions by the interpolation polynomials within constructed elements are foreseen:

i) on the quadrilateral element

$$u_i(\mathbf{x})|_{S_q} = \sum_{n=1}^8 u_i(\mathbf{x}_{qn}) N^n(\xi_1, \xi_2), \quad p_i(\mathbf{x})|_{S_q} = \sum_{n=1}^8 p_i(\mathbf{x}_{qn}) N^n(\xi_1, \xi_2), \quad i = 1, 2, 3; \quad (11)$$

ii) on the triangular element

$$u_i(\mathbf{x})|_{S_q} = \sum_{n=1}^6 u_i(\mathbf{x}_{qn}) M^n(\xi_1, \xi_2), \quad p_i(\mathbf{x})|_{S_q} = \sum_{n=1}^6 p_i(\mathbf{x}_{qn}) M^n(\xi_1, \xi_2), \quad i = 1, 2, 3. \quad (12)$$

The collocation technique is proposed for obtaining the discrete analogues of boundary integral equations as systems of linear algebraic equations relative to the interfacial quantities (both displacements and tractions) at the nodal points. The stability of proposed BIEM-BEM algorithm is provided by consideration of numerical properties of the matrices of discrete analogues. The standard Gaussian schemes of integration over nonsingular elements (under determination of nondiagonal coefficients in the matrix) are exploited. Special adaptive methodology is implemented for the correct evaluation of the singular integrals, which represent the diagonal coefficients in the matrixes. It foresees using the triangular polar coordinates to reduce the order of singularity of the singular elements by one degree and to carry out the integration over the mappings (13) of the singular elements onto plane squares (Fig. 2).

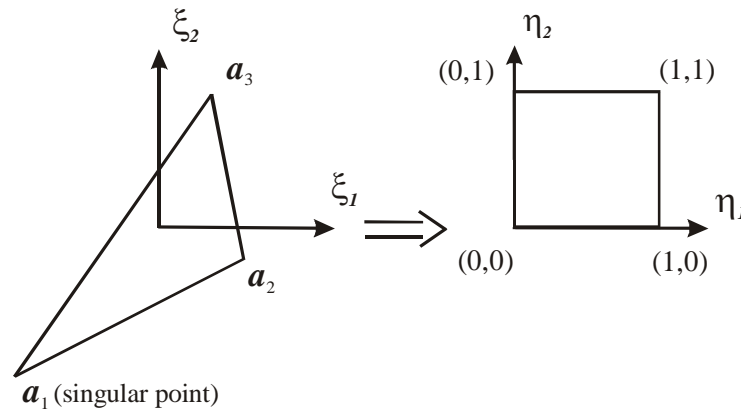


Fig. 2

$$\xi = (1 - \eta_1) \mathbf{a}_1 + \eta_1 (1 - \eta_2) \mathbf{a}_2 + \eta_1 \eta_2 \mathbf{a}_3 \quad (13)$$

This strategy results in good numerical approximations of singular integrals existing in the Cauchy principal value sense and converts weakly singular integrals into integrals over smooth functions. Besides, both the interpolation polynomials of different orders for the interfacial quantities approximations (as example, first order approximations for the traction functions and second order approximations for the displacement function) and boundary elements of different sizes are involved in the numerical analysis.

The software codes (in FORTRAN) are generated for implementation of the above algorithm. In consequence, the 3D elastostatic problems for composite solid formed by infinite elastic matrix and perfectly bonded volumetric elastic inclusion of shape of finite cylinder with smoothed edges are brought to numerical results. Fig. 1 is a representation of the inclusion boundary described in the cylindrical coordinate system and in the half-space $z \geq 0$ by the surface ($2H$ is the inclusion height, a is the radius of inclusion cross-section, R is the radius of rounding of inclusion's edges):

$$\begin{cases} r = a, & \text{when } z \leq H - R; \\ z = H, & \text{when } r \leq a - R; \\ (r - a + R)^2 + (z - H + R)^2 = R^2, & \text{when } z > H - R, r > a - R, \end{cases} \quad (14)$$

which reduces to a sphere and cylinder with smoothed edges in the limiting cases $H = a = R$ and $R = a$, respectively. The mesh for this inclusion configuration is shown in the Fig. 1.

The actual interfacial quantities (both displacements and tractions) are estimated from the discretized BIE with six types of the right parts, that characterize the displacement main field due to the remote unit tensile and shear

loadings in three perpendicular X,Y,Z directions. Different relations between the elastic modulus of the solid constituents and two shape parameters (first parameter describes the relation between the height and radius of the cylinder cross-section, in other words the inclusion aspect ratio, the second one – the degree of rounding of inclusion’s edges) are involved in the analysis. Obtained results allow us to calculate the inhomogeneous stress field at any point inside the inclusion. As consequence, we obtain six-rank tensors, which are necessary at including the homogenization ideas and hypotheses for study of the influence of inclusion shape on the statistical averages of effective stresses and stresses in the inclusions, when 3D matrix containing statistically homogeneous set of inclusions of nonclassical shapes is considered.

The procedures for accuracy-stability verification of the proposed method are foreseen in the computer programs through the possibilities to change the boundary element sizes and to proceed to the simplest solutions, which are obtained analytically. As a test of accuracy of the proposed BIEM-BEM technique, the single spherical inclusion in an infinite elastic matrix subjected to homogeneous stress σ^0 at infinity is considered. The obtained BIEM-BEM results for the stresses in inclusion are compared with the Eshelby’s analytical solutions for different relations between the inclusion-matrix elastic modulus (Tables 1-4). In all cases the dependences of errors versus discretization parameter of numerical scheme are established. On this base the optimal meshes and approximations are defined (in our case 182 boundary elements are used, quadratic approximation for the displacement and linear approximation for the tractions are employed).

$$\text{Case I: } \nu^M = \nu^I = 0,45; \quad \frac{E^M}{E^I} = \frac{\mu^M}{\mu^I} = 0,1$$

Analytical solution

	σ_{11}/σ^0	σ_{22}/σ^0	σ_{33}/σ^0	σ_{12}/σ^0	σ_{13}/σ^0	σ_{23}/σ^0
Tension along Ox_1	1.758	-0.318	-0.318	0	0	0
Tension along Ox_2	-0.318	1.758	-0.318	0	0	0
Tension along Ox_3	-0.318	-0.318	1.758	0	0	0
Shear in plane x_1Ox_2	0	0	0	2.075	0	0
Shear in plane x_1Ox_3	0	0	0	0	2.075	0
Shear in plane x_2Ox_3	0	0	0	0	0	2.075

Table 1

Numerical solution

	σ_{11}/σ^0	σ_{22}/σ^0	σ_{33}/σ^0	σ_{12}/σ^0	σ_{13}/σ^0	σ_{23}/σ^0
Tension along Ox_1	1.769	-0.310	-0.310	0	0	0
Tension along Ox_2	-0.310	1.769	-0.310	0	0	0
Tension along Ox_3	-0.310	-0.310	1.769	0	0	0
Shear in plane x_1Ox_2	0	0	0	2.156	0	0
Shear in plane x_1Ox_3	0	0	0	0	2.156	0
Shear in plane x_2Ox_3	0	0	0	0	0	2.156

Table 2

$$\text{Case II: } \nu^M = \nu^I = 0,45; \quad \frac{E^M}{E^I} = \frac{\mu^M}{\mu^I} = 0,01$$

Analytical solution

	σ_{11}/σ^0	σ_{22}/σ^0	σ_{33}/σ^0	σ_{12}/σ^0	σ_{13}/σ^0	σ_{23}/σ^0
Tension along Ox_1	1.929	-0.396	-0.396	0	0	0
Tension along Ox_2	-0.396	1.929	-0.396	0	0	0
Tension along Ox_3	-0.396	-0.396	1.929	0	0	0
Shear in plane x_1Ox_2	0	0	0	2.326	0	0
Shear in plane x_1Ox_3	0	0	0	0	2.326	0
Shear in plane x_2Ox_3	0	0	0	0	0	2.326

Table 3

Numerical solution

	σ_{11}/σ^0	σ_{22}/σ^0	σ_{33}/σ^0	σ_{12}/σ^0	σ_{13}/σ^0	σ_{23}/σ^0
Tension along Ox_1	2.103	-0.362	-0.362	0	0	0
Tension along Ox_2	-0.362	2.103	-0.362	0	0	0
Tension along Ox_3	-0.362	-0.362	2.103	0	0	0
Shear in plane x_1Ox_2	0	0	0	2.368	0	0
Shear in plane x_1Ox_3	0	0	0	0	2.368	0
Shear in plane x_2Ox_3	0	0	0	0	0	2.368

Table 4

The 3D BIEM-BEM results are very close to the exact test solutions even when a small number of both quadrilateral and triangular isoparametric surface elements are employed on the interface (this is the main advantage of the BEM over the FEM, in which a large number of finite elements is needed for the analysis), besides, it is preferable to use the advanced BIEM-BEM formulations based on the preliminary regularization and adaptive procedures.

On the basis of integral representation formulas (7) and obtained interfacial quantities at the nodal points, six stress components inside the inclusion of finite cylinder shape, embedded in elastic matrix, under tensile and shear loading are computed. The discrete analogues of these relations are constructed by the implementation of the standard Gaussian quadratures to deal with regular integrals as well as subdivision technique to deal with nearly-singular integrals, which occur when the field point is very close to but still off the surface of integration. As a numerical example, the inclusion with smoothed edges (Fig. 1, $R = a$) is considered. The stresses as function of the position vector of inclusion internal point are estimated for different relations between the elastic modulus of the solid constituents and inclusion aspect ratios. The curves on the Figs. 3-8 show the stress distributions inside the inclusion in the plane $x_3 = 0$ under homogeneous tension $\sigma^0 = const$ of the matrix along the axis Ox_3 : 1 – $H/R = 1.0$; 2 – $H/R = 1.3$; 3 – $H/R = 1.5$; 4 – $H/R = 2.0$.

$$\text{Case I: } \nu^M = \nu^I = 0,45; \quad \frac{E^M}{E^I} = \frac{\mu^M}{\mu^I} = 0,1$$

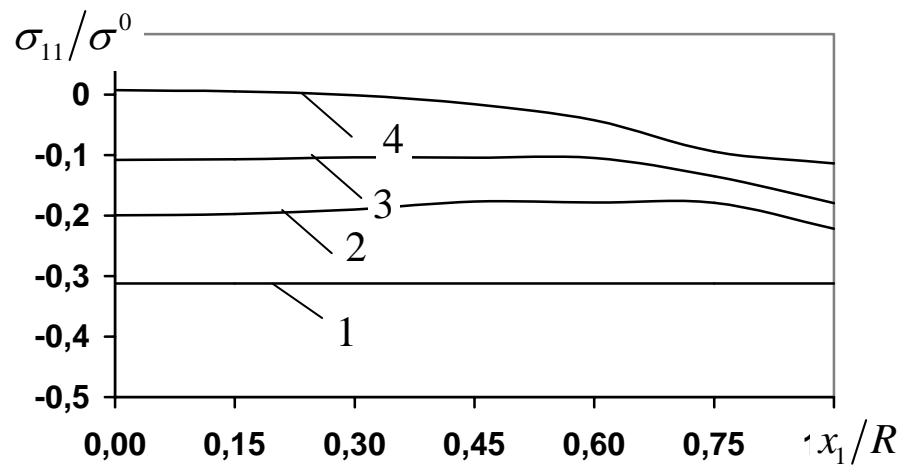


Fig. 3

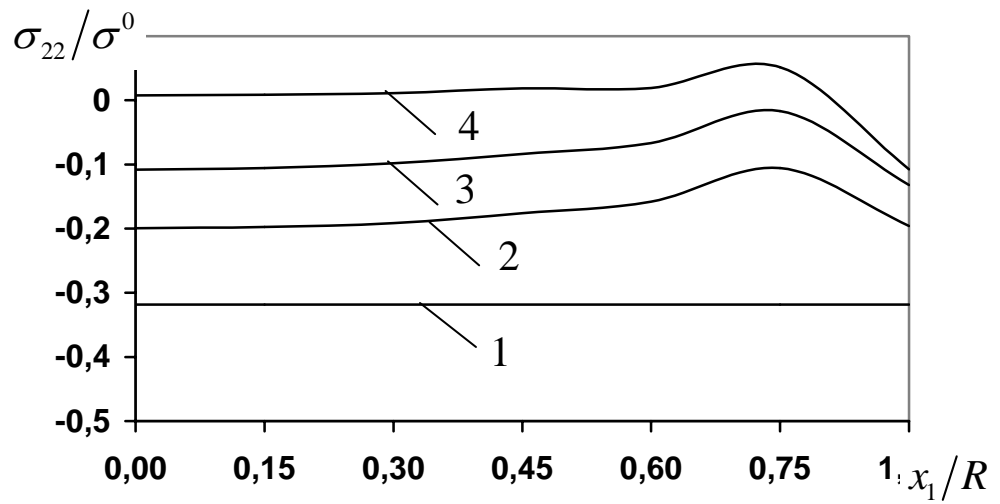


Fig. 4

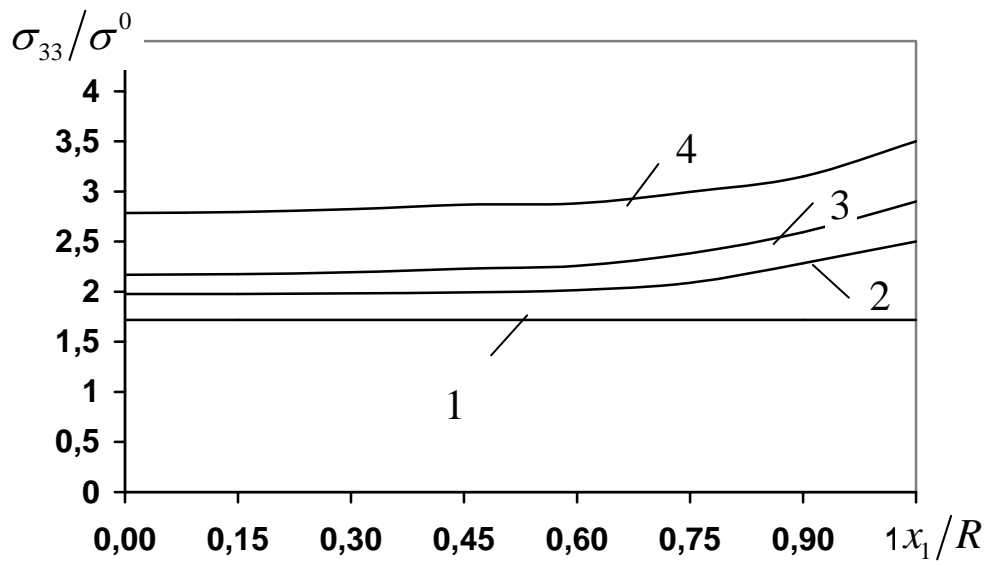


Fig. 5

Case II: $\nu^M = \nu^I = 0,45$; $\frac{E^M}{E^I} = \frac{\mu^M}{\mu^I} = 0,01$

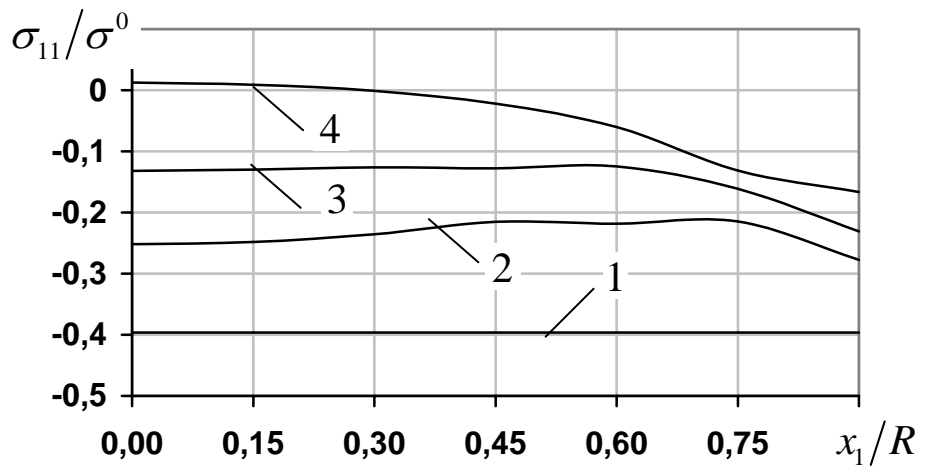


Fig. 6

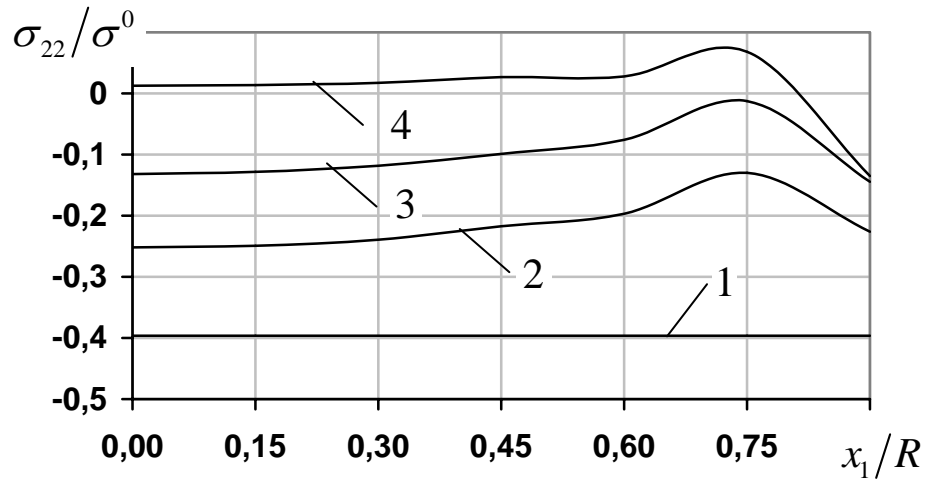


Fig. 7

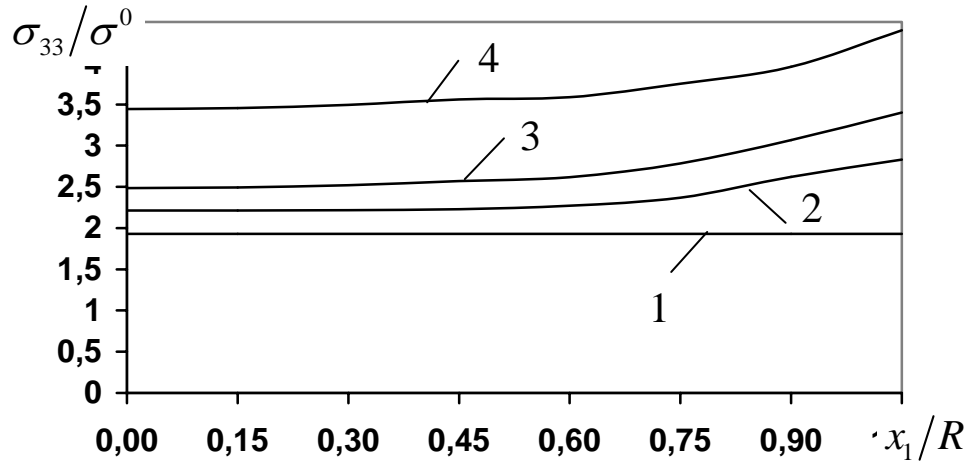


Fig. 8

As a very important example, the inclusions of the same shape with high aspect ratios are included in the BEM analyses using nonhomogeneous meshes. The curves on the Figs. 9-10 demonstrate the normal stress distributions inside the inclusion along the axis Ox_3 ($x_1 = x_2 = 0$) under homogeneous tension σ^0 of the matrix along axis Ox_3 (1 - $E^M / E^I = 0.01$; 2 - $E^M / E^I = 0.1$; 3 - $E^M / E^I = 10.0$). The Fig. 9 correspond to the relation $H / R = 20$, the Fig. 10 correspond to the relation $H / R = 100$,

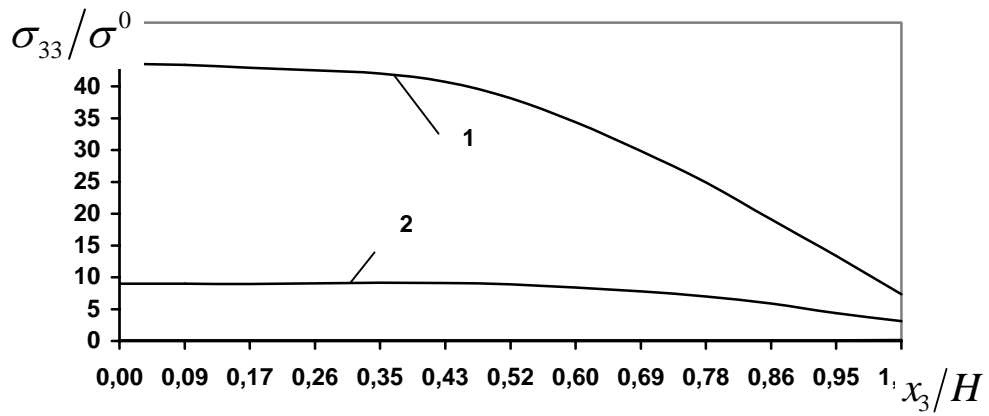


Fig. 9

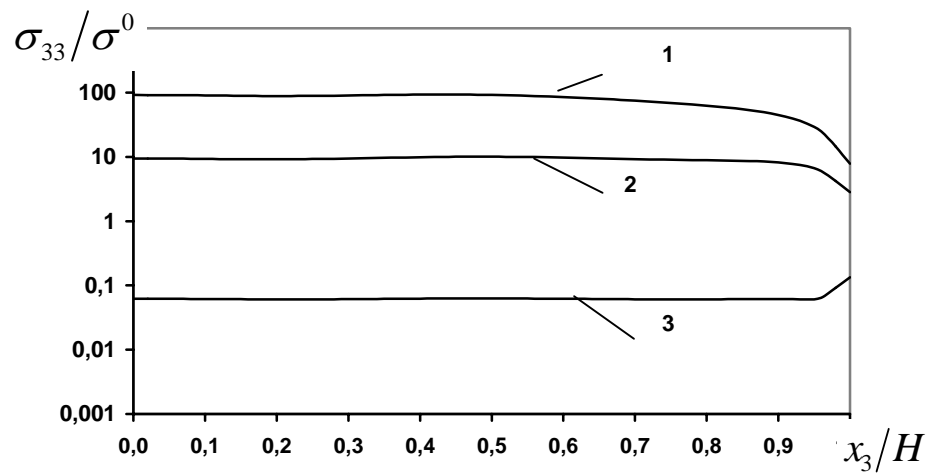


Fig. 10

3.2 Investigation of Effective Elastic Properties of 3-D Aligned Structure Composites using Boundary Element Method

By the multiparticle effective field method in conjunction with the previously obtained boundary element solutions of 3D one-particle problem for the uniform tensile and shear loading as well as uniform fictitious eigenstrains conditions, the effective elastic properties of random structure composites for arbitrary inclusion shape are estimated. The influence of the nonspherical shape of inclusions (on the example of finite cylinder with the smooth ends) on the effective elastic moduli of a composite material is investigated. The dependences of the effective elastic moduli versus the concentration of inhomogeneities are constructed and studied from the point of view of the reinforcing effects. The distribution of the statistical averages of the stresses in the fiber-like inclusions is obtained for different external loadings of composite, the relations between the elastic moduli of its constituents, the inclusion aspect ratios, as well as the dilute and nondilute concentration of inhomogeneities.

As 3D object of continuum analysis, a linearly elastic medium of isotropic constituents, which consists of a homogeneous matrix Ω^M containing a statistically homogeneous random set of aligned inclusions Ω_i ($i=1,2,\dots$) of any shapes and concentration c , is considered. Then the ensemble averaging is replaced by volume averaging for the random quantities description in such composite structure, namely:

$$\langle f \rangle = \frac{1}{\Omega} \int_{\Omega} f(\mathbf{x}) d\Omega_{\mathbf{x}} \quad (15)$$

The following formula for the 6×6 effective compliance tensor is exploited, which takes into account the “quasi-cristalline” approximation of the inclusion interactions:

$$\mathbf{M}^* = \mathbf{M}^M + \left[\langle \mathbf{R}^{\Omega} V \rangle^{-1} - \mathbf{Q}^0 \right]^{-1}, \quad (16)$$

where \mathbf{M}^* is the tensor of the effective elastic moduli of the composite material, \mathbf{M}^M and \mathbf{M}^I is the tensor of the elastic moduli of the matrix material and inclusion material respectively, $\Omega = \cup \Omega_i$, $V(\mathbf{x}) = \sum V_i(\mathbf{x})$, V_i is a characteristic function of Ω_i ,

$$\mathbf{R}_i(\mathbf{x}) = \bar{\Omega}_i (\mathbf{M}^I - \mathbf{M}^M) \mathbf{B}_i(\mathbf{x}). \quad (17)$$

The estimation of statistical averages of the inhomogeneous stresses $\langle \bar{\sigma} \rangle_i$ in the inclusions bases on the relation

$$\langle \bar{\sigma} \rangle_i(\mathbf{x}) = \mathbf{B}_i(\mathbf{x}) \left[\mathbf{I} - \mathbf{Q}^0 \langle \mathbf{R}^{\Omega} V \rangle \right]^{-1} \langle \sigma \rangle \quad (18)$$

Two tensors are included in the calculation formulas (16) and (18). The tensor \mathbf{B}_i corresponds to the inhomogeneous stresses inside a single i th inclusion due to six types of loadings of the matrix, namely the remote unit tensile and shear loadings in three perpendicular X,Y,Z-directions. Its components are defined by the relations

$$B_{i|jm}(\mathbf{x}) = \sigma_m(\mathbf{x}), \quad \mathbf{x} \in \Omega_i, \quad \text{when } \sigma_j^0 = 1, \quad \sigma_k^0 = 0 \quad (j \neq k), \quad (19)$$

$$j, m = 1, 2, \dots, 6$$

The tensor \mathbf{Q}^0 corresponds to the inhomogeneous stresses inside a single inclusion due to six types of fictitious unit eigenstrains in the same directions:

$$Q_{i|jm}(\mathbf{x}) = \sigma_m(\mathbf{x}), \quad \mathbf{x} \in \Omega_i^0, \quad \text{when } \varepsilon_j^0 = 1, \quad \varepsilon_k^0 = 0 \quad (j \neq k),$$

$$j, m = 1, 2, \dots, 6$$
(20)

where Ω_i^0 is the correlation hole domain. In the numerical scheme we use the spherical correlation hole, then $Q^0 = \text{const}$.

The previously created computer codes in FORTRAN on the base of boundary element method are applied with the purpose of mentioned tensors determination. The accurate estimation of analogous tensors with averaged stresses is performed by the optimal selection of nodal field points along the radial and angular coordinates inside the inclusion. Then the proposed numerical scheme is implemented for the homogenization analysis of composite with the cylinder shape inclusions with the smoothed ends and aligned orientation (Fig. 1, $a = R$). Different relations between the elastic modulus of the solid constituents and fiber aspect ratios are involved in the study. The effective Young's moduli in the directions along and crosswise the limit fibers as functions of concentration of inhomogeneities are computed and compared with the matrix counterpart. The behaviour of the effective stresses, when the concentration (both dilute and nondilute) of inclusions changes, is investigated.

Case I.

$$\nu^I = \nu^M = 0,45; \quad \frac{E^M}{E^I} = 0.1$$

The matrixes of averaged stresses (matrixes $\langle \mathbf{B} \rangle$) inside the single fiber-like inclusion for different aspect ratios.

$H/R = 1.0$

	$\langle \sigma_{11} \rangle / \sigma^0$	$\langle \sigma_{22} \rangle / \sigma^0$	$\langle \sigma_{33} \rangle / \sigma^0$	$\langle \sigma_{12} \rangle / \sigma^0$	$\langle \sigma_{13} \rangle / \sigma^0$	$\langle \sigma_{23} \rangle / \sigma^0$
Tension along $O x_1$	1.758	-0.318	-0.318	0	0	0
Tension along $O x_2$	-0.318	1.758	-0.318	0	0	0
Tension along $O x_3$	-0.318	-0.318	1.758	0	0	0
Shear in plane $x_1 O x_2$	0	0	0	2.075	0	0
Shear in plane $x_1 O x_3$	0	0	0	0	2.075	0
Shear in plane $x_2 O x_3$	0	0	0	0	0	2.075

$H/R = 1.3$

	$\langle \sigma_{11} \rangle / \sigma^0$	$\langle \sigma_{22} \rangle / \sigma^0$	$\langle \sigma_{33} \rangle / \sigma^0$	$\langle \sigma_{12} \rangle / \sigma^0$	$\langle \sigma_{13} \rangle / \sigma^0$	$\langle \sigma_{23} \rangle / \sigma^0$
Tension along $O x_1$	1.637	-0.308	-0.442	0	0	0
Tension along $O x_2$	-0.308	1.637	-0.442	0	0	0
Tension along $O x_3$	-0.235	-0.235	2.024	0	0	0
Shear in plane $x_1 O x_2$	0	0	0	1.944	0	0
Shear in plane $x_1 O x_3$	0	0	0	0	2.099	0
Shear in plane $x_2 O x_3$	0	0	0	0	0	2.099

$H/R = 1.5$

	$\langle \sigma_{11} \rangle / \sigma^0$	$\langle \sigma_{22} \rangle / \sigma^0$	$\langle \sigma_{33} \rangle / \sigma^0$	$\langle \sigma_{12} \rangle / \sigma^0$	$\langle \sigma_{13} \rangle / \sigma^0$	$\langle \sigma_{23} \rangle / \sigma^0$
Tension along $O x_1$	1.602	-0.300	-0.527	0	0	0
Tension along $O x_2$	-0.300	1.602	-0.527	0	0	0
Tension along $O x_3$	-0.209	-0.209	2.216	0	0	0
Shear in plane $x_1 O x_2$	0	0	0	1.902	0	0
Shear in plane $x_1 O x_3$	0	0	0	0	2.107	0
Shear in plane $x_2 O x_3$	0	0	0	0	0	2.107

$H/R = 2.0$

	$\langle \sigma_{11} \rangle / \sigma^0$	$\langle \sigma_{22} \rangle / \sigma^0$	$\langle \sigma_{33} \rangle / \sigma^0$	$\langle \sigma_{12} \rangle / \sigma^0$	$\langle \sigma_{13} \rangle / \sigma^0$	$\langle \sigma_{23} \rangle / \sigma^0$
Tension along $O x_1$	1.528	-0.300	-0.742	0	0	0
Tension along $O x_2$	-0.300	1.528	-0.742	0	0	0
Tension along $O x_3$	-0.165	-0.165	2.681	0	0	0
Shear in plane $x_1 O x_2$	0	0	0	1.827	0	0
Shear in plane $x_1 O x_3$	0	0	0	0	2.076	0
Shear in plane $x_2 O x_3$	0	0	0	0	0	2.076

The matrixes of stresses (matrix \mathbf{Q}^0) inside the spherical correlation hole

$$\mathbf{Q}^0 = \begin{pmatrix} 0.6674 & 0.2702 & 0.2702 & 0.0 & 0.0 & 0.0 \\ 0.2702 & 0.6674 & 0.2702 & 0.0 & 0.0 & 0.0 \\ 0.2702 & 0.2702 & 0.6674 & 0.0 & 0.0 & 0.0 \\ 0.0 & 0.0 & 0.0 & 0.397 & 0.0 & 0.0 \\ 0.0 & 0.0 & 0.0 & 0.0 & 0.397 & 0.0 \\ 0.0 & 0.0 & 0.0 & 0.0 & 0.0 & 0.397 \end{pmatrix}$$

The dependences of the effective Young's modulus versus the inclusion concentration C (Figs. 11-12) on the base of one particle "quasi-crystalline" approximation: 1 - $H/R = 1.0$; 2 - $H/R = 1.3$; 3 - $H/R = 1.5$; 4 - $H/R = 2.0$.

$$\frac{E_{11}^*}{E^0}$$

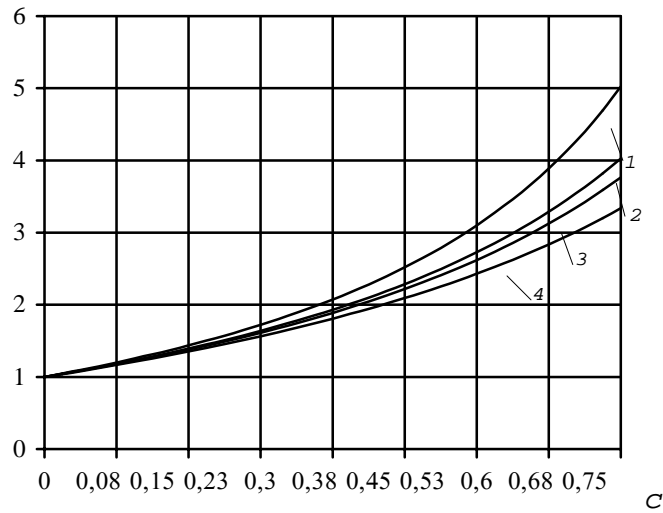


Fig. 11

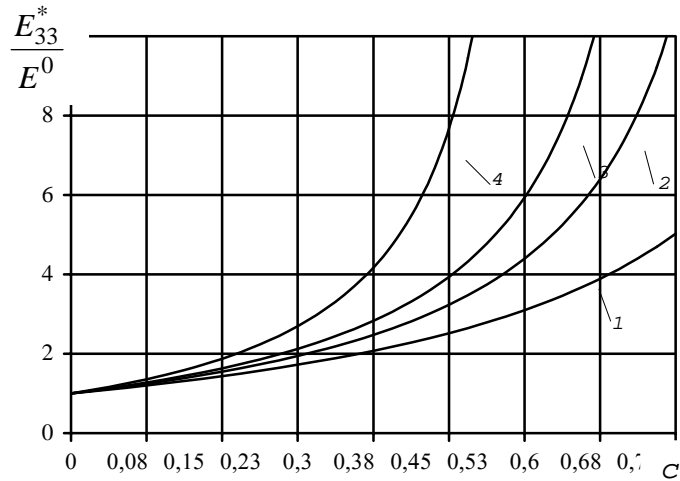


Fig. 12

The curves on the Fig. 13 demonstrate the distributions of normal effective stresses inside the inclusion with the aspect ratio $H/R = 2.0$ along the axis Ox_3 ($x_1 = x_2 = 0$) under homogeneous tension σ^0 of the matrix along axis Ox_3 : 1- $c = 0.0$ (single inclusion); 2- $c = 0.1$; 3- $c = 0.5$; 4- $c = 0.7$.

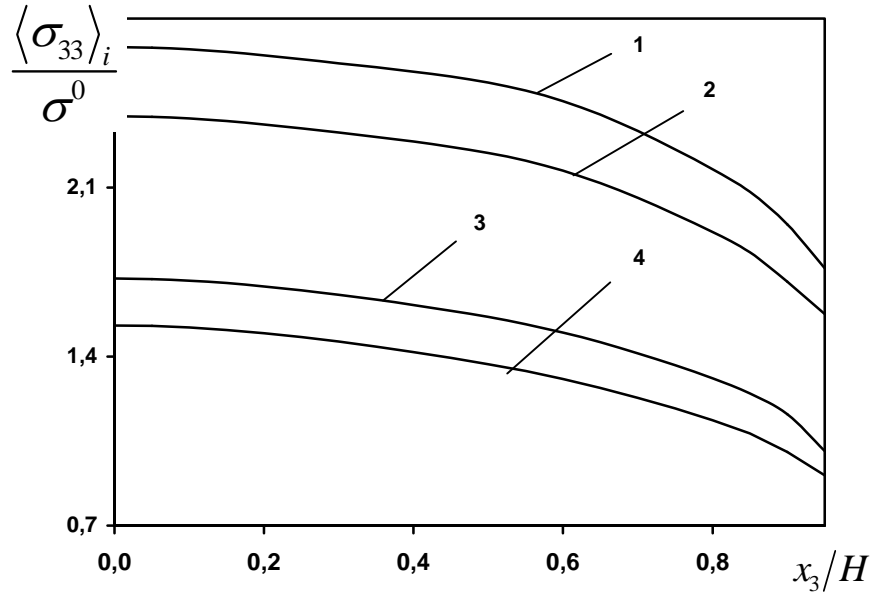


Fig. 13

Case II.

$$\nu^I = \nu^M = 0,45; \quad \frac{E^M}{E^I} = 0.01$$

The matrixes of averaged stresses (matrixes $\langle \mathbf{B} \rangle$) inside the single fiber-like inclusion for different aspect ratios.

$H/R = 1.0$

	$\langle \sigma_{11} \rangle / \sigma^0$	$\langle \sigma_{22} \rangle / \sigma^0$	$\langle \sigma_{33} \rangle / \sigma^0$	$\langle \sigma_{12} \rangle / \sigma^0$	$\langle \sigma_{13} \rangle / \sigma^0$	$\langle \sigma_{23} \rangle / \sigma^0$
Tension along $O x_1$	1.929	-0.402	-0.402	0	0	0
Tension along $O x_2$	-0.402	1.929	-0.402	0	0	0
Tension along $O x_3$	-0.402	-0.402	1.929	0	0	0
Shear in plane $x_1 O x_2$	0	0	0	2.326	0	0
Shear in plane $x_1 O x_3$	0	0	0	0	2.326	0
Shear in plane $x_2 O x_3$	0	0	0	0	0	2.326

$l = 1.3$

	$\langle \sigma_{11} \rangle / \sigma^0$	$\langle \sigma_{22} \rangle / \sigma^0$	$\langle \sigma_{33} \rangle / \sigma^0$	$\langle \sigma_{12} \rangle / \sigma^0$	$\langle \sigma_{13} \rangle / \sigma^0$	$\langle \sigma_{23} \rangle / \sigma^0$
Tension along $O x_1$	1.764	-0.374	-0.563	0	0	0
Tension along $O x_2$	-0.374	1.764	-0.563	0	0	0
Tension along $O x_3$	-0.300	-0.300	2.286	0	0	0
Shear in plane $x_1 O x_2$	0	0	0	2.139	0	0
Shear in plane $x_1 O x_3$	0	0	0	0	2.366	0

Shear in plane $x_2 O x_3$	0	0	0	0	0	2.366
----------------------------	---	---	---	---	---	-------

$H/R = 1.5$

	$\langle \sigma_{11} \rangle / \sigma^0$	$\langle \sigma_{22} \rangle / \sigma^0$	$\langle \sigma_{33} \rangle / \sigma^0$	$\langle \sigma_{12} \rangle / \sigma^0$	$\langle \sigma_{13} \rangle / \sigma^0$	$\langle \sigma_{23} \rangle / \sigma^0$
Tension along $O x_1$	1.721	-0.361	-0.687	0	0	0
Tension along $O x_2$	-0.361	1.721	-0.687	0	0	0
Tension along $O x_3$	-0.272	-0.272	2.560	0	0	0
Shear in plane $x_1 O x_2$	0	0	0	2.083	0	0
Shear in plane $x_1 O x_3$	0	0	0	0	2.387	0
Shear in plane $x_2 O x_3$	0	0	0	0	0	2.387

$l = 2.0$

	$\langle \sigma_{11} \rangle / \sigma^0$	$\langle \sigma_{22} \rangle / \sigma^0$	$\langle \sigma_{33} \rangle / \sigma^0$	$\langle \sigma_{12} \rangle / \sigma^0$	$\langle \sigma_{13} \rangle / \sigma^0$	$\langle \sigma_{23} \rangle / \sigma^0$
Tension along $O x_1$	1.652	-0.349	-1.014	0	0	0
Tension along $O x_2$	-0.349	1.652	-1.014	0	0	0
Tension along $O x_3$	-0.231	-0.231	3.281	0	0	0
Shear in plane $x_1 O x_2$	0	0	0	1.931	0	0
Shear in plane $x_1 O x_3$	0	0	0	0	2.415	0
Shear in plane $x_2 O x_3$	0	0	0	0	0	2.415

The matrixes of stresses (matrix \mathbf{Q}^0) inside the spherical correlation hole

$$\mathbf{Q}^0 = \begin{pmatrix} 0.6706 & 0.2736 & 0.2736 & 0.0 & 0.0 & 0.0 \\ 0.2736 & 0.6706 & 0.2736 & 0.0 & 0.0 & 0.0 \\ 0.2736 & 0.2736 & 0.6706 & 0.0 & 0.0 & 0.0 \\ 0.0 & 0.0 & 0.0 & 0.3971 & 0.0 & 0.0 \\ 0.0 & 0.0 & 0.0 & 0.0 & 0.3971 & 0.0 \\ 0.0 & 0.0 & 0.0 & 0.0 & 0.0 & 0.3971 \end{pmatrix}$$

The dependences of the effective Young's modulus versus the inclusion concentration c (Figs. 14-15) on the base of one particle "quasi-crystalline" approximation: 1 - $H/R = 1.0$; 2 - $H/R = 1.3$; 3 - $H/R = 1.5$; 4 - $H/R = 2.0$.

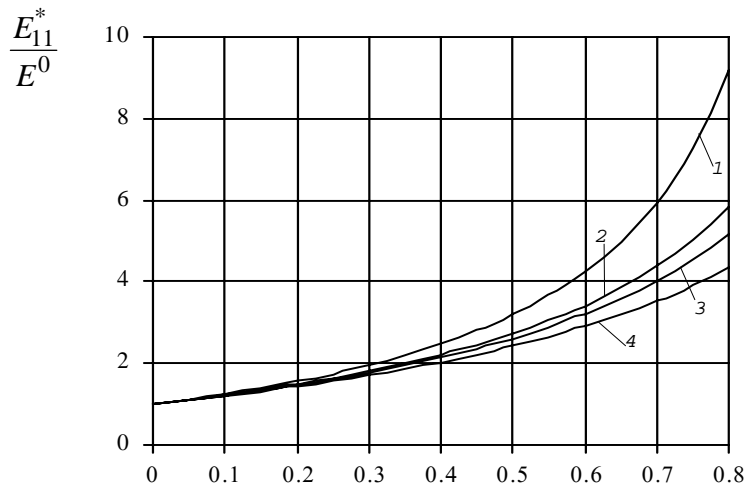


Fig. 14

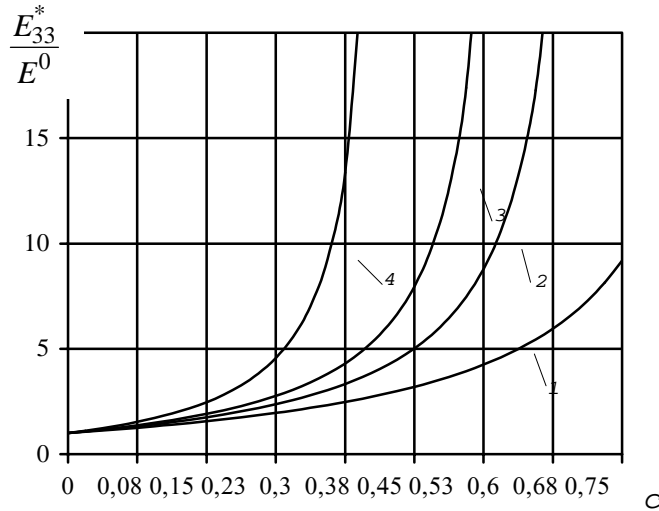
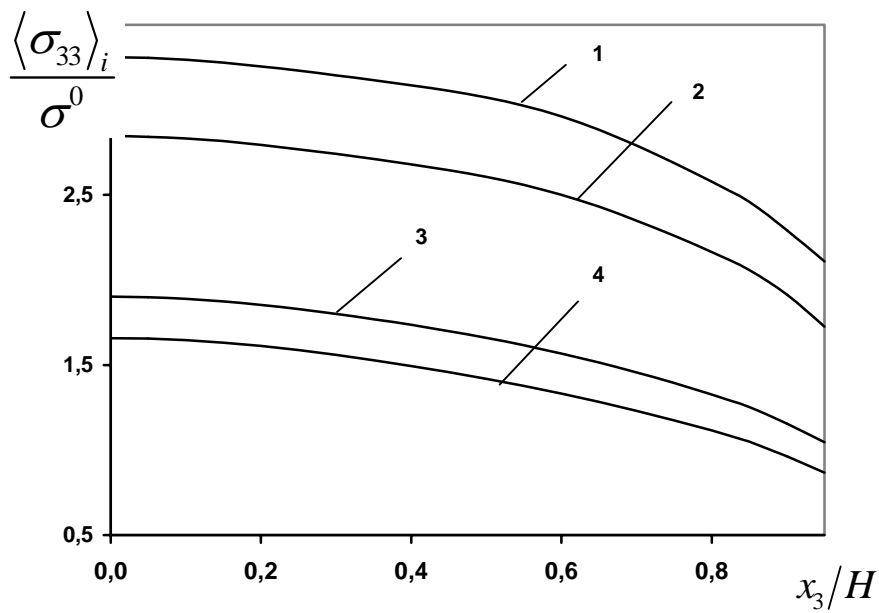


Fig. 15

The curves on the Fig. 16 demonstrate the distributions of normal effective stresses inside the inclusion with the aspect ratio $H/R = 2.0$ along the axis Ox_3 ($x_1 = x_2 = 0$) under homogeneous tension σ^0 of the matrix along axis Ox_3 : 1- $c = 0.0$ (single inclusion); 2- $c = 0.1$; 3 - $c = 0.5$; 4 - $c = 0.7$.



The character of monotonical increasing the effective elastic moduli, when the concentration (both dilute and nondilute) of inclusions increases, is investigated. This dependence is most expressive for the composites with the constituents, which have a large contrast relative to the elastic properties. In the domain of nondilute concentration of inclusions the essential variation of effective elastic moduli under considered changing of the shape parameter is revealed. It is demonstrated, that the predicted isotropic effective moduli of composites with the aligned limited fiber-like fillers in the direction of fibers are stiffer than the effective elastic moduli of composites with the spherical inclusions. An opposite effect is fixed in the perpendicular direction. It is shown, that the stress distributions are essentially inhomogeneous along the axis and cross-section of inclusions for any concentration. The comparison of the localization places of concentration zones for the different effective stress components is fulfilled.

3.3 Micromechanics of 3D Particulate Composites with Crack-Like Damages

Next, the composite material containing arbitrarily located inhomogeneities with limiting geometric properties and contrast rigidities – N^I stiff disk-shaped inclusions in the plane domains $S^{(n)I}$ ($n = 1, 2, \dots, N^I$) and N^C crack-like defects in the plane domains $S^{(n)C}$ ($n = 1, 2, \dots, N^C$) – under inhomogeneous outer field $\mathbf{u}^0, \sigma_{ij}^0$ (Fig. 17) is investigated.

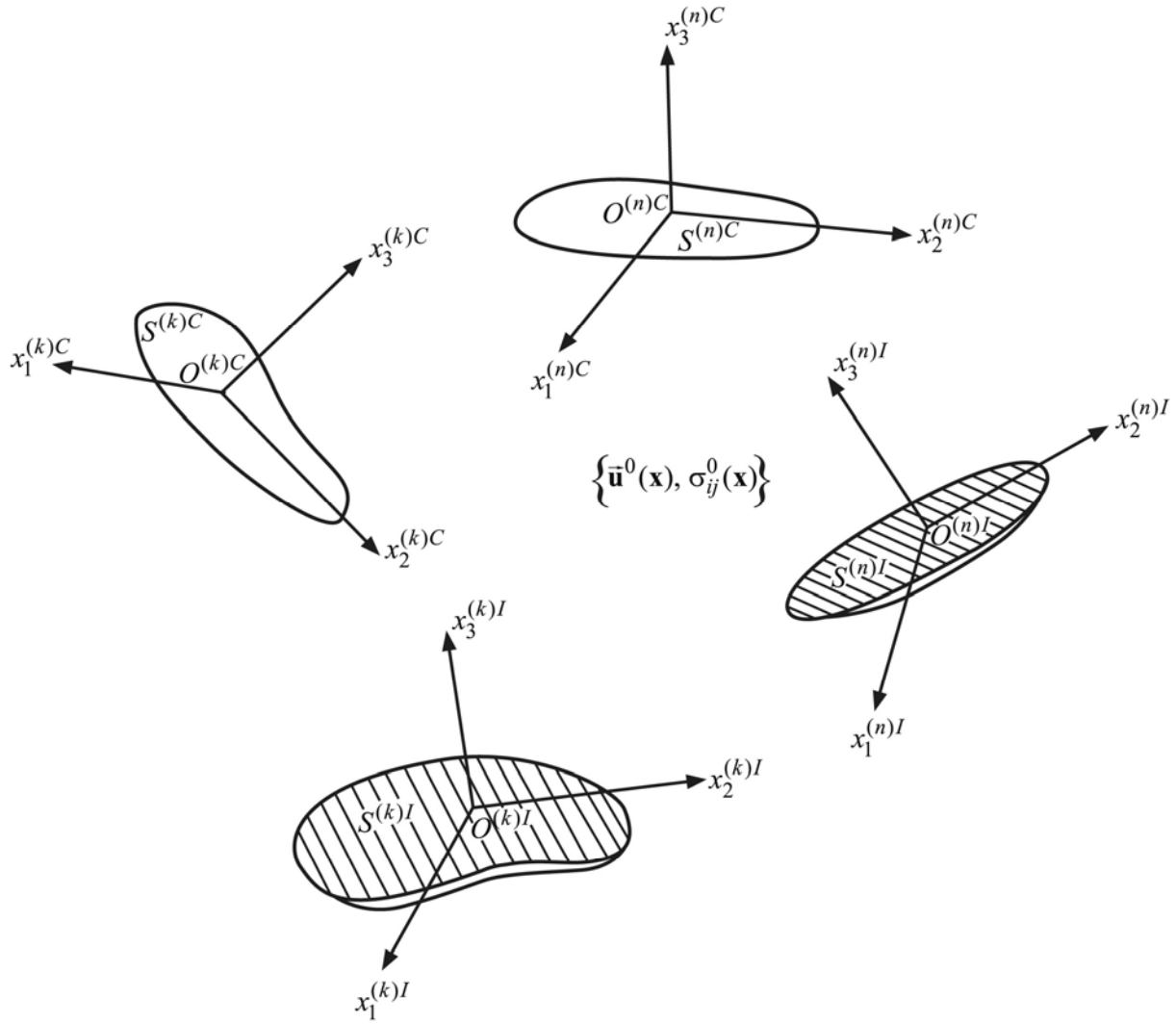


Fig. 17

The effective boundary conditions (the linearity of displacement components in the inclusion domains and load-free conditions in the crack domains) are suggested, namely:

$$\begin{aligned}
 u_j(\mathbf{x}^{(n)I}) &= U_j^{(n)} + (-1)^j \Omega_3^{(n)} x_{3-j}^{(n)I}, \quad j=1,2, \\
 u_3(\mathbf{x}^{(n)I}) &= U_3^{(n)} + \Omega_1^{(n)} x_2^{(n)I} - \Omega_2^{(n)} x_1^{(n)I}, \\
 \mathbf{x}^{(n)I} &\in S^{(n)I}, \quad n=1,2,\dots,N^I.
 \end{aligned}
 \tag{21}$$

$$\sigma_{j3}(\mathbf{x}^{(n)C}) = 0, \quad j=1,2,3, \quad \mathbf{x}^{(n)C} \in S^{(n)C}, \quad n=1,2,\dots,N^C,$$

where constants $U_j^{(n)}, \Omega_j^{(n)}$ describe the translation and rotation of the n -th inclusion (to simplify the current and subsequent mathematical representations we use the local coordinate systems associated with the corresponding object (Fig. 17)).

Then the boundary integral formulation of problems is achieved via the superposition principle, when the total field in the matrix is formed from the fields caused by effects of separate disperse objects, in the form

$$\mathbf{u} = \mathbf{u}^0 + \sum_{k=1}^{N^I} \mathbf{u}^{(k)I} + \sum_{k=1}^{N^C} \mathbf{u}^{(k)C}. \quad (22)$$

The representations for the functions $\mathbf{u}^{(k)I}$, $\mathbf{u}^{(k)C}$ in terms of surface integrals are obtained. Finally, we can write

$$\begin{aligned} u_j^{(k)I}(\mathbf{x}^{(k)I}) &= \frac{1}{G^M} \iint_{S^{(k)I}} \frac{\Delta \sigma_j^{(k)}(\boldsymbol{\xi}^{(k)I})}{|\mathbf{x}^{(k)I} - \boldsymbol{\xi}^{(k)I}|} dS_{\boldsymbol{\xi}} - \frac{1}{4(1-\nu^M)} \frac{\partial}{\partial x_j^{(k)I}} \iint_{S^{(k)I}} \left[\Delta \sigma_1^{(k)}(\boldsymbol{\xi}^{(k)I}) \frac{\partial}{\partial x_1^{(k)I}} + \right. \\ &\quad \left. + \Delta \sigma_2^{(k)}(\boldsymbol{\xi}^{(k)I}) \frac{\partial}{\partial x_2^{(k)I}} + \Delta \sigma_3^{(k)}(\boldsymbol{\xi}^{(k)I}) \frac{\partial}{\partial x_3^{(k)I}} \right] |\mathbf{x}^{(k)I} - \boldsymbol{\xi}^{(k)I}| dS_{\boldsymbol{\xi}}, \quad j = 1, 2, 3, \\ u_j^{(k)C}(\mathbf{x}^{(k)C}) &= \frac{\partial}{\partial x_3^{(k)C}} \iint_{S^{(k)C}} \frac{\Delta u_j^{(k)}(\boldsymbol{\xi}^{(k)C})}{|\mathbf{x}^{(k)C} - \boldsymbol{\xi}^{(k)C}|} dS_{\boldsymbol{\xi}} - \frac{1-2\nu^M}{2(1-\nu^M)} \frac{\partial}{\partial x_j^{(k)C}} \iint_{S^{(k)C}} \frac{\Delta u_3^{(k)C}(\boldsymbol{\xi}^{(k)C})}{|\mathbf{x}^{(k)C} - \boldsymbol{\xi}^{(k)C}|} dS_{\boldsymbol{\xi}} + \\ &\quad + \frac{1-2\nu^M}{2(1-\nu^M)} \delta_{j3} \iint_{S^{(k)C}} \left[\Delta u_1^{(k)}(\boldsymbol{\xi}^{(k)C}) \frac{\partial}{\partial x_1^{(k)C}} + \Delta u_2^{(k)}(\boldsymbol{\xi}^{(k)C}) \frac{\partial}{\partial x_2^{(k)C}} + \Delta u_3^{(k)}(\boldsymbol{\xi}^{(k)C}) \frac{\partial}{\partial x_3^{(k)C}} \right] \frac{dS_{\boldsymbol{\xi}}}{|\mathbf{x}^{(k)C} - \boldsymbol{\xi}^{(k)C}|} - \\ &\quad (23) \\ &\quad + \frac{x_3^{(k)C}}{2(1-\nu^M)} \frac{\partial}{\partial x_j^{(k)C}} \iint_{S^{(k)C}} \left[\Delta u_1^{(k)}(\boldsymbol{\xi}^{(k)C}) \frac{\partial}{\partial x_1^{(k)I}} + \Delta u_2^{(k)}(\boldsymbol{\xi}^{(k)C}) \frac{\partial}{\partial x_2^{(k)C}} + \right. \\ &\quad \left. + \Delta u_3^{(k)}(\boldsymbol{\xi}^{(k)C}) \frac{\partial}{\partial x_3^{(k)C}} \right] \frac{dS_{\boldsymbol{\xi}}}{|\mathbf{x}^{(k)C} - \boldsymbol{\xi}^{(k)C}|}, \quad j = 1, 2, 3. \end{aligned}$$

In the case of thin-walled (disk-shaped) inclusions and cracks the roles of unknown densities play the jumps of interfacial stresses and displacements across the inhomogeneities, respectively. Following relations explain the physical sense of the densities:

$$\begin{aligned} \Delta \sigma_j^{(k)}(\boldsymbol{\xi}^{(k)I}) &= \frac{1}{4\pi} \left[\sigma_{j3}^-(\xi_1^{(k)I}, \xi_2^{(k)I}) - \sigma_{j3}^+(\xi_1^{(k)I}, \xi_2^{(k)I}) \right], \quad j = \overline{1,3}, \\ \boldsymbol{\xi}^{(k)I}(\xi_1^{(k)I}, \xi_2^{(k)I}) &\in S^{(k)I}, \quad \sigma_{j3}^{\pm}(x_1^{(k)I}, x_2^{(k)I}) = \lim_{x_3^{(k)I} \rightarrow \pm 0} \sigma_{j3}(x^{(k)I}), \\ \Delta u_j^{(k)}(\boldsymbol{\xi}^{(k)C}) &= \frac{1}{4\pi} \left[u_j^-(\xi_1^{(k)C}, \xi_2^{(k)C}) - u_j^+(\xi_1^{(k)C}, \xi_2^{(k)C}) \right], \quad j = \overline{1,3}, \\ \boldsymbol{\xi}^{(k)C}(\xi_1^{(k)C}, \xi_2^{(k)C}) &\in S^{(k)C}, \quad u_j^{\pm}(x_1^{(k)C}, x_2^{(k)C}) = \lim_{x_3^{(k)C} \rightarrow \pm 0} u_j(x^{(k)C}). \end{aligned} \quad (24)$$

The boundary integral equations for these functions are deduced by satisfying the boundary conditions (21). So we arrive at the system of $3(N^I + N^C)$ equations, as follows

$$\begin{aligned}
& (3-4\nu^M) \iint_{S^{(n)I}} \Delta\sigma_j^{(n)}(\xi^{(n)I}) \frac{dS_\xi}{|\mathbf{x}^{(n)I} - \xi^{(n)I}|} + (1-\delta_{3j}) \iint_{S^{(n)I}} \left[\Delta\sigma_j^{(n)}(\xi^{(n)I}) \left(x_j^{(n)I} - \xi_j^{(n)I} \right)^2 + \right. \\
& + \Delta\sigma_{3-j}^{(n)}(\xi^{(n)I}) \left(x_1^{(n)I} - \xi_1^{(n)I} \right) \left(x_2^{(n)I} - \xi_2^{(n)I} \right) \left. \right] \frac{dS_\xi}{|\mathbf{x}^{(n)I} - \xi^{(n)I}|^3} + \sum_{k=1}^{N^I} (1-\delta_{kn}) \sum_{r=1}^3 \iint_{S^{(k)I}} \Delta\sigma_r^{(k)}(\xi^{(k)I}) \times \\
& \times R_{jr}^{(kn)I}(\mathbf{x}^{(kn)I}, \xi^{(k)I}) dS_\xi + \sum_{k=1}^{N^C} \sum_{r=1}^3 \iint_{S^{(k)C}} \Delta u_r^{(k)}(\xi^{(k)C}) L_{jr}^{(kn)CI}(\mathbf{x}^{(kn)CI}, \xi^{(k)C}) dS_\xi - \\
& - 4(1-\nu^M) G^M \left\{ U_j^{(n)} + \delta_{3j} (\Omega_1^{(n)} x_2^{(n)I} - \Omega_2^{(n)} x_1^{(n)I}) + (1-\delta_{3j}) (-1)^j \Omega_3^{(n)} x_{3-j}^{(n)I} \right\} = \\
& = -4(1-\nu^M) G^M u_j^{(0)}(\mathbf{x}^{(n)I}), \quad j=1,2,3, \quad n=1,2,\dots,N^I, \quad (25) \\
& \left[\delta_{3j} + (1-\delta_{3j})(1-2\nu^M) \right] \iint_{S^{(n)C}} \Delta u_j^{(n)}(\xi^{(n)C}) \frac{dS_\xi}{|\mathbf{x}^{(n)C} - \xi^{(n)C}|^3} + \\
& + 3\nu^M (1-\delta_{3j}) \iint_{S^{(n)C}} \left[\Delta u_j^{(n)}(\xi^{(n)C}) \left(x_j^{(n)C} - \xi_j^{(n)C} \right)^2 + \right. \\
& + \Delta u_{3-j}^{(n)}(\xi^{(n)C}) \left(x_1^{(n)C} - \xi_1^{(n)C} \right) \left(x_2^{(n)C} - \xi_2^{(n)C} \right) \left. \right] \frac{dS_\xi}{|\mathbf{x}^{(n)C} - \xi^{(n)C}|^5} + \sum_{k=1}^{N^C} (1-\delta_{kn}) \sum_{r=1}^3 \iint_{S^{(k)C}} \Delta u_r^{(k)}(\xi^{(k)C}) \times \\
& \times R_{jr}^{(kn)C}(\mathbf{x}^{(kn)C}, \xi^{(k)C}) dS_\xi + \sum_{k=1}^{N^I} \sum_{r=1}^3 \iint_{S^{(k)I}} \Delta\sigma_r^{(k)}(\xi^{(k)I}) L_{jr}^{(kn)IC}(\mathbf{x}^{(kn)IC}, \xi^{(k)I}) dS_\xi = -\frac{1-\nu^M}{G^M} \sigma_{j3}^{(0)}(\mathbf{x}^{(n)C}), \\
& j=1,2,3, \quad n=1,2,\dots,N^C.
\end{aligned}$$

In the first $3N^I$ equations, the characteristic part with weakly singularities coincides with the integral operator of 3D problem of isolated inclusion in the elastic matrix, the regular kernels $R_{jr}^{(kn)I}$ and $L_{jr}^{(kn)CI}$ describe, respectively, the influence of the k th inclusion and k th crack on the n th inclusion. In the remaining $3N^C$ equations, the characteristic part with hypersingularities coincides with the integral operator of 3D problem of isolated crack in the elastic matrix, the regular kernels $R_{jr}^{(kn)C}$ and $L_{jr}^{(kn)IC}$ describe, respectively, the influence of the k th crack and k th inclusion on the n th crack. In the resulting integral equations these regular kernels are obtained in the explicit form, what guarantees their numerical discretization by standard approaches.

For completeness the $6N^I$ equilibrium equations for the inclusions as rigid unities are added to the obtained integral equations in the form

$$\begin{aligned}
& \iint_{S^{(n)I}} \Delta\sigma_j^{(n)}(\xi^{(n)I}) dS_\xi = 0, \quad j=1,2,3, \quad n=1,2,\dots,N^I, \\
& \iint_{S^{(n)I}} \left[\xi_2^{(n)I} \Delta\sigma_1^{(n)}(\xi^{(n)I}) - \xi_1^{(n)I} \Delta\sigma_2^{(n)}(\xi^{(n)I}) \right] dS_\xi = 0, \quad n=1,2,\dots,N^I, \quad (26) \\
& \iint_{S^{(n)I}} \xi_{3-j}^{(n)I} \Delta\sigma_3^{(n)}(\xi^{(n)I}) dS_\xi = 0, \quad j=1,2, \quad n=1,2,\dots,N^I.
\end{aligned}$$

The behavior of both displacement and stress fields in the vicinity of thin-walled inhomogeneity fronts, where stress concentration takes place, is considered exactly by square-root extraction from the functions, which are determined. In particular, in the case of circular inhomogeneities with radii $a^{(n)I}, a^{(n)C}$ we assume:

$$\begin{aligned}\Delta\sigma_j^{(n)}(\mathbf{x}^{(n)I}) &= \left[\left(a^{(n)I} \right)^2 - \left(x_1^{(n)I} \right)^2 - \left(x_2^{(n)I} \right)^2 \right]^{-1/2} \alpha_j^{(n)}(\mathbf{x}^{(n)I}), \\ \mathbf{x}^{(n)I} &\in S^{(n)I}, \quad n = 1, 2, \dots, N^I, \quad j = 1, 2, 3, \\ \Delta u_j^{(n)}(\mathbf{x}^{(n)C}) &= \left[\left(a^{(n)C} \right)^2 - \left(x_1^{(n)C} \right)^2 - \left(x_2^{(n)C} \right)^2 \right]^{1/2} \beta_j^{(n)}(\mathbf{x}^{(n)C}), \\ \mathbf{x}^{(n)C} &\in S^{(n)C}, \quad n = 1, 2, \dots, N^C, \quad j = 1, 2, 3,\end{aligned}\tag{27}$$

where $\alpha_j^{(n)}, \beta_j^{(n)}$ are new smooth unknown functions, which can be approximated with a good accuracy as piecewise-constants in the practical calculations.

This fact finally yields the direct and more accurate definition of fracture parameters. Indeed, it is easily to show, that the mixed mode stress intensity factors in the vicinity of n th crack are expressed by the solutions of boundary integral equations as

$$\begin{aligned}K_I^{(n)C}(\varphi) &= -\frac{2\pi G^M \sqrt{\pi a^{(n)C}}}{1-\nu^M} \beta_3^{(n)}(\mathbf{x}^{(n)C}) \Big|_{\mathbf{x}^{(n)C}|=a^{(n)C}}, \\ K_{II}^{(n)C}(\varphi) &= -\frac{2\pi G^M \sqrt{\pi a^{(n)C}}}{1-\nu^M} \left[\cos \varphi \beta_1^{(n)}(\mathbf{x}^{(n)C}) \Big|_{\mathbf{x}^{(n)C}|=a^{(n)C}} + \sin \varphi \beta_2^{(n)}(\mathbf{x}^{(n)C}) \Big|_{\mathbf{x}^{(n)C}|=a^{(n)C}} \right], \\ K_{III}^{(n)C}(\varphi) &= -2\pi G^M \sqrt{\pi a^{(n)C}} \left[\sin \varphi \beta_1^{(n)}(\mathbf{x}^{(n)C}) \Big|_{\mathbf{x}^{(n)C}|=a^{(n)C}} - \cos \varphi \beta_2^{(n)}(\mathbf{x}^{(n)C}) \Big|_{\mathbf{x}^{(n)C}|=a^{(n)C}} \right].\end{aligned}\tag{28}$$

The approach for the regularization and boundary element discretization of Eqs. (25), (26) rests on the lowering of the order of singularity by the integration by parts in conjunction with the application of the mapping procedures and using collocation technique. During calculation 176 boundary elements C^0 -type are used on each inhomogeneity, Poisson's ratio was chosen as $\nu^M = 0.3$.

For the testing a single stiff circular disk-shaped inclusion in the homogeneous stress field is considered (then the exact analytical solution exists). This case is reached in the limit $d \rightarrow \infty$ and demonstrates excellent agreement (less than 0.1%).

As the example of methodology implementation, the normalized mode I stress intensity factor as function of angular coordinate φ of crack front point for the interacting pair stiff disk-shaped inclusion – penny-shaped crack under uniaxial homogeneous loading P is showed (Fig. 18, where $a^I = a^C$). Reinforcing properties of dispersed phase are revealed by comparing the peak values of stress intensity factor in the crack vicinity in the cases of presence and absence of neighboring inclusion under the same disturbances of the solid. Also the influence of the distance between inhomogeneities on the interaction phenomena is evaluated. Also within this Project the attempt to extend such approach concerning thin-walled inclusions to the time-harmonic (Fig. 19, where $a^C/a^I = 0.1$) and transient (Fig. 20) cases is made.

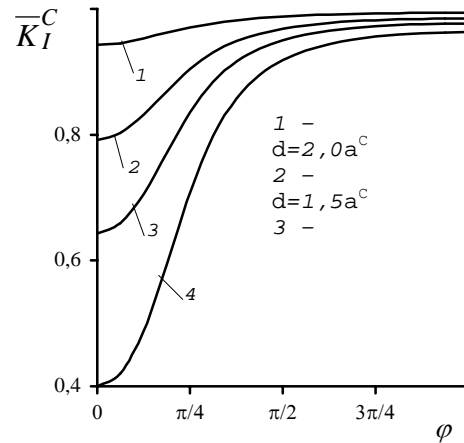
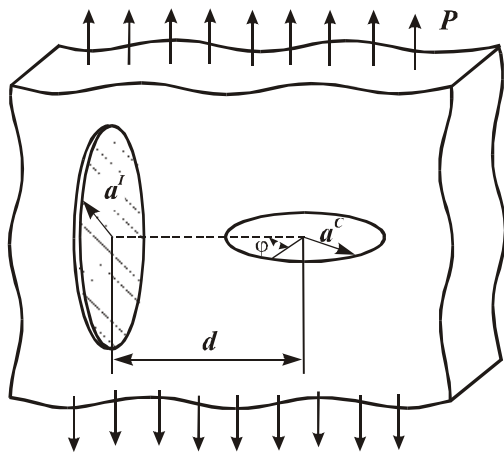


Fig. 18

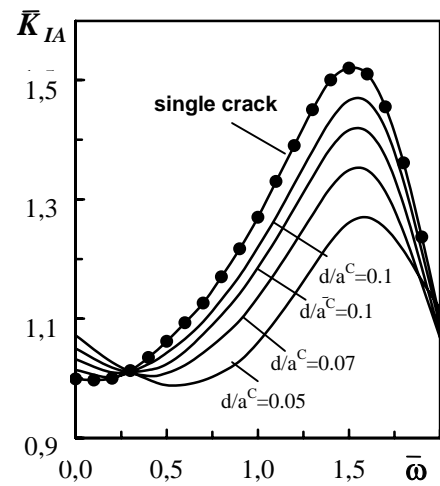
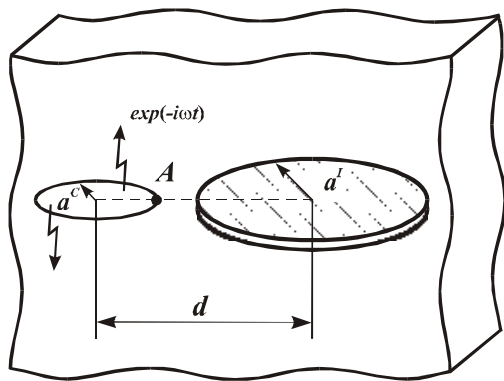


Fig. 19

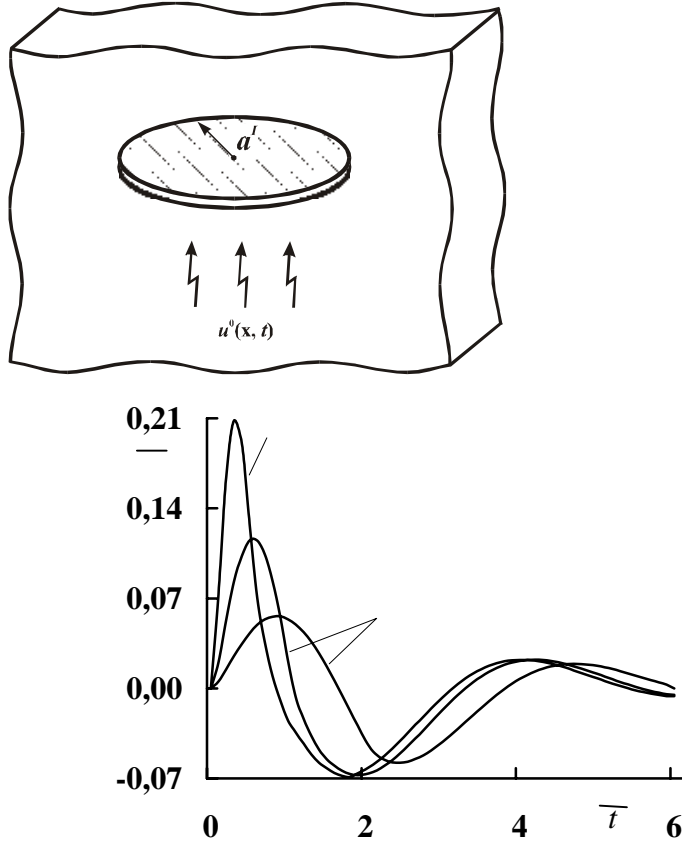


Fig. 20

3. Conclusions

The numerical tool, based on the advanced BIEM-BEM formulations, is developed and applied for the solution of three-dimensional elastostatic problems for remotely inhomogeneous loaded matrix with the perfectly bonded inclusions. Proposed approach is not sensitive to the geometry of inclusions (both volumetric and thin-walled inhomogeneities of complex shapes are involved to the analysis), their physical-mechanical properties and mutual localization in the solid, also to the loading conditions. In conjunction with the average schemes of multiparticle effective field method (MEFM) it is implemented for the macroanalysis (with obtaining of all necessary effective parameters) of composites, which are models by 3D homogeneous matrix containing a statistically homogeneous set of aligned fiber-like inclusions.

Summary of Personnel Commitments

Mykhas'kiv V.V.

- Development of general approaches for the boundary integral formulations of 3-D elastostatic multiple inclusion problems.
- Elaboration of general scheme for discretization and numerical solution of boundary integral equations of 3-D elastostatic problems for an infinite matrix with a single volumetric or thin-walled inclusion. Obtaining the discretized relations for computation of the strain-stress state at the inner points of matrix and inclusion by means of interfacial quantities (solutions of boundary integral equations).
- Selection of 3D test inclusion-matrix models with most demonstrative field distributions and formulation of particular examples and conditions for verification the numerical results. Creation of alternative regularization, conversation and discretization procedures for obtaining key matrices with the best numerical properties.

- Statement of the actual problems of BIEM–BEM elastic field analysis for 3D partially-homogeneous solids with a selection of input and output parameters. Elaboration of the approaches for the optimal (from the point of view of CPU time and memory) computational coding of problems.
- BIEM–BEM analysis of stress field inside volumetric and thin-walled elastic inclusion of nonclassical shapes. Elaboration of the approaches for the optimal computational coding of problems. Analysis and estimation of obtained numerical results.
- Implementation of BIEM–BEM strategy for the investigation of the stress fields both in the discrete and averaged forms inside the elastic inclusions of nonclassical shapes. Revealing the regularities of the stress behaviors and selection of the most demonstrative distributions for presentation of the numerical results obtained.
- Development of general scheme for the homogenization analysis of 3D particulate composite materials using boundary element technique. Estimation of the tensors of stresses inside the inclusion of complex shape in the discrete and averaged forms. Analysis of the effective elastic moduli of 3D composites with the limit fiber-like inclusions.
- Development of general scheme for the study of the effective stress concentration in 3D particulate composite materials using boundary element technique. Analysis of the effective properties of 3D composites with the limit fiber-like inclusions.

Stasyuk B.M.

- Obtaining regularized boundary integral equations of 3-D elastostatic multiple volumetric inclusion problems.
- Obtaining the discretized boundary integral equations of 3-D elastostatic problems for an infinite matrix with inclusion of finite cylinder shape. Creation of software codes directed on the determination of interfacial displacements and tractions for this type of inclusion.
- Testing of BIEM-BEM results for volumetric elastic inclusion and generation on this base the improved numerical procedures.
- Generation and realization of improved numerical procedures and codes within BIEM-BEM for the analysis of stress field inside volumetric elastic inclusion of nonclassical shape.
- Obtaining the discrete relations for the analysis of stress field inside volumetric elastic inclusion of nonclassical shape. Calculation of stress components at the internal nodes on the different meshes.
- Numerical realization of averaging procedures for stresses inside a cylinder shape inclusion. Construction and estimation of the six-rank tensors with averaged stresses (strains) as components for different geometric and mechanical parameters of the inclusion.
- Estimation of tensors of inhomogeneous stresses inside the single inclusion of limit cylinder shape due to the remote uniform tensile and shear loadings in three perpendicular directions. Obtaining the analogous tensors with the volume averaging of stresses.
- Numerical estimation of effective normal stresses inside the aligned inclusions of limit cylinder shape due to the remote uniform tensile and shear loadings in the three perpendicular directions.

Stepanyuk O.I.

- Obtaining regularized integral equations of 3-D elastostatic multiple thin-walled inclusion problems.
- Obtaining the discretized boundary integral equations of 3-D elastostatic problems for an infinite matrix with disk-shaped inclusion. Creation of software codes directed on the determination of interfacial displacements and tractions for this type of inclusion.
- Testing of BIEM-BEM results for inclusion with contrast geometrical and mechanical properties and generation on this base the improved numerical procedures.
- Generation and realization of improved numerical procedures and codes within BIEM-BEM for the analysis of stress intensity factors near the interacting inclusions with contrast geometrical and mechanical properties.
- Obtaining the discrete relations for the analysis of stress concentration near the interacting inclusions with contrast geometrical and mechanical properties.
- Numerical determination of the stress components inside a cylinder shape inclusion under six types of tensile and shear loadings of the matrix. Analysis of these quantities as functions of the field point in 3D space.

- Estimation of tensors of inhomogeneous stresses inside the single inclusion of limit cylinder shape due to the uniform fictitious tensile and shear eigenstrains in three perpendicular directions. Obtaining the analogous tensors with the volume averaging of stresses.
- Numerical estimation of effective tangential stresses inside the aligned inclusions of limit cylinder shape due to the remote uniform tensile and shear loadings in the three perpendicular directions.

4. Solution of the two-dimensional micromechanics problem for the fiber reinforced bounded and unbounded solids. Investigation of effective local and nonlocal thermoelastic properties, stress concentration factors, and edge effect

1.1 Theoretical part

The 2-D problem for a plain domain with inclusions is considered. Generally the problem may be presented in the form shown on Fig. 1.1.1

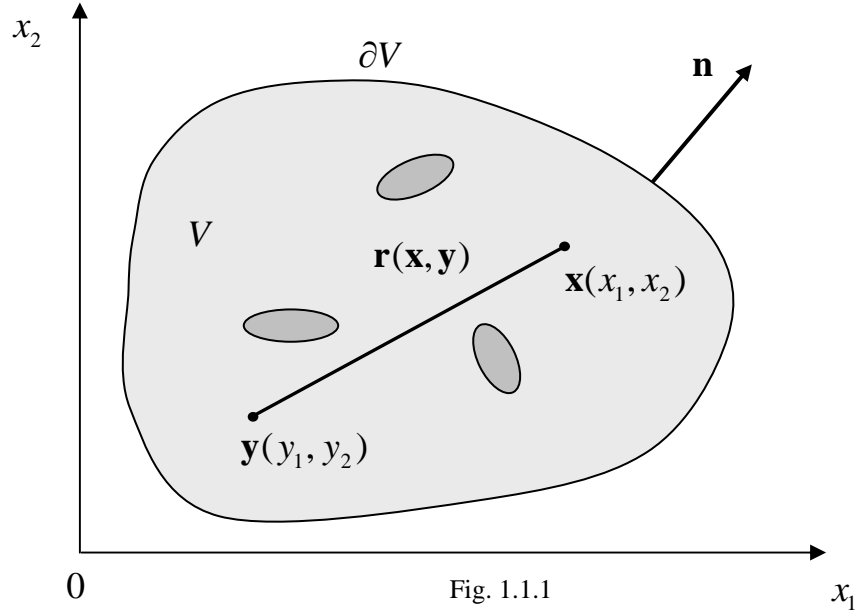


Fig. 1.1.1

The general solution of the 2-D problem can be presented by the integral identities of the Somigliano type for displacements in the form

$$u_i(\mathbf{y}) = \int_{\partial V} \{p_j(\mathbf{x})U_{ij}(\mathbf{x} - \mathbf{y}) - u_j(\mathbf{x})W_{ij}(\mathbf{x}, \mathbf{y})\} dS + \int_V b_j(\mathbf{x})U_{ij}(\mathbf{x} - \mathbf{y}) dV, \quad i, j = 1, 2 \quad (1.1.1)$$

here and bellow we use conventional index notation, summation over any pair of repeated indices is understood.

Notations:

$u_i(\mathbf{y})$ are components of the displacements vector in a point \mathbf{y} in the direction

of the axis x_i ;

$p_j(\mathbf{x})$ are components of the traction vector in a point \mathbf{x} in the direction of the axis x_j ;

$b_j(\mathbf{x})$ are components of the body forces vector in a point \mathbf{x} in the direction of axis x_j ;

$r = r(\mathbf{x}, \mathbf{y}) = \sqrt{(x_1 - y_1)^2 + (x_2 - y_2)^2}$ is the distance between points \mathbf{x} and \mathbf{y} ;

$\mathbf{x} = \mathbf{x}(x_1, x_2)$ is the point to which loading is put in;

$\mathbf{y} = \mathbf{y}(y_1, y_2)$ is the point in which we search displacements; $\mathbf{x}, \mathbf{y} \in V \setminus \partial V$;

$\partial V = \partial V_b + \bigcup_{i=1}^N \Gamma_i$ where ∂V_b is the boundary of the body and Γ_i is the boundary of a inclusion.

Tractions also can be defined by the formulas of the Somigliano type in the form

$$p_i(\mathbf{y}) = \int_{\partial V} \{p_j(\mathbf{x})K_{ij}(\mathbf{x}, \mathbf{y}) - u_i(\mathbf{x})C_{ij}(\mathbf{x}, \mathbf{y})\}dS + \int_V b_j(\mathbf{x})B_{ij}(\mathbf{x}, \mathbf{y})dV. \quad (1.1.2)$$

In order to obtain the boundary integral equations (BIE) from the integral representations (1.1.1) and (1.1.2) we have to turn out points \mathbf{y} to the boundary ∂V .

From the integral representation (1.1.1) we obtain BIE of the form

$$\frac{1}{2} \cdot u_i(\mathbf{y}) = \int_{\partial V} \{p_j(\mathbf{x})U_{ij}(\mathbf{x} - \mathbf{y}) - u_j(\mathbf{x})W_{ij}(\mathbf{x}, \mathbf{y})\}dS + \int_V b_j(\mathbf{x})U_{ij}(\mathbf{x} - \mathbf{y})dV. \quad (1.1.3)$$

From the integral representation (1.1.2) we obtain BIE of the form

$$\frac{1}{2} p_i(\mathbf{y}) = \int_{\partial V} \{p_j(\mathbf{x})K_{ij}(\mathbf{x}, \mathbf{y}) - u_i(\mathbf{x})F_{ij}(\mathbf{x}, \mathbf{y})\}dS + \int_V b_j(\mathbf{x})K_{ij}(\mathbf{x}, \mathbf{y})dV. \quad (1.1.4)$$

Now the two-dimensional problem under consideration has the dimension 1.

Integral identities of the Somigliano type for displacements (1.1.1) in matrix form:

$$\begin{aligned} \frac{1}{2} \begin{bmatrix} u_1(\mathbf{y}) \\ u_2(\mathbf{y}) \end{bmatrix} = \int_{\partial \Omega} \left\{ \begin{bmatrix} U_{11}(\mathbf{x} - \mathbf{y}) & U_{12}(\mathbf{x} - \mathbf{y}) \\ U_{21}(\mathbf{x} - \mathbf{y}) & U_{22}(\mathbf{x} - \mathbf{y}) \end{bmatrix} \cdot \begin{bmatrix} p_1(\mathbf{x}) \\ p_2(\mathbf{x}) \end{bmatrix} - \begin{bmatrix} W_{11}(\mathbf{x}, \mathbf{y}) & W_{12}(\mathbf{x}, \mathbf{y}) \\ W_{21}(\mathbf{x}, \mathbf{y}) & W_{22}(\mathbf{x}, \mathbf{y}) \end{bmatrix} \cdot \begin{bmatrix} u_1(\mathbf{x}) \\ u_2(\mathbf{x}) \end{bmatrix} \right\} dS + \\ + \int_V \begin{bmatrix} U_{11}(\mathbf{x} - \mathbf{y}) & U_{12}(\mathbf{x} - \mathbf{y}) \\ U_{21}(\mathbf{x} - \mathbf{y}) & U_{22}(\mathbf{x} - \mathbf{y}) \end{bmatrix} \cdot \begin{bmatrix} b_1(\mathbf{x}) \\ b_2(\mathbf{x}) \end{bmatrix} dV \end{aligned} \quad (1.1.5)$$

or in vector form

$$\frac{1}{2} \mathbf{u}(\mathbf{y}) = \int_{\partial \Omega} \{U(\mathbf{x} - \mathbf{y}) \cdot \mathbf{u}(\mathbf{x}) + W(\mathbf{x}, \mathbf{y}) \cdot \mathbf{p}(\mathbf{x})\}dS + \int_V U(\mathbf{x} - \mathbf{y}) \cdot \mathbf{b}(\mathbf{x})dV. \quad (1.1.6)$$

where – displacements $\mathbf{u}(\mathbf{x}) = \begin{bmatrix} u_1(\mathbf{x}) \\ u_2(\mathbf{x}) \end{bmatrix}$

– traction
$$\mathbf{p}(\mathbf{x}) = \begin{bmatrix} p_1(\mathbf{x}) \\ p_2(\mathbf{x}) \end{bmatrix}$$

– matrix fundamental solutions

– for displacements
$$U(\mathbf{x} - \mathbf{y}) = \begin{bmatrix} U_{11}(\mathbf{x} - \mathbf{y}) & U_{12}(\mathbf{x} - \mathbf{y}) \\ U_{21}(\mathbf{x} - \mathbf{y}) & U_{22}(\mathbf{x} - \mathbf{y}) \end{bmatrix}$$

– for traction
$$W(\mathbf{x}, \mathbf{y}) = \begin{bmatrix} W_{11}(\mathbf{x}, \mathbf{y}) & W_{12}(\mathbf{x}, \mathbf{y}) \\ W_{21}(\mathbf{x}, \mathbf{y}) & W_{22}(\mathbf{x}, \mathbf{y}) \end{bmatrix}$$

– body forces
$$\mathbf{b}(\mathbf{x}) = \begin{bmatrix} b_1(\mathbf{x}) \\ b_2(\mathbf{x}) \end{bmatrix}$$

for tractions we have the equations in vector and matrix form:

$$\frac{1}{2} \mathbf{p}(\mathbf{y}) = \int_{\partial\Omega} \{K(\mathbf{x}, \mathbf{y}) \cdot \mathbf{p}(\mathbf{x}) - F(\mathbf{x}, \mathbf{y}) \cdot \mathbf{u}(\mathbf{x})\} dS + \int_V K(\mathbf{x}, \mathbf{y}) \cdot \mathbf{b}(\mathbf{x}) dV. \quad (1.1.7)$$

$$\frac{1}{2} \begin{bmatrix} p_1(\mathbf{y}) \\ p_2(\mathbf{y}) \end{bmatrix} = \int_{\partial\Omega} \left\{ \begin{bmatrix} K_{11}(\mathbf{x}, \mathbf{y}) & K_{12}(\mathbf{x}, \mathbf{y}) \\ K_{21}(\mathbf{x}, \mathbf{y}) & K_{22}(\mathbf{x}, \mathbf{y}) \end{bmatrix} \cdot \begin{bmatrix} p_1(\mathbf{x}) \\ p_2(\mathbf{x}) \end{bmatrix} - \begin{bmatrix} F_{11}(\mathbf{x}, \mathbf{y}) & F_{12}(\mathbf{x}, \mathbf{y}) \\ F_{21}(\mathbf{x}, \mathbf{y}) & F_{22}(\mathbf{x}, \mathbf{y}) \end{bmatrix} \cdot \begin{bmatrix} u_1(\mathbf{x}) \\ u_2(\mathbf{x}) \end{bmatrix} \right\} dS + \int_V \begin{bmatrix} K_{11}(\mathbf{x}, \mathbf{y}) & K_{12}(\mathbf{x}, \mathbf{y}) \\ K_{21}(\mathbf{x}, \mathbf{y}) & K_{22}(\mathbf{x}, \mathbf{y}) \end{bmatrix} \cdot \begin{bmatrix} b_1(\mathbf{x}) \\ b_2(\mathbf{x}) \end{bmatrix} dV \quad (1.1.8)$$

1.2 The boundary integral equations analysis

For more compact record and analysis of the BIE (1.1.6) and (1.1.7) and we will introduce the following notations for potentials:

– boundary potentials from the expression (1.1.6)

$$U_{ij}(p_j, \mathbf{x}, \partial\Omega) = \int_{\partial V} p_j(\mathbf{x}) U_{ij}(\mathbf{x} - \mathbf{y}) dS. \quad (1.2.1)$$

$$W_{ij}(u_j, \mathbf{x}, \partial\Omega) = \int_{\partial V} u_j(\mathbf{x}) W_{ij}(\mathbf{x}, \mathbf{y}) dS. \quad (1.2.2)$$

– body potentials from the expression (1.1.6)

$$U_{ij}(b_j, \mathbf{x}, \Omega) = \int_V b_j(\mathbf{x}) U_{ij}(\mathbf{x} - \mathbf{y}) dV. \quad (1.2.3)$$

– boundary potentials from the expression (1.1.7)

$$K_{ij}(p_j, \mathbf{x}, \partial\Omega) = \int_{\partial V} p_j(\mathbf{x}) K_{ij}(\mathbf{x}, \mathbf{y}) dS. \quad (1.2.4)$$

$$F_{ij}(u_i, \mathbf{x}, \partial\Omega) = \int_{\partial V} u_i(\mathbf{x}) F_{ij}(\mathbf{x}, \mathbf{y}) dS. \quad (1.2.5)$$

– body potentials from the expression (1.1.7)

$$K_{ij}(b_j, \mathbf{x}, \Omega) = \int_V b_j(\mathbf{x}) K_{ij}(\mathbf{x}, \mathbf{y}) dV. \quad (1.2.6)$$

Thus, using notations (1.2.1-6), the BIEs (1.1.6) and (1.1.7) may be presented in the form

$$\pm \frac{1}{2} \cdot u_i(\mathbf{y}) = U_{ij}(p_j, \mathbf{x}, \partial\Omega) - W_{ij}(u_j, \mathbf{x}, \partial\Omega) + U_{ij}(b_j, \mathbf{x}, \Omega). \quad (1.2.7)$$

$$\pm \frac{1}{2} \cdot p_i(\mathbf{y}) = K_{ij}(p_j, \mathbf{x}, \partial\Omega) - F_{ij}(u_i, \mathbf{x}, \partial\Omega) + B_{ij}(b_j, \mathbf{x}, \Omega). \quad (1.2.8)$$

Exactly form of the BIEs, obtained from the expression (1.2.7) and (1.2.8), depends on the type of the boundary conditions. As it is known, in the classic case scope terms can be Dirihle and Neymana. The mixed case is also possible.

Let us consider mixed boundary conditions. In this case on the part of the boundary ∂V_u the displacements vector is known, and there on the part of the boundary ∂V_p the vector of the traction is known consequently,

$$u_i(\mathbf{y}) = \varphi(\mathbf{y}), \quad \forall \mathbf{y} \in \partial V_u \quad \text{and} \quad p_i(\mathbf{y}) = \psi_i(\mathbf{y}), \quad \forall \mathbf{y} \in \partial V_p. \quad (1.2.9)$$

Thus, for mixed boundary conditions it is possible to write the following BIEs.

The Type 1

$$U_{ij}(p_j, \mathbf{x}, \partial\Omega) - W_{ij}(u_j, \mathbf{x}, \partial\Omega) = \pm \frac{1}{2} \cdot \varphi_i(\mathbf{y}) - U_{ij}(b_j, \mathbf{x}, \Omega), \quad \forall \mathbf{y} \in \partial V_u$$

$$\pm \frac{1}{2} \cdot u_i(\mathbf{y}) - U_{ij}(p_j, \mathbf{x}, \partial\Omega) + W_{ij}(u_j, \mathbf{x}, \partial\Omega) = U_{ij}(b_j, \mathbf{x}, \Omega) \quad \forall \mathbf{y} \in \partial V_p \quad (1.2.10)$$

The potentials here contain only weekly singular and singular integrals.

The Type 2

$$\pm \frac{1}{2} \cdot p_i(\mathbf{y}) - K_{ij}(p_j, \mathbf{x}, \partial\Omega) + F_{ij}(u_i, \mathbf{x}, \partial\Omega) = B_{ij}(b_j, \mathbf{x}, \Omega), \quad \forall \mathbf{y} \in \partial V_u$$

$$K_{ij}(p_j, \mathbf{x}, \partial\Omega) - F_{ij}(u_i, \mathbf{x}, \partial\Omega) = \pm \frac{1}{2} \cdot \psi_i(\mathbf{y}) - B_{ij}(b_j, \mathbf{x}, \Omega) \quad \forall \mathbf{y} \in \partial V_p \quad (1.2.11)$$

The potentials here contain only singular and hypersingular integrals.

The Type 3.

$$U_{ij}(p_j, \mathbf{x}, \partial\Omega) - W_{ij}(u_j, \mathbf{x}, \partial\Omega) = \pm \frac{1}{2} \cdot \varphi_i(\mathbf{y}) - U_{ij}(b_j, \mathbf{x}, \Omega), \quad \forall \mathbf{y} \in \partial V_u$$

$$K_{ij}(p_j, \mathbf{x}, \partial\Omega) - F_{ij}(u_i, \mathbf{x}, \partial\Omega) = \pm \frac{1}{2} \cdot \psi_i(\mathbf{y}) - B_{ij}(b_j, \mathbf{x}, \Omega) \quad \forall \mathbf{y} \in \partial V_p \quad (1.2.12)$$

The potentials here contain weekly singular, singular and hypersingular integrals.

The Type 4.

$$\pm \frac{1}{2} \cdot p_i(\mathbf{y}) - K_{ij}(p_j, \mathbf{x}, \partial\Omega) + F_{ij}(u_i, \mathbf{x}, \partial\Omega) = B_{ij}(b_j, \mathbf{x}, \Omega), \quad \forall \mathbf{y} \in \partial V_u$$

$$\pm \frac{1}{2} \cdot u_i(\mathbf{y}) - U_{ij}(p_j, \mathbf{x}, \partial\Omega) + W_{ij}(u_j, \mathbf{x}, \partial\Omega) = U_{ij}(b_j, \mathbf{x}, \Omega) \quad \forall \mathbf{y} \in \partial V_p \quad (1.2.13)$$

The potentials here contain weekly singular, singular and hypersingular integrals.

1.3. Fundamental solutions U and W (general case)

The fundamental solutions for equation (1.1.3) and its derivatives have the form:

$$U_{ij}(\mathbf{x} - \mathbf{y}) = \frac{-1}{8\pi\mu(1-\nu)} \left\{ (3-4\nu)\ln(r)\delta_{ij} - \frac{\partial r}{\partial x_i} \frac{\partial r}{\partial x_j} \right\}, \quad (1.3.1)$$

or

$$U_{ij}(\mathbf{x} - \mathbf{y}) = \frac{-1}{8\pi\mu(1-\nu)} \left\{ (3-4\nu)\ln(r)\delta_{ij} - \frac{x_i - y_i}{r} \frac{x_j - y_j}{r} \right\}, \quad (1.3.2)$$

$$i=1, j=1$$

$$U_{11}(\mathbf{x} - \mathbf{y}) = \frac{-1}{8\pi\mu(1-\nu)} \left\{ (3-4\nu)\ln(r) - \left(\frac{\partial r}{\partial x_1} \right)^2 \right\} \quad (1.3.3)$$

$$U_{11}(\mathbf{x} - \mathbf{y}) = \frac{-1}{8\pi\mu(1-\nu)} \left\{ (3-4\nu)\ln(r) - \left(\frac{x_1 - y_1}{r} \right)^2 \right\} \quad (1.3.4)$$

$i = 1, j = 2$

$$U_{12}(\mathbf{x} - \mathbf{y}) = \frac{1}{8\pi\mu(1-\nu)} \frac{\partial r}{\partial x_1} \frac{\partial r}{\partial x_2} \quad (1.3.5)$$

$$U_{12}(\mathbf{x} - \mathbf{y}) = \frac{1}{8\pi\mu(1-\nu)} \frac{x_1 - y_1}{r} \frac{x_2 - y_2}{r}, \quad (1.3.6)$$

$i = 2, j = 1$

$$U_{21}(\mathbf{x} - \mathbf{y}) = \frac{1}{8\pi\mu(1-\nu)} \frac{\partial r}{\partial x_1} \frac{\partial r}{\partial x_2}, \quad (1.3.7)$$

$$U_{21}(\mathbf{x} - \mathbf{y}) = \frac{1}{8\pi\mu(1-\nu)} \frac{x_1 - y_1}{r} \frac{x_2 - y_2}{r}, \quad (1.3.8)$$

$i = 2, j = 2$

$$U_{22}(\mathbf{x} - \mathbf{y}) = \frac{-1}{8\pi\mu(1-\nu)} \left\{ (3-4\nu)\ln(r) - \left(\frac{\partial r}{\partial x_2} \right)^2 \right\} \quad (1.3.9)$$

$$U_{22}(\mathbf{x} - \mathbf{y}) = \frac{-1}{8\pi\mu(1-\nu)} \left\{ (3-4\nu)\ln(r) - \left(\frac{x_2 - y_2}{r} \right)^2 \right\} \quad (1.3.10)$$

1) Here we use definition of the delta function

$$\delta_{ij} = \begin{cases} 1 & \text{при } i = j \\ 0 & \text{при } i \neq j \end{cases}$$

2) It is clear that,

$$U_{12}(\mathbf{x} - \mathbf{y}) = U_{21}(\mathbf{x} - \mathbf{y}) \quad (1.3.11)$$

The fundamental solution W can be obtained from the fundamental solution U by use of the following operator:

$$W_{ij} = \lambda n_i(\mathbf{x}) \frac{\partial U_{ij}}{\partial x_j} + \mu \left(\delta_{ij} \frac{\partial U_{ij}}{\partial n(\mathbf{x})} + n_j(\mathbf{x}) \frac{\partial U_{ij}}{\partial x_i} \right), \quad (1.3.12)$$

where $\lambda = \frac{E}{(1+\nu)(1-2\nu)}$, $\mu = \frac{E}{2(1+\nu)}$.

Fundamental solution W has the form

$$W_{ij}(\mathbf{x}, \mathbf{y}) = \frac{1}{4\pi(1-\nu)r} \left\{ (1-2\nu) \left(n_j(\mathbf{x}) \frac{\partial r}{\partial x_i} - n_i(\mathbf{x}) \frac{\partial r}{\partial x_j} \right) - \left((1-2\nu) \delta_{ij} + 2 \frac{\partial r}{\partial x_i} \frac{\partial r}{\partial x_j} \right) \frac{\partial r}{\partial n(\mathbf{x})} \right\}$$

(1.3.13)

$i=1, j=1$

$$W_{11}(\mathbf{x}, \mathbf{y}) = \frac{-1}{4\pi(1-\nu)r} \left\{ (1-2\nu) + 2 \left(\frac{\partial r}{\partial x_1} \right)^2 \right\} \frac{\partial r}{\partial n(\mathbf{x})}$$

(1.3.14)

$$W_{11}(\mathbf{x}, \mathbf{y}) = \frac{-1}{4\pi(1-\nu)r} \left\{ (1-2\nu) + 2 \left(\frac{x_1 - y_1}{r} \right)^2 \right\} \left(\frac{x_1 - y_1}{r} n_1(\mathbf{x}) + \frac{x_2 - y_2}{r} n_2(\mathbf{x}) \right)$$

(1.3.15)

$i=1, j=2$

$$W_{12}(\mathbf{x}, \mathbf{y}) = \frac{1}{4\pi(1-\nu)r} \left\{ (1-2\nu) \left(n_2(\mathbf{x}) \frac{\partial r}{\partial x_1} - n_1(\mathbf{x}) \frac{\partial r}{\partial x_2} \right) - 2 \frac{\partial r}{\partial x_1} \frac{\partial r}{\partial x_2} \frac{\partial r}{\partial n(\mathbf{x})} \right\}$$

(1.3.16)

$$W_{12}(\mathbf{x}, \mathbf{y}) = \frac{1}{4\pi(1-\nu)r} \left\{ (1-2\nu) \left(\frac{x_1 - y_1}{r} n_2(\mathbf{x}) - \frac{x_2 - y_2}{r} n_1(\mathbf{x}) \right) - 2 \frac{x_1 - y_1}{r} \frac{x_2 - y_2}{r} \left(\frac{x_1 - y_1}{r} n_1(\mathbf{x}) + \frac{x_2 - y_2}{r} n_2(\mathbf{x}) \right) \right\}$$

1.3.17

$i=2, j=1$

$$W_{21}(\mathbf{x}, \mathbf{y}) = \frac{1}{4\pi(1-\nu)r} \left\{ (1-2\nu) \left(n_1(\mathbf{x}) \frac{\partial r}{\partial x_2} - n_2(\mathbf{x}) \frac{\partial r}{\partial x_1} \right) - 2 \frac{\partial r}{\partial x_1} \frac{\partial r}{\partial x_2} \frac{\partial r}{\partial n(\mathbf{x})} \right\} \quad (1.3.18)$$

$$W_{21}(\mathbf{x}, \mathbf{y}) = \frac{1}{4\pi(1-\nu)r} \left\{ (1-2\nu) \left(\frac{x_2 - y_2}{r} n_1(\mathbf{x}) - \frac{x_1 - y_1}{r} n_2(\mathbf{x}) \right) - \right. \\ \left. - 2 \frac{x_1 - y_1}{r} \frac{x_2 - y_2}{r} \left(\frac{x_1 - y_1}{r} n_1(\mathbf{x}) + \frac{x_2 - y_2}{r} n_2(\mathbf{x}) \right) \right\} \quad (1.3.19)$$

$i = 2, j = 2$

$$W_{22}(\mathbf{x}, \mathbf{y}) = \frac{-1}{4\pi(1-\nu)r} \left\{ (1-2\nu) + 2 \left(\frac{\partial r}{\partial x_2} \right)^2 \right\} \frac{\partial r}{\partial n(\mathbf{x})} \quad (1.3.20)$$

$$W_{22}(\mathbf{x}, \mathbf{y}) = \frac{-1}{4\pi(1-\nu)r} \left\{ (1-2\nu) + 2 \left(\frac{x_2 - y_2}{r} \right)^2 \right\} \left(\frac{x_1 - y_1}{r} n_1(\mathbf{x}) + \frac{x_2 - y_2}{r} n_2(\mathbf{x}) \right) \quad (1.3.21)$$

Here we use the following notations:

$$\frac{\partial r}{\partial x_i} = \frac{x_i - y_i}{r} \quad \text{-- partial space derivative with respect to } x_i \quad (1.3.22)$$

derivative in the normal direction –

$$\frac{\partial n(\mathbf{x})}{\partial n(\mathbf{x})} = \frac{\partial r}{\partial x_1} n_1(\mathbf{x}) + \frac{\partial r}{\partial x_2} n_2(\mathbf{x}) = \frac{x_1 - y_1}{r} n_1(\mathbf{x}) + \frac{x_2 - y_2}{r} n_2(\mathbf{x}). \quad (1.3.23)$$

$n_i(\mathbf{x}), n_j(\mathbf{x})$ - cosines in the direction perpendicular to axis i и j correspondently.

Cosines in direction

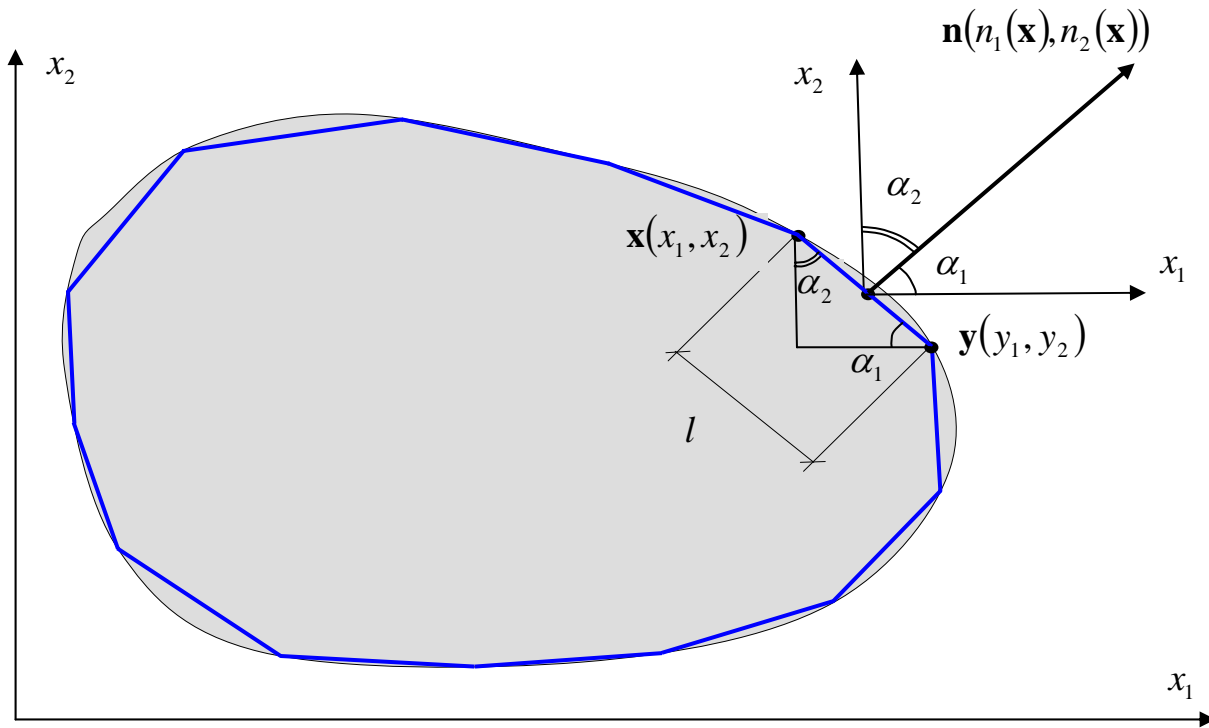


Fig. 1.3.1

It is visible from the Fig. 1.3.1, that the position of the boundary element can be set through the co-ordinates of unit normal vector $\mathbf{n}(\mathbf{x})$:

$$n_1(\mathbf{x}) = \cos \alpha_1 = \sin \alpha_2,$$

$$n_2(\mathbf{x}) = \sin \alpha_1 = \cos \alpha_2 \tag{1.3.24}$$

In coordinate form:

$$\boxed{n_1(\mathbf{x}) = \cos \alpha_1 = \frac{x_1 - y_1}{r} \quad \text{and} \quad n_2(\mathbf{x}) = \sin \alpha_1 = \frac{x_2 - y_2}{r},} \tag{1.3.25}$$

where $r = r(\mathbf{x}, \mathbf{y}) = \sqrt{(x_1 - y_1)^2 + (x_2 - y_2)^2}$ is the distance between points $\mathbf{x}(x_1, x_2)$

and $\mathbf{y}(y_1, y_2)$.

1.4 Fundamental solutions K and F (general case)

The fundamental solution K can be obtained from the fundamental solution U by use of the following operator:

$$K_{ij} = \lambda n_i(\mathbf{y}) \frac{\partial U_{ij}}{\partial y_j} + \mu \left(\delta_{ij} \frac{\partial U_{ij}}{\partial n(\mathbf{y})} + n_j(\mathbf{y}) \frac{\partial U_{ij}}{\partial y_i} \right) \quad (1.4.1)$$

and the fundamental solution F

$$F_{ij} = \lambda n_i(\mathbf{y}) \frac{\partial W_{ij}}{\partial y_j} + \mu \left(\delta_{ij} \frac{\partial W_{ij}}{\partial n(\mathbf{y})} + n_j(\mathbf{y}) \frac{\partial W_{ij}}{\partial y_i} \right) \quad (1.4.2)$$

The fundamental solutions for equation (1.1.4) and its derivatives have the form:

$$K_{ij}(\mathbf{x}, \mathbf{y}) = \frac{1}{4\pi(1-\nu)r} \left[(1-2\nu) \left(\frac{\partial r}{\partial t} \delta_{ij} + \frac{\partial r}{\partial x_j} t_i - \frac{\partial r}{\partial x_i} t_j \right) + 2 \frac{\partial r}{\partial x_i} \frac{\partial r}{\partial x_j} \frac{\partial r}{\partial t} \right] \quad (1.4.3)$$

or concretely for $i, j = 1, 2$

$$K_{11}(\mathbf{x}, \mathbf{y}) = \frac{1}{4\pi(1-\nu)r} \left[(1-2\nu) \frac{\partial r}{\partial t} + 2 \left(\frac{\partial r}{\partial x_1} \right)^2 \frac{\partial r}{\partial t} \right] \quad (1.4.4)$$

$$K_{12}(\mathbf{x}, \mathbf{y}) = \frac{1}{4\pi(1-\nu)r} \left[(1-2\nu) \left(\frac{\partial r}{\partial x_2} t_1 - \frac{\partial r}{\partial x_1} t_2 \right) + 2 \frac{\partial r}{\partial x_1} \frac{\partial r}{\partial x_2} \frac{\partial r}{\partial t} \right] \quad (1.4.5)$$

$$K_{21}(\mathbf{x}, \mathbf{y}) = \frac{1}{4\pi(1-\nu)r} \left[(1-2\nu) \left(\frac{\partial r}{\partial x_1} t_2 - \frac{\partial r}{\partial x_2} t_1 \right) + 2 \frac{\partial r}{\partial x_1} \frac{\partial r}{\partial x_2} \frac{\partial r}{\partial t} \right] \quad (1.4.6)$$

$$K_{22}(\mathbf{x}, \mathbf{y}) = \frac{1}{4\pi(1-\nu)r} \left[(1-2\nu) \frac{\partial r}{\partial t} + 2 \left(\frac{\partial r}{\partial x_2} \right)^2 \frac{\partial r}{\partial t} \right] \quad (1.4.7)$$

Other notation of the fundamental solutions has the form

$$K_{ij}(\mathbf{x}, \mathbf{y}) = \frac{-1}{4\pi(1-\nu)r} \left[- (1-2\nu) \left(\left(\frac{x_1 - y_1}{r} n_1(\mathbf{y}) + \frac{x_2 - y_2}{r} n_2(\mathbf{y}) \right) \delta_{ij} - \frac{x_i - y_i}{r} n_j(\mathbf{y}) + \frac{x_j - y_j}{r} n_i(\mathbf{y}) \right) - 2 \left(\frac{x_1 - y_1}{r} n_1(\mathbf{y}) + \frac{x_2 - y_2}{r} n_2(\mathbf{y}) \right) \frac{x_i - y_i}{r} \frac{x_j - y_j}{r} \right]$$

(1.4.8)

where:

$$\frac{\partial r}{\partial y_i} = - \frac{x_i - y_i}{r} \text{ - derivative with respect to } y_i \quad \dots\dots \quad (1.4.9)$$

derivative in the normal direction –

$$\frac{\partial n(\mathbf{y})}{\partial n(\mathbf{y})} = \frac{\partial r}{\partial y_1} n_1(\mathbf{y}) + \frac{\partial r}{\partial y_2} n_2(\mathbf{y}) = - \frac{x_1 - y_1}{r} n_1(\mathbf{y}) - \frac{x_2 - y_2}{r} n_2(\mathbf{y}) - \quad (1.4.10)$$

$n_i(\mathbf{y}), n_j(\mathbf{y})$ - cosines in the direction perpendicular to axis i и j correspondently.

And

$$i=1, j=1$$

$$K_{11}(\mathbf{x}, \mathbf{y}) = \frac{-1}{4\pi(1-\nu)r} \left[- (1-2\nu) \left(\left(\frac{x_1 - y_1}{r} n_1(\mathbf{y}) + \frac{x_2 - y_2}{r} n_2(\mathbf{y}) \right) \right) - \right. \\ \left. - 2 \left(\frac{x_1 - y_1}{r} n_1(\mathbf{y}) + \frac{x_2 - y_2}{r} n_2(\mathbf{y}) \right) \left(\frac{x_1 - y_1}{r} \right)^2 \right] \\ K_{11}(\mathbf{x}, \mathbf{y}) = \frac{1}{4\pi(1-\nu)r} \left[\left((1-2\nu) + 2 \left(\frac{x_1 - y_1}{r} \right)^2 \right) \left(\frac{x_1 - y_1}{r} n_1(\mathbf{y}) + \frac{x_2 - y_2}{r} n_2(\mathbf{y}) \right) \right] \quad (1.4.11)$$

$$K_{11}(\mathbf{x}, \mathbf{y}) = \frac{1}{4\pi(1-\nu)r} \left[\left((1-2\nu) + 2 \left(\frac{\partial r}{\partial x_1} \right)^2 \right) \frac{\partial r}{\partial n(\mathbf{y})} \right] \quad (1.4.12)$$

$i=1, j=2$

$$K_{12}(\mathbf{x}, \mathbf{y}) = \frac{1}{4\pi(1-\nu)r} \left[(1-2\nu) \left(\frac{x_2 - y_2}{r} n_1(\mathbf{y}) - \frac{x_1 - y_1}{r} n_2(\mathbf{y}) \right) + \right. \\ \left. + 2 \left(\frac{x_1 - y_1}{r} n_1(\mathbf{y}) + \frac{x_2 - y_2}{r} n_2(\mathbf{y}) \right) \frac{x_1 - y_1}{r} \frac{x_2 - y_2}{r} \right] \quad (1.4.13)$$

$$K_{12}(\mathbf{x}, \mathbf{y}) = \frac{1}{4\pi(1-\nu)r} \left[(1-2\nu) \left(\frac{\partial r}{\partial x_2} n_1(\mathbf{y}) - \frac{\partial r}{\partial x_1} n_2(\mathbf{y}) \right) + 2 \frac{\partial r}{\partial n(\mathbf{y})} \frac{\partial r}{\partial y_1} \frac{\partial r}{\partial y_2} \right] \quad (1.4.14)$$

$i=2, j=1$

$$K_{21}(\mathbf{x}, \mathbf{y}) = \frac{-1}{4\pi(1-\nu)r} \left[-\frac{x_2 - y_2}{r} n_1(\mathbf{y}) + \frac{x_1 - y_1}{r} n_2(\mathbf{y}) - \right. \\ \left. - 2 \left(\frac{x_1 - y_1}{r} n_1 + \frac{x_2 - y_2}{r} n_2 \right) \frac{x_1 - y_1}{r} \frac{x_2 - y_2}{r} \right] \quad (1.4.15)$$

$$K_{21}(\mathbf{x}, \mathbf{y}) = \frac{-1}{4\pi(1-\nu)r} \left[(1-2\nu) \left(\frac{\partial r}{\partial y_2} \cdot n_1(\mathbf{y}) - \frac{\partial r}{\partial y_1} \cdot n_2(\mathbf{y}) \right) + 2 \frac{\partial r}{\partial n(\mathbf{y})} \frac{\partial r}{\partial y_1} \frac{\partial r}{\partial y_2} \right] \quad (1.4.16)$$

$i=2, j=2$

$$K_{22}(\mathbf{x}, \mathbf{y}) = \frac{-1}{4\pi(1-\nu)r} \left[-(1-2\nu) \left(\frac{x_1 - y_1}{r} n_1(\mathbf{y}) + \frac{x_2 - y_2}{r} n_2(\mathbf{y}) \right) - \right. \\ \left. - 2 \left(\frac{x_1 - y_1}{r} n_1(\mathbf{y}) + \frac{x_2 - y_2}{r} n_2(\mathbf{y}) \right) \left(\frac{x_2 - y_2}{r} \right)^2 \right] =$$

$$K_{22}(\mathbf{x}, \mathbf{y}) = \frac{-1}{4\pi(1-\nu)r} \left[\left(-(1-2\nu) - 2 \left(\frac{x_2 - y_2}{r} \right)^2 \right) \left(\frac{x_1 - y_1}{r} n_1(\mathbf{y}) + \frac{x_2 - y_2}{r} n_2(\mathbf{y}) \right) \right] \quad (1.4.17)$$

$$K_{22}(\mathbf{x}, \mathbf{y}) = \frac{-1}{4\pi(1-\nu)r} \left[\left((1-2\nu) + 2 \left(\frac{\partial r}{\partial y_2} \right)^2 \right) \frac{\partial r}{\partial n(\mathbf{y})} \right] \quad (1.4.18)$$

Fundamental solution F has the form:

$$F_{ij}(\mathbf{x}, \mathbf{y}) = \frac{\mu}{2\pi(1-\nu)r^2} \left\{ 2 \frac{\partial r}{\partial y_j} \left[(1-2\nu)\delta_{ij} \frac{\partial r}{\partial n(\mathbf{y})} + \nu \left(n_i(\mathbf{y}) \frac{\partial r}{\partial y_j} + n_j(\mathbf{y}) \frac{\partial r}{\partial y_i} \right) - 4 \frac{\partial r}{\partial y_i} \frac{\partial r}{\partial y_j} \frac{\partial r}{\partial n(\mathbf{y})} \right] + \right. \\ \left. + 2\nu \left(n_i(\mathbf{y}) \frac{\partial r}{\partial y_j} \frac{\partial r}{\partial n(\mathbf{y})} + n_j(\mathbf{y}) \frac{\partial r}{\partial y_i} \frac{\partial r}{\partial n(\mathbf{y})} \right) + 2(1-2\nu) \left(\frac{\partial r}{\partial y_i} \frac{\partial r}{\partial y_j} + 2n_i(\mathbf{y})n_j(\mathbf{y}) \right) - (1-4\nu)\delta_{ij} \right\}$$

(1.4.19)

Or in specific cases

$$F_{11}(\mathbf{x}, \mathbf{y}) = \frac{\mu}{\pi(1-\nu)r^2} \left\{ \left(\frac{x_1 - y_1}{r} \right)^2 n_1(\mathbf{y})t_1(\mathbf{y}) + \frac{1}{2} \frac{(x_1 - y_1)(x_2 - y_2)}{r} (n_2(\mathbf{y})t_1(\mathbf{y}) + n_1(\mathbf{y})t_2(\mathbf{y})) + \right. \\ \left. + \frac{1}{2} n_1(\mathbf{y})t_1(\mathbf{y}) - 4 \left(\frac{x_1 - y_1}{r} \right)^2 \frac{\partial r}{\partial n(\mathbf{y})} \frac{\partial r}{\partial t(\mathbf{y})} \right\}$$

(1.4.20)

$$F_{12}(\mathbf{x}, \mathbf{y}) = \frac{\mu}{\pi(1-\nu)r^2} \left\{ \frac{(x_1 - y_1)(x_2 - y_2)}{r} n_1(\mathbf{y})t_2(\mathbf{y}) - 4 \left(\frac{x_1 - y_1}{r} \right)^2 \frac{\partial r}{\partial n(\mathbf{y})} \frac{\partial r}{\partial t(\mathbf{y})} + \right. \\ \left. + \frac{1}{2} (n_2(\mathbf{y})t_1(\mathbf{y}) + n_1(\mathbf{y})t_2(\mathbf{y})) \right\}$$

(1.4.21)

$$F_{21}(\mathbf{x}, \mathbf{y}) = \frac{\mu}{\pi(1-\nu)r^2} \left\{ \frac{(x_1 - y_1)(x_2 - y_2)}{r} n_2(\mathbf{y})t_1(\mathbf{y}) - 4 \frac{(x_1 - y_1)(x_2 - y_2)}{r} \frac{\partial r}{\partial n(\mathbf{y})} \frac{\partial r}{\partial t(\mathbf{y})} + \right. \\ \left. + \frac{1}{2} (n_2(\mathbf{y})t_1(\mathbf{y}) + n_1(\mathbf{y})t_2(\mathbf{y})) \right\}$$

(1.4.22)

$$F_{22}(\mathbf{x}, \mathbf{y}) = \frac{\mu}{\pi(1-\nu)r^2} \left\{ \left(\frac{x_2 - y_2}{r} \right)^2 n_2(\mathbf{y}) t_2(\mathbf{y}) + \frac{1}{2} \frac{(x_1 - y_1)(x_2 - y_2)}{r} (n_2(\mathbf{y}) t_1(\mathbf{y}) + n_1(\mathbf{y}) t_2(\mathbf{y})) + \frac{1}{2} n_2(\mathbf{y}) t_2(\mathbf{y}) - 4 \left(\frac{x_2 - y_2}{r} \right)^2 \frac{\partial r}{\partial n(\mathbf{y})} \frac{\partial r}{\partial t(\mathbf{y})} \right\}$$

(1.4.23)

1.5 Analysis of the fundamental solutions for the main elements

The boundary potentials (fundamental solutions) contain divergent integrals which arise up when point \mathbf{y} move to the boundary of region. The analysis of these integrals shows that they contain:

– $U_{ij}(\mathbf{x} - \mathbf{y})$ weak singularity, i.e.,

$$U_{ij}(\mathbf{x} - \mathbf{y}) \rightarrow \ln(r). \quad (1.5.1)$$

– $W_{ij}(\mathbf{x}, \mathbf{y})$ and $K_{ij}(\mathbf{x}, \mathbf{y})$ singularity in the Cauchy sense:

$$W_{ij}(\mathbf{x}, \mathbf{y}) \rightarrow \frac{1}{r}, \quad K_{ij}(\mathbf{x}, \mathbf{y}) \rightarrow \frac{1}{r}. \quad (1.5.2)$$

– $F_{ij}(\mathbf{x}, \mathbf{y})$ – strong singularity in the Hadamard sense, i.e.,

$$F_{ij}(\mathbf{x}, \mathbf{y}) \rightarrow \frac{1}{r^2}. \quad (1.5.3)$$

1.6 Inclusion problem

We consider the 2-D domain V_1 with an inclusion V_2 (Fig. 1.6.1).

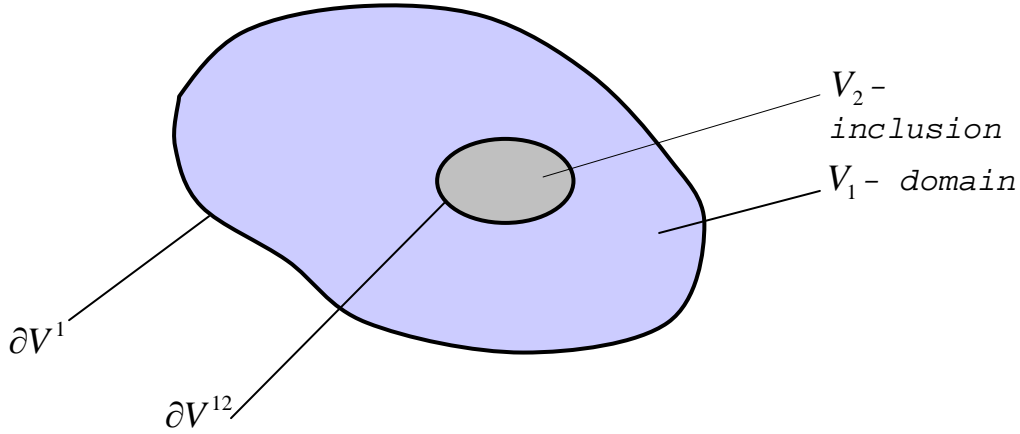


Fig. 1.6.1

BIEs for the domain V_1 have the form

$$\frac{1}{2}u_i^1(\mathbf{y}) = \int_{\partial V^1} \{p_j^1(\mathbf{x})U_{ij}^1(\mathbf{x}-\mathbf{y}) - u_j^1(\mathbf{x})W_{ij}^1(\mathbf{x},\mathbf{y})\}dS + \int_{\partial V^{12}} \{p_j^{12}(\mathbf{x})U_{ij}^1(\mathbf{x}-\mathbf{y}) - u_j^{12}(\mathbf{x})W_{ij}^1(\mathbf{x},\mathbf{y})\}dS \tag{1.6.1}$$

BIEs for the inclusion V_2 have the form

$$\frac{1}{2}u_i^{21}(\mathbf{y}) = \int_{\partial V^{12}} \{p_j^{21}(\mathbf{x})U_{ij}^2(\mathbf{x}-\mathbf{y}) - u_j^{21}(\mathbf{x})W_{ij}^2(\mathbf{x},\mathbf{y})\}dS \tag{1.6.2}$$

On the boundary between domain and inclusion ∂V_{12} the following conditions have to fulfill

$$u_j^{21}(\mathbf{x}) = u_j^{12}(\mathbf{x}), \quad p_j^{21}(\mathbf{x}) = -p_j^{12}(\mathbf{x}) \tag{1.6.3}$$

Therefore (1.6.2) has the form

$$\frac{1}{2}u_i^{12}(\mathbf{y}) = - \int_{\partial V^{12}} \{p_j^{12}(\mathbf{x})U_{ij}^2(\mathbf{x}-\mathbf{y}) + u_j^{12}(\mathbf{x})W_{ij}^2(\mathbf{x},\mathbf{y})\}dS \tag{1.6.4}$$

As result we obtain the system of BIEs in the form

$$\left\{ \begin{aligned} \frac{1}{2}u_i^1(\mathbf{y}) &= \int_{\partial V^1} \{p_j^1(\mathbf{x})U_{ij}^1(\mathbf{x}-\mathbf{y}) - u_j^1(\mathbf{x})W_{ij}^1(\mathbf{x},\mathbf{y})\}dS + \int_{\partial V^{12}} \{p_j^{12}(\mathbf{x})U_{ij}^1(\mathbf{x}-\mathbf{y}) - u_j^{12}(\mathbf{x})W_{ij}^1(\mathbf{x},\mathbf{y})\}dS \\ \frac{1}{2}u_i^{12}(\mathbf{y}) &= - \int_{\partial V^{12}} \{p_j^{12}(\mathbf{x})U_{ij}^2(\mathbf{x}-\mathbf{y}) + u_j^{12}(\mathbf{x})W_{ij}^2(\mathbf{x},\mathbf{y})\}dS \end{aligned} \right.$$

(1.6.5)

We rewrite the system (1.6.5) in the matrix form. For that we change order of equations in (1.6.5) and write them in more details:

$$\left\{ \begin{aligned} \frac{1}{2}u_1^1(\mathbf{y}) &= \int_{\partial V^1} \{ (p_1^1(\mathbf{x})U_{11}^1(\mathbf{x}-\mathbf{y}) + p_2^1(\mathbf{x})U_{12}^1(\mathbf{x}-\mathbf{y})) - (u_1^1(\mathbf{x})W_{11}^1(\mathbf{x},\mathbf{y}) + u_2^1(\mathbf{x})W_{12}^1(\mathbf{x},\mathbf{y})) \} dS + \\ &\quad + \int_{\partial V^{12}} \{ (p_1^{12}(\mathbf{x})U_{11}^1(\mathbf{x}-\mathbf{y}) + p_2^{12}(\mathbf{x})U_{12}^1(\mathbf{x}-\mathbf{y})) - (u_1^{12}(\mathbf{x})W_{11}^1(\mathbf{x},\mathbf{y}) + u_2^{12}(\mathbf{x})W_{12}^1(\mathbf{x},\mathbf{y})) \} dS \\ \frac{1}{2}u_1^{12}(\mathbf{y}) &= - \int_{\partial V^{12}} \{ (p_1^{12}(\mathbf{x})U_{11}^2(\mathbf{x}-\mathbf{y}) + p_2^{12}(\mathbf{x})U_{12}^2(\mathbf{x}-\mathbf{y})) + (u_1^{12}(\mathbf{x})W_{11}^2(\mathbf{x},\mathbf{y}) + u_2^{12}(\mathbf{x})W_{12}^2(\mathbf{x},\mathbf{y})) \} dS \\ \frac{1}{2}u_2^1(\mathbf{y}) &= \int_{\partial V^1} \{ (p_1^1(\mathbf{x})U_{21}^1(\mathbf{x}-\mathbf{y}) + p_2^1(\mathbf{x})U_{22}^1(\mathbf{x}-\mathbf{y})) - (u_1^1(\mathbf{x})W_{21}^1(\mathbf{x},\mathbf{y}) + u_2^1(\mathbf{x})W_{22}^1(\mathbf{x},\mathbf{y})) \} dS + \\ &\quad + \int_{\partial V^{12}} \{ (p_1^{12}(\mathbf{x})U_{21}^1(\mathbf{x}-\mathbf{y}) + p_2^{12}(\mathbf{x})U_{22}^1(\mathbf{x}-\mathbf{y})) - (u_1^{12}(\mathbf{x})W_{21}^1(\mathbf{x},\mathbf{y}) + u_2^{12}(\mathbf{x})W_{22}^1(\mathbf{x},\mathbf{y})) \} dS \\ \frac{1}{2}u_2^{12}(\mathbf{y}) &= - \int_{\partial V^{12}} \{ (p_1^{12}(\mathbf{x})U_{21}^2(\mathbf{x}-\mathbf{y}) + p_2^{12}(\mathbf{x})U_{22}^2(\mathbf{x}-\mathbf{y})) + (u_1^{12}(\mathbf{x})W_{21}^2(\mathbf{x},\mathbf{y}) + u_2^{12}(\mathbf{x})W_{22}^2(\mathbf{x},\mathbf{y})) \} dS \end{aligned} \right.$$

(1.6.6)

or in matrix form:

$$\frac{1}{2} \begin{pmatrix} u_1^1(\mathbf{y}) \\ u_1^{12}(\mathbf{y}) \\ u_2^1(\mathbf{y}) \\ u_2^{12}(\mathbf{y}) \end{pmatrix} = \begin{pmatrix} \int_{\partial V^1} U_{11}^1(\mathbf{x}-\mathbf{y})dS & \int_{\partial V^{12}} U_{11}^1(\mathbf{x}-\mathbf{y})dS & \int_{\partial V^1} U_{12}^1(\mathbf{x}-\mathbf{y})dS & \int_{\partial V^{12}} U_{12}^1(\mathbf{x}-\mathbf{y})dS \\ 0 & - \int_{\partial V^{12}} U_{11}^2(\mathbf{x}-\mathbf{y})dS & 0 & - \int_{\partial V^{12}} U_{12}^2(\mathbf{x}-\mathbf{y})dS \\ \int_{\partial V^1} U_{21}^1(\mathbf{x}-\mathbf{y})dS & \int_{\partial V^{12}} U_{21}^1(\mathbf{x}-\mathbf{y})dS & \int_{\partial V^1} U_{22}^1(\mathbf{x}-\mathbf{y})dS & \int_{\partial V^{12}} U_{22}^1(\mathbf{x}-\mathbf{y})dS \\ 0 & - \int_{\partial V^{12}} U_{21}^2(\mathbf{x}-\mathbf{y})dS & 0 & - \int_{\partial V^{12}} U_{22}^2(\mathbf{x}-\mathbf{y})dS \end{pmatrix} \cdot \begin{pmatrix} p_1^1(\mathbf{x}) \\ p_1^{12}(\mathbf{x}) \\ p_2^1(\mathbf{x}) \\ p_2^{12}(\mathbf{x}) \end{pmatrix} -$$

$$\begin{pmatrix} \int_{\partial V^1} W_{11}^1(\mathbf{x},\mathbf{y})dS & \int_{\partial V^{12}} W_{11}^1(\mathbf{x},\mathbf{y})dS & \int_{\partial V^1} W_{12}^1(\mathbf{x},\mathbf{y})dS & \int_{\partial V^{12}} W_{12}^1(\mathbf{x},\mathbf{y})dS \\ 0 & - \int_{\partial V^{12}} W_{11}^2(\mathbf{x},\mathbf{y})dS & 0 & - \int_{\partial V^{12}} W_{12}^2(\mathbf{x},\mathbf{y})dS \\ \int_{\partial V^1} W_{21}^1(\mathbf{x},\mathbf{y})dS & \int_{\partial V^{12}} W_{21}^1(\mathbf{x},\mathbf{y})dS & \int_{\partial V^1} W_{22}^1(\mathbf{x},\mathbf{y})dS & \int_{\partial V^{12}} W_{22}^1(\mathbf{x},\mathbf{y})dS \\ 0 & - \int_{\partial V^{12}} W_{21}^2(\mathbf{x},\mathbf{y})dS & 0 & - \int_{\partial V^{12}} W_{22}^2(\mathbf{x},\mathbf{y})dS \end{pmatrix} \cdot \begin{pmatrix} u_1^1(\mathbf{x}) \\ u_1^{12}(\mathbf{x}) \\ u_2^1(\mathbf{x}) \\ u_2^{12}(\mathbf{x}) \end{pmatrix} dS$$

(1.6.7)

Matrices in equation (1.6.7) have the block structure. Let N – is the number of boundary elements at the boundary of domain.

Block $\int_{\partial V^1} U_{11}^1(\mathbf{x}-\mathbf{y})dS$ has the form

$$\int_{\partial V^1} U_{11}^1(\mathbf{x}-\mathbf{y})dS = \int_{\partial V^1} \underbrace{\begin{pmatrix} U_{11}^1(x_1 - x_1) & U_{11}^1(x_2 - x_1) & \dots & U_{11}^1(x_{N/2} - x_1) \\ U_{11}^1(x_1 - x_2) & U_{11}^1(x_2 - x_2) & \dots & U_{11}^1(x_{N/2} - x_2) \\ \dots & \dots & \dots & \dots \\ U_{11}^1(x_1 - x_{N/2}) & U_{11}^1(x_2 - x_{N/2}) & \dots & U_{11}^1(x_{N/2} - x_{N/2}) \end{pmatrix}}_{\frac{N}{2}} dS \left. \vphantom{\int_{\partial V^1}} \right\} \frac{N}{2}$$

The traces of each block contain kernels with singularity.

1.7 Solution of the problem for the domain with an inclusion by the boundary integral equations method

We consider the following rectangular domain with the circular inclusion (Fig.1.7.1)

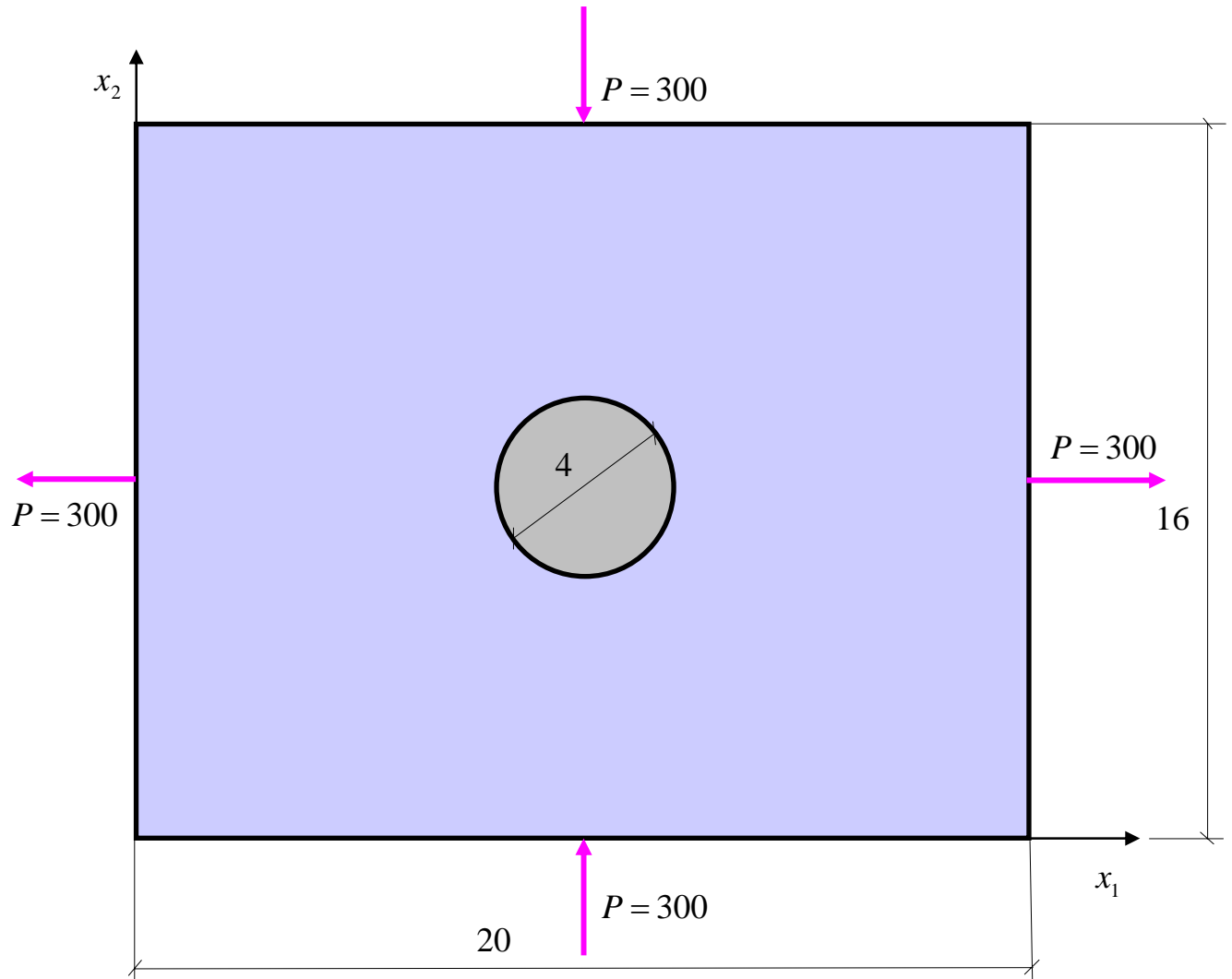


Fig.1.7.1

Mechanical characteristics :

- domain: module of elasticity $E = 20000$, Poisson ratio $\mu = 0.1$;
- inclusion: module of elasticity $E = 100000$, Poisson ratio $\mu = 0.2$.

Each boundary contains 20 boundary elements.

The singular kernels have been calculated analytically and regular kernels have been calculated using the Gauss formulas with constant weight.

Forces applied as it is shown in (Fig.1.7.1).

Bellow we present data for calculation using our FORTRAN program.

1) General data:

NUMBER OF BOUNDARY ELEMENTS = 40

NUMBER OF INTERNAL POINTS = 2

DOMAIN SHEAR MODULUS = 0.2000000E+05

DOMAIN POISSON RATIO = 0.1000000E+00

INCLUSION SHEAR MODULUS = 0.1000000E+06

INCLUSION POISSON RATIO = 0.2000000E+00

2) Coordinates of boundary elements:

a) rectangular domain:

	X1	X2
1	0.0000000E+00	0.0000000E+00
2	0.0000000E+00	0.3200000E+01
3	0.0000000E+00	0.6400000E+01
4	0.0000000E+00	0.9600000E+01
5	0.0000000E+00	0.1280000E+02
6	0.0000000E+00	0.1600000E+02
7	0.4000000E+01	0.1600000E+02
8	0.8000000E+01	0.1600000E+02
9	0.1200000E+02	0.1600000E+02
10	0.1600000E+02	0.1600000E+02
11	0.2000000E+02	0.1600000E+02
12	0.2000000E+02	0.1280000E+02
13	0.2000000E+02	0.9600000E+01
14	0.2000000E+02	0.6400000E+01
15	0.2000000E+02	0.3200000E+01
16	0.2000000E+02	0.0000000E+00
17	0.1600000E+02	0.0000000E+00
18	0.1200000E+02	0.0000000E+00
19	0.8000000E+01	0.0000000E+00
20	0.4000000E+01	0.0000000E+00

6) Inclusion:

	X1	X2
21	0.1000000E+02	0.6000000E+01
22	0.9382000E+01	0.6097900E+01
23	0.8824400E+01	0.6382000E+01

24	0.8382000E+01	0.6824400E+01
25	0.8097900E+01	0.7382000E+01
26	0.8000000E+01	0.8000000E+01
27	0.8097900E+01	0.8618000E+01
28	0.8382000E+01	0.9175600E+01
29	0.8824400E+01	0.9618000E+01
30	0.9382000E+01	0.9904000E+01
31	0.1000000E+02	0.1000000E+02
32	0.1061800E+02	0.9902100E+01
33	0.1117560E+02	0.9618000E+01
34	0.1161800E+02	0.9175600E+01
35	0.1190210E+02	0.8618000E+01
36	0.1200000E+02	0.8000000E+01
37	0.1190210E+02	0.7382000E+01
38	0.1161800E+02	0.6824400E+01
39	0.1117560E+02	0.6382000E+01
40	0.1061800E+02	0.6097900E+01

3) Boundary conditions

	X1 DIRECTION	X2 DIRECTION
1	0.0000000E+00	0.0000000E+00
2	0.0000000E+00	0.0000000E+00
3	-0.3000000E+03	0.0000000E+00
4	0.0000000E+00	0.0000000E+00
5	0.0000000E+00	0.0000000E+00
6	0.0000000E+00	0.0000000E+00
7	0.0000000E+00	0.0000000E+00
8	0.0000000E+00	-0.3000000E+03
9	0.0000000E+00	0.0000000E+00
10	0.0000000E+00	0.0000000E+00
11	0.0000000E+00	0.0000000E+00
12	0.0000000E+00	0.0000000E+00
13	0.3000000E+03	0.0000000E+00
14	0.0000000E+00	0.0000000E+00
15	0.0000000E+00	0.0000000E+00
16	0.0000000E+00	0.0000000E+00
17	0.0000000E+00	0.0000000E+00

18	0.000000E+00	0.300000E+03
19	0.000000E+00	0.000000E+00
20	0.000000E+00	0.000000E+00
21	0.000000E+00	0.000000E+00
22	0.000000E+00	0.000000E+00
23	0.000000E+00	0.000000E+00
24	0.000000E+00	0.000000E+00
25	0.000000E+00	0.000000E+00
26	0.000000E+00	0.000000E+00
27	0.000000E+00	0.000000E+00
28	0.000000E+00	0.000000E+00
29	0.000000E+00	0.000000E+00
30	0.000000E+00	0.000000E+00
31	0.000000E+00	0.000000E+00
32	0.000000E+00	0.000000E+00
33	0.000000E+00	0.000000E+00
34	0.000000E+00	0.000000E+00
35	0.000000E+00	0.000000E+00
36	0.000000E+00	0.000000E+00
37	0.000000E+00	0.000000E+00
38	0.000000E+00	0.000000E+00
39	0.000000E+00	0.000000E+00
40	0.000000E+00	0.000000E+00

4) Coordinates of the centers of the boundary elements

	X1	X2
1	0.000000E+00	0.160000E+01
2	0.000000E+00	0.480000E+01
3	0.000000E+00	0.800000E+01
4	0.000000E+00	0.112000E+02
5	0.000000E+00	0.144000E+02
6	0.200000E+01	0.160000E+02
7	0.600000E+01	0.160000E+02
8	0.100000E+02	0.160000E+02
9	0.140000E+02	0.160000E+02
10	0.180000E+02	0.160000E+02
11	0.200000E+02	0.144000E+02

12	0.2000000E+02	0.1120000E+02
13	0.2000000E+02	0.8000000E+01
14	0.2000000E+02	0.4800000E+01
15	0.2000000E+02	0.1600000E+01
16	0.1800000E+02	0.0000000E+00
17	0.1400000E+02	0.0000000E+00
18	0.1000000E+02	0.0000000E+00
19	0.6000000E+01	0.0000000E+00
20	0.2000000E+01	0.0000000E+00
21	0.9691000E+01	0.6048950E+01
22	0.9103200E+01	0.6239950E+01
23	0.8603200E+01	0.6603200E+01
24	0.8239950E+01	0.7103200E+01
25	0.8048950E+01	0.7691000E+01
26	0.8048950E+01	0.8309000E+01
27	0.8239950E+01	0.8896800E+01
28	0.8603200E+01	0.9396800E+01
29	0.9103200E+01	0.9761000E+01
30	0.9691000E+01	0.9952000E+01
31	0.1030900E+02	0.9951050E+01
32	0.1089680E+02	0.9760050E+01
33	0.1139680E+02	0.9396800E+01
34	0.1176005E+02	0.8896800E+01
35	0.1195105E+02	0.8309000E+01
36	0.1195105E+02	0.7691000E+01
37	0.1176005E+02	0.7103200E+01
38	0.1139680E+02	0.6603200E+01
39	0.1089680E+02	0.6239950E+01
40	0.1030900E+02	0.6048950E+01

5) Results of the calculations in some points of the domain:

X1	X2	SIGMA X1	TAU X1X2	SIGMA X2
0.1240000E+02	0.1020000E+02	0.3476998E+02	0.1663189E+02	0.2616725E+02
0.1000000E+02	0.8000000E+01	-0.7020971E+02	-0.9875047E+01	0.5356906E+02

1.8 Numerical example for the two-dimensional problem with an inclusion located non-symmetrically

Let us consider the following rectangular domain V_1 (Aluminum, mechanical characteristics: the Young module of elasticity $E = 70$ GPa, the Poisson ratio $\nu = 0.33$, the material density $\rho = 2700$ kg/m³) with the circular inclusion V_2 (Iron, the Young module of elasticity $E = 200$ GPa, the Poisson ratio $\nu = 0.29$, the material density $\rho = 7870$ kg/m³) under static tension. The circular inclusions located non-symmetrically, so $V_1 = \{-a \leq x_1 \leq a, -b \leq x_2 \leq b\}$ and $V_2 = \{(x_1 - s)^2 + (x_2 - t)^2 \leq c^2\}$ (see Figure 1.8.1).

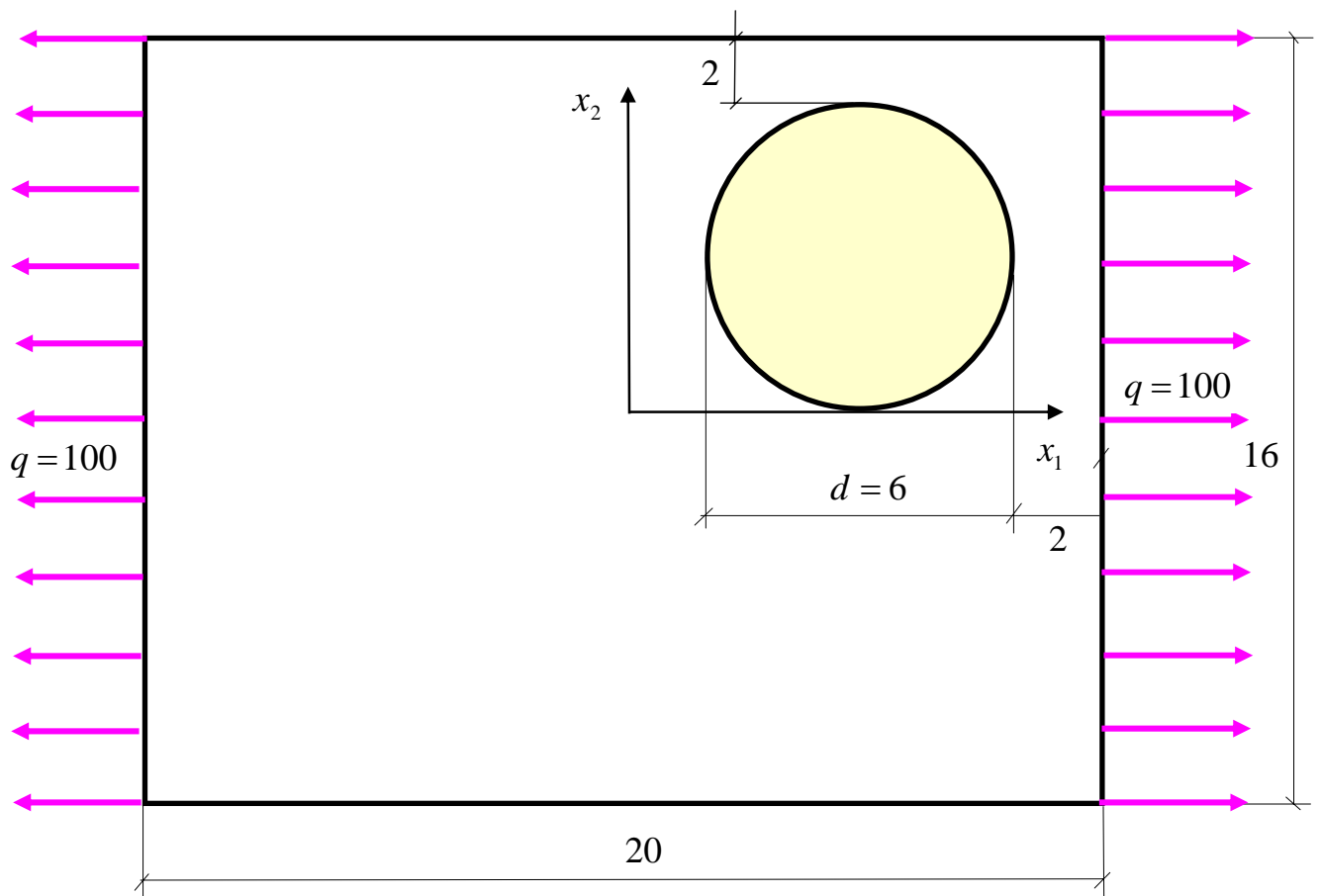


Figure 1.8.1

The distributions of the normal stress and the normal displacement on the section $S = \{-a \leq x_1 \leq a, x_2 = t\}$ have been shown in Figures 1.8.2 and 1.8.3 for the case $a = 10, b = 8, c = 3, s = 5, t = 3$.

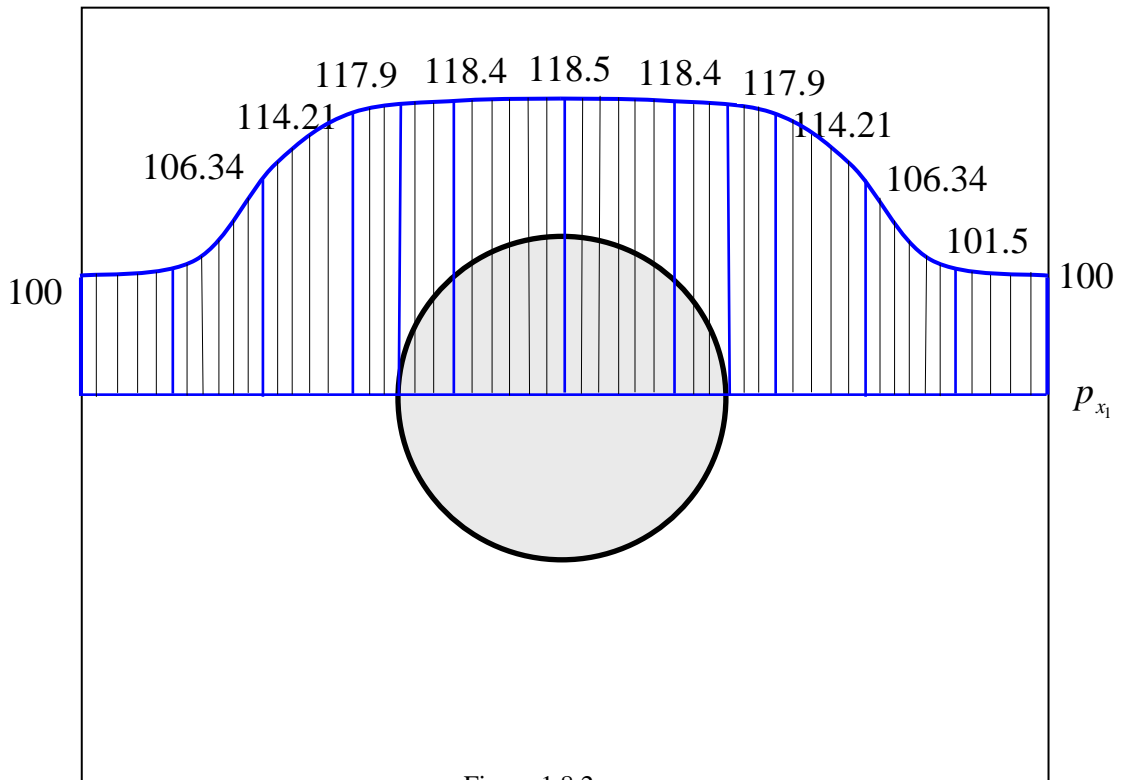
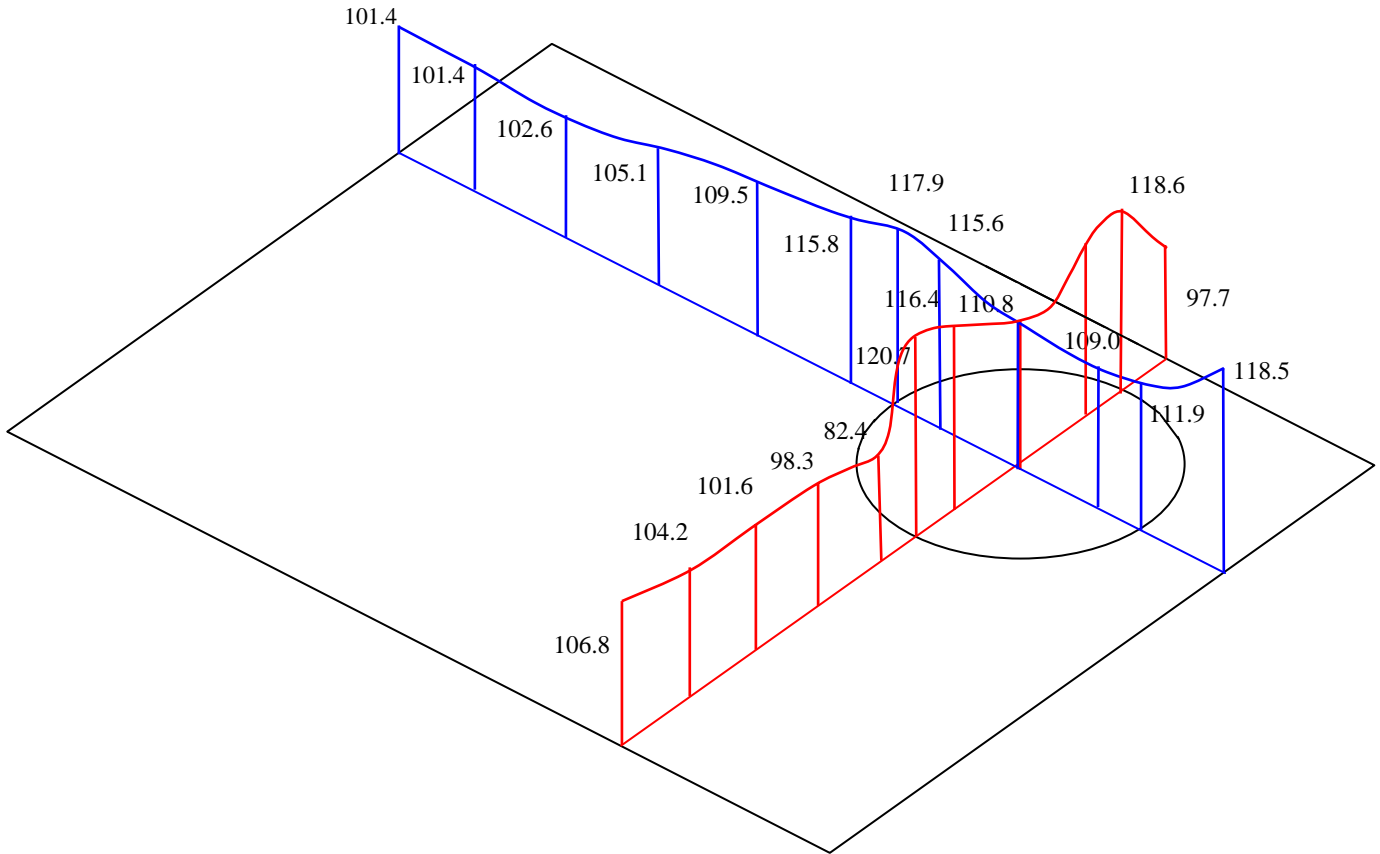


Figure 1.8.2.
Normal stress

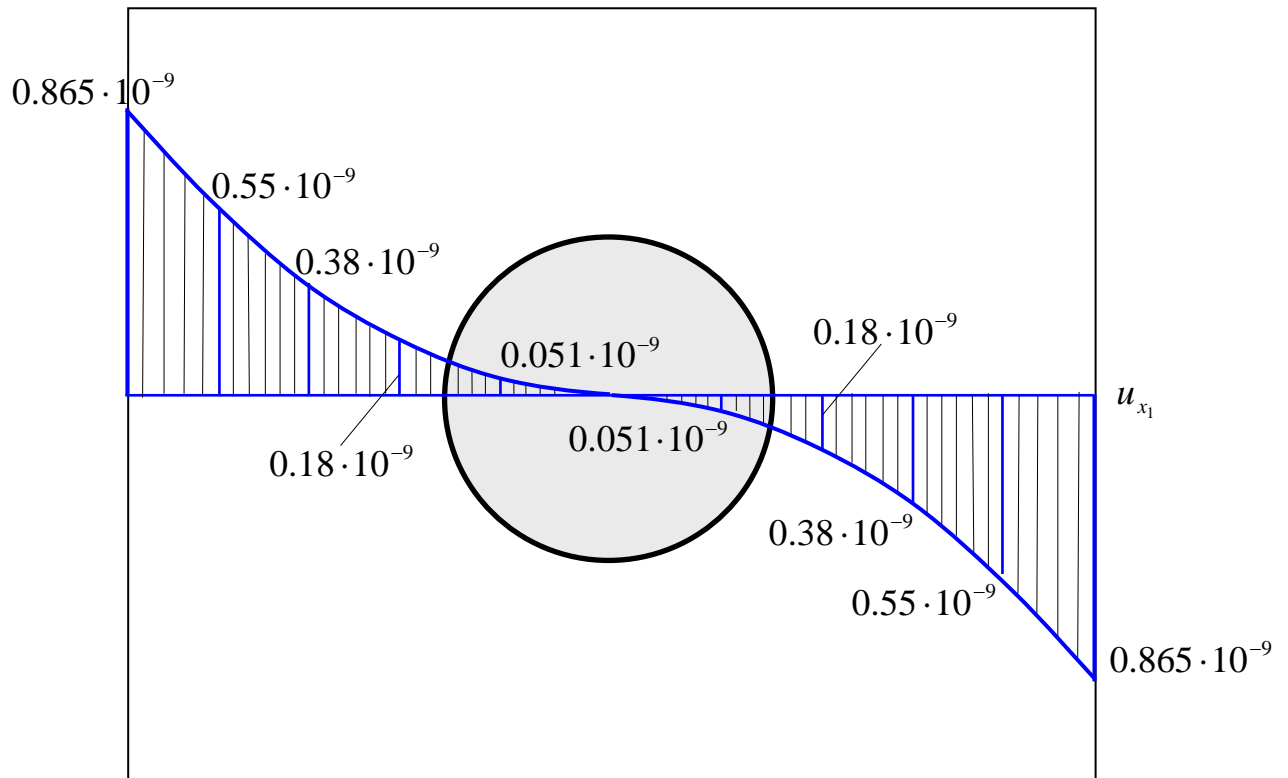


Figure 1.8.3. Normal displacement.

1.9 Computer codes

The initial data for the program is the text file "date_Include.txt"; the results file is the text file "result.txt".

```

!-----
!
! PROGRAM BEM_INCLUD_V3
!-----
!
! THIS PROGRAM SOLVES TWO-DIMENSIONAL ELASTIC PROBLEMS FOR THE DOMAIN WITH INCLUSION USING BOUNDARY
ELEMENTS
!
! (USING BOUNDARY INTEGRAL EQUATIONS METHOD)
!
! CHARACTER*20 FILEIN,FILEOUT
!
! COMMON/MATU/ U(1000,1000)
! COMMON/MATW/ W(1000,1000)
! COMMON N,L,NC(5),M,GE,XNU,INP,IPR,GE1,XNU1
! DIMENSION X(501),Y(501),XM(500),YM(500),FI(1000),DFI(1000)
! DIMENSION CODE(1000),CX(500),CY(500),SSOL(1000),DSOL(1000)
!
! NX - MAXIMUN DIMENSION OF THE SYSTEM OF EQUATIONS (NX)
!
! NX=1000
!
! ASSIGN NUMBERS FOR INPUT AND OUTPUT FILES
!
! INP=7
! IPR=8

```

```

!
! READ DATES FROM FILE "date_Include.txt" AND WRITES REZULTS IN FILE result.txt
! (IN COMMON FOLDER, WHERE IS PROGRAM)
!
      OPEN(INP,FILE='date_Include.txt')
      OPEN(IPR,FILE='result.txt')
!
! READ DATA
!
      CALL INPUTEC(CX,CY,X,Y,CODE,FI)
!
! COMPUTE W AND U MATRICES AND FORM SYSTEM
!
      CALL UWMATEC(X,Y,XM,YM,U,W,FI,DFI,CODE,NX)
!
! SOLVE SLAE
!
      NN=2*N
      CALL SLNPD(U,DFI,D,NN,NX)
!
! COMPUTE STRESS AND DISPLACEMENT AT INTERNAL POINTS
!
      CALL INTEREC(FI,DFI,CODE,CX,CY,X,Y,SSOL,DSOL)
!
! PRINT RESULTS
!
      CALL OUTPTEC(XM,YM,FI,DFI,CX,CY,SSOL,DSOL)
!
      CLOSE (INP)
      CLOSE (IPR)
!
      STOP
      END PROGRAM BEM_INCLUD_V3
!
!-----
      SUBROUTINE INPUTEC(CX,CY,X,Y,CODE,FI)
!-----
!
      CHARACTER*80 TITLE
      DIMENSION CX(1),CY(1),X(1),Y(1),CODE(1),FI(1)
      COMMON N,L,NC(5),M,GE,XNU,INP,IPR,GE1,XNU1
!
! N - NUMBER OF HALF BOUNDARY NODES (= NUMBER OF ELEMENTS)
! L - NUMBER OF INTERNAL POINTS WHERE DISPLACEMENT AND STRESS
!     ARE CALCULATED
! M - NUMBER OF DIFFERENT BOUNDARIES
! NC(I) - LAST NODE OF BOUNDARY I
! GE - DOMAIN SHEAR MODULUS
! XNU - DOMAIN POISSON MODULUS
! GE1 - INCLUDE SHEAR MODULUS
! XNU1 - INCLUDE POISSON MODULUS
!
      WRITE(IPR,20)
      20 FORMAT(' ',3('BEM_INCLUDE V.2 '))
!
! READ-WRITE TITLE
!
      READ(INP,'(A)') TITLE
      WRITE(IPR,'(A)') TITLE
!
! READ NUMBER OF NODES, INTERNAL POINTS AND DIFFERENT BOUNDARIES;
! READ LAST NODES OF THESE BOUNDARIES AND MATERIAL PROPERTIES
!
      READ(INP,*)N,L,M,(NC(K),K=1,5),GE,XNU,GE1,XNU1
      WRITE(IPR,300)N,L,GE,XNU,GE1,XNU1
      300 FORMAT(/' DATA'//2X,'NUMBER OF BOUNDARY ELEMENTS =',I3/2X,
      1 'NUMBER OF INTERNAL POINTS =',I3/2X,

```

```

2  'DOMAIN SHEAR MODULUS   =',E14.7/2X,
3  'DOMAIN POISSON RATIO  =',E14.7/2X,
4  'INCLUDE SHEAR MODULUS  =',E14.7/2X,
5  'INCLUDE POISSON RATIO  =',E14.7/2X)
  IF(M)40,40,30
30  WRITE(IPR,999)M,(NC(K),K=1,M)
999  FORMAT(2X,'NUMBER OF DIFFERENT BOUNDARIES=',I3/2X, 'LAST NODES OF THESE BOUNDARIES =',5(2X,I3))
!
! READ COORDINATES OF EXTREME POINTS OF THE BOUNDARY
! ELEMENTS IN ARRAYS X AND Y
!
40  WRITE(IPR,500)
500  FORMAT(/2X,'COORDINATES OF THE EXTREME POINTS OF,' THE BOUNDARY ELEMENTS OF
DOMAIN'//4X,'POINT',10X,'X',18X,'Y')
  READ(INP,*) (X(I),Y(I),I=1,N)
  DO I=1,N/2
    WRITE(IPR,700)I,X(I),Y(I)
  END DO
700  FORMAT(5X,I3,2(5X,E14.7))
!
  WRITE(IPR,501)
501  FORMAT(/2X,'COORDINATES OF THE EXTREME POINTS OF,' THE BOUNDARY ELEMENTS OF
INCLUDE'//4X,'POINT',10X,'X',18X,'Y')
  DO I=N/2+1,N
    WRITE(IPR,701)I,X(I),Y(I)
  END DO
701  FORMAT(5X,I3,2(5X,E14.7))
!
! READ BOUNDARY CONDITIONS IN FI(I) VECTOR, IF CODE(I)=0 THE FI(I)
! VALUE IS A KNOWN DISPLACEMENT; IF CODE(I)=1 THE FI(I) VALUE IS A
! KNOWN TRACTION.
!
  WRITE(IPR,800)
800  FORMAT(/2X,'BOUNDARY CONDITIONS'//15X,'PRESCRIBED VALUE',15X,
1  'PRESCRIBED VALUE'/5X,'NODE',9X,'X DIRECTION',8X,'CODE',8X,'Y DIRECTION',8X,'CODE')
  DO I=1,N
    READ(INP,*) CODE(2*I-1),FI(2*I-1),CODE(2*I),FI(2*I)
    WRITE(IPR,950)I,FI(2*I-1),CODE(2*I-1),FI(2*I),CODE(2*I)
  END DO
950  FORMAT(5X,I3,8X,E14.7,8X,I1,8X,E14.7,8X,I1)
!
! READ COORDINATES OF THE INTERNAL POINTS
!
  IF(L.EQ.0) GO TO 50
  READ(INP,*) (CX(I),CY(I),I=1,L)
50  RETURN
  END SUBROUTINE INPUTEC
!
!-----
!
SUBROUTINE UWMATEC(X,Y,XM,YM,U,W,FI,DFI,CODE,NX)
!-----
!
! THIS SUBROUTINE COMPUTES THE U AND W MATRICES AND
! FORMS THE SYSTEM OF EQUATIONS A X = F
!
  DIMENSION U(NX,NX),W(NX,NX)
  DIMENSION X(1),Y(1),XM(1),YM(1),FI(1)
  DIMENSION CODE(1),DFI(1)
  COMMON N,L,NC(5),M,GE,XNU,INP,IPR,GE1,XNU1
!
! COMPUTE THE NODAL COORDINATES AND STORE IN ARRAYS XM AND YM
!
  DO I=1,N/2-1
    XM(I)=(X(I)+X(I+1))/2
10  YM(I)=(Y(I)+Y(I+1))/2

```

```

END DO
XM(N/2)=(X(1)+X(N/2))/2
YM(N/2)=(Y(1)+Y(N/2))/2
!
DO I=N/2+1,N-1
  XM(I)=(X(I)+X(I+1))/2
  YM(I)=(Y(I)+Y(I+1))/2
END DO
XM(N)=(X(N/2+1)+X(N))/2
YM(N)=(Y(N/2+1)+Y(N))/2
!
! PRINT XM AND YM IN FILE "result"
!
  WRITE(IPR,501)
501 FORMAT(/2X,'COORDINATES CENTERS OF BOUNDARY ELEMENT ',(NODES IN ARRAYS XM AND
YM)//4X,'POINT',10X,'XM',18X,'YM')
  DO I=1,N
    WRITE(IPR,701)I,XM(I),YM(I)
  END DO
701 FORMAT(5X,I3,2(5X,E14.7))
!
! CALCULATE COORDINATS INTERNAL NODES
!
  IF(M-1)15,15,12
12 XM(NC(1))=(X(NC(1))+X(1))/2
  YM(NC(1))=(Y(NC(1))+Y(1))/2
  DO K=2,M
    XM(NC(K))=(X(NC(K))+X(NC(K-1)+1))/2
    YM(NC(K))=(Y(NC(K))+Y(NC(K-1)+1))/2
  END DO
!
! COMPUTE THE COEFFICIENTS OF U AND W MATRICES
!
15 DO 30 I=1,N
  DO 30 J=1,N
    IF(M-1)16,16,17
17 IF(J-NC(1))19,18,19
18 KK=1
  GO TO 23
19 DO 22 K=2,M
    IF(J-NC(K))22,21,22
21 KK=NC(K-1)+1
  GO TO 23
22 CONTINUE
16 KK=J+1
23 IF(I-J)20,25,20
!
!
20 CALL EXTINEC(XM(I),YM(I),X(J),Y(J),X(KK),Y(KK),
1 W((2*I-1),(2*J-1)),W((2*I-1),(2*J)),
2 W((2*I),(2*J-1)),W((2*I),(2*J)),
3 U((2*I-1),(2*J-1)),U((2*I-1),(2*J)),
4 U((2*I),(2*J)))
!
  U((2*I),(2*J-1))=U((2*I-1),(2*J))
  GO TO 26
25 CALL LOCINEC(X(J),Y(J),X(KK),Y(KK),U((2*I-1),(2*J-1)),U((2*I-1),(2*J)),U((2*I),(2*J)))
!
! DIAGONAL
  IF (1<=I<=N/2) THEN
    IF (1<=J<=N/2) THEN
      W(I,J)=0.5
    END IF
  END IF
!
  IF (N/2+1<=I<=2*N/2) THEN
    IF (N/2+1<=J<=2*N/2) THEN
      W(I,J)=0.5
    END IF

```

```

END IF
!
IF (2*N/2+1<=I<=3*N/2) THEN
  IF (2*N/2+1<=J<=3*N/2) THEN
    W(I,J)=0.5
  END IF
END IF
!
IF (3*N/2+1<=I<=4*N/2) THEN
  IF (3*N/2+1<=J<=4*N/2) THEN
    W(I,J)=0.5
  END IF
END IF
!
! ETS DIAGONAL
!
IF (1<=I<=N/2) THEN
  IF (N/2+1<=J<=2*N/2) THEN
    IF (I==J-N/2) THEN
      W(I,J)=0.
    END IF
  END IF
END IF
!
IF (1<=J<=N/2) THEN
  IF (N/2+1<=I<=2*N/2) THEN
    IF (I==J-N/2) THEN
      W(I,J)=0.
    END IF
  END IF
END IF
!
IF (2*N/2+1<=I<=3*N/2) THEN
  IF (3*N/2+1<=J<=4*N/2) THEN
    IF (I==J-N/2) THEN
      W(I,J)=0.
    END IF
  END IF
END IF
!
IF (3*N/2+1<=I<=4*N/2) THEN
  IF (2*N/2+1<=J<=3*N/2) THEN
    IF (J==I-N/2) THEN
      W(I,J)=0.
    END IF
  END IF
END IF
!
U((2*I),(2*J-1))=U((2*I-1),(2*J))
!
26 CONTINUE

30 CONTINUE
!
! REORDER THE COLUMNS OF THE SYSTEM OF EQUATIONS IN ACCORDANCE
! WITH THE BOUNDARY CONDITIONS AND FORM SYSTEM MATRIX A WHICH
! IS STORED IN U
!
NN=2*N
!


---


IF (N/2+1<=I<=N) THEN
  IF (J<=N/2) THEN
    U(I,J)=0
    W(I,J)=0
  END IF
END IF
!
IF (N/2+1<=I<=N) THEN

```

```

      IF (N+1<=J<=N+N/2) THEN
        U(I,J)=0
        W(I,J)=0
      END IF
    END IF
  !
  IF (N/2+N+1<=I<=2*N) THEN
    IF (J<=N/2) THEN
      U(I,J)=0
      W(I,J)=0
    END IF
  END IF
  !
  IF (N/2+N+1<=I<=2*N) THEN
    IF (N+1<=J<=N+N/2) THEN
      U(I,J)=0
      W(I,J)=0
    END IF
  END IF
  !
  IF (N/2+1<=I<=N) THEN
    IF (N/2+1<=J<=N) THEN
      U(I,J)=-U(I,J)
      W(I,J)=-W(I,J)
    END IF
  END IF
  !
  IF (N/2+1<=I<=N) THEN
    IF (N+N/2+1<=J<=2*N) THEN
      U(I,J)=-U(I,J)
      W(I,J)=-W(I,J)
    END IF
  END IF
  !
  IF (N+N/2+1<=I<=2*N) THEN
    IF (N/2+1<=J<=N) THEN
      U(I,J)=-U(I,J)
      W(I,J)=-W(I,J)
    END IF
  END IF
  !
  IF (N+N/2+1<=I<=2*N) THEN
    IF (N+N/2+1<=J<=2*N) THEN
      U(I,J)=-U(I,J)
      W(I,J)=-W(I,J)
    END IF
  END IF
  !
  !-----
  !
  !
  DO 50 J=1,NN
    IF(CODE(J))43,43,40
40  DO 42 I=1,NN
      CH=U(I,J)
      U(I,J)=-W(I,J)
42  W(I,J)=-CH
      GO TO 50
43  DO 45 I=1,NN
      IF (I<=N) THEN
        U(I,J)=U(I,J)*GE
      END IF
      IF (I>N) THEN
        U(I,J)=U(I,J)*GE1
45  END IF
50 CONTINUE
  !
  ! FORM THE RIGHT HAND SIDE VECTOR F WHICH IS STORED IN DFI
  !
  DO 60 I=1,NN

```

```

      DFI(I)=0.
      DO 60 J=1,NN
        DFI(I)=DFI(I)+W(I,J)*FI(J)
60 CONTINUE
      RETURN
      END SUBROUTINE UWMATEC
!
!-----
      SUBROUTINE EXTINEC(XP,YP,X1,Y1,X2,Y2,H11,H12,
1          H21,H22,G11,G12,G22)
!
!
! THIS SOUBROUTINE COMPUTES THE U AND W MATRICES
! COEFFICIENTS THAT RELATE A COLLOCATION POINT WITH A DIFFERENT
! ELEMENT USING GAUSS QUADRATURE
!
! DIST= DISTANCE FROM THE COLOCATION POINT TO THE
! LINE TANGENT TO THE ELEMENT
! RA= DISTANCE FROM THE COLOCATION POINT TO THE
! GAUSS INTEGRATION POINT AT THE BOUNDARY ELEMENT
!
      DIMENSION XCO(4),YCO(4),GI(4),OME(4)
      COMMON N,L,NC(5),M,GE,XNU,INP,IPR,GE1,XNU1
      DATA GI/0.86113631,-0.86113631,0.33998104,-0.33998104/
      DATA OME/0.34785485,0.34785485,0.65214515,0.65214515/
!
      IF (I<=N/2) THEN
        IF (J<=N/2) THEN
          NU=XNU
          MU=GE
        END IF
      END IF
!
      IF (I<=N/2) THEN
        IF (J>N/2) THEN
          NU=XNU
          MU=GE
        END IF
      END IF
!
      IF (I>N/2) THEN
        IF (J<=N/2) THEN
          NU=XNU1
          MU=GE1
        END IF
      END IF
!
      IF (I>N/2) THEN
        IF (J>N/2) THEN
          NU=XNU1
          MU=GE1
        END IF
      END IF
!
      AX=(X2-X1)/2
      BX=(X2+X1)/2
      AY=(Y2-Y1)/2
      BY=(Y2+Y1)/2
!   ETA1=(Y2-Y1)/(2*SQRT(AX**2+AY**2))
!   ETA2=(X1-X2)/(2*SQRT(AX**2+AY**2))
      IF (I<=N/2) THEN
        IF (J<=N/2) THEN
          ETA1=(Y2-Y1)/(2*SQRT(AX**2+AY**2))
          ETA2=(X1-X2)/(2*SQRT(AX**2+AY**2))
        END IF
      END IF
!
      IF (I<=N/2) THEN
        IF (J>N/2) THEN

```

```

      ETA1=(Y2-Y1)/(2*SQRT(AX**2+AY**2))
      ETA2=(X1-X2)/(2*SQRT(AX**2+AY**2))
    END IF
  END IF
!
  IF (I>N/2) THEN
    IF (J<=N/2) THEN
      ETA1=-(Y2-Y1)/(2*SQRT(AX**2+AY**2))
      ETA2=-(X1-X2)/(2*SQRT(AX**2+AY**2))
    END IF
  END IF
!
  IF (I>N/2) THEN
    IF (J>N/2) THEN
      ETA1=-(Y2-Y1)/(2*SQRT(AX**2+AY**2))
      ETA2=-(X1-X2)/(2*SQRT(AX**2+AY**2))
    END IF
  END IF
!
! COMPUTE THE DISTANCE FROM THE POINT TO THE LINE OF THE ELEMENT
!
  IF(AX)10,20,10
10  TA=AY/AX
    DIST=ABS((TA*XP-YP+Y1-TA*X1)/SQRT(TA**2+1))
    GO TO 30
20  DIST=ABS(XP-X1)
!
! DETERMINE THE DIRECTION OF THE OUTWARD NORMAL
!
30  SIG=(X1-XP)*(Y2-YP)-(X2-XP)*(Y1-YP)
    IF(SIG)31,32,32
31  DIST=-DIST
32  H11=0.
    H12=0.
    H21=0.
    H22=0.
    G11=0.
    G12=0.
    G22=0.
!
! COMPUTE U AND W COEFFICIENTS
!
  DE=4*3.141592*(1-NU)
  DO 40 I=1,4
    XCO(I)=AX*GI(I)+BX
    YCO(I)=AY*GI(I)+BY
    RA=SQRT((XP-XCO(I))**2+(YP-YCO(I))**2)
    RD1=(XCO(I)-XP)/RA
    RD2=(YCO(I)-YP)/RA
    G11=G11+((3-4*NU)*ALOG(1./RA)+RD1**2)*OME(I)*SQRT(AX**2+AY**2)/(2*DE*MU)
!
  WRITE(IPR,332)G11
! 332  FORMAT('G11=',E14.7/2X)

  G12=G12+RD1*RD2*OME(I)*SQRT(AX**2+AY**2)/(2*DE*MU)
  G22=G22+((3-4*NU)*ALOG(1./RA)+RD2**2)*OME(I)*SQRT(AX**2+AY**2)/(2*DE*MU)
  H11=H11-DIST*((1-2*NU)+2*RD1**2)/(RA**2*DE)*OME(I)*SQRT(AX**2+AY**2)
  H12=H12-(DIST*2*RD1*RD2/RA+(1-2*NU)*(ETA1*RD2-ETA2*RD1))*OME(I)*SQRT(AX**2+AY**2)/(RA*DE)
  H21=H21-(DIST*2*RD1*RD2/RA+(1-2*NU)*(ETA2*RD1-ETA1*RD2))*OME(I)*SQRT(AX**2+AY**2)/(RA*DE)
40  H22=H22-DIST*((1-2*NU)+2*RD2**2)*OME(I)*SQRT(AX**2+AY**2)/(RA**2*DE)
  RETURN
END SUBROUTINE EXTINEC
!
!
!
!-----
SUBROUTINE LOCINEC(X1,Y1,X2,Y2,G11,G12,G22)
!
!
!

```

! THIS SUBROUTINE COMPUTES THE VALUES OF THE MATRIX U COEFFICIENTS
! THAT RELATE AN ELEMENT WITH ITSELF

```
!
COMMON N,L,NC(5),M,GE,XNU,INP,IPR,GE1,XNU1
!
IF (I<=N/2) THEN
  IF (J<=N/2) THEN
    NU=XNU
    MU=GE
  END IF
END IF
!
IF (I<=N/2) THEN
  IF (J>N/2) THEN
    NU=XNU
    MU=GE
  END IF
END IF
!
IF (I>N/2) THEN
  IF (J<=N/2) THEN
    NU=XNU1
    MU=GE1
  END IF
END IF
!
IF (I>N/2) THEN
  IF (J>N/2) THEN
    NU=XNU1
    MU=GE1
  END IF
END IF
!
AX=(X2-X1)/2
AY=(Y2-Y1)/2
SR=SQRT(AX**2+AY**2)
DE=4*3.141592*MU*(1-NU)
G11=SR*((3-4*NU)*(1-ALOG(SR))+(X2-X1)**2/(4*SR**2))/DE
G22=SR*((3-4*NU)*(1-ALOG(SR))+(Y2-Y1)**2/(4*SR**2))/DE
G12=(X2-X1)*(Y2-Y1)/(4*SR*DE)
RETURN
END SUBROUTINE LOCINEC
!
```

SUBROUTINE SLNPD(A,B,D,N,NX)

! SOLUTION OF LINEAR SYSTEMS OF EQUATIONS
! BY THE GAUSS ELIMINATION METHOD PROVIDING
! FOR INTERCHANGING ROWS WHEN ENCOUNTERING A
! ZERO DIAGONAL COEFFICIENT

! A : SYSTEM MATRIX
! B : ORIGINALLY IT CONTAINS THE INDEPENDENT
! COEFFICIENTS. AFTER SOLUTION IT CONTAINS
! THE VALUES OF THE SYSTEM UNKNOWNNS.

! N : ACTUAL NUMBER OF UNKNOWNNS
! NX: ROW AND COLUMN DIMENSION OF A

```
!
COMMON NMUDO,LMUDO,NCMUDO(5),MMUDO,INP,IPR
DIMENSION B(NX),A(NX,NX)
```

```
!
TOL=1.E-5
```

```
!
N1=N-1
```

```
DO 100 K=1,N1
  K1=K+1
```

```

C=A(K,K)
IF(ABS(C)-TOL)1,1,3
1   DO 7 J=K1,N
!
! TRY TO INTERCHANGE ROWS TO GET NON ZERO DIAGONAL COEFFICIENT
!
      IF(ABS((A(J,K)))-TOL)7,7,5
5     DO 6 L=K,N
        C=A(K,L)
        A(K,L)=A(J,L)
6     A(J,L)=C
        C=B(K)
        B(K)=B(J)
        B(J)=C
        C=A(K,K)
        GO TO 3
7     CONTINUE
      GO TO 8
!
! DIVIDE ROW BY DIAGONAL COEFFICIENT
!
3     C=A(K,K)
      DO 4 J=K1,N
4     A(K,J)=A(K,J)/C
      B(K)=B(K)/C
!
! ELIMINATE UNKNOWN X(K) FROM ROW I
!
      DO 10 I=K1,N
        C=A(I,K)
        DO 9 J=K1,N
9     A(I,J)=A(I,J)-C*A(K,J)
10    B(I)=B(I)-C*B(K)
100  CONTINUE
!
! COMPUTE LAST UNKNOWN
!
      IF(ABS((A(N,N)))-TOL)8,8,101
101  B(N)=B(N)/A(N,N)
!
! APPLY BACKSUBSTITUTION PROCESS TO COMPUTE REMAINING UNKNOWNNS
!
      DO 200 L=1,N1
        K=N-L
        K1=K+1
        DO 200 J=K1,N
200  B(K)=B(K)-A(K,J)*B(J)
!
! COMPUTE VALUE OF DETERMINANT
!
      D=1.
      DO 250 I=1,N
250  D=D*A(I,I)
      GO TO 300
8    WRITE(IPR,2) K
2    FORMAT(' **** SINGULARITY IN ROW',I5)
      D=0.
300  RETURN
      END SUBROUTINE SLNPD
!
!
!
!-----
SUBROUTINE INTEREC(FI,DFI,CODE,CX,CY,X,Y,SSOL,DSOL)
!
! THIS SUBROUTINE COMPUTES THE VALUES OF THE STRESS AND DISPLACEMENT
! COMPONENTS AT INTERNAL POINTS

```

```

!
! DIMENSION CX(1),CY(1),SSOL(1),DSOL(1)
! DIMENSION FI(1),DFI(1),CODE(1),X(1),Y(1)
! COMMON N,L,NC(5),M,GE,XNU,INP,IPR,GE1,XNU1
!
! REARRANGE FI AND DFI ARRAYS TO STORE ALL THE VALUES
! OF THE DISPLACEMENT IN FI AND ALL THE VALUES OF THE TRACTIONS IN DFI
!
! NN=2*N
! DO 20 I=1,NN
!
! IF (I<=20) THEN
!   IF (J<=20) THEN
!     NU=XNU
!     MU=GE
!   END IF
! END IF
!
! IF (I<=20) THEN
!   IF (J>20) THEN
!     NU=XNU
!     MU=GE
!   END IF
! END IF
!
! IF (I>20) THEN
!   IF (J<=20) THEN
!     NU=XNU1
!     MU=GE1
!   END IF
! END IF
!
! IF (I>20) THEN
!   IF (J>20) THEN
!     NU=XNU1
!     MU=GE1
!   END IF
! END IF
!
! IF(CODE(I)) 15,15,10
10   CH=FI(I)
!     FI(I)=DFI(I)
!     DFI(I)=CH
!     GO TO 20
15   DFI(I)=DFI(I)*MU
20 CONTINUE
!
! COMPUTE THEIR VALUES OF STRESSES AND DISPLACEMENTS AT INTERNAL POINTS.
!
! IF(L.EQ.0) GO TO 50
! DO 40 K=1,L
!   DSOL(2*K-1)=0.
!   DSOL(2*K)=0.
!   SSOL(3*K-2)=0.
!   SSOL(3*K-1)=0.
!   SSOL(3*K)=0.
!   DO 30 J=1,N
!     IF(M-1)28,28,22
22   IF(J-NC(1))24,23,24
23   KK=1
!     GO TO 29
24   DO 26 LK=2,M
!     IF(J-NC(LK))26,25,26
25   KK=NC(LK-1)+1
!     GO TO 29
26   CONTINUE
28   KK=J+1
29   CALL EXTINEC(CX(K),CY(K),X(J),Y(J),X(KK),Y(KK),H11,H12, H21,H22,G11,G12,G22)
!     DSOL(2*K-1)=DSOL(2*K-1)+DFI(2*J-1)*G11+DFI(2*J)*G12-FI(2*J-1)*H11-FI(2*J)*H12

```

```

DSOL(2*K)=DSOL(2*K)+DFI(2*J-1)*G12+DFI(2*J)*G22-FI(2*J-1)*H21-FI(2*J)*H22
CALL SIGMAEC(CX(K),CY(K),X(J),Y(J),X(KK),Y(KK),D111,D211,D112,D212,D122,D222,S111,S211,S112,S212,S122,S222)
SSOL(3*K-2)=SSOL(3*K-2)+DFI(2*J-1)*D111+DFI(2*J)*D211-FI(2*J-1)*S111-FI(2*J)*S211
SSOL(3*K-1)=SSOL(3*K-1)+DFI(2*J-1)*D112+DFI(2*J)*D212-FI(2*J-1)*S112-FI(2*J)*S212
30  SSOL(3*K)=SSOL(3*K)+DFI(2*J-1)*D122+DFI(2*J)*D222-FI(2*J-1)*S122-FI(2*J)*S222
40  CONTINUE
50  RETURN
    END SUBROUTINE INTEREC
!
!
!
!-----
SUBROUTINE SIGMAEC(XP,YP,X1,Y1,X2,Y2,D111,D211,D112,D212,D122, D222,S111,S211,S112,S212,S122,S222)
!
! THIS SUBROUTINE COMPUTES THE VALUES OF THE S AND D MATRICES
! USING GAUSS QUADRATURE IN ORDER TO COMPUTE THE STRESSES
! AT ANY INTERNAL POINT
!
! RA= DISTANCE FROM THE POINT TO THE GAUSS INTEGRATION POINTS
!   ON THE BOUNDARY ELEMENTS
! DIST= DISTANCE FROM THE POINT TO THE LINE TANGENT
!   TO THE ELEMENT
! RD1,RD2= DERIVATIVES OF RA
! ETA1,ETA2= COMPONENTS OF THE UNIT NORMAL TO THE ELEMENT
!
  DIMENSION XCO(4),YCO(4),GI(4),OME(4)
  COMMON N,L,NC(5),M,GE,XNU,INP,IPR,GE1,XNU1
  DATA GI/0.86113631,-0.86113631,0.33998104,-0.33998104/
  DATA OME/0.34785485,0.34785485,0.65214515,0.65214515/
!
  AX=(X2-X1)/2
  BX=(X2+X1)/2
  AY=(Y2-Y1)/2
  BY=(Y2+Y1)/2
!
  IF (I<=N/2) THEN
    IF (J<=N/2) THEN
      ETA1=(Y2-Y1)/(2*SQRT(AX**2+AY**2))
      ETA2=(X1-X2)/(2*SQRT(AX**2+AY**2))
    END IF
  END IF
!
  IF (I<=N/2) THEN
    IF (J>N/2) THEN
      ETA1=(Y2-Y1)/(2*SQRT(AX**2+AY**2))
      ETA2=(X1-X2)/(2*SQRT(AX**2+AY**2))
    END IF
  END IF
!
  IF (I>N/2) THEN
    IF (J<=N/2) THEN
      ETA1=-(Y2-Y1)/(2*SQRT(AX**2+AY**2))
      ETA2=-(X1-X2)/(2*SQRT(AX**2+AY**2))
    END IF
  END IF
!
  IF (I>N/2) THEN
    IF (J>N/2) THEN
      ETA1=-(Y2-Y1)/(2*SQRT(AX**2+AY**2))
      ETA2=-(X1-X2)/(2*SQRT(AX**2+AY**2))
    END IF
  END IF
!
  IF (I<=N/2) THEN
    IF (J<=N/2) THEN
      NU=XNU
      MU=GE

```

```

        END IF
    END IF
!
    IF (I<=N/2) THEN
        IF (J>N/2) THEN
            NU=XNU
            MU=GE
        END IF
    END IF
!
    IF (I>N/2) THEN
        IF (J<=N/2) THEN
            NU=XNU1
            MU=GE1
        END IF
    END IF
!
    IF (I>N/2) THEN
        IF (J>N/2) THEN
            NU=XNU1
            MU=GE1
        END IF
    END IF
!
! COMPUTE THE DISTANCE FROM THE POINT TO THE LINE OF THE ELEMENT
!
    IF(AX)10,20,10
10  TA=AY/AX
    DIST=ABS((TA*XP-YP+Y1-TA*X1)/SQRT(TA**2+1))
    GO TO 30
20  DIST=ABS(XP-X1)
!
! DETERMINE THE DIRECTION OF THE OUTWARD NORMAL
!
30  SIG=(X1-XP)*(Y2-YP)-(X2-XP)*(Y1-YP)
    IF(SIG)31,32,32
31  DIST=-DIST
32  D111=0.
    D211=0.
    D112=0.
    D212=0.
    D122=0.
    D222=0.
    S111=0.
    S211=0.
    S112=0.
    S212=0.
    S122=0.
    S222=0.
!
! COMPUTE D AND S COEFFICIENTS
!
    FA=1-4*NU
    AL=1-2*NU
    DE=4*3.141592*(1-NU)
    DO 40 I=1,4
        XCO(I)=AX*GI(I)+BX
        YCO(I)=AY*GI(I)+BY
        RA=SQRT((XP-XCO(I))**2+(YP-YCO(I))**2)
        RD1=(XCO(I)-XP)/RA
        RD2=(YCO(I)-YP)/RA
        D111=D111+(AL*RD1+2*RD1**3)*OME(I)*SQRT(AX**2+AY**2)/(DE*RA)
        D211=D211+(2*RD1**2*RD2-AL*RD2)*OME(I)*SQRT(AX**2+AY**2)/(DE*RA)
        D112=D112+(AL*RD2+2*RD1**2*RD2)/(DE*RA)*OME(I)*SQRT(AX**2+AY**2)
        D212=D212+(AL*RD1+2*RD1*RD2**2)/(DE*RA)*OME(I)*SQRT(AX**2+AY**2)
        D122=D122+(2*RD1*RD2**2-AL*RD1)/(DE*RA)*OME(I)*SQRT(AX**2+AY**2)
        D222=D222+(AL*RD2+2*RD2**3)/(DE*RA)*OME(I)*SQRT(AX**2+AY**2)
        S111=S111+(2*DIST/RA*(AL*RD1+NU*2*RD1-4*RD1**3)+4*NU*ETA1*
1      RD1**2+AL*(2*ETA1*RD1**2+2*ETA1)-FA*ETA1)*2*MU/(DE*RA**2)*OME(I)*SQRT(AX**2+AY**2)

```

```

S211=S211+(2*DIST/RA*(AL*RD2-4*RD1**2*RD2)+4*NU*ETA1*RD1*RD2+
1 AL*2*ETA2*RD1**2-FA*ETA2)*2*MU/(DE*RA**2)*OME(I)*SQRT(AX**2+AY**2)
S112=S112+(2*DIST/RA*(NU*RD2-4*RD1**2*RD2)+2*NU*(ETA1*RD2*RD1+
1 ETA2*RD1**2)+AL*(2*ETA1*RD1*RD2+ETA2))*2*MU/(DE*RA**2)*OME(I)*SQRT(AX**2+AY**2)
S212=S212+(2*DIST/RA*(NU*RD1-4*RD1*RD2**2)+2*NU*(ETA1*RD2**2+
1 ETA2*RD1*RD2)+AL*(2*ETA2*RD1*RD2+ETA1))*2*MU/(DE*RA**2)*OME(I)*SQRT(AX**2+AY**2)
S122=S122+(2*DIST/RA*(AL*RD1-4*RD1*RD2**2)+4*NU*ETA2*RD1*RD2+
1 AL*2*ETA1*RD2**2-FA*ETA1)*2*MU/(DE*RA**2)*OME(I)*SQRT(AX**2+AY**2)
40 S222=S222+(2*DIST/RA*(AL*RD2+2*NU*RD2-4*RD2**3)+4*NU*ETA2*
1 RD2**2+AL*(2*ETA2*RD2**2+2*ETA2)-FA*ETA2)*2*MU/(DE*RA**2)*OME(I)*SQRT(AX**2+AY**2)
RETURN
END SUBROUTINE SIGMAEC
!
!-----
SUBROUTINE OUTPTEC(XM,YM,FI,DFI,CX,CY,SSOL,DSOL)
!
!
! THIS SUBROUTINE PRINTS THE VALUES OF THE DISPLACEMENTS
! AND TRACTIONS AT BOUNDARY NODES. IT ALSO PRINTS THE VALUES
! OF DISPLACEMENTS AND STRESSES AT INTERNAL POINTS
!
DIMENSION XM(1),YM(1),FI(1),DFI(1)
DIMENSION CX(1),CY(1),SSOL(1),DSOL(1)
COMMON N,L,NC(5),M,GE,XNU,INP,IPR,GE1,XNU1
!
WRITE(IPR,100)
100 FORMAT(' ',79('*'))/35X,'RESULTS'/2X,'BOUNDARY NODES'/6X, 'X',12X,'Y',9X,'DISPL. X',5X,'DISPL. Y',4X, 'TRACTION
X',3X,'TRACTION Y'/
DO 10 I=1,N
10 WRITE(IPR,200) XM(I),YM(I),FI(2*I-1),FI(2*I),DFI(2*I-1),DFI(2*I)
200 FORMAT(6(1X,E12.5))
!
IF(L.EQ.0.) GO TO 30
WRITE(IPR,300)
300 FORMAT(/2X,'INTERNAL POINTS DISPLACEMENTS'/8X,'X',15X,'Y',10X, 'DISPLACEMENT X',5X,'DISPLACEMENT Y')
DO 20 K=1,L
20 WRITE(IPR,400)CX(K),CY(K),DSOL(2*K-1),DSOL(2*K)
WRITE(IPR,350)
350 FORMAT(/2X,'INTERNAL POINTS STRESSES'/8X,'X',15X,'Y',12X, 'SIGMA X',10X,'TAU XY',9X,'SIGMA Y')
DO 25 K=1,L
25 WRITE(IPR,450) CX(K),CY(K),SSOL(3*K-2),SSOL(3*K-1),SSOL(3*K)
400 FORMAT(2(2X,E14.7),2(5X,E14.7))
450 FORMAT(5(2X,E14.7))
30 WRITE(IPR,500)
500 FORMAT(' ',79('*'))
RETURN
END SUBROUTINE OUTPTEC

```

2. Solution of the three-dimensional micromechanics problem for the fiber reinforced bounded and unbounded solids. Investigation of effective local and non-local thermo-elastic properties, stress concentration factors, and edge effect

The general statement of the spatial fracture mechanics problem for the bounded solid with inclusions has been considered. The boundary integral equations method was used in order to solve the problem. Several fundamental solutions of the static theory of elasticity have been obtained.

2.1 Theoretical part

The three-dimensional problem with inclusions is considered. Generally the geometry of the problem may be presented in the form shown on Fig. 2.1.1.

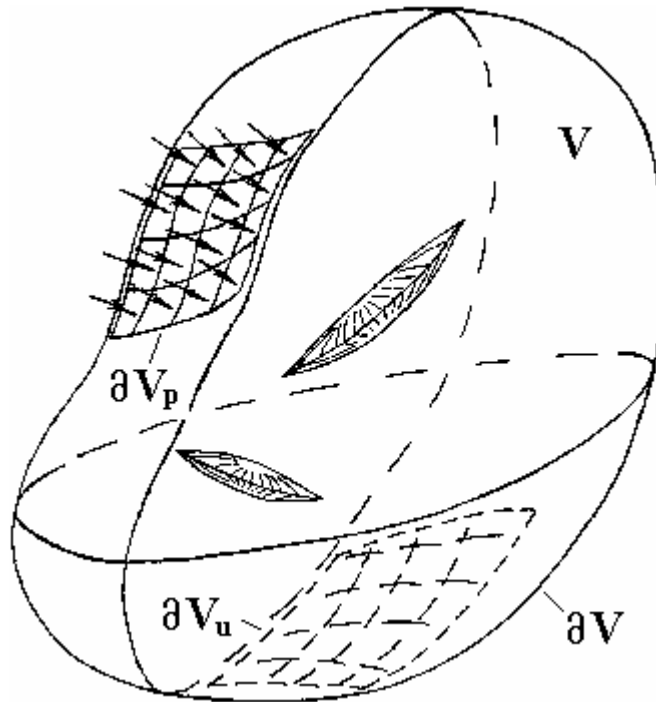


Fig. 2.1.1

The general solution of the 3-D problem can be presented by the integral identities of the Somigliano type for displacements in the form

$$u_i(\mathbf{y}) = \int_{\partial V} \{p_j(\mathbf{x})U_{ij}(\mathbf{x}-\mathbf{y}) - u_j(\mathbf{x})W_{ij}(\mathbf{x},\mathbf{y})\}dS + \int_V b_j(\mathbf{x})U_{ij}(\mathbf{x}-\mathbf{y})dV, \quad i, j = \overline{1,3}. \quad (2.1.1)$$

Notations:

$u_i(\mathbf{y})$ are components of the displacements vector in a point \mathbf{y} in the direction of the axis x_i ;

$p_j(\mathbf{x})$ are components of the traction vector in a point \mathbf{x} in the direction of the axis x_j ;

$b_j(\mathbf{x})$ are components of the body forces vector in a point \mathbf{x} in the direction of axis x_j ;

$r = r(\mathbf{x},\mathbf{y}) = \sqrt{(x_1 - y_1)^2 + (x_2 - y_2)^2 + (x_3 - y_3)^2}$ is the distance between points \mathbf{x} and \mathbf{y} ;

$\mathbf{x} = (x_1, x_2, x_3)$ is the point to which loading is put in;

$\mathbf{y} = (y_1, y_2, y_3)$ is the point in which we search displacements; $\mathbf{x}, \mathbf{y} \in V \setminus \partial V$.

Tractions also can be defined by the formulas of the Somigliano type in the form

$$p_i(\mathbf{y}) = \int_{\partial V} \{p_j(\mathbf{x})K_{ij}(\mathbf{x}, \mathbf{y}) - u_i(\mathbf{x})F_{ij}(\mathbf{x}, \mathbf{y})\}dS + \int_V b_j(\mathbf{x})B_{ij}(\mathbf{x}, \mathbf{y})dV. \quad (2.1.2)$$

In order to obtain boundary integral equations (BIE) from integral representations (2.1.1) and (2.1.2) we have to turn out points \mathbf{y} to the boundary ∂V .

From integral representation (2.1.1) we obtain BIEs of the form

$$\frac{1}{2} \cdot u_i(\mathbf{y}) = \int_{\partial V} \{p_j(\mathbf{x})U_{ij}(\mathbf{x} - \mathbf{y}) - u_j(\mathbf{x})W_{ij}(\mathbf{x}, \mathbf{y})\}dS + \int_V b_j(\mathbf{x})U_{ij}(\mathbf{x} - \mathbf{y})dV. \quad (2.1.3)$$

From integral representation (2.1.2) we obtain BIEs of the form

$$\frac{1}{2} p_i(\mathbf{y}) = \int_{\partial \Omega} \{p_j(\mathbf{x})K_{ij}(\mathbf{x}, \mathbf{y}) - u_i(\mathbf{x})F_{ij}(\mathbf{x}, \mathbf{y})\}dS + \int_V b_j(\mathbf{x})K_{ij}(\mathbf{x}, \mathbf{y})dV. \quad (2.1.4)$$

Integral identities of the Somigliano type for displacements (2.1.1) in matrix form:

$$\begin{aligned} \frac{1}{2} \begin{bmatrix} u_1(\mathbf{y}) \\ u_2(\mathbf{y}) \\ u_3(\mathbf{y}) \end{bmatrix} &= \int_{\partial \Omega} \begin{bmatrix} U_{11}(\mathbf{x} - \mathbf{y}) & U_{12}(\mathbf{x} - \mathbf{y}) & U_{13}(\mathbf{x} - \mathbf{y}) \\ U_{21}(\mathbf{x} - \mathbf{y}) & U_{22}(\mathbf{x} - \mathbf{y}) & U_{23}(\mathbf{x} - \mathbf{y}) \\ U_{31}(\mathbf{x} - \mathbf{y}) & U_{32}(\mathbf{x} - \mathbf{y}) & U_{33}(\mathbf{x} - \mathbf{y}) \end{bmatrix} \cdot \begin{bmatrix} p_1(\mathbf{x}) \\ p_2(\mathbf{x}) \\ p_3(\mathbf{x}) \end{bmatrix} dS - \\ &\int_{\partial \Omega} \begin{bmatrix} W_{11}(\mathbf{x}, \mathbf{y}) & W_{12}(\mathbf{x}, \mathbf{y}) & W_{13}(\mathbf{x}, \mathbf{y}) \\ W_{21}(\mathbf{x}, \mathbf{y}) & W_{22}(\mathbf{x}, \mathbf{y}) & W_{23}(\mathbf{x}, \mathbf{y}) \\ W_{31}(\mathbf{x}, \mathbf{y}) & W_{32}(\mathbf{x}, \mathbf{y}) & W_{33}(\mathbf{x}, \mathbf{y}) \end{bmatrix} \cdot \begin{bmatrix} u_1(\mathbf{x}) \\ u_2(\mathbf{x}) \\ u_3(\mathbf{x}) \end{bmatrix} dS + \\ &\int_V \begin{bmatrix} U_{11}(\mathbf{x} - \mathbf{y}) & U_{12}(\mathbf{x} - \mathbf{y}) & U_{13}(\mathbf{x} - \mathbf{y}) \\ U_{21}(\mathbf{x} - \mathbf{y}) & U_{22}(\mathbf{x} - \mathbf{y}) & U_{23}(\mathbf{x} - \mathbf{y}) \\ U_{31}(\mathbf{x} - \mathbf{y}) & U_{32}(\mathbf{x} - \mathbf{y}) & U_{33}(\mathbf{x} - \mathbf{y}) \end{bmatrix} \cdot \begin{bmatrix} b_1(\mathbf{x}) \\ b_2(\mathbf{x}) \\ b_3(\mathbf{x}) \end{bmatrix} dV, \end{aligned} \quad (2.1.5)$$

or in the vector form



$$\frac{1}{2} \mathbf{u}(\mathbf{y}) = \int_{\partial\Omega} \{U(\mathbf{x} - \mathbf{y}) \cdot \mathbf{u}(\mathbf{x}) + W(\mathbf{x}, \mathbf{y}) \cdot \mathbf{p}(\mathbf{x})\} dS + \int_V U(\mathbf{x} - \mathbf{y}) \cdot \mathbf{b}(\mathbf{x}) dV. \quad (2.1.6)$$

where – displacements $\mathbf{u}(\mathbf{x}) = \begin{bmatrix} u_1(\mathbf{x}) \\ u_2(\mathbf{x}) \\ u_3(\mathbf{x}) \end{bmatrix},$

– traction $\mathbf{p}(\mathbf{x}) = \begin{bmatrix} p_1(\mathbf{x}) \\ p_2(\mathbf{x}) \\ p_3(\mathbf{x}) \end{bmatrix},$

– body forces $\mathbf{b}(\mathbf{x}) = \begin{bmatrix} b_1(\mathbf{x}) \\ b_2(\mathbf{x}) \\ b_3(\mathbf{x}) \end{bmatrix};$

– matrix fundamental solutions

– for displacements $U(\mathbf{x} - \mathbf{y}) = \begin{bmatrix} U_{11}(\mathbf{x} - \mathbf{y}) & U_{12}(\mathbf{x} - \mathbf{y}) & U_{13}(\mathbf{x} - \mathbf{y}) \\ U_{21}(\mathbf{x} - \mathbf{y}) & U_{22}(\mathbf{x} - \mathbf{y}) & U_{23}(\mathbf{x} - \mathbf{y}) \\ U_{31}(\mathbf{x} - \mathbf{y}) & U_{32}(\mathbf{x} - \mathbf{y}) & U_{33}(\mathbf{x} - \mathbf{y}) \end{bmatrix},$

– for traction $W(\mathbf{x}, \mathbf{y}) = \begin{bmatrix} W_{11}(\mathbf{x}, \mathbf{y}) & W_{12}(\mathbf{x}, \mathbf{y}) & W_{13}(\mathbf{x}, \mathbf{y}) \\ W_{21}(\mathbf{x}, \mathbf{y}) & W_{22}(\mathbf{x}, \mathbf{y}) & W_{23}(\mathbf{x}, \mathbf{y}) \\ W_{31}(\mathbf{x}, \mathbf{y}) & W_{32}(\mathbf{x}, \mathbf{y}) & W_{33}(\mathbf{x}, \mathbf{y}) \end{bmatrix}.$

For tractions we have the equations in vector and matrix form:

$$\frac{1}{2} \mathbf{p}(\mathbf{y}) = \int_{\partial\Omega} \{K(\mathbf{x}, \mathbf{y}) \cdot \mathbf{p}(\mathbf{x}) - F(\mathbf{x}, \mathbf{y}) \cdot \mathbf{u}(\mathbf{x})\} dS + \int_V K(\mathbf{x}, \mathbf{y}) \cdot \mathbf{b}(\mathbf{x}) dV. \quad (2.1.7)$$

$$\begin{aligned}
\frac{1}{2} \begin{bmatrix} p_1(\mathbf{y}) \\ p_2(\mathbf{y}) \\ p_3(\mathbf{y}) \end{bmatrix} &= \int_{\partial\Omega} \begin{bmatrix} K_{11}(\mathbf{x}, \mathbf{y}) & K_{12}(\mathbf{x}, \mathbf{y}) & K_{13}(\mathbf{x}, \mathbf{y}) \\ K_{21}(\mathbf{x}, \mathbf{y}) & K_{22}(\mathbf{x}, \mathbf{y}) & K_{23}(\mathbf{x}, \mathbf{y}) \\ K_{31}(\mathbf{x}, \mathbf{y}) & K_{32}(\mathbf{x}, \mathbf{y}) & K_{33}(\mathbf{x}, \mathbf{y}) \end{bmatrix} \cdot \begin{bmatrix} p_1(\mathbf{x}) \\ p_2(\mathbf{x}) \\ p_3(\mathbf{x}) \end{bmatrix} dS - \\
&\int_{\partial\Omega} \begin{bmatrix} F_{11}(\mathbf{x}, \mathbf{y}) & F_{12}(\mathbf{x}, \mathbf{y}) & F_{13}(\mathbf{x}, \mathbf{y}) \\ F_{21}(\mathbf{x}, \mathbf{y}) & F_{22}(\mathbf{x}, \mathbf{y}) & F_{23}(\mathbf{x}, \mathbf{y}) \\ F_{31}(\mathbf{x}, \mathbf{y}) & F_{32}(\mathbf{x}, \mathbf{y}) & F_{33}(\mathbf{x}, \mathbf{y}) \end{bmatrix} \cdot \begin{bmatrix} u_1(\mathbf{x}) \\ u_2(\mathbf{x}) \\ u_3(\mathbf{x}) \end{bmatrix} dS + \\
&\int_V \begin{bmatrix} K_{11}(\mathbf{x}, \mathbf{y}) & K_{12}(\mathbf{x}, \mathbf{y}) & K_{13}(\mathbf{x}, \mathbf{y}) \\ K_{21}(\mathbf{x}, \mathbf{y}) & K_{22}(\mathbf{x}, \mathbf{y}) & K_{23}(\mathbf{x}, \mathbf{y}) \\ K_{31}(\mathbf{x}, \mathbf{y}) & K_{32}(\mathbf{x}, \mathbf{y}) & K_{33}(\mathbf{x}, \mathbf{y}) \end{bmatrix} \cdot \begin{bmatrix} b_1(\mathbf{x}) \\ b_2(\mathbf{x}) \\ b_3(\mathbf{x}) \end{bmatrix} dV.
\end{aligned} \tag{2.1.8}$$

2.2 Fundamental solutions

In order to evaluate the integral kernels $U_{ij}(\mathbf{x}-\mathbf{y})$, $W_{ij}(\mathbf{x}, \mathbf{y})$, $K_{ij}(\mathbf{x}, \mathbf{y})$, $F_{ij}(\mathbf{x}, \mathbf{y})$ from expressions (2.1.1)–(2.1.8) we use the following three-dimensional fundamental Green displacement tensor

$$U_{ij}(\mathbf{x}-\mathbf{y}) = \frac{1}{4\pi\rho c_2^2} \left\{ \delta_{ij}\psi - \chi \frac{\partial r}{\partial x_i} \frac{\partial r}{\partial x_j} \right\}, \tag{2.2.1}$$

where δ_{ij} is the Kronecker symbol; $r = \sqrt{\sum_{i=1}^3 (x_i - y_i)^2}$ is the distance between points \mathbf{x} и \mathbf{y} ; and

$$\frac{\partial r}{\partial x_s} = \frac{x_s - y_s}{r}, \quad s = \overline{1,3}.$$

In the three-dimensional case functions χ and ψ from (2.2.1) have the following form:

$$\psi = \frac{3-4\nu}{4(1-\nu)} \frac{1}{r}, \quad \chi = \frac{1}{4(1-\nu)}. \tag{2.2.2}$$

It follows from (2.2.1), that

$$U_{11}(\mathbf{x}-\mathbf{y}) = \frac{1}{4\pi\rho c_2^2} \left\{ \psi - \chi \frac{\partial r}{\partial x_1} \frac{\partial r}{\partial x_1} \right\}, \tag{2.2.3}$$

$$U_{11}(\mathbf{x} - \mathbf{y}) = \frac{1}{16(1-\nu)\pi\rho c_2^2 r} \left\{ 3 - 4\nu - \frac{(x_1 - y_1)^2}{r} \right\},$$

$$U_{12}(\mathbf{x} - \mathbf{y}) = U_{21}(\mathbf{x} - \mathbf{y}) = -\frac{\chi}{4\pi\rho c_2^2} \frac{\partial r}{\partial x_1} \frac{\partial r}{\partial x_2}, \quad (2.2.4)$$

$$U_{12}(\mathbf{x} - \mathbf{y}) = U_{21}(\mathbf{x} - \mathbf{y}) = -\frac{1}{16(1-\nu)\pi\rho c_2^2 r} \frac{(x_1 - y_1)(x_2 - y_2)}{r},$$

$$U_{13}(\mathbf{x} - \mathbf{y}) = U_{31}(\mathbf{x} - \mathbf{y}) = -\frac{\chi}{4\pi\rho c_2^2} \frac{\partial r}{\partial x_1} \frac{\partial r}{\partial x_3}, \quad (2.2.5)$$

$$U_{13}(\mathbf{x} - \mathbf{y}) = U_{31}(\mathbf{x} - \mathbf{y}) = -\frac{1}{16(1-\nu)\pi\rho c_2^2 r} \frac{(x_1 - y_1)(x_3 - y_3)}{r},$$

$$U_{22}(\mathbf{x} - \mathbf{y}) = \frac{1}{4\pi\rho c_2^2} \left\{ \psi - \chi \frac{\partial r}{\partial x_2} \frac{\partial r}{\partial x_2} \right\}, \quad (2.2.6)$$

$$U_{22}(\mathbf{x} - \mathbf{y}) = \frac{1}{16(1-\nu)\pi\rho c_2^2 r} \left\{ 3 - 4\nu - \frac{(x_2 - y_2)^2}{r} \right\},$$

$$U_{23}(\mathbf{x} - \mathbf{y}) = U_{32}(\mathbf{x} - \mathbf{y}) = -\frac{\chi}{4\pi\rho c_2^2} \frac{\partial r}{\partial x_2} \frac{\partial r}{\partial x_3}, \quad (2.2.7)$$

$$U_{23}(\mathbf{x} - \mathbf{y}) = U_{32}(\mathbf{x} - \mathbf{y}) = -\frac{1}{16(1-\nu)\pi\rho c_2^2 r} \frac{(x_2 - y_2)(x_3 - y_3)}{r},$$

$$U_{33}(\mathbf{x} - \mathbf{y}) = \frac{1}{4\pi\rho c_2^2} \left\{ \psi - \chi \frac{\partial r}{\partial x_3} \frac{\partial r}{\partial x_3} \right\}, \quad (2.2.8)$$

$$U_{33}(\mathbf{x} - \mathbf{y}) = \frac{1}{16(1-\nu)\pi\rho c_2^2 r} \left\{ 3 - 4\nu - \frac{(x_3 - y_3)^2}{r} \right\}.$$

Partial derivatives from functions χ and ψ with respect to the distance r have the form:

$$\frac{\partial \chi}{\partial r} = 0, \quad (2.2.9)$$

$$\frac{\partial^2 \chi}{\partial r^2} = 0, \quad (2.2.10)$$

$$\frac{\partial \psi}{\partial r} = -\frac{3-4\nu}{4(1-\nu)} \frac{1}{r^2} = -\frac{\psi}{r}, \quad (2.2.11)$$

$$\frac{\partial^2 \psi}{\partial r^2} = \frac{3-4\nu}{2(1-\nu)} \frac{1}{r^3} = \frac{2\psi}{r^2}. \quad (2.2.12)$$

Then we evaluate several partial derivatives from the tensor $U_{ij}(\mathbf{x} - \mathbf{y})$ with respect to the space coordinates, which will be used in future

$$\frac{\partial}{\partial x_k} U_{ij}(\mathbf{x} - \mathbf{y}) = \frac{1}{\alpha\pi\rho c_2^2} \cdot \left\{ \delta_{ij} \frac{\partial r}{\partial x_k} \frac{\partial \psi}{\partial r} - \frac{\chi}{r} \left[\delta_{ik} \frac{\partial r}{\partial x_j} + \delta_{jk} \frac{\partial r}{\partial x_i} \right] \right\}, \quad (2.2.13)$$

$$\begin{aligned}
 \frac{\partial}{\partial y_l} \frac{\partial}{\partial x_k} U_{ij}(\mathbf{x} - \mathbf{y}) &= \\
 &= \frac{1}{\alpha\pi\rho c_2^2} \times \left\{ \frac{\delta_{ij}}{r} \frac{\partial\psi}{\partial r} \left(\frac{\partial r}{\partial x_k} \frac{\partial r}{\partial x_l} - \delta_{kl} \right) - \delta_{ij} \frac{\partial^2\psi}{\partial r^2} \frac{\partial r}{\partial x_k} \frac{\partial r}{\partial x_l} + \right. \\
 &\quad \left. \frac{\chi}{r^2} (\delta_{ki}\delta_{lj} + \delta_{kj}\delta_{li}) - \frac{2\chi}{r^2} \times \left(\delta_{ki} \frac{\partial r}{\partial x_j} \frac{\partial r}{\partial x_l} + \delta_{kj} \frac{\partial r}{\partial x_i} \frac{\partial r}{\partial x_l} + \right. \right. \\
 &\quad \left. \left. \delta_{kl} \frac{\partial r}{\partial x_i} \frac{\partial r}{\partial x_j} + \delta_{li} \frac{\partial r}{\partial x_k} \frac{\partial r}{\partial x_j} + \delta_{lj} \frac{\partial r}{\partial x_k} \frac{\partial r}{\partial x_i} - 4 \frac{\partial r}{\partial x_i} \frac{\partial r}{\partial x_j} \frac{\partial r}{\partial x_k} \frac{\partial r}{\partial x_l} \right) \right\}, \tag{2.2.14}
 \end{aligned}$$

where $c_1 = \sqrt{(\lambda + 2\mu)/\rho}$ and $c_2 = \sqrt{\mu/\rho}$ are the velocities of the longitudinal and transverse waves, respectively; λ and μ are the Lamé constants; ρ is the density of the material.

Kernels $W_{ij}(\mathbf{x}, \mathbf{y})$ can be obtain from kernels $U_{ij}(\mathbf{x} - \mathbf{y})$, using the differential operator P_{ik} :

$$P_{ik} : u_k \rightarrow p_i, P_{ik}[\bullet, (\mathbf{y})] = \lambda n_i(\mathbf{y}) \frac{\partial[\bullet]}{\partial y_k} + \mu \left[\delta_{ik} \frac{\partial[\bullet]}{\partial n(\mathbf{y})} + n_k(\mathbf{y}) \frac{\partial[\bullet]}{\partial y_i} \right]. \tag{2.2.15}$$

Then the expression for the kernel $W_{ij}(\mathbf{x}, \mathbf{y})$ has the following form:

$$\begin{aligned}
 W_{ij}(\mathbf{x}, \mathbf{y}) &= P_{ik}(\bullet, (\mathbf{x})) U_{kj}(\mathbf{x} - \mathbf{y}) = \\
 &= \lambda n_i(\mathbf{x}) \frac{\partial}{\partial x_k} U_{kj}(\mathbf{x} - \mathbf{y}) + \mu n_k(\mathbf{x}) \left[\frac{\partial}{\partial x_k} U_{ij}(\mathbf{x} - \mathbf{y}) + \frac{\partial}{\partial x_i} U_{kj}(\mathbf{x} - \mathbf{y}) \right]. \tag{2.2.16}
 \end{aligned}$$

From (2.2.16) we obtain for the derivatives $\frac{\partial}{\partial x_k} U_{ij}(\mathbf{x} - \mathbf{y})$:

$$\begin{aligned}
 \frac{\partial}{\partial x_k} U_{kj}(\mathbf{x} - \mathbf{y}) &= \frac{1}{\alpha\pi\rho c_2^2} \left\{ \delta_{kj} \frac{\partial r}{\partial x_k} \frac{\partial\psi}{\partial r} - \frac{\chi}{r} \left[\frac{\partial r}{\partial x_j} + \delta_{jk} \frac{\partial r}{\partial x_i} \right] \right\}, \\
 \frac{\partial}{\partial x_k} U_{ij}(\mathbf{x} - \mathbf{y}) &= \frac{1}{\alpha\pi\rho c_2^2} \left\{ \delta_{ij} \frac{\partial r}{\partial x_k} \frac{\partial\psi}{\partial r} - \frac{\chi}{r} \left[\delta_{ik} \frac{\partial r}{\partial x_j} + \delta_{jk} \frac{\partial r}{\partial x_i} \right] \right\}, \tag{*}
 \end{aligned}$$

$$\frac{\partial}{\partial x_i} U_{kj}(\mathbf{x}-\mathbf{y}) = \frac{1}{\alpha\pi\rho c_2^2} \left\{ \delta_{kj} \frac{\partial r}{\partial x_i} \frac{\partial \psi}{\partial r} - \frac{\chi}{r} \left[\delta_{ik} \frac{\partial r}{\partial x_j} + \delta_{ij} \frac{\partial r}{\partial x_k} \right] \right\}.$$

Then, with allowance for $\lambda = \rho(c_1^2 - 2c_2^2)$ and $\mu = \rho c_2^2$, after some transformations we have:

$$\begin{aligned} W_{ij}(\mathbf{x}, \mathbf{y}) = & \frac{1}{\alpha\pi} \left\{ \left[\frac{\partial \psi}{\partial r} - \frac{\chi}{r} \right] \left(\delta_{ij} \frac{\partial r}{\partial n(\mathbf{x})} + n_j(\mathbf{x}) \frac{\partial r}{\partial x_i} \right) - \right. \\ & \left. \frac{2\chi}{r} \left[n_i(\mathbf{x}) \frac{\partial r}{\partial x_j} - 2 \frac{\partial r}{\partial x_i} \frac{\partial r}{\partial x_j} \frac{\partial r}{\partial n(\mathbf{x})} \right] + \left(\frac{c_1^2}{c_2^2} - 2 \right) n_i(\mathbf{x}) \frac{\partial r}{\partial x_j} \frac{\partial \psi}{\partial r} \right\}, \end{aligned} \quad (2.2.17)$$

where $\frac{\partial}{\partial n(\mathbf{x})} = \sum_{l=1}^3 n_l(\mathbf{x}) \frac{\partial r}{\partial x_l}$ is the normal derivative.

So, we have for kernel $W_{ij}(\mathbf{x}, \mathbf{y})$:

$$\begin{aligned} W_{11}(\mathbf{x}, \mathbf{y}) = & \frac{1}{\alpha\pi} \left\{ \left[\frac{\partial \psi}{\partial r} - \frac{\chi}{r} \right] \left(\frac{\partial r}{\partial n(\mathbf{x})} + n_1(\mathbf{x}) \frac{\partial r}{\partial x_1} \right) - \right. \\ & \left. \frac{2\chi}{r} \left[n_1(\mathbf{x}) \frac{\partial r}{\partial x_1} - 2 \frac{\partial r}{\partial x_1} \frac{\partial r}{\partial x_1} \frac{\partial r}{\partial n(\mathbf{x})} \right] + \left(\frac{c_1^2}{c_2^2} - 2 \right) n_1(\mathbf{x}) \frac{\partial r}{\partial x_1} \frac{\partial \psi}{\partial r} \right\}, \end{aligned} \quad (2.2.18)$$

$$\begin{aligned} W_{11}(\mathbf{x}, \mathbf{y}) = & \frac{-1}{2\alpha\pi(1-\nu)r^2} \left\{ \frac{1}{2} \left(\frac{3-4\nu}{r} + 1 \right) [2n_1(\mathbf{x})(x_1 - y_1) + n_2(\mathbf{x})(x_2 - y_2) + n_3(\mathbf{x})(x_3 - y_3)] + \right. \\ & (x_1 - y_1) \left[n_1(\mathbf{x}) - 2 \frac{(x_1 - y_1)}{r^2} [n_1(\mathbf{x})(x_1 - y_1) + n_2(\mathbf{x})(x_2 - y_2) + n_3(\mathbf{x})(x_3 - y_3)] \right] + \\ & \left. \frac{3-4\nu}{2} \left(\frac{c_1^2}{c_2^2} - 2 \right) n_1(\mathbf{x}) \frac{(x_1 - y_1)}{r^3} \right\}, \end{aligned}$$

$$W_{12}(\mathbf{x}, \mathbf{y}) = \frac{1}{\alpha\pi} \left\{ \left[\frac{\partial\psi}{\partial r} - \frac{\chi}{r} \right] n_2(\mathbf{x}) \frac{\partial r}{\partial x_1} - \frac{2\chi}{r} \left[n_1(\mathbf{x}) \frac{\partial r}{\partial x_2} - 2 \frac{\partial r}{\partial x_1} \frac{\partial r}{\partial x_2} \frac{\partial r}{\partial \mathbf{n}(\mathbf{x})} \right] + \left(\frac{c_1^2}{c_2^2} - 2 \right) n_1(\mathbf{x}) \frac{\partial r}{\partial x_2} \frac{\partial\psi}{\partial r} \right\}, \quad (2.2.19)$$

$$W_{12}(\mathbf{x}, \mathbf{y}) = \frac{-1}{4\alpha\pi(1-\nu)r^2} \left\{ n_2(\mathbf{x})(x_1 - y_1) + 2n_1(\mathbf{x})(x_2 - y_2) + \frac{(3-4\nu)}{r} n_2(\mathbf{x})(x_1 - y_1) + \frac{(3-4\nu)}{r} \left(\frac{c_1^2}{c_2^2} - 2 \right) n_1(\mathbf{x})(x_2 - y_2) - \frac{2}{r^2} (x_1 - y_1)(x_2 - y_2) [n_1(\mathbf{x})(x_1 - y_1) + n_2(\mathbf{x})(x_2 - y_2) + n_3(\mathbf{x})(x_3 - y_3)] \right\},$$

$$W_{13}(\mathbf{x}, \mathbf{y}) = \frac{1}{\alpha\pi} \left\{ \left[\frac{\partial\psi}{\partial r} - \frac{\chi}{r} \right] n_3(\mathbf{x}) \frac{\partial r}{\partial x_1} - \frac{2\chi}{r} \left[n_1(\mathbf{x}) \frac{\partial r}{\partial x_3} - 2 \frac{\partial r}{\partial x_1} \frac{\partial r}{\partial x_3} \frac{\partial r}{\partial \mathbf{n}(\mathbf{x})} \right] + \left(\frac{c_1^2}{c_2^2} - 2 \right) n_1(\mathbf{x}) \frac{\partial r}{\partial x_3} \frac{\partial\psi}{\partial r} \right\}, \quad (2.2.20)$$

$$W_{13}(\mathbf{x}, \mathbf{y}) = \frac{-1}{4\alpha\pi(1-\nu)r^2} \left\{ n_3(\mathbf{x})(x_1 - y_1) + 2n_1(\mathbf{x})(x_3 - y_3) + \frac{(3-4\nu)}{r} n_3(\mathbf{x})(x_1 - y_1) + \frac{(3-4\nu)}{r} \left(\frac{c_1^2}{c_2^2} - 2 \right) n_1(\mathbf{x})(x_3 - y_3) - \frac{2}{r^2} (x_1 - y_1)(x_3 - y_3) [n_1(\mathbf{x})(x_1 - y_1) + n_2(\mathbf{x})(x_2 - y_2) + n_3(\mathbf{x})(x_3 - y_3)] \right\},$$

$$W_{21}(\mathbf{x}, \mathbf{y}) = \frac{1}{\alpha\pi} \left\{ \left[\frac{\partial\psi}{\partial r} - \frac{\chi}{r} \right] n_1(\mathbf{x}) \frac{\partial r}{\partial x_2} - \frac{2\chi}{r} \left[n_2(\mathbf{x}) \frac{\partial r}{\partial x_1} - 2 \frac{\partial r}{\partial x_2} \frac{\partial r}{\partial x_1} \frac{\partial r}{\partial \mathbf{n}(\mathbf{x})} \right] + \left(\frac{c_1^2}{c_2^2} - 2 \right) n_2(\mathbf{x}) \frac{\partial r}{\partial x_1} \frac{\partial\psi}{\partial r} \right\}, \quad (2.2.21)$$

$$W_{21}(\mathbf{x}, \mathbf{y}) = \frac{-1}{4\alpha\pi(1-\nu)r^2} \left\{ n_1(\mathbf{x})(x_2 - y_2) + 2n_2(\mathbf{x})(x_1 - y_1) + \right. \\ \left. \frac{(3-4\nu)}{r} n_1(\mathbf{x})(x_2 - y_2) + \frac{(3-4\nu)}{r} \left(\frac{c_1^2}{c_2^2} - 2 \right) n_2(\mathbf{x})(x_1 - y_1) - \right. \\ \left. \frac{2}{r^2} (x_1 - y_1)(x_2 - y_2) [n_1(\mathbf{x})(x_1 - y_1) + n_2(\mathbf{x})(x_2 - y_2) + n_3(\mathbf{x})(x_3 - y_3)] \right\},$$

$$W_{22}(\mathbf{x}, \mathbf{y}) = \frac{1}{\alpha\pi} \left\{ \left[\frac{\partial\psi}{\partial r} - \frac{\chi}{r} \right] \left[\frac{\partial r}{\partial \mathbf{n}(\mathbf{x})} + n_2(\mathbf{x}) \frac{\partial r}{\partial x_2} \right] - \right. \\ \left. \frac{2\chi}{r} \left[n_2(\mathbf{x}) \frac{\partial r}{\partial x_2} - 2 \frac{\partial r}{\partial x_2} \frac{\partial r}{\partial x_2} \frac{\partial r}{\partial \mathbf{n}(\mathbf{x})} \right] + \left(\frac{c_1^2}{c_2^2} - 2 \right) n_2(\mathbf{x}) \frac{\partial r}{\partial x_2} \frac{\partial\psi}{\partial r} \right\}, \quad (2.2.22)$$

$$W_{22}(\mathbf{x}, \mathbf{y}) = \frac{-1}{2\alpha\pi(1-\nu)r^2} \left\{ \left(\frac{3-4\nu}{r} + 1 \right) [n_1(\mathbf{x})(x_1 - y_1) + 2n_2(\mathbf{x})(x_2 - y_2) + n_3(\mathbf{x})(x_3 - y_3)] - \right. \\ \left. (x_2 - y_2) \left[n_2(\mathbf{x}) - 2 \frac{(x_2 - y_2)}{r^2} [n_1(\mathbf{x})(x_1 - y_1) + n_2(\mathbf{x})(x_2 - y_2) + n_3(\mathbf{x})(x_3 - y_3)] \right] - \right. \\ \left. \frac{3-4\nu}{4(1-\nu)} \left(\frac{c_1^2}{c_2^2} - 2 \right) n_2(\mathbf{x}) \frac{(x_2 - y_2)}{r^3} \right\},$$

$$W_{23}(\mathbf{x}, \mathbf{y}) = \frac{1}{\alpha\pi} \left\{ \left[\frac{\partial\psi}{\partial r} - \frac{\chi}{r} \right] n_3(\mathbf{x}) \frac{\partial r}{\partial x_2} - \right. \\ \left. \frac{2\chi}{r} \left[n_2(\mathbf{x}) \frac{\partial r}{\partial x_3} - 2 \frac{\partial r}{\partial x_2} \frac{\partial r}{\partial x_3} \frac{\partial r}{\partial \mathbf{n}(\mathbf{x})} \right] + \left(\frac{c_1^2}{c_2^2} - 2 \right) n_2(\mathbf{x}) \frac{\partial r}{\partial x_3} \frac{\partial\psi}{\partial r} \right\}, \quad (2.2.23)$$

$$\begin{aligned}
W_{23}(\mathbf{x}, \mathbf{y}) &= \frac{-1}{4\alpha\pi(1-\nu)r^2} \{n_3(\mathbf{x})(x_2 - y_2) + 2n_2(\mathbf{x})(x_3 - y_3) + \\
&\quad \frac{(3-4\nu)}{r} n_3(\mathbf{x})(x_2 - y_2) + \frac{(3-4\nu)}{r} \left(\frac{c_1^2}{c_2^2} - 2 \right) n_2(\mathbf{x})(x_3 - y_3) - \\
&\quad \frac{2}{r^2} (x_3 - y_3)(x_2 - y_2) [n_1(\mathbf{x})(x_1 - y_1) + n_2(\mathbf{x})(x_2 - y_2) + n_3(\mathbf{x})(x_3 - y_3)] \}, \\
W_{31}(\mathbf{x}, \mathbf{y}) &= \frac{1}{\alpha\pi} \left\{ \left[\frac{\partial\psi}{\partial r} - \frac{\chi}{r} \right] n_1(\mathbf{x}) \frac{\partial r}{\partial x_2} - \right. \\
&\quad \left. \frac{2\chi}{r} \left[n_3(\mathbf{x}) \frac{\partial r}{\partial x_1} - 2 \frac{\partial r}{\partial x_3} \frac{\partial r}{\partial x_1} \frac{\partial r}{\partial \mathbf{n}(\mathbf{x})} \right] + \left(\frac{c_1^2}{c_2^2} - 2 \right) n_3(\mathbf{x}) \frac{\partial r}{\partial x_1} \frac{\partial\psi}{\partial r} \right\}, \quad (2.2.24)
\end{aligned}$$

$$\begin{aligned}
W_{31}(\mathbf{x}, \mathbf{y}) &= \frac{-1}{4\alpha\pi(1-\nu)r^2} \{n_1(\mathbf{x})(x_3 - y_3) + 2n_3(\mathbf{x})(x_1 - y_1) + \\
&\quad \frac{(3-4\nu)}{r} n_1(\mathbf{x})(x_3 - y_3) + \frac{(3-4\nu)}{r} \left(\frac{c_1^2}{c_2^2} - 2 \right) n_3(\mathbf{x})(x_1 - y_1) - \\
&\quad \frac{2}{r^2} (x_1 - y_1)(x_3 - y_3) [n_1(\mathbf{x})(x_1 - y_1) + n_2(\mathbf{x})(x_2 - y_2) + n_3(\mathbf{x})(x_3 - y_3)] \},
\end{aligned}$$

$$\begin{aligned}
W_{32}(\mathbf{x}, \mathbf{y}) &= \frac{1}{\alpha\pi} \left\{ \left[\frac{\partial\psi}{\partial r} - \frac{\chi}{r} \right] n_2(\mathbf{x}) \frac{\partial r}{\partial x_3} - \right. \\
&\quad \left. \frac{2\chi}{r} \left[n_3(\mathbf{x}) \frac{\partial r}{\partial x_2} - 2 \frac{\partial r}{\partial x_3} \frac{\partial r}{\partial x_2} \frac{\partial r}{\partial \mathbf{n}(\mathbf{x})} \right] + \left(\frac{c_1^2}{c_2^2} - 2 \right) n_3(\mathbf{x}) \frac{\partial r}{\partial x_2} \frac{\partial\psi}{\partial r} \right\}, \quad (2.2.25)
\end{aligned}$$

$$\begin{aligned}
W_{32}(\mathbf{x}, \mathbf{y}) &= \frac{-1}{4\alpha\pi(1-\nu)r^2} \{n_2(\mathbf{x})(x_3 - y_3) + 2n_3(\mathbf{x})(x_2 - y_2) + \\
&\quad \frac{(3-4\nu)}{r} n_2(\mathbf{x})(x_3 - y_3) + \frac{(3-4\nu)}{r} \left(\frac{c_1^2}{c_2^2} - 2 \right) n_3(\mathbf{x})(x_2 - y_2) - \\
&\quad \frac{2}{r^2} (x_2 - y_2)(x_3 - y_3) [n_1(\mathbf{x})(x_1 - y_1) + n_2(\mathbf{x})(x_2 - y_2) + n_3(\mathbf{x})(x_3 - y_3)] \},
\end{aligned}$$

$$W_{33}(\mathbf{x}, \mathbf{y}) = \frac{1}{\alpha\pi} \left\{ \left[\frac{\partial\psi}{\partial r} - \frac{\chi}{r} \right] \left(\frac{\partial r}{\partial \mathbf{n}(\mathbf{x})} + n_3(\mathbf{x}) \frac{\partial r}{\partial x_3} \right) - \frac{2\chi}{r} \left[n_3(\mathbf{x}) \frac{\partial r}{\partial x_3} - 2 \frac{\partial r}{\partial x_3} \frac{\partial r}{\partial x_3} \frac{\partial r}{\partial \mathbf{n}(\mathbf{x})} \right] + \left(\frac{c_1^2}{c_2^2} - 2 \right) n_3(\mathbf{x}) \frac{\partial r}{\partial x_3} \frac{\partial \psi}{\partial r} \right\}, \quad (2.2.26)$$

$$W_{33}(\mathbf{x}, \mathbf{y}) = \frac{-1}{2\alpha\pi(1-\nu)r^2} \left\{ \frac{1}{2} \left(\frac{3-4\nu}{r} + 1 \right) [n_1(\mathbf{x})(x_1 - y_1) + n_2(\mathbf{x})(x_2 - y_2) + 2n_3(\mathbf{x})(x_3 - y_3)] + (x_3 - y_3) \left[n_3(\mathbf{x}) - 2 \frac{(x_3 - y_3)}{r^2} [n_1(\mathbf{x})(x_1 - y_1) + n_2(\mathbf{x})(x_2 - y_2) + n_3(\mathbf{x})(x_3 - y_3)] \right] + \frac{3-4\nu}{2r} \left(\frac{c_1^2}{c_2^2} - 2 \right) n_3(\mathbf{x})(x_3 - y_3) \right\}.$$

Expressions for integral kernels from BIEs (2.1.4) can be obtained analogously.

$$K_{ij}(\mathbf{x}, \mathbf{y}) = P_{ik}(\bullet, (\mathbf{y})) U_{kj}(\mathbf{x} - \mathbf{y}) = = \lambda n_i(\mathbf{y}) \frac{\partial}{\partial y_k} U_{jk}(\mathbf{x} - \mathbf{y}) + \mu n_k(\mathbf{y}) \left[\frac{\partial}{\partial y_k} U_{ji}(\mathbf{x} - \mathbf{y}) + \frac{\partial}{\partial y_i} U_{jk}(\mathbf{x} - \mathbf{y}) \right]. \quad (2.2.27)$$

In order to evaluate the integral kernel $F_{ik}(\mathbf{x}, \mathbf{y})$ we apply the differential operator (2.2.21) to the kernel

$W_{ij}(\mathbf{x}, \mathbf{y})$:

$$F_{ij}(\mathbf{x}, \mathbf{y}) = P_{ik}(\bullet, (\mathbf{y})) W_{jk}(\mathbf{x}, \mathbf{y}) = = \lambda n_i(\mathbf{y}) \frac{\partial}{\partial y_r} W_{kr}(\mathbf{x}, \mathbf{y}) + \mu n_r(\mathbf{y}) \left[\frac{\partial}{\partial y_r} W_{ki}(\mathbf{x}, \mathbf{y}) + \frac{\partial}{\partial y_i} W_{kr}(\mathbf{x}, \mathbf{y}) \right]. \quad (2.2.28)$$

Use the expression (2.2.28) we obtain for $F_{ik}(\mathbf{x}, \mathbf{y})$ the following:

$$\begin{aligned}
F_{ik}(\mathbf{x}, \mathbf{y}) &= \lambda^2 n_i(\mathbf{y}) n_k(\mathbf{x}) \frac{\partial}{\partial y_r} \frac{\partial}{\partial x_l} U_{lr}(\mathbf{x} - \mathbf{y}) + \\
&\lambda \mu \left[n_i(\mathbf{y}) n_l(\mathbf{x}) \left(\frac{\partial}{\partial y_r} \frac{\partial}{\partial x_l} U_{kr}(\mathbf{x} - \mathbf{y}) + \frac{\partial}{\partial y_r} \frac{\partial}{\partial x_k} U_{lr}(\mathbf{x} - \mathbf{y}) \right) + \right. \\
&n_r(\mathbf{y}) n_k(\mathbf{x}) \left. \left(\frac{\partial}{\partial y_r} \frac{\partial}{\partial x_l} U_{li}(\mathbf{x} - \mathbf{y}) + \frac{\partial}{\partial y_i} \frac{\partial}{\partial x_l} U_{lr}(\mathbf{x} - \mathbf{y}) \right) \right] + \\
&\mu^2 n_r(\mathbf{y}) n_l(\mathbf{x}) \left[\frac{\partial}{\partial y_r} \frac{\partial}{\partial x_l} U_{ki}(\mathbf{x} - \mathbf{y}) + \frac{\partial}{\partial y_r} \frac{\partial}{\partial x_k} U_{li}(\mathbf{x} - \mathbf{y}) + \right. \\
&\left. \frac{\partial}{\partial y_i} \frac{\partial}{\partial x_l} U_{kr}(\mathbf{x} - \mathbf{y}) + \frac{\partial}{\partial y_i} \frac{\partial}{\partial x_k} U_{lr}(\mathbf{x} - \mathbf{y}) \right]. \tag{2.2.29}
\end{aligned}$$

It follows from (*), with allowance for the fact, that $\frac{\partial r}{\partial x_l} \frac{\partial r}{\partial x_l} = 1$, we have for terms from (2.2.29)

following expressions:

$$\begin{aligned}
n_i(\mathbf{y}) n_k(\mathbf{x}) \frac{\partial}{\partial y_r} \frac{\partial}{\partial x_l} U_{lr}(\mathbf{x} - \mathbf{y}) &= \frac{n_i(\mathbf{y}) n_k(\mathbf{x}) 2\chi}{\alpha \pi \rho c_2^2 r^2}, \\
n_i(\mathbf{y}) n_l(\mathbf{x}) \left(\frac{\partial r}{\partial y_r} \frac{\partial r}{\partial x_l} U_{kr}(\mathbf{x} - \mathbf{y}) + \frac{\partial r}{\partial y_r} \frac{\partial r}{\partial x_k} U_{lr}(\mathbf{x} - \mathbf{y}) \right) &= \\
= \frac{2n_i(\mathbf{y}) n_l(\mathbf{x})}{\alpha \pi \rho c_2^2} \left\{ \frac{1}{r} \frac{\partial \psi}{\partial r} \left(\frac{\partial r}{\partial x_l} \frac{\partial r}{\partial x_k} - \delta_{lk} \right) - \frac{\partial^2 \psi}{\partial r^2} \frac{\partial r}{\partial x_l} \frac{\partial r}{\partial x_k} - \frac{2\chi}{r^2} \left(2 \frac{\partial r}{\partial x_k} \frac{\partial r}{\partial x_l} - \delta_{lk} \right) \right\}, \\
n_r(\mathbf{y}) n_k(\mathbf{x}) \left(\frac{\partial r}{\partial y_r} \frac{\partial r}{\partial x_l} U_{li}(\mathbf{x} - \mathbf{y}) + \frac{\partial r}{\partial y_i} \frac{\partial r}{\partial x_l} U_{lr}(\mathbf{x} - \mathbf{y}) \right) &= \\
= \frac{2n_r(\mathbf{y}) n_k(\mathbf{x})}{\alpha \pi \rho c_2^2} \left\{ \frac{1}{r} \frac{\partial \psi}{\partial r} \left(\frac{\partial r}{\partial x_i} \frac{\partial r}{\partial x_r} - \delta_{ir} \right) - \frac{\partial^2 \psi}{\partial r^2} \frac{\partial r}{\partial x_i} \frac{\partial r}{\partial x_r} - \frac{2\chi}{r^2} \left(2 \frac{\partial r}{\partial x_r} \frac{\partial r}{\partial x_i} - \delta_{ri} \right) \right\},
\end{aligned}$$

$$\begin{aligned}
& n_r(\mathbf{y})n_l(\mathbf{x}) \left[\frac{\partial}{\partial y_r} \frac{\partial}{\partial x_l} U_{ki}(\mathbf{x} - \mathbf{y}) + \frac{\partial}{\partial y_r} \frac{\partial}{\partial x_k} U_{li}(\mathbf{x} - \mathbf{y}) + \right. \\
& \left. \frac{\partial}{\partial y_i} \frac{\partial}{\partial x_l} U_{kr}(\mathbf{x} - \mathbf{y}) + \frac{\partial}{\partial y_i} \frac{\partial}{\partial x_k} U_{lr}(\mathbf{x} - \mathbf{y}) \right] = \frac{n_r(\mathbf{y})n_l(\mathbf{x})}{\alpha\pi\rho c_2^2} \times \\
& \left\{ \frac{1}{r} \frac{\partial \psi}{\partial r} \left[\delta_{ki} \left(\frac{\partial r}{\partial x_r} \frac{\partial r}{\partial x_l} - \delta_{rl} \right) + \delta_{li} \left(\frac{\partial r}{\partial x_r} \frac{\partial r}{\partial x_k} - \delta_{kr} \right) + \delta_{kr} \left(\frac{\partial r}{\partial x_i} \frac{\partial r}{\partial x_l} - \delta_{il} \right) + \right. \right. \\
& \left. \left. \delta_{lr} \left(\frac{\partial r}{\partial x_i} \frac{\partial r}{\partial x_k} - \delta_{ik} \right) \right] - \frac{\partial^2 \psi}{\partial r^2} \left(\delta_{ki} \frac{\partial r}{\partial x_r} \frac{\partial r}{\partial x_l} + \delta_{li} \frac{\partial r}{\partial x_r} \frac{\partial r}{\partial x_k} + \delta_{kr} \frac{\partial r}{\partial x_i} \frac{\partial r}{\partial x_l} + \delta_{lr} \frac{\partial r}{\partial x_i} \frac{\partial r}{\partial x_k} \right) - \right. \\
& \left. \frac{2\chi}{r^2} \left[-2\delta_{lk}\delta_{ri} - \delta_{kr}\delta_{li} - \delta_{ki}\delta_{lr} + 4\delta_{kl} \frac{\partial r}{\partial x_i} \frac{\partial r}{\partial x_r} + 4\delta_{ri} \frac{\partial r}{\partial x_l} \frac{\partial r}{\partial x_k} + 3\delta_{ki} \frac{\partial r}{\partial x_r} \frac{\partial r}{\partial x_l} + 3\delta_{rk} \frac{\partial r}{\partial x_i} \frac{\partial r}{\partial x_l} + \right. \right. \\
& \left. \left. 3\delta_{li} \frac{\partial r}{\partial x_k} \frac{\partial r}{\partial x_r} + 3\delta_{rl} \frac{\partial r}{\partial x_k} \frac{\partial r}{\partial x_i} - 16 \frac{\partial r}{\partial x_i} \frac{\partial r}{\partial x_r} \frac{\partial r}{\partial x_k} \frac{\partial r}{\partial x_l} \right] \right\}.
\end{aligned}$$

And in the end we obtain:

$$\begin{aligned}
F_{ik}(\mathbf{x}, \mathbf{y}) &= \frac{\rho(c_1^2 - 2c_2^2)^2}{\alpha\pi c_2^2} n_i(\mathbf{y}) n_k(\mathbf{x}) \frac{2\chi}{r^2} + \\
&\frac{2\rho(c_1^2 - 2c_2^2)}{\alpha\pi} \left[n_r(\mathbf{y}) n_k(\mathbf{x}) \left\{ \frac{1}{r} \frac{\partial\psi}{\partial r} \left(\frac{\partial r}{\partial x_i} \frac{\partial r}{\partial x_r} - \delta_{ir} \right) - \frac{\partial^2\psi}{\partial r^2} \frac{\partial r}{\partial x_i} \frac{\partial r}{\partial x_r} + \right. \right. \\
&\left. \left. \frac{\chi}{r^2} (3\delta_{ri} + \delta_{ri}) - \frac{2\chi}{r^2} \left(2 \frac{\partial r}{\partial x_r} \frac{\partial r}{\partial x_i} + \delta_{ri} \right) \right\} + \right. \\
&n_i(\mathbf{y}) n_l(\mathbf{x}) \left\{ \frac{1}{r} \frac{\partial\psi}{\partial r} \left(\frac{\partial r}{\partial x_l} \frac{\partial r}{\partial x_k} - \delta_{lk} \right) - \frac{\partial^2\psi}{\partial r^2} \frac{\partial r}{\partial x_l} \frac{\partial r}{\partial x_k} + \right. \\
&\left. \left. \frac{\chi}{r^2} (3\delta_{lk} + \delta_{lk}) - \frac{2\chi}{r^2} \left(2 \frac{\partial r}{\partial x_k} \frac{\partial r}{\partial x_l} + \delta_{lk} \right) \right\} \right] + \frac{\rho c_2^2}{\alpha\pi} n_r(\mathbf{y}) n_l(\mathbf{x}) \left\{ \frac{1}{r} \frac{\partial\psi}{\partial r} \times \right. \\
&\left[\delta_{ki} \left(\frac{\partial r}{\partial x_r} \frac{\partial r}{\partial x_l} - \delta_{rl} \right) + \delta_{li} \left(\frac{\partial r}{\partial x_r} \frac{\partial r}{\partial x_k} - \delta_{kr} \right) + \delta_{kr} \left(\frac{\partial r}{\partial x_i} \frac{\partial r}{\partial x_l} - \delta_{il} \right) + \right. \\
&\left. \delta_{lr} \left(\frac{\partial r}{\partial x_i} \frac{\partial r}{\partial x_k} - \delta_{ik} \right) \right] - \frac{\partial^2\psi}{\partial r^2} \left(\delta_{ki} \frac{\partial r}{\partial x_r} \frac{\partial r}{\partial x_l} + \delta_{li} \frac{\partial r}{\partial x_r} \frac{\partial r}{\partial x_k} + \delta_{kr} \frac{\partial r}{\partial x_i} \frac{\partial r}{\partial x_l} + \delta_{lr} \frac{\partial r}{\partial x_i} \frac{\partial r}{\partial x_k} \right) + \\
&\frac{2\chi}{r^2} (2\delta_{lk} \delta_{ri} + \delta_{kr} \delta_{li} + \delta_{ki} \delta_{lr}) - \\
&\frac{2\chi}{r^2} \left[4\delta_{kl} \frac{\partial r}{\partial x_i} \frac{\partial r}{\partial x_r} + 4\delta_{ri} \frac{\partial r}{\partial x_l} \frac{\partial r}{\partial x_k} + 3\delta_{ki} \frac{\partial r}{\partial x_r} \frac{\partial r}{\partial x_l} + \right. \\
&\left. 3\delta_{rk} \frac{\partial r}{\partial x_i} \frac{\partial r}{\partial x_l} + 3\delta_{li} \frac{\partial r}{\partial x_k} \frac{\partial r}{\partial x_r} + 3\delta_{rl} \frac{\partial r}{\partial x_k} \frac{\partial r}{\partial x_i} - 16 \frac{\partial r}{\partial x_i} \frac{\partial r}{\partial x_r} \frac{\partial r}{\partial x_k} \frac{\partial r}{\partial x_l} \right] \left. \right\}. \tag{2.2.30}
\end{aligned}$$

The fundamental solutions (2.2.1), (2.2.17), (2.2.27), (2.2.29) contain singularities of different kinds, which arise, when the observation point \mathbf{y} tends to the load point \mathbf{x} :

$-U_{ij}(\mathbf{x} - \mathbf{y})$ has the weak singularity:

$$U_{ij}(\mathbf{x} - \mathbf{y}) \rightarrow \frac{1}{r}. \tag{2.2.31}$$

– $W_{ij}(\mathbf{x}, \mathbf{y})$ and $K_{ij}(\mathbf{x}, \mathbf{y})$ have the singularity in the Cauchy sense:

$$W_{ij}(\mathbf{x}, \mathbf{y}) \rightarrow \frac{1}{r^2}, \quad K_{ij}(\mathbf{x}, \mathbf{y}) \rightarrow \frac{1}{r^2}. \quad (2.2.32)$$

– $F_{ij}(\mathbf{x}, \mathbf{y})$ has the strong (hyper) singularity in the Hadamard sense:

$$F_{ij}(\mathbf{x}, \mathbf{y}) \rightarrow \frac{1}{r^3}. \quad (2.2.33)$$

2.3 Equations of the boundary element method

So, in accordance with previous results, we have following integral identities of the Somigliano type:

$$\frac{1}{2}u_1(\mathbf{y}) = \int_{\partial V} (p_j(\mathbf{x})U_{1j}(\mathbf{x} - \mathbf{y}) - u_j(\mathbf{x})W_{1j}(\mathbf{x}, \mathbf{y}))d\mathbf{x} + \int_V b_j(\mathbf{x})U_{1j}(\mathbf{x} - \mathbf{y})d\mathbf{x}, \quad (2.3.1)$$

and

$$\frac{1}{2}p_1(\mathbf{y}) = \int_{\partial V} (p_j(\mathbf{x})K_{1j}(\mathbf{x}, \mathbf{y}) - u_j(\mathbf{x})F_{1j}(\mathbf{x}, \mathbf{y}))d\mathbf{x} + \int_V b_j(\mathbf{x})K_{1j}(\mathbf{x} - \mathbf{y})d\mathbf{x}, \quad (3.3.2)$$

Use the boundary element method to solve the problem under consideration. Subdivide the surface ∂V into N plain polygonal elements $\Omega_j, j = \overline{1, N}$. Then

$$\partial V = \bigcup_{j=1}^N \Omega_j; \quad \Omega_i \cap \Omega_j = \emptyset, \text{ if } i \neq j.$$

and every function $f(\mathbf{x}), \mathbf{x} \in \partial V$ will be approximately presented in the form

$$f(\mathbf{x}) \approx \sum_{j=1}^N \sum_{q=1}^{Q_j} f^j(\mathbf{x}^q) \varphi_{jq}(\mathbf{x}), \mathbf{x} \in \partial V$$

where $f^j(\mathbf{x}) = f(\mathbf{x}), \mathbf{x} \in \Omega_j$; points $\mathbf{x}^q, q = \overline{1, Q_j}$ are the nodal points located on the boundary element Ω_j ; and functions $\varphi_{jq}(\mathbf{x}), \mathbf{x} \in \partial V$ are the functions of the form of the boundary element Ω_j .

Use the constant approximation on the every boundary element, the functions $\varphi_{jq}(\mathbf{x}), \mathbf{x} \in \partial V$ do not depend on the form of the boundary element Ω_j , so

$$\varphi_{jq}(\mathbf{x}) = \begin{cases} 1, & \mathbf{x} \in \Omega_j; \\ 0, & \mathbf{x} \in \Omega_j. \end{cases}$$

Then from systems of boundary integral equations (2.3.1) and (2.3.2), in the absence of body forces, we obtain the following approximately systems of equations for \mathbf{y}^i , $i = \overline{1, N}$:

$$\begin{cases} \frac{1}{2}u_1(\mathbf{y}^i) + \sum_{j=1}^3 \sum_{l=1}^N \int_{\Omega_l} W_{1j}(\mathbf{x}^l, \mathbf{y}^i) u_j(\mathbf{x}^l) d\mathbf{x} = \sum_{j=1}^3 \sum_{l=1}^N \int_{\Omega_l} U_{1j}(\mathbf{x}^l - \mathbf{y}^i) d\mathbf{x} p_j(\mathbf{x}^l) \\ \frac{1}{2}u_2(\mathbf{y}^i) + \sum_{j=1}^3 \sum_{l=1}^N \int_{\Omega_l} W_{2j}(\mathbf{x}^l, \mathbf{y}^i) u_j(\mathbf{x}^l) d\mathbf{x} = \sum_{j=1}^3 \sum_{l=1}^N \int_{\Omega_l} U_{2j}(\mathbf{x}^l - \mathbf{y}^i) d\mathbf{x} p_j(\mathbf{x}^l) \\ \frac{1}{2}u_3(\mathbf{y}^i) + \sum_{j=1}^3 \sum_{l=1}^N \int_{\Omega_l} W_{3j}(\mathbf{x}^l, \mathbf{y}^i) u_j(\mathbf{x}^l) d\mathbf{x} = \sum_{j=1}^3 \sum_{l=1}^N \int_{\Omega_l} U_{3j}(\mathbf{x}^l - \mathbf{y}^i) d\mathbf{x} p_j(\mathbf{x}^l) \end{cases} \quad (2.3.3)$$

and

$$\begin{cases} \frac{1}{2}p_1(\mathbf{y}^i) - \sum_{j=1}^3 \sum_{l=1}^N \int_{\Omega_l} K_{1j}(\mathbf{x}^l, \mathbf{y}^i) p_j(\mathbf{x}^l) d\mathbf{x} = -\sum_{j=1}^3 \sum_{l=1}^N \int_{\Omega_l} F_{1j}(\mathbf{x}^l, \mathbf{y}^i) d\mathbf{x} u_j(\mathbf{x}^l) \\ \frac{1}{2}p_2(\mathbf{y}^i) + \sum_{j=1}^3 \sum_{l=1}^N \int_{\Omega_l} K_{2j}(\mathbf{x}^l, \mathbf{y}^i) p_j(\mathbf{x}^l) d\mathbf{x} = \sum_{j=1}^3 \sum_{l=1}^N \int_{\Omega_l} F_{2j}(\mathbf{x}^l, \mathbf{y}^i) d\mathbf{x} u_j(\mathbf{x}^l) \\ \frac{1}{2}p_3(\mathbf{y}^i) + \sum_{j=1}^3 \sum_{l=1}^N \int_{\Omega_l} K_{3j}(\mathbf{x}^l, \mathbf{y}^i) p_j(\mathbf{x}^l) d\mathbf{x} = \sum_{j=1}^3 \sum_{l=1}^N \int_{\Omega_l} F_{3j}(\mathbf{x}^l, \mathbf{y}^i) d\mathbf{x} u_j(\mathbf{x}^l) \end{cases} \quad (2.3.4)$$

where points \mathbf{x}^j and \mathbf{y}^j are located in the geometrical center of boundary element Ω_j .

2.4 Regularization of divergent integrals

To calculate of coefficients of linear algebraic equations systems (2.3.3) and (2.4.4) it follows from expressions for the fundamental solutions of the elastostatic problem, that different divergent integrals

$$J_{\gamma}^{\alpha, \beta}(\mathbf{x}, \Omega_j) = \int_{\Omega_j} \frac{(x_1 - y_1)^{\alpha} (x_2 - y_2)^{\beta}}{r^{\gamma}} d\Omega,$$

over polygonal elements Ω_j , $j = \overline{1, N}$ should be regularized and calculated.

In (Zozulya and Gonzalez-Chi 1999) it has been shown that for regularization of the divergent integrals the second Green theorem may be used

$$\int_{\Omega} \varphi(\mathbf{x}) \Delta g(\mathbf{x}) d\Omega = \int_{\Omega} g(\mathbf{x}) \Delta \varphi(\mathbf{x}) d\Omega + \int_{\partial\Omega} [\varphi(\mathbf{x}) \partial_n g(\mathbf{x}) - g(\mathbf{x}) \partial_n \varphi(\mathbf{x})] dl,$$

where $\partial\Omega$ is contour of area Ω .

Particularly for weakly singular integrals it has been obtained the following regular representations

$$J_1^{0,0}(\mathbf{x}, \Omega_j) = - \int_{\partial\Omega_j} \left[\frac{x_1 - y_1}{r} n_1(\mathbf{y}) + \frac{x_2 - y_2}{r} n_2(\mathbf{y}) \right] d\mathbf{y},$$

$$J_3^{1,1}(\mathbf{x}, \Omega_j) = \frac{1}{5} \int_{\partial\Omega_j} \left[\frac{x_1 - y_1}{r} n_2(\mathbf{y}) + \frac{x_2 - y_2}{r} n_1(\mathbf{y}) - \right. \\ \left. - 3 \frac{(x_1 - y_1)^2 (x_2 - y_2)}{r^3} n_1(\mathbf{y}) - 3 \frac{(x_1 - y_1)(x_2 - y_2)^2}{r^3} n_2(\mathbf{y}) \right] d\mathbf{y},$$

$$J_3^{2,0}(\mathbf{x}, \Omega_j) = \\ \frac{1}{5} \int_{\partial\Omega_j} \left[-2 \frac{x_2 - y_2}{r} n_2(\mathbf{y}) - 3 \frac{(x_1 - y_1)^3}{r^3} n_1(\mathbf{y}) - 3 \frac{(x_1 - y_1)^2 (x_2 - y_2)}{r^3} n_2(\mathbf{y}) \right] d\mathbf{y},$$

$$J_3^{0,2}(\mathbf{x}, \Omega_j) = \\ \frac{1}{5} \int_{\partial\Omega_j} \left[-2 \frac{x_1 - y_1}{r} n_1(\mathbf{y}) - 3 \frac{(x_2 - y_2)^3}{r^3} n_2(\mathbf{y}) - 3 \frac{(x_1 - y_1)(x_2 - y_2)^2}{r^3} n_1(\mathbf{y}) \right] d\mathbf{y}.$$

For hypersingular kernels it has been obtained the following regular representations

$$J_3^{0,0}(\mathbf{x}, \Omega_j) = \int_{\partial\Omega_j} \left[\frac{x_1 - y_1}{r^3} n_1(\mathbf{y}) + \frac{x_2 - y_2}{r^3} n_2(\mathbf{y}) \right] d\mathbf{y},$$

$$J_5^{1,1}(\mathbf{x}, \Omega_j) = \frac{1}{5} \int_{\partial\Omega_j} \left[\frac{x_1 - y_1}{r^3} n_2(\mathbf{y}) + \frac{x_2 - y_2}{r^3} n_1(\mathbf{y}) - \right. \\ \left. - \frac{(x_1 - y_1)^2 (x_2 - y_2)}{r^5} n_1(\mathbf{y}) - \frac{(x_1 - y_1)(x_2 - y_2)^2}{r^5} n_2(\mathbf{y}) \right] d\mathbf{y},$$

$$J_5^{2,0}(\mathbf{x}, \Omega_j) = \\ \frac{1}{5} \int_{\partial\Omega_j} \left[4 \frac{x_1 - y_1}{r^3} n_1(\mathbf{y}) + 2 \frac{x_2 - y_2}{r^3} n_2(\mathbf{y}) - \frac{(x_1 - y_1)^3}{r^5} n_1(\mathbf{y}) - \frac{(x_1 - y_1)^2 (x_2 - y_2)}{r^5} n_2(\mathbf{y}) \right] d\mathbf{y},$$

$$J_5^{0,2}(\mathbf{x}, \Omega_j) = \frac{1}{5} \int_{\partial\Omega_j} \left[4 \frac{x_2 - y_2}{r^3} n_2(\mathbf{y}) + 2 \frac{x_1 - y_1}{r^3} n_1(\mathbf{y}) - \frac{(x_2 - y_2)^3}{r^5} n_2(\mathbf{y}) - \frac{(x_1 - y_1)(x_2 - y_2)^2}{r^5} n_1(\mathbf{y}) \right] d\mathbf{y}.$$

In (Zozulya and Gonzalez-Chi 1999) it also has been presented the equations that permit the easy calculation of the weakly singular, the singular and the hypersingular integrals over any convex polygonal element with s angles.

We ave following convenient expressions for calculation above mentioned weakly singular integrals

$$J_1^{0,0}(\mathbf{x}, \Omega_j) = \sum_{l=1}^s \sqrt{A_l} [-x_1 n_{l,1} - (x_2 - \beta_l) n_{l,2}] I_{1,0}(\Gamma_{j,l}),$$

$$J_3^{1,1}(\mathbf{x}, \Omega_j) = \sum_{l=1}^s \frac{\sqrt{A_l}}{5} \left\{ -3 [x_1^2 (x_2 - \beta_l) n_{l,1} + x_1 (x_2 - \beta_l)^2 n_{l,2}] I_{3,0}(\Gamma_{j,l}) + \right.$$

$$+ 3 [(\alpha_l x_1^2 + 2x_1 (x_2 - \beta_l)) n_{l,1} + (2\alpha_l x_1 (x_2 - \beta_l) + (x_2 - \beta_l)^2) n_{l,2}] I_{3,1}(\Gamma_{j,l}) +$$

$$+ 3 [(\beta_l - x_2 - 2\alpha_l x_1) n_{l,1} - (\alpha_l^2 x_1 + 2\alpha_l (x_2 - \beta_l)) n_{l,2}] I_{3,2}(\Gamma_{j,l}) +$$

$$\left. + [(x_2 - \beta_l) n_{l,1} + x_1 n_{l,2}] I_{1,0}(\Gamma_{j,l}) + [\alpha_l n_{l,1} + n_{l,2}] I_{1,1}(\Gamma_{j,l}) \right\}$$

$$J_3^{2,0}(\mathbf{x}, \Omega_j) = \sum_{l=1}^s \frac{\sqrt{A_l}}{5} \left\{ -3 [x_1^3 n_{l,1} - x_1^2 (x_2 - \beta_l) n_{l,2}] I_{3,0}(\Gamma_{j,l}) + \right.$$

$$+ 3 [3x_1^2 n_{l,1} + x_1 (2x_2 - 2\beta_l + \alpha_l x_1) n_{l,2}] I_{3,1}(\Gamma_{j,l}) - 2(x_2 - \beta_l) n_{l,2} I_{1,0}(\Gamma_{j,l}) +$$

$$\left. + 2\alpha_l n_{l,2} I_{1,1}(\Gamma_{j,l}) + 3 [3x_1 n_{l,1} - (x_2 - \beta_l + 2\alpha_l x_1) n_{l,2}] I_{3,2}(\Gamma_{j,l}) \right\}$$

$$J_3^{0,2}(\mathbf{x}, \Omega_j) = \sum_{l=1}^s \frac{\sqrt{A_l}}{5} \left\{ -3 [x_1 (x_2 - \beta_l)^2 n_{l,1} - (x_2 - \beta_l)^3 n_{l,2}] I_{3,0}(\Gamma_{j,l}) + \right.$$

$$+ 3 [(2\alpha_l x_1 (x_2 - \beta_l) + (x_2 - \beta_l)^2) n_{l,1} + 3\alpha_l (x_2 - \beta_l)^2 n_{l,2}] I_{3,1}(\Gamma_{j,l}) - 2(x_2 - \beta_l) n_{l,2} I_{1,0}(\Gamma_{j,l}) +$$

$$\left. + 2\alpha_l n_{l,2} I_{1,1}(\Gamma_{j,l}) - 3 [(\alpha_l^2 x_1 + 2\alpha_l (x_2 - \beta_l)) n_{l,1} + 3\alpha_l^2 (x_2 - \beta_l) n_{l,2}] I_{3,2}(\Gamma_{j,l}) \right\}$$

and for hypersingular integrals

$$J_3^{0,0}(\mathbf{x}, \Omega_j) = \sum_{l=1}^s \sqrt{A_l} [x_1 n_{l,1} + (x_2 - \beta_l) n_{l,2}] I_{3,0}(\Gamma_{j,l}),$$

$$\begin{aligned}
J_5^{1,1}(\mathbf{x}, \Omega_j) = & \sum_{l=1}^s \frac{\sqrt{A_l}}{5} \left\{ [(x_2 - \beta_l)n_{l,1} + x_1 n_{l,2}] I_{3,0}(\Gamma_{j,l}) - \right. \\
& - [\alpha_l n_{l,1} + n_{l,2}] I_{3,1}(\Gamma_{j,l}) - [x_1^2 (x_2 - \beta_l)n_{l,1} + x_1 (x_2 - \beta_l)^2 n_{l,2}] I_{5,0}(\Gamma_{j,l}) - \\
& - [-x_1 (2(x_2 - \beta_l) + \alpha_l x_1)n_{l,1} + (2\alpha_l \beta_l x_1 + 2\beta_l x_2 - 2\alpha_l x_1 x_2 - x_2^2 - \beta_l^2)n_{l,2}] I_{5,1}(\Gamma_{j,l}) + \\
& \left. - [(x_2 - \beta_l - 2\alpha_l x_1)n_{l,1} + \alpha_l (2x_2 + \alpha_l x_1 - 2\beta_l)n_{l,2}] I_{5,2}(\Gamma_{j,l}) \right\}
\end{aligned}$$

$$\begin{aligned}
J_5^{2,0}(\mathbf{x}, \Omega_j) = & \sum_{l=1}^s \frac{\sqrt{A_l}}{5} \left\{ 2[2x_1 n_{l,1} + (x_2 - \beta_l)n_{l,2}] I_{3,0}(\Gamma_{j,l}) - \right. \\
& - 2n_{l,1} I_{3,1}(\Gamma_{j,l}) - [x_1^3 n_{l,1} + x_1^2 (x_2 - \beta_l)n_{l,2}] I_{5,0}(\Gamma_{j,l}) + \\
& \left. + [3x_1^2 n_{l,1} + x_1 (2(x_2 - \beta_l) + \alpha_l x_1)n_{l,2}] I_{5,1}(\Gamma_{j,l}) - [3x_1 n_{l,1} + (x_2 + 2\alpha_l x_1 - \beta_l)n_{l,2}] I_{5,2}(\Gamma_{j,l}) \right\}
\end{aligned}$$

$$J_5^{0,2}(\mathbf{x}, \Omega_j) = J_3^{0,0}(\mathbf{x}, \Omega_j) - J_5^{2,0}(\mathbf{x}, \Omega_j).$$

Note, that integrals $I_{a,b}(\Gamma_{j,l})$ are regular ones and they have following form

$$I_{a,b}(\Gamma_{j,l}) = \int_{\Gamma_{j,l}} \frac{y^b dy}{(\sqrt{A_l y^2 + B_l y + C_l})^a}$$

where $\Gamma_{j,l}$ is the l -th side of contour $\partial\Omega_j$ given by the equation of the line with coefficients α_l, β_l ; $A_l = 1 + \alpha_l^2, B_l = 2(\alpha_l \beta_l - x_1 - \alpha_l x_2), C_l = x_1^2 + (x_2 - \beta_l)^2$; $n_{l,1}$ and $n_{l,2}$ are components of the unit vector normal to the $\Gamma_{j,l}$.

Integrals $I_{a,b}(\Gamma_{j,l})$ could be easy calculated analytically or numerically, using any quadrature formulas, for example, the Gauss formulas.

2.5. Problem for the domain with the penny-shaped inclusion, boundary integral equations and the system of linear equations

In accordance with previous results, in three-dimensional case we have following integral identities of the Somigliano type:

$$\frac{1}{2}u_i(\mathbf{y}) = \int_{\partial V} (p_j(\mathbf{x})U_{ij}(\mathbf{x}-\mathbf{y}) - u_j(\mathbf{x})W_{ij}(\mathbf{x},\mathbf{y}))d\mathbf{x} + \int_V b_j(\mathbf{x})U_{ij}(\mathbf{x}-\mathbf{y})d\mathbf{x}, \quad (2.5.1)$$

and

$$\frac{1}{2}p_i(\mathbf{y}) = \int_{\partial V} (p_j(\mathbf{x})K_{ij}(\mathbf{x},\mathbf{y}) - u_j(\mathbf{x})F_{ij}(\mathbf{x},\mathbf{y}))d\mathbf{x} + \int_V b_j(\mathbf{x})K_{ij}(\mathbf{x}-\mathbf{y})d\mathbf{x}, \quad (2.5.2)$$

for $\mathbf{y} \in \partial V$ and $i = \overline{1,3}$.

The integral kernels $U_{ij}(\mathbf{x}-\mathbf{y})$, $W_{ij}(\mathbf{x},\mathbf{y})$, $K_{ij}(\mathbf{x},\mathbf{y})$, $F_{ij}(\mathbf{x},\mathbf{y})$ are fundamental solutions of the static theory of the elasticity (See section 2.2).

Let us consider the cylindrical domain V_1 with the central penny-shaped inclusion V_2 (see Figure 2.5.1).

In order to solve the problem considered we use the boundary elements method with constant approximation on every boundary element Ω_j . To simplify the problem we use for the numerical solution the system of boundary integral equations (2.5.1). In the absence of body forces, we obtain the following approximately system of equations for \mathbf{y}^i , $i = \overline{1,N}$:

$$\begin{cases} \frac{1}{2}u_1(\mathbf{y}^i) + \sum_{j=1}^3 \sum_{l=1}^N \int_{\partial V} W_{1j}(\mathbf{x}^l, \mathbf{y}^i) u_j(\mathbf{x}^l) d\mathbf{x} = \sum_{j=1}^3 \sum_{l=1}^N \int_{\partial V} U_{1j}(\mathbf{x}^l - \mathbf{y}^i) d\mathbf{x} p_j(\mathbf{x}^l) \\ \frac{1}{2}u_2(\mathbf{y}^i) + \sum_{j=1}^3 \sum_{l=1}^N \int_{\partial V} W_{2j}(\mathbf{x}^l, \mathbf{y}^i) u_j(\mathbf{x}^l) d\mathbf{x} = \sum_{j=1}^3 \sum_{l=1}^N \int_{\partial V} U_{2j}(\mathbf{x}^l - \mathbf{y}^i) d\mathbf{x} p_j(\mathbf{x}^l) \\ \frac{1}{2}u_3(\mathbf{y}^i) + \sum_{j=1}^3 \sum_{l=1}^N \int_{\partial V} W_{3j}(\mathbf{x}^l, \mathbf{y}^i) u_j(\mathbf{x}^l) d\mathbf{x} = \sum_{j=1}^3 \sum_{l=1}^N \int_{\partial V} U_{3j}(\mathbf{x}^l - \mathbf{y}^i) d\mathbf{x} p_j(\mathbf{x}^l) \end{cases} \quad (2.5.3)$$

where points \mathbf{x}^j and \mathbf{y}^j are located in the geometrical center of the plain boundary element Ω_j , and the boundary surface $\partial V = \partial V_1 \cup \partial V_2 \cup \partial V_3 \cup \partial V_4 \cup \partial V_5$.

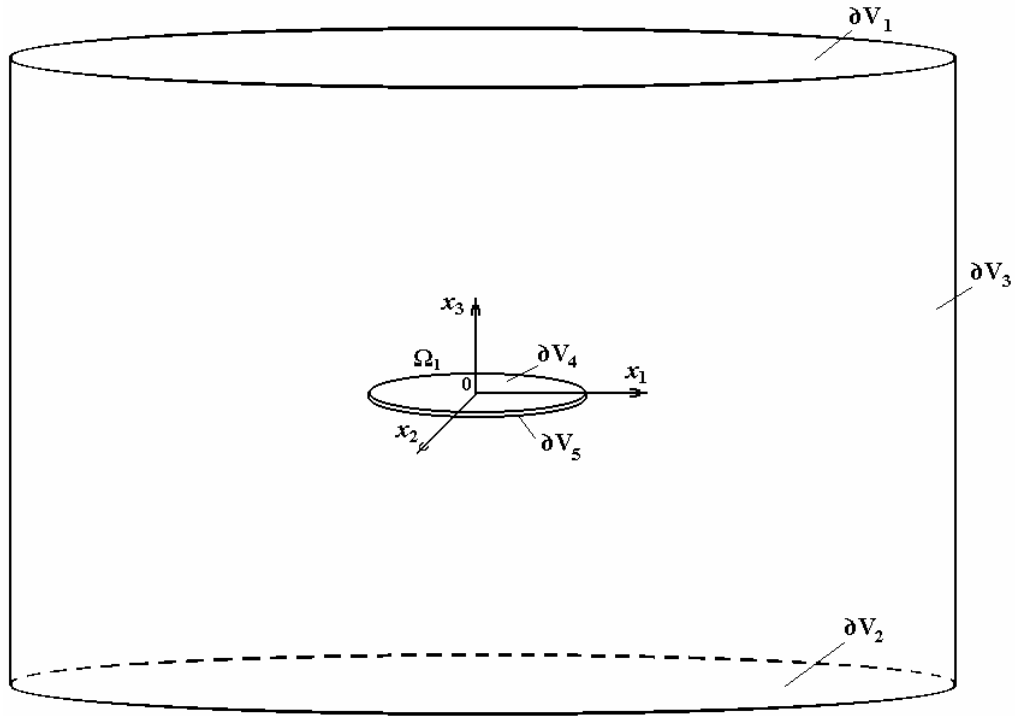


Figure 2.5.1

In order to evaluate the integral kernels $U_{ij}(\mathbf{x}-\mathbf{y})$, $W_{ij}(\mathbf{x},\mathbf{y})$ from system (2.5.3) we use the corresponding results from section 2.2.

Therefore, we have

$$U_{11}(\mathbf{x}-\mathbf{y}) = \frac{1}{16(1-\nu)\pi\rho c_2^2 r} \left\{ 3 - 4\nu - \frac{(x_1 - y_1)^2}{r} \right\},$$

$$U_{12}(\mathbf{x}-\mathbf{y}) = U_{21}(\mathbf{x}-\mathbf{y}) = -\frac{1}{16(1-\nu)\pi\rho c_2^2 r} \frac{(x_1 - y_1)(x_2 - y_2)}{r},$$

$$U_{13}(\mathbf{x}-\mathbf{y}) = U_{31}(\mathbf{x}-\mathbf{y}) = -\frac{1}{16(1-\nu)\pi\rho c_2^2 r} \frac{(x_1 - y_1)(x_3 - y_3)}{r},$$

$$U_{22}(\mathbf{x}-\mathbf{y}) = \frac{1}{16(1-\nu)\pi\rho c_2^2 r} \left\{ 3 - 4\nu - \frac{(x_2 - y_2)^2}{r} \right\},$$

$$U_{23}(\mathbf{x}-\mathbf{y}) = U_{32}(\mathbf{x}-\mathbf{y}) = -\frac{1}{16(1-\nu)\pi\rho c_2^2 r} \frac{(x_2 - y_2)(x_3 - y_3)}{r},$$

$$U_{33}(\mathbf{x} - \mathbf{y}) = \frac{1}{16(1-\nu)\pi\rho c_2^2 r} \left\{ 3 - 4\nu - \frac{(x_3 - y_3)^2}{r} \right\}.$$

Kernels $W_{ij}(\mathbf{x}, \mathbf{y})$ have been obtained from kernels $U_{ij}(\mathbf{x} - \mathbf{y})$ using the space derivation, and we have:

$$W_{ij}(\mathbf{x}, \mathbf{y}) = \frac{1}{\alpha\pi} \left\{ \left[\frac{\partial\psi}{\partial r} - \frac{\chi}{r} \right] \left(\delta_{ij} \frac{\partial r}{\partial n(\mathbf{x})} + n_j(\mathbf{x}) \frac{\partial r}{\partial x_i} \right) - \frac{2\chi}{r} \left[n_i(\mathbf{x}) \frac{\partial r}{\partial x_j} - 2 \frac{\partial r}{\partial x_i} \frac{\partial r}{\partial x_j} \frac{\partial r}{\partial n(\mathbf{x})} \right] + \left(\frac{c_1^2}{c_2^2} - 2 \right) n_i(\mathbf{x}) \frac{\partial r}{\partial x_j} \frac{\partial\psi}{\partial r} \right\},$$

where $c_1 = \sqrt{(\lambda + 2\mu)/\rho}$ is the velocity of the longitudinal wave.

So, we have for $\mathbf{x} \in \partial V_1 \cup \partial V_2 \cup \partial V_4 \cup \partial V_5$:

$$W_{11}(\mathbf{x}, \mathbf{y}) = \mp \frac{(x_3 - y_3)}{2\alpha\pi(1-\nu)r^2} \left\{ \frac{1}{2} \left(\frac{3-4\nu}{r} + 1 \right) - 2 \frac{(x_1 - y_1)^2}{r^2} \right\},$$

where the sign \mp depends on the orientation of the external normal unit vector, and for $\mathbf{x} \in \partial V_3$:

$$W_{11}(\mathbf{x}, \mathbf{y}) = \frac{-1}{2\alpha\pi(1-\nu)r^2} \left\{ \frac{1}{2} \left(\frac{3-4\nu}{r} + 1 \right) \left[2n_1(\mathbf{x})(x_1 - y_1) + n_2(\mathbf{x})(x_2 - y_2) \right] + (x_1 - y_1) \left[n_1(\mathbf{x}) - 2 \frac{(x_1 - y_1)}{r^2} \left[n_1(\mathbf{x})(x_1 - y_1) + n_2(\mathbf{x})(x_2 - y_2) \right] \right] + \frac{3-4\nu}{2} \left(\frac{c_1^2}{c_2^2} - 2 \right) n_1(\mathbf{x}) \frac{(x_1 - y_1)}{r^3} \right\}.$$

Analogously, we have for $\mathbf{x} \in \partial V_1 \cup \partial V_2 \cup \partial V_4 \cup \partial V_5$:

$$W_{12}(\mathbf{x}, \mathbf{y}) = \pm \frac{(x_1 - y_1)(x_2 - y_2)(x_3 - y_3)}{2\alpha\pi(1-\nu)r^4},$$

and for $\mathbf{x} \in \partial V_3$:

$$W_{12}(\mathbf{x}, \mathbf{y}) = \frac{-1}{4\alpha\pi(1-\nu)r^2} \{n_2(\mathbf{x})(x_1 - y_1) + 2n_1(\mathbf{x})(x_2 - y_2) + \frac{(3-4\nu)}{r}n_2(\mathbf{x})(x_1 - y_1) + \frac{(3-4\nu)}{r} \left(\frac{c_1^2}{c_2^2} - 2 \right) n_1(\mathbf{x})(x_2 - y_2) - \frac{2}{r^2}(x_1 - y_1)(x_2 - y_2)[n_1(\mathbf{x})(x_1 - y_1) + n_2(\mathbf{x})(x_2 - y_2)]\}.$$

For $\mathbf{x} \in \partial V_1 \cup \partial V_2 \cup \partial V_4 \cup \partial V_5$:

$$W_{13}(\mathbf{x}, \mathbf{y}) = \mp \frac{(x_1 - y_1)}{4\alpha\pi(1-\nu)r^2} \left\{ 1 + \frac{(3-4\nu)}{r} - \frac{2}{r^2}(x_3 - y_3)(x_3 - y_3) \right\},$$

and for $\mathbf{x} \in \partial V_3$:

$$W_{13}(\mathbf{x}, \mathbf{y}) = \frac{-1}{4\alpha\pi(1-\nu)r^2} \left\{ 2n_1(\mathbf{x})(x_3 - y_3) \frac{(3-4\nu)}{r} \left(\frac{c_1^2}{c_2^2} - 2 \right) n_1(\mathbf{x})(x_3 - y_3) - \frac{2}{r^2}(x_1 - y_1)(x_3 - y_3)[n_1(\mathbf{x})(x_1 - y_1) + n_2(\mathbf{x})(x_2 - y_2)] \right\}.$$

For $\mathbf{x} \in \partial V_1 \cup \partial V_2 \cup \partial V_4 \cup \partial V_5$:

$$W_{21}(\mathbf{x}, \mathbf{y}) = \pm \frac{(x_1 - y_1)(x_2 - y_2)(x_3 - y_3)}{2\alpha\pi(1-\nu)r^4},$$

and for $\mathbf{x} \in \partial V_3$:

$$W_{21}(\mathbf{x}, \mathbf{y}) = \frac{-1}{4\alpha\pi(1-\nu)r^2} \{n_1(\mathbf{x})(x_2 - y_2) + 2n_2(\mathbf{x})(x_1 - y_1) + \frac{(3-4\nu)}{r}n_1(\mathbf{x})(x_2 - y_2) + \frac{(3-4\nu)}{r} \left(\frac{c_1^2}{c_2^2} - 2 \right) n_2(\mathbf{x})(x_1 - y_1) - \frac{2}{r^2}(x_1 - y_1)(x_2 - y_2)[n_1(\mathbf{x})(x_1 - y_1) + n_2(\mathbf{x})(x_2 - y_2)]\}.$$

For $\mathbf{x} \in \partial V_1 \cup \partial V_2 \cup \partial V_4 \cup \partial V_5$:

$$W_{22}(\mathbf{x}, \mathbf{y}) = \mp \frac{(x_3 - y_3)}{2\alpha\pi(1-\nu)r^2} \left\{ \left(\frac{3-4\nu}{r} + 1 \right) + 2 \frac{(x_2 - y_2)^2(x_3 - y_3)}{r^2} \right\},$$

and for $\mathbf{x} \in \partial V_3$:

$$W_{22}(\mathbf{x}, \mathbf{y}) = \frac{-1}{2\alpha\pi(1-\nu)r^2} \left\{ \left(\frac{3-4\nu}{r} + 1 \right) [n_1(\mathbf{x})(x_1 - y_1) + 2n_2(\mathbf{x})(x_2 - y_2)] - \right. \\ \left. (x_2 - y_2) \left[n_2(\mathbf{x}) - 2 \frac{(x_2 - y_2)}{r^2} [n_1(\mathbf{x})(x_1 - y_1) + n_2(\mathbf{x})(x_2 - y_2)] \right] - \right. \\ \left. \frac{3-4\nu}{4(1-\nu)} \left(\frac{c_1^2}{c_2^2} - 2 \right) n_2(\mathbf{x}) \frac{(x_2 - y_2)}{r^3} \right\}.$$

For $\mathbf{x} \in \partial V_1 \cup \partial V_2 \cup \partial V_4 \cup \partial V_5$:

$$W_{23}(\mathbf{x}, \mathbf{y}) = \mp \frac{(x_2 - y_2)}{4\alpha\pi(1-\nu)r^2} \left\{ 1 + \frac{(3-4\nu)}{r} - \frac{2}{r^2} (x_3 - y_3)(x_3 - y_3) \right\},$$

and for $\mathbf{x} \in \partial V_3$:

$$W_{23}(\mathbf{x}, \mathbf{y}) = \frac{-(x_3 - y_3)}{4\alpha\pi(1-\nu)r^2} \left\{ 2n_2(\mathbf{x}) + \frac{(3-4\nu)}{r} \left(\frac{c_1^2}{c_2^2} - 2 \right) n_2(\mathbf{x}) - \right. \\ \left. \frac{2}{r^2} (x_2 - y_2) [n_1(\mathbf{x})(x_1 - y_1) + n_2(\mathbf{x})(x_2 - y_2)] \right\}.$$

For $\mathbf{x} \in \partial V_1 \cup \partial V_2 \cup \partial V_4 \cup \partial V_5$:

$$W_{31}(\mathbf{x}, \mathbf{y}) = \mp \frac{(x_1 - y_1)}{4\alpha\pi(1-\nu)r^2} \left\{ 2 + \frac{(3-4\nu)}{r} \left(\frac{c_1^2}{c_2^2} - 2 \right) - \frac{2}{r^2} (x_3 - y_3)(x_3 - y_3) \right\},$$

and for $\mathbf{x} \in \partial V_3$:

$$W_{31}(\mathbf{x}, \mathbf{y}) = \frac{-(x_3 - y_3)}{4\alpha\pi(1-\nu)r^2} \left\{ n_1(\mathbf{x}) + \frac{(3-4\nu)}{r} n_1(\mathbf{x}) - \right. \\ \left. \frac{2}{r^2} (x_1 - y_1) [n_1(\mathbf{x})(x_1 - y_1) + n_2(\mathbf{x})(x_2 - y_2)] \right\}.$$

For $\mathbf{x} \in \partial V_1 \cup \partial V_2 \cup \partial V_4 \cup \partial V_5$:

$$W_{32}(\mathbf{x}, \mathbf{y}) = \mp \frac{(x_2 - y_2)}{4\alpha\pi(1-\nu)r^2} \left\{ 2 + \frac{(3-4\nu)}{r} \left(\frac{c_1^2}{c_2^2} - 2 \right) - \frac{2}{r^2} (x_3 - y_3)^2 \right\},$$

and for $\mathbf{x} \in \partial V_3$:

$$W_{32}(\mathbf{x}, \mathbf{y}) = \frac{-(x_3 - y_3)}{4\alpha\pi(1-\nu)r^2} \left\{ n_2(\mathbf{x}) + \frac{(3-4\nu)}{r} n_2(\mathbf{x}) - \frac{2}{r^2} (x_2 - y_2) [n_1(\mathbf{x})(x_1 - y_1) + n_2(\mathbf{x})(x_2 - y_2)] \right\}.$$

For $\mathbf{x} \in \partial V_1 \cup \partial V_2 \cup \partial V_4 \cup \partial V_5$:

$$W_{33}(\mathbf{x}, \mathbf{y}) = \mp \frac{(x_3 - y_3)}{2\alpha\pi(1-\nu)r^2} \left\{ \frac{1}{2} \left(\frac{3-4\nu}{r} + 1 \right) 2 + \left[1 - 2 \frac{(x_3 - y_3)^2}{r^2} \right] + \frac{3-4\nu}{2r} \left(\frac{c_1^2}{c_2^2} - 2 \right) \right\},$$

and for $\mathbf{x} \in \partial V_3$:

$$W_{33}(\mathbf{x}, \mathbf{y}) = \frac{n_1(\mathbf{x})(x_1 - y_1) + n_2(\mathbf{x})(x_2 - y_2)}{2\alpha\pi(1-\nu)r^2} \left\{ 2 \frac{(x_3 - y_3)^2}{r^2} - \frac{1}{2} \left(\frac{3-4\nu}{r} + 1 \right) \right\}.$$

Current status of the project.

No evidence of delays is recorded; the current technical stage of the Project may be regarded as being in a full accordance with schedule.

Summary of personnel commitment.

1. Dr. B. Maslov, Ph.D. V. Bystrov and Ph.D. M.Lavrenyuk are involved into investigation of the stress and strain concentration problem for n -coated ellipsoidal inclusion embedded in non-linear elastic matrix. The refined approach of conditional-moment method (CMM) with hypothesis of multi-particle effective field method (MFFM) proposed here to investigate local stress fields in inclusions with n -layered coatings. We consider here a non linear elastic composite medium with stress free strains, which consists of a homogeneous matrix containing a homogeneous and statistically uniform random set of coated ellipsoidal or spheroidal inclusions having all the same form, orientation and mechanical properties. The user interface "Micro-mechanics of fiber reinforced bounded and unbounded solids: effective local and non-local thermo-elastic properties, stress concentration factors and edge effect" is developed, being a part of the entire program complex for numerical solution of multi-scale static problems of material with inclusions. The abbreviation of the program complex is MSSPMI (Multi-Scale Static Problems of Materials with Inclusions). The complex is developed in Lahey/Fujitsu Fortran 95 LF95 environment by use of user-interface and graphics development tool-set Winterector Starter Kit (WiSK). Separate applied programs are developed by use of programming systems Delphi 6. The environment of a program complex is integrated at a level of a source code with applied programs which are developed in language LF95, initiates start of programs and access to the input and output data of the programs developed with use of other programming units.

2. Dr. V. Kushch, Ph.D. V. Dutka and S. Shmegeera deal with the following tasks. An accurate analytical multipole-expansion based solution is obtained for an elastic half-space containing a finite array of inclusions in 2D (long fibers) as well as in 3D (spherical inclusions); the relevant computer codes are under development; the edge effect on micro stress concentration being investigated is expressed as the solutions that will serve as a benchmark for a numerical, integral equations based method. Also, the multipole expansion technique can be incorporated into a general scheme of the Boundary Element Method to improve its numerical efficiency.

3. Dr. V. Mykhas'kiv, O. Stepanyuk and B. Stasjuk are involved in to the execution of the next milestones. The problem of boundary (volume) integral formulations of 3-D static and dynamic problems of inclusion interaction is considered. By using the general reciprocity principles and fundamental solutions, the boundary integral representations of elastic displacements and stresses in statically loaded solid consisting of 3-D matrix with N interacting volumetric inclusions are constructed. The densities of involved integrals characterize the displacements as well as tractions at the interfaces. To define these densities the systems of $6N$ boundary integral equations of the second kind are obtained by satisfaction of contact conditions at the interfaces. The alternative volume integral equations are also deduced for this type of problems resting on the effective body force distribution in the inclusion areas. The boundary integral formulations of 3-D problems of interaction between crack-like inhomogeneities and thin-walled inclusions in an elastic wave field are proposed.

4. Dr. V. Zozulya, Ph.D. O. Lukin and Ph.D. O. Menshikov have developed a general approach to creation of powerful numerical tool for the micro-macro solution of elastostatic 2-D and 3-D problem of multiple inclusions of different scale interaction in micromechanics of fiber reinforced bounded and unbounded solids is made. This implies a creation of new and adoption of know relations of BIE and VIE for the specific problem of numerical modeling fiber reinforced elastic composite materials, defining analytical expressions for corresponding fundamental solutions and investigating their properties.

Description of travels.

As stated in the Work plan of the P-110 Project, alongside with research activities on site the appropriate arrangements were made to register for coming conferences to present and discuss the achievements made in the framework of the Project in the scientific society. The paper of Dr. B. Maslov entitled "Nonlinear overall viscoelastic properties of the random multi-component media" was presented at the 21st International Congress of Theoretical and Applied Mechanics, (ICTAM04), which took place in August 15-20, 2004 in Warsaw.

Information about major equipment and materials acquired, other direct costs, related to the project.

- The purchase of equipment and all travel expenses are in full agreement with what was previously stated in the work plan with no overdraft occurring.
- All shifts in participants' payment and changes of equipment costs that were officially agreed during the reported period of working on the P-110 Project are provided in the cumulative **Table Redirection** below, which keeps all changes in chronological order.

Table Redirection

Reference documents & date (1)	New requested category, or old category with new cost (2)	Requested cost (new) (3)	Original (old) category (4)	Estimated cost (old) (5)	Redirected cost (6) old – new
Quarter 2					
Invoice number 1718, 27.11.2003	4-Equipment Non-Capital #1 Pentium 4 computer, peripherals	1636	4-Equipment Non-Capital #1 Pentium 4 computer, periphery	1497	-139
	4-Equipment Non-Capital #2 Pentium 4 computer, peripherals	1358	4-Equipment Non-Capital #2 Pentium 4 computer, periphery	1497	+139
Total by L01					0
Quarter 3					
Letter of Redirection L03 18 March, 2003	3-Pers. № 5, Qtr3-Qtr8 Grants of Menshykov Oleksandr	0	3-Pers. № 5, Qtr3-Qtr8 Grants of Menshykov Oleksandr	2100	-2100
	3-Pers. № 10, Qtr1-Qtr8 Grants of Kushch Volodymyr	12100	3-Pers. № 10, Qtr1-Qtr8 Grants of Kushch Volodymyr	10000	+2100
Total by L02					0

Quarter 4					
Letter of Redirection L04 16 April, 2004	3-Pers. № 2, Qtr3-Qtr8 Grants of Zozulya Vladimir	0	3-Pers. № 2, Qtr3-Qtr8 Grants of Zozulya Vladimir	9000	-9000
	3-Pers. № 5, Qtr4-Qtr8 Grants of Kushch Volodymyr	9100	3-Pers. № 5, Qtr4-Qtr8 Grants of Kushch Volodymyr	8000	+1100
	3-Pers. New, Qtr4-Qtr8 Grants of S. Shmegeera	3944	3-Pers. New, Qtr4-Qtr8 Grants of S. Shmegeera	0	+3944
	3-Pers. New, Qtr4-Qtr8 Grants of V. Dutka	3944	3-Pers. New, Qtr4-Qtr8 Grants of V. Dutka	0	+3944
Total by L04					-12
Quarter 5					
Letter of Redirection L05 18 July, 2004	8-Travel. Outside Ukraine № 2, Qtr3 Conference Germany, Bonn	0	8-Travel. Outside Ukraine № 2, Qtr3 Conference Germany, Bonn	200	-200
	8-Travel. Inside Ukraine № 1, Qtr4 Conference Ukraine, Lviv	0	8-Travel. Inside Ukraine № 1, Qtr4 Conference Ukraine, Lviv	55	-55
	8-Travel. Inside Ukraine № 2, Qtr4 Conference Ukraine, Kyiv	0	8-Travel. Inside Ukraine № 2, Qtr4 Conference Ukraine, Kyiv	55	-55
	8-Travel. Outside Ukraine № 3, Qtr4 Conference GB, London	0	8-Travel. Outside Ukraine № 3, Qtr4 Conference GB, London	200	-200
	8-Travel. Outside Ukraine № 4, Qtr4 Conference Greece, Thessaloniki	0	8-Travel. Outside Ukraine № 4, Qtr4 Conference Greece, Thessaloniki	445	-445
	8-Travel. Outside Ukraine № 1, Qtr6 Conference Poland, Warsaw	0	8-Travel. Outside Ukraine № 1, Qtr6 Conference Poland, Warsaw	500	-500
	8-Travel. Outside Ukraine № 2, Qtr8 Conference Germany, Bonn	350	8-Travel. Outside Ukraine № 2, Qtr8 Conference Germany, Bonn	0	+350
	8-Travel. Outside Ukraine № 1, Qtr5 Conference Poland, Warsaw	1105	8-Travel. Outside Ukraine № 1, Qtr5 Conference Poland, Warsaw	0	+1105
Total by L05					0

! Note. After the hard copy of this document, attach copies of technical reports (milestones), completed to the date. Associated files should be collected in the directory "Annual_0/Final". >

Mesomechanics of bounded and unbounded composites: effective local and nonlocal elastic properties, stress concentration factors, and edge effect

Project manager: Maslov Borys Petrovich, Dr. Sc. In Physics and Mathematics
Phone: +380-44-454-7764, Fax: –, E-mail: maslov@inmech.kiev.ua
Institutions: S.P. Timoshenko Institute of Mechanics
Financing parties: USA, European Office of Aerospace Research and Development (EOARD)
Operative commencement date: 01.07.2003
Project duration: 2 years
Project technical area: materials, composites
Reported stage: #8 An approximate estimation of statistical moments of stress concentrator factors in random structure half space
Date of submission: 15.07.2005

Summary

The new approaches in the theory of bounded and unbounded composites have been created that would be a fruitful tools in meso-mechanics of materials. Mathematical multi-paricle model is taken as a foundation. The methods of prediction the elastic and strength properties of the multi-component unidirectional composites with linear and physically non-linear matrix, polymer or metallic is worked out. Random structure of material is adopted. The feature new is that the matrix is assumed be weakened by mesoscopic damage so the effective properties are the function not only of the volume concentrations of the constituents but of the new material parameter reflecting the damage evolution mechanisms. Stress concentration in the composite laminates containing macroscopic risers of holes, cutouts and bolted joints type. An edge effects and adhesive bonded joints are investigated. The boundary element method and MEFM model is involved to obtain the solution of the theory elasticity's problems of the first and second type. Model of singularities at the fiber-matrix interfaces and at the free edge of composite specimen is suggested. The investigation of the stress concentration near macroscopic stress risers in the composites with initial residual stress in components and prediction the life-time and fatigue resistance parameters for materials with micro-structural damage is done. Composite media is assumed consisting of a homogeneous non-linear matrix containing a random set of inclusions of ellipsoidal shape. In contrast to the Finite Element Method the hybrid BIE and VIE method is considered in this project enables one to restrict discretisation to the inclusions only, and an inhomogeneous structure of inclusions presents no problem in the framework of the same numerical scheme as compared to the standard BIE method. A fundamental role of an edge effect yielding to the redistribution of local stresses in a boundary layer region is taken into account. In so doing, the eventual abandonment of so-called hypothesis of statistically homogeneous fields leads to a non-local coupling between statistical averages of stresses and the strains tensors when the statistical average stress is given by an integral of the field quantity weighted by some tensor function, i.e. the non-local effective elastic properties take place. Results of P-110 project give a possibility to assume a local nature of constitutive law of continuum mechanics at the mesoscale based in turn on the assumption that a field scale such as internal stress inhomogeneity infinitely exceeds a material scale.

	Summary	PAGE 1
	Content of technical report for the 1-8 stage	PAGE 2
	Introduction	PAGE 2
	Technical approach	PAGE 2
1	Effective properties, local stresses and edge effects in multi-component materials with n-coated inclusions	PAGE 4
2	The statistical moments of stress concentration factors in continuum estimation	PAGE 61
3	Boundary 3D element analysis in the continuum estimation of effective thermoelastic properties of nanocomposites	PAGE 62
4.	Solution of the two-dimensional micromechanics problem for the fiber reinforced bounded and unbounded solids. Investigation of effective local and nonlocal thermoelastic properties, stress concentration factors, and edge effect	PAGE 92
	Conclusions	PAGE 4 of T08 and in chapters text of FF 110
	References	PAGE 4 of T08 and in text of FF 110

Introduction

The final stage #8 of P-110 project is accomplished. Consideration of random structure composites is performed using the Multi-particle Effective Field Method based on the theory of functions of random variables and Green's functions. Within this method one constructs a hierarchy of statistical moment equations for conditional averages of stresses in the inclusions; the interaction of different inclusions is taken into account. The influence of the ellipsoidal shape, coating structure and orientation on inclusions on the effective local and non-local properties as well as stress concentrator factors will be estimated. For a finite number of interacting inclusions in a half space the iteration hybrid BIE and VIE method is used. Combined with judicious choice of initial approximation of interacting inclusions with random distribution of size, shape, orientation and properties in a half space, the advanced version of Multi-particle Effective Field Method without effective field hypothesis is proposed. A finite-size or infinite composite solid is considered consisting of a homogeneous matrix containing a random set of inclusions of ellipsoidal shape (2-D and 3-D cases). For a finite number of interacting inclusions in a half space the iteration hybrid BIE and VIE method combined with judicious choice of initial approximation of interacting inclusions with random distribution of size, shape, orientation and properties in a half space is used. A proper approximation is provided by solving the multi-particle model problem by means of the multipole expansion technique. To study local and macro stress in a composite of realistic disordered structure with the full account for particle-particle interactions, the advanced multi-particle unit cell model is applied as well. Based on theoretical analysis, the efficient numerical algorithms and relevant computer codes have been developed providing a detailed analysis of stress fields and macroscopic thermoelastic behavior of a wide class of modern composites.

Technical approach

1. Effective properties, local stresses and edge effects in multi-component materials with n -coated inclusions

1.1 Nonlinear meso-mechanics of multi-component materials

Strength and reliability of constructions built up with composite materials is largely a multi-parametrical problem, one of its solutions being the evaluation of stress concentration in microstructure elements and the formulation of

required criteria of durability which correspond to classical methods of strength theory. The service life of units made up of composite materials is dependent on average or maximum cyclic stresses both in matrix, inclusions and coatings. The number of load cycles is very important, amplitude etc. Moreover, many behavior singularities of non-homogeneous material as it was mentioned in can be given only in terms of nonlinear mechanics. More detailed considerations of the mechanical behavior of composite materials require the analysis of the interface between the reinforcement and the matrix. These interfaces may represent: weak interfacial layer due to imperfect bonding between the two phases; inter-diffusion or chemical interaction zones with properties varying through the thickness and/or along the surface at the interface between the two phases. It is well known that the overall effective properties of composite materials are significantly influenced by the properties of the interfaces between the constituents. First, the interface controls the in situ reinforcement's, particles or fibers, strength and hence the strength of the composite. Secondly, defects and damage are likely to occur at the interface (for example debonding, sliding and interface cracks, damage etc.) and these interfacial defects control the degradation of the composite. So to evaluate more accurately the effective properties of a composite non-linear especially, the behavior and structures of interfaces have been taken into consideration. Some type of conditional statistical averages of the general integral equation is being done leading to an infinite system of integral equations. In order to simplify originally the exact system the main hypothesis of MEFM, the so-called effective field hypothesis is applied. The effective linear and nonlinear properties as well as stress concentrator factors are estimated. The accuracy and efficiency of the method are examined through comparison with results obtained from boundary element analysis and some analytical two-dimensional solutions.

The refined approach of conditional-moment method (CMM) with hypothesis of multi-particle effective field method (MEFM) have been proposed here to investigate local stress fields in inclusions with n -layered coatings. We consider here a non linear elastic composite medium with stress free strains, which consists of a homogeneous matrix containing a homogeneous and statistically uniform random set of coated ellipsoidal or spheroidal inclusions having all the same form, orientation and mechanical properties. We are using the refined approach of CMM with the powerful hypothesis of many micro-mechanical methods, according to which each inclusion is located inside a homogeneous so-called effective or equivalent field. It is shown, in the framework of the effective field hypothesis, that from a solution of the classical linear elastic problem with zero stress free strains for the composite the relations for effective non linear, stored energy and average elastic strains inside the components can be found. This way one obtains the generalization of the known formulae, which are exact for two-component composites. The proposed theory is applied to the example of composites reinforced with particles with thin inhomogeneous along inclusion surface coatings. For a single coated inclusion the micro-mechanical approach is based on the Green function technique as well as on the interfacial Hill operators.

2 The statistical moments of stress concentration factors in continuum estimation

2.1 Multi-particle models in study the local micro stress and effective elastic moduli of bounded and unbounded fiber reinforced composites

An accurate solutions have been obtained of the 2D and 3D elastostatics problem for a piece-homogeneous half-space containing a finite array of non-overlapping ellipsoidal inclusions of arbitrary size, aspect ratio, location and elastic properties. The method combines the multipole expansion solution in terms of partial vector solutions of Navier equation for unbounded space with the expansion formulas and integral transforms to obtain a complete solution of the composite half-space problem. By exact satisfaction of all the matrix-inclusion interfaces and flat boundary conditions, a primary boundary-value problem stated on a complicated heterogeneous domain has been reduced to an ordinary well-posed set of linear algebraic equations. Properly chosen structure of general solution provides remarkably simple form of resolving equations and thus an efficient computational algorithm. The advanced structure model of composite half-plane involving a number ellipsoidal inclusions, cavities and/or cracks with an accurate account for the microstructure statistics and interaction effects can be considered in this way. The statistical moments of stress concentration factors in the random structure fibrous composite have been evaluated from the numerical experiments on the generalized periodic structure model being a periodicity unit cell with a number of inclusions. The relevant numerical code has been developed and a wide series of numerical experiments has been performed with 50 to 100 randomly placed inclusions per cell and statistically meaningful results were obtained for the statistical moments of stress concentration factors in phases and interfaces of a random structure fibrous composite. They include, in particular, the second moment of stress playing a fundamental role in a wide class of non-linear elasticity problems, damage initiation, etc. The developed method finds a variety of applications in the composite mechanics: so, combined with the MEFM, a micro mechanical model has been built to predict the thermoelastic behavior of random structure nanocomposites reinforced by the aligned silicate nanoplate clusters of deterministic structure. Numerical (finite element) solution has been obtained of the "solid with a coated high-aspect ratio inclusion" anisotropic elastostatics problem in 2D and 3D. The both platelet-like and rod-like inclusions with

rounded edge were studied. Parametric analysis of the problem has been performed and local as well as averaged stress in and around the inclusion were evaluated. Alternatively, the developed model can be thought as the "correlation hole" scheme in the continuum estimation of effective thermoelastic properties of composites by means of FEA. The developed solution has been applied to evaluate the stress concentrator factors and other relevant local and averaged tensors entering the general theory of the MEFM. The special emphasis was made on the problem of the continuum estimation of effective thermoelastic properties of nanocomposites. For a finite number of interacting inclusions (with the elastic properties estimated from molecular structural model) in a half space, the hybrid FEA and BIE method combined with the multipole expansion method and MEFM will be used for analysis of composites reinforced by the nanoelements with random location, orientation, and arrangement (statistically homogeneous clustered, and functionally graded structure).

Conclusions

The evolution of composites to its anticipated level of importance to society in general significantly depends on the contributions from modeling and simulation. Computational approaches are currently limited to the some kind of scale and cannot deal with the micro-length scales which are traditionally analyzed by a continuum mechanics approach. These main results of P-110 project give a possibility to assume a local nature of constitutive law of continuum mechanics at the mesoscale based in turn on the assumption that a field scale such as internal stress inhomogeneity infinitely exceeds a material scale. So evaluation of the solid mechanics approaches correctness can be contribute to our understanding of the bridging mechanism between the coupled scales. The results of the computer simulation have been executed would be incorporated in a hierarchical model of estimation of effective properties of composites by MEFM which is really a milestone in the progress of mathematical materials science.

References

1. Maslov B.P. Nonlinear overall visco-elastic properties of the random multi-component media. – in Proceeding of 21st International Congress of Theoretical and Applied Mechanics, ICTAM04.-Warsaw.-2004.
2. Maslov B.P., Shatylo L.V. The equation of fatigue crack growth in damaged material with strengthening // Kyiv University Visnyk.-2005.-N1.-pp.32-39.
3. Kushch, V.I., Shmegeera, S.V. and Buryachenko, V.A. (2005). Interacting elliptic inclusions by the method of complex potentials. *International Journal of Solids and Structures*, 42(20), 5491–5512.
4. Kushch, V.I., Shmegeera, S.V. and Buryachenko, V.A. (2005). Elastic equilibrium of a half plane containing a finite array of elliptic inclusions. *International Journal of Solids and Structures*, 42(22).
5. Mykhas'kiv V.V. Transient response of a plane rigid inclusion to an incident wave in an elastic solid // *Wave Motion*. – 2005.- 41, No 2.- P. 133-144.

Dr. B. Maslov

Project manager

Chapter 2

Multi-particle models in study the local micro stress and effective elastic moduli of bounded and unbounded fiber reinforced composites: an analytical approach

2.1 Effective transverse elastic moduli of composites at non-dilute concentration of a random field of aligned fibers

2.1.1 Introduction

The prediction of the behavior of composite materials by the use of mechanical properties of constituents and their microstructure is a central problem of micromechanics, which is evidently reduced to the estimation of stress fields in the constituents. Appropriate, but by no means exhaustive, references for the estimation of effective elastic moduli of statistically homogeneous media are provided by the reviews Buryachenko (2001), Torquato (2002). Accurate estimation of polynomial dependence of effective elastic moduli \mathbf{L}^* on the small concentration c of inclusions is a classical direction in micromechanics. It is well known that for the estimation of the coefficient of the c^2 , it is necessary to take into account both the radial distribution function of inclusion random locations and inclusion-pair interactions within the composite. This problem was accurately solved by Chen and Acrivos (1976) for the identical composites containing the isotropic identical spherical inclusions (see for the references of different approximative solutions Chen and Acrivos (1976) as well as Buryachenko, 2001). The estimation of particle-particle interaction were based on the Boussinesq-Papkovich stress function approach and made use of the multipole expansion technique in which the solutions are expanded into series of spherical harmonic with respect to the centers of two spheres. Numerical results were obtained for well-steered approximation of a radial distribution function of center locations of cavities and rigid spheres. We will consider the generalization of the approach by Chen and Acrivos (1976) for the aligned fiber composites for any ratio of the moduli of two phases.

The particle-particle interaction will be estimated by the Kolosov-Muskhelishvili complex potential method which is simple and powerful tool of solving a variety of the plane linear elastic problems.

The problem we consider is an elastic equilibrium of a fibrous composite half space. Provided the surface load and far stress field do not vary in fiber direction, the problem can be thought as two-dimensional (2D), namely, an elastic half plane with a finite number $N > 1$ of circular inclusions. And, likewise the majority of 2D linear elasticity problems, the powerful method of complex potentials can be applied here to obtain an accurate analytical solution.

The surveys of the work done up to the date can be found in the book by Savin (1961) and in the comprehensive review by Buryachenko (2001), among others. What is somewhat surprising, after more than 80 years after the pioneering work by Jeffery (1920) had been published, this problem continues to be relevant and attracts attention of investigators. Among the recent publications, we mention the papers by Kooi and Verruijt (2001) and Verruijt (1998) who used the method of complex potentials and applied conformal mapping to reduce the half plane with hole problem to the problem for circular ring. The principal drawback of this approach is that, as well as in the Jeffery's solution, only a single inclusion problem can be considered by this way. Dong et al. (2004) tested three numerical methods on the problem for a half plane containing two circular inclusions. Although only well-separated and distant from the flat boundary inclusions were considered, discrepancy in the numerical data generated by the different methods compared has been observed.

In the present section, the complete analytical solution has been obtained for a half plane containing a finite or infinite quasi-periodic array of arbitrarily placed non-overlapping circular inclusions. The stress state of inhomogeneous half plane is governed by the uniform far stress field and arbitrary load applied at the flat boundary. To get an accurate solution of the problem, the Kolosov-Muskhelishvili method of complex potentials (Muskhelishvili, 1953) has been combined with the Fourier integral transforms technique. By exact satisfaction of all the boundary conditions, the primary boundary-value problem is reduced to an ordinary well-posed set of linear algebraic equations and this provides high computation efficiency and accuracy of the method developed.

2.1.2 Preliminaries

In the mesodomain w with space dimensionality $d = 2$ containing a set $X = (V_i, \mathbf{x}_i, \omega_i)$, ($i = 1, 2, \dots$) of identical circle aligned fibers v_i with centers x_i , radii a , a characteristic function W is defined; $V(\mathbf{x}) = \sum V_i(\mathbf{x})$, and $V_i(\mathbf{x})$ is a characteristic function of v_i which equals 1 at $\mathbf{x} \in v_i$ and 0 otherwise, ($i = 1, 2, \dots$). Here and in the following the upper index (k) numbers the components, and the lower index i numbers the individual inclusions. It is assumed that all inclusions have identical mechanical and geometrical properties and are grouped into the component $v^{(1)}$. For the sake of definiteness, in the 2- D case we will consider a plane-strain problem.

Let stresses and strains be related to each other via the constitutive equation $\boldsymbol{\varepsilon}(\mathbf{x}) = \mathbf{M}(\mathbf{x})\boldsymbol{\sigma}(\mathbf{x})$, where $\mathbf{M}(\mathbf{x}) \equiv (\mathbf{L}(\mathbf{x}))^{-1}$ and $\mathbf{L} = (dK_{[d]}, 2G_{[d]}) \equiv dK_{[d]}\mathbf{N}_1 + 2G_{[d]}\mathbf{N}_2$, $\mathbf{N}_1 = \boldsymbol{\delta} \otimes \boldsymbol{\delta}/d$, $\mathbf{N}_2 = \mathbf{I} - \mathbf{N}_1$; $K_{[d]}$ and $G_{[d]}$ are the bulk and shear modulus, respectively in the space dimensionality d ; $\boldsymbol{\delta}$ and \mathbf{I} are the unit second-order and fourth-order tensors. For example, for the plane strain $G_{[2]} = G_{[3]}$, $K_{[2]} = K_{[3]} + G_{[3]}/3$, $E_{[2]} = E_{[3]}/(1 + \nu_{[3]})(1 -$

$\nu_{[3]}$), $\nu_{[2]} = \nu_{[3]}/(1 - \nu_{[3]})$ and for the plane stress $G_{[2]} = G_{[3]}$, $K_{[2]} = 9K_{[3]}G_{[3]}/(3K_{[3]} + 4G_{[3]})$, $E_{[2]} = E_{[3]}$, $\nu_{[2]} = \nu_{[3]}$ where E and ν are the Young modulus and Poisson's ratio, respectively. The local strain and stress tensors satisfy the linearized strain-displacement relations and the equilibrium equation, respectively. We consider a mesodomain w , subjected to the uniform traction boundary conditions $\boldsymbol{\sigma}^0 \mathbf{n}(\mathbf{x}) = \mathbf{T}(\mathbf{x})$, $\mathbf{x} \in \partial w$, where $\mathbf{T}(\mathbf{x})$ is the traction vector at the external boundary ∂w , \mathbf{n} is its unit outward normal, and $\boldsymbol{\sigma}^0$ is a given symmetric tensor, representing the macroscopic stress state.

In the matrix $v^{(0)} = w \setminus v^{(1)}$ and in the inclusions $v^{(1)}$, the tensor $\mathbf{f}(\mathbf{x})$ ($\mathbf{f} = \mathbf{L}, \mathbf{M}$, $\mathbf{M} \equiv \mathbf{L}^{-1}$) is assumed to be constant: $\mathbf{f}(\mathbf{x}) = \mathbf{f}^{(0)}$ for $\mathbf{x} \in v^{(0)}$ and $\mathbf{f}(\mathbf{x}) = \mathbf{f}^{(0)} + \mathbf{f}_1(\mathbf{x}) = \mathbf{f}^{(0)} + \mathbf{f}_1^{(1)}$ for $\mathbf{x} \in v^{(1)}$; the subscript 1 denotes a jump of the corresponding quantity (e.g. of the material tensor). The phases are perfectly bonded. All the random quantities under discussion are statistically homogeneous, and, hence, the ensemble averaging could be replaced by volume averaging $\langle (\cdot) \rangle = \bar{w}^{-1} \int (\cdot) W(\mathbf{x}) d\mathbf{x}$, $\langle (\cdot) \rangle^{(k)} = [\bar{v}^{(k)}]^{-1} \int (\cdot) V^{(k)}(\mathbf{x}) d\mathbf{x}$, where the bar appearing above the region represents its measure, e.g. $\bar{v} \equiv \text{mes } v$. The average over component $v^{(k)}$ agrees with the ensemble average over an individual inclusion $v_i \in v^{(k)}$ ($i = 1, 2, \dots$): $\langle (\cdot) \rangle_i = \langle (\cdot) \rangle^{(k)}$. The notation $\langle (\cdot) \rangle_i(\mathbf{x})$ at $\mathbf{x} \in v_i \subset v^{(k)}$ means the average over an ensemble realization of surrounding inclusions (but not over the volume v_i of a particular inclusion, in contrast to $\langle (\cdot) \rangle_i$). For the description of the random statistically homogeneous structure of a composite material, let us introduce a conditional probability density $\varphi(v_j, \mathbf{x}_j | v_i, \mathbf{x}_i)$, which is a probability density to find the j -th inclusion with the center \mathbf{x}_j in the domain v_j with fixed inclusion v_i with the centers \mathbf{x}_i . The notation $\varphi(v_j, \mathbf{x}_j | v_i, \mathbf{x}_i)$ denotes the case $\mathbf{x}_j \neq \mathbf{x}_i$. Of course, $\varphi(v_j, \mathbf{x}_j | v_i, \mathbf{x}_i)$ for values of \mathbf{x}_j lying inside the ‘‘included volumes’’ (called also the correlation hole) $\cup v_{ji}^0$, where $v_{ji}^0 \supset v_i$ with characteristic functions V_{0m} (since inclusions cannot overlap), and $\varphi(v_j, \mathbf{x}_j | v_i, \mathbf{x}_i) \rightarrow \varphi(v_j, \mathbf{x}_j)$ at $|\mathbf{x}_j - \mathbf{x}_i| \rightarrow \infty$ (since no long-range order is assumed); it is assumed that $v_{ji}^0 \equiv v_j^0$ are the circles with the radii $2a$; $j, i = 1, 2, \dots$). Only if the pair distribution function $g(\mathbf{x}_i - \mathbf{x}_j) \equiv \varphi(v_i, \mathbf{x}_i | v_j, \mathbf{x}_j)/n^{(1)}$ depends on $|\mathbf{x}_j - \mathbf{x}_i|$ it is called the radial distribution function. $\varphi(v_i, \mathbf{x}_i)$ is a number density $n^{(1)}$ of component $v^{(1)} \ni v_i$ and $c^{(k)}$ is the concentration, i.e. volume fraction, of the component $v^{(k)}$: $c^{(1)} = \langle V^{(1)} \rangle = \bar{v}_i n^{(1)}$ $i = 1, 2, \dots$), $c^{(0)} = 1 - \langle V \rangle$.

2.1.3 Integral equations and effective elastic properties

The well-known integral equations for microinhomogeneous medium (see for references and details Buryachenko, 2001) can be recast for conditional statistical averages at the fixed inclusion $v_i \ni \mathbf{x}$

$$\langle \boldsymbol{\varepsilon} \rangle(\mathbf{x}) = \langle \boldsymbol{\varepsilon} \rangle + \mathbf{P}(v_i^0) \langle \boldsymbol{\xi} \rangle + \int \mathbf{U}(\mathbf{x} - \mathbf{y}) [\langle \boldsymbol{\xi} | v_i, \mathbf{x}_i \rangle(\mathbf{y}) - (1 - V_i^0(\mathbf{y})) \langle \boldsymbol{\xi} \rangle] d\mathbf{y}, \quad (2.1)$$

$$\langle \boldsymbol{\sigma} \rangle(\mathbf{x}) = \langle \boldsymbol{\sigma} \rangle + \mathbf{Q}(v_i^0) \langle \boldsymbol{\eta} \rangle + \int \boldsymbol{\Gamma}(\mathbf{x} - \mathbf{y}) [\langle \boldsymbol{\eta} | v_i, \mathbf{x}_i \rangle(\mathbf{y}) - (1 - V_i^0(\mathbf{y})) \langle \boldsymbol{\eta} \rangle] d\mathbf{y}, \quad (2.2)$$

where the tensors $\boldsymbol{\xi}(\mathbf{y}) = \mathbf{L}_1(\mathbf{y})\boldsymbol{\varepsilon}(\mathbf{y})$ and $\boldsymbol{\eta}(\mathbf{y}) = \mathbf{M}_1(\mathbf{y})\boldsymbol{\sigma}(\mathbf{y})$ are called the stress polarization tensor and the strain polarization tensor, respectively, and are simply a notational convenience. In Eq. (2.2) the integral kernel $\boldsymbol{\Gamma}(\mathbf{x} - \mathbf{y}) = -\mathbf{L}^c[\mathbf{I}\delta(\mathbf{x} - \mathbf{y}) + \mathbf{U}(\mathbf{x} - \mathbf{y})\mathbf{L}^c]$ is the even homogeneous generalized function of the order $-d$ defined by the second derivative of the Green tensor \mathbf{G} : $U_{ijkl}(\mathbf{x}) = [\nabla_j \nabla_l G_{ik}(\mathbf{x})]_{(ij)(kl)}$, where the notation indicates

symmetrization on (ij) and (kl) , and \mathbf{G} is the infinite-homogeneous-body Green's function of the Navier equation with an elastic moduli tensor $\mathbf{L}^{(0)}$,

$\nabla \{ \mathbf{L}^c [\nabla \otimes \mathbf{G}(\mathbf{x}) + (\nabla \otimes \mathbf{G}(\mathbf{x}))^\top] / 2 \} = -\delta\delta(\mathbf{x})$. The tensors $\mathbf{P}(v_i^0)$ and $\mathbf{Q}(v_i^0)$ are defined by the Eshelby tensor $\mathbf{S}(v_i^0)$ for the domain v_i^0 by the equalities $\mathbf{S}(v_i^0) = \mathbf{P}(v_i^0)\mathbf{L}^{(0)}$ and $\mathbf{S}(v_i^0) = \mathbf{I} - \mathbf{M}^{(0)}\mathbf{Q}(v_i^0)$.

A constitutive equation for microinhomogeneous medium can be presented in the form

$$\langle \boldsymbol{\sigma} \rangle = \mathbf{L}^{(0)} \langle \boldsymbol{\varepsilon} \rangle + \langle \boldsymbol{\xi} \rangle, \quad \langle \boldsymbol{\varepsilon} \rangle = \mathbf{M}^{(0)} \langle \boldsymbol{\sigma} \rangle + \langle \boldsymbol{\eta} \rangle. \quad (2.3)$$

If $c \ll 1$, so that the interaction between fibers can be neglected, the average $\langle \boldsymbol{\xi} \rangle$ and $\langle \boldsymbol{\eta} \rangle$ can be approximated by the tensor $n\mathbf{R}^\varepsilon \langle \boldsymbol{\varepsilon} \rangle$ and $n\mathbf{R}^\sigma \langle \boldsymbol{\sigma} \rangle$ obtained from the single-fiber solution with applied homogeneous strain $\langle \boldsymbol{\varepsilon} \rangle$ and the stress $\langle \boldsymbol{\sigma} \rangle$ at the infinity, respectively:

$$\bar{v}_i \boldsymbol{\xi}(\mathbf{x}) = \mathbf{R}^\varepsilon \langle \boldsymbol{\varepsilon} \rangle, \quad \bar{v}_i \boldsymbol{\eta}(\mathbf{x}) = \mathbf{R}^\sigma \langle \boldsymbol{\sigma} \rangle, \quad (2.4)$$

where $\mathbf{R}^\varepsilon = \bar{v}_i \mathbf{L}_1^{(1)} \mathbf{A}$, $\mathbf{R}^\sigma = \bar{v}_i \mathbf{M}_1^{(1)} \mathbf{B}$, and the strain $\mathbf{A} = (\mathbf{I} + \mathbf{P}\mathbf{L}_1^{(1)})^{-1}$ and stress $\mathbf{B} = (\mathbf{I} + \mathbf{Q}\mathbf{M}_1^{(1)})^{-1}$ concentrator factors are defined by the Eshelby tensor \mathbf{S} for the domain v_i by the equalities $\mathbf{S} = \mathbf{P}\mathbf{L}^{(0)}$ and $\mathbf{S} = \mathbf{I} - \mathbf{M}^{(0)}\mathbf{Q}$. In such a case, (2.3) becomes $\langle \boldsymbol{\sigma} \rangle = \mathbf{L}^{(0)} \langle \boldsymbol{\varepsilon} \rangle + n\mathbf{R}^\varepsilon \langle \boldsymbol{\varepsilon} \rangle$, $\langle \boldsymbol{\varepsilon} \rangle = \mathbf{M}^{(0)} \langle \boldsymbol{\sigma} \rangle + n\mathbf{R}^\sigma \langle \boldsymbol{\sigma} \rangle$.

The next step is taking the binary interaction of fibers into account that reduces, for example, Eq. (3.3₁), to the following one ($\mathbf{x} \in v_i$)

$$\begin{aligned} \langle \boldsymbol{\sigma} \rangle &= \mathbf{L}^{(0)} \langle \boldsymbol{\varepsilon} \rangle + n\mathbf{R}^\varepsilon \langle \boldsymbol{\varepsilon} \rangle + n \int \left[[\langle \boldsymbol{\xi}(\mathbf{x}) |; v_j, \mathbf{y} \rangle_{(i)} - \mathbf{R}^\varepsilon \langle \boldsymbol{\varepsilon} \rangle] \phi(v_j, \mathbf{y}; v_i, \mathbf{x}_i) \right. \\ &\quad \left. - n \{ \mathbf{X}\boldsymbol{\varepsilon}'(\mathbf{x}_i) \} \right] d\mathbf{y}. \end{aligned} \quad (2.5)$$

Here $\langle \boldsymbol{\xi}(\mathbf{x}) |; v_j, \mathbf{y} \rangle_{(i)}$ is the volume average of stress polarization tensor $\mathbf{L}_1 \boldsymbol{\varepsilon}$ in the inclusion v_i at the condition that the center of the inclusion $v_j \neq v_i$ is located in the point \mathbf{y}_j , and the pair of inclusions v_i and v_j placed in the infinite homogeneous matrix $\mathbf{L}^{(0)}$ is subjected to the homogeneous field $\bar{\boldsymbol{\varepsilon}}_{ij}$ (called effective field, see for referenses and details Buryachenko, 2001) which, in the framework of the considered model, coincides with the remote strain $\langle \boldsymbol{\varepsilon} \rangle$. Chen and Acrivos (1976) have introduced the second summand of the integrand in the brace as an item $\mathbf{X}\boldsymbol{\varepsilon}'$ where $\boldsymbol{\varepsilon}' \equiv \boldsymbol{\varepsilon}'(\mathbf{x}_i) = \boldsymbol{\varepsilon}(\mathbf{x}_i) - \langle \boldsymbol{\varepsilon} \rangle$ is a perturbation strain at the \mathbf{x}_i due to a single inclusion being at \mathbf{y} subjected to the applied strain $\langle \boldsymbol{\varepsilon} \rangle$ at the infinity. The constant tensor \mathbf{X} determined so that the integral will be absolutely convergent has been chosen as \mathbf{R} . Therefore the item in the brace can be uniquely determined in the term of the solution (2.4₁) $\mathbf{X}\boldsymbol{\varepsilon}' = \mathbf{R}^\varepsilon \mathbf{T}_j^\varepsilon(\mathbf{x}_i - \mathbf{y}_j) \mathbf{R}^\varepsilon \langle \boldsymbol{\varepsilon} \rangle$. Hereinafter $\mathbf{T}_j^\varepsilon(\mathbf{x} - \mathbf{y}_j) = \langle \mathbf{U}(\mathbf{x} - \mathbf{y}) \rangle_j(\mathbf{x})$ at $\mathbf{x} \notin v_j$ and $\mathbf{T}_j^\varepsilon(\mathbf{x} - \mathbf{y}_j) = -(\bar{v}_i)^{-1} \mathbf{P}$ for $\mathbf{x} \in v_j$; $\mathbf{T}_{ij}^\varepsilon(\mathbf{x}_i - \mathbf{y}_j) = \langle \mathbf{T}_j^\varepsilon(\mathbf{x} - \mathbf{y}_j) \rangle_i$. The proposed approximative representation is based on the assumption that the field $\boldsymbol{\varepsilon}' \equiv \text{const.}$ in the area v_i . The last limitation can be easily avoided in the framework of the original scheme by Chen and Acrivos (1976). Indeed, the item in the brace should be replaced by the relation $\langle \boldsymbol{\xi}^0(\mathbf{x}) |; v_j, \mathbf{y} \rangle_{(i)} - \mathbf{R}^\varepsilon \langle \boldsymbol{\varepsilon} \rangle$, where $\langle \boldsymbol{\xi}^0(\mathbf{x}) |; v_j, \mathbf{y} \rangle_{(i)}$ is the average stress polarization tensor $\langle \mathbf{L}_1 \boldsymbol{\xi} \rangle_{(i)}$ in the inclusion v_i subjected to both the homogeneous remote field $\langle \boldsymbol{\varepsilon} \rangle$ and the inhomogeneous field $\mathbf{T}_j^\varepsilon(\mathbf{x} - \mathbf{y}_j) \mathbf{R}^\varepsilon \langle \boldsymbol{\varepsilon} \rangle$.

$$\begin{aligned} \langle \boldsymbol{\sigma} \rangle &= \mathbf{L}^{(0)} \langle \boldsymbol{\varepsilon} \rangle + n\mathbf{R}^\varepsilon \langle \boldsymbol{\varepsilon} \rangle + n^2 \mathbf{R}^\varepsilon \mathbf{P}(v_i^0) \mathbf{R}^\varepsilon \langle \boldsymbol{\varepsilon} \rangle \\ &\quad + n \int \left[[\langle \boldsymbol{\xi}(\mathbf{x}) |; v_j, \mathbf{y} \rangle_{(i)} - \mathbf{R}^\varepsilon \langle \boldsymbol{\varepsilon} \rangle] \phi(v_j, \mathbf{y}; v_i, \mathbf{x}_i) \right. \\ &\quad \left. - n(1 - V_i^0(\mathbf{y})) \{ \langle \boldsymbol{\xi}^0(\mathbf{x}) |; v_j, \mathbf{y} \rangle_{(i)} - \mathbf{R}^\varepsilon \langle \boldsymbol{\varepsilon} \rangle \} \right] d\mathbf{y}, \end{aligned} \quad (2.6)$$

where the domain v_i^0 was extracted from the integration area analogously to Eq. (2.1). It should be mentioned that the inhomogeneous tensor $\langle \boldsymbol{\varepsilon} \rangle + \mathbf{T}_j^\varepsilon(\mathbf{x} - \mathbf{y}_j) \mathbf{R}^\varepsilon \langle \boldsymbol{\varepsilon} \rangle$ ($\mathbf{x} \in v_i$) has a sense of the inhomogeneous strain field outside of the inclusion v_j in the area v_i , which can be estimated by the different methods not just by the use of the tensors $\mathbf{T}_j^\varepsilon(\mathbf{x} - \mathbf{y}_j)$ and \mathbf{R}^ε . A new representation coincides with the old one $\langle \boldsymbol{\xi}^0(\mathbf{y}) | v_j, \mathbf{y} \rangle_{(i)} = \mathbf{R}^\varepsilon \mathbf{T}_{ij}^\varepsilon(\mathbf{x}_i - \mathbf{y}_j) \mathbf{R}^\varepsilon \langle \boldsymbol{\varepsilon} \rangle + \mathbf{R}^\varepsilon \langle \boldsymbol{\varepsilon} \rangle$ just in the framework of both the case of homogeneous ellipsoidal inclusions and the effective field hypothesis **H1**) according to which each inclusion v_i is located in the homogeneous effective field (see for references and details Buryachenko, 2001)

$$\bar{\boldsymbol{\varepsilon}}_i = \text{const.} \quad (2.7)$$

In a similar manner, Eq. (2.3₂) can be reduced to the equation ($\mathbf{x} \in v_i$)

$$\begin{aligned} \langle \boldsymbol{\varepsilon} \rangle &= \mathbf{M}^{(0)} \langle \boldsymbol{\sigma} \rangle + n \mathbf{R}^\sigma \langle \boldsymbol{\sigma} \rangle + n^2 \mathbf{R}^\sigma \mathbf{Q}(v_i^0) \mathbf{R}^\sigma \langle \boldsymbol{\sigma} \rangle \\ &+ n \int \left[\langle \boldsymbol{\eta}(\mathbf{x}) | v_j, \mathbf{y} \rangle_{(i)} - \mathbf{R}^\sigma \langle \boldsymbol{\sigma} \rangle \right] \phi(v_j, \mathbf{y}; v_i, \mathbf{x}_i) \\ &- n(1 - V_i^0(\mathbf{x})) \{ \langle \boldsymbol{\eta}^0(\mathbf{y}) | v_j, \mathbf{y} \rangle_{(i)} - \mathbf{R}^\sigma \langle \boldsymbol{\sigma} \rangle \} d\mathbf{y}, \end{aligned} \quad (2.8)$$

where the conditional averages of the strain polarization tensors $\langle \boldsymbol{\eta}(\mathbf{y}) | v_j, \mathbf{y} \rangle_{(i)}$ and $\langle \boldsymbol{\eta}^0(\mathbf{y}) | v_j, \mathbf{y} \rangle_{(i)}$ are defined analogously to the conditional averages of the stress polarization tensors $\langle \boldsymbol{\xi}(\mathbf{y}) | v_j, \mathbf{y} \rangle_{(i)}$ and $\langle \boldsymbol{\xi}^0(\mathbf{y}) | v_j, \mathbf{y} \rangle_{(i)}$, respectively, with the replacement of the homogeneous field $\langle \boldsymbol{\varepsilon} \rangle$ acting on two inclusions v_i and v_j by the homogeneous field $\langle \boldsymbol{\sigma} \rangle$. Introduction of new tensors proportional to the involved polarization tensors $\langle \boldsymbol{\xi}(\mathbf{y}) | v_j, \mathbf{y} \rangle_{(i)} = \langle \boldsymbol{\xi}^\varepsilon(\mathbf{y}) | v_j, \mathbf{y} \rangle_{(i)} \langle \boldsymbol{\varepsilon} \rangle$, $\langle \boldsymbol{\xi}^0(\mathbf{y}) | v_j, \mathbf{y} \rangle_{(i)} = \langle \boldsymbol{\xi}^{0\varepsilon}(\mathbf{y}) | v_j, \mathbf{y} \rangle_{(i)} \langle \boldsymbol{\varepsilon} \rangle$, $\langle \boldsymbol{\eta}(\mathbf{y}) | v_j, \mathbf{y} \rangle_{(i)} = \langle \boldsymbol{\eta}^\sigma(\mathbf{y}) | v_j, \mathbf{y} \rangle_{(i)} \langle \boldsymbol{\sigma} \rangle$, $\langle \boldsymbol{\eta}^0(\mathbf{y}) | v_j, \mathbf{y} \rangle_{(i)} = \langle \boldsymbol{\eta}^{0\sigma}(\mathbf{y}) | v_j, \mathbf{y} \rangle_{(i)} \langle \boldsymbol{\sigma} \rangle$, makes it possible to estimate from Eqs. (2.6) and (2.8) the effective elastic stiffness and compliances, respectively

$$\begin{aligned} \mathbf{L}^* &= \mathbf{L}^{(0)} + n \mathbf{R}^\varepsilon + n^2 \mathbf{R}^\varepsilon \mathbf{P}(v_i^0) \mathbf{R}^\varepsilon + n \int \left[\langle \boldsymbol{\xi}^\varepsilon(\mathbf{y}) | v_j, \mathbf{y} \rangle_{(i)} - \mathbf{R}^\varepsilon \right] \phi(v_j, \mathbf{y}; v_i, \mathbf{x}_i) \\ &- n(1 - V_i^0(\mathbf{y})) \{ \langle \boldsymbol{\xi}^{0\varepsilon}(\mathbf{y}) | v_j, \mathbf{y} \rangle_{(i)} - \mathbf{R}^\varepsilon \} d\mathbf{y} \end{aligned} \quad (2.9)$$

$$\begin{aligned} \mathbf{M}^* &= \mathbf{M}^{(0)} + n \mathbf{R}^\sigma + n^2 \mathbf{R}^\sigma \mathbf{Q}(v_i^0) \mathbf{R}^\sigma + n \int \left[\langle \boldsymbol{\eta}^\sigma(\mathbf{y}) | v_j, \mathbf{y} \rangle_{(i)} - \mathbf{R}^\sigma \right] \phi(v_j, \mathbf{y}; v_i, \mathbf{x}_i) \\ &- n(1 - V_i^0(\mathbf{y})) \{ \langle \boldsymbol{\eta}^{0\sigma}(\mathbf{y}) | v_j, \mathbf{y} \rangle_{(i)} - \mathbf{R}^\sigma \} d\mathbf{y}. \end{aligned} \quad (2.10)$$

For the well-stirred radial distribution function $g(\mathbf{x}_i - \mathbf{y}_j) \equiv 1$ at $|\mathbf{x}_i - \mathbf{y}_j| > 2a$, the isotropic effective elastic moduli $\mathbf{L}^* = (2k^*, 2\mu^*)$ have polynomial dependance on the fiber concentration $k^*/k^{(0)} = 1 + a_1^k c + a_2^k c^2$ and $\mu^*/\mu^{(0)} = 1 + a_1^\mu c + a_2^\mu c^2$. The integrals in Eqs. (2.9) and (2.10) are absolutely convergent and, because of this, don't depend on the the shape of the integration domains. However, the choice of circular shape of these domains leads to the vanishing of a contribution produced by the summands in the braces and they can be omitted.

Let us compare Eqs. (2.9) and (2.10) with Mori-Tanaka estimations which coincide with the variational lower bounds by Hashin (1965) when the fibers are stiffer than the matrix, and with the upper bounds when the fibers are weaker than the matrix. To $O(c^2)$, the relevant representations by the MT method (called $O(c^2)$ approximation of the MT method) for the effective stiffness and compliance coincide with Eqs. (2.9) and (2.10),

respectively, if in the last representation the integral items are neglected. The absence of integral items in Eqs. (2.9) and (2.10) is equivalent to ignoring binary interaction of fibers provided by the one-particle approximation $\langle \boldsymbol{\xi}(\mathbf{x}) |; v_j, \mathbf{y}_j \rangle_i \equiv \langle \boldsymbol{\xi} \rangle_i$ (called also quasi-crystalline approximation by Lax, see for references and details Buryachenko, 2001; Willis and Acton, 1976) The authors of [15] have estimated the effective elastic moduli to $O(c^2)$ for the particular matrix composites through the use of an integral equation method in the framework of the far-field solution $O((a/R)^6)$ accompanied by the effective field hypothesis (2.7), where $R = |\mathbf{x}_i - \mathbf{y}_j|$ is a distance between the centers of inclusions v_i and v_j . These estimations are yielded as a limiting case from more general representations by Buryachenko (2001) at $c \rightarrow 0$; the analogous results for the fiber composites were obtained in the work by Buryachenko *et al.* (2003) from where the following representations yield at $c \rightarrow 0$

$$\begin{aligned} \mathbf{L}^* &= \mathbf{L}^{(0)} + n\mathbf{R}^\varepsilon + n^2\mathbf{R}^\varepsilon\mathbf{P}(v_i^0)\mathbf{R}^\varepsilon \\ &+ n \int \mathbf{R}^\varepsilon \mathbf{T}_{ij}^\varepsilon(\mathbf{x}_i - \mathbf{y}_j) \mathbf{R}^\varepsilon \mathbf{T}_{ij}^\varepsilon(\mathbf{x}_i - \mathbf{y}_j) \mathbf{R}^\varepsilon \phi(v_j, \mathbf{y}_j |; v_i, \mathbf{x}_i) d\mathbf{y}, \end{aligned} \quad (2.11)$$

$$\begin{aligned} \mathbf{M}^* &= \mathbf{M}^{(0)} + n\mathbf{R}^\sigma + n^2\mathbf{R}^\sigma\mathbf{Q}(v_i^0)\mathbf{R}^\sigma \\ &+ n \int \mathbf{R}^\sigma \mathbf{T}_{ij}^\sigma(\mathbf{x}_i - \mathbf{y}_j) \mathbf{R}^\sigma \mathbf{T}_{ij}^\sigma(\mathbf{x}_i - \mathbf{y}_j) \mathbf{R}^\sigma \phi(v_j, \mathbf{y}_j |; v_i, \mathbf{x}_i) d\mathbf{y}, \end{aligned} \quad (2.12)$$

where the items analogous to ones in the braces in Eqs. (2.9) and (2.10) were omitted due to choice of the circular integration areas in Eqs. (2.11) and (2.12). It should be mentioned that a natural reciprocity between stiffness and compliance of effective properties $\mathbf{L}^* = (\mathbf{M}^*)^{-1}$ is not valid for the representations (2.9) and (2.10) as well as for Eqs. (2.11) and (2.12).

2.1.4 A finite number of circular fibers in an unbounded solid

We keep the basic notations introduced by Muskhelishvili (1953) to write a general solution in the form

$$(u_1 + iu_2) = \varkappa\varphi(z) - \overline{z\varphi'(z)} - \overline{\psi(z)}, \quad (2.13)$$

where u_i are the Cartesian components of displacement vector $\mathbf{u} = (u_1, u_2)^T$ and $i = \sqrt{-1}$. Also, $z = (x_1 + ix_2)$ is a complex variable representing the point $\mathbf{x} = (x_1, x_2)^T$ in the complex plane Ox_1x_2 and \varkappa is the constant factor equal to $3 - 4\nu$ or $(3 - \nu)/(1 + \nu)$ depending on the plane strain or plane stress problem is considered, respectively. In the polar coordinates (r, ϕ) corresponding to the Cartesian ones (x_1, x_2) , $z = re^{i\phi}$ and the vector \mathbf{u} components are related by

$$(u_r + iu_\phi) = (u_1 + iu_2) e^{-i\phi}. \quad (2.14)$$

In (2.13), the functions $\varphi(z)$ and $\psi(z)$ are the complex potentials; what is important, components of the corresponding to \mathbf{u} stress tensor σ also can be expressed in terms of these potentials:

$$\begin{aligned} \sigma_{11} + \sigma_{22} &= 8G \operatorname{Re} [\varphi'(z)]; \\ \sigma_{22} - \sigma_{11} + 2i\sigma_{12} &= 4G [\overline{z}\varphi''(z) + \psi'(z)]. \end{aligned} \quad (2.15)$$

Here, as well as in (2.13), \bar{z} means the complex conjugate of z : $\bar{z} = (x_1 + ix_2) = re^{-i\phi}$. In what follows, we need also the curvilinear components of the tensor σ given by the formula

$$\begin{aligned} (\sigma_r - i\sigma_{r\phi}) &= \frac{1}{2} [\sigma_{11} + \sigma_{22} - (\sigma_{22} - \sigma_{11} + 2i\sigma_{12}) e^{2i\phi}] \\ &= 2G \{ 2 \operatorname{Re} [\varphi'(z)] - [\bar{z}\varphi''(z) + \psi'(z)] e^{2i\phi} \}. \end{aligned} \quad (2.16)$$

The specific form of φ and ψ is problem-dependent: in our case, we can separate the far field term by taking $\varphi(z) = \Gamma_1 z + \varphi_0(z)$ and $\psi(z) = \Gamma_2 z + \psi_0(z)$, where Γ_1 and Γ_2 are the complex-valued constants and $\varphi_0(z)$ and $\psi_0(z)$ are the functions vanishing at infinity. So, suppose we have the homogeneous remote strain $\langle \varepsilon \rangle$ prescribed. It follows from (2.13) that

$$(u_1 + iu_2) \rightarrow (\varkappa - 1) \Gamma_1 z - \bar{\Gamma}_2 \bar{z} \quad (2.17)$$

as $|z| \rightarrow \infty$. On the other hand, $\mathbf{u} \rightarrow \mathbf{u}_\infty = \langle \varepsilon \rangle \mathbf{x}$ and we get immediately

$$\Gamma_1 = \frac{\langle \varepsilon_{11} \rangle + \langle \varepsilon_{22} \rangle}{2(\varkappa - 1)}; \quad \Gamma_2 = \frac{1}{2} (\langle \varepsilon_{22} \rangle - \langle \varepsilon_{11} \rangle + 2i \langle \varepsilon_{12} \rangle). \quad (2.18)$$

Now, we apply the above theory to derive an accurate, asymptotically exact series solution for an infinite solid containing a finite array of fibers perfectly bonded with the matrix. First, we introduce the global Cartesian coordinate system Ox_1x_2 arbitrarily. In this basis, position of the p -th fiber center is given by $Z_p = (x_{1p} - ix_{2p})$, $p = 1, 2, \dots, N$. Also, we shall use the variables $z_p = z - Z_p$ of local coordinate systems with origins located in the points Z_p . To construct a solution in the multiply-connected matrix domain we make use the generalized superposition principle (see, e.g., Kushch 1996) to write

$$\mathbf{u}_m = \mathbf{u}_\infty + \sum_{p=1}^N \mathbf{U}_p(z_p) \quad (2.19)$$

where \mathbf{u}_∞ (2.17) represents the far field whereas \mathbf{U}_p is the vanishing at infinity disturbance field due to p -th inhomogeneity which can be written in the form (2.13). The explicit expression of (2.19) is

$$\mathbf{u}_m = (\varkappa_0 - 1) \Gamma_1 z - \bar{\Gamma}_2 \bar{z} + \sum_{p=1}^N \left[\varkappa_0 \varphi_{0p}(z_p) - z_p \overline{\varphi'_{0p}(z_p)} - \overline{\psi_{0p}(z_p)} \right], \quad (2.20)$$

where the potentials φ_{0p} and ψ_{0p} are taken as a singular part of the Loran's series

$$\varphi_{0p}(z) = \sum_{n=1}^{\infty} \frac{A_n^{(p)}}{z^n}, \quad \psi_{0p}(z) = \sum_{n=1}^{\infty} \frac{B_n^{(p)}}{z^n}, \quad (2.21)$$

with $A_n^{(p)}$ and $B_n^{(p)}$ being the series expansion coefficients to be determined. It is quite clear that such a choice of φ_{0p} and ψ_{0p} provides the proper behavior of \mathbf{u}_m at infinity.

On the contrary, the displacement field inside the fiber has no singularity and, thus, the regular part only has to be retained in the Loran's series expansion of the corresponding complex potentials. Thus, the displacement in the q -th fiber can be written as

$$\mathbf{u}_i^{(q)} = \varkappa_q \varphi_q(z_q) - z_q \overline{\varphi'_q(z_q)} - \overline{\psi_q(z_q)}, \quad (2.22)$$

where $\varkappa_q = \varkappa(\nu_q)$,

$$\varphi_q(z) = \sum_{n=1}^{\infty} C_{-n}^{(p)} z^n, \quad \psi_q(z) = \sum_{n=1}^{\infty} D_{-n}^{(p)} z^n, \quad (2.23)$$

and $C_{-n}^{(p)}$ and $D_{-n}^{(p)}$ are the unknown constants. Likewise the $A_n^{(p)}$ and $B_n^{(p)}$, they should be chosen so that to satisfy the matrix-fiber interface boundary conditions

$$\left(\mathbf{u}_m - \mathbf{u}_i^{(q)} \right) \Big|_{|z_q|=R_q} = 0; \quad \left[\mathbf{T}_n(\mathbf{u}_m) - \mathbf{T}_n(\mathbf{u}_i^{(q)}) \right] \Big|_{|z_q|=R_q} = 0; \quad (2.24)$$

where $\mathbf{T}_n = \sigma \mathbf{n}$ is the traction vector and R_q is the radius of q -th fiber. In our case of circular fiber, the unit normal vector $\mathbf{n} = \mathbf{e}_r$ and $\mathbf{T}_n = (\sigma_r, \sigma_{r\phi})^T$.

To get a resolving set of equations for $A_n^{(p)}$, $B_n^{(p)}$, $C_{-n}^{(p)}$ and $D_{-n}^{(p)}$, we substitute the expressions of \mathbf{u}_m (2.20) and $\mathbf{u}_i^{(q)}$ (2.22) into the first of conditions (2.24) and equate the corresponding power series coefficients in the opposite parts of equation. However, we need first to represent (2.20) as a function of local variable z_q ; note that the separate terms of (2.19) are written in variables of different coordinate systems. Such a transformation uses the following easy-to-prove formula

$$\frac{1}{(z+Z)^n} = \sum_{k=0}^{\infty} H_{nk}(Z) z^k, \quad H_{nk}(Z) = (-1)^k \frac{(n+k-1)!}{k!(n-1)!} Z^{-(n+k)}. \quad (2.25)$$

Taking into account $z_p = z_q + Z_{pq}$ ($Z_{pq} = Z_q - Z_p$) and applying (2.25) to all the sum terms in (2.20) but that one with $p = q$, we get, in particular,

$$\sum_{\substack{p=1 \\ (p \neq q)}}^N \varphi_{0p}(z_p) = \sum_{\substack{p=1 \\ (p \neq q)}}^N \sum_{n=1}^{\infty} \frac{A_n^{(p)}}{(z_q + Z_{pq})^n} = \sum_{k=0}^{\infty} A_{-k}^{(q)} (z_q)^k. \quad (2.26)$$

where

$$A_{-k}^{(q)} = \sum_{\substack{p=1 \\ (p \neq q)}}^N \sum_{n=1}^{\infty} A_n^{(p)} H_{nk}(Z_{pq}). \quad (2.27)$$

The desired representation is

$$\mathbf{u}_m(z_q) = \mathbf{U}_{0q} + (\varkappa_0 - 1) \Gamma_1 z_q - \overline{\Gamma_2 z_q} + \varkappa_0 \varphi_{0\Sigma}(z_q) - \overline{z_q \varphi'_{0\Sigma}(z_q)} - \overline{\psi_{0\Sigma}(z_q)}, \quad (2.28)$$

where

$$\begin{aligned} \mathbf{U}_{0q} &= (\varkappa_0 - 1) \Gamma_1 Z_q - \overline{\Gamma_2 Z_q}; \\ \varphi_{0\Sigma}(z) &= \sum_{n=-\infty}^{\infty} \frac{A_n^{(q)}}{z^n}, \quad \psi_{0\Sigma}(z) = \sum_{n=-\infty}^{\infty} \frac{B_n^{(q)}}{z^n} \end{aligned} \quad (2.29)$$

and

Now, we substitute (2.28) and (2.22) into the first of conditions (2.24). Taking into account that at the interface

$$B_{-k}^{(q)} = \sum_{\substack{p=1 \\ (p \neq q)}}^N \sum_{n=1}^{\infty} \left[B_n^{(p)} - \frac{Z_{pq}}{Z_{pq}} (k+n) A_n^{(p)} \right] H_{nk}(Z_{pq}). \quad (2.30)$$

$z_q = R_q e^{i\phi}$, $z_q \bar{z}_q = (R_q)^2$ and $(z_q)^2 = (R_q)^2 e^{2i\phi}$, we come, after somewhat tedious algebra, to the infinite set of linear equations

$$\begin{aligned} \varkappa_0 \frac{A_k^{(q)}}{(R_q)^{2k}} - (R_q)^2 (k+2) \overline{A_{-(k+2)}^{(q)}} - \overline{B_{-k}^{(q)}} &= \delta_{k1} \overline{\Gamma_2} - (R_q)^2 (k+2) \overline{C_{-(k+2)}^{(q)}} - \overline{D_{-k}^{(q)}}; \\ \frac{B_k^{(q)}}{(R_q)^{2k}} - \varkappa_0 \overline{A_{-k}^{(q)}} - \frac{(k-2)}{(R_q)^{2k-2}} A_{k-2}^{(q)} &= \delta_{k1} \left[(\varkappa_0 - 1) \Gamma_1 + C_{-k}^{(q)} \right] - \varkappa_q \overline{C_{-k}^{(q)}}; \end{aligned} \quad (2.31)$$

$$q = 1, 2, \dots, N; \quad k = 1, 2, \dots$$

To satisfy the second of conditions (2.24), we recognize first that the stress in matrix domain can be written as

$$\begin{aligned} \sigma_{11} + \sigma_{22} &= \langle \sigma_{11} \rangle + \langle \sigma_{22} \rangle + 8G_0 \sum_{p=1}^N \operatorname{Re} [\varphi'_{0p}(z_p)]; \\ \sigma_{22} - \sigma_{11} + 2i\sigma_{12} &= \langle \sigma_{22} \rangle - \langle \sigma_{11} \rangle + 2i \langle \sigma_{12} \rangle + 4G_0 \sum_{p=1}^N [\bar{z}_p \varphi''_{0p}(z_p) + \psi'_{0p}(z_p)]; \end{aligned} \quad (2.32)$$

and that the formula for a traction vector $\mathbf{T}_n = (\sigma_r + i\sigma_{r\phi})$ is simply the complex conjugate of (2.16). By substituting (2.32) into (2.16) and carrying out the transforms analogous to those described above we obtain another set of algebraic equations

$$\begin{aligned} \frac{A_k^{(q)}}{(R_q)^{2k}} + (R_q)^2 (k+2) \overline{A_{-(k+2)}^{(q)}} + \overline{B_{-k}^{(q)}} &= -\delta_{k1} \overline{\Gamma_2} + \lambda_q \left[(R_q)^2 (k+2) \overline{C_{-(k+2)}^{(q)}} + \overline{D_{-k}^{(q)}} \right]; \\ \frac{B_k^{(q)}}{(R_q)^{2k}} - \frac{(k-2)}{(R_q)^{2k-2}} A_{k-2}^{(q)} + \overline{A_{-k}^{(q)}} &= -2\delta_{k1} \Gamma_1 + \lambda_q \left(\delta_{k1} C_{-k}^{(q)} + \overline{C_{-k}^{(q)}} \right); \end{aligned} \quad (2.33)$$

where $\lambda_q = G_q/G_0$.

Together with (2.31), these equalities form a closed infinite set of linear algebraic equations. We simplify it further by excluding the unknowns $C_{-k}^{(q)}$ and $D_{-k}^{(q)}$ and obtain the final form of the resolving system containing the unknowns $A_k^{(q)}$ and $B_k^{(q)}$ only:

$$\begin{aligned} \frac{\Omega_1}{(R_q)^{2k}} \left[(R_q)^2 (k-2) A_{k-2}^{(q)} - B_k^{(q)} \right] + \sum_{\substack{p=1 \\ (p \neq q)}}^N \sum_{n=1}^{\infty} A_n^{(p)} H_{nk}(Z_{pq}) &= -\delta_{k1} \Gamma_1; \\ \frac{\Omega_2}{(R_q)^{2k}} A_k^{(q)} + \sum_{\substack{p=1 \\ (p \neq q)}}^N \sum_{n=1}^{\infty} \left\{ \overline{A_n^{(p)}} \left[(k+n) \frac{Z_{pq}}{Z_{pq}} \overline{H_{nk}(Z_{pq})} - (k+2) (R_q)^2 \overline{H_{n,k+2}(Z_{pq})} \right] \right. \\ \left. + \overline{B_n^{(p)}} H_{nk}(Z_{pq}) \right\} &= -\delta_{k1} \Gamma_1; \\ q = 1, 2, \dots, N; \quad k = 1, 2, \dots; \end{aligned} \quad (2.34)$$

where

$$\Omega_1 = \frac{(2\lambda_q + \varkappa_q - 1)}{2[\lambda_q(\varkappa_0 - 1) + (\varkappa_q - 1)]} \text{ for } k = 1, \quad \Omega_1 = \frac{(\lambda_q + \varkappa_q)}{2(\lambda_q \varkappa_0 - \varkappa_q)} \text{ for } k > 1$$

and

$$\Omega_2 = \frac{(\lambda_q \varkappa_0 + 1)}{2(\lambda_q - 1)}.$$

After we solved (2.34) for $A_k^{(q)}$ and $B_k^{(q)}$, we can utilize either (2.31) or (2.33) to calculate $C_{-k}^{(q)}$ and $D_{-k}^{(q)}$.

It can be shown that (2.34) is the infinite linear system with normal determinant (see, e.g., Kantorovich and Krylov, 1962) provided that the non-touching condition is satisfied for every pair of fibers. Thus, its approximate numerical solution can be obtained by the truncation method which assumes retaining in (2.34) the unknowns and equations with $k, n \leq n_h$. With n_h increased, these approximate solutions converge to the exact one, providing evaluation of the stress tensor in every point of a composite domain with any desirable accuracy by taking n_h sufficiently large.

2.1.5 Half plane containing a finite array of fibers

Half plane with a circular hole: conductivity problem

Let us consider a half plane $x_2 \leq 0$, containing a number of circular inclusions of holes of radii R_q (Fig.2.1) centered in the points O_q with coordinates (X_{1q}, X_{2q}) . Besides the global Cartesian coordinate system Ox_1x_2 , we introduce the local ones with origins O_q . Also, we introduce the following complex-valued variables

$$z = x_1 + ix_2, \quad z_q = x_{1q} + ix_{2q}; \quad (2.35)$$

Clearly, $z = z_q + Z_q$, where $Z_q = X_{1q} + iX_{2q}$.

We consider first a steady state conductivity problem for a half plane with single hole ($N = 1$). The temperature field T in the matrix material satisfies the Laplace equation

$$\left(\frac{\partial^2}{\partial x_1^2} + \frac{\partial^2}{\partial x_2^2} \right) T = 0; \quad (2.36)$$

as to the boundary conditions, we prescribe constant heat flux $\mathbf{q} = -\lambda \nabla T$ at the flat boundary $x_2 = 0$

$$(\mathbf{q} \cdot \mathbf{n}) \Big|_{x_2 = 0} = Q; \quad (2.37)$$

whereas the hole's surface is assumed to be thermally isolated:

$$(\mathbf{q} \cdot \mathbf{n}) \Big|_{|z_q| = R_q} = 0. \quad (2.38)$$

We shall solve the problem stated using the complex potentials based approach. It is common knowledge that T can be found as

$$T = \text{Re}(\varphi) = \frac{1}{2} (\varphi + \bar{\varphi}); \quad (2.39)$$

where φ is an analytical function of complex variable z or \bar{z} , \bar{z} being the complex conjugate of z . It follows directly from the fact that the eqn (2.36) can be written in complex variables as

$$\frac{\partial^2}{\partial z \partial \bar{z}} T = 0, \quad \text{where } \frac{\partial}{\partial z} = \frac{1}{2} \left(\frac{\partial}{\partial x_1} - i \frac{\partial}{\partial x_2} \right) \text{ and } \frac{\partial}{\partial \bar{z}} = \frac{1}{2} \left(\frac{\partial}{\partial x_1} + i \frac{\partial}{\partial x_2} \right). \quad (2.40)$$

To find φ , we make use of the superposition principle. Because the multiple-connected domain we consider is an intersection of two infinite areas, one being a half plane and another being a plane with circular hole, it is natural to write φ as a sum of appropriate potentials. Specifically, we take φ in the form

$$\varphi = \Gamma \bar{z} + G(z_q) + H(\bar{z}), \quad (2.41)$$

where $\Gamma \bar{z}$ ($\Gamma = \Gamma_1 + i\Gamma_2$ is a constant) represents far field solution, whereas $G(z_q)$ and $H(\bar{z})$ are the disturbance fields caused by the hole and flat boundary, respectively. From the physical consideration, we require both the $G(z_q)$ and $H(\bar{z})$ to vanish at infinity.

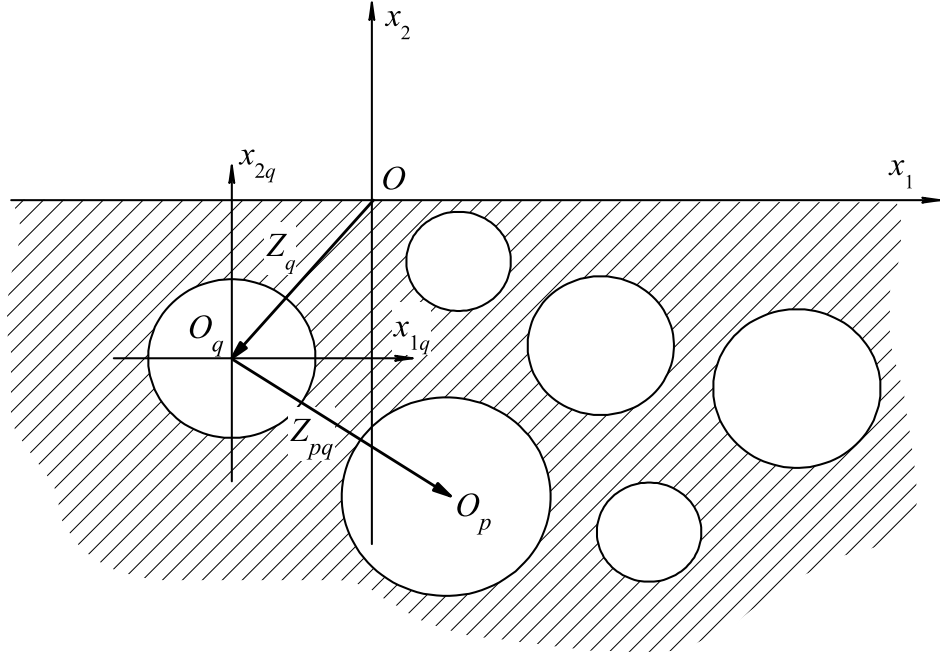


Fig.2.1 Geometry of the problem

Specific form of G and H has to be taken that to satisfy the boundary conditions (2.37), ((2.38) in a simplest way. The natural choice for G is singular part of the Loran series

$$G(z_q) = \sum_{n=1}^{\infty} \frac{a_n}{(z_q)^n}, \quad (2.42)$$

where a_n are the unknown complex-valued series coefficients. On the other hand, H is taken in the form for Fourier integral:

$$H(z) = \int_{-\infty}^{\infty} h(\beta) \exp(i\beta z) d\beta \quad (2.43)$$

with unknown complex-valued density $h(\beta)$.

As a first step, we rewrite (2.37) as

$$\left. \frac{\partial T}{\partial x_2} \right|_{x_2=0} = -\frac{Q}{\lambda};$$

this condition is satisfied provided we put

$$\Gamma_1 = 0, \quad \Gamma_2 = -\frac{Q}{\lambda} \quad \text{and} \quad \left. \frac{\partial}{\partial x_2} [G(z_q) + H(\bar{z})] \right|_{x_2=0} = 0. \quad (2.44)$$

The eqn (2.44) will be used to specify $h(\beta)$; for this purpose, we take into account the following Fourier integral transform (Erdeley et al., 1954)

$$\int_{-\infty}^{\infty} \frac{\exp(-i\eta t)}{i\gamma + t} dt = \begin{cases} -2\pi i \exp(-\eta\gamma), & \eta > 0; \quad \text{Re } \gamma > 0; \\ 0, & \eta < 0. \end{cases} \quad (2.45)$$

With replace t to x_1 , γ to x_2 and η to β , the inverse transform gives for $x_2 > 0$

$$\frac{1}{z} = -i \int_{-\infty}^{\infty} \exp(i\beta z) d\beta; \quad (2.46)$$

by its differentiation, one obtains

$$\frac{1}{z^n} = \int_{-\infty}^{\infty} \xi_n^-(\beta) \exp(i\beta z) d\beta, \quad \text{where} \quad \xi_n^-(\beta) = \begin{cases} (-i)^n \beta^{(n-1)} / (n-1)! & \text{for } \beta > 0; \\ 0, & \text{otherwise.} \end{cases} \quad (2.47)$$

Note that in our geometry (Fig.2.1), $x_{2q} > 0$ at the half plane boundary; therefore, we can use (2.47) to represent $G(z_q)$ (2.42) in the form

$$G(z_q) = \int_{-\infty}^{\infty} \sum_{n=1}^{\infty} a_n \xi_n^-(\beta) \exp[i\beta(z - Z_q)] d\beta. \quad (2.48)$$

Substituting (2.48) and (2.43) into (2.44) gives us

$$\int_{-\infty}^{\infty} i\beta \left[h(\beta) - \sum_{n=1}^{\infty} a_n \xi_n^-(\beta) \exp(-i\beta Z_q) \right] \exp(i\beta x_1) d\beta = 0. \quad (2.49)$$

We require (2.49) to be valid for arbitrary x_1 ; this is possible only when

$$h(\beta) = \sum_{n=1}^{\infty} a_n \xi_n^-(\beta) \exp(-i\beta Z_q). \quad (2.50)$$

Likewise to $\xi_n^-(\beta)$, the density $h(\beta) \equiv 0$ for $\beta < 0$.

The remaining unknown coefficients will be utilized to satisfy the boundary condition (2.38) at the hole $r_q = |z_q| = R_q$, which can be rewritten as

$$\left. \frac{\partial T}{\partial r_q} \right|_{r_q = R_q} = 0,$$

the last being a consequence of more general condition

$$\left. \frac{\partial \varphi}{\partial r_q} \right|_{r_q = R_q} = 0.$$

At the circle $r_q = R_q$, $z_q = R_q \exp(i\phi_q)$ and $(z_q)^n = (R_q)^n \exp(in\phi_q)$ are the functions of angular coordinate only and, thus, $G(z_q)$ in the form (2.42) is already suitable for our purpose. Representation of other terms of (2.41) in a form similar to (2.42) is rather straightforward and gives

$$\Gamma \bar{z} = \Gamma_2 \bar{Z}_q + \Gamma_2 r_q \exp(-i\phi_q); \quad (2.51)$$

$$H(z) = \int_{-\infty}^{\infty} h(\beta) \exp [i\beta(\bar{z}_q + \bar{Z}_q)] d\beta = \sum_{k=0}^{\infty} b_k (\bar{z}_q)^k, \quad (2.52)$$

where

$$b_k = \frac{1}{k!} \int_0^{\infty} (i\beta)^k h(\beta) \exp(i\beta \bar{Z}_q) d\beta, \quad k = 1, 2, \dots \quad (2.53)$$

For the specific form (2.50) of $h(\beta)$, the expression (2.53) can be simplified greatly: we have

$$b_k = \frac{1}{k!} \int_0^{\infty} (i\beta)^k \sum_{n=1}^{\infty} a_n \frac{(-i)^n \beta^{(n-1)}}{(n-1)!} \exp [i\beta(\bar{Z}_q - Z_q)] d\beta = \quad (2.54)$$

$$\sum_{n=1}^{\infty} a_n \frac{i^{n-k} (n+k-1)!}{k! (n-1)! (2X_{2q})^{(n+k)}},$$

where the use is made of the Euler's integral for Gamma-function (Abramowitz and Stegun, 1964):

$$\int_0^{\infty} \beta^{n+1} \exp(\beta Z) d\beta = \frac{n!}{Z^n}.$$

The final step is substituting the expressions (2.42), (2.51) and (2.52) into the condition $\partial\varphi/\partial r_q = 0$ ($r_q = R_q$); after simple algebra, we get

$$\sum_{k=1}^{\infty} \left\{ \frac{(-k) \exp(-ik\phi_q)}{(R_q)^{k+1}} a_k + k (R_q)^{k-1} \exp(-ik\phi_q) b_k + \delta_{k1} \Gamma_2 \exp(-i\phi_q) \right\} = 0; \quad (2.55)$$

where δ_{ij} is the Kronecker's delta. Taking account of the orthogonality property of the complex harmonics $\exp(ik\phi_q)$ reduces (2.55) to a set of algebraic relations

$$a_k = \frac{(R_q)^{2k}}{k!} \left(b_k - \delta_{k1} \frac{Q}{\lambda} \right), \quad k = 1, 2, \dots; \quad (2.56)$$

which, together with (2.54), form a closed infinite set of linear algebraic equations, from where the unknown coefficients a_k are to be determined. The explicit dimensionless form of it is ($\tilde{a}_n = a_n / (R_q)^n$):

$$\tilde{a}_k - \sum_{n=1}^{\infty} \left[\frac{i^{n-k} (n+k-1)!}{k! (n-1)!} \left(\frac{R_q}{2X_{2q}} \right)^{(n+k)} \right] \tilde{a}_n = -\delta_{k1} \frac{Q}{\lambda}. \quad (2.57)$$

Remark 1. *Expectably, the solution obtained does not contain X_{1q} as a parameter and is invariant to the particular choice of global coordinate system origin at the boundary $x_2 = 0$.*

Half plane with a circular hole: elasticity problem

Next, we consider an equilibrium stress state of a half plane with circular hole subjected to uniform far stress field $\mathbf{S} = \{S_{ij}\}$. By analogy with above analysis (2.41), we construct solution as a superposition of three terms,

$$u = u_1 + iu_2 = u_0 + u_s + u_h, \quad (2.58)$$

u_0 being the far field solution, u_s and u_h are the disturbance fields induced by hole and flat boundary, respectively. The form of the first two terms are essentially the same as those in (Buryachenko and Kushch, 2004); here, we give a brief summary of the formulas to be used below.

So, the basic representation of u in terms of scalar complex potentials (Muskhelishvili, 1953) is

$$u_1 + iu_2 = \varkappa_0 \varphi(z) - z \overline{\varphi'(z)} - \overline{\psi(z)}, \quad (2.59)$$

where $\varkappa_0 = 3 - 4\nu_0$ for the plane strain problem and ν_0 is the Poisson ratio of the halfplane material. The corresponding to u (2.59) components of the stress tensor $\sigma = \{\sigma_{ij}\}$ are given by the formulas (Muskhelishvili, 1953)

$$\begin{aligned} \sigma_{11} + \sigma_{22} &= 4G_0 \left(\varphi'(z) + \overline{\varphi'(z)} \right); \\ \sigma_{22} - \sigma_{11} + 2i\sigma_{12} &= 4G_0 [\bar{z}\varphi''(z) + \psi'(z)]. \end{aligned} \quad (2.60)$$

The potentials, corresponding to the uniform far field u_0 , are $\varphi_0(z) = \Gamma_1 z$ and $\psi_0(z) = \Gamma_2 z$ ($\text{Im } \Gamma_1 = 0$); from (2.59),

$$u_0 = (\varkappa_0 - 1) \Gamma_1 z - \overline{\Gamma_2 z}. \quad (2.61)$$

The values of Γ_1 and Γ_2 are

$$\Gamma_1 = \frac{E_{11} + E_{22}}{2(\varkappa_0 - 1)}; \quad \Gamma_2 = \frac{1}{2} (E_{22} - E_{11} + 2iE_{12}) \quad (2.62)$$

for the uniform strain far field $\mathbf{E} = \{E_{ij}\}$, and

$$\Gamma_1 = \frac{S_{11} + S_{22}}{8G_0}; \quad \Gamma_2 = \frac{1}{4G_0} (S_{22} - S_{11} + 2iS_{12}) \quad (2.63)$$

when the uniform stress far field $\mathbf{S} = \{S_{ij}\}$ prescribed; G_0 is a shear modulus of the halfplane's material. In both the cases, Γ_1 and Γ_2 represent hydrostatic and deviatoric,

respectively, parts of solution. Induced by hole disturbance field u_s also is taken as (2.59), where we put $z = z_q$, $\varphi = \varphi_s$ and $\psi = \psi_s$; these potentials, by analogy with (2.42), are given by singular part of the Loran's series, namely

$$\varphi_s(z) = \sum_{n=1}^{\infty} \frac{a_n}{z^n}, \quad \psi_s(z) = \sum_{n=1}^{\infty} \frac{b_n}{z^n}. \quad (2.64)$$

For the half plane disturbance solution u_h the following, somewhat different from (2.59) and (2.60) representation

$$\begin{aligned} u &= \varkappa_0 \overline{\varphi(\bar{z})} - (z - \bar{z})\varphi'(\bar{z}) - \psi(\bar{z}); \\ \sigma_{11} + \sigma_{22} &= 4G_0 \left(\varphi'(\bar{z}) + \overline{\varphi'(\bar{z})} \right); \\ \sigma_{22} - \sigma_{11} + 2i\sigma_{12} &= 4G_0 \left[(\bar{z} - z)\overline{\varphi''(\bar{z})} - \overline{\varphi'(\bar{z})} + \overline{\psi'(\bar{z})} \right]; \end{aligned} \quad (2.65)$$

is more appropriate. The corresponding potentials have the form analogous to (2.43):

$$\varphi_h(z) = \int_{-\infty}^{\infty} p(\beta) \exp(i\beta z) d\beta; \quad \psi_h(z) = \int_{-\infty}^{\infty} q(\beta) \exp(i\beta z) d\beta. \quad (2.66)$$

It is rather straightforward to show that defined by (2.65) displacement and stress fields satisfy the elastic equilibrium equations.

To specify the problem, we assume the surface of hole to be traction-free:

$$\mathbf{T}_r = \sigma_r \mathbf{e}_r + \sigma_{r\phi} \mathbf{e}_\phi = 0 \quad \text{or, equivalently,} \quad (\sigma_r - i\sigma_{r\phi}) \Big|_{r_q = R_q} = 0. \quad (2.67)$$

The following well known formula is useful for evaluation σ_r and $\sigma_{r\phi}$:

$$\tau_r = \sigma_r - i\sigma_{r\phi} = \frac{1}{2} [(\sigma_{11} + \sigma_{22}) - (\sigma_{22} - \sigma_{11} + 2i\sigma_{12}) e^{2i\phi}]; \quad (2.68)$$

with account for (2.60) and (2.65), it gives an explicit representation of σ_r and $\sigma_{r\phi}$ in terms of complex potentials derivatives. Similarly, the components of the traction vector at the flat boundary $x_2 = 0$ $\mathbf{T}_n = \sigma_{12} \mathbf{e}_1 + \sigma_{22} \mathbf{e}_2$ can be written in terms of potentials φ and ψ using

$$\tau_n = \sigma_{22} + i\sigma_{12} = \frac{1}{2} [(\sigma_{11} + \sigma_{22}) + (\sigma_{22} - \sigma_{11} + 2i\sigma_{12})]. \quad (2.69)$$

For the time being, we apply at the flat boundary the uniform load compatible with the far stress field:

$$\tau_n(u) \Big|_{x_2 = 0} = S_{22} + iS_{12}. \quad (2.70)$$

It is obvious that u_0 (2.61) with Γ_1 and Γ_2 in the form (2.63) satisfies (2.70) and reduces it to a homogeneous boundary condition

$$\tau_n(u_s + u_h) \Big|_{x_2 = 0} = 0, \quad (2.71)$$

equivalent to (2.44) in the conductivity problem. We make use of (2.71) to express $p(\beta)$ and $q(\beta)$ in terms of the potentials (2.66). So, their substitution into the eqns (2.65) gives

$$\begin{aligned}\varphi'_h(\bar{z}) + \overline{\varphi'_h(\bar{z})} &= \int_{-\infty}^{\infty} (i\beta) \left[p(\beta) \exp(i\beta\bar{z}) - \overline{p(\beta)} \exp(-i\beta z) \right] d\beta; \quad (2.72) \\ (\bar{z} - z)\overline{\varphi''_h(\bar{z})} - \overline{\varphi'_h(\bar{z})} + \psi'_h(\bar{z}) &= \int_{-\infty}^{\infty} (i\beta) \left[\overline{p(\beta)} - \overline{q(\beta)} + 2\beta x_2 \overline{p(\beta)} \right] \exp(-i\beta z) d\beta.\end{aligned}$$

From (2.65), (2.69) and (2.72) we obtain for $x_2 = 0$

$$\frac{\tau_n(u_h)}{2G_0} = \int_{-\infty}^{\infty} (i\beta) \left[p(\beta) \exp(i\beta x_1) + \overline{q(\beta)} \exp(-i\beta x_1) \right] d\beta. \quad (2.73)$$

On the other hand, from (2.60) and (2.69) one finds that

$$\begin{aligned}\frac{\tau_n(u_s)}{2G_0} &= \varphi'_s(z_q) + \overline{\varphi'_s(z_q)} + \overline{z_q} \varphi''_s(z_q) + \psi'_s(z_q) \quad (2.74) \\ &= \sum_{n=1}^{\infty} (-n) \left[\frac{a_n + b_n}{(z_q)^{n+1}} + \frac{\bar{a}_n}{(\bar{z}_q)^{n+1}} - (n+1) \frac{a_n \bar{z}_q}{(z_q)^{n+2}} \right].\end{aligned}$$

By applying the transformation rule (2.47) to (2.74), we obtain after some algebra

$$\begin{aligned}\frac{\tau_n(u_s)}{2G_0} \Big|_{x_2=0} &= \int_{-\infty}^{\infty} (i\beta) \left\{ [Q(\beta) - R(\beta) - 2\beta X_{2q} P(\beta)] \exp(-i\beta Z_q) \exp(i\beta x_1) \right. \quad (2.75) \\ &\quad \left. - P(\beta) \exp(i\beta \bar{Z}_q) \exp(-i\beta x_1) \right\} d\beta,\end{aligned}$$

where

$$P(\beta) = \sum_{n=1}^{\infty} a_n \xi_n^-(\beta), \quad Q(\beta) = \sum_{n=1}^{\infty} b_n \xi_n^-(\beta) \quad \text{and} \quad R(\beta) = \sum_{n=1}^{\infty} n a_n \xi_n^-(\beta). \quad (2.76)$$

Substitution of (2.73) and (2.75) into (2.71) gives us the finite relations between $p(\beta)$, $q(\beta)$ and a_n , b_n :

$$\begin{aligned}p(\beta) &= [R(\beta) - Q(\beta) + 2\beta X_{2q} P(\beta)] \exp(-i\beta Z_q); \quad (2.77) \\ q(\beta) &= -P(\beta) \exp(-i\beta Z_q).\end{aligned}$$

Again, $p(\beta) = q(\beta) \equiv 0$ for $\beta < 0$.

Remark 2. *The boundary condition in the form of eqn (2.70) is obviously not the only choice; by analogy, we can consider in the same way the displacement or mixed-mode condition at the flat boundary of half plane: moreover, these conditions can be inhomogeneous. E.g., let (2.70) has the form*

$$\tau_n(u) \Big|_{x_2=0} = S_{22} + F_{22}(x_1) + i(S_{12} + F_{12}(x_1)),$$

where

$$F(x_1) = F_{22}(x_1) + iF_{12}(x_1) = \int_{-\infty}^{\infty} f(x_1) dx_1 = 0;$$

Noteworthy, zero mean value of F is required only to provide total (surface plus far field) force balance and is not limiting in any way. In this case, the condition (2.71) has non-zero right-hand side:

$$\tau_n(u_s + u_h) \Big|_{x_2 = 0} = \int_{-\infty}^{\infty} f(\beta) \exp(i\beta x_1) d\beta,$$

where $f(\beta)$ is given by inverse Fourier transform

$$\int_{-\infty}^{\infty} f(\beta) = \frac{1}{2\pi} \int_{-\infty}^{\infty} F(x_1) \exp(-i\beta x_1) dx_1.$$

It results in the additional right-hand terms, namely $f(\beta)$ and $\overline{f(-\beta)}$ in the expressions (2.77) which, however, do not affect flow of solution.

To obtain a resolving set of equations for a_n and b_n from the condition (2.67), we need first to expand all the terms, $\tau_n(u_0)$, $\tau_n(u_s)$ and $\tau_n(u_h)$ into the Loran series in a vicinity of the point O_q . The formulas (2.63) and (2.68) give us immediately

$$\frac{\tau_n(u_0)}{2G_0} \Big|_{r_q = R_q} = 2\Gamma_1 - \Gamma_2 \exp(-2i\phi_q). \quad (2.78)$$

The term u_s is written initially in the local coordinates z_q ; by substituting (2.60) into (2.68), we get

$$\frac{\tau_n(u_s)}{2G_0} \Big|_{r_q = R_q} = \exp(i\phi_q) \sum_{k=1}^{\infty} \frac{(-k)}{(R_q)^{k+1}} \{ \bar{a}_k \exp(ik\phi_q) + [(k-2)a_{k-2}(R_q)^2 - b_k] \exp(-ik\phi_q) \}. \quad (2.79)$$

Transformation of $\tau_n(u_h)$ is similar to (2.52) and (2.53) although somewhat more involved. Omitting the algebra, we give the resulting formulae to be substituted into (2.68):

$$\begin{aligned} \frac{\sigma_{11} + \sigma_{22}}{4G_0} &= \varphi'_{qh}(\bar{z}_q) + \overline{\varphi'_{qh}(\bar{z}_q)}; \\ \frac{\sigma_{22} - \sigma_{11} + 2i\sigma_{12}}{4G_0} &= (\bar{z}_q - z_q) \overline{\varphi''_{qh}(\bar{z}_q)} - \overline{\varphi'_{qh}(\bar{z}_q)} + \overline{\psi'_{qh}(\bar{z}_q)}; \end{aligned} \quad (2.80)$$

here,

$$\varphi_{qh}(z) = \sum_{k=0}^{\infty} A_k^{(q)} z^k \quad \text{and} \quad \psi_s(z) = \sum_{k=0}^{\infty} B_k^{(q)} z^k, \quad (2.81)$$

where, analogously to (2.53),

$$\begin{aligned} A_k^{(q)} &= \frac{1}{k!} \int_0^{\infty} (i\beta)^k p(\beta) \exp(i\beta \bar{Z}_q) d\beta, \\ B_k^{(q)} &= \frac{1}{k!} \int_0^{\infty} (i\beta)^k [q(\beta) - 2\beta X_{2q} p(\beta)] \exp(i\beta \bar{Z}_q) d\beta, \\ k &= 1, 2, \dots \end{aligned} \quad (2.82)$$

And, likewise to (2.53), these expressions can be simplified to

$$\begin{aligned} A_k^{(q)} &= -\sum_{n=1}^{\infty} \frac{i^{k-n}(n+k-1)!}{k!(n-1)!(2X_{2q})^{(n+k)}} (ka_n + b_n), \\ B_k^{(q)} &= -\sum_{n=1}^{\infty} \frac{i^{k-n}(n+k-1)!}{k!(n-1)!(2X_{2q})^{(n+k)}} a_n + 2iX_{2q}(k+1)A_{k+1}^{(q)}, \end{aligned} \quad (2.83)$$

where the explicit expressions of $p(\beta)$ and $q(\beta)$ are taken into account.

The resulting local expansion is

$$\begin{aligned} \frac{\tau_n(u_h)}{2G_0} \Big|_{r_q = R_q} &= \exp(i\phi_q) \sum_{k=1}^{\infty} k (R_q)^{k-1} \left\{ \left(A_k^{(q)} + \delta_{k1} \overline{A_k^{(q)}} \right) \exp(-ik\phi_q) \right. \\ &\quad \left. + \left[k \overline{A_k^{(q)}} - \overline{B_k^{(q)}} - (k+2) (R_q)^2 \overline{A_{k+2}^{(q)}} \right] \exp(ik\phi_q) \right\}. \end{aligned} \quad (2.84)$$

We substitute it together with (2.78) and (2.80) into (2.67) to obtain an infinite set of equalities:

$$\begin{aligned} a_k - (R_q)^{2k} \left[k \overline{A_k^{(q)}} - \overline{B_k^{(q)}} - (R_q)^2 (k+2) \overline{A_{k+2}^{(q)}} \right] &= -\Gamma_2 \delta_{k1}; \\ b_k - (R_q)^2 (k-2) a_{k-2} + (R_q)^{2k} \left(A_k^{(q)} + \delta_{k1} \overline{A_k^{(q)}} \right) &= -2\Gamma_1 \delta_{k1}; \end{aligned}$$

in a pair with (2.80) they form a closed set of linear algebraic equations, from where the unknowns a_n and b_n can be found and, thus, the problem has been solved.

A finite array of inclusions

Now, we consider an elastic halfplane $x_2 \leq 0$ with elastic moduli ν_0 and G_0 , containing a finite number N of elastic circular inclusions of radii R_q with elastic properties ν_q and G_q , $q = 1, 2, \dots, N$. As before, the stress state of inhomogeneous halfplane is governed by the uniform far stress field $\mathbf{S} = \{S_{ij}\}$. At the matrix - fiber interfaces, the conditions of perfect bonding, or adhesion

$$\begin{aligned} \left(u_m - u_i^{(q)} \right) \Big|_{r_q = R_q} &= 0; \quad \left[\tau_n(u_m) - \tau_n(u_i^{(q)}) \right] \Big|_{r_q = R_q} = 0; \\ q &= 1, 2, \dots, N. \end{aligned} \quad (2.85)$$

are assumed. Here, u_m and $u_i^{(q)}$ represent displacement in the matrix and q th inclusion, respectively. At the boundary $x_2 = 0$, the stress boundary condition is taken in the form (2.70).

In accordance with analysis by Buryachenko and Kushch (2004), we write solution in the multiple-connected matrix domain as

$$u = u_0 + \sum_{p=1}^N u_{ps} + u_h, \quad (2.86)$$

where u_0 and u_h are given by the eqns (2.61) and (2.65)-(2.66), respectively; for u_{ps} , we accept (2.59) with $z = z_q$, $\varphi = \varphi_{ps}$ and $\psi = \psi_{ps}$ given by

$$\varphi_{ps}(z) = \sum_{n=1}^{\infty} \frac{a_n^{(p)}}{z^n}, \quad \psi_{ps}(z) = \sum_{n=1}^{\infty} \frac{b_n^{(p)}}{z^n}. \quad (2.87)$$

Displacement $u_i^{(q)}$ in the q th fiber is given by

$$u_i^{(q)} = \varkappa_q \varphi_{qr}(z_q) - z_{qr} \overline{\varphi'_{qr}(z_q)} - \overline{\psi_{qr}(z_q)}, \quad (2.88)$$

$$\varphi_{qr}(z) = \sum_{n=0}^{\infty} \frac{c_n^{(q)}}{z^n}, \quad \psi_{qr}(z) = \sum_{n=0}^{\infty} \frac{d_n^{(q)}}{z^n}.$$

Analysis similar to that performed in the previous subsection reduces the surface traction condition (2.70) to

$$\tau_n \left(\sum_{p=1}^N u_{ps} + u_h \right) \Big|_{x_2=0} = 0,$$

provided Γ_1 and Γ_2 are taken in the form (2.63). The following results are quite close to those presented in the previous subsection and we give them here without derivation. So, the density functions $p(\beta)$ and $q(\beta)$ in (2.66) are given now by

$$p(\beta) = \sum_{p=1}^N [R^{(p)}(\beta) - Q^{(p)}(\beta) + 2\beta X_{2p} P^{(p)}(\beta)] \exp(-i\beta Z_p); \quad (2.89)$$

$$q(\beta) = -\sum_{p=1}^N P^{(p)}(\beta) \exp(-i\beta Z_p);$$

where

$$P^{(p)}(\beta) = \sum_{n=1}^{\infty} a_n^{(p)} \xi_n^-(\beta), \quad Q^{(p)}(\beta) = \sum_{n=1}^{\infty} b_n^{(p)} \xi_n^-(\beta) \quad \text{and} \quad R^{(p)}(\beta) = \sum_{n=1}^{\infty} n a_n^{(p)} \xi_n^-(\beta).$$

The local expansion of u_h around the point O_q has the form (2.66) with the potentials given by (2.81), where the values of expansion coefficients $A_k^{(q)}$ and $B_k^{(q)}$ are now

$$A_k^{(q)} = \sum_{p=1}^N \sum_{n=1}^{\infty} [G_{nk}^{pq} (n a_n^{(p)} - b_n^{(p)}) + 2i X_{2q} n G_{n+1,k}^{pq} a_n^{(p)}]; \quad (2.90)$$

$$B_k^{(q)} = -\sum_{p=1}^N \sum_{n=1}^{\infty} G_{nk}^{pq} a_n;$$

$$G_{nk}^{pq} = \frac{(-1)^k (n+k-1)!}{k!(n-1)!} (\bar{Z}_q - Z_p)^{-(n+k)}.$$

The remaining part of solving procedure, namely, local expansion of u_{ps} in the vicinity of O_q for $p \neq q$ and matching the interface conditions (2.85) resembles that described

elsewhere (Buryachenko and Kushch, 2004) and we do not reproduce it here. The resolving set of linear equations corresponding to (2.85) is

$$\begin{aligned}
\mathcal{K}_0 \frac{a_k^{(q)}}{(R_q)^{2k}} - (R_q)^2 (k+2) \left(\overline{a_{-k-2}^{(q)}} + A_{k+2}^{(q)} \right) - \left(\overline{b_{-k}^{(q)}} + B_k^{(q)} \right) + k A_k^{(q)} & \quad (2.91) \\
= \delta_{k1} \overline{\Gamma_2} - (R_q)^2 (k+2) \overline{c_{-(k+2)}^{(q)}} - \overline{d_{-k}^{(q)}}; \\
\frac{b_k^{(q)}}{(R_q)^{2k}} - (k-2) \frac{a_{k-2}^{(q)}}{(R_q)^{2k-2}} - \mathcal{K}_0 \left(\overline{a_{-k}^{(q)}} + A_k^{(q)} \right) + \delta_{k1} \overline{A_k^{(q)}} & \\
= \delta_{k1} \left[(\mathcal{K}_0 - 1) \Gamma_1 + c_{-k}^{(q)} \right] - \mathcal{K}_q \overline{c_{-k}^{(q)}}; \\
\frac{a_k^{(q)}}{(R_q)^{2k}} + (R_q)^2 (k+2) \left(\overline{a_{-k-2}^{(q)}} + A_{k+2}^{(q)} \right) + \left(\overline{b_{-k}^{(q)}} + B_k^{(q)} \right) - k A_k^{(q)} & \\
= -\delta_{k1} \overline{\Gamma_2} + \lambda_q \left[(R_q)^2 (k+2) \overline{c_{-(k+2)}^{(q)}} + \overline{d_{-k}^{(q)}} \right]; \\
\frac{b_k^{(q)}}{(R_q)^{2k}} - (k-2) \frac{a_{k-2}^{(q)}}{(R_q)^{2k-2}} + \left(\overline{a_{-k}^{(q)}} + A_k^{(q)} \right) + \delta_{k1} \overline{A_k^{(q)}} & \\
= -2\delta_{k1} \Gamma_1 + \lambda_q \left(\delta_{k1} c_{-k}^{(q)} + \overline{c_{-k}^{(q)}} \right); \\
q = 1, 2, \dots, N; \quad k = 1, 2, \dots .
\end{aligned}$$

In (2.91), $\lambda_q = G_q/G_0$,

$$\begin{aligned}
a_{-k}^{(q)} &= \sum_{\substack{p=1 \\ (p \neq q)}}^N \sum_{n=1}^{\infty} a_n^{(p)} H_{nk}^{pq}, \\
B_{-k}^{(q)} &= \sum_{\substack{p=1 \\ (p \neq q)}}^N \sum_{n=1}^{\infty} \left[B_n^{(p)} - \frac{Z_{pq}}{Z_p} (k+n) A_n^{(p)} \right] H_{nk}^{pq}; \\
H_{nk}^{pq} &= (-1)^k \frac{(n+k-1)!}{k!(n-1)!} (Z_{pq})^{-(n+k)} \quad \text{and} \quad Z_{pq} = Z_q - Z_p.
\end{aligned} \quad (2.92)$$

By excluding the unknowns $c_{-k}^{(q)}$ and $d_{-k}^{(q)}$, the system (2.91) is reduced to

$$\begin{aligned}
\frac{\Omega_1}{(R_q)^{2k}} \left[(R_q)^2 (k-2) a_{k-2}^{(q)} - b_k^{(q)} \right] + \overline{a_{-k}^{(q)}} + A_k^{(q)} &= -\delta_{k1} \Gamma_1; \\
\frac{\Omega_2}{(R_q)^{2k}} a_k^{(q)} - (k+2) (R_q)^2 \left(\overline{a_{-k-2}^{(q)}} + A_{k+2}^{(q)} \right) - \left(\overline{b_{-k}^{(q)}} + B_k^{(q)} \right) + k A_k^{(q)} &= \delta_{k1} \overline{\Gamma_2}; \\
q = 1, 2, \dots, N; \quad k = 1, 2, \dots ;
\end{aligned} \quad (2.93)$$

where

$$\Omega_1 = \frac{(2\lambda_q + \mathcal{K}_q - 1)}{2[\lambda_q(\mathcal{K}_0 - 1) + (\mathcal{K}_q - 1)]} \text{ for } k = 1, \quad \Omega_1 = \frac{(\lambda_q + \mathcal{K}_q)}{2(\lambda_q \mathcal{K}_0 - \mathcal{K}_q)} \text{ for } k > 1$$

and

$$\Omega_2 = \frac{(\lambda_q \mathcal{K}_0 + 1)}{2(\lambda_q - 1)}.$$

After we have (2.93) solved for $a_k^{(q)}$ and $b_k^{(q)}$, the following finite relations can be utilized to evaluate $c_{-k}^{(q)}$ and $d_{-k}^{(q)}$:

$$\begin{aligned}
c_{-k}^{(q)} &= \frac{(\varkappa_0 + 1)}{(\lambda_q + \varkappa_q)} \left(a_k^{(q)} + \overline{A_k^{(q)}} \right), \quad k > 1; \\
\operatorname{Re} c_{-1}^{(q)} &= \frac{(\varkappa_0 + 1)}{(2\lambda_q + \varkappa_q - 1)} \operatorname{Re} \left(a_1^{(q)} + \overline{A_1^{(q)}} + \Gamma_1 \right); \\
\operatorname{Im} c_{-1}^{(q)} &= \frac{(\varkappa_0 + 1)}{(\varkappa_q + 1)} \operatorname{Im} \left(a_1^{(q)} - \overline{A_1^{(q)}} \right); \\
d_{-k}^{(q)} &= \frac{(\varkappa_0 + 1)}{(\lambda_q - 1)} \frac{\overline{a_k^{(q)}}}{(R_q)^{2k}} - (R_q)^2 (k + 2) \overline{c_{-(k+2)}^{(q)}}, \quad k \geq 1; \\
d_0^{(q)} &= 2(R_q)^2 \left(a_{-2}^{(q)} + \overline{A_2^{(q)}} - c_{-2}^{(q)} \right) + b_0^{(q)} + \overline{B_0^{(q)}} \\
&\quad - \varkappa_0 \left(\overline{a_0^{(q)}} + A_0^{(q)} \right) - (\varkappa_0 - 1) \Gamma_1 Z_q + \overline{\Gamma_2 Z_q}.
\end{aligned}$$

2.1.6 Numerical study

In order to check the accuracy of the numerical method the influence of the interaction between two identical circular inclusions (e.g. fibers) on the stress field in the inclusions is studied. Let the elastic properties of the matrix and the inclusions be $\mu^{(0)} = 1$, $\nu^{(0)} = 0.5$ and $\mu^{(1)} = 1000$, $\nu^{(1)} = 0.5$. Let us consider a plane strain problem and the pair of inclusions v_i and v_j loaded by the tension $\langle \boldsymbol{\sigma} \rangle = (\langle \sigma_{11} \rangle, 0, 0)^\top$ along the line linked to the inclusion centers $\mathbf{x}_2 = (Da, 0)^\top$ and $\mathbf{x}_1 = (0, 0)^\top$, D is a normalized distance between the inclusion centers. In Fig.2.2 the numerical results of the normal tractional component $\sigma_{rr} = \sigma_{rr}(\phi)$ at the interface of the first fiber $\mathbf{x} = a(\cos(\phi), \sin(\phi))^\top \in v_1$ obtained

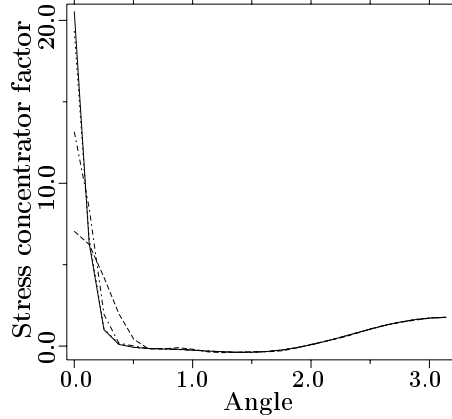


Figure 2.2: Stress concentration factor $\sigma_{11}(\mathbf{z})/\langle \sigma_{11} \rangle$ at the fiber matrix interface $\mathbf{z} = (a, 0)^\top$ vs normalized distance D : $n_h = 120$ (solid curve), $n_h = 40$ (dotted curve), $n_h = 20$ (dot-dashed curve), $n_h = 10$ (dashed curve).

for the numbers of harmonics $n_h = 120, 40, 20, 10$ are presented at $D = 2.01$ that demonstrate the error 5.8%, 35% and 65% of the solution with the $n_h = 40, 20$, and $n_h = 10$, respectively, in comparison with the solution corresponding to $n_h = 120$. The CPU times expended for the solution at a PC with a 2.0 GHz processor equal 150 sec. and 0.5 sec. for $n_h = 120$ and $n_h = 30$, respectively. The error less 0.1% is provided by

the number of harmonics $n_h = 70$. It can be seen that as the fibers approach each other, the accuracy using the Kolosov-Muskhelishvili complex potentials decreases rapidly, and a little improvement in accuracy up to 0.1% can be provided just by significantly increasing the number of harmonics used to $n_h = 95$ at $D = 2.005$.

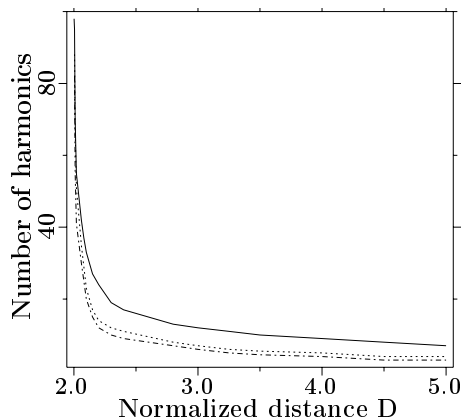


Figure 2.3: The number n_h of harmonics providing the error less 0.1% (solid curve), 1.0% (dotted curve), and 5.0% (dot-dashed curve) vs the normalized distance D between the inclusion centers.

In a similar manner, the number of approximating harmonics providing the error less 0.1%, 1%, and 5% were estimated in Fig.2.3 as a function of the relative distances between the fibers D . Although the present numerical estimation for the local stress field in the fiber loses accuracy (that can be protected by increasing of the number n_h of harmonics) when the fibers almost touch, this does not affect the accuracy of the estimated coefficient of the $O(c^2)$ term which, being dependent on the smoothing integral operator, is very insensitive to the exact local stress distribution in the fibers when $D \rightarrow 2$. The integrals in Eq. (2.9) and (2.10) are estimated for the well stirred radial distribution function $g(|\mathbf{x}_i - \mathbf{y}_j|) \equiv 1$ at $|\mathbf{x}_i - \mathbf{y}_j| > 2a$ and varying number $n_h = n_h(|\mathbf{x}_i - \mathbf{y}_j|)$ presented in Fig.2.3 and corresponding to the error 0.1%.

Similarly to Chen and Acrivos (1978) we present the coefficient a_2^μ in the form $a_2^\mu = a_1^\mu H$ where the parameter H was estimated

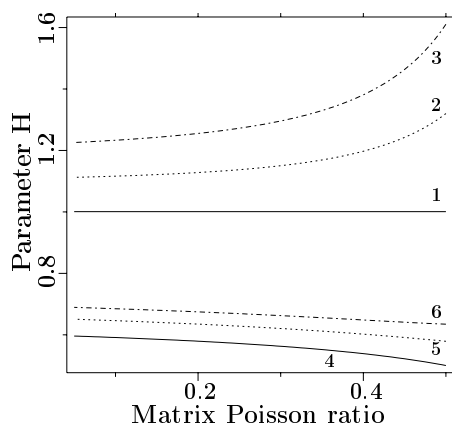


Figure 2.4: The estimation of the coefficient H vs the matrix Poisson ratio $\nu^{(0)}$: $O(c^2)$ approximation of the MT method (solid curves 1, 4), Eq. (2.11) (dotted curves 2, 5), Eq. (2.9) (dot-dashed curve 3, 6). The curves 1, 2, 3 are estimated for $\mu^{(1)} = 1000$, and the curves 4, 5, 6 - for $\mu^{(1)} = 3$.

in Fig. 2.4 by the different methods as a function of the Poisson ratio $\nu^{(0)}$ for two different values $\mu^{(1)} = 1000$ and $\mu^{(1)} = 3$ (another elastic moduli are fixed: $\mu^{(0)} = 1$, $\nu^{(1)} =$

0.5). It was used the methods (2.9), (2.11) as well as the $O(c^2)$ approximation of the MT method. As can be seen, using the accurate solution (2.9) leads to significant refinement of the results obtained. The coefficients H estimated for the different varying numbers $n_h = n_h(|\mathbf{x}_i - \mathbf{y}_j|)$ corresponding to the errors 0.1% and 1.0% differ from one another on 0.002%. In order to demonstrate the comparison of the available experimental data with the predicting capability of the proposed method, we will consider the estimation of the effective elastic moduli \mathbf{L}^* (4.9). Assume the matrix is epoxy resin ($k^{(0)} = 4.27$ GPa and $\mu^{(0)} = 1.53$ GPa) which contains identical circular glass fibers ($k^{(1)} = 50.89$ GPa and $\mu^{(1)} = 35.04$ GPa). In Fig.2.5 the experimental data by Lee and Mykkanen (1987)

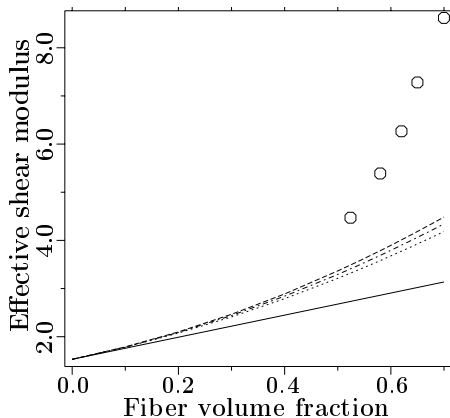


Figure 2.5: Estimation of the relative effective shear modulus $\mu^*/\mu^{(0)}$ as a function of a fiber volume fraction c . Experimental data \circ and curves calculated by the linear approximation (solid line), by $O(c^2)$ approximation of Mori-Tanaka method (dotted curve), by Eq. (2.11) (dot-dashed line), (2.9) (dashed line).

are compared with the estimations of the effective shear modulus μ^* obtained by the use of Eqs. (2.9), (2.11), by the $O(c^2)$ approximation of the MT method, which is equivalent to the vanishing of the integral item in Eq. (2.11) as well as by the linear approximation $O(c)$ of Eq. (2.9). As can be seen from Fig.2.5, the use of method (2.9) and especially by using method (2.11), slightly improves the approximation of experimental data in comparison with the $O(c^2)$ approximation of the MT approach. Only an insignificant difference of the mentioned curved is explained by a slight variation of the considered composite material of the parameter $H = 0.932, 1.073, 1.200$ estimated by the $O(c^2)$ approximation of the MT method, by (2.9) and by (2.11) methods, respectively (compared with the analogous parameter H in Fig.2.4 for the rigid fibers in the incompressible matrix). The next improvement of the proposed method (2.9) will be considered in forthcoming publications by the authors in the framework of the multiparticle effective field method (MEFM, Buryachenko, 2001) with a non-well-stirred radial distribution function $g(|\mathbf{x}_i - \mathbf{y}_j|) \neq \text{const.}$ at $|\mathbf{x}_i - \mathbf{y}_j| > 2a$ estimated by the authors of by Buryachenko *et al.* (2003). It should be mentioned that the MT method is invariant with respect to the radial distribution function $g(|\mathbf{x}_i - \mathbf{y}_j|)$ in opposition to the MEFM.

Below, we give a few numerical examples to show numerical efficiency and accuracy of the method developed in application to the composite half space problems. All the practical calculations were performed with $t_{\max} = 30$, where t_{\max} is a max number of harmonics retained in the truncated system (2.93). As analysis shows, this provides practical convergence of solution and, thus, sufficient accuracy of calculations: so, relative error of stress evaluation is well below 1% for geometry where gap between the inclusions and/or

flat boundary of half plane is $0.1R$ or greater. The smaller is gap, the higher harmonics are to be taken into account to provide accuracy of numerical data: this relationship was studied in detail elsewhere (Buryachenko and Kushch, 2005).

The obtained solution contains an additional integral term, evaluation of which requires a considerable computational effort. It is possible, however, to avoid direct integration, at least in the case where the surface load is taken in the form (2.70). Before starting the practical calculations, we derive some useful formulas; their application makes the solution for inhomogeneous half plane comparable in efficiency with that for an unbounded plane with inclusions. Taking into account the explicit expressions of the integral densities $p(\beta)$ and $q(\beta)$ (2.89) allows us, with aid of the mentioned already Euler's integral for Gamma-function, to find representation of the potentials (2.66) by the rational functions. So, we have

$$\begin{aligned} \psi_h(\bar{z}) &= \int_{-\infty}^{\infty} q(\beta) \exp(i\beta\bar{z}) d\beta = - \sum_{p=1}^N \sum_{n=1}^{\infty} a_n^{(p)} \int_{-\infty}^{\infty} \xi_n^-(\beta) \exp[-i\beta(\bar{z} - Z_p)] d\beta = \\ &= - \sum_{p=1}^N \sum_{n=1}^{\infty} a_n^{(p)} \int_{-\infty}^{\infty} \xi_n^-(\beta) \exp[-i\beta(\bar{z} - Z_p)] d\beta = - \sum_{p=1}^N \sum_{n=1}^{\infty} \frac{a_n^{(p)}}{(\bar{z} - Z_p)^n}. \end{aligned}$$

In a similar way we get also

$$\varphi_h(\bar{z}) = \int_{-\infty}^{\infty} p(\beta) \exp(i\beta\bar{z}) d\beta = \sum_{p=1}^N \sum_{n=1}^{\infty} \frac{1}{(\bar{z} - Z_p)^n} \left[na_n^{(p)} \frac{(\bar{z} - \bar{Z}_p)}{(\bar{z} - Z_p)} - b_n^{(p)} \right].$$

Note, first, that these formulae are *exact* and provide the most efficient way of the displacement and stress disturbance fields evaluation using the formulas (2.65). Second, and possibly even more important, they give a clear idea of how the solution for half plane could be constructed in rational functions only. Such a solution is, however, restricted to the case of uniform surface load (2.70); the method of solution exposed in the present communication is rather general and allows us to find stress field due to *arbitrary* surface load.

Below, some numerical data for a series of test one- and two inclusion in half space problems are presented. So, the plots at the Fig.2.6 show the stress $\sigma_{11}(x_1)$ at $x_2 = 0$ induced by far stress $S_{11} = 1$ for five different values of distance dH between the hole surface and flat boundary of half plane: $X_{1q} = 0$, $X_{2q} = -(R_q + dH)$. Here and below, we put $R_q = 1$. It is clearly seen considerable stress concentration in the case where hole is close to surface. These data agree well with those reported by Dong et al. (2004) who considered a single hole distant from the half plane edge ($dH = 3$, solid points at the Fig.2.6)

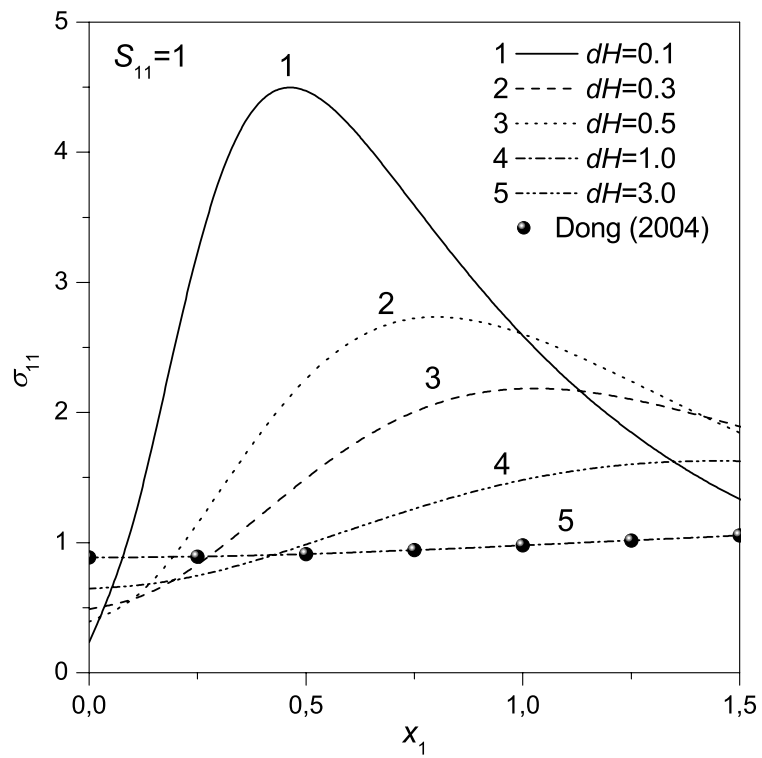


Fig.2.6 Stress σ_{11} variation along the flat boundary of half plane with a single hole

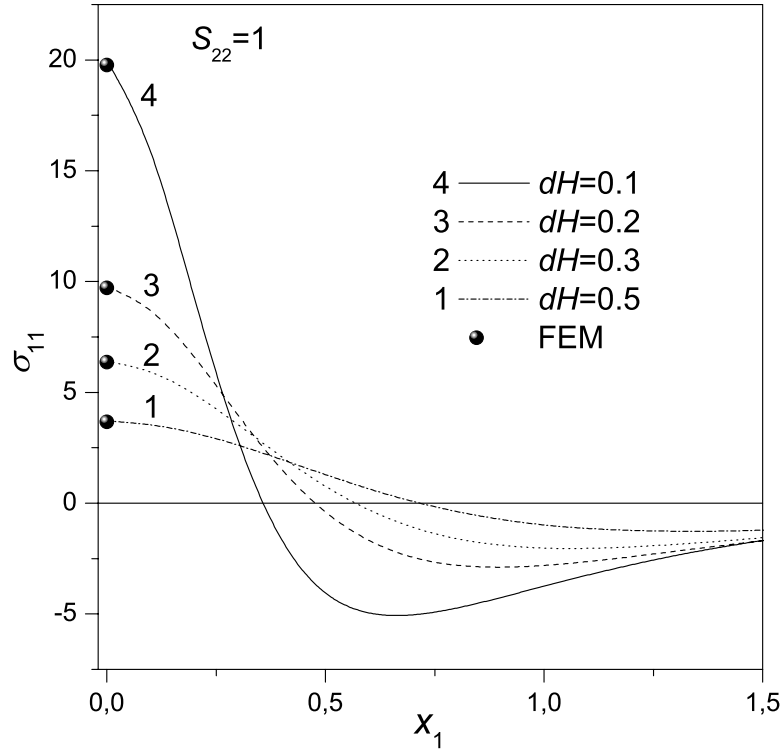


Fig.2.7 Stress σ_{11} variation along the flat boundary of half plane with a single hole

The curves at the Fig.2.7 represent $\sigma_{11}(x_1)$ at $x_2 = 0$ induced by far stress $S_{22} = 1$. As calculations show, uniform load applied to the half plane surface produces very high (up to 20 times) stress concentration for $dH = 0.1$. The solid points at this plot represent the data obtained by FEA using the fine mesh of quadratic 6-node triangular elements. As seen from the picture, agreement between the data compared is very good.

In the last two examples, we analyze stress σ_{11} distribution along the negative x_2 semi axis in the half plane containing two equal circular inclusions. due to load $S_{11} = 1$. Position of the inclusions is given by coordinates $X_{1q} = (-1)^q(R_q + dH/2)$; $X_{2q} = -(R_q + dH)$. Curves at the Fig.2.8 correspond to the case of soft inclusions $E_i/E_m = 0.5$; the solid points represent data by Dong (2004) for $dH = 1$. In this case, the stress concentration shows only slightly dependent on dH . On the contrary, stress between the two hard inclusions $E_i/E_m = 100$ grow rapidly as the inclusions are drawn toward each other and to the flat boundary of half plane (Fig.2.9).

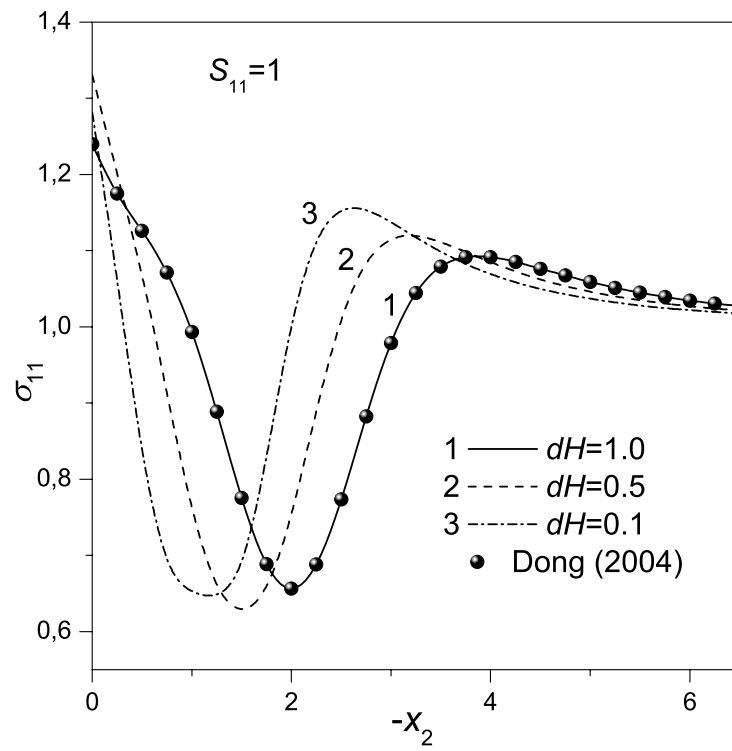


Fig.2.8 Stress σ_{11} variation along the x_2 axis ($x_1 = 0$) in half plane with two inclusions, $S_{11} = 1$

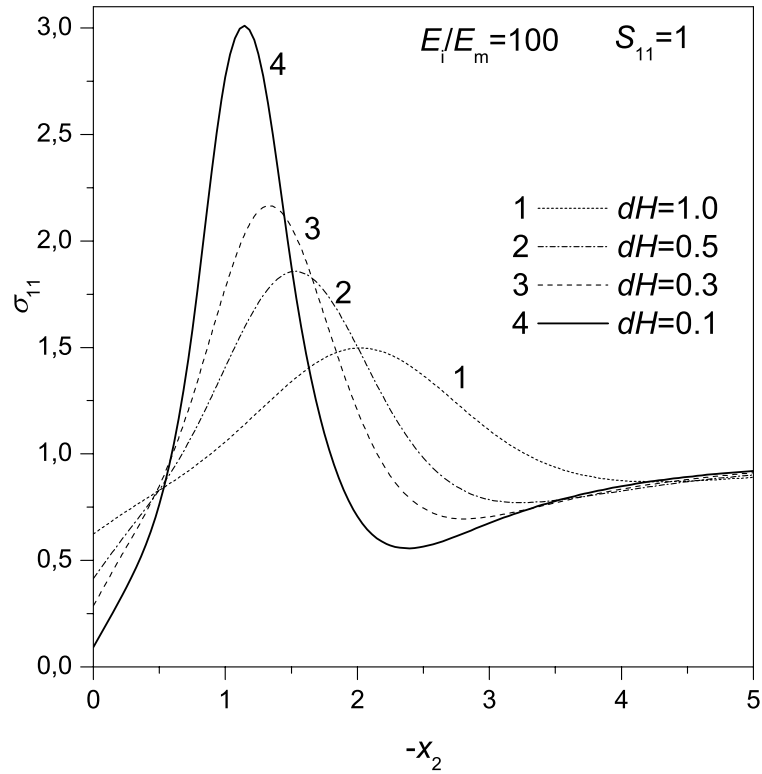


Fig.2.9 Stress σ_{11} variation along the x_2 axis ($x_1 = 0$) in half plane with two hard inclusions, $S_{11} = 1$

2.1.7 Conclusions

An accurate analytical method has been developed to solve for stress in a half plane containing a finite array of circular inclusions, the last being a model of near-to-surface domain of fibrous composite. The method combines technique of complex potentials with the Fourier integral transforms to reduce a primary boundary-value elasticity problem for a complicated multiple-connected domain to an ordinary well-posed set of linear algebraic equations. Moreover, the resulting expression of the matrix coefficients are given by the rational algebraic expressions and do not involve the integral terms. This provides high numerical efficiency of the method, accuracy of which is controlled entirely by a number of harmonics retained in the truncated series for practical calculations. Up to several hundred of interacting inclusions can be considered in this way which makes the model of composite half plane realistic and flexible enough to account for the micro structure statistics. The method has been effectively applied to evaluate the local micro stress and macroscopic transverse elastic moduli of composites at non-dilute concentration of a random field of aligned fibers. The numerical results are given which demonstrate accuracy and high numerical efficiency of the developed method and can serve as a benchmark for the approximate and numerical methods.

2.2 The multi-particle cell model to study effective elastic properties and stress moments in the fibrous composite of random structure

2.2.1 Preliminaries

In the mesodomain $w \subset R^d$ containing a set $X = (V_i, \mathbf{x}_i, \omega_i)$, ($i = 1, 2, \dots$) of ellipsoids v_i with characteristic functions V_i , centers x_i , semi-axes a_i^j ($j = 1, 2, 3$) and an aggregate of Euler angles ω_i , a characteristic function W and space dimensionality d ($d = 2$ and $d = 3$ for 2- D and 3- D problems, respectively). are defined. It is assumed that all inclusions have identical mechanical and geometrical properties and are grouped into the component $v^{(1)}$. The local strain tensor $\boldsymbol{\varepsilon}$ is related to the displacements \mathbf{u} via the linearized strain-displacement equation $\boldsymbol{\varepsilon} = \frac{1}{2}[\nabla \otimes \mathbf{u} + (\nabla \otimes \mathbf{u})^\top]$. Here \otimes denotes tensor product, and $(\cdot)^\top$ denotes matrix transposition. The stress tensor, $\boldsymbol{\sigma}$, satisfies the equilibrium equation: $\nabla \cdot \boldsymbol{\sigma} = \mathbf{0}$. Stresses and strains are related to each other via the constitutive equations $\boldsymbol{\sigma}(\mathbf{x}) = \mathbf{L}(\mathbf{x})\boldsymbol{\varepsilon}(\mathbf{x}) + \boldsymbol{\alpha}(\mathbf{x})$ or $\boldsymbol{\varepsilon}(\mathbf{x}) = \mathbf{M}(\mathbf{x})\boldsymbol{\sigma}(\mathbf{x}) + \boldsymbol{\beta}(\mathbf{x})$, where $\mathbf{L}(\mathbf{x})$ and $\mathbf{M}(\mathbf{x}) \equiv \mathbf{L}(\mathbf{x})^{-1}$ are the known phase stiffness and compliance fourth-order tensors, and the common notation for contracted products has been employed: $\mathbf{L}\boldsymbol{\varepsilon} = L_{ijkl}\varepsilon_{kl}$. $\boldsymbol{\beta}(\mathbf{x})$ and $\boldsymbol{\alpha}(\mathbf{x}) \equiv -\mathbf{L}(\mathbf{x})\boldsymbol{\beta}(\mathbf{x})$ are second-order tensors of local eigenstrains and eigenstresses. In particular, for isotropic constituents the local stiffness tensor $\mathbf{L}(\mathbf{x})$ is given in terms of the local bulk modulus $k(\mathbf{x})$ and the local shear modulus $\mu(\mathbf{x})$, and the local eigenstrain $\boldsymbol{\beta}(\mathbf{x})$ is given in terms of the bulk component $\beta_0(\mathbf{x})$ by the relations:

$$\mathbf{L}(\mathbf{x}) = (dk, 2\mu) \equiv d[k(\mathbf{x}) + (1 - d/3)\mu(\mathbf{x})]\mathbf{N}^1 + 2\mu(\mathbf{x})\mathbf{N}^2, \quad \boldsymbol{\beta}(\mathbf{x}) = \beta_0(\mathbf{x})\boldsymbol{\delta}, \quad (2.94)$$

$\mathbf{N}_1 = \boldsymbol{\delta} \otimes \boldsymbol{\delta}/d$, $\mathbf{N}_2 = \mathbf{I} - \mathbf{N}_1$ ($d = 2$ or 3); $\boldsymbol{\delta}$ and \mathbf{I} are the unit second-order and fourth-order tensors, and \otimes denotes tensor product. The interrelations among the planar $\mathbf{L}_{[2]}$ and three-dimensional $\mathbf{L}_{[3]}$ moduli can be found, e.g., in Torquato (2002). For example, for plane strain $\mu_{[2]} = \mu_{[3]}$, $K_{[2]} = K_{[3]} + \mu_{[3]}/3$, $E_{[2]} = E_{[3]}/(1 + \nu_{[3]})(1 - \nu_{[3]})$, $\nu_{[2]} = \nu_{[3]}/(1 - \nu_{[3]})$ and for plane stress $\mu_{[2]} = \mu_{[3]}$, $K_{[2]} = 9K_{[3]}\mu_{[3]}/(3K_{[3]} + 4\mu_{[3]})$, $E_{[2]} = E_{[3]}$, $\nu_{[2]} = \nu_{[3]}$ where E and ν are the Young modulus and Poisson's ratio. The local strain and stress tensors satisfy the linearized strain-displacement relations and the equilibrium equation, respectively. We consider a mesodomain w , subjected to the uniform traction boundary conditions.

In the matrix $v^{(0)} = w \setminus v^{(1)}$ and in the inclusions $v^{(1)}$ the tensor $\mathbf{f}(\mathbf{x})$ ($\mathbf{f} = \mathbf{L}, \mathbf{M}$, $\mathbf{M} \equiv \mathbf{L}^{-1}$) is assumed to be constant: $\mathbf{f}(\mathbf{x}) = \mathbf{f}^{(0)}$ for $\mathbf{x} \in v^{(0)}$ and $\mathbf{f}(\mathbf{x}) = \mathbf{f}^{(0)} + \mathbf{f}_1(\mathbf{x}) = \mathbf{f}^{(0)} + \mathbf{f}_1^{(1)}$ for $\mathbf{x} \in v^{(1)}$. The upper index of the material properties tensor put in parentheses shows the number of the respective component. The subscript 1 denotes a jump of the corresponding quantity (e.g. of the material tensor). The phases are perfectly bonded.

For random structure composites, we introduce a conditional probability density $\varphi(v_m, \mathbf{x}_m | v_i, \mathbf{x}_i)$, which describes the probability density of finding the m -th inclusion in the domain v_m with the center \mathbf{x}_m , the inclusions in the domains v_i with the centers $\mathbf{x}_i \neq \mathbf{x}_m$ being treated as fixed. We will consider statistically homogeneous media, when all the random quantities under discussion are statistically homogeneous and, hence, the ensemble averaging could be replaced by volume averaging

$$\langle (\cdot) \rangle = \bar{w}^{-1} \int (\cdot) W(\mathbf{x}) d\mathbf{x}, \quad \langle (\cdot) \rangle^{(k)} = [\bar{v}^{(k)}]^{-1} \int (\cdot) V^{(k)}(\mathbf{x}) d\mathbf{x}, \quad (2.95)$$

where $\sum V^{(1)} = \sum V_i$, $i = 1, 2, \dots$, and the bar appearing above the region represents its measure, e.g. $\bar{v} \equiv \text{mes } v$. Of course, $\varphi(v_m, \mathbf{x}_m | v_i, \mathbf{x}_i) = 0$ for values of \mathbf{x}_m lying inside the “included volumes” $\cup v_{im}^0$ ($m = 1, \dots, n$), where $v_{im}^0 \supset v_m$ with characteristic functions V_{im}^0 (since inclusions cannot overlap). $\varphi(v_i)$ is a number density n of component $v^{(1)} \ni v_i$ and $c^{(k)}$ ($k = 0, 1$) is the concentration, i.e. volume fraction, of the component $v^{(k)}$: $c^{(1)} = \langle V^{(1)}(\mathbf{x}) \rangle = \bar{v}_i n^{(1)}$ ($k = 1; i = 1, 2, \dots$), $c^{(0)} = 1 - \langle V \rangle$. The notation $\langle (\cdot) \rangle_k$ denotes the average over the component $v^{(k)}$ ($k = 0, 1$). The notation $\langle (\cdot) \rangle(\mathbf{x})$ will be used for the average taken for the ensemble of a statistically inhomogeneous field $X = (v_i)$ in the point \mathbf{x} .

Only if the pair distribution function $g(\mathbf{x}_i - \mathbf{x}_m) \equiv \varphi(v_i, \mathbf{x}_i | v_m, \mathbf{x}_m) / n^{(k)}$ depends on $|\mathbf{x}_m - \mathbf{x}_i|$ it is called the radial distribution function (RDF). The RDFs estimated from experimental data utilized a digital image processing technique to identify fiber centroids and describe the stochastic structure of the material through estimation of the statistical parameters and functions that describe the radial fiber distribution (see Buryachenko *et al.*, 2003). The numerical simulation was carried out by the modified Collective Rearrangement Model (CRM) accompanied by the random shaking procedure, creating the most homogeneous and mixed structures that do not depend on the initial protocol of particle generations (see for detail Buryachenko *et al.*, 2003).

2.2.2 Multi-particle cell model of a random composite

The many-particle cell models of fibrous composite layer/space/half-space, shown in Fig.2.10a, b, represent a natural next step in the development of the “finite array of inclusions” model studied in Buryachenko and Kushch(2005). Namely, we consider a periodicity cell with sides a and b along the axes Ox_1 and Ox_2 , respectively, containing a certain number of aligned in x_3 direction, circular in cross-section fibers. Within such a cell, the inclusions can be placed arbitrarily but without overlapping with other fibers and, in the case of layer, with its flat edges $x_2 = 0$ and $x_2 = -b$. Number N of fibers inside the cell may be taken large enough (say, from 50 to 100) which, as will be shown below, provides efficient simulation of both disordered and regular structure of actual composite specimen in the framework of the same structural model. Sometimes, the geometry shown in the Fig.2.10 is referred as a quasi-random or generalized periodic structure model (Golovchan *et al.*, 1993; Bystroem, 2003, among others).

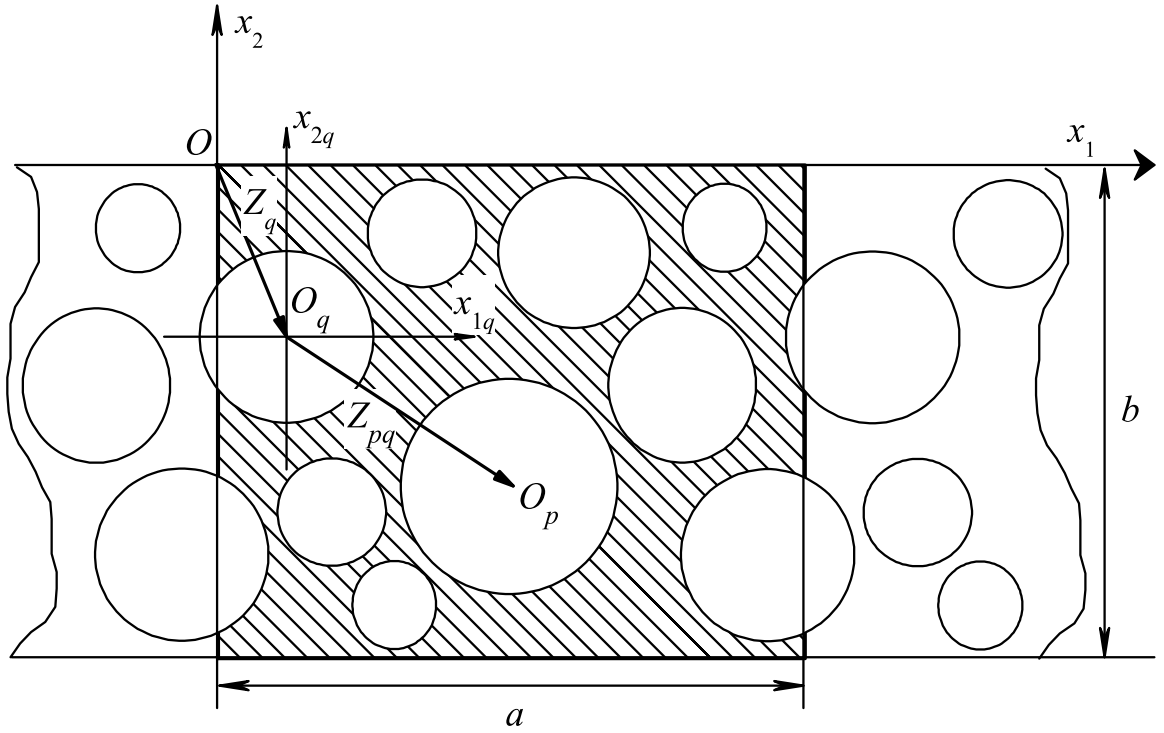


Fig.2.10a. Geometry of the composite layer cell model

This model is rather general in the sense that it can be applied equally to several problems of composite mechanics. The most straightforward application is an elastic response of uni- or cross-directional composite parts loaded/supported on both the flat boundaries. Next, by prescribing on one side of layer the conditions simulating a joint with dissimilar material, we come to a "composite layer on substrate" problem, which is also of practical interest. By equalizing the elastic moduli of substrate material to bulk effective moduli of fibrous composite under study, we get probably the most advanced and realistic model of composite half-plane. Finally, imposing the periodicity condition on the opposite sides of layer transforms the given model into a "cell" (more precisely, "sandwich") model of bulk composite material.

In what follows, we assume that the boundary conditions at the flat boundaries are periodic in x_1 (constants, as a particular case); in this case, one can expect the stress field to be periodic in x_1 with period a as well. In turn, it gives a chance to

- a) reformulate the primary "composite layer" or "composite space" problem as a problem for a piece-homogeneous finite-sized cell, and
- b) confine finding the solution of relevant BVP to the class of periodic functions.

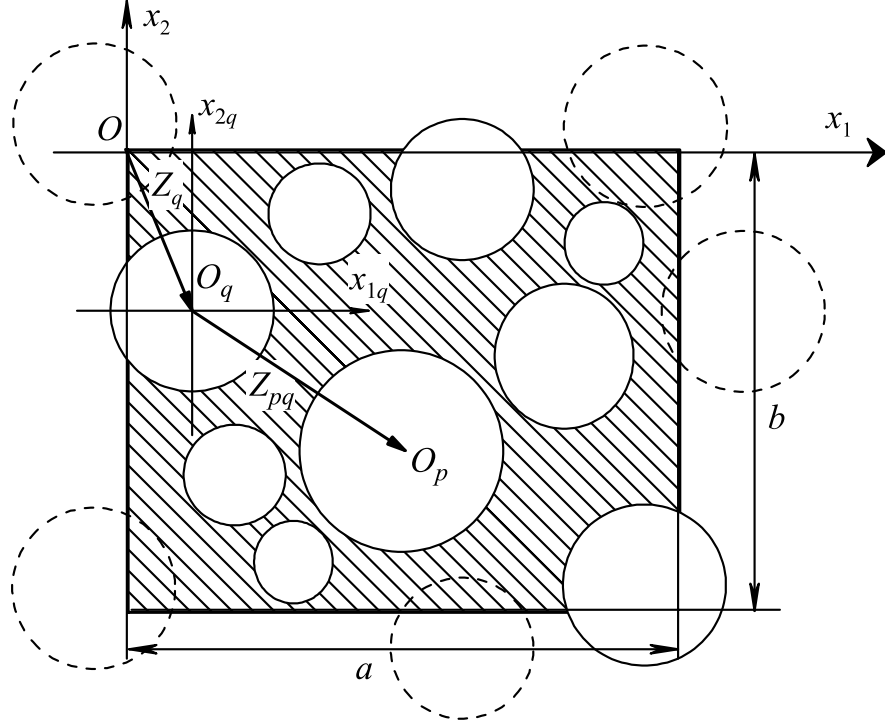


Fig.2.10b. Geometry of the composite space cell model

Geometry of the cell is given by its length a , height b , centers of inclusions O_q with coordinates (X_{1q}, X_{2q}) and their radii R_q . Besides the global Cartesian coordinate system Ox_1x_2 , we introduce the local, inclusion-related coordinate systems $Ox_{1q}x_{2q}$ with origins in O_q . Also, we will use the following complex-valued variables

$$z = x_1 + ix_2, \quad z_q = x_{1q} + ix_{2q}; \quad (2.96)$$

clearly, $z = z_q + Z_q$, where $Z_q = X_{1q} + iX_{2q}$. We denote $u_m = u_{m1} + iu_{m2}$ the displacement in a matrix material with elastic moduli G_0 and ν_0 ; $u_i^{(q)}$, G_q and ν_q refer to displacement and elastic moduli, respectively, of q th fiber, $q = 1, 2, \dots, N$. At the matrix-fiber interfaces, the adhesion conditions

$$\left. (u_m - u_i^{(q)}) \right|_{r_q = R_q} = 0; \quad \left. [\tau_n(u_m) - \tau_n(u_i^{(q)})] \right|_{r_q = R_q} = 0; \quad (2.97)$$

$$q = 1, 2, \dots, N;$$

where $\tau_n = \sigma_{rr} + i\sigma_{r\varphi}$, are assumed. The stress state of a composite space is governed by a set of far loads applied at infinity, and the stress state of a composite layer is governed by a self-equilibrated set of load applied to the flat boundaries of layer. To be specific, we prescribe the kinematic boundary conditions on both edge surfaces of layer, namely

$$u_m \Big|_{x_2 = -b} = 0; \quad u_m \Big|_{x_2 = 0} = i\delta. \quad (2.98)$$

It will be seen from the below analysis that the stress or mixed (say, normal displacement plus tangential stress) boundary conditions case can be treated in a quite similar way.

In the framework of generalized cell model, a composite sample can be thought as a set of cells. As we mentioned already, periodicity of structure results in periodicity of relevant physical fields: i.e.,

$$\sigma_{ij}(z+a) = \sigma_{ij}(z) \quad (2.99)$$

for a layer and

$$\sigma_{ij}(z+a) = \sigma_{ij}(z+ib) = \sigma_{ij}(z) \quad (2.100)$$

for an unbounded composite is an additional to (2.97) condition to be satisfied in order to provide continuity of displacement and stress fields between the adjacent cells. One natural and highly computational cost-efficient way to match (2.100) is to find solution of the boundary-value problem in the class of periodic (rather than doubly-periodic) functions. Likewise the 2D problem considered in Buryachenko and Kushch (2004), the Kolosov-Muskhelishvili's method of complex potentials seems to be most appropriate solving technique for a given problem. However, unlike the case of a finite array of inclusions, periodicity of problem implies introducing the relevant periodic complex potentials. A brief summary of the theory of periodic potentials is given in the next subsection; for more details, see Golovchan et al. (1993).

2.2.3 Theoretical background: periodic potentials

Let us consider the functions defined by the convergent series

$$t_n(z) = \sum_k \frac{1}{(z-ka)^n}, \quad n = 1, 2, \dots \quad (2.101)$$

These functions are periodic in x_1 with period a and possess a countable set of n th order poles in the points $z = ka$. For $x_1 \neq 0$ these functions are continuous and, thus, allow expansion into the Fourier series with respect to x_1 . It has been found elsewhere (Golovchan et al., 1993) that these series have the form

$$t_n(z) = \sum_{m=0}^{\infty} t_{nm}^{\pm} \exp(\pm i\beta_m z), \quad x_2 \gtrless 0; \quad (2.102)$$

where $\beta_m = 2\pi m/a$ and $t_{nm}^{\pm} = \frac{2\pi}{a} \varepsilon_m (\beta_m)^{n-1} \frac{(\mp i)^n}{(n-1)!}$; $\varepsilon_0 = \frac{1}{2}$, $\varepsilon_m = 1$ for $m > 1$.

The expressions (2.102) are particularly useful when it comes to executing the boundary conditions at the flat boundaries $x_2 = \text{const}$. It is clear from (2.102) that $t_n(z) \rightarrow 0$ when $|x_2| \rightarrow \infty$ for all $n > 1$, whereas $t_1(z) \rightarrow t_{10}^{\pm} = \mp 2\pi i/a$ as $x_2 \rightarrow \pm\infty$. Thus, the functions (2.101) can be thought as singular periodic potentials whereas the functions $\exp(\pm i\beta_m z)$ may be considered as the regular periodic potentials for a half plane.

On the other hand, to match the matrix-fiber interface conditions (2.97), the functions (2.101) are to be expanded into the Laurent's power series around a certain point. These expansions can be obtained by applying termwise the formula

$$\frac{1}{(z+Z)^n} = \sum_{k=0}^{\infty} H_{nk}(Z) z^k, \quad H_{nk}(Z) = (-1)^k \frac{(n+k-1)!}{k!(n-1)!} Z^{-(n+k)}. \quad (2.103)$$

followed by a proper change of summation order. So, local expansion around the pole $z = 0$ is given by

$$t_n(z) = \frac{1}{z^n} + \sum_{m=0}^{\infty} H_{nm}^*(0) z^m, \quad |z| < a; \quad (2.104)$$

where

$$H_{nm}^*(0) = \sum_{k \neq 0} H_{nm}(ak) = [(-1)^n + (-1)^m] \frac{(n+m-1)!}{m!(n-1)!} \zeta(n+m). \quad (2.105)$$

With the fact that $\zeta(n) = \sum_{k=1}^{\infty} \frac{1}{k^n}$ is the Euler's ζ -function taken into account, evaluation of (2.105) is rather simple: first, $H_{nm}^*(0) \equiv 0$ for $(n+m)$ odd. Then, $\zeta(2) = \pi^2/6$ and $\zeta(4) = \pi^4/90$ (Abramovitz and Stegun, 1965); for $(n+m) \geq 6$ direct summation is rapid.

Local expansion in a vicinity of regularity point can be written in the following, convenient for subsequent usage form:

$$t_n(z_p) = \sum_{m=0}^{\infty} H_{nm}^*(Z_{pq}) z_q^m, \quad z_p = z_q + Z_{pq} \quad (Z_{pq} \neq ka); \quad (2.106)$$

where now

$$H_{nm}^*(Z_{pq}) = \sum_k H_{nm}(Z_{pq} - ak) = (-1)^m \frac{(n+m-1)!}{m!(n-1)!} t_{n+m}(Z_{pq}). \quad (2.107)$$

To evaluate $t_{n+m}(Z_{pq})$ numerically, three following case-dependent methods are applicable:

- a) direct summation provided $(n+m)$ is sufficiently large; otherwise,
- b) Fourier series expansion (2.102), if $|X_{2pq}| > \delta$; and, the last,
- c) expansion of type (2.104) in the case $|X_{2pq}| \leq \delta$.

Local expansion of "halfplane" regular potentials $\exp(\pm i\beta_m z)$ is rather simple:

$$\exp(\pm i\beta_m z) = \sum_{k=0}^{\infty} \frac{(\pm i\beta_m)^k}{k!} z^k. \quad (2.108)$$

2.2.4 Composite band

We apply first the periodic potential introduced above to solve for a "composite band" obtained by removing upper and bottom edges of cell (Fig.2.10a) or, equivalently, by putting $b = \infty$. In fact, we study a plane containing several periodic rows of inclusions embedded. We focus on this problem only to demonstrate the technique of reducing the boundary-value problem to linear set of algebraic equations. In the next Section, a composite space will be considered with the boundary conditions on the flat edges incorporated.

The method of solution we apply is well-known method of complex potentials by Kolosov-Muskhelishvili, with minor modifications. First, we use the following representation of displacement

$$u = u_1 + iu_2 = \kappa\varphi(z) - (z - \bar{z}) \overline{z\varphi'(z)} - \overline{\psi(z)}, \quad (2.109)$$

slightly different of that suggested in the original Muskhelishvili's (1953) book. It is rather straightforward to show that these two representations are equivalent. At the same time,

as we will see later on, presence of the multiplier $(z - \bar{z}) = 2ix_2$ instead of z in the bi-harmonic term simplifies the solving procedure greatly: namely, it enables using the periodic potentials in exactly the same way we worked with the conventional potentials of type z^n in the "finite array of inclusion" problem. Corresponding to (2.109) stress tensor is given by

$$\begin{aligned}\sigma_{11} + \sigma_{22} &= 4G_0 \left(\varphi'(z) + \overline{\varphi'(z)} \right); \\ \sigma_{22} - \sigma_{11} + 2i\sigma_{12} &= 4G_0 [(\bar{z} - z)\varphi''(z) - \varphi'(z) + \psi'(z)].\end{aligned}\quad (2.110)$$

Following Buryachenko and Kushch (2004), we write general solution for a plane containing a *finite* row of circular inclusions with centers $Z_k = ak$

$$u_m = u_0(z) + \sum_{k=-K}^K \left[\varkappa_0 \varphi_k(z_k) - (z_k - \bar{z}_k) \overline{\varphi'_k(z_k)} - \overline{\psi_k(z_k)} \right], \quad (2.111)$$

where

$$\varphi_k(z_k) = \sum_{n=1}^{\infty} \frac{a_n^{(k)}}{(z_k)^n}, \quad \psi_k(z_k) = \sum_{n=1}^{\infty} \frac{b_n^{(k)}}{(z_k)^n}, \quad (2.112)$$

u_0 is a far displacement field and $z_k = z - Z_k$. Note, that in this specific case $(z_k - \bar{z}_k)$ is independent of index k and, thus, (2.111) can be rewritten in the form (2.109), with potentials

$$\varphi_{\Sigma}(z) = \sum_{k=-K}^K \varphi_k(z_k); \quad \psi_{\Sigma}(z) = \sum_{k=-K}^K \psi_k(z_k). \quad (2.113)$$

Now, we recognize that solution for a plane with an *infinite* row on inclusions may be thought as a limiting case of (2.111)-(2.113) as $K \rightarrow \infty$. Moreover, periodicity of solution implies $a_n^{(k)} = a_n$ and $b_n^{(k)} = b_n$ for any k . As easy to see, by change of summation order in (2.112) and (2.113) we come again to solution in the form (2.109), with periodic potentials

$$\varphi(z) = \sum_{n=1}^{\infty} a_n t_n(z) \quad \text{and} \quad \psi(z) = \sum_{n=1}^{\infty} b_n t_n(z). \quad (2.114)$$

Quite analogous consideration shows also that for a more general model involving several, say N , infinite rows of fibers a general solution will be

$$u_m = u_0(z) + \sum_{p=1}^N u_{ps}(z_p), \quad (2.115)$$

where

$$u_{ps}(z_p) = \varkappa_0 \varphi_{ps}(z_p) - (z_p - \bar{z}_p) \overline{\varphi'_{ps}(z_p)} - \overline{\psi_{ps}(z_p)} \quad (2.116)$$

and

$$\varphi_{ps}(z_p) = \sum_{n=1}^{\infty} a_n^{(p)} t_n(z_p), \quad \psi_{ps}(z_p) = \sum_{n=1}^{\infty} b_n^{(p)} t_n(z_p). \quad (2.117)$$

In (2.117), $a_n^{(p)}$ and $b_n^{(p)}$ are the unknown complex-valued coefficients. For simplicity sake, we take u_0 to be linear:

$$u_0(z) = \Gamma_0 + (\varkappa_0 - 1) \Gamma_1 z - (\overline{\Gamma_2} - \Gamma_1) \bar{z}. \quad (2.118)$$

Two governing parameters, Γ_1 and Γ_2 , relate the far field strains E_{ij} in a way defined below (eqn(2.170)); for a while, we consider them as arbitrary complex-valued constants.

Due to generic periodicity of solution, it suffices to satisfy the interface conditions (2.97) for the fibers with centers lying inside the unit cell. We write displacement in q th fiber as

$$u_i^{(q)} = \varkappa_q \varphi_{qr}(z_q) - (z_q - \bar{z}_q) \overline{\varphi'_{qr}(z_q)} - \overline{\psi_{qr}(z_q)}, \quad (2.119)$$

where the potentials

$$\varphi_{qr}(z_q) = \sum_{n=0}^{\infty} c_{-n}^{(q)}(z_q)^n, \quad \psi_{qr}(z_q) = \sum_{n=0}^{\infty} d_{-n}^{(q)}(z_q)^n \quad (2.120)$$

are the regular analytical functions.

Noteworthy, $u_i^{(q)}$ are written in local coordinates of q th fiber. To match the conditions (2.97), one has to find first a local expansion of u_m in a vicinity of O_q as well. For u_0 , such an expansion is straightforward:

$$u_0 = U_{0q} + R_q [(\varkappa_0 - 1) \Gamma_1 \exp(i\phi_q) - (\bar{\Gamma}_2 - \Gamma_1) \exp(-i\phi_q)], \quad (2.121)$$

where

$$U_{0q} = \Gamma_0 + (\varkappa_0 - 1) \Gamma_1 Z_q - (\bar{\Gamma}_2 - \Gamma_1) \bar{Z}_q. \quad (2.122)$$

Transformation of $u_{ps}(z_p)$ (2.116) is based on the formulas (2.104)-(2.107); taking account of $z_p = z_q - Z_{pq}$, we have

$$\begin{aligned} \sum_{p=1}^N \varphi_{ps}(z_p) &= \sum_{p=1}^N \sum_{n=1}^{\infty} a_n^{(p)} t_n(z_p) = \\ \sum_{p=1}^N \sum_{n=1}^{\infty} a_n^{(p)} \left[\frac{\delta_{pq}}{(z_q)^n} + \sum_{m=0}^{\infty} H_{nm}^*(Z_{pq}) (z_q)^m \right] &= \sum_n a_n^{(q)} (z_q)^{-n}; \end{aligned} \quad (2.123)$$

where

$$a_{-n}^{(q)} = \sum_{p=1}^N \sum_{m=1}^{\infty} a_m^{(p)} H_{mn}^*(Z_{pq}), \quad n = 0, 1, 2, \dots \quad (2.124)$$

Applying the same procedure to the rest of terms in (2.115) and (2.116) gives us, after simple algebra, the following local expansion:

$$u_m = \varkappa_0 \sum_n a_n^{(q)} (z_q)^{-n} - (z_q - \bar{z}_q) \sum_n (-n) \overline{a_n^{(q)}} (\bar{z}_q)^{-n-1} - \sum_n \overline{b_n^{(q)}} (\bar{z}_q)^{-n}, \quad (2.125)$$

where

$$\begin{aligned} b_{-n}^{(q)} &= \sum_{p=1}^N \sum_{m=1}^{\infty} \left[b_m^{(p)} H_{mn}^*(Z_{pq}) + (n+1) (\bar{Z}_{pq} - Z_{pq}) a_m^{(p)} H_{m,n+1}^*(Z_{pq}) \right], \\ n &= 0, 1, 2, \dots \end{aligned} \quad (2.126)$$

The final step is substitution of (2.125) together with (2.119) into the interface conditions (2.97). This procedure resembles that described by Buryachenko and Kushch (2004)

and we do not reproduce it here. The final form of linear set of equations, obtained after excluding the unknowns $c_n^{(p)}$ and $d_n^{(p)}$, is

$$\begin{aligned} \frac{\Omega_1}{(R_q)^{2k}} \left[(R_q)^2 (k-2) a_{k-2}^{(q)} - \left(b_k^{(q)} + k a_k^{(q)} \right) \right] + \overline{a_{-k}^{(q)}} &= -\delta_{k1} \Gamma_1; \\ \frac{\Omega_2}{(R_q)^{2k}} a_k^{(q)} - (k+2) (R_q)^2 \overline{a_{-k-2}^{(q)}} - \left(\overline{b_{-k}^{(q)}} - k a_{-k}^{(q)} \right) &= \delta_{k1} (\overline{\Gamma_2} - \Gamma_1); \\ q = 1, 2, \dots, N; \quad k = 1, 2, \dots; \end{aligned} \quad (2.127)$$

where

$$\Omega_1 = \frac{(2\tilde{G}_q + \varkappa_q - 1)}{2 \left[\tilde{G}_q (\varkappa_0 - 1) + (\varkappa_q - 1) \right]} \text{ for } k = 1, \quad \Omega_1 = \frac{(\tilde{G}_q + \varkappa_q)}{2 (\tilde{G}_q \varkappa_0 - \varkappa_q)} \text{ for } k > 1 \quad (2.128)$$

and

$$\Omega_2 = \frac{(\tilde{G}_q \varkappa_0 + 1)}{2 (\tilde{G}_q - 1)}; \quad \tilde{G}_q = G_q / G_0.$$

The eqns (2.127) together with (2.125) and (2.125) form a closed infinite well-posed set of linear equations. Based on the results by Golovchan et al. (1993), it is rather straightforward to show that this system belongs to the class of systems with normal type determinant (add more) and thus its solution can be obtained by the truncation method. After we have $a_n^{(p)}$ and $b_n^{(p)}$ found from (2.127), the coefficients $c_n^{(p)}$ and $d_n^{(p)}$ are calculated according to

$$\begin{aligned} c_{-k}^{(q)} &= \frac{(\varkappa_0 + 1)}{(\tilde{G}_q + \varkappa_q)} a_k^{(q)}, \quad k > 1; \\ \text{Re } c_{-1}^{(q)} &= \frac{(\varkappa_0 + 1)}{(2\tilde{G}_q + \varkappa_q - 1)} \text{Re} \left(a_1^{(q)} + \Gamma_1 \right); \\ \text{Im } c_{-1}^{(q)} &= \frac{(\varkappa_0 + 1)}{(\varkappa_q + 1)} \text{Im} \left(a_1^{(q)} \right); \\ d_{-k}^{(q)} &= k c_{-k}^{(q)} + \frac{(\varkappa_0 + 1)}{(\tilde{G}_q - 1)} \frac{\overline{a_k^{(q)}}}{(R_q)^{2k}} - (R_q)^2 (k+2) \overline{c_{-(k+2)}^{(q)}}, \quad k \geq 1; \\ d_0^{(q)} &= 2 (R_q)^2 \left(a_{-2}^{(q)} - c_{-2}^{(q)} \right) + b_0^{(q)} + \overline{B_0^{(q)}} \\ &\quad - \varkappa_0 \overline{a_0^{(q)}} - (\varkappa_0 - 1) \Gamma_1 Z_q + (\overline{\Gamma_2} - \Gamma_1) \overline{Z_q} - U_{0q}; \end{aligned} \quad (2.129)$$

and, thus, the solution has been completed.

2.2.5 Finite thickness composite layer

Local stress field

Now, we come back to the problem stated in the Section 1 (Fig.2.10a) and show how to provide the flat edge boundary conditions (2.98). To this end, we introduce the potentials

$$\varphi_h(z) = \sum_{m \neq 0} p_m \exp(i\beta_m z), \quad \psi_h(z) = \sum_{m \neq 0} q_m \exp(i\beta_m z); \quad \beta_m = 2\pi m/a \quad (2.130)$$

written in global variables. In accordance with the superposition principle, general solution in the matrix domain u_m (2.115) takes the form

$$u_m = u_0(z) + \sum_{p=1}^N u_{ps}(z_p) + u_h(z) \quad (2.131)$$

where u_h is the boundary-related term, which by analogy with (??) can be expressed as

$$\begin{aligned} u_h &= \varkappa_0 \varphi_h(z) - (z - \bar{z}) \overline{\varphi_h'(z)} - \overline{\psi_h(z)} \\ &= \sum_{m \neq 0} \{ \varkappa_0 p_m \exp(i\beta_m z) + [(z - \bar{z}) i\beta_m \overline{p_m} - \overline{q_m}] \exp(-i\beta_m \bar{z}) \}. \end{aligned} \quad (2.132)$$

This extra term takes account of the flat boundaries provided the complex-valued Fourier series coefficients p_m and q_m are chosen so that the kinematic conditions (2.98) were satisfied. To find them, we note first that in our model $-b < X_{2p} < 0$, $p = 1, 2, \dots, N$.

By definition, $z = z_p + Z_p$; therefore, $x_{2p} > 0$ when $x_2 = 0$ (upper edge of layer) and $x_{2p} < 0$ when $x_2 = -b$ (bottom one). We expand (2.131) into a Fourier series in x_1 . By applying (2.102), we get for the singular part of u_m , namely $u_s = \sum_{p=1}^N u_{ps}(z_p)$

$$\begin{aligned} u_m \Big|_{x_2=0} &= \sum_{m=0}^{\infty} \left\{ \exp(i\beta_m x_1) \left[\varkappa_0 \sum_{p=1}^N P_m^{(p)+} \exp(-i\beta_m Z_p) \right] \right. \\ &\quad \left. + \exp(-i\beta_m x_1) \sum_{p=1}^N \left[i\beta_m (\overline{Z_p} - Z_p) \overline{P_m^{(p)+}} - \overline{Q_m^{(p)+}} \right] \exp(i\beta_m \overline{Z_p}) \right\}; \\ u_m \Big|_{x_2=-b} &= \sum_{m=0}^{\infty} \exp(-\beta_m b) \left\{ \exp(-i\beta_m x_1) \left[\varkappa_0 \sum_{p=1}^N P_m^{(p)-} \exp(i\beta_m Z_p) \right] \right. \\ &\quad \left. + \exp(i\beta_m x_1) \sum_{p=1}^N \left[-\beta_m \langle 2b + i(\overline{Z_p} - Z_p) \rangle \overline{P_m^{(p)-}} - \overline{Q_m^{(p)-}} \right] \exp(-i\beta_m \overline{Z_p}) \right\}; \end{aligned} \quad (2.133)$$

where

$$P_m^{(p)\pm} = \sum_{n=1}^{\infty} a_n^{(p)} t_{nm}^{\pm}, \quad Q_m^{(p)\pm} = \sum_{n=1}^{\infty} b_n^{(p)} t_{nm}^{\pm}. \quad (2.134)$$

After substitution (2.132) and (2.133) into (2.98), we obtain for $m > 0$

$$\begin{aligned} \varkappa_0 p_m - \overline{q_{-m}} &= R_1; & \varkappa_0 p_m \exp(2\beta_m b) - 2\beta_m b \overline{p_{-m}} - \overline{q_{-m}} &= R_3; \\ \varkappa_0 p_{-m} - \overline{q_m} &= R_2; & \varkappa_0 p_{-m} - (2\beta_m b \overline{p_m} - \overline{q_m}) \exp(2\beta_m b) &= R_4; \end{aligned} \quad (2.135)$$

where

$$\begin{aligned}
R_1 &= -\varkappa_0 \sum_{p=1}^N P_m^{(p)+} \exp(-i\beta_m Z_p); \\
R_2 &= \sum_{p=1}^N \left[i\beta_m (\overline{Z}_p - Z_p) \overline{P_m^{(p)+}} - \overline{Q_m^{(p)+}} \right] \exp(i\beta_m \overline{Z}_p); \\
R_3 &= \sum_{p=1}^N \left[-\beta_m \langle 2b + i(\overline{Z}_p - Z_p) \rangle \overline{P_m^{(p)-}} - \overline{Q_m^{(p)-}} \right] \exp(-i\beta_m \overline{Z}_p); \\
R_4 &= \varkappa_0 \sum_{p=1}^N P_m^{(p)-} \exp(i\beta_m Z_p).
\end{aligned} \tag{2.136}$$

By solving (2.135) for p_m and q_m , one finds

$$\begin{aligned}
p_m &= \frac{\Delta_m \varkappa_0 (R_3 - R_1) + 2\beta_m b \Delta_m \overline{R}_2 - 2\beta_m b (\overline{R}_4 - \overline{R}_2)}{(\Delta_m \varkappa_0)^2 - [2\beta_m b \exp(2\beta_m b)]^2}; \\
q_m &= p_m 2\beta_m b \exp(2\beta_m b) / \Delta_m - (\overline{R}_4 - \overline{R}_2) / \Delta_m; \\
p_{-m} &= \varkappa_0 \overline{p}_m - \overline{R}_1; \quad p_{-m}^- = (R_2 + \overline{q}_m) / \varkappa_0;
\end{aligned} \tag{2.137}$$

where $\Delta_m = \exp(2\beta_m b) - 1$.

The separate case is $m = 0$, where we have

$$\begin{aligned}
u_m \Big|_{x_2=0} &= -\frac{\pi i}{a} \sum_{p=1}^N \left(\varkappa_0 a_1^{(p)} + b_1^{(p)} \right) = i\delta; \\
u_m \Big|_{x_2=-b} &+ \frac{\pi i}{a} \sum_{p=1}^N \left(\varkappa_0 a_1^{(p)} + b_1^{(p)} \right) = 0.
\end{aligned} \tag{2.138}$$

From here, the constant term in u_m is

$$\Gamma_0 = i\delta + \frac{\pi i}{a} \sum_{p=1}^N \left(\varkappa_0 a_1^{(p)} + b_1^{(p)} \right) \tag{2.139}$$

whereas the linear term coefficients Γ_1 and Γ_2 are given by

$$\Gamma_1 = \frac{E_{11} + E_{22}}{2(\varkappa_0 - 1)}; \quad \Gamma_2 = \frac{1}{2} (E_{22} - E_{11} + 2iE_{12}), \tag{2.140}$$

with

$$E_{22} = \frac{\delta}{b} + \frac{2\pi}{ab} \sum_{p=1}^N \left(\varkappa_0 a_1^{(p)} + b_1^{(p)} \right); \quad E_{ij} = 0 \quad (i, j \neq 2). \tag{2.141}$$

Thus, p_m and q_m chosen in the form (2.137) and Γ_i taken from (2.139) and (2.141) satisfy the boundary conditions (2.98) accurately. It is quite evident that the described procedure of executing the flat boundary conditions remains valid for any self-balanced set of loads not violating the periodicity condition (2.99).

The edge disturbance u_h affects the stress field around inclusions and has to be taken into account as well by proper modification of the procedure described in the previous Section. By applying the formula (2.108) to (2.132) one finds easily the local expansion of u_h in a vicinity of Z_q :

$$u_h(z) = u_h(z_q + Z_q) = \varkappa_0 \varphi_{hq}(z_q) - (z_q - \bar{z}_q) \overline{\varphi'_{hq}(z_q)} - \overline{\psi_{hq}(z_q)}, \quad (2.142)$$

where

$$\varphi_{hq}(z_q) = \sum_{k=0}^{\infty} A_k^{(q)}(z_q)^k, \quad \psi_{hq}(z_q) = B_k^{(q)}(z_q)^k \quad (2.143)$$

and

$$A_k^{(q)} = \sum_{m \neq 0} p_m \frac{(i\beta_m)^k}{k!} \exp(i\beta_m Z_q); \quad (2.144)$$

$$B_k^{(q)} = - \sum_{m \neq 0} [i\beta_m (Z_q - \bar{Z}_q) p_m - q_m] \frac{(i\beta_m)^k}{k!} \exp(i\beta_m Z_q).$$

Remarkably, the local expansion (2.142) is identical in form to that of the regular part of (2.125). Hence, derivation of the resolving set of equations follows the same way as described above, with replace $a_{-k}^{(q)}$ to $(a_{-k}^{(q)} + A_k^{(q)})$ and $b_{-k}^{(q)}$ to $(b_{-k}^{(q)} + B_k^{(q)})$ and gives (??) with $A_k^{(q)}$ and $B_k^{(q)}$ standing in the right hand side

$$\frac{\Omega_1}{(R_q)^{2k}} \left[(R_q)^2 (k-2) a_{k-2}^{(q)} - (b_k^{(q)} + k a_k^{(q)}) \right] + \overline{a_{-k}^{(q)}} = -\delta_{k1} \Gamma_1 - \overline{A_k^{(q)}}; \quad (2.145)$$

$$\frac{\Omega_2}{(R_q)^{2k}} a_k^{(q)} - (k+2) (R_q)^2 \overline{a_{-k-2}^{(q)}} - (\overline{b_{-k}^{(q)}} - k a_{-k}^{(q)}) = \delta_{k1} (\overline{\Gamma_2} - \Gamma_1)$$

$$+ (k+2) (R_q)^2 \overline{A_{k+2}^{(q)}} + \overline{B_k^{(q)}} - k A_k^{(q)};$$

$$q = 1, 2, \dots, N; \quad k = 1, 2, \dots;$$

The eqn (2.145) together with (2.124), (2.126), (2.137) and (2.144) constitute a closed set of linear equations which can be solved by means of standard computer algebra. In doing so, any desirable accuracy can be achieved by retaining a sufficient number of harmonics in numerical solution.

In principle, it is possible to reduce a number of variables by excluding $A_k^{(q)}$ and $B_k^{(q)}$ from (2.145). The following iterative algorithm, however, seems to be more appropriate here. We start with the solution of (2.145) where $A_k^{(q)} = B_k^{(q)} = 0$ and $E_{22} = \delta/b$ ((2.127), composite band problem), then evaluate $A_k^{(q)}$, $B_k^{(q)}$ and E_{22} from (2.144) and (2.141), respectively. Next, we substitute the obtained values into the right hand side of (2.145) and solve it again, etc. This algorithm is more flexible because the eqns (2.141) and (2.144) may vary depending on the specific conditions assumed at the flat boundaries of layer and, to account for them, only minor modification of numerical code has to be made. Yet another argument in favor of the above iterative scheme is that the cell model (Fig.2.10) with many (say, $N = 100$) inclusions requires a set of several thousand of linear equations to be solved. The well-known fact is that for such a large system an iterative solver is preferable and, often, the only option.

Effective transverse stiffness

The stress field obtained from the above solution can be integrated to estimate macroscopic, or effective, stiffness C^* defined by

$$\langle \sigma_{ij} \rangle = C_{ijkl}^* \langle \varepsilon_{kl} \rangle, \quad (2.146)$$

where $\langle \cdot \rangle$ means averaging over the representative volume element (RVE). In the model considered by us, RVE coincides with the periodicity cell. Moreover, it follows from (2.98) and (2.99) that

$$\langle \varepsilon_{22} \rangle = E_{22} = \delta/b; \quad \langle \varepsilon_{ij} \rangle = 0 \quad (i, j \neq 2). \quad (2.147)$$

On the other hand, we can evaluate $\langle \sigma_{22} \rangle$ as

$$\langle \sigma_{22} \rangle = \frac{1}{a} \int_0^a \sigma_{22} \Big|_{x_2=0} dx_1. \quad (2.148)$$

The simplest way to integrate (2.148) uses the Fourier series expansion of σ_{22} , from where one finds easily:

$$\frac{\langle \sigma_{22} \rangle}{2G_0} = \Gamma_1 + \Gamma_2 = \frac{(\varkappa_0 + 1)}{2(\varkappa_0 - 1)} \left[\frac{\delta}{b} + \frac{2\pi}{ab} \sum_{p=1}^N \left(\varkappa_0 a_1^{(p)} + b_1^{(p)} \right) \right]. \quad (2.149)$$

Noteworthy, $C_{2222}^{(0)} = G_0 (\varkappa_0 + 1) / (\varkappa_0 - 1)$; combining it with (2.149), we obtain remarkably simple expression for dimensionless transverse stiffness

$$\frac{C_{2222}^*}{C_{2222}^{(0)}} = 1 + \frac{2\pi}{ab} \sum_{p=1}^N \left(\varkappa_0 a_1^{(p)} + b_1^{(p)} \right) \quad (2.150)$$

C_{2222}^* in which contributions from matrix and each inclusion are clearly separated.

In a similar way, longitudinal and shear stiffness of composite layer can be evaluated. One particular but important application of the model under study is the composite bulk, which may be thought as a "sandwich" made of composite layers. To simulate behavior of composite material, we impose, instead of (2.98), the periodicity condition on the opposite sides of layer:

$$(\sigma_{22} + i\sigma_{12}) \Big|_{x_2 = -b} = (\sigma_{22} + i\sigma_{12}) \Big|_{x_2 = 0} \quad (2.151)$$

These two problems (composite bulk and layer) coincide in the simplest case $N = 1$ (composite with an orthogonal lattice of fibers). To simplify the problem even more, we put $b = a$ and $R = 1$; in this case, the unit cell is a square containing a single circular inclusion. Volume fraction of fibers $c = \pi/a^2$, or $a = \sqrt{\pi/4c}$. For a composite given, $C_{1111}^* = C_{2222}^*$ can be evaluated from (2.150); the corresponding numerical data for $\nu_0 = 0.3, \nu_1 = 0.2$ and a series of $\lambda_1 = G_1/G_0$ are given in the Table 1.

Table 2.1. Effective transverse stiffness of a fibrous composite monolayer ($N = 1$)

c	$b = a$	$C_{2222}^*/C_{2222}^{(0)}$		
		$G_1 = 0$	$G_1 = 10G_0$	$G_1 = 1000G_0$
0	∞	1.0	1.0	1.0
0.1	5.605	0.7430	1.133	1.167
0.2	3.963	0.5742	1.303	1.392
0.3	3.236	0.4495	1.519	1.702
0.4	2.802	0.3492	1.799	2.147
0.5	2.507	0.2636	2.167	2.828
0.6	2.288	0.1852	2.672	4.030
0.7	2.118	0.1075	3.421	6.990

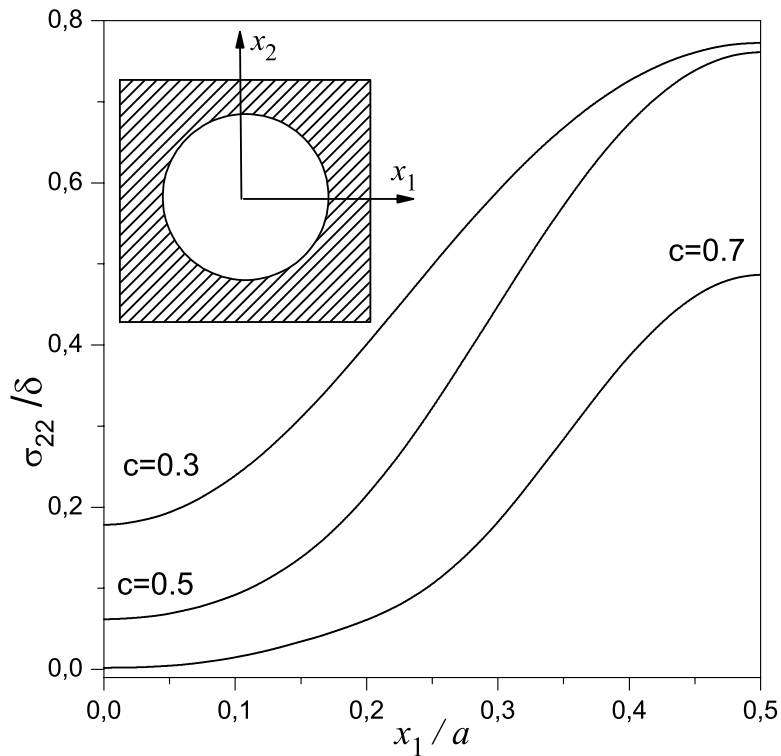


Fig.2.11. Normalized stress $\sigma_{22}/\delta G_0$ variation along the x_1 axis ($x_2 = 0$) in a layer with circular pores

In the Figs 2.11 and 2.12, the local stress $\sigma_{22}/\delta G_0|_{x_2=0}$ (2.148) distribution is shown, from where effect of volume content and elastic stiffness of reinforcing fibers on surface stress concentration is clearly seen. So, near-to-surface pore reduces stress concentration; for low porosity, this effect is localized in a vicinity of $x_1 = 0$ (above the pore, Fig.2.11). For high porosity ($c > 0.5$), when σ_{22} at $x_1 = 0$ is close to zero, we observe also considerable stress reduction in the area between the adjacent pores. On the contrary, in the layer reinforced by high-moduli fibers, σ_{22} stress concentration grows together with c and reaches value of almost 30 at $c = 0.7$ (Fig.2.12).

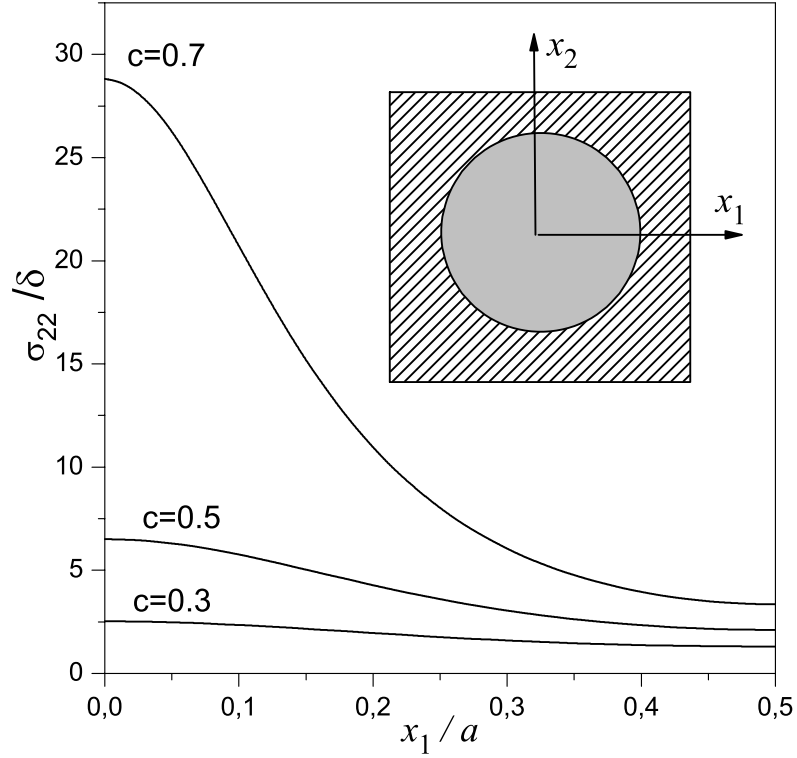


Fig.2.12. Normalized stress $\sigma_{22}/\delta G_0$ variation along the x_1 axis ($x_2 = 0$) in composite layer, $G_1 = 1000G_0$

2.2.6 Quasi-random composite space

Local stress field

Now, we consider application of cell model method to come back to the quasi-random composite space problem stated in the Section 1 (Fig.2.10b) and show how to provide the periodicity conditions (2.100) in x_2 direction, namely

$$T_n(z - bi) = T_n(z), \text{ where } T_n = \sigma_{22} + i\sigma_{12}. \quad (2.152)$$

To this end, we follow the same way as described in the previous section: namely, we take general solution in the matrix domain u_m (2.115) in the form (2.131) where the boundary-related term u_h is given by analogy with (2.132). The complex-valued Fourier series coefficients p_m and q_m in this extra term are to be chosen so that the conditions (2.152) were satisfied.

To find them, we expand (2.131) into the Fourier series in x_1 . By applying (2.102), we

get for the singular part of T_n , namely $T_s = T_n(u_s) = \sum_{p=1}^N T_n [u_{ps}(z_p)]$

$$\begin{aligned}
T_s(z) &= \sum_{p=1}^N \sum_{m=0}^{\infty} \left\{ \exp(i\beta_m z) \left[(i\beta_m)^2 (\bar{z} - z - \bar{Z}_p + Z_p) P_m^{(p)+} + i\beta_m Q_m^{(p)+} \right] \exp(-i\beta_m Z_p) \right. \\
&\quad \left. + i\beta_m \exp(-i\beta_m \bar{z}) \overline{P_m^{(p)+}} \exp(i\beta_m \bar{Z}_p) \right\}; \\
T_s(z - bi) &= \sum_{p=1}^N \sum_{m=0}^{\infty} \exp(-\beta_m b) \left\{ \exp(-i\beta_m z) \right. \\
&\quad \times \left[(i\beta_m)^2 (\bar{z} - z + 2bi - \bar{Z}_p + Z_p) P_m^{(p)+} + i\beta_m Q_m^{(p)+} \right] \exp(i\beta_m Z_p) \\
&\quad \left. - i\beta_m \exp(i\beta_m \bar{z}) \overline{P_m^{(p)-}} \exp(-i\beta_m \bar{Z}_p) \right\};
\end{aligned} \tag{2.153}$$

where

$$P_m^{(p)\pm} = \sum_{n=1}^{\infty} a_n^{(p)} t_{nm}^{\pm}, \quad Q_m^{(p)\pm} = \sum_{n=1}^{\infty} b_n^{(p)} t_{nm}^{\pm}. \tag{2.154}$$

After substitution (2.132) and (2.153) into (2.152), we obtain for $m > 0$

$$\begin{aligned}
p_{\pm m} &= \frac{1}{\Delta_m} \sum_{p=1}^N P_m^{(p)\pm} \exp(\mp i\beta_m Z_p); \\
q_{\pm m} &= \frac{1}{\Delta_m} \sum_{p=1}^N \left\{ \left[2b \frac{\exp(\beta_m b)}{\Delta_m} \pm i (Z_p - \bar{Z}_p) \right] \beta_m P_m^{(p)\pm} + Q_m^{(p)\pm} \right\} \exp(\mp i\beta_m Z_p);
\end{aligned} \tag{2.155}$$

where $\Delta_m = \exp(2\beta_m b) - 1$.

Thus, p_m and q_m chosen in the form (2.155) satisfy the boundary conditions (2.152) accurately. In turn, the edge disturbance u_h affects the stress field around inclusions and has to be taken into account as well by proper modification of the procedure described in the previous Section. By applying the formula (2.108) to (2.132) one finds easily the local expansion of u_h in a vicinity of Z_q :

$$u_h(z) = u_h(z_q + Z_q) = \varkappa_0 \varphi_{hq}(z_q) - (z_q - \bar{z}_q) \overline{\varphi'_{hq}(z_q)} - \overline{\psi_{hq}(z_q)}, \tag{2.156}$$

where

$$\varphi_{hq}(z_q) = \sum_{k=0}^{\infty} A_k^{(q)} (z_q)^k, \quad \psi_{hq}(z_q) = B_k^{(q)} (z_q)^k \tag{2.157}$$

and

$$\begin{aligned}
A_k^{(q)} &= \sum_{m \neq 0} p_m \frac{(i\beta_m)^k}{k!} \exp(i\beta_m Z_q); \\
B_k^{(q)} &= - \sum_{m \neq 0} [i\beta_m (Z_q - \bar{Z}_q) p_m - q_m] \frac{(i\beta_m)^k}{k!} \exp(i\beta_m Z_q).
\end{aligned} \tag{2.158}$$

Remarkably, the local expansion (2.156) is identical in form to that of the regular part of (2.125). Hence, derivation of the resolving set of equations follows the same way as described above, with replace $a_{-k}^{(q)}$ to $(a_{-k}^{(q)} + A_k^{(q)})$ and $b_{-k}^{(q)}$ to $(b_{-k}^{(q)} + B_k^{(q)})$ and gives (2.127) with $A_k^{(q)}$ and $B_k^{(q)}$ standing in the right hand side

$$\begin{aligned} \frac{\Omega_1}{(R_q)^{2k}} \left[(R_q)^2 (k-2) a_{k-2}^{(q)} - \left(b_k^{(q)} + k a_k^{(q)} \right) \right] + \overline{a_{-k}^{(q)}} &= -\delta_{k1} \Gamma_1 - \overline{A_k^{(q)}}; \\ \frac{\Omega_2}{(R_q)^{2k}} a_k^{(q)} - (k+2) (R_q)^2 \overline{a_{-k-2}^{(q)}} - \left(\overline{b_{-k}^{(q)}} - k a_{-k}^{(q)} \right) &= \delta_{k1} (\overline{\Gamma_2} - \Gamma_1) \\ + (k+2) (R_q)^2 \overline{A_{k+2}^{(q)}} + \overline{B_k^{(q)}} - k A_k^{(q)}; & \\ q = 1, 2, \dots, N; \quad k = 1, 2, \dots; & \end{aligned} \quad (2.159)$$

The eqns (2.159) together with (2.124), (2.126), (2.157) and (2.158) constitute a closed set of linear equations which can be solved by means of standard computer algebra. In doing so, any desirable accuracy can be achieved by retaining a sufficient number K of harmonics in numerical solution.

In principle, it is possible to reduce a number of variables by excluding $A_k^{(q)}$ and $B_k^{(q)}$ from (2.159). The following iterative algorithm, however, seems to be more appropriate here. We start with the solution of (2.159) where $A_k^{(q)} = B_k^{(q)} = 0$, then evaluate $A_k^{(q)}$, $B_k^{(q)}$ from (2.158). Next, we substitute the obtained values into the right hand side of (2.159) and solve it again, etc. The argument in favor of the above iterative scheme is that the cell model (Fig 2.10) with many (say, $N = 100$) inclusions requires a set of several thousand of linear equations to be solved. The well-known fact is that for a large linear system an iterative solver is preferable and, often, the only option.

Effective stiffness

The stress field obtained from the above solution can be integrated to estimate macroscopic, or effective, stiffness tensor C^* defined by

$$\langle \sigma_{ij} \rangle = C_{ijkl}^* \langle \varepsilon_{kl} \rangle, \quad (2.160)$$

where $\langle \cdot \rangle$ means averaging over the representative volume element (RVE). In the model considered by us, RVE coincides with the periodicity cell and, due to periodicity of structure,

$$\langle f \rangle = \frac{1}{V} \int_V f \, dV \quad (2.161)$$

where V is a cell volume. In our case, $V = ab$.

We assume the stress field to be macroscopically uniform which means the corresponding strain $\mathbf{E} = \{E_{ij}\} = \{\langle \varepsilon_{ij} \rangle\}$ and stress $\mathbf{S} = \{S_{ij}\} = \{\langle \sigma_{ij} \rangle\}$ tensors were constant. To evaluate $\langle \varepsilon_{ij} \rangle$, we write

$$\langle \varepsilon_{ij} \rangle = \frac{1}{2V} \int_V (u_{i,j} + u_{j,i}) \, dV = \frac{1}{2V} \left[\left(\int_{V_m} + \sum_{p=1}^N \int_{V_p} \right) (u_{i,j} + u_{j,i}) \, dV \right]. \quad (2.162)$$

Now, we apply the Gauss' theorem to reduce the volume integrals to surface ones: taking into account also the first of adhesion conditions (2.97) we get simple and predictable result:

$$\langle \varepsilon_{ij} \rangle = \frac{1}{2V} \int_{\Sigma} (u_i n_j + u_j n_i) dS, \quad (2.163)$$

where Σ is the cell outer surface and n_i are the components of unit normal vector.

Evaluation of (2.97) uses periodicity property of u : so,

$$E_{11} = \frac{1}{ab} \int_{\Sigma} u_1 n_1 dS = \frac{1}{ab} \int_0^b [u_1(z+a) - u_1(z)] dx_2. \quad (2.164)$$

It follows from (2.131) and (2.118) that $u_m(z+a) - u_m(z) = a(\varkappa_0 \Gamma_1 - \Gamma_2)$. Considering $u_1 = \operatorname{Re} u$ gives us

$$E_{11} = \operatorname{Re}(\varkappa_0 \Gamma_1 - \Gamma_2). \quad (2.165)$$

Similarly,

$$E_{22} = \frac{1}{ab} \int_{\Sigma} u_2 n_2 dS = \frac{1}{ab} \int_0^a [u_2(z+bi) - u_2(z)] dx_1, \quad u_2 = \operatorname{Im} u_m; \quad (2.166)$$

based on the expansion (2.102), one finds

$$u_m(z+bi) - u_m(z) = bi(\varkappa_0 \Gamma_1 - \overline{\Gamma_1}) - bi(\overline{\Gamma_1} - \overline{\Gamma_2}) - 2bi\Gamma_{\Sigma}, \quad (2.167)$$

and

$$E_{22} = \operatorname{Re}[(\varkappa_0 - 2)\Gamma_1 + \Gamma_2 - 2\Gamma_{\Sigma}], \quad \text{where } \Gamma_{\Sigma} = \frac{\pi}{ab} \sum_{p=1}^N (\varkappa_0 a_1^{(p)} + \overline{b_1^{(p)}}). \quad (2.168)$$

In the same way we obtain

$$E_{12} = \operatorname{Im}(\Gamma_2 - \Gamma_1 + \Gamma_{\Sigma}). \quad (2.169)$$

From here we can derive the eqns determining the parameters Γ_1 and Γ_2 :

$$\begin{aligned} (\varkappa_0 - 1)\Gamma_1 &= \frac{E_{11} + E_{22}}{2} + \Gamma_{\Sigma}; \\ \Gamma_2 &= \Gamma_1 + \frac{E_{22} - E_{11}}{2} + iE_{12} + \overline{\Gamma_{\Sigma}}; \end{aligned} \quad (2.170)$$

and, thus, completing the problem statement.

Evaluating the macroscopic stress follows the same way:

$$\langle \sigma_{ij} \rangle = \frac{1}{V} \int_V \sigma_{ij} dV = \frac{1}{2V} \left[\left(\int_{V_m} + \sum_{p=1}^N \int_{V_p} \right) (2G\varepsilon_{ij} + \delta_{ij}\lambda\theta) dV \right]; \quad (2.171)$$

after some algebra, we come to

$$\begin{aligned} \frac{S_{ij}}{2G_0} &= E_{ij} + \delta_{ij} (E_{11} + E_{22}) + \left(\tilde{G}_p - 1 \right) \frac{f_p}{V_p} \int_{V_p} \varepsilon_{ij} dV \\ &+ \delta_{ij} \left(\tilde{G}_p \frac{\nu_p}{1 - 2\nu_p} - \frac{\nu_0}{1 - 2\nu_0} \right) \frac{f_p}{V_p} \int_{V_p} \theta dV, \quad f_p = \frac{V_p}{V} \end{aligned} \quad (2.172)$$

Thus the problem has been reduced to evaluating the

$$\frac{1}{V_p} \int_{V_p} \varepsilon_{ij} dV = \frac{1}{2\pi R_p^2} \int_{L_p} (u_i n_j + u_j n_i) dl = \frac{1}{2\pi R_p} \int_0^{2\pi} (u_i n_j + u_j n_i) d\varphi. \quad (2.173)$$

On the circle $r_p = R_p$, $n = n_1 + in_2 = \exp(i\varphi)$; with account for the explicit form (2.119), (2.120) of displacement inside the p th fiber integration in (2.173) is rather trivial task, leading to

$$\begin{aligned} \frac{1}{V_p} \int_{V_p} (\varepsilon_{11} + \varepsilon_{22}) dV &= 2(\varkappa_p - 1) \operatorname{Re} c_{-1}^{(p)}; \\ \frac{1}{2V_p} \int_{V_p} (\varepsilon_{22} - \varepsilon_{11} + 2i\varepsilon_{12}) dV &= d_{-1}^{(p)} - c_{-1}^{(p)} + 3R_p^2 c_{-3}^{(p)}. \end{aligned} \quad (2.174)$$

Combining (2.174) with (2.172) gives an explicit expressions of (2.160) written in compact form as

$$\begin{aligned} \frac{S_{11} + S_{22}}{2G_0} &= \frac{E_{11} + E_{22}}{(\varkappa_0 - 1)} + 2f_p \left(\tilde{G}_p \frac{\nu_p}{1 - 2\nu_p} - \frac{\nu_0}{1 - 2\nu_0} \right) (\varkappa_p - 1) \operatorname{Re} c_{-1}^{(p)}; \\ \frac{S_{22} - S_{11} + 2iS_{12}}{2G_0} &= E_{22} - E_{11} + 2iE_{12} + 2f_p \left(\tilde{G}_p - 1 \right) \left(d_{-1}^{(p)} - c_{-1}^{(p)} + 3R_p^2 c_{-3}^{(p)} \right). \end{aligned} \quad (2.175)$$

As a last step, we utilize the relations (2.129) to express S_{ij} in terms of variables $a_n^{(p)}$ and $b_n^{(p)}$ entering the resolving system (2.127) and get the final exact, finite-form result:

$$\begin{aligned} \frac{S_{11} + S_{22}}{2G_0} &= \frac{E_{11} + E_{22}}{(\varkappa_0 - 1)} + \frac{2\pi(\varkappa_0 + 1)}{ab(\varkappa_0 - 1)} \left(a_1^{(p)} + b_1^{(p)} \right); \\ \frac{S_{22} - S_{11} + 2iS_{12}}{2G_0} &= E_{22} - E_{11} + 2iE_{12} + \frac{2\pi}{ab} (\varkappa_0 + 1) a_1^{(p)}. \end{aligned} \quad (2.176)$$

Together with (2.160), these relations provide evaluation of all components of stiffness tensor C^* .

2.2.7 Statistical analysis of stress distributions

Let us consider N realisations of a random field of inclusions v_i^j with the centers $\mathbf{x}_i^j \in \Omega$ in a unite cell $\Omega = [0, A] \times [0, A]$ with n^j inclusions in j 's realisation. We will create two sorts of meshes. The square meshes

$$\mathbf{y} = \left\{ (x_1, x_2)^\top \mid (p-1) \frac{A}{N\Omega} < x_1 < p \frac{A}{N\Omega}, (q-1) \frac{A}{N\Omega} < x_2 < q \frac{A}{N\Omega} \right\}, \quad (2.177)$$

will be used for coordinates of matrix points where the stresses will be estimated. Here $p, q = 1, \dots, N^\Omega$, $A/N^\Omega \ll a$, for example $A/N^\Omega = a/10$. The domains of inclusions v_i^j ($i = 1, \dots, n^j$, $j = 1, \dots, N$) are discretized along the polar angle and the radius in the local polar coordinate system with the centers \mathbf{x}_i^j . Then the points

$$\mathbf{z} = \left\{ (r, \varphi) \mid (p-1)\frac{2\pi}{l} < \varphi < p\frac{2\pi}{l}, (q-1)\frac{a_i}{m} < r < q\frac{a_i}{m} \right\} \quad (2.178)$$

($p = 1, 2, \dots, l$; $q = 1, 2, \dots, m$) represent the coordinates of points of the meshes of v_i^j where the stresses will be estimated that is not optimized, but is efficient. We will use piecewise-constant elements of the meshes which are not very cost-efficient but are very easy for computer programming, and the discretization (2.177) permits the analysis of nonregular shape of the matrix. For simplicity estimation of integrals involved we will utilize the basic numerical integrations formulas of Simpson's rule for the uniform meshes (2.177) and (2.178).

We can estimate a statistical average of stresses inside the representative inclusion v^r as

$$\langle \boldsymbol{\sigma} \rangle^N(\mathbf{z}) = \frac{1}{Nn^j} \sum_{j=1}^N \sum_{i=1}^{n^j} \boldsymbol{\sigma}_i^j(\mathbf{x}_i + \mathbf{z}) \quad (2.179)$$

where $\boldsymbol{\sigma}_i^j(\mathbf{x}_i + \mathbf{z})$ is a stresses in a local coordinate system connected with the inclusion centers of the inclusion i in a realisation j . It is expected a fundamentally new result such as inhomogeneity of statistical average stresses $\langle \boldsymbol{\sigma} \rangle^N(\mathbf{z})$ inside the representative inclusion v^r .

Moreover, we can estimate a histogram of stress distribution inside each point \mathbf{z} of the representative inclusion $\mathbf{z} \in v^r$.

The next step is estimation of a statistical average of the second moment of stresses inside the inclusions

$$\langle \boldsymbol{\sigma} \otimes \boldsymbol{\sigma} \rangle^N(\mathbf{z}) = \frac{1}{Nn^j} \sum_{j=1}^N \sum_{i=1}^{n^j} \boldsymbol{\sigma}_i^j(\mathbf{x}_i + \mathbf{z}) \otimes \boldsymbol{\sigma}_i^j(\mathbf{x}_i + \mathbf{z}), \quad (2.180)$$

which is not coincide with the second moment of statistical average of stresses $\langle \boldsymbol{\sigma} \otimes \boldsymbol{\sigma} \rangle^N(\mathbf{z}) \neq \langle \boldsymbol{\sigma} \rangle^N(\mathbf{z}) \otimes \langle \boldsymbol{\sigma} \rangle^N(\mathbf{z})$. In so doing, estimation of statistical average of an arbitrary function \mathbf{f} (e.g. $f = \boldsymbol{\sigma}$, $\boldsymbol{\sigma} \otimes \boldsymbol{\sigma}$) is carried out by the formula

$$\langle \mathbf{f} \rangle^{N+1} = \frac{1}{N+1} \left[N \langle \mathbf{f} \rangle^N + \sum_{i=1}^{n^{N+1}} \mathbf{f}_i^{N+1} \right]. \quad (2.181)$$

The second moment of stresses plays a fundamental role in a wide class of nonlinear problems such as e.g. nonlinear elasticity, failure initiation, plasticity (see for references Buryachenko, 2001). In particular, the problem of failure initiation is based on the estimation of the statistical averages of the second moments of the normal and tangential components (see Eq. (5.7) by Buryachenko and Shoepner, 2004)

$$\max_{\mathbf{n}} \langle \Pi^2(\mathbf{n}) \rangle^N = 1, \quad (2.182)$$

$$\Pi^2(\mathbf{n}) = \frac{(\mathbf{N}^n \boldsymbol{\sigma}^-(\mathbf{n}))(\mathbf{N}^n \boldsymbol{\sigma}^-(\mathbf{n}))}{(\sigma_n^{\max})^2} + \frac{(\mathbf{T}^n \boldsymbol{\sigma}^-(\mathbf{n}))(\mathbf{T}^n \boldsymbol{\sigma}^-(\mathbf{n}))}{(\sigma_\tau^{\max})^2}, \quad (2.183)$$

where the interface stresses $\boldsymbol{\sigma}_{\mathbf{n}}^- \equiv \boldsymbol{\sigma}^-(\mathbf{n})\mathbf{n}$ can be partitioned as $\boldsymbol{\sigma}_{\mathbf{n}}^- = \mathbf{N}^{\mathbf{n}}\boldsymbol{\sigma}^-(\mathbf{n}) + \mathbf{T}^{\mathbf{n}}\boldsymbol{\sigma}^-(\mathbf{n})$, where $\mathbf{N}^{\mathbf{n}}$ and $\mathbf{T}^{\mathbf{n}}$ are the three-rank functions of the normal \mathbf{n} such that

$$N_{ikl}^{\mathbf{n}} = n_i n_k n_l, \quad T_{ikl}^{\mathbf{n}} = \frac{1}{2}(\delta_{ik} n_l + \delta_{il} n_k) - n_i n_k n_l, \quad (2.184)$$

where the tensors $N_{ikl}^{\mathbf{n}}$ and $T_{ikl}^{\mathbf{n}}$ symmetrical under the interchanges $k \leftrightarrow l$ generate the normal $\boldsymbol{\sigma}_n^- = \mathbf{N}^{\mathbf{n}}\boldsymbol{\sigma}^-(\mathbf{n})$ and tangential components $\boldsymbol{\sigma}_\tau^- = \mathbf{T}^{\mathbf{n}}\boldsymbol{\sigma}^-(\mathbf{n})$ of the traction $\boldsymbol{\sigma}^-\mathbf{n}$ with the magnitudes $\sigma_n \equiv \|\boldsymbol{\sigma}_n^-\| = \sigma_{kl}^- n_k n_l$ and $\sigma_\tau \equiv \|\boldsymbol{\sigma}_\tau^-\| = \sqrt{\sigma_{kl}^- \sigma_{kl}^- - (\sigma_n)^2}$, respectively. Therefore, our goal is estimation of $\langle (\mathbf{N}^{\mathbf{n}}\boldsymbol{\sigma}^-(\mathbf{n})) (\mathbf{N}^{\mathbf{n}}\boldsymbol{\sigma}^-(\mathbf{n})) \rangle^N$ and $\langle (\mathbf{T}^{\mathbf{n}}\boldsymbol{\sigma}^-(\mathbf{n})) (\mathbf{T}^{\mathbf{n}}\boldsymbol{\sigma}^-(\mathbf{n})) \rangle^N$ (and their histogram) and comparison of its with

$$\langle (\mathbf{N}^{\mathbf{n}}\boldsymbol{\sigma}^-(\mathbf{n})) \rangle^N \langle (\mathbf{N}^{\mathbf{n}}\boldsymbol{\sigma}^-(\mathbf{n})) \rangle^N \text{ and } \langle (\mathbf{T}^{\mathbf{n}}\boldsymbol{\sigma}^-(\mathbf{n})) \rangle^N \langle (\mathbf{T}^{\mathbf{n}}\boldsymbol{\sigma}^-(\mathbf{n})) \rangle^N, \text{ respectively.}$$

In a similar manner the statistical averages of both stresses and their second moments can be estimated over the whole matrix

$$\langle \boldsymbol{\sigma} \rangle^{(0)N} = \frac{1}{N n^{0j}} \sum_{j=1}^N \sum_{i=1}^{n^{0j}} \boldsymbol{\sigma}_i^j(\mathbf{y}), \quad (2.185)$$

$$\langle \boldsymbol{\sigma} \otimes \boldsymbol{\sigma} \rangle^{(0)N} = \frac{1}{N n^{0j}} \sum_{j=1}^N \sum_{i=1}^{n^{0j}} \boldsymbol{\sigma}_i^j(\mathbf{y}) \otimes \boldsymbol{\sigma}_i^j(\mathbf{y}), \quad (2.186)$$

where n^{0j} is a number of mesh nodes (2.177) belonging to the matrix and \mathbf{y} passes through all these nodes in the global coordinate system connected with Ω . We can also plot the histogram distributions of the first and second moments of stresses in the matrix. In more general sense for any nonlinear function \mathbf{f} of $\boldsymbol{\sigma}$ (e.g. $\mathbf{f} = \boldsymbol{\sigma}(\mathbf{z}), \boldsymbol{\sigma}(\mathbf{y}), \boldsymbol{\sigma}(\mathbf{z}) \otimes \boldsymbol{\sigma}(\mathbf{z}), \boldsymbol{\sigma}(\mathbf{y}) \otimes \boldsymbol{\sigma}(\mathbf{y}), \mathbf{\Pi}^2(\mathbf{n})$), we can estimate a histogram of \mathbf{f} which can be used e.g. for estimation of a measure of the part of the matrix where an ejection of the random process \mathbf{f} takes place: $|\mathbf{f}| \geq t$ (see Lipton, 2003).

It should be mentioned that all averages mentioned above are estimated for three different remote stresses $\langle \boldsymbol{\sigma} \rangle = (1, 0, 0)^\top, (0, 1, 0)^\top$ and $(0, 0, 1)^\top$. Therefore, the stresses presented in Eqs. (2.179)-(2.184) in reality have a dimensions 3×3 rather than 3 (in Voigt notations). So, the effective compliance can be estimated as

$$\mathbf{M}^* = \mathbf{M}^{(0)} + (\mathbf{M}^{(1)} - \mathbf{M}^{(0)}) \frac{1}{\bar{v}^r} \int_{v^r} \langle \boldsymbol{\sigma} \rangle^N(\mathbf{z}) d\mathbf{z}. \quad (2.187)$$

It is interesting that the second moment of stresses averaged over the volume of the phase can be estimated exactly if the functional dependence $\mathbf{M}^* \sim \mathbf{M}^{(k)}$ ($k = 0, 1$) is known (see for details Section 5.1 by Buryachenko, 2001)

$$\langle \boldsymbol{\sigma} \otimes \boldsymbol{\sigma} \rangle^{(k)} = \frac{1}{c^{(k)}} \frac{\partial \mathbf{M}^*}{\partial \mathbf{M}^{(k)}} \langle \boldsymbol{\sigma} \rangle \otimes \langle \boldsymbol{\sigma} \rangle. \quad (2.188)$$

For isotropic materials $\mathbf{M}^{(k)} = (3p^{(k)}, 2q^{(k)})$, the formula (2.188) can be recast for the invariants $\sigma_m = \text{tr} \boldsymbol{\sigma} / 3$ and $\sigma_{\text{eq}} = \sqrt{2 \boldsymbol{\sigma}_d : \boldsymbol{\sigma}_d / 3}$ ($\boldsymbol{\sigma}_d = \mathbf{N}^2 : \boldsymbol{\sigma}$)

$$\langle \sigma_m^2 \rangle^{(k)} = \frac{\partial \mathbf{M}^*}{9 \partial p^{(k)}} :: (\langle \boldsymbol{\sigma} \rangle \otimes \langle \boldsymbol{\sigma} \rangle), \quad (2.189)$$

$$\langle \sigma_{\text{eq}}^2 \rangle^{(k)} = \frac{\partial \mathbf{M}^*}{3 \partial q^{(k)}} :: (\langle \boldsymbol{\sigma} \rangle \otimes \langle \boldsymbol{\sigma} \rangle). \quad (2.190)$$

Thus, $\langle \sigma_m^2 \rangle^{(k)}$ and $\langle \sigma_{\text{eq}}^2 \rangle^{(k)}$ can be estimated by two different methods. The first one is based on direct estimations of the second moments of stresses averages over the phase volumes, see Eqs. (2.180) and (2.186). The second method is a perturbation method (2.189) and (2.190).

2.2.8 Numerical study

Three main parameters governing convergence and accuracy of results in the below statistical analysis are

- a) number K of harmonics retained in the numerical solution;
- b) number N of inclusions with centers inside the periodicity unit cell;
- c) number M of random structure realizations taken for averaging.

Obviously, all these numbers should be taken sufficiently large to provide the reliable numerical results. On the other hand, computational effort of such a study scales as $(NK)^\alpha M$, where $\alpha = 2$ or 3 depending on the linear solver type (iterative or direct) utilized and, to avoid exceedingly large total computational time, the reasonably high values of K, M and N are to be taken. The motivated choice can be made based on convergence rate study of solution with each separate parameter increased.

First, we evaluate number of harmonics K we need to keep in the numerical solution in order to get statistically meaningful results. Specifically, we consider uniaxial tension $S_{22} = 1$ of a composite with volume fraction of equal-sized fibers $c = 0.5$. The elastic properties of composite phases are $\nu_0 = 0.3, \nu_p = 0.2$ and $G_p = 100G_0, p = 1, 2, \dots, N$. In the Fig.2.13, σ_{22} radial variation in x_2 direction ($0 < r_p < R_p, \varphi_p = \pi/2$) is shown averaged over $M = 50$ configurations of $N = 50$ inclusions inside the cell. As seen from the Fig.2.13, the runs with $K = 20$ and $K = 30$ give practically coinciding numbers

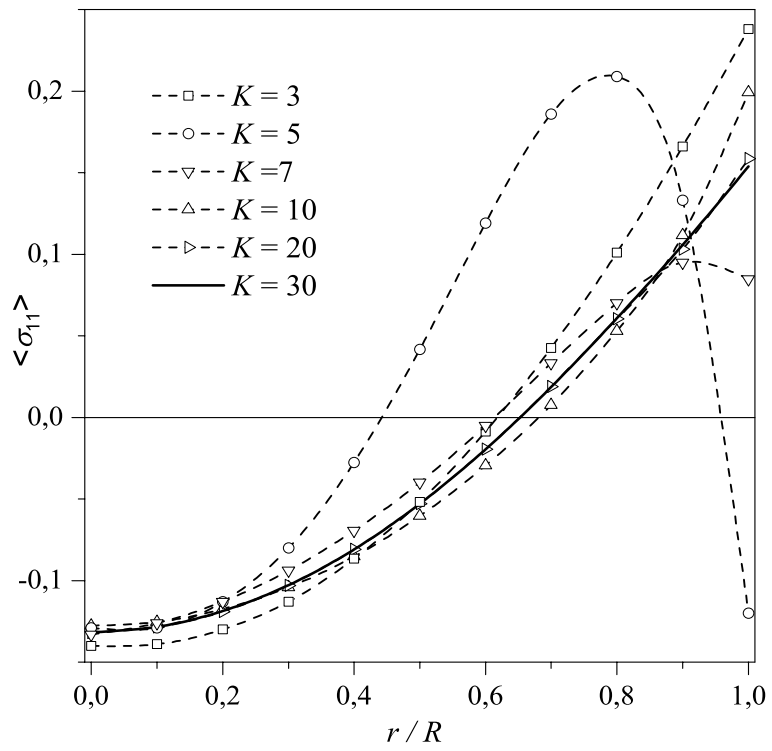


Fig.2.13. Convergence of the fiber interface stress with number of inclusions N inside the cell increased

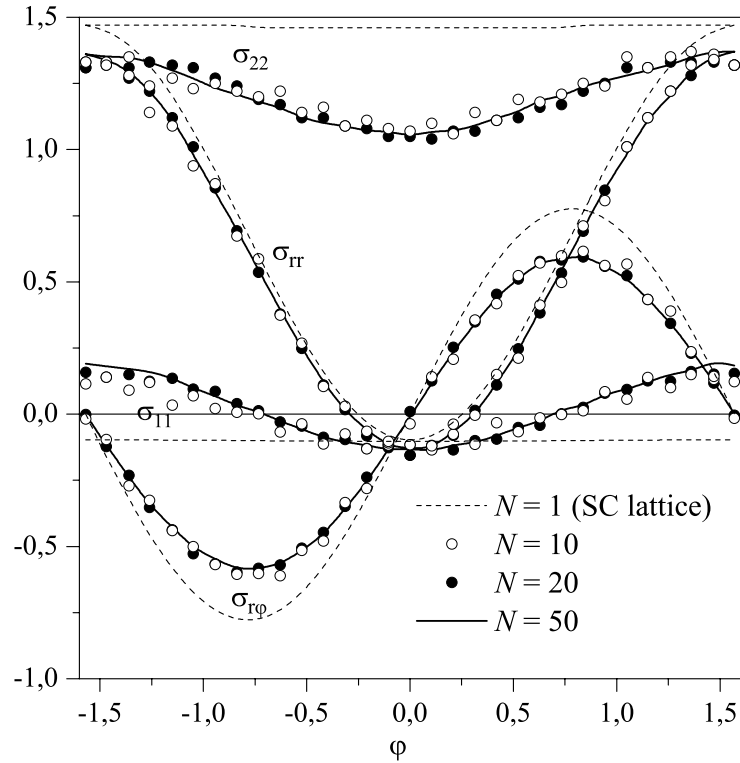


Fig.2.14. Convergence of the fiber interface stress with number of inclusions N inside the cell increased

The next issue is a number of particles N inside the unit cell. In the Fig.2.14, the interface stress variation for $-\pi/2 < \varphi < \pi/2$ is shown averaged over $M = 50$ configurations of $N = 1$ (dashed lines), $N = 10$ (open circles), $N = 20$ (solid circles) and $N = 50$ (solid lines). In the case $N = 1$ we have a simple square lattice of inclusions which is essentially deterministic structure. In the last two cases, stress values are practically the same; smoothness and symmetry of curves for $N = 50$ is yet another reliability confirmation of the results being obtained

The data in the Table below are the averaged over 50 configurations mean stress inside the fibers given in the form $\langle \sigma_{ij} \rangle / C_{ijkl}^0 = MEAN \pm SEM$. The standard deviation (SD) is calculated as follows: $SD = \sqrt{Var}$ where $Var = \frac{1}{(M-1)} \sum_{m=1}^M (X_m - \tilde{X})^2$, M is the sample size and \tilde{X} is the mean: $\tilde{X} = \frac{1}{M} \sum_{m=1}^M X_m$. The standard error of the mean (SEM) is calculated as follows: $SEM = SD / \sqrt{M}$. Assuming far loading is the uniaxial macroscopic strain $E_{kl} = 1$, these data represent as well the effective elastic moduli of a fibrous composite: $C_{ijkl}^* = \langle \sigma_{ij} \rangle$.

Table 2.2. Effective stiffness of a fibrous composite: convergence and isotropy checking

	$\langle \sigma_{11} \rangle / C_{1111}^0$	$\langle \sigma_{22} \rangle / C_{2222}^0$	$\langle \sigma_{12} \rangle / C_{1212}^0$
$N = 20, E_{11} = 1$	2.685 ± 0.016	2.242 ± 0.012	0.009 ± 0.012
$N = 20, E_{22} = 1$	2.242 ± 0.011	2.659 ± 0.016	0.009 ± 0.012
$N = 50, E_{11} = 1$	2.683 ± 0.011	2.270 ± 0.008	-0.006 ± 0.008
$N = 50, E_{22} = 1$	2.271 ± 0.008	2.671 ± 0.010	-0.005 ± 0.009

It is seen from the Table 2.2 that the values obtained for $N = 20$ and $N = 50$ are rather close which clearly indicates convergence of solution with respect to N . These data can also be useful in testifying isotropy of the random structure model. Ideally, one must get for macroscopically isotropic composite material $\langle \sigma_{11} \rangle |_{E_{11}=1} = \langle \sigma_{22} \rangle |_{E_{22}=1}$, $\langle \sigma_{22} \rangle |_{E_{11}=1} = \langle \sigma_{11} \rangle |_{E_{22}=1}$ and $\langle \sigma_{12} \rangle \equiv 0$. As calculations show, already for $N = 20$ the anisotropy degree is less than 1% and demonstrates a clear tendency to decrease with growth of N .

The next figure shows how number of realizations effects the results of statistical averaging. Here, the normalized effective Young modulus E_{eff}/E_0 is shown averaged over different sample size. The open circles correspond to $N = 20$ whereas the solid circles correspond to $N = 50$. The conclusion can be made based on these observations that in both the cases $M = 50$ provides practically convergent solution. This value together with $K = 25$ and $N = 50$ was taken for the subsequent computations.

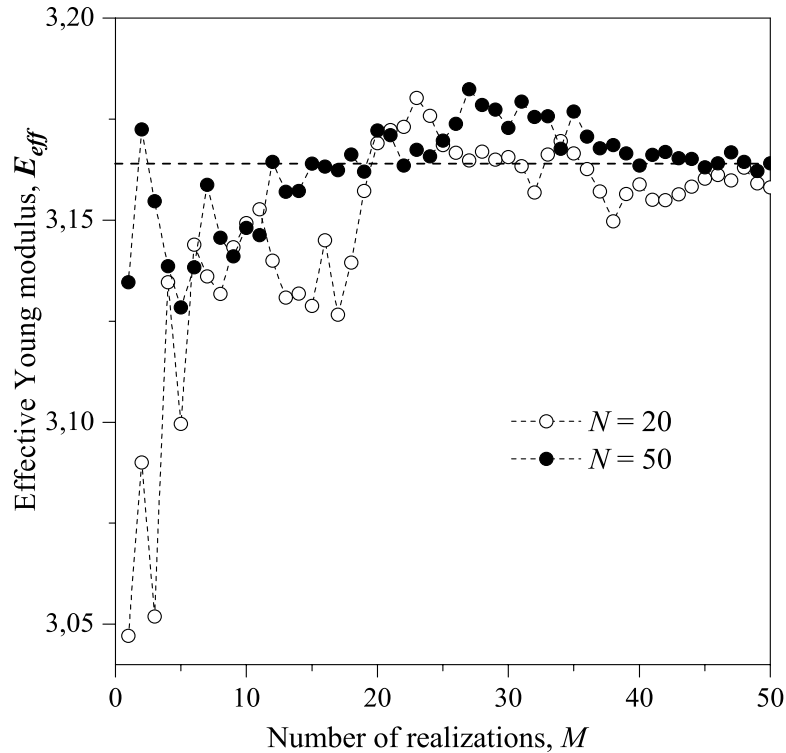


Fig.2.15. Convergence of effective Young modulus E_{eff} of a fibrous composite ($c = 0.5$) with number of realizations M increased

In the Fig.2.16, the statistical average of stress σ_{22} radial distribution ($0 < r < R$, $\varphi = 0$) is shown. The fundamentally new result we observe here is an inhomogeneity of statistical average stresses $\langle \sigma_{22} \rangle^N(z)$ inside the representative inclusion. The inhomogeneity degree is growing up with volume fraction of fibers c increased; at the same time, absolute stress value is a decaying function of c which qualitatively agrees with most existing theories.

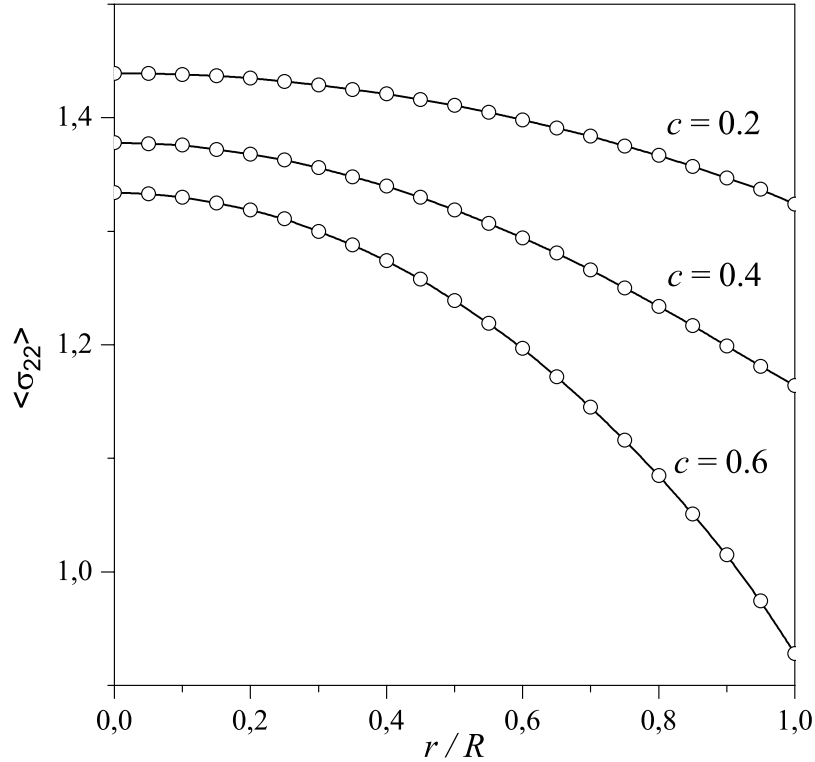


Fig.2.16. stress s_{22} radial variation as a function of volume fraction of fibers

In Fig.2.17, estimation of a statistical average of the second moment of stress $\langle \sigma_{22}^2 \rangle^N(z)$ inside the inclusions is shown. It is clearly seen that it is not coincide with the second moment of statistical average of stresses: $\langle \sigma \otimes \sigma \rangle^N(z) \neq \langle \sigma^N(z) \rangle \otimes \langle \sigma^N(z) \rangle$. As the calculations show, difference between the values compared grows up with c ; likewise $\langle \sigma_{22} \rangle^N(z)$, they are essentially inhomogeneous inside the fiber.

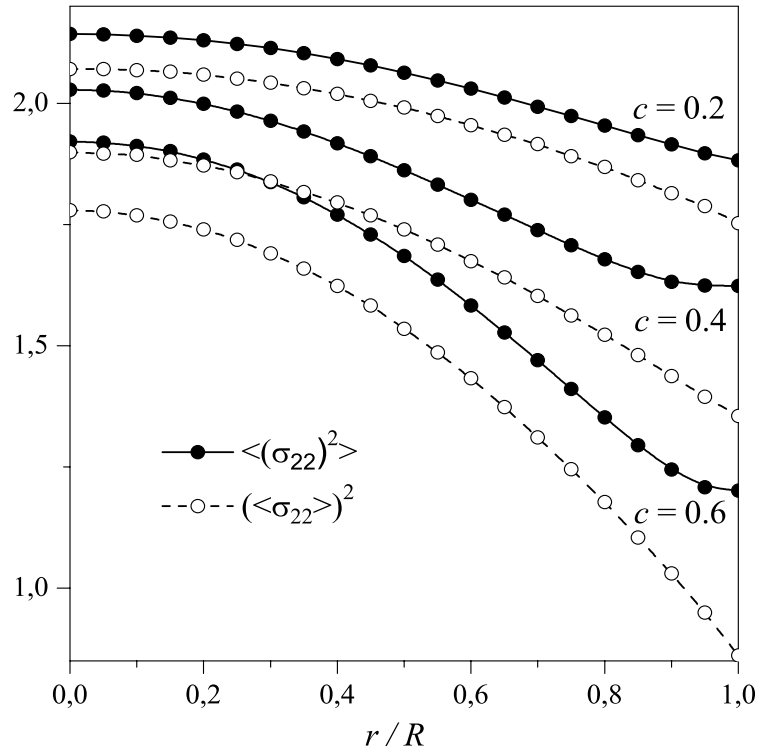


Fig.2.17. Second moment of stress σ_{22} radial variation as a function of volume fraction of fibers

The second moment of stresses plays a fundamental role in a wide class of nonlinear problems such as e.g. nonlinear elasticity, failure initiation, plasticity (see for references Buryachenko, 2001). In particular, the problem of failure initiation is based on the estimation of the statistical averages of the second moments of the normal and tangential components (Buryachenko and Shoepner, 2004). In the Fig.2.18., the second moments $\langle \sigma_{rr}^2 \rangle^N$ and $\langle \sigma_{r\varphi}^2 \rangle^N$ are compared with $(\langle \sigma_{rr} \rangle^N)^2$ and $(\langle \sigma_{r\varphi} \rangle^N)^2$, respectively. In this example, $c = 0.5$; the plot shows their variation along the matrix-fiber interface $r = R$, $-\pi/2 < \varphi < \pi/2$.

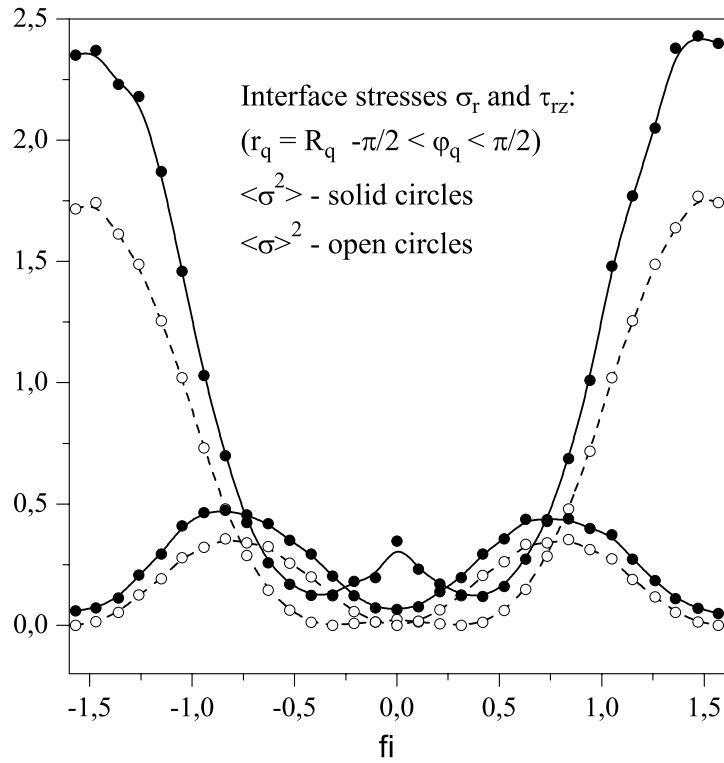


Fig.2.18. Second moment of interface stress σ_{rr} variation

2.2.9 Conclusions

An accurate analytical method has been developed to solve for stress in a plane an infinite quasi-random array of circular inclusions, the last being a "cell model" of non-ordered fibrous composite. The method combines technique of periodic complex potentials with the Fourier series expansion to reduce a primary boundary-value elasticity problem for a complicated multiple-connected domain to an ordinary well-posed set of linear algebraic equations. It provides high numerical efficiency of the method, accuracy of which is controlled entirely by a number of harmonics in the truncated series retained for practical calculations. Up to several hundred of interacting inclusions can be considered in this way which makes the model sufficiently realistic and flexible to account for the micro structure statistics and this able to model geometry and elastic behavior of stochastic structure composite. The numerical results are given for the statistical average of local phase and interface stress and their second moments.

Chapter 5

The high aspect-ratio rod-like inclusion: Eshelby-type problem by the Finite Element Method

5.1 The problem statement

The linear elasticity problem under study is a stress field in and around the inclusions with extremely high (of order 1000) ratio of the major and minor dimensions, say, slender rods, platelets, etc. We consider a single isotropic inclusion, embedded in an infinite solid, or matrix. The displacement \mathbf{u} and normal fraction $\mathbf{T}_n = \boldsymbol{\sigma} \cdot \mathbf{n}$, where $\boldsymbol{\sigma}$ is a stress tensor, $\boldsymbol{\sigma} = \mathbf{L}\boldsymbol{\varepsilon} + \boldsymbol{\alpha}$ and $\boldsymbol{\varepsilon} = \frac{1}{2}[\nabla\mathbf{u} + (\nabla\mathbf{u})^\top]$, are assumed to be continuous through the matrix-inclusion interface:

$$[[\mathbf{u}]] = 0; \quad [[\boldsymbol{\sigma} \cdot \mathbf{n}]] = 0. \quad (5.1)$$

Here, $[[f]]$ means a jump of the function f through the interface; so, $[[\mathbf{u}]] = \mathbf{u}^{(0)} - \mathbf{u}^{(1)}$, where the upper indices "0" and "1" refer to matrix and inclusion, respectively. Also, $\mathbf{L} = \mathbf{L}(G, \nu)$ is the isotropic stiffness tensor, with the shear modulus G and Poisson's ratio ν : $G = G_0, \nu = \nu_0$ in the matrix and $G = G_1, \nu = \nu_1$ in the inclusion.

The stress in the piece-homogeneous solid is induced by the the far stress field $\boldsymbol{\sigma}_0$ or, what is equivalent in the math sense, the eigenstress tensor $\boldsymbol{\alpha} = \{\alpha_{ij}\}$, non-zero constant in the inclusion and zero in the matrix. It is well-known and commonly used in the composite mechanics fact, that for the inclusion of ellipsoidal shape the resulting stress inside the inclusion also were constant (Eshelby solution). In the real world, however, such a shape is rather exception than a rule: the more common are the fiber-like and penny-like shapes. In such the inclusions, the stress is non-uniform even for the constant far stress or eigenstress. The problem of practical importance is the shape effect on local and mean (averaged) stress concentration in the inclusions. The latter is indicating ability of inclusion to transfer the load and, thus, to improve overall elastic stiffness of composite.

Inclusion's shape is rarely considered in studies of fiber–matrix interactions. The previous analytical (Goh et al. 1999) and FE analyzes (Goh et al. 2000) have been concerned with the effect of fibre shape when the surrounding matrix is plastic. Studies of elastic load transfer by photoelasticity (Schuster & Scala 1964) and FE analysis (Carrara & McGarry 1968) demonstrated stress concentrations in the matrix surrounding the cylindrical fibre end and that these were reduced at a tapered fibre end. However, these conclusions

were not complete; ever recent publications (Goh et al. 2004) deal with the simplified (namely, axisymmetric geometry based) models.

The aim of this study is twofold. The first goal to obtain convergent (and, thus, reliable) solution of the 3D Eshelby-type problem by the finite element method (FEM) in the case of very high aspect ratio inclusion. The second one is to investigate way and extent to which local and average stress in and around the inclusion is affected by its shape. In doing so, we address the following question: *is it possible (and, if yes, then how) to define an ellipsoid, "equivalent" in the averaged stress sense to a rod or platelet of high aspect ratio?* From the macroscopic description of composite mechanics standpoint, the averaged stress inside the inclusions are of primary interest. Keeping in mind a lot of work done already for composites of ellipsoidal inclusions, the idea to suggest some "equivalent ellipsoid" concept providing application of numerous available theories for the composites of ellipsoidal inclusions to the "real-world" composite materials seems very attractive.

In what follows, we give a brief theory account of the numerical method first. Then, we start numerical study with the 2D Eshelby-type problem (plane strain formulation) and evaluate the local stress variation in the major axis direction as well as the averaged over the inclusion stress for various aspect ratio and ratio of shear moduli of inclusion and matrix. An accuracy of numerical algorithm was tested on the problem for a plane with elliptic inclusion known to possess an exact analytical solution; another was the convergence check consisting in comparison of the numerical data obtained on a given and refined meshes. Then, the same problem is studied in 3D in the axisymmetric statement. In turn, these results along with the Eshelby solution for three-axial ellipsoid are utilized for testing and accuracy estimation sake when a general 3D problem is solved. Parametric numerical study of the 3D models (both the rods and platelets) and proof of the "equivalent ellipsoid" hypothesis completes this work.

5.2 FEM theory

5.2.1 Elasticity theory equations

The force balance equation is

$$\nabla \cdot \boldsymbol{\sigma} + \mathbf{p} = 0. \quad (5.2)$$

Here, $\boldsymbol{\sigma}$ is a stress tensor, \mathbf{p} is a body force vector and ∇ is the nabla-operator (Hamilton's operator):

$$\nabla = \frac{\partial}{\partial x_k} \mathbf{e}_k \quad (5.3)$$

where \mathbf{e}_k is basis vector of coordinate system, " \cdot " is the scalar product operation. The stress tensor $\boldsymbol{\sigma}$ is related to strain tensor $\boldsymbol{\varepsilon}$ and tensor of initial (say, thermal) stress $\boldsymbol{\alpha}$ by the Lamé formula

$$\boldsymbol{\sigma} = \mathbf{L}\boldsymbol{\varepsilon} + \boldsymbol{\alpha}. \quad (5.4)$$

Here tensor $\mathbf{L} = \mathbf{L}(G, \nu)$ is the elastic stiffness tensor. The strain tensor $\boldsymbol{\varepsilon}$ is related to the displacement vector \mathbf{u} by

$$\boldsymbol{\varepsilon} = 0.5[\nabla\mathbf{u} + (\nabla\mathbf{u})^T]. \quad (5.5)$$

On the surface S of the volume V the following boundary conditions are considered:

1) on the part S_1 the displacements vector \mathbf{u} is specified:

$$\mathbf{u} = \mathbf{f}(\mathbf{r}, t), \quad \mathbf{r} \in S_1. \quad (5.6)$$

2) on the part S_2 the surface forces \mathbf{F} are specified:

$$\mathbf{n} \cdot \boldsymbol{\sigma}(\mathbf{r}, t) = \mathbf{F}(\mathbf{r}, t), \quad \mathbf{r} \in S_2. \quad (5.7)$$

3) on the part S_3 the normal displacement and shear forces are absent:

$$\mathbf{n} \cdot \mathbf{u}(\mathbf{r}, t) = 0, \quad \mathbf{n} \times [(\mathbf{n} \cdot \boldsymbol{\sigma}(\mathbf{r}, t)) \times \mathbf{n}] = \mathbf{0}, \quad \mathbf{r} \in S_3. \quad (5.8)$$

Here, \mathbf{n} is the outer normal unit vector to surface S .

5.2.2 FEM equations

Let us consider solution of the elasticity theory problem by the Finite Element Method (FEM). To obtain the equations of resolving linear system, we apply the Bubnov-Galerkin procedure. First, we multiply equation (5.2) by the shape function N_m (associated with the node index $m = 1, 2, \dots, K$, where K is a total node number of FE mesh of V) and then integrate over the volume V . Then, we rewrite equation (5.2) in the "weak" form:

$$\int_V \nabla \cdot \boldsymbol{\sigma} N_m dV + \int_V \mathbf{p} N_m dV = 0. \quad (5.9)$$

By applying the identities

$$\nabla \cdot (\boldsymbol{\sigma} N_m) = \nabla N_m \cdot \boldsymbol{\sigma} + N_m \nabla \cdot \boldsymbol{\sigma}, \quad (5.10)$$

$$\int_V \nabla \cdot \boldsymbol{\sigma} dV = \int_S \mathbf{n} \cdot \boldsymbol{\sigma} dS, \quad (5.11)$$

we obtain from (5.9)

$$\int_V \boldsymbol{\sigma} \cdot \nabla N_m dV = \int_V \mathbf{p} N_m dV + \int_S N_m \mathbf{n} \cdot \boldsymbol{\sigma} dS. \quad (5.12)$$

Next, we substitute the formulas (5.4) and (5.5) in (5.12) and make use of the boundary conditions (5.7) to obtain from (5.12) the equation

$$\begin{aligned} & \frac{1}{2} \int_V [\mathbf{L}(\nabla \mathbf{u} + (\nabla \mathbf{u})^T)] \cdot \nabla N_m dV \\ & = \int_V \mathbf{p} N_m dV - \int_V \boldsymbol{\alpha} \cdot \nabla N_m dV + \int_S N_m \mathbf{F}(\mathbf{r}, t) dS. \end{aligned} \quad (5.13)$$

Following the FEM scheme, we approximate the \mathbf{u} , \mathbf{p} , $\boldsymbol{\alpha}$ and \mathbf{F} on each finite element as

$$W = W_p N_p, \quad p = 1, 2, \dots, K^e \quad (W = (\mathbf{u}, \mathbf{p}, \mathbf{F}, \boldsymbol{\alpha})), \quad (5.14)$$

where K^e is node number of element with number e , $e = 1, 2, \dots, M$, M is a total number of finite elements.

Finally, substituting the expressions (5.14) into (5.13) gives us the equations for nodal values of the displacement vector $\mathbf{u}(\mathbf{r}_k, t) = \mathbf{U}_k(t) \equiv \mathbf{U}_k$:

$$\begin{aligned} & \frac{1}{2} \sum_{e=1}^M \int_{V^e} [\mathbf{L}(\nabla(\mathbf{U}_k N_k) + (\nabla(\mathbf{U}_k N_k))^{\mathbf{T}})] \cdot \nabla N_m dV \\ & = \sum_{e=1}^M \left[\int_{V^e} \mathbf{p}_k N_k N_m dV - \int_{V^e} \boldsymbol{\alpha}_k N_k \cdot \nabla N_m dV + \int_{S^e} \mathbf{F}_k N_m dS \right]. \end{aligned} \quad (5.15)$$

After calculation of the volume and surface integrals in (5.15) and assembling the equations (5.15) over all the finite elements, we come to a global system of lineal algebraic equations with unknown vector $\{\mathbf{U}\}$ of the nodal displacements:

$$[A] \{\mathbf{U}\} = \{\mathbf{R}\}. \quad (5.16)$$

Here, vector $\{\mathbf{R}\}$ is a sum over the elements of the RHS of the equations (5.15) and the matrix $[A]$ with dimensions $K \times K$ is the symmetric and positively defined matrix.

5.3 2D problem (plane strain)

In this part, we consider a 2D solid with the inclusions of two kinds: a rod with rounded edge of length $2L_x$ and thickness $2L$, Fig.5.1 and an ellipse with semi-axes a and b , Fig.5.2. Inside the inclusion, we assume the uniform eigenstress $\alpha = \text{const}$ to be applied. Two loading cases will be considered, namely $\alpha_{11} = 1$ and/or $\alpha_{22} = 1$; in the 2D plane strain problem, we have also $\alpha_{33} = \nu_1(\alpha_{11} + \alpha_{22})$. All other components of the tensor $\boldsymbol{\alpha}$ are equal to zero. The disturbance caused by inhomogeneity, decays as R^{-2} , where R is a distance from inclusion. E.g., at the distance $R = 30L_x$, from inclusion the matrix stress is about three orders of magnitude below the applied stress in the inclusion. Therefore, instead of use the special, so-called "infinite" elements to solve for an unbounded solid, we can alternatively consider a finite matrix domain, sufficiently large to make effect of the free outer boundary on the stress in the vicinity of inclusion negligibly small. A square with the side length equal to $100L_x$ was found to be quite sufficient and thus was accepted for practical computations. Moreover, due to symmetry of the model problems with eigenstress taken in the form $\alpha_{ij} = \delta_{kl}$, it is possible to reduce our numerical analysis to the first quadrant only

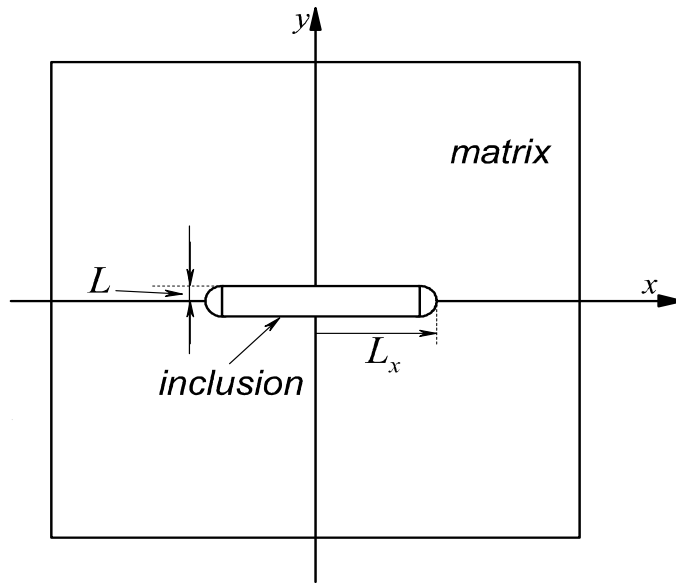


Fig.5.1. Model 1: plane with the rod-like inclusion

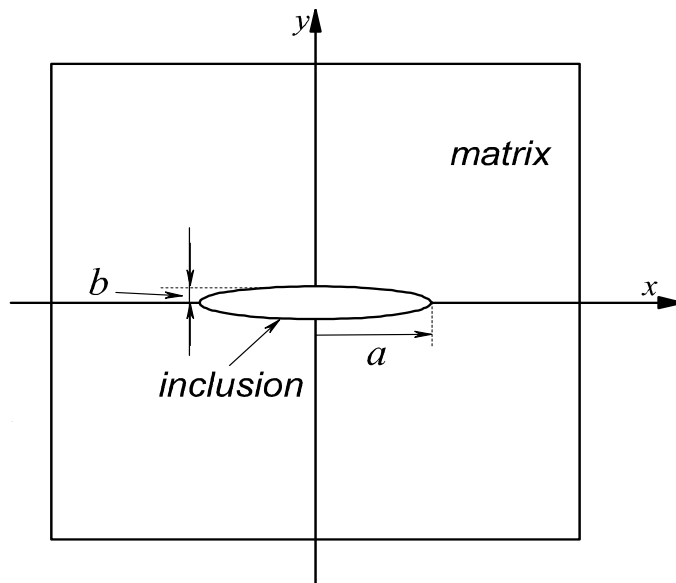


Fig.5.2. Model 2: plane with the elliptic inclusion

In all the subsequent calculations, we accept $\nu_1 = \nu_0 = 0.25$. Two varying parameters were a) aspect ratio $A_r = 10, 20, 50, 100, 200, 500, 1000$; and b) the shear moduli ratio $G_{rat} = G_1/G_0 = 0.1, 1, 10, 100$ and 1000 . In Fig.5.3- Fig.5.4, a typical finite-element mesh is shown for a whole domain as well as in the vicinity of inclusion with $A_r = 10$. To ensure adequate approximation of the highly inhomogeneous stress field near the matrix-

inclusion interface, the fine mesh was used in and around the inclusions. The special care was taken in the case of high (> 100) aspect ratio to ensure sufficiently fine mesh in the area of stress steep variation and, in the same time, to prevent the total number of DOFs from getting exceedingly large.

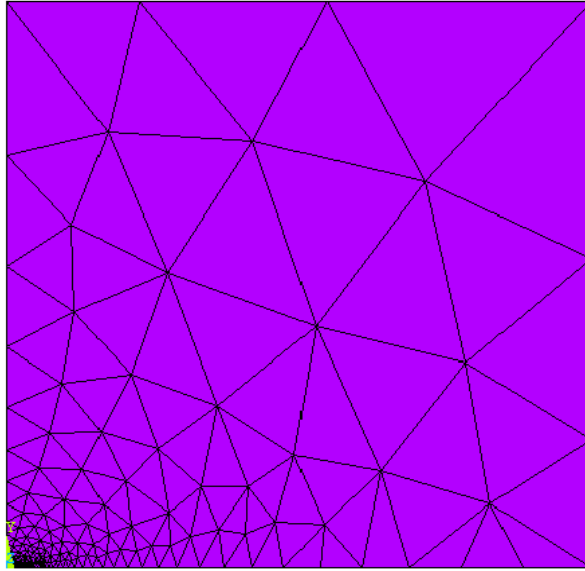


Fig.5.3. FE mesh in the first quadrant.

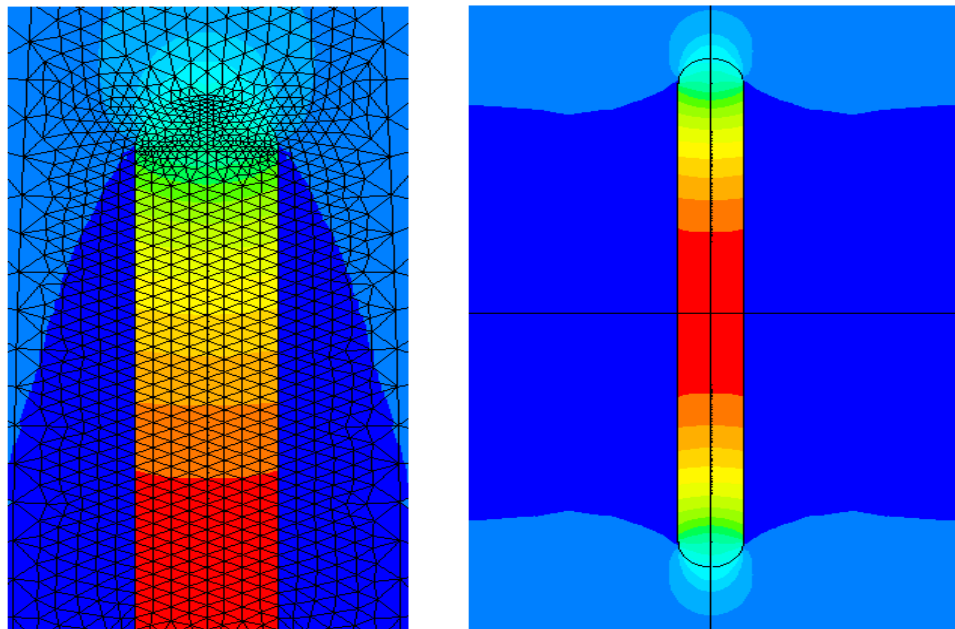


Fig.5.4. FE mesh around the rod-like inclusion and symmetry of solution.

Below, some results of the of FE model testing are given. So, in Fig.5.5 the obtained by FEM numerical (circles - for aspect ratio $A_e=20$ and triangles - for aspect ratio $A_e=200$) and analytical (solid and dot lines, respectively) solutions for $G_{rat}=10$ corresponding to hydrostatic eigenstress $\alpha_{11}=\alpha_{22}=1$ in the elliptic inclusion are shown. As follows from Fig.5.5 and similar results for $G_{rat}=0.1, 1, 10, 100$ and 1000 and $A_r=10, 20, 50, 100, 200, 500$ and 1000 , the numerical and analytical solutions agree quite well for a whole range of parameters. Expectedly, stress is constant in the inclusion and tends to zero outside of it. Noteworthy, σ_{22} is smaller than σ_{11} and drops to zero with the aspect ratio A_r growing up.

In Fig.5.6-av the value of average stress $\langle\sigma_{11}\rangle$ in the strip-like inclusion (solid lines) and in the elliptic inclusion (dotted lines) are shown. As seen from the plots, both G_{rat} and A_r influence greatly the average stress $\langle\sigma_{11}\rangle$ in the inclusion. Interestingly, the moduli ratio G_{rat}^0 exists (≈ 0.5), where the average stress in inclusion is practically invariant of the aspect ratio A_r . At $G_{rat} = G_{rat}^0$, the average stress $\langle\sigma_{11}\rangle$ is practically constant and equal to 0.67. However, for G_{rat} different from G_{rat}^0 , the aspect ratio A_r affects average stress in the inclusion. Namely, for $G_{rat} < G_{rat}^0$ value of the $\langle\sigma_{11}\rangle$ decreases with the aspect ratio A_r increased, and for $G_{rat} > G_{rat}^0$ $\langle\sigma_{11}\rangle$ increases with increasing the aspect ratio A_r .

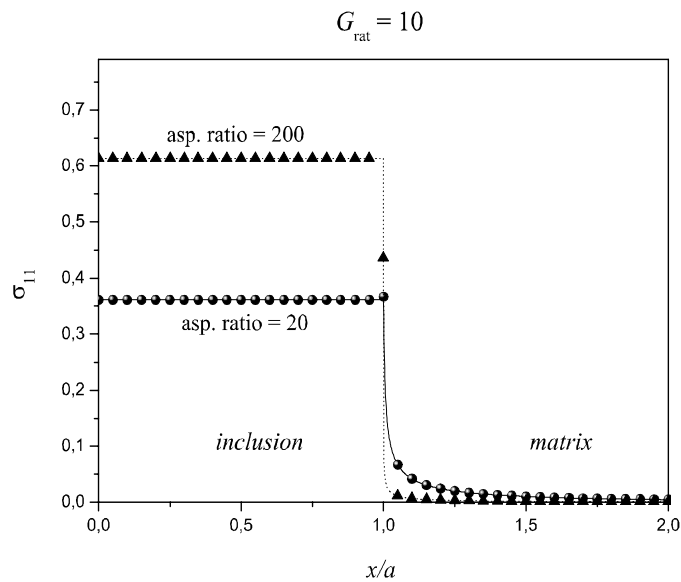


Fig.5.5. σ_{11} variation along a x -coordinate, $G_{rat} = 10$

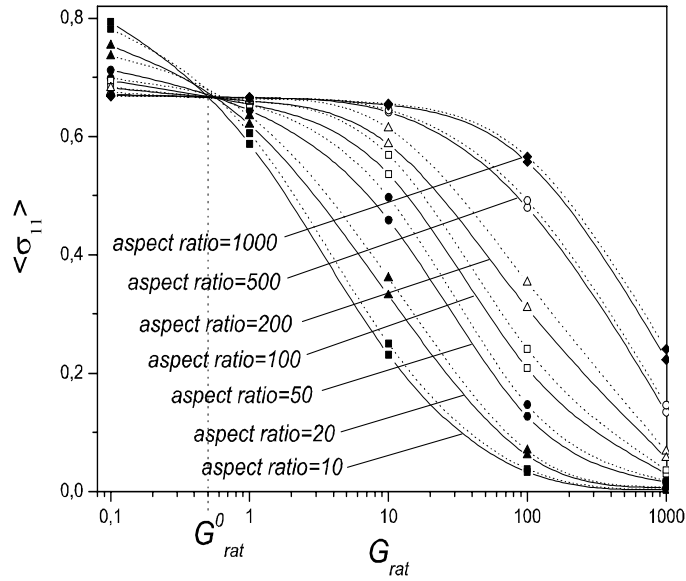


Fig.5.6-av. Average stress $\langle \sigma_{11} \rangle$ in inclusion (at initial stress $\sigma_{11}=1$, $\sigma_{22}=1$; solid lines - for strip-like inclusion, dot lines - for ellipse).

Now, we consider the Eshelby-type problem for a strip-like inclusion (Fig.5.1) with the eigenstress $\alpha_{11} = 1$ prescribed. The results of numerical solution are presented in Fig.5.6a-Fig.5.6d with signs circle ($A_r = 10$), square ($A_r = 50$), triangle ($A_r = 200$), and circumference ($A_r = 1000$). Also, in Figures 5.6 (a-d) the analytical solution is shown for elliptic inclusion of the same aspect ratio (solid lines for $A_r = 10$, dashed lines for $A_r = 50$, dotted lines for $A_r = 200$, and dash-dotted lines for $A_r = 1000$).

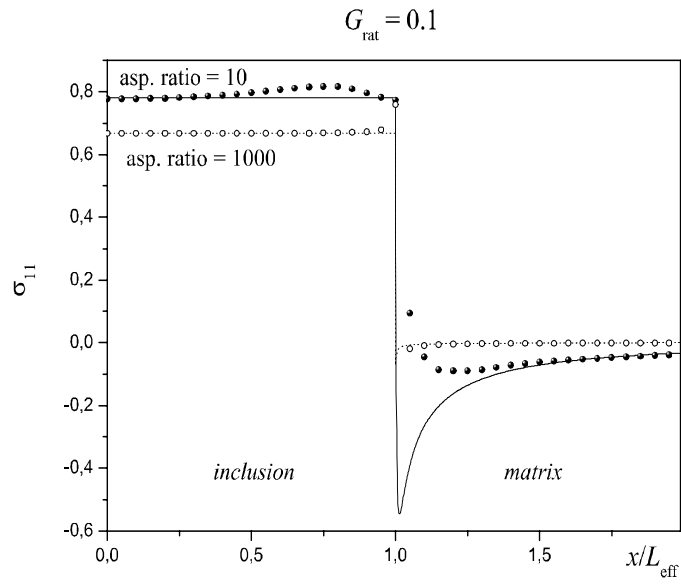


Fig.5.6a. σ_{11} variation along a x -coordinate, $G_{rat} = 0.1$

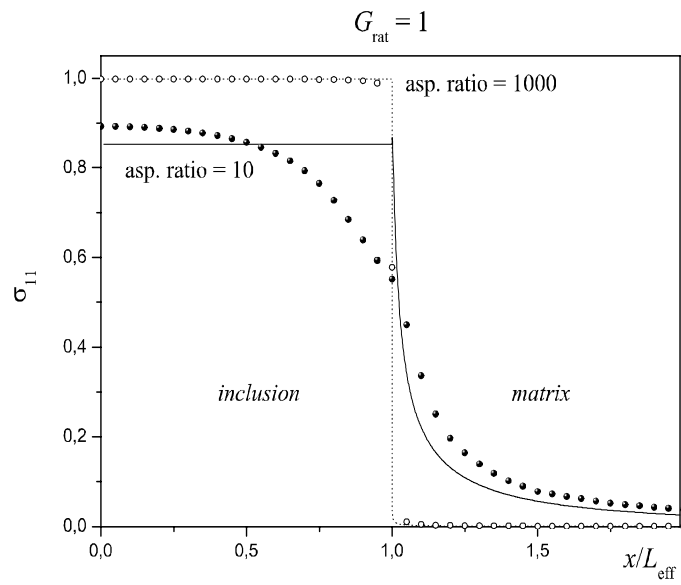


Fig.5.6b. $G_{rat} = 1$

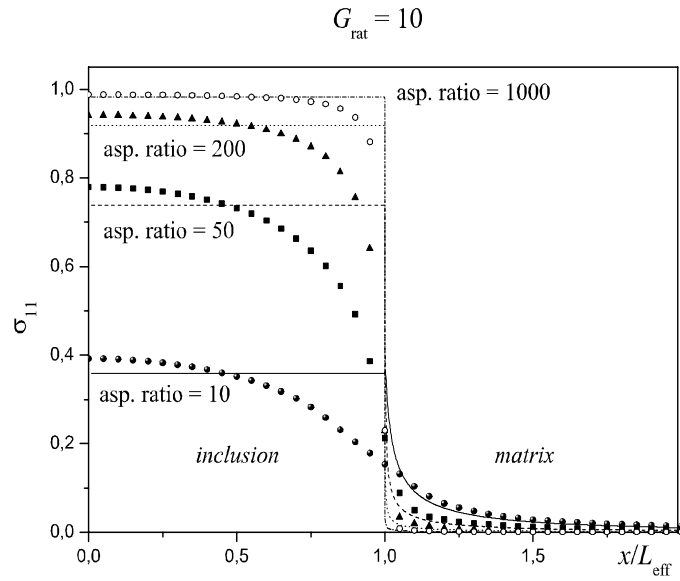


Fig.5.6c. $G_{rat} = 10$

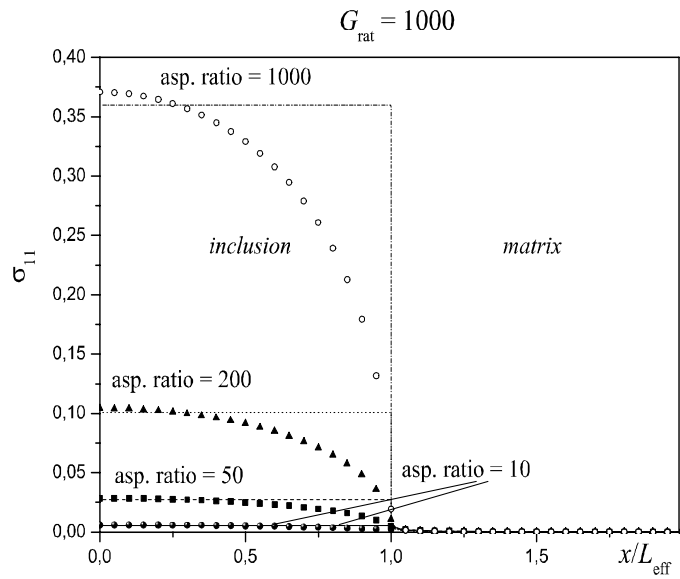


Fig.5.6d. $G_{rat} = 1000$

In Table 5.1, the results of calculations of average stress $\langle \sigma_{11} \rangle$ in the inclusion are presented. In this and the next tables, the columns labeled "num." contain the results obtained with numerical (FEM) method for solid with strip-like inclusion and the columns labeled "exact" show the analytical solution for a solid with elliptic inclusion. Noteworthy, the qualitative behavior and absolute values of mean stress for the compared inclusions

Table 5.1: Average values of $\langle \sigma_{11} \rangle$ obtained with numerical (FEM) method (num.) and with exact solution (exact)

G_{rat}	A_r							
	10		50		200		1000	
	num.	exact	num.	exact	num.	exact	num.	exact
0.1	0.980	0.989	0.996	0.998	0.999	1.0	1.0	1.0
1	0.821	0.854	0.948	0.969	0.983	0.992	0.998	0.998
10	0.331	0.359	0.681	0.738	0.878	0.919	0.979	0.983
100	0.048	0.053	0.188	0.219	0.464	0.529	0.835	0.849
1000	0.005	0.005	0.023	0.027	0.083	0.101	0.335	0.360

are rather similar. Such a comparison is somewhat conditional because it is not obvious how to compare the inclusions of different shapes. One way is to compare the inclusions of equal aspect ratio (Table 5.1 and Fig.5.7a). Probably, more physically motivated choice is to compare inclusions of equal dimensions (major axis and area): then, their aspect ratios relate approximately by $A_r/A_e = \pi/4$. At first sight, in this case agreement of the compared data looks much better, see Fig.5.7b; however, it is a subject of the careful asymptotic analysis.

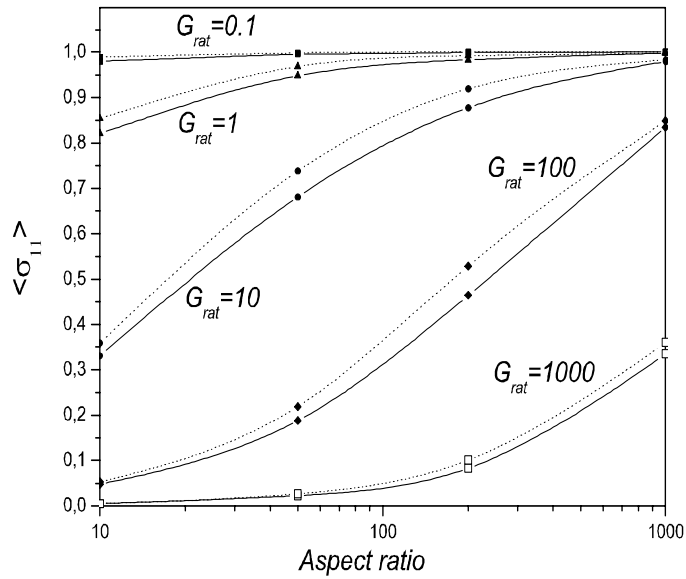


Fig.5.7a. Comparison: equal aspect ratio.

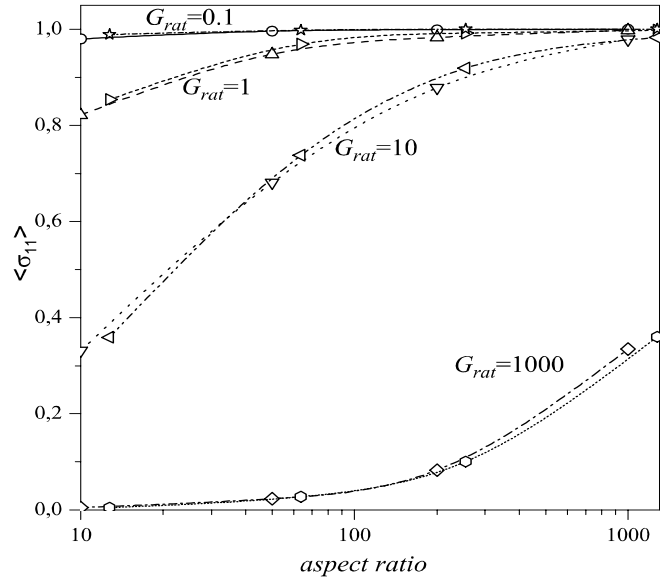


Fig.5.7b. Comparison: equal area and length.

In Fig.5.8a–Fig.5.8d, the results of numerical and analytical solutions presented for the eigenstress $\alpha_{22} = 1$. In this case, as before, at increasing of the value of aspect ratio A_r from 10 to 1000 value of stress σ_{22} rapidly descends and tends to zero.

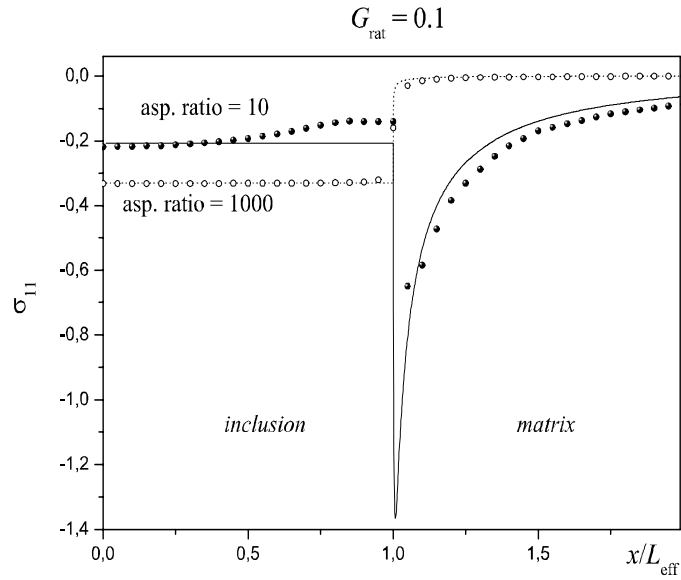


Fig.5.8a. σ_{11} variation along a x -coordinate, $G_{rat} = 0.1$

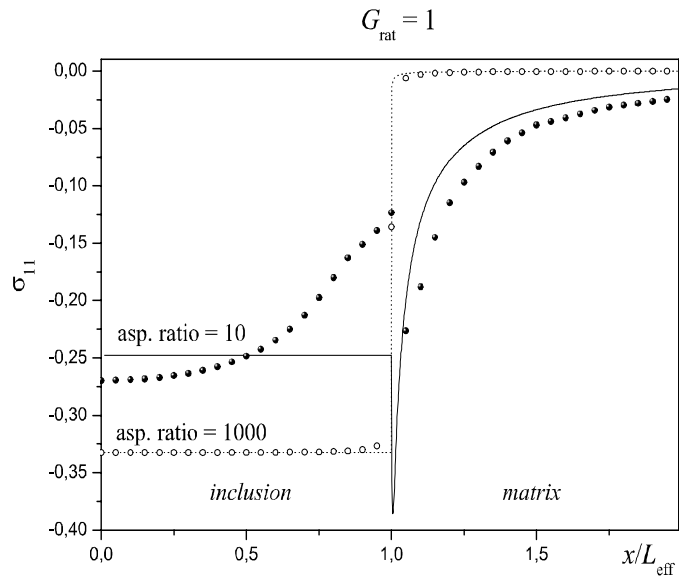


Fig.5.8b. $G_{rat} = 1$

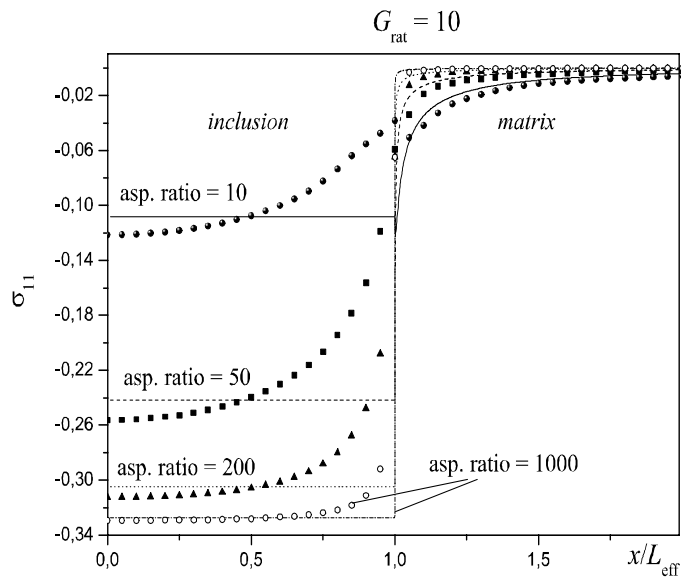


Fig.5.8c. $G_{rat} = 10$

Table 5.2: Average values of $\langle \sigma_{xx} \rangle$ obtained with numerical (FEM) method (num.) and with exact solution (exact)

G_{rat}	A_r							
	10		50		200		1000	
	num.	exact	num.	exact	num.	exact	num.	exact
0.1	-0.186	-0.207	-0.283	-0.300	-0.317	-0.324	-0.331	-0.332
1	-0.233	-0.248	-0.303	-0.314	-0.324	-0.328	-0.332	-0.332
10	-0.100	-0.108	-0.222	-0.242	-0.291	-0.305	-0.326	-0.327
100	-0.015	-0.016	-0.062	-0.072	-0.154	-0.176	-0.278	-0.283
1000	-0.0015	-0.0017	-0.0075	-0.0089	-0.028	-0.033	-0.111	-0.120

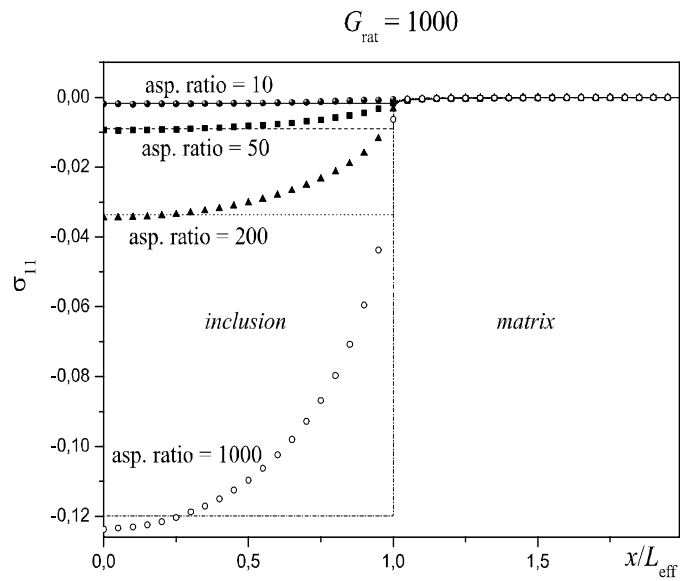


Fig.5.8d. $G_{rat} = 1000$

In Table 5.2, the results of calculations of average stress concentration $\langle \sigma_{11} \rangle / \alpha_{22}$ are given. Comparison of these data as well as those shown in Figs 9a, b leads to a conclusion analogous to that we made above: evaluation of averaged stress in the strip-like inclusion can be performed using the Eshelby solution for an ellipse with some "equivalent" aspect ratio; however, local stress fields in the compared inclusions are quite different (uniform in the ellipse and varying steeply near the interface in the strip-like inclusion).

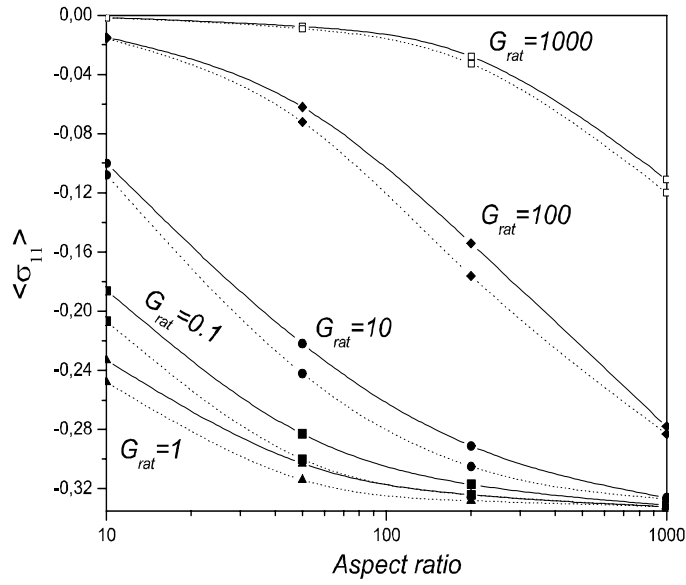


Fig.5.9a. Comparison - equal aspect ratio.

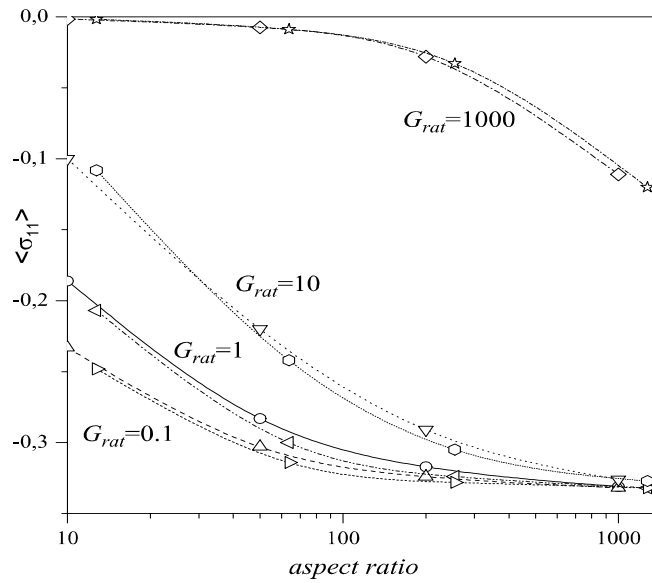


Fig.5.9b. Comparison - equal area and length.

5.4 3D problem: spherocylinder (long capped rod)

In this part, we analyse stress in a solid with inclusions of two kinds. They are long fiber with rounded ends and its counterpart, prolate ellipsoid of revolution (spheroid). The

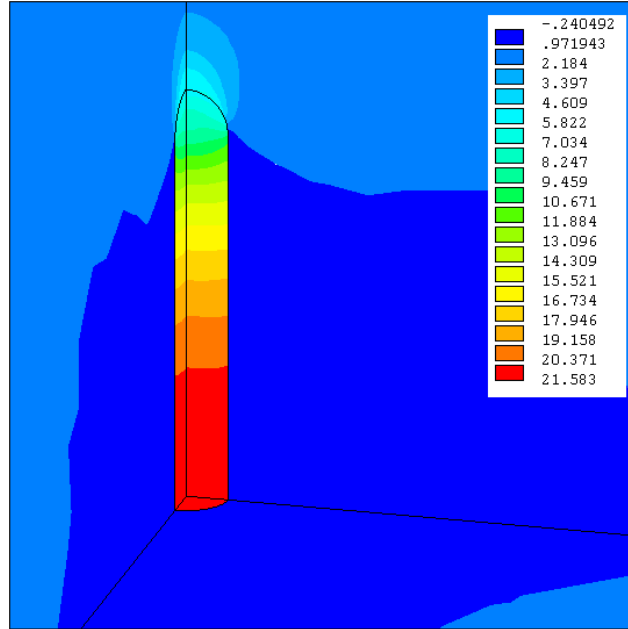


Figure 5.10: Stress σ_{33} in the 1st octant due to far field $\langle\sigma_{33}\rangle = 1$

both shapes are axially symmetric: however, the uniform eigenstress $\alpha = const$ prescribed there makes the problem essentially three-dimensional.

The finite element analysis of 3D problem is, in general, much more time-expensive as compared with the two-dimensional problems. Fortunately, in the 3D case disturbance, caused by inhomogeneity, decays as R^{-3} , where R is a distance from inclusion. Thus, unlike 2D case, the matrix stress is about three orders of magnitude below the eigenstress in the inclusion already at the distance $R = 10L_x$. A finite matrix domain, sufficiently large to make effect of the free outer boundary on the stress in the vicinity of inclusion negligibly small, was found to be $30L_x$ and this value was accepted for practical calculations. Moreover, due to linearity of the problem and symmetry of the domain geometry, an analysis of the specific problems of type $\alpha_{ij} = \delta_{kl}$ can be confined to the first octant only and thus reducing greatly the computational effort.

The typical stress distribution in and around the inclusion are shown by the isolines in the Figures from 5.10 to 5.14: the Fig.5.10-5.12 correspond to the axial far stress $\langle\sigma_{33}\rangle = 1$ whereas in the Fig.5.13 and Fig.5.14 the stress components induced by the transversal to the rod axis direction far stress $\langle\sigma_{11}\rangle = 1$ are given. To make the pictures more informative, a moderate aspect ratio $A_r = 10$ was taken. However, even in this case, the tendency common for long rods is clearly seen. Namely, the stress in the middle part of inclusion is nearly uniform, whereas near the tips we observe considerable and highly localized stress concentration.

In the case where the eigenstress instead of far field were prescribed, the situation is quite analogous. For, in the Figs from 15 to 20 the stress induced by the load taken in the form $\alpha_{ij} = \delta_{kl}$ are presented. In the Figs from 16 to 20, the stress isolines in Oxz cross-section is shown, Oz being the fiber direction.

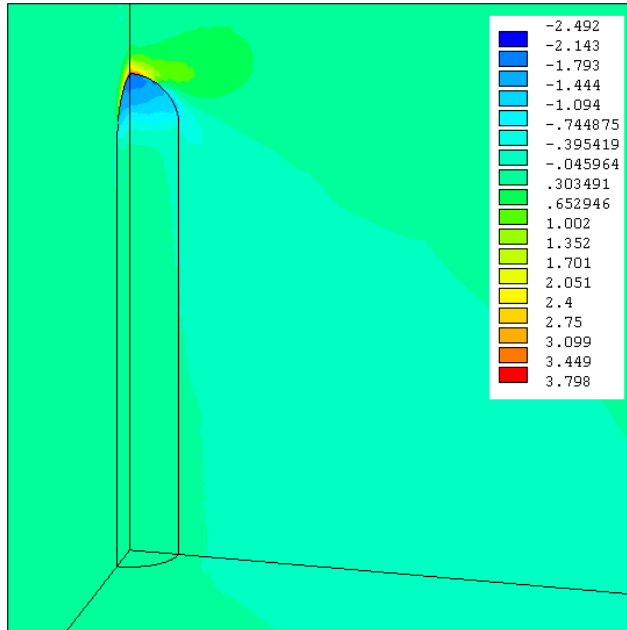


Figure 5.11: Stress σ_{11} in the 1st octant due to far field $\langle \sigma_{33} \rangle = 1$

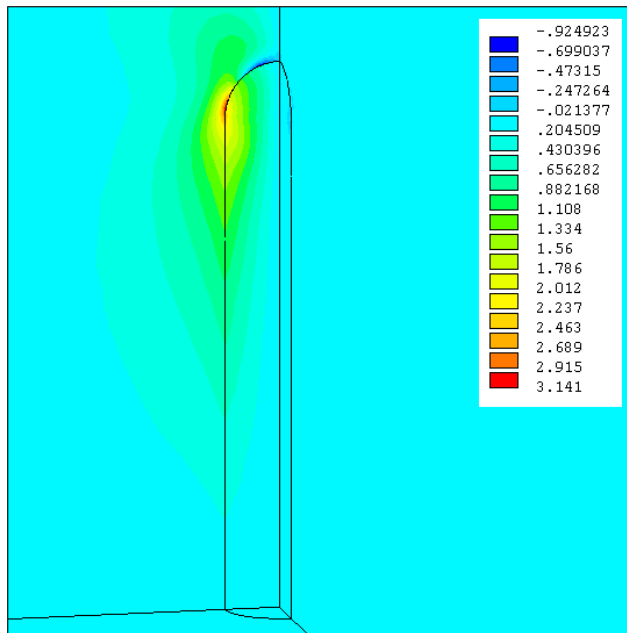


Figure 5.12: Stress τ_{13} in the 1st octant due to far field $\langle \sigma_{33} \rangle = 1$

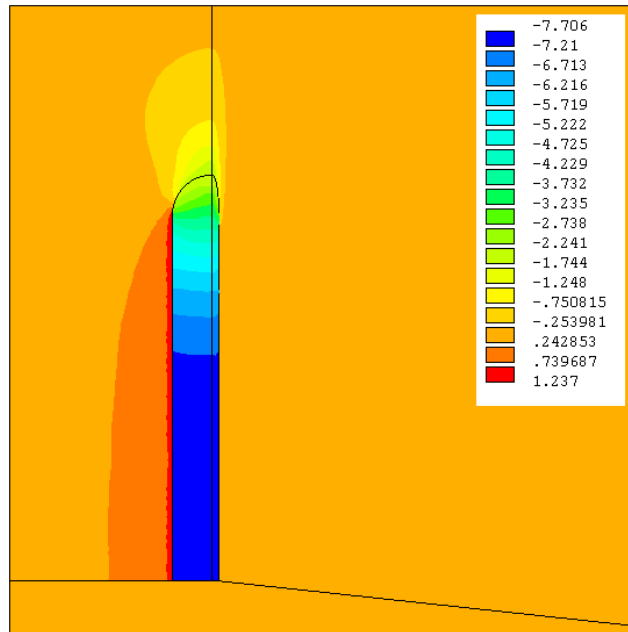


Figure 5.13: Stress σ_{33} in the 1st octant due to far field $\langle \sigma_{11} \rangle = 1$

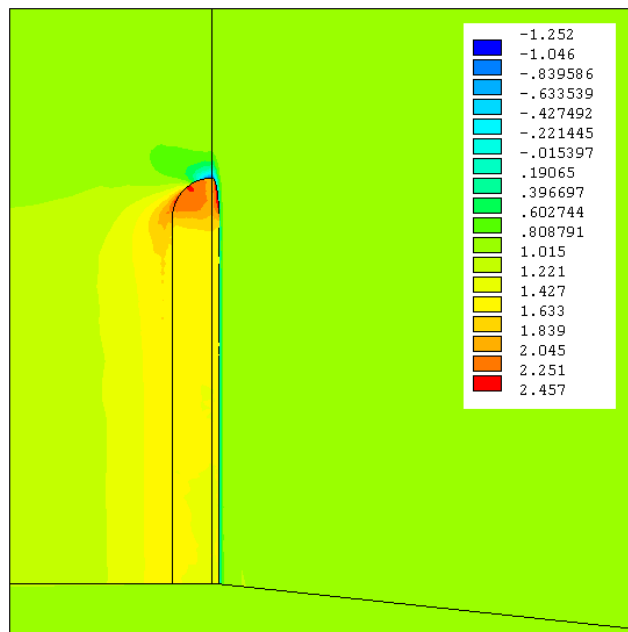


Figure 5.14: Stress σ_{11} in the 1st octant due to far field $\langle \sigma_{11} \rangle = 1$

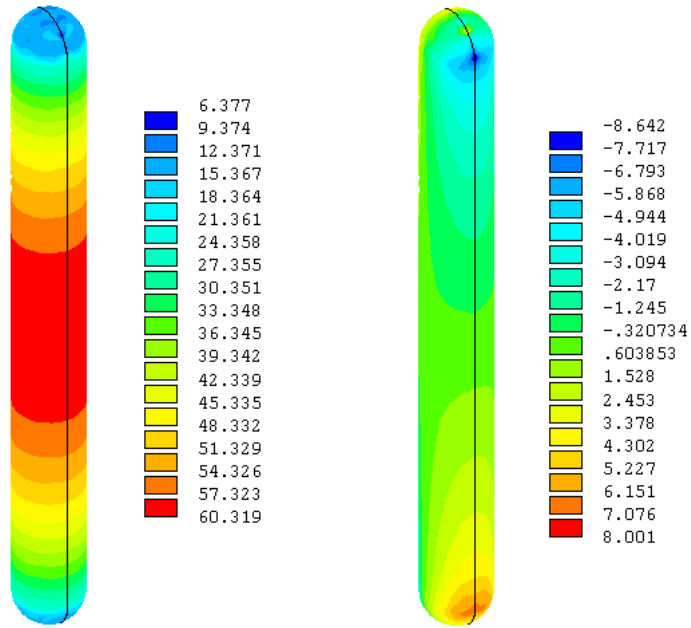


Figure 5.15: Stress σ_{33} and τ_{13} at the surface of the fiber, $\beta_{33} = 1$

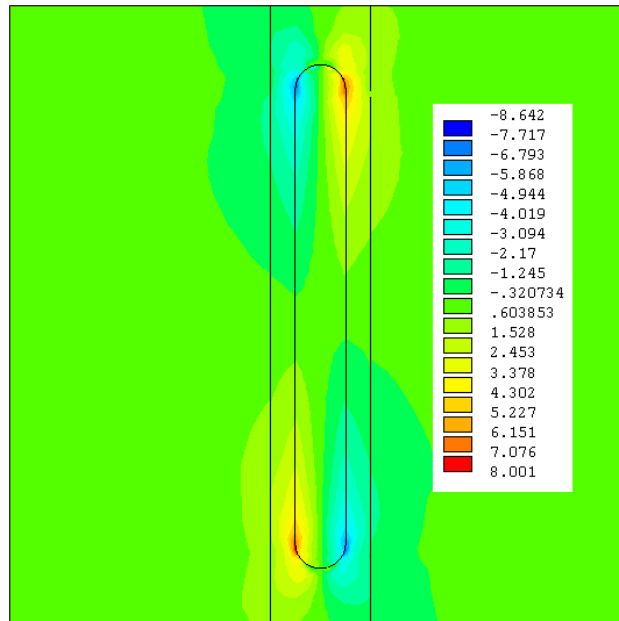


Figure 5.16: Stress τ_{13} inside the fiber, $\beta_{33} = 1$

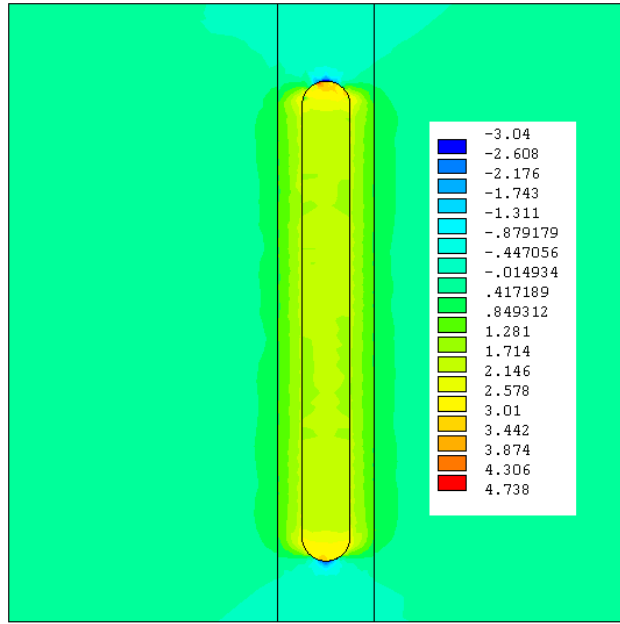


Figure 5.17: Stress σ_{11} inside the fiber, $\beta_{11} = 1$

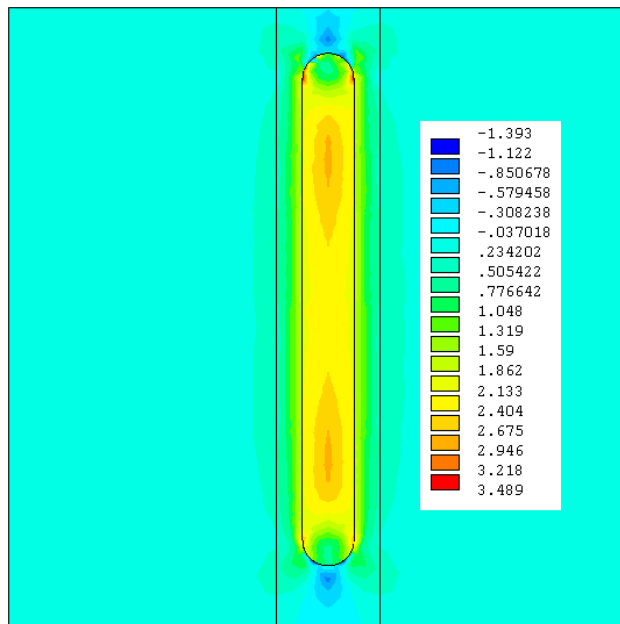


Figure 5.18: Stress τ_{13} inside the fiber, $\beta_{13} = 1$

Two particular but important loading cases we consider below are $\alpha_{22} = \alpha_{11} = 1$ and $\alpha_{33} = 1$ where the problem possesses an axial symmetry and can be effectively solved using the FEM software and mesh developed for 2D case. On the one hand, it simplifies and accelerates numerical study of the problem; on the other hand, it provides the necessary benchmark for testing workability and accuracy of the 3D FEM solver and the obtained numerical data.

The last problem we consider here is $\alpha_{22} = \alpha_{11} = 1$. The calculations using FEM for four values of material ratio $G_{rat} = 0.1, 1, 10$ and 1000 and five values of the aspect ratio $A_r = 10, 50, 200, 500$ and 1000 have been performed. Also, we obtain the analytical and numerical solutions of the analogous axisymmetric problem for a solid with inclusion in form of spheroid with z -axis of rotational symmetry. In Fig.5.19(a – d), the stress σ_{33} variation along the axial symmetry axis (z -axis) for various G_{rat} values are presented.

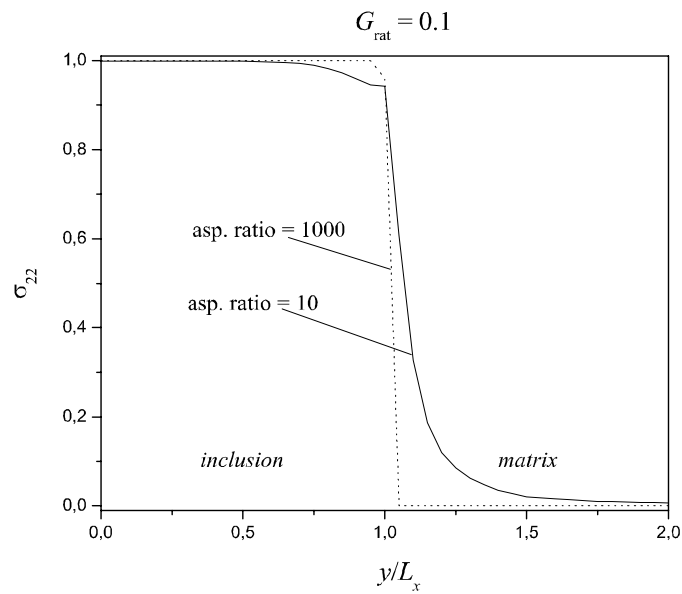


Fig.5.19a. σ_{33} variation along a z -coordinate, $G_{rat} = 0.1$

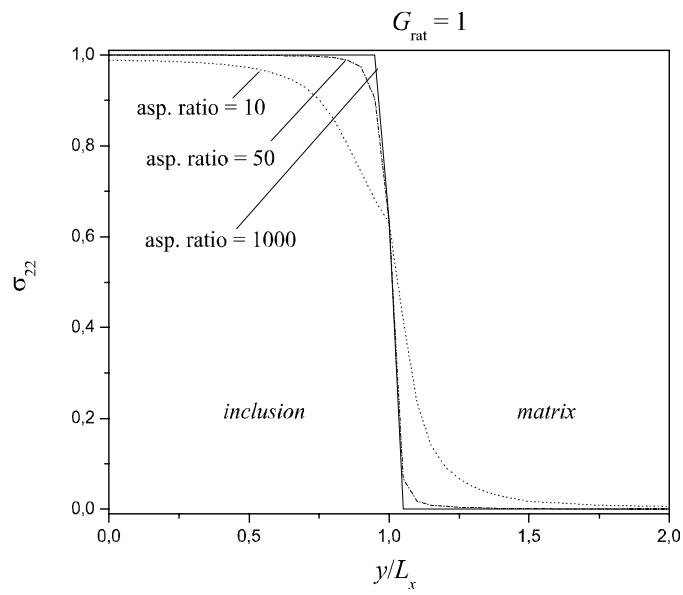


Fig.5.19b. $G_{rat} = 1$

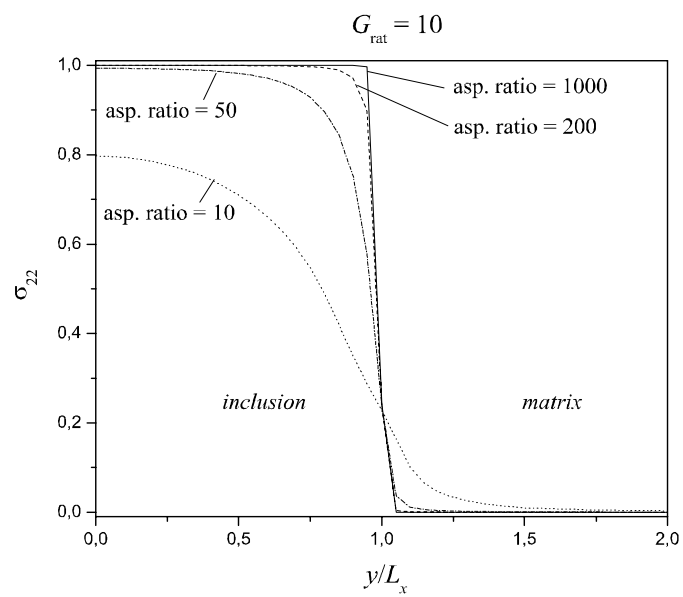


Fig.5.19c. $G_{rat} = 10$

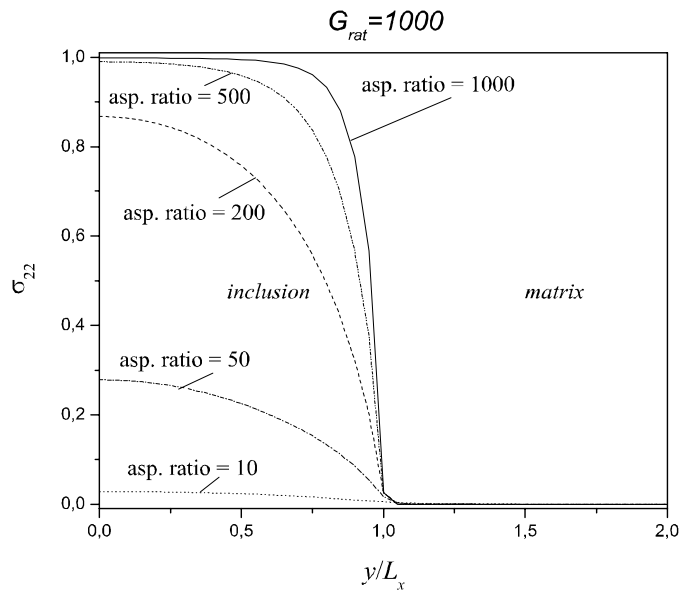


Fig.5.19d. $G_{rat} = 1000$

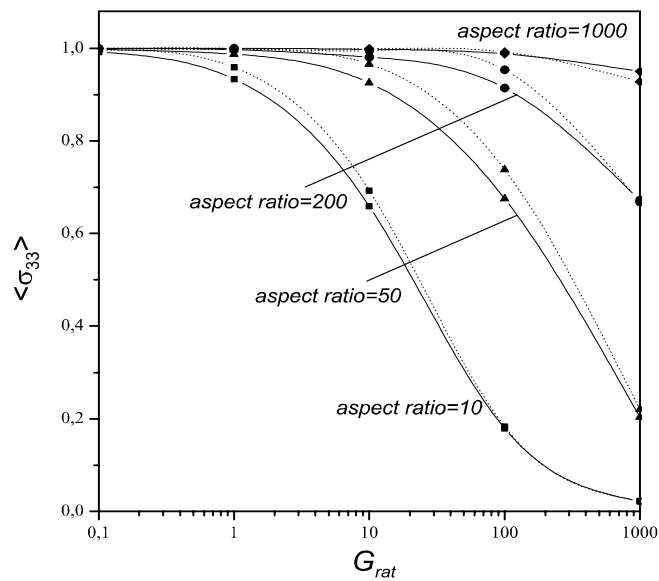


Fig. 5.20. Comparison of $\langle \sigma_{33} \rangle$ - equal aspect ratio.

As our comparative analysis shows, both the 2D and 3D codes give the close results for the axisymmetric problem which, in turn, agree well with analytical solution in the spheroidal inclusion case. It confirms the software workability and reliability of the numerical data obtained with it. Also, it is seen from the Fig.5.20 that, likewise the above

Table 5.3: Average values of $\langle \sigma_{33} \rangle$ obtained with numerical (FEM) method (num.) for a solid with a fiber with round end, and (exact) for a solid with long ellipsoid

G_{rat}	A_r									
	10		50		200		500		1000	
	num.	exact								
0.1	0.992	0.996	0.998	1.0	1.0	1.0	1.0	1.0	1.0	1.0
1	0.934	0.959	0.987	0.997	0.997	1.0	0.999	1.0	1.0	1.0
10	0.659	0.693	0.925	0.966	0.981	0.995	0.995	0.998	0.998	0.999
100	0.179	0.183	0.675	0.738	0.914	0.953	0.976	0.984	0.988	0.992
1000	0.022	0.022	0.203	0.220	0.672	0.668	0.898	0.859	0.950	0.928

considered 2D problem, the qualitative behavior and absolute values of mean stress for the compared inclusions are quite similar.

5.5 Brief conclusions:

- the reliable numerical FE solution has been obtained for a solid with a high-aspect ratio inclusion in 2D and 3D;
- the parametric study of the problem has been performed and local as well as averaged stress inside and outside the inclusion were evaluated;
- an “equivalent” ellipsoid concept has been suggested and confirmed for both the long rods and platelets by comparison with the analytical Eshelby’s solution for a single ellipsoidal inclusion in an unbounded solid.

5.6 References

- Carrara, A. S. & McGarry, F. J. 1968 Matrix and interface stresses in a discontinuous fibre composite model. *J. Compos. Mater.* **2**, 222–241.
- Goh, K. L., Aspden, R. M., Mathias, K. J. & Hukins, D. W. L. 1999 Effect of fibre shape on the stresses within fibres in fibre-reinforced composite materials. *Proc. R. Soc. Lond. A* **455**, 3351–3361.
- Goh, K. L., Mathias, K. J., Aspden, R. M. & Hukins, D. W. L. 2000 Finite element analysis of the effect of fibre shape on stresses in an elastic fibre surrounded by a plastic matrix. *J. Mater. Sci.* **35**, 2493–2497.
- Goh, K. L., Aspden, R. M., Mathias, K. J. & Hukins, D. W. L. 2004 Finite-element analysis of the effect of material properties and fibre shape on stresses in an elastic fibre embedded in an elastic matrix in a fibre-composite material *Proc. R. Soc. Lond. A* **460**, 2339–2352.
- Schuster, D. M. & Scala, E. 1964 The mechanical interaction of sapphire whiskers with a birefringent matrix. *Trans. AIME* **230**, 1635–1640.

2.4 A finite cluster of spheroidal inclusions in an elastic solid subjected to inhomogeneous external field: the method of analysis

2.4.1 The problem statement

Let us consider an infinite elastic solid with shear modulus μ_0 and Poisson ratio ν_0 , containing a finite number N of spheroidal inclusions made from material with shear modulus μ_p and Poisson ratio ν_p , $p = 1, 2, \dots, N$. Size and shape of p th spheroid is given by its semi-axes l_3^p (along the axis of revolution) and l_1^p (in perpendicular direction).

To describe geometry of the problem, we introduce arbitrarily the global Cartesian coordinate system $Ox_1x_2x_3$ and the inclusion-related local Cartesian coordinate systems $O^p x_1^p x_2^p x_3^p$, $p = 1, 2, \dots, N$; the last being introduced so that its origin O^p lies in the center of mass of p th spheroid whereas the axis $O^p x_3^p$ coincides with the its revolution axis. Position of p th local system (or, the same, p th inclusion) with respect to global coordinate frame is defined by the translation vector $\mathbf{X}_p = (X_1^p, X_2^p, X_3^p)$ being the global Cartesian coordinates the center of p th spheroid and the rotation matrix $\mathbf{\Omega}_p = \{\Omega_{ij}^p\}$; $(\mathbf{\Omega}_p)^T = (\mathbf{\Omega}_p)^{-1}$ and $\det(\mathbf{\Omega}_p) = 1$. So, the local coordinates of arbitrary point \mathbf{x} are related to global ones by

$$x_i^p = \Omega_{ij}^p (x_j - X_j^p); \quad (2.358)$$

Cartesian projections of the vector \mathbf{u} transform according to

$$u_i^p = \Omega_{ij}^p u_j. \quad (2.359)$$

Also, we introduce local curvilinear (spheroidal) coordinates for each inclusion in such a way that the matrix-inclusion interface

$$\left(\frac{x_1^p}{l_1^p}\right)^2 + \left(\frac{x_2^p}{l_1^p}\right)^2 + \left(\frac{x_3^p}{l_3^p}\right)^2 = 1 \quad (2.360)$$

would coincide with the coordinate surface $\xi^p = \xi_0^p$. Namely, (ξ, η, φ) are the spheroidal coordinates related to the Cartesian ones by (Hobson 1931)

$$\begin{aligned} x_1 + ix_2 &= d\bar{\xi}\bar{\eta}\exp(i\varphi), & x_3 &= d\xi\eta; \\ \bar{\xi}^2 &= \xi^2 - 1, & \bar{\eta}^2 &= 1 - \eta^2; \\ 1 &\leq \xi < \infty, & |\eta| &\leq 1, & 0 &\leq \varphi < 2\pi. \end{aligned} \quad (2.361)$$

The relations (2.361) at $Re(d) > 0$ describe the family of confocal prolate spheroids with inter-foci distance $2d$. In the case of an oblate spheroid, one must replace ξ on $i\bar{\xi}$ and d on $(-id)$ in this and all other relevant formulae.

So defined composite domain is subjected to an inhomogeneous external, or far, stress field. We *do not* assume any analytical expression for it nor specify its nature: it can be, say, numerical solution for a stress concentrator (crack, hole, etc.). In what follows, we postulate only that the displacement vector $\mathbf{U}(x_j)$ corresponding to above mentioned far stress tensor is known in any point of the interfaces S_p , $p = 1, 2, \dots, N$. On these surfaces,

the conditions of perfect mechanical contact, which are continuity of the displacement vector and normal traction vector through the interface:

$$\begin{aligned} (\mathbf{u}_q - \mathbf{u})_{S_q} = 0; \quad [\mathbf{T}_n(\mathbf{u}_q) - \mathbf{T}_n(\mathbf{u})]_{S_q} = 0; \\ q = 1, 2, \dots, N. \end{aligned} \quad (2.362)$$

Here, \mathbf{u} and \mathbf{u}_q are the displacement vectors in matrix domain and q th inclusion, respectively; they, as well as the far field \mathbf{U} , satisfy the equilibrium equation

$$\nabla \cdot \sigma = (1 - 2\nu) \Delta \mathbf{u} + \nabla (\nabla \cdot \mathbf{u}) = 0. \quad (2.363)$$

The traction vector

$$\mathbf{T}_n = \sigma \mathbf{n} = (\mathbf{L}\varepsilon - \beta) \mathbf{n} \quad (2.364)$$

where σ is the stress tensor, \mathbf{n} is the outside normal to interface, \mathbf{L} is the fourth-rank elastic stiffness tensor and

$$\varepsilon = \frac{1}{2} \left[\nabla \mathbf{u} + (\nabla \mathbf{u})^T \right] \quad (2.365)$$

is the strain tensor. Finally, β in (2.364) represents so-called strain-free, or transformation (e.g., residual or thermal) stress.

2.4.2 Theoretical background.

Partial vectorial solutions of the Lamé equation in spheroidal coordinates

The following sets of the partial vectorial solutions of Lamé equation have been introduced by Kushch (1997): constrained at $\|\mathbf{x}\| \rightarrow \infty$, or singular $\mathbf{F}_{ts}^{(i)} = \mathbf{F}_{ts}^{(i)}(\mathbf{x}, d)$:

$$\mathbf{F}_{ts}^{(1)} = \mathbf{e}_1 F_{t+1}^{s-1} - \mathbf{e}_2 F_{t+1}^{s+1} + \mathbf{e}_3 F_{t+1}^s; \quad (2.366)$$

$$\mathbf{F}_{ts}^{(2)} = \frac{1}{t} \left[\mathbf{e}_1 (t+s) F_t^{s-1} + \mathbf{e}_2 (t-s) F_t^{s+1} + \mathbf{e}_3 s F_t^s \right];$$

$$\begin{aligned} \mathbf{F}_{ts}^{(3)} = & \mathbf{e}_1 \left\{ -(x_1 - ix_2) D_2 F_{t-1}^{s-1} - \left[(\xi^{(0)})^2 - 1 \right] d D_1 F_t^s + (t+s-1)(t+s) \beta_{-(t+1)} F_{t-1}^{s-1} \right\} \\ & + \mathbf{e}_2 \left\{ (x_1 + ix_2) D_1 F_{t-1}^{s+1} - \left[(\xi^{(0)})^2 - 1 \right] d D_2 F_t^s - (t-s-1)(t-s) \beta_{-(t+1)} F_{t-1}^{s+1} \right\} \\ & + \mathbf{e}_3 \left[x_3 D_3 F_{t-1}^s - (\xi^{(0)})^2 d D_3 F_t^s + C_{-(t+1),s} F_{t-1}^s \right]; \end{aligned}$$

constrained at $\|\mathbf{x}\| \rightarrow 0$, or regular $\mathbf{f}_{ts}^{(i)} = \mathbf{f}_{ts}^{(i)}(\mathbf{x}, d)$:

$$\mathbf{f}_{ts}^{(1)} = \mathbf{e}_1 f_{t-1}^{s-1} - \mathbf{e}_2 f_{t-1}^{s+1} + \mathbf{e}_3 f_{t-1}^s; \quad (2.367)$$

$$\mathbf{f}_{ts}^{(2)} = \frac{1}{t+1} \left[\mathbf{e}_1 (t-s+1) f_t^{s-1} + \mathbf{e}_2 (t+s+1) f_t^{s+1} - \mathbf{e}_3 s f_t^s \right];$$

$$\begin{aligned} \mathbf{f}_{ts}^{(3)} = & \mathbf{e}_1 \left\{ -(x_1 - ix_2) D_2 f_{t+1}^{s-1} - \left[(\xi^{(0)})^2 - 1 \right] d D_1 f_t^s + (t-s+1)(t-s+2) \beta_t f_{t+1}^{s-1} \right\} \\ & + \mathbf{e}_2 \left\{ (x_1 + ix_2) D_1 f_{t+1}^{s+1} - \left[(\xi^{(0)})^2 - 1 \right] d D_2 f_t^s - (t+s+1)(t+s+2) \beta_t f_{t+1}^{s+1} \right\} \\ & + \mathbf{e}_3 \left[x_3 D_3 f_{t+1}^s - (\xi^{(0)})^2 d D_3 f_t^s - C_{ts} f_{t+1}^s \right]; \end{aligned}$$

where

$$\beta_t = \frac{t+5-4\nu}{(t+1)(2t+3)}, \quad C_{ts} = (t+s+1)(t-s+1)\beta_t; \quad t = 0, 1, \dots; \quad |s| \leq t.$$

In (2.366) and (2.367) the following notations are used:

$$\begin{aligned} \mathbf{e}_1 &= (\mathbf{i} + i\mathbf{j})/2, & \mathbf{e}_2 &= \overline{\mathbf{e}_1} = (\mathbf{i} - i\mathbf{j})/2, & \mathbf{e}_3 &= \mathbf{k}; \\ D_1 &= (\partial/\partial x_1 - i\partial/\partial x_2), & D_2 &= \overline{D_1} = (\partial/\partial x_1 + i\partial/\partial x_2), & D_3 &= \partial/\partial x_3. \end{aligned} \quad (2.368)$$

The functions $F_t^s = F_t^s(\mathbf{x}, d)$ and $f_t^s = f_t^s(\mathbf{x}, d)$ are the singular and regular, respectively, solid scalar spheroidal harmonics of the form

$$F_t^s(\mathbf{x}, d) = Q_t^{-s}(\xi)P_t^s(\eta) \exp(is\varphi), \quad f_t^s(\mathbf{x}, d) = P_t^{-s}(\xi)P_t^s(\eta) \exp(is\varphi), \quad (2.369)$$

In (2.369), P_t^s and Q_t^s are the associated Legendre polynomials of the first and second kind, respectively.

Re-expansion formulae for the singular solutions of Lamé equation

Translation of a reference coordinate system. Let $O_p x_p y_p z_p$ and $O_q x_q y_q z_q$ are two equally oriented coordinate systems, $\mathbf{x}_p = \mathbf{X}_{pq} + \mathbf{x}_q$. Then,

$$\begin{aligned} \mathbf{F}_{ts}^{(i)}(\mathbf{x}_p, d_p) &= \sum_{j=1}^3 \sum_{k=0}^{\infty} \sum_{l=-k}^k \eta_{tksl}^{(i)(j)}(\mathbf{X}_{pq}, d_p, d_q) \mathbf{f}_{kl}^{(j)}(\mathbf{x}_q, d_q), \\ i &= 1, 2, 3; \quad t = 0, 1, \dots; \quad |s| \leq t; \end{aligned} \quad (2.370)$$

where

$$\begin{aligned} \eta_{tksl}^{(1)(2)} &= \eta_{tksl}^{(1)(3)} = \eta_{tksl}^{(2)(3)} = 0; & \eta_{tksl}^{(i)(i)} &= \eta_{t+2-i, k-2+i}^{s-l}; \\ \eta_{tksl}^{(2)(1)} &= \left(\frac{s}{t} + \frac{l}{k}\right) \eta_{t, k-1}^{s-l} & \eta_{tksl}^{(3)(2)} &= 2 \left(\frac{s}{t} + \frac{l}{k}\right) \eta_{t-1, k}^{s-l}; \\ \eta_{tksl}^{(3)(1)} &= \left\{ 2 \frac{l}{k} \left[\frac{s}{t} + \frac{l}{(k-1)} \right] + C_{k-2, l} - C_{-(t+1), s} \right\} \eta_{t-1, k-1}^{s-l} \\ &+ (2k-1) \sum_{m=0}^{\infty} \left[(-1)^m \frac{Z_{pq}}{d_q} \eta_{t-1, k+2m}^{s-l} - d_p (\xi_p^{(0)})^2 \eta_{t, k+2m}^{s-l} + d_q (\xi_q^{(0)})^2 \eta_{t-1, k+2m+1}^{s-l} \right] \\ k &> 1; \\ \eta_{t1s0}^{(3)(1)} &= C_{-t-1, s} \eta_{t-1, 0}^s, \\ \eta_{t1s1}^{(3)(1)} &= (t+s-1) [1 + (t+s)\beta_{-t-1}] \eta_{t-1, 0}^{s-1}, \\ \eta_{t1s, -1}^{(3)(1)} &= (t-s-1) [1 + (t-s)\beta_{-t-1}] \eta_{t-1, 0}^{s+1}. \end{aligned} \quad (2.371)$$

In (2.371) η_{tk}^{s-l} are the expansion coefficients in the addition theorem for the solid spheroidal harmonics F_t^s (Kusch, 1998)

$$F_t^s(\mathbf{x}_p + \mathbf{X}_{pq}, d_p) = \sum_{k=0}^{\infty} \sum_{l=-k}^k \eta_{tk}^{s-l}(\mathbf{X}_{pq}, d_p, d_q) f_k^l(\mathbf{x}_q, d_q).$$

Noteworthy, at least two different expressions of η_{tk}^s exist. The most general form is

$$\eta_{tk}^s(\mathbf{X}_{pq}, d_p, d_q) = {}^{(1)}\eta_{tk}^s = a_{tk} \sum_{r=0}^{\infty} N_{tkr}(d_p, d_q) F_{t+k+2r}^s(\mathbf{X}_{pq}, d_p + d_q), \quad (2.372)$$

where

$$N_{tkr} = (t+k+2r+1/2) \sum_{j=0}^r \frac{(-1)^j}{j!} \left(\frac{d_p}{d_p+d_q} \right)^{2r-2j} \Gamma(t+k+2r-j+1/2) M_{tk,r-j}(d_p, d_q),$$

$$M_{tkj}(d_p, d_q) = \sum_{i=0}^j \frac{(d_q/d_p)^{2i}}{i! (j-i)! \Gamma(t+j-i+3/2) \Gamma(k+i+3/2)}$$

and

$$a_{tk} = (-1)^k \sqrt{\pi} (k+1/2) \left(\frac{d_p}{2} \right)^{t+1} \left(\frac{d_q}{2} \right)^k$$

In particular, for $d_p = d_q$ the expression of M_{tkj} reduces to

$$M_{tkj} = \frac{(t+k+j+2)_j}{j! \Gamma(t+j+3/2) \Gamma(k+j+3/2)},$$

where $\Gamma(z)$ is the Gamma-function and $(n)_m = \Gamma(n+m)/\Gamma(n)$ is the Pochhammer's symbol.

The formulas (2.370) – (2.372) are valid for any two aligned coordinate systems. In the case of well-separated particles, namely for $\|\mathbf{X}_{pq}\| > d_p + d_q$, the more simple expression of η_{tk}^s exists:

$$\eta_{tk}^s(\mathbf{X}_{pq}, d_p, d_q) = {}^{(2)}\eta_{tk}^s = (-1)^s \sqrt{\pi} a_{tk} \sum_{r=0}^{\infty} L_{tkr}(d_p, d_q) S_{t+k+2r}^s(\mathbf{X}_{pq}) \quad (2.373)$$

where the functions $S_t^s(\mathbf{r}) = (t-s)! r^{-t-1} Y_t^s(\theta, \varphi)$ are the singular solid spherical harmonics and

$$L_{tkr} = \left(\frac{d_p}{2} \right)^{2r} M_{tkr}(d_p, d_q).$$

In (2.371), we must also define $\eta_{t-1,k-1}^{s-l}$ for $|s-l| = t+k$. So, for $\|\mathbf{X}_{pq}\| > d_p + d_q$ the coefficient η_{tk}^{t+k+2} takes the form

$${}^{(2)}\eta_{tk}^{t+k+2} = \frac{(-1)^{t+k} \sqrt{\pi} a_{tk}}{\Gamma(t+1/2) \Gamma(k+1/2)} (X_{pq} + iY_{pq}) S_{t+k+1}^{t+k+1}(\mathbf{X}_{pq});$$

in a general case,

$${}^{(1)}\eta_{tk}^{t+k+2} = \frac{a_{tk}}{\Gamma(t+3/2) \Gamma(k+3/2)} \sum_{r=0}^{\infty} \frac{(-1)^r}{r!} \Gamma(t+k+r+3/2) \left[\frac{t+k+2r+5/2}{r+1} \cdot F_{t+k+2r+2}^{t+k+2}(\mathbf{X}_{pq}, d_p + d_q) - 2(t+k+2r+3/2) \frac{X_{pq} + iY_{pq}}{d_p + d_q} F_{t+k+2r+1}^{t+k+1}(\mathbf{X}_{pq}, d_p + d_q) \right].$$

As to an infinite sum in the expression of $\eta_{tksl}^{(3)(1)}$ (2.371), no problems arise with its calculation: by change the summation order it reduces to the form, analogous to (2.372), (2.373).

Rotation of a reference coordinate system. Now, we consider two coordinate systems $O_p x_p y_p z_p$ and $O_q x_q y_q z_q$ with common origin $O_p = O_q$: $\mathbf{x}_p = \mathbf{O}_{pq} \cdot \mathbf{x}_q$.

The transformation formulae for the partial regular solutions (2.367) due to rotation of coordinate frame are the exact and finite (Kushch, 1998):

$$\mathbf{f}_{ts}^{(i)}(\mathbf{x}_p, d_p) = \sum_{j=1}^3 \sum_{k=0}^{t+i-j} \sum_{l=-k}^k Q_{tksl}^{(i)(j)}(\mathbf{w}_{pq}, d_p, d_q) \mathbf{f}_{kl}^{(j)}(\mathbf{x}_q, d_q), \quad (2.374)$$

where

$$Q_{tksl}^{(i)(j)} = \sum_{\alpha=j}^i \sum_{m=k+j-\alpha}^{t+i-\alpha} {}^{(1)}K_{t, m+\alpha-i, s}^{(i)(\alpha)}(d_p) {}^{(2)}K_{m, k+j-\alpha, l}^{(\alpha)(j)}(d_q) \frac{(m-l)!(m+l)!}{(m-s)!(m+s)!} \quad (2.375)$$

$$\times S_{2m}^{m-s, m-l}(\mathbf{w}_{pq}) + \delta_{i3} \delta_{j1} (2k-1) \sum_{n=k}^t \left[(\xi_p^{(0)}) Q_{tnsl}^{(3)(3)} - (\xi_q^{(0)}) Q_{tnsl}^{(2)(2)} \right].$$

In (2.374), we keep in mind that the vectorial functions standing in the opposite sides of equality are written in their local coordinates and components. The functions $S_t^{s,l}$ entering (2.375) are the spherical harmonics in a four-dimensional space (Bateman & Erdelyi, 1953) and $\mathbf{w} = \{w_1, w_2, w_3, w_4\}$, $\|\mathbf{w}\| = 1$ is the vector determining uniquely the rotation matrix

$$\mathbf{O} = \begin{pmatrix} w_2^2 - w_1^2 - w_3^2 + w_4^2 & 2(w_2 w_3 - w_1 w_4) & 2(w_1 w_2 + w_3 w_4) \\ 2(w_2 w_3 + w_1 w_4) & w_3^2 - w_1^2 - w_2^2 + w_4^2 & 2(w_1 w_3 - w_2 w_4) \\ 2(w_1 w_2 - w_3 w_4) & 2(w_1 w_3 + w_2 w_4) & w_1^2 - w_2^2 - w_3^2 + w_4^2 \end{pmatrix}. \quad (2.376)$$

Also,

$${}^{(1)}K_{tks}^{(i)(j)} = 0 \text{ for } i < j; \quad {}^{(1)}K_{tks}^{(i)(i)} = K_{t+i-2, k+i-2}^{(1)}, \quad (2.377)$$

$${}^{(1)}K_{tks}^{(2)(1)} = \left(\frac{s}{k+1} - \frac{s}{t+1} \right) K_{tk}^{(1)}, \quad {}^{(1)}K_{tks}^{(3)(2)} = 2 \left(\frac{s}{k+1} - \frac{s}{t+1} \right) K_{t+1, k+1}^{(1)},$$

$${}^{(1)}K_{tks}^{(3)(1)} = \left[C_{-(t+3), s} - C_{-(k+3), s} + \frac{2s}{t+1} \left(\frac{s}{k+2} - \frac{s}{t+2} \right) \right] K_{t+1, k+1}^{(1)}$$

and

$$K_{tk}^{(1)}(d) = \frac{(-1)^{(t-k)/2}}{\sqrt{\pi}} \left(\frac{2}{d} \right)^k \Gamma \left(\frac{t+k}{2} + \frac{1}{2} \right) / \left(\frac{t-k}{2} \right)!$$

for $t-k$ even and $K_{tk}^{(1)}(d) = 0$ otherwise. The expressions of ${}^{(2)}K_{tks}^{(i)(j)}$ are defined by (2.377), with $K_{tk}^{(1)}$ replaced by

$$K_{tk}^{(2)}(d) = \sqrt{\pi} \left(\frac{d}{2} \right)^t \left(k + \frac{1}{2} \right) / \Gamma \left(\frac{t+k}{2} + \frac{3}{2} \right) / \left(\frac{t-k}{2} \right)!;$$

$K_{tk}^{(2)}(d) = 0$ for $t-k$ odd.

The formulae (2.374) are written for the most general case $d_p \neq d_q$ and $\xi_p^{(0)} \neq \xi_q^{(0)}$. In the context of this paper, we use them for $p = q$ only: in this case, the expression of expansion coefficients (2.375) is simplified substantially.

2.4.3 Formal solution

To solve the boundary-value problem (2.362), (2.363) for displacements, we shall follow the approach developed by Kushch (1997, 1998a) for the uniform external loading. First, due to linearity of the problem, we apply the superposition principle to decompose the displacement field in the matrix domain into a sum of far field \mathbf{U} and disturbances, or near fields, induced by each inhomogeneity:

$$\mathbf{u}(\mathbf{x}) = \mathbf{U}(\mathbf{x}) + \sum_{p=1}^N \mathbf{U}_p(\mathbf{x}_p). \quad (2.378)$$

The disturbance \mathbf{U}_p caused by each separate inclusion vanishes at infinity and, therefore, can be expanded into a series over the singular partial solutions $\mathbf{F}_{ts}^{(i)}$ of Lamé equation (2.363) (formula (2.366)):

$$\mathbf{U}_p(\mathbf{x}_p) = \sum_{j=1}^3 \sum_{k=0}^{\infty} \sum_{l=-k}^k A_{kl}^{(j)(p)} \mathbf{F}_{kl}^{(j)}(\mathbf{x}_p, d_p), \quad (2.379)$$

where $A_{kl}^{(j)(p)}$ are the unknown series coefficients.

On the other hand, since displacement field inside the inclusions is continuous and constrained, its series expansion contains the regular partial solutions $\mathbf{f}_{ts}^{(i)}$ (2.367) only, written in the local coordinates of a given inclusion with index q :

$$\mathbf{u}_q = \sum_{i=1}^3 \sum_{t=0}^{\infty} \sum_{s=-t}^t D_{ts}^{(i)(q)} \mathbf{f}_{ts}^{(i)}(\mathbf{x}_q, d_q) \quad (2.380)$$

where $D_{ts}^{(i)(q)}$, as well as the $A_{ts}^{(i)(p)}$ in (2.379), are the constants to be determined. And, since the set of functions (2.366), (2.367) is full and linearly independent, the displacement vector (2.378) in the vicinity of this inclusion allows expansion of the form

$$\mathbf{u} = \sum_{i=1}^3 \sum_{t=0}^{\infty} \sum_{s=-t}^t \left[A_{ts}^{(i)(q)} \mathbf{F}_{ts}^{(i)}(\mathbf{x}_q, d_q) + a_{ts}^{(i)(q)} \mathbf{f}_{ts}^{(i)}(\mathbf{x}_q, d_q) \right]. \quad (2.381)$$

To obtain the coefficients $a_{ts}^{(i)(q)}$, we have to rewrite all the terms in (2.378) but one with $p = q$ in variables of q th local coordinate system.

Provided we have the expansion (2.381) obtained in that or another way, the rest of solving procedure resembles that described by Kushch (1997,1998a). To get a resolving set of linear algebraic equations for determining the series coefficients $A_{ts}^{(i)(p)}$ and $D_{ts}^{(i)(q)}$, we substitute the expressions (2.380) and (2.381) into the first of the interfacial boundary conditions (2.362). Note, that the functions $\mathbf{F}_{ts}^{(i)}$ and $\mathbf{f}_{ts}^{(i)}$ are introduced so that to simplify to a maximum possible extent satisfying the boundary conditions at the coordinate surfaces $\xi^q = \xi_0^q$. On the spheroidal surface (index q is omitted for the time being), the

following representation of $\mathbf{F}_{ts}^{(i)}$ take a place:

$$\begin{aligned}\mathbf{F}_{ts}^{(1)} \Big|_{\xi=\xi^{(0)}} &= \mathbf{e}_1 Q_{t+1}^{s-1} Y_{t+1}^{s-1} - \mathbf{e}_2 Q_{t+1}^{s+1} Y_{t+1}^{s+1} + \mathbf{e}_3 Q_{t+1}^s Y_{t+1}^s; \\ \mathbf{F}_{ts}^{(2)} \Big|_{\xi=\xi^{(0)}} &= \mathbf{e}_1 \frac{(t+s)}{t} Q_t^{s-1} Y_t^{s-1} + \mathbf{e}_2 \frac{(t-s)}{t} Q_t^{s+1} Y_t^{s+1} + \mathbf{e}_3 \frac{s}{t} Q_t^s Y_t^s; \\ \mathbf{F}_{ts}^{(3)} \Big|_{\xi=\xi^{(0)}} &= \mathbf{e}_1 \left\{ -(t-s+1)\xi^{(0)} Q_t^{s-1} + (t+s-1) [1 + (t+s)\beta_{-(t+1)}] Q_{t-1}^{s-1} \right\} Y_{t-1}^{s-1} \\ &\quad + \mathbf{e}_2 \left\{ (t-s-1)\xi^{(0)} Q_t^{s+1} - (t-s-1) [1 + (t-s)\beta_{-(t+1)}] Q_{t-1}^{s+1} \right\} Y_{t-1}^{s+1} \\ &\quad + \mathbf{e}_3 \left\{ -(t-s)\xi^{(0)} Q_t^s - C_{-(t+1),s} Q_{t-1}^s \right\} Y_{t-1}^s;\end{aligned}\tag{2.382}$$

where $Q_t^s = Q_t^s(\xi^{(0)})$ and $Y_t^s(\eta, \varphi) = \frac{(t-s)!}{(t+s)!} P_t^s(\eta) \exp(is\varphi)$. are the scalar surface harmonics.

The analogous expressions of the functions $\mathbf{f}_{ts}^{(i)}$ (2.367) take a form

$$\begin{aligned}\mathbf{f}_{ts}^{(1)} \Big|_{\xi=\xi^{(0)}} &= \mathbf{e}_1 P_{t-1}^{s-1} Y_{t-1}^{s-1} - \mathbf{e}_2 P_{t-1}^{s+1} Y_{t-1}^{s+1} + \mathbf{e}_3 P_{t-1}^s Y_{t-1}^s; \\ \mathbf{f}_{ts}^{(2)} \Big|_{\xi=\xi^{(0)}} &= \mathbf{e}_1 \frac{(t-s+1)}{t+1} P_t^{s-1} Y_t^{s-1} + \mathbf{e}_2 \frac{(t+s+1)}{t+1} P_t^{s+1} Y_t^{s+1} + \mathbf{e}_3 \frac{s}{t+1} P_t^s Y_t^s; \\ \mathbf{f}_{ts}^{(3)} \Big|_{\xi=\xi^{(0)}} &= \mathbf{e}_1 \left\{ (t+s)\xi^{(0)} P_t^{s-1} + (t-s+2) [-1 + (t-s+1)\beta_t] P_{t+1}^{s-1} \right\} Y_{t+1}^{s-1} \\ &\quad + \mathbf{e}_2 \left\{ (t+s+2)\xi^{(0)} P_t^{s+1} + (t+s+2) [-1 + (t+s+1)\beta_t] P_{t+1}^{s+1} \right\} Y_{t+1}^{s+1} \\ &\quad + \mathbf{e}_3 \left\{ (t+s+1)\xi^{(0)} P_t^s - C_{ts} P_{t+1}^s \right\} Y_{t+1}^s.\end{aligned}\tag{2.383}$$

The formulas (2.382) and (2.383) can be written in a compact form as

$$\mathbf{F}_{ts}^{(i)}(\mathbf{x}, d) = \sum_{j=1}^3 F_{ts}^{(i)(j)} \mathbf{e}_j Y_{t+2-i}^{s_j}(\eta, \varphi); \quad \mathbf{f}_{ts}^{(i)}(\mathbf{x}, d) = \sum_{j=1}^3 f_{ts}^{(i)(j)} \mathbf{e}_j Y_{t-2+i}^{s_j}(\eta, \varphi) \tag{2.384}$$

where $s_1 = s-1$, $s_2 = s+1$ and $s_3 = s$. Using the orthogonality property of the complex-valued vectors \mathbf{e}_i (2.368) and surface harmonics Y_t^s , it is rather straightforward, by means of standard algebra, to reduce the vectorial functional equality (2.362) to an infinite linear algebraic system. A suitable for the computer algebra form of this system is

$$\begin{aligned}UG_t(\nu_0) \mathbf{A}_t^{(q)} + UM_t(\nu_0) \mathbf{a}_t^{(q)} &= UM_t(\nu_q) \mathbf{D}_t^{(q)}, \\ t = 1, 2, \dots; \quad q = 1, 2, \dots, N;\end{aligned}\tag{2.385}$$

where the vector $\mathbf{A}_t^{(q)}$ contains the unknowns $A_{t+i-2,s}^{(i)(q)}$, the vectors $\mathbf{a}_t^{(q)}$ and $\mathbf{D}_t^{(q)}$ include the values $a_{t-i+2,s}^{(i)(q)}$ and $D_{t-i+2,s}^{(i)(q)}$, respectively.

Obtaining the second set of equations from the traction vector continuity condition follows the quite analogous way. By taking into account that $\mathbf{n} = \mathbf{e}_\xi$ is the unit vector normal to spheroidal surface, the traction vector \mathbf{T}_n can be represented as

$$\begin{aligned}\mathbf{T}_n &= \sigma_\xi \mathbf{e}_\xi + \tau_{\xi\eta} \mathbf{e}_\eta + \tau_{\xi\varphi} \mathbf{e}_\varphi \\ &= 2\mu \left(\frac{\nu}{1-2\nu} \mathbf{e}_\xi \nabla \cdot \mathbf{u} + \frac{\bar{\xi} h}{d} \frac{\partial}{\partial \xi} \mathbf{u} + \frac{1}{2} \mathbf{e}_\xi \times \nabla \times \mathbf{u} \right) - \beta \mathbf{n}.\end{aligned}\tag{2.386}$$

Substituting the series (2.380) and (2.381) into the second of the contact conditions (2.362) written in the form (2.386) gives us another set of equations (for more details, see Kuchsh (1997)):

$$TG_t(\nu_0) \mathbf{A}_t^{(q)} + TM_t(\nu_0) \mathbf{a}_t^{(q)} = TM_t(\nu_q) \mathbf{D}_t^{(q)} + \delta_{t1} (\mathbf{T}_\beta^0 - \mathbf{T}_\beta^q), \tag{2.387}$$

where \mathbf{T}_β is the right-hand side vector obtained by expansion of the strain-free term $\beta \cdot \mathbf{n}$,

$$\mathbf{T}_\beta = (\beta_{33}, (\beta_{13} - i\beta_{23})/2, (\beta_{11} + \beta_{22})e, \beta_{13} - i\beta_{23}, (\beta_{11} - \beta_{22} - 2i\beta_{12})e, 0)^T, \quad (2.388)$$

δ_{t1} is the Kronecker delta and $e = l_3/l_1 = \xi_0/\bar{\xi}_0$ is an aspect ratio of spheroid.

Now, we combine (2.385) and (2.387) to exclude $D_{ts}^{(i)(q)}$ from consideration; after some algebra, one obtains

$$\begin{aligned} M_1 \mathbf{A}_t^{(q)} + M_2 \mathbf{a}_t^{(q)} &= \delta_{t1} (\mathbf{T}_\beta^0 - \mathbf{T}_\beta^q); \\ M_1 &= TM_t(\nu_q) (UM_t(\nu_q))^{-1} UG_t(\nu_0) - TG_t(\nu_0); \\ M_2 &= TM_t(\nu_q) (UM_t(\nu_q))^{-1} UG_t(\nu_0) - TG_t(\nu_0); \\ &t = 1, 2, \dots; \quad q = 1, 2, \dots, N. \end{aligned} \quad (2.389)$$

To get a closed set of linear algebraic equations, we need to make the last remaining step, namely, to express the coefficients $a_{ts}^{(i)(q)}$ in terms of $A_{ts}^{(i)(p)}$ and \mathbf{U} .

2.4.4 Local expansion

In (Kushch, 1997), the far field displacement vector was taken in the form $\mathbf{U} = \widehat{\mathbf{E}} \cdot \mathbf{x}$, $\widehat{\mathbf{E}}$ being the second-rank symmetric constant tensor. For this particular problem, it is possible to find analytical expression of $a_{ts}^{(i)(q)}$. Our situation is different, however: we do not suggest any specific analytical form of \mathbf{U} . Therefore, some numerical technique has to be applied in order to determine $a_{ts}^{(i)(q)}$ accurately.

Let us proceed with the local expansion of \mathbf{U} in the vicinity of q th inclusion (more exactly, of the point O^q), assumed in the form

$$\mathbf{U} = \mathbf{U}_k \mathbf{e}_k = \sum_{i=1}^3 \sum_{t=0}^{\infty} \sum_{s=-t}^t a_{ts}^{(i)(0)(q)} \mathbf{f}_{ts}^{(i)}(\mathbf{x}_q, d_q). \quad (2.390)$$

First, we express the left side of (2.390) in projections on the local complex-valued basis vectors:

$$\mathbf{U} = \mathbf{U}_k \mathbf{e}_k = \mathbf{U}_i^q \mathbf{e}_i^q; \quad (2.391)$$

to find \mathbf{U}_i^q , we make use the relationship between \mathbf{e}_k and \mathbf{e}_i^q :

$$\mathbf{e}_i^q = \Omega_{ik}^{*q} \mathbf{e}_k, \quad \text{where } \Omega^{*q} = \mathbf{D}^{-1} \Omega^q \mathbf{D} \quad \text{and} \quad D = \begin{pmatrix} 1 & 1 & 0 \\ -i & i & 0 \\ 0 & 0 & 1 \end{pmatrix}. \quad (2.392)$$

Then, with account for the (2.384), we transform the projections of (2.389) to

$$\begin{aligned} \mathbf{U}_j^q &= \sum_{i=1}^3 \sum_{t=0}^{\infty} \sum_{s=-t}^t a_{ts}^{(i)(0)(q)} f_{ts}^{(i)(j)} Y_{t+i-2}^{s_j}(\eta^q, \varphi^q) \\ &= \sum_{t=0}^{\infty} \sum_{s=-t}^t \left(\sum_{i=1}^3 a_{t+2-i, \tilde{s}_j}^{(i)(0)(q)} f_{t+2-i, \tilde{s}_j}^{(i)(j)} \right) Y_t^s(\eta^q, \varphi^q), \end{aligned} \quad (2.393)$$

where $\tilde{s}_1 = s + 1$, $\tilde{s}_2 = s - 1$ and $\tilde{s}_3 = s$.

Integrating (2.393) over $-1 \leq \eta^q \leq 1$ and $0 \leq \varphi^q < 2\pi$ with weight $\overline{Y_t^s(\eta^q, \varphi^q)}$ and taking the orthogonality property of the spherical harmonics into account, we obtain a set of equations

$$\sum_{i=1}^3 a_{t+2-i, \tilde{s}_j}^{(i)(0)(q)} f_{t+2-i, \tilde{s}_j}^{(i)(j)} = \Phi_{ts}^{(j)(q)}; \quad (2.394)$$

$$j = 1, 2, 3; \quad t = 1, 2, \dots; \quad |s| \leq t;$$

In (2.394),

$$\Phi_{ts}^{(j)(q)} = \frac{1}{N_{ts}} \int_0^{2\pi} \int_{-1}^1 \mathbf{U}_j^q \overline{Y_t^s(\eta^q, \varphi^q)} d\eta^q d\varphi^q, \quad (2.395)$$

where

$$N_{ts} = \int_0^{2\pi} \int_{-1}^1 Y_t^s \overline{Y_t^s} d\eta d\varphi = \frac{4\pi}{2t+1} \frac{(t-s)!}{(t+s)!}. \quad (2.396)$$

For each t , we have a separate set of $3(2t+1)$ independent linear equations, determining the unknowns $a_{t+2-i, \tilde{s}}^{(i)(0)(q)}$ uniquely and, thus, the expansion (2.390) is established.

Finding the expansions of \mathbf{U}_p in (2.378) for $p \neq q$ follows the same way: we have no need to expand \mathbf{U}_q written already in variables of q th local coordinate system. As to other terms, we note that, with representation of \mathbf{U}_p (2.379) taken into account, it suffices to obtain the expansions of kind (2.390) for the separate terms in (2.379), i.e., for the singular partial solutions $\mathbf{F}_{ts}^{(i)}$. Application of the exposed above procedure gives us a set of equalities

$$\mathbf{F}_{kl}^{(j)}(\mathbf{x}_p, d_p) = \sum_{i=1}^3 \sum_{t=0}^{\infty} \sum_{s=-t}^t \eta_{klls}^{(j)(i)}(\mathbf{X}_{pq}, \mathbf{\Omega}_{pq}, d_p, d_q) \mathbf{f}_{ts}^{(i)}(\mathbf{x}_q, d_q) \quad (2.397)$$

where $\mathbf{X}_{pq} = \mathbf{X}_q - \mathbf{X}_p$ and $\mathbf{\Omega}_{pq} = (\mathbf{\Omega}_p)^{-1} \mathbf{\Omega}_q$ define relative position and orientation of p th and q th local coordinate systems. Now, we recognize that the relations (2.397) are nothing more nor less than the re-expansion formulae, or addition theorems, derived elsewhere (Kushch, 1997, 1998a). There, the explicit analytical expressions of $\eta_{klls}^{(j)(i)}$ had been obtained in terms of infinite series of special functions: they are summarized in "Theoretical background" subsection. Thus, we have two independent ways to evaluate $\eta_{klls}^{(j)(i)}$, one analytical (although rather involved) and another mostly numerical. Their comparison will be given below; here we note only that the exact analytical results may serve as a benchmark to estimate accuracy of the numerical technique developed here. However, without regard to the specific evaluation method chosen, after we have the formulae (2.397) established we substitute them into (2.379) to obtain the expansion of \mathbf{U}_p in the form (2.390), with the coefficients

$$a_{ts}^{(i)(p)(q)} = \sum_{j=1}^3 \sum_{k=0}^{\infty} \sum_{l=-k}^k A_{kl}^{(j)(p)} \eta_{klls}^{(j)(i)}(\mathbf{X}_{pq}, \mathbf{\Omega}_{pq}, d_p, d_q), \quad (2.398)$$

$$p = 1, 2, \dots, N \quad (p \neq q).$$

Collecting all these terms together, we get

$$\mathbf{a}_{ts}^{(i)(q)} = \sum_{\substack{p=0 \\ p \neq q}}^N \mathbf{a}_{ts}^{(i)(p)(q)}, \quad (2.399)$$

or, in the matrix form adopted,

$$\mathbf{a}_t^{(q)} = \sum_{p \neq q} \sum_{k=1}^{\infty} \eta_{kt}^{(p)(q)} \mathbf{A}_k^{(p)}. \quad (2.400)$$

The (2.398) and (2.399) are exactly the formulae we need to transform (2.389) into a closed set of linear algebraic equations with the unknowns $A_{ts}^{(i)(p)}$.

2.4.5 Numerical solution

Numerical realization of the method exposed is rather simple and consists mostly in generating and solving the truncated set of equations (2.389), where the equations and unknowns with $t \leq t_{\max}$ are only retained. It has been shown elsewhere (Kushch, 1998b) that obtained in such a way approximate solutions converge to exact one with $t_{\max} \rightarrow \infty$ provided the domains, occupied by inclusions, do not intersect. There, an efficient iterative solving procedure has been also suggested which does not require the full matrix of linear system formation and reduces greatly the total computational effort. Even simplest iterative scheme, following directly from (2.389)

$$\mathbf{A}_{t, m+1}^{(q)} = - (M_1)^{-1} \left[M_2 \cdot \mathbf{a}_{t, m}^{(q)} + \delta_{t1} (\mathbf{T}_\beta^q - \mathbf{T}_\beta^0) \right]; \quad (2.401)$$

where $\mathbf{a}_{t, m}^{(q)}$ is calculated according to (2.398) and (2.399) for $\mathbf{A}_{t, m}^{(q)}$, is of order $(N_{eq})^2$ (N_{eq} is a number of equations retained in the truncated linear system) and obviously preferable in comparison with direct $O(N_{eq})^3$ Gauss-like linear solver. Applying the method of conjugate gradients in the form of so-called GMRES routine (Frayse, Giraud and Gratton (1998)) allows to reduce computational time even more substantially.

The algorithm exposed above involves numerical integration over the spheroidal surfaces and, in order to ensure convergence of computational scheme, the surface integrals must be evaluated with sufficient accuracy. The scheme applied by Kushch et al. (2002) seems to be most appropriate for this aim. It assumes uniform distribution of integration points in azimuthal direction (φ -integral) and Gauss-Legendre formula for integration over η :

$$\int_0^{2\pi} \int_{-1}^1 f(\eta, \varphi) d\eta d\varphi = \frac{1}{2\pi n} \sum_{i=1}^n \sum_{j=1}^n \omega_i f(\eta_i, \varphi_j); \quad (2.402)$$

where $\varphi_j = 2\pi j/n$; for the tabulated values of Gauss' integration points η_i and weights ω_i , see e.g. Abramovitz and Stegun (1964). With n integration points taken in each direction, (2.402) is exact for the spherical harmonics up to order $(2n - 1)$. As a consequence, this scheme allows to calculate the expansion coefficients with high accuracy: e.g., the relative error of the numerically obtained values $\eta_{kltts}^{(j)(i)}$ is of order $10^{-6} \div 10^{-7}$, comparable with accuracy of series summation in the analytical formulae. Notheworthy, computational

effort of numerical integration only slightly (~ 1.2 times) exceeds that of the analytical method. The main advantage of numerical integration is, however, in that it does not require the involved math to be used and makes the numerical realization of the method exposed much simpler and, at the same time, more general and robust.

2.4.6 Elastic half space containing a finite array of spheroidal inclusions

Integral transforms of the singular solutions of Lamé equation

For the problems for a composite half-space or layer there is a need in representation of solution, convenient for executing the boundary conditions on the plane surfaces. Such a representation can be obtained by using the appropriate Fourier integral transforms. The transforms for the singular solutions of the Lamé equation in spherical basis were developed by Golovchan et al.(1993); we will derive them in the case of spheroidal coordinate system.

Let us consider, for beginning, representation by the double Fourier integral of the scalar harmonic functions F_t^s (2.369). For this purpose, it is sufficient to use the analogous formulae for the singular solutions of Laplace equation in spherical basis:

$$Y_t^s(\mathbf{x}) = \frac{(t-s)!}{r^{t+1}} P_t^s(\cos \theta) \exp(is\varphi) = (\mp 1)^{t+s} \int_{-\infty}^{\infty} \int_{-\infty}^{\infty} \xi_{\alpha\beta}^{ts} E_{\alpha\beta}^{\pm}(\mathbf{x}) d\alpha d\beta, \quad (2.403)$$

$$t = 1, 2, \dots, |s| \leq t;$$

where the upper and lower signs in this and all subsequent formulae correspond to the cases $z < 0$ and $z > 0$, respectively and

$$\xi_{\alpha\beta}^{ts} = \delta^{t-s-1} (\beta - i\alpha)^s, \quad \delta^2 = \alpha^2 + \beta^2,$$

$$E_{\alpha\beta}^{\pm}(\mathbf{x}) = \exp(\pm \delta z) F_{\alpha\beta}(x, y), \quad F_{\alpha\beta}(x, y) = \exp[i(\alpha x + \beta y)];$$

Now, we take the series expansion (Kushch, 1998b)

$$F_t^s(\mathbf{x}, d) = \sqrt{\pi} (-1)^s \sum_{l=0}^{\infty} \frac{(d/2)^{2l+t+l}}{l! \Gamma(t+l+3/2)} Y_l^s(\mathbf{x}), \quad \|\mathbf{x}\| > \text{Re}(d);$$

into account. After substitution of it into (2.403), we get

$$F_t^s(\mathbf{x}, d) = \sqrt{\pi} (-1)^s \sum_{l=0}^{\infty} \frac{(d/2)^{2l+t+l}}{l! \Gamma(t+l+3/2)} (\mp 1)^{t+s} \int_{-\infty}^{\infty} \int_{-\infty}^{\infty} \xi_{\alpha\beta}^{t+2l,s} E_{\alpha\beta}^{\pm}(\mathbf{x}) d\alpha d\beta. \quad (2.404)$$

Because of $\xi_{\alpha\beta}^{t+2l,s} = \delta^{2l} \xi_{\alpha\beta}^{ts}$, we change order of integration and summation to obtain

$$F_t^s(\mathbf{x}, d) = (\mp 1)^{t+s} \left(\frac{d}{2}\right)^{t+l} \sqrt{\pi} (-1)^s \int_{-\infty}^{\infty} \int_{-\infty}^{\infty} \xi_{\alpha\beta}^{ts} E_{\alpha\beta}^{\pm}(\mathbf{x}) \sum_{l=0}^{\infty} \frac{(\delta d/2)^{2l}}{l! \Gamma(t+l+3/2)} d\alpha d\beta.$$

Note that the series (Abramovitz and Stegun, 1964)

$$\sum_{l=0}^{\infty} \frac{(z/2)^{2l+\nu}}{l! \Gamma(\nu + l + 1)} = I_{\nu}(z)$$

coincides with the internal sum at $\nu = t + 1/2$ and we cm to the following Fourier integral transform:

$$F_t^s(\mathbf{x}, d) = (\mp 1)^{t+s} \int_{-\infty}^{\infty} \int_{-\infty}^{\infty} \zeta_{\alpha\beta}^{ts} E_{\alpha\beta}^{\pm}(\mathbf{x}) d\alpha d\beta, \quad z \leq \mp \operatorname{Re}(d), \quad (2.405)$$

where

$$\zeta_{\alpha\beta}^{ts} = \frac{(-1)^s}{\delta^2} \left(\frac{\beta - i\alpha}{\delta} \right)^s \sqrt{\frac{\pi\delta d}{2}} I_{t+1/2}(\delta d).$$

The inverse integral transforms have the form

$$(\mp 1)^{t+s} \zeta_{\alpha\beta}^{ts} \exp(\pm \delta z) = \frac{1}{2\pi} \int_{-\infty}^{\infty} \int_{-\infty}^{\infty} F_t^s(\mathbf{x}, d) \overline{F_{\alpha\beta}(x, y)} dx dy, \quad z \leq \operatorname{Re}(d)$$

$$t = 1, 2, \dots; \quad |s| \leq t.$$

Representation of a general solution of Lamé equation, bounded in half-spaces $z \leq 0$ is

$$\mathbf{u}(\mathbf{x}) = \int_{-\infty}^{\infty} \int_{-\infty}^{\infty} \sum_{j=1}^3 G_j(\alpha, \beta) \mathbf{H}_{\alpha\beta}^{(j)\pm}(\mathbf{x}) d\alpha d\beta, \quad z \geq 0; \quad (2.406)$$

where G_j are the integral densities. The vectorial functions

$$\mathbf{H}_{\alpha\beta}^{(1)\pm} = \frac{\nabla E_{\alpha\beta}^{\pm}}{(\pm\delta)}, \quad \mathbf{H}_{\alpha\beta}^{(2)\pm} = \frac{\nabla \times (\mathbf{e}_3 E_{\alpha\beta}^{\pm})}{(\pm\delta)}, \quad (2.407)$$

$$\mathbf{H}_{\alpha\beta}^{(3)\pm} = \frac{1}{(\pm\delta)} [\nabla (z E_{\alpha\beta}^{\pm}) + 4(1 - \nu) \mathbf{e}_3 E_{\alpha\beta}^{\pm}]$$

can be thought as the regular solutions of Lamé equation for a half-space. We note their properties

$$\nabla \cdot \mathbf{H}_{\alpha\beta}^{(1)\pm} = \nabla \cdot \mathbf{H}_{\alpha\beta}^{(2)\pm} = \nabla \times \mathbf{H}_{\alpha\beta}^{(1)\pm} = 0; \quad \nabla \cdot \mathbf{H}_{\alpha\beta}^{(3)\pm} = (\pm\delta) 2(2\nu - 1) \mathbf{E}_{\alpha\beta}^{\pm}; \quad (2.408)$$

$$d \nabla \times \mathbf{H}_{\alpha\beta}^{(3)\pm} = \pm\delta \mathbf{H}_{\alpha\beta}^{(1)\pm}; \quad \nabla \times \mathbf{H}_{\alpha\beta}^{(3)\pm} = (\pm\delta) 4(\nu - 1) \mathbf{H}_{\alpha\beta}^{(2)\pm}.$$

The functions (2.407) were introduced in (Golovchan et al 1993). It was shown there that to satisfy the boundary conditions on the planes $z = \text{const}$ is convenient to expand these functions over the full and orthogonal set of vectorial harmonics (Ulitko 1979)

$$\mathbf{L}_{\alpha\beta}(x, y) = \mathbf{e}_z F_{\alpha\beta}, \quad \mathbf{M}_{\alpha\beta}(x, y) = \frac{1}{\delta} \nabla \times F_{\alpha\beta} = \left(\frac{i\alpha}{\delta} \mathbf{e}_x + \frac{i\beta}{\delta} \mathbf{e}_y \right) F_{\alpha\beta},$$

$$\mathbf{N}_{\alpha\beta}(x, y) = \frac{1}{\delta} \nabla \times (\mathbf{e}_z F_{\alpha\beta}) = \left(\frac{i\beta}{\delta} \mathbf{e}_x - \frac{i\alpha}{\delta} \mathbf{e}_y \right) F_{\alpha\beta}. \quad (2.409)$$

These expansions have the form

$$\begin{aligned}\mathbf{H}_{\alpha\beta}^{(1)\pm} &= (\mathbf{L}_{\alpha\beta} \pm \mathbf{M}_{\alpha\beta}) \exp(\pm\delta z), & \mathbf{H}_{\alpha\beta}^{(2)\pm} &= \pm\mathbf{N}_{\alpha\beta} \exp(\pm\delta z), \\ \mathbf{H}_{\alpha\beta}^{(3)\pm} &= \frac{1}{(\pm\delta)} [(4\nu - 3 \pm \delta z)\mathbf{L}_{\alpha\beta} + \delta z\mathbf{M}_{\alpha\beta}] \exp(\pm\delta z)\end{aligned}$$

By analogy with (2.406), we will find the integral transforms as

$$\begin{aligned}\mathbf{F}_{ts}^{(i)}(\mathbf{x}, d) &= (\mp 1)^{t+s+i-1} \int_{-\infty}^{\infty} \int_{-\infty}^{\infty} \sum_{j=1}^3 \zeta_{\alpha\beta ts}^{(i)(j)\pm}(\alpha, \beta) \mathbf{H}_{\alpha\beta}^{(j)\pm}(\mathbf{x}) d\alpha d\beta, & (2.410) \\ z &\leq \mp \operatorname{Re}(d), \quad t = 1, 2, \dots; \quad |s| \leq t.\end{aligned}$$

In doing so, as well as for derivation of addition theorems, the properties (2.408) of partial solutions introduced and above integral transforms of scalar harmonic functions (2.405), (2.406) are used essentially. So, calculating divergence and curl from both the parts of eqn (2.410) we obtain $\zeta_{\alpha\beta ts}^{(i)(j)\pm} = 0$ for $j > i$. Projection of (2.410) on the unit basic vector \mathbf{e}_3 gives also

$$\mathbf{F}_{ts}^{(1)} \cdot \mathbf{e}_z = F_{t+1}^s = (\mp 1)^{t+s} \int_{-\infty}^{\infty} \int_{-\infty}^{\infty} \zeta_{\alpha\beta ts}^{(1)(1)\pm} E_{\alpha\beta}^{\pm} d\alpha d\beta.$$

By comparison with (2.405) we find $\zeta_{\alpha\beta ts}^{(1)(1)\pm} = \pm\zeta_{\alpha\beta}^{t+1, s}$.

For the second equality in (2.410) calculation of curl form left-hand part gives $d\nabla \times \mathbf{F}_{ts}^{(2)} = -i\tilde{\mathbf{F}}_{ts}^{(1)}$, projecting of the expression found on \mathbf{e}_3 leads to

$$-\frac{i}{d} D_{t+1}^s = -i \frac{\partial}{\partial z} F_t^s = (-i)(\mp 1)^{t+s} \int_{-\infty}^{\infty} \int_{-\infty}^{\infty} (\pm\delta) \zeta_{\alpha\beta}^{ts} E_{\alpha\beta}^{\pm} d\alpha d\beta.$$

Calculating the curl of right-hand part and taking (2.408) into account we obtain

$$(\mp 1)^{t+s+1} \int_{-\infty}^{\infty} \int_{-\infty}^{\infty} (\pm\delta) \zeta_{\alpha\beta ts}^{(2)(2)\pm} \mathbf{H}_{\alpha\beta}^{(1)\pm} d\alpha d\beta,$$

or, in projection on \mathbf{e}_3 ,

$$(\mp 1)^{t+s+1} \int_{-\infty}^{\infty} \int_{-\infty}^{\infty} (\pm\delta) \zeta_{\alpha\beta ts}^{(2)(2)\pm} E_{\alpha\beta}^{\pm} d\alpha d\beta.$$

From here, obviously, $\zeta_{\alpha\beta ts}^{(2)(2)\pm} = \pm i \zeta_{\alpha\beta}^{ts}$. Finally, we project on \mathbf{e}_3 the initial equality to obtain

$$\frac{s}{t} F_t^s = (\mp 1)^{t+s} \frac{s}{t} \int_{-\infty}^{\infty} \int_{-\infty}^{\infty} \zeta_{\alpha\beta}^{ts} E_{\alpha\beta}^{\pm} d\alpha d\beta = (\mp 1)^{t+s+1} \int_{-\infty}^{\infty} \int_{-\infty}^{\infty} \zeta_{\alpha\beta ts}^{(2)(1)\pm} E_{\alpha\beta}^{\pm} d\alpha d\beta,$$

i.e.,

$$\zeta_{\alpha\beta ts}^{(2)(1)\pm} = \mp \frac{S}{t} \zeta_{\alpha\beta}^{ts}.$$

For the third equality in (2.410) calculation of divergence gives

$$\begin{aligned} \nabla \cdot \mathbf{F}_{ts}^{(3)} &= \frac{2(2\nu - 1)}{d} D_t^s = 2(2\nu - 1)(\mp 1)^{t+s-1} \int_{-\infty}^{\infty} \int_{-\infty}^{\infty} (\pm\delta) \zeta_{\alpha\beta}^{t-1,s} E_{\alpha\beta}^{\pm} d\alpha d\beta = \\ &2(2\nu - 1)(\mp 1)^{t+s} \int_{-\infty}^{\infty} \int_{-\infty}^{\infty} (\pm\delta) \zeta_{\alpha\beta ts}^{(3)(3)\pm} E_{\alpha\beta}^{\pm} d\alpha d\beta, \end{aligned}$$

from where $\zeta_{\alpha\beta ts}^{(3)(3)\pm} = \mp \zeta_{\alpha\beta}^{t-1,s}$. By calculation of curl we find

$$\begin{aligned} \nabla \times \mathbf{F}_{ts}^{(3)} &= \frac{4i}{d} (\nu - 1) \tilde{\mathbf{F}}_{ts}^{(2)} = (\mp 1)^{t+s} \int_{-\infty}^{\infty} \int_{-\infty}^{\infty} (\pm\delta) \left[4(\nu - 1) \zeta_{\alpha\beta ts}^{(3)(3)\pm} \mathbf{H}_{\alpha\beta}^{(2)\pm} + \right. \\ &\left. \zeta_{\alpha\beta ts}^{(3)(2)\pm} \mathbf{H}_{\alpha\beta}^{(1)\pm} \right] d\alpha d\beta, \end{aligned}$$

and, using the value $\zeta_{\alpha\beta ts}^{(3)(3)\pm}$, calculated before,

$$\begin{aligned} 4i(\nu - 1) \frac{S}{t} \frac{\partial}{\partial z} F_{t-1}^s &= 4i(\nu - 1) \frac{S}{t} (\mp 1)^{t+s-1} \int_{-\infty}^{\infty} \int_{-\infty}^{\infty} (\pm\delta) \zeta_{\alpha\beta}^{t-1,s} E_{\alpha\beta}^{\pm} d\alpha d\beta = \\ &(\mp 1)^{t+s} \int_{-\infty}^{\infty} \int_{-\infty}^{\infty} (\pm\delta) \zeta_{\alpha\beta ts}^{(3)(2)\pm} E_{\alpha\beta}^{\pm} d\alpha d\beta; \\ \zeta_{\alpha\beta ts}^{(3)(2)\pm} &= \mp 4i(\nu - 1) \frac{S}{t} \zeta_{\alpha\beta}^{t-1,s}. \end{aligned}$$

Projecting of (2.410) for $i = 3$ on the complex Cartesian unit vectors completes calculation of $\zeta_{\alpha\beta ts}^{(i)(j)\pm}$. Equalizing the coefficients near the harmonic parts (the coefficients near the biharmonics are identical), we obtain

$$\zeta_{\alpha\beta ts}^{(3)(1)\pm} = \pm [4\nu - 3 + C_{-(t+1),s}] \zeta_{\alpha\beta}^{t-1,s} \mp d \zeta_0^2 \delta \zeta_{\alpha\beta}^{ts}.$$

and, thus the double vectorial Fourier integral transforms are established.

In turn, to satisfy the boundary conditions on spheroidal surfaces the solution (2.406) must be transformed to the corresponding local spheroidal basis. Such a transformation uses the relations

$$\mathbf{H}_{\alpha\beta}^{(i)\pm}(\mathbf{x}) = \sum_{j=1}^3 \sum_{t=0}^{\infty} \sum_{s=-t}^t (\pm 1)^{t+s} \omega_{\alpha\beta ts}^{(i)(j)\pm} \mathbf{f}_{ts}^{(j)}(\mathbf{x}, d), \quad i = 1, 2, 3; \quad (2.411)$$

The way to find the coefficients $\omega_{\alpha\beta ts}^{(i)(j)\pm}$ is quite analogous to that exposed above. So, using the expansion of scalar harmonics for a half-space into a series over the partial solutions of Laplace equation in spherical coordinates (Golovchan 1987)

$$E_{\alpha\beta}^{\pm}(\mathbf{x}) = \sum_{t=0}^{\infty} \sum_{s=-t}^t (\pm 1)^{t+s} \delta^{t+s} (\beta - i\alpha)^{-s} y_t^s(\mathbf{x}),$$

and expansion

$$y_t^s(\mathbf{x}) = \sqrt{\pi} \left(\frac{d}{2}\right)^t \sum_{k=|s|}^t \left(k + \frac{1}{2}\right) \frac{f_k^s(\mathbf{x}, d)}{\left(\frac{t-k}{2}\right)! \Gamma\left(\frac{t-k}{2} + \frac{3}{2}\right)}$$

we have

$$E_{\alpha\beta}^{\pm} = \sum_{t=0}^{\infty} \sum_{s=-t}^t (\pm 1)^{t+s} \delta^{t+s} (\beta - i\alpha)^{-s} \sqrt{\pi} \left(\frac{d}{2}\right)^t \times \sum_{k=|s|}^t \left(k + \frac{1}{2}\right) \frac{f_k^s(\mathbf{x}, d)}{\left(\frac{t-k}{2}\right)! \Gamma\left(\frac{t-k}{2} + \frac{3}{2}\right)} .$$

After change of summation order, we easily recognize that the internal power series, as before, is the nothing else but the spherical Bessel's function. Hence,

$$E_{\alpha\beta}^{\pm}(\mathbf{x}) = \sum_{t=0}^{\infty} \sum_{s=-t}^t (\pm 1)^{t+s} \omega_{\alpha\beta}^{ts} f_t^s(\mathbf{x}, d) , \quad (2.412)$$

where

$$\omega_{\alpha\beta}^{ts} = (2t+1) \left(\frac{\beta + i\alpha}{\delta}\right)^s \sqrt{\frac{\pi}{2\delta d}} I_{t+1/2}(\delta d) .$$

This formula provides determination of the expansion coefficients in (2.411). Say, because divergence of $\mathbf{H}_{\alpha\beta}^{(i)\pm}$ and $\mathbf{f}_{ts}^{(j)}$ for $j=1,2$ is zero, then, evidently, $\omega_{\alpha\beta ts}^{(i)(j)\pm} = 0$, $j > i$. Projection of the first expansion in (2.411) on \mathbf{e}_i is

$$\mathbf{H}_{\alpha\beta}^{(1)\pm} \cdot \mathbf{e}_z = E_{\alpha\beta}^{\pm} = \sum_{t=0}^{\infty} \sum_{s=-t}^t (\pm 1)^{t+s} \omega_{\alpha\beta ts}^{(1)(1)\pm} f_{t-1}^s .$$

Also, (2.412) can be written as

$$E_{\alpha\beta}^{\pm} = \sum_{t=0}^{\infty} \sum_{s=-t}^t (\pm 1)^{t+s-1} \omega_{\alpha\beta}^{t-1,s} f_{t-1}^s \quad (f_t^s \equiv 0 \text{ for } |s| > t)$$

therefore, $\omega_{\alpha\beta ts}^{(1)(1)\pm} = \pm \omega_{\alpha\beta}^{t-1,s}$.

The expression of $\mathbf{H}_{\alpha\beta}^{(2)\pm}$ in projections on \mathbf{e}_1 , \mathbf{e}_2 has a form

$$\mathbf{H}_{\alpha\beta}^{(2)\pm} = \pm i E_{\alpha\beta}^{\pm} \left[\mathbf{e}_1 \frac{(\beta + i\alpha)}{\delta} + \mathbf{e}_2 \frac{(\beta - i\alpha)}{\delta} \right] ;$$

developing $E_{\alpha\beta}^{\pm}$ into a series (2.412), one obtain

$$\begin{aligned} \mathbf{H}_{\alpha\beta}^{(2)\pm} &= i \sum_{t=0}^{\infty} \sum_{s=-t}^t (\pm 1)^{t+s+1} (\mathbf{e}_1 \omega_{\alpha\beta}^{t,s+1} + \mathbf{e}_2 \omega_{\alpha\beta}^{t,s-1}) f_t^s = \\ &= i \sum_{t=0}^{\infty} \sum_{s=-t}^t (\pm 1)^{t+s} \omega_{\alpha\beta}^{ts} (\mathbf{e}_1 f_t^s + \mathbf{e}_2 f_t^{s-1}) . \end{aligned}$$

Now, we recognize that the expression in the brackets is exactly $\mathbf{f}_{ts}^{(2)} + \frac{s}{(t+1)} \mathbf{f}_{t+1,s}^{(1)}$, hence

$$\mathbf{H}_{\alpha\beta}^{(2)\pm} = i \sum_{t=0}^{\infty} \sum_{s=-t}^t (\pm 1)^{t+s} \left(\pm \frac{s}{t} \omega_{\alpha\beta}^{t,s-1} \mathbf{f}_{ts}^{(1)} + \omega_{\alpha\beta}^{ts} \mathbf{f}_{ts}^{(2)} \right) ,$$

from where

$$\omega_{\alpha\beta ts}^{(2)(2)\pm} = \omega_{\alpha\beta}^{ts} , \quad \omega_{\alpha\beta ts}^{(2)(1)\pm} = \pm \frac{s}{t} \omega_{\alpha\beta}^{t-1,s} .$$

Taking into account the relations

$$\begin{aligned} \mathbf{H}_{\alpha\beta}^{(3)\pm} &= z \nabla E_{\alpha\beta}^{\pm} + (4\nu - 3) E_{\alpha\beta}^{\pm} \mathbf{e}_3 , \\ \mathbf{f}_{ts}^{(3)} &= z \nabla f_{t+1}^s - \mathbf{e}_1 (t - s + 2) f_{t+1}^{s-1} + \mathbf{e}_2 (t + s + 2) f_{t+1}^{s+1} + (t + 1)(2t + 3) \beta_t \mathbf{m}_{ts}^{(3)} \end{aligned}$$

valid for the functions $\mathbf{H}_{\alpha\beta}^{(3)\pm}$ and $\mathbf{f}_{ts}^{(3)}$, we equalize the coefficients of bi-harmonic terms in both the parts of equality to obtain $\omega_{\alpha\beta ts}^{(3)(3)\pm} = \pm \omega_{\alpha\beta}^{t+1,s}$. Calculation of curl of the third equality in (2.411) and its projection on the complex Cartesian unit vectors \mathbf{e}_i finalizes the procedure; after some algebra we have

$$\begin{aligned} \omega_{\alpha\beta ts}^{(3)(2)\pm} &= 4(1 - \nu) \frac{s}{t} \omega_{\alpha\beta}^{ts} ; \\ \omega_{\alpha\beta ts}^{(3)(2)\pm} &= \mp C_{-(t+1),s} \omega_{\alpha\beta}^{t-1,s} \pm d\xi_0^2 \frac{2(2t-1)}{2t+1} \delta \omega_{\alpha\beta}^{ts} ; \end{aligned}$$

and the expansion formulae (2.411) are obtained.

Stress in an elastic half space containing a finite array of spheroidal inclusions

Investigation of stress and strain near the free or loaded boundary is of primary interest from the standpoint of developing the micro-mechanical strength theory of composites, since, in many cases, the fracture is a consequence of surface defects. In this subsection, the indicated problem will be considered in the framework of generalized self-consistent method using the half-space $z_0 < 0$ will be considered which contained N spheroidal inclusions as geometrical model of composite half-space. Previously this problem was considered by Mura (1982) and Tsuchida et al (1987) in one-inclusion approximation and and in the axisymmetric statement only.

The stress state of a half space is determined by the displacement vector $\mathbf{u}_0 = \hat{E} \cdot \mathbf{x}$; also, it is assumed that a plane boundary is traction-free

$$\mathbf{T}_z(\mathbf{u}^{(0)})_{z=0} = 0 , \quad (2.413)$$

where

$$\frac{1}{2\mu} \mathbf{T}_z(\mathbf{u}) = \frac{\nu}{1-2\nu} (\nabla \cdot \mathbf{u}) \mathbf{e}_z + \frac{\partial}{\partial z} \mathbf{u} + \frac{1}{2} \mathbf{e}_z \times (\nabla \times \mathbf{u})$$

is the traction vector on the surface $z = const$. If on the elements of the matrix \hat{E} the following restrictions

$$E_{13} = E_{13} = 0 ; \quad \nu(E_{11} + E_{22}) + (1 - \nu)E_{33} = 0 ;$$

are imposed then the traction vector (corresponding to \mathbf{u}_0) is zero for $z = \text{const}$. Conditions on the matrix-inclusion interfaces $\xi_n = \xi_0^{(n)}$ are in the form (2.362); for the sake of simplicity, we assume that the axes of spheroids are parallel to the normal $\mathbf{n} = n_z \mathbf{e}_z$.

In accordance with the superposition principle, we represent the displacement vector in matrix in the form

$$\begin{aligned} \mathbf{u}^{(0)} = & \mathbf{u}_0 + \int_{-\infty}^{\infty} \int_{-\infty}^{\infty} \sum_{j=1}^3 G_j(\alpha, \beta) \mathbf{H}_{\alpha\beta}^{(j)\pm}(\mathbf{r}_0) d\alpha d\beta \\ & + \sum_{q=1}^N \sum_{i=1}^3 \sum_{t=0}^{\infty} \sum_{s=-t}^t A_{ts}^{(i)(q)} \mathbf{F}_{ts}^{(i)}(\mathbf{x}_q, d_q), \end{aligned}$$

where the integral densities G_j and the arbitrary constants $A_{ts}^{(i)(q)}$ must be determined from the conditions (2.362) and (2.413); the expression for the displacement vector in the points of the q th inclusion has the form (2.380). To satisfy the condition (2.403), we transform the second part of (2.405) \mathbf{u}_2 to the Cartesian basis (x_0, y_0, z_0) . This transformation uses integral representations of the exterior partial solutions $\mathbf{F}_{ts}^{(i)}$ (2.366) and the directly verified relations

$$\mathbf{H}_{\alpha\beta}^{(j)\pm}(\mathbf{x}_q) = E_{\alpha\beta}^{\pm}(-\mathbf{X}_{0q}) \left[\mathbf{H}_{\alpha\beta}^{(j)\pm}(\mathbf{x}_0) - \delta_j^3 Z_{0q} \mathbf{H}_{\alpha\beta}^{(1)\pm}(\mathbf{x}_0) \right]. \quad (2.414)$$

After corresponding substitutions and the change of an order of summation we arrive at the following expression

$$\begin{aligned} \mathbf{u}_2 = & \int_{-\infty}^{\infty} \int_{-\infty}^{\infty} \left\{ \sum_{j=1}^3 \mathbf{H}_{\alpha\beta}^{(j)-}(\mathbf{x}_0) E_{\alpha\beta}^{-}(-\mathbf{X}_{0q}) \sum_{q=1}^N \sum_{i=1}^3 \sum_{t=0}^{\infty} \sum_{s=-t}^t A_{ts}^{(i)(q)} \right. \\ & \times \left. \left[\zeta_{\alpha\beta ts}^{(i)(j)-}(d_q) - \delta_j^1 Z_{0q} \zeta_{\alpha\beta ts}^{(i)(3)-}(d_q) \right] d\alpha d\beta \right\}, \end{aligned}$$

Substituting (2.404) in (2.405) and, next, in (2.403) and taking into account the accepted condition $\mathbf{T}_z(\mathbf{u}_0) = 0$, we have

$$\begin{aligned} \int_{-\infty}^{\infty} \int_{-\infty}^{\infty} \left\{ \sum_{j=1}^3 G_j \mathbf{T}_z \left(\mathbf{H}_{\alpha\beta}^{(j)+} \right) + \sum_{j=1}^3 \mathbf{T}_z \left(\mathbf{H}_{\alpha\beta}^{(j)-} \right) \sum_{q=1}^N E_{\alpha\beta}^{\pm}(-\mathbf{X}_{0q}) \right. \\ \times \left. \sum_{i=1}^3 \sum_{t=0}^{\infty} \sum_{s=-t}^t A_{ts}^{(i)(q)} \hat{\zeta}_{\alpha\beta ts}^{(i)(j)-} d\alpha d\beta \right\} = 0, \end{aligned}$$

where

$$\hat{\zeta}_{\alpha\beta ts}^{(i)(j)\pm}(d_q, Z_{0q}) = \left[\zeta_{\alpha\beta ts}^{(i)(j)\pm}(d_q) \pm \delta_j^1 Z_{0q} \zeta_{\alpha\beta ts}^{(i)(3)\pm}(d_q) \right].$$

Calculation of the expressions $\mathbf{T}_z \left(\mathbf{H}_{\alpha\beta}^{(j)+} \right)$ is not a problem in view of the properties

(2.408). In the terms of the vector harmonics $\mathbf{L}_{\alpha\beta}$, $\mathbf{M}_{\alpha\beta}$ and $\mathbf{N}_{\alpha\beta}$ (2.409) we have

$$\begin{aligned}\frac{1}{2\mu}\mathbf{T}_z\left(\mathbf{H}_{\alpha\beta}^{(1)\pm}\right) &= (\pm\delta)\left[\mathbf{L}_{\alpha\beta}\pm\mathbf{M}_{\alpha\beta}\right]\exp(\pm\delta z); \\ \frac{1}{2\mu}\mathbf{T}_z\left(\mathbf{H}_{\alpha\beta}^{(2)\pm}\right) &= \frac{(\pm\delta)}{2}\mathbf{N}_{\alpha\beta}\exp(\pm\delta z); \\ \frac{1}{2\mu}\mathbf{T}_z\left(\mathbf{H}_{\alpha\beta}^{(3)\pm}\right) &= (\pm\delta)\left[(2\nu-2\pm\delta z)\mathbf{L}_{\alpha\beta}\pm(2\nu-1\pm\delta z)\mathbf{M}_{\alpha\beta}\right]\exp(\pm\delta z).\end{aligned}$$

Substituting (2.409) into (2.408) and taking into account of an orthogonality of these harmonics, we get to a set of three algebraic equations which (in write matrix) have the following form

$$TZ_{\alpha\beta}^+(0)\cdot\mathbf{G}_{\alpha\beta}+TZ_{\alpha\beta}^-(0)\cdot\sum_{q=1}^NE_{\alpha\beta}^-(-\mathbf{X}_{0q})\mathbf{g}_{\alpha\beta}^{(q)}=0, \quad (2.415)$$

where

$$\begin{aligned}\mathbf{G}_{\alpha\beta} &= \left[G_{\alpha\beta}^{(1)}, G_{\alpha\beta}^{(2)}, G_{\alpha\beta}^{(3)}\right]^T, \quad \mathbf{g}_{\alpha\beta}^{(q)} = \left[g_{\alpha\beta}^{(1)(q)}, g_{\alpha\beta}^{(2)(q)}, g_{\alpha\beta}^{(3)(q)}\right]^T, \\ g_{\alpha\beta}^{(i)(q)}(d_q, Z_{0q}) &= \sum_{i=1}^3\sum_{t=0}^{\infty}\sum_{s=-t}^t A_{ts}^{(i)(q)}\hat{\zeta}_{\alpha\beta ts}^{(i)(j)-},\end{aligned} \quad (2.416)$$

$$TZ_{\alpha\beta}^{\pm}(z) = \begin{pmatrix} 1 & 0 & (1-2\nu)/(\pm\delta)+z \\ 0 & 1/2 & 0 \\ \pm\delta & 0 & \pm\delta z-2\nu \end{pmatrix}.$$

Since $\det(TZ_{\alpha\beta}^{\pm}(z))\neq 0$ for $z=0$, the set (2.410) is uniquely solvable for the integral densities vector $\mathbf{G}_{\alpha\beta}$. In the case when a traction is non-zero on the surface $z_0=0$ the right-hand side of (2.410) will have additional expression obtained by expansion of the traction vector with respect to the set of the functions (2.409).

Satisfaction of contact conditions (2.362) requires transformation of the solution $\mathbf{u}^{(0)}$ to local coordinate system. So, in n th spheroid's coordinate system the expression \mathbf{u}_2 have the following form

$$\mathbf{u}_2 = \sum_{i=1}^3\sum_{t=0}^{\infty}\sum_{s=-t}^t \left[A_{ts}^{(i)(n)}\mathbf{F}_{ts}^{(i)}(\mathbf{x}_n, d_n)+a_{ts}^{(i)(n)}\mathbf{f}_{ts}^{(i)}(\mathbf{x}_n, d_n)\right], \quad (2.417)$$

where $a_{ts}^{(i)(n)}$ is clear from the formula (2.411). By applying the relations inverse to (2.414), for \mathbf{u}_1 we find

$$\begin{aligned}\mathbf{u}_1 &= \int_{-\infty}^{\infty}\int_{-\infty}^{\infty} E_{\alpha\beta}^+(X_{0n})\sum_{j=1}^3 G_j(\alpha, \beta)\left[\mathbf{H}_{\alpha\beta}^{(j)+}(\mathbf{x}_n)+\delta_j^3 Z_{0n}\mathbf{H}_{\alpha\beta}^{(j)+}(\mathbf{x}_n)\right]d\alpha d\beta \\ &= \int_{-\infty}^{\infty}\int_{-\infty}^{\infty} E_{\alpha\beta}^+(\mathbf{X}_{0n})\sum_{j=1}^3 \tilde{G}_j(\alpha, \beta)\mathbf{H}_{\alpha\beta}^{(j)+}(\mathbf{x}_n)d\alpha d\beta,\end{aligned}$$

where $\tilde{G}_j = G_j + \delta_j^1 Z_{0n} G_3$. Substituting the formulae (2.411) into the last expression, after some transformations, gives us

$$\mathbf{u}_1 = \sum_{i=1}^3 \sum_{t=0}^{\infty} \sum_{s=-t}^t \mathbf{f}_{ts}^{(i)}(\mathbf{x}_n, d_n) \int_{-\infty}^{\infty} \int_{-\infty}^{\infty} [E_{\alpha\beta}^+(\mathbf{X}_{0n}) \sum_{j=1}^3 \omega_{\alpha\beta ts}^{(j)(i)\pm} \tilde{G}_j(\alpha, \beta)] d\alpha d\beta. \quad (2.418)$$

Relations (2.381), (2.417) and (2.418) determine the form of displacement vector (2.405) in the n th base, completely. Further run for solution of the problem repeats, with minor deviations, that was exposed in the previous subsection; the only difference is the term (2.418). As a result, we arrive at an infinite set of linear algebraic equations of the type (2.389), in so doing, the equation (2.411) is used to exclude the unknown vector from this set. Numerical solution of this system enables calculation of the displacement vector, stress and strain tensor in the matrix and in the inclusion with accuracy determining by the maximum value of the index t into the expression for displacement vector $\mathbf{u}^{(0)}$ (2.405), used in practical calculations. Noteworthy, using more complicated math for solution of these problem makes numerical realization of the method more involved in comparison with the method used for unbounded composite study.

It may be noted also that the assumption regarding orientation of spheroids is not restrictive. The case of their arbitrary orientation can be considered analogously. In so doing, transformation of \mathbf{u}_2 to the form (2.404) uses also the re-expansion formulae due to rotation of the coordinate system (2.374), (2.375).

2.4.7 Application to the composite mechanics problems

Averaged stress $\langle \sigma \rangle_{(q)}$

The general solution derived above provides fast and accurate local stress field evaluation in any point of the piece-homogeneous domain with spheroidal interfaces. Based on it, the "phase-averaged" stress playing an important role in the micromechanics can be readily evaluated; yet another advantage of the analytical framework developed here is that such an averaging can be done analytically and gives the simple and exact finite-form formulae.

Let us find an expression of

$$\langle \sigma \rangle_{(q)} = \frac{1}{v_q} \iiint_{v_q} \sigma(\mathbf{x}) d\mathbf{x}, \quad (2.419)$$

where $v_q = \frac{4}{3}\pi (l_1^q)^2 l_3^q$ is the volume of q th inclusion. Inside this inclusion, in accordance with (2.364) and (2.365),

$$\sigma(\mathbf{x}) = \mathbf{L}^{(q)} \frac{1}{2} [\nabla \mathbf{u}_q + (\nabla \mathbf{u}_q)^T] - \beta_q, \quad (2.420)$$

where the displacement \mathbf{u}_q is given by eqn (2.380). Substituting (2.420) into (2.419) and applying the Gauss' theorem gives us

$$\langle \sigma \rangle_{(q)} = \mathbf{L}^{(q)} \frac{1}{2v_q} \iint_{S_q} (\mathbf{n} \mathbf{u}_q + \mathbf{u}_q \mathbf{n}) ds - \beta_q, \quad (2.421)$$

and, thus, the problem is reduced to evaluation of the integrals of kind $\iint_{S_q} n_i u_j ds$, or, with the (2.367) taken into account, $\iint_{S_q} n_i f_t^s(\mathbf{x}_q, d_q) ds$. As shown elsewhere (Kushch, 1998b), only a few of them are nonzero, namely

$$\begin{aligned} \iint_{S_q} n_3 f_1^0(\mathbf{x}_q, d_q) ds &= \frac{4}{3}\pi \left(d_q \bar{\xi}_0^q\right)^2 \xi_0^q = \frac{v_q}{d_q}; \\ \iint_{S_q} (n_1 + in_2) f_1^{-1}(\mathbf{x}_q, d_q) ds &= -\iint_{S_q} (n_1 - in_2) f_1^1(\mathbf{x}_q, d_q) ds = -\frac{v_q}{2d_q}. \end{aligned} \quad (2.422)$$

After simple algebra, one obtains the averaged strains

$$\begin{aligned} d_q \langle \varepsilon_{11} \rangle_{(q)} &= \gamma_0^{(q)} D_{00}^{(3)(q)} - \frac{1}{2} \left(D_{20}^{(1)(q)} - \text{Re } D_{22}^{(1)(q)} \right); \\ d_q \langle \varepsilon_{22} \rangle_{(q)} &= \gamma_0^{(q)} D_{00}^{(3)(q)} - \frac{1}{2} \left(D_{20}^{(1)(q)} + \text{Re } D_{22}^{(1)(q)} \right); \\ d_q \langle \varepsilon_{33} \rangle_{(q)} &= \gamma_0^{(q)} D_{00}^{(3)(q)} + D_{20}^{(1)(q)}; \\ d_q \left(\langle \varepsilon_{13} \rangle_{(q)} - i \langle \varepsilon_{23} \rangle_{(q)} \right) &= D_{21}^{(1)(q)}; \\ d_q \langle \varepsilon_{12} \rangle_{(q)} &= -\frac{1}{2} \text{Im } D_{22}^{(1)(q)}; \end{aligned} \quad (2.423)$$

where $\gamma_0^{(q)} = 2(2\nu_q - 1)/3$.

Noteworthy, the right hand sides of (2.423) contain the expansion coefficients $D_{ts}^{(i)(q)}$ entering the vector

$$\mathbf{D}_1^{(q)} = \left(D_{00}^{(3)(q)}, D_{10}^{(2)(q)}, D_{11}^{(2)(q)}, D_{20}^{(1)(q)}, D_{21}^{(1)(q)}, D_{22}^{(1)(q)} \right)^T \quad (2.424)$$

only. Using also standard reduction notation for the symmetric second-rank tensors (e.g., $\beta_1 = \beta_{11}, \beta_2 = \beta_{22}, \beta_3 = \beta_{33}, \beta_4 = \beta_{13}, \beta_5 = \beta_{23}$ and $\beta_6 = \beta_{12}$), we rewrite eqn (2.423) in the matrix form:

$$\langle \varepsilon \rangle_{(q)} = \mathbf{P}^{(q)} \mathbf{D}_1^{(q)}, \quad (2.425)$$

where

$$\mathbf{P}^{(q)} = \frac{1}{d_q} \begin{pmatrix} \gamma_0^{(q)} & 0 & 0 & -1/2 & 0 & 1/2 \\ \gamma_0^{(q)} & 0 & 0 & -1/2 & 0 & -1/2 \\ \gamma_0^{(q)} & 0 & 0 & 1 & 0 & 0 \\ 0 & 0 & 0 & 0 & 1 & 0 \\ 0 & 0 & 0 & 0 & i & 0 \\ 0 & 0 & 0 & 0 & 0 & i/2 \end{pmatrix}. \quad (2.426)$$

The resulting expression of average stress

$$\langle \sigma \rangle_{(q)} = \mathbf{L}^{(q)} \mathbf{P}^{(q)} \mathbf{D}_1^{(q)} - \beta_q \quad (2.427)$$

is valid for any geometry, phase elastic properties and loading type provided β_q is constant in the domain occupied by q th inclusion.

One-inclusion problem: explicit expression

In what follows, we will need a solution of one-inclusion problem being a simple particular case of many-inclusion problem considered above. Specifically, we put $\mathbf{L}^{(p)} = \mathbf{L}^{(0)}$ ($p = 1, 2, \dots, N$) and $\beta_p = 0$ ($p \neq q$) to get a problem where the transformation stress β_q is a sole governing parameter. The well-known fact is that such a problem possesses an analytical, Eshelby-type solution: we recover it from the general one (2.389) by putting $\mathbf{a}_t^{(q)} = 0$ and $t = 1$. In this solution, only the unknowns, or multipole strengths, $A_{ts}^{(i)(q)}$ entering the vector

$$\mathbf{A}_1^{(q)} = \left(A_{00}^{(1)(q)}, A_{10}^{(2)(q)}, A_{11}^{(2)(q)}, A_{20}^{(3)(q)}, A_{21}^{(3)(q)}, A_{22}^{(3)(q)} \right)^T \quad (2.428)$$

are nonzero and can be found from (2.389) as

$$\mathbf{A}_1^{(q)} = -(M_1)^{-1} \mathbf{T}_\beta^q, \text{ where } M_1 = TM_1(\nu_0) (UM_1(\nu_0))^{-1} UG_1(\nu_0) - TG_1(\nu_0). \quad (2.429)$$

Despite rather complicated structure of the matrix M_1 , the resulting explicit expressions

$$\begin{aligned} A_{00}^{(1)(q)} &= \frac{\gamma_0^{(0)} v_q^*}{4\mu_0(1-\nu_0)} (\beta_{q|11} + \beta_{q|22} + \beta_{q|33}); \\ A_{10}^{(2)(q)} &= \frac{v_q^*}{2\mu_0} (\beta_{q|11} + \beta_{q|22}); \\ A_{11}^{(2)(q)} &= \frac{v_q^*}{4\mu_0} (1 - 1/2e_q) (\beta_{q|13} - i\beta_{q|23}); \\ A_{20}^{(3)(q)} &= \frac{v_q^*}{8\mu_0(1-\nu_0)} (\beta_{q|11} + \beta_{q|22} - 2\beta_{q|33}); \\ A_{21}^{(3)(q)} &= \frac{v_q^*}{8\mu_0(1-\nu_0)} (1 + 1/2e_q) (\beta_{q|13} - i\beta_{q|23}); \\ A_{22}^{(3)(q)} &= \frac{v_q^*}{16\mu_0(1-\nu_0)} (\beta_{q|22} - \beta_{q|11} + 2i\beta_{q|12}); \end{aligned} \quad (2.430)$$

are amazingly simple and give clear insight into the nature of the singular vectorial functions $\mathbf{F}_{ts}^{(i)}$ (2.366). In the eqn (2.430), $v_q^* = \xi_0^q (\bar{\xi}_0^q)^2$ and $e_q = \xi_0^q / \bar{\xi}_0^q$. It is convenient to rewrite (2.430) as

$$\mathbf{A}_1^{(q)} = \mathbf{R}^{(q)} \beta_q, \quad (2.431)$$

where

$$\mathbf{R}^{(q)} = \frac{v_q^*}{2\mu_0(1-\nu_0)} \left\{ \begin{array}{cccccc} \gamma_0^{(0)}/2 & \gamma_0^{(0)}/2 & \gamma_0^{(0)}/2 & 0 & 0 & 0 \\ (1-\nu_0) & (1-\nu_0) & 0 & 0 & 0 & 0 \\ 0 & 0 & 0 & \frac{(1-\nu_0)}{2} \left(1 - \frac{1}{2e_q}\right) & \frac{1}{2i} \left(1 - \frac{1}{2e_q}\right) & 0 \\ 1/4 & 1/4 & -1/2 & 1 & 0 & 0 \\ 0 & 0 & 0 & \frac{(1-\nu_0)}{4} \left(1 + \frac{1}{2e_q}\right) & \frac{1}{4i} \left(1 + \frac{1}{2e_q}\right) & 0 \\ -1/8 & -1/8 & 0 & 0 & 0 & i/4 \end{array} \right\}. \quad (2.432)$$

Given $\mathbf{A}_1^{(q)}$, the coefficients $\mathbf{D}_1^{(q)}$ can be obtained, say, from (2.385), where we put $\mathbf{a}_t^{(q)} = 0$ and $t = 1$ as well:

$$\mathbf{D}_1^{(q)} = (UM_1(\nu_0))^{-1} UG_1(\nu_0)\mathbf{A}_1^{(q)} = \mathbf{Q}^{(q)}\mathbf{A}_1^{(q)}, \quad (2.433)$$

where the following elements of the matrix $\mathbf{Q}^{(q)} = \{Q_{ij}^{(q)}\}$ are nonzero (for brevity sake, the index q is omitted):

$$\begin{aligned} Q_{11} &= \frac{1}{3\gamma_0^{(0)}\xi(\bar{\xi})^2}; & Q_{22} &= Q_1^1/\bar{\xi}; & Q_{33} &= 2Q_1^0/\xi - Q_1^1/\bar{\xi}; \\ Q_{44} &= -\frac{2}{3\xi} \left(\xi Q_2^0 + 4\gamma_0^{(0)} Q_1^0 \right) + \frac{1}{3\bar{\xi}} \left[-\xi Q_2^1 + (1 - 2\gamma_0^{(0)}) Q_1^1 \right]; \\ Q_{55} &= \frac{1}{2\xi} \left(-\xi Q_2^1 + 3\gamma_0^{(0)} Q_1^1 \right) + \frac{1}{2\bar{\xi}} \left[-\xi Q_2^0 + 2(1 - 3\gamma_0^{(0)}) Q_1^0 \right]; \\ Q_{66} &= \frac{1}{\bar{\xi}} \left[-\xi Q_2^1 + 3(1 - 4\gamma_0^{(0)}) Q_1^1 \right]; \\ Q_{41} &= \frac{1}{3} (2Q_1^0/\xi + Q_1^1/\bar{\xi}); & Q_{53} &= \frac{1}{2} (2Q_1^0/\xi + Q_1^1/\bar{\xi}); \\ Q_{14} &= \frac{1}{(1 - 2\nu_0)\xi} \left(\xi Q_2^0 - 2\gamma_0^{(0)} Q_1^0 \right) + \frac{1}{2(1 - 2\nu_0)\bar{\xi}} \left[-\xi Q_2^1 + (1 - 2\gamma_0^{(0)}) Q_1^1 \right]. \end{aligned} \quad (2.434)$$

Here, $\xi = \xi_0^{(q)}$ and $Q_t^s = Q_t^s(\xi_0^{(q)})$ are the associated Legendre functions of second kind.

Thus, the displacement caused by the transformation stress β_q takes the following finite form:

$$\mathbf{u}_q = \sum_{i=1}^3 \sum_{|s| \leq (i-1)}^t D_{i-1,s}^{(4-i)(q)} \mathbf{f}_{i-1,s}^{(4-i)}(\mathbf{x}_q, d_q) \quad (2.435)$$

inside the q th inclusion and

$$\mathbf{u} = \sum_{i=1}^3 \sum_{|s| \leq (i-1)}^t A_{i-1,s}^{(i)(q)} \mathbf{F}_{i-1,s}^{(i)}(\mathbf{x}_q, d_q) \quad (2.436)$$

outside of it. The corresponding stress tensor is given by

$$\sigma(\mathbf{x}) = \begin{cases} \mathbf{L}^{(0)} \frac{1}{2} \left[\nabla \mathbf{u}_q + (\nabla \mathbf{u}_q)^T \right] - \beta_q, & \mathbf{x} \in v_q; \\ \mathbf{L}^{(0)} \frac{1}{2} \left[\nabla \mathbf{u} + (\nabla \mathbf{u})^T \right], & \text{otherwise;} \end{cases} \quad (2.437)$$

and, after substitution here the eqns (2.435) and (2.436), can be written as

$$\sigma(\mathbf{x}) = \begin{cases} \mathbf{L}^{(0)} \phi^{(q)}(\mathbf{x} - \mathbf{X}_q) \mathbf{D}_1^{(q)} - \beta_q, & \mathbf{x} \in v_q; \\ \mathbf{L}^{(0)} \Phi^{(q)}(\mathbf{x} - \mathbf{X}_q) \mathbf{A}_1^{(q)}, & \text{otherwise;} \end{cases} \quad (2.438)$$

where the matrices ϕ and Φ are obtained by differentiating the functions $\mathbf{f}_{i-1,s}^{(4-i)}$ and $\mathbf{F}_{i-1,s}^{(i)}$, respectively, with respect to local Cartesian coordinates. Note, finally, that unlike the Eshelby's solution, the formulae derived apply equally to the prolate and oblate spheroids including the limiting cases of needle-like and penny-like shapes.

Evaluation of the tensors \mathbf{T}_q and \mathbf{T}_{pq}

The theory exposed can be applied, in particular, to evaluate the tensor $\mathbf{T}_q(\mathbf{x} - \mathbf{X}_q)$ introduced as (Buryachenko and Pagano, 2003)

$$\sigma(\mathbf{x}) = \int \Gamma(\mathbf{x} - \mathbf{y}) V_q d\mathbf{y} \beta_q = v_q \mathbf{T}_q(\mathbf{x} - \mathbf{X}_q) \beta_q. \quad (2.439)$$

Indeed, substitution of (2.431) and (2.433) into (2.438) and subsequent comparison with (2.439) gives the desired explicit representation

$$v_q \mathbf{T}_q(\mathbf{x} - \mathbf{X}_q) = \begin{cases} \mathbf{L}^{(0)} \phi^{(q)}(\mathbf{x} - \mathbf{X}_q) \mathbf{Q}^{(q)} \mathbf{R}^{(q)} - \mathbf{I}, & \mathbf{x} \in v_q; \\ \mathbf{L}^{(0)} \Phi^{(q)}(\mathbf{x} - \mathbf{X}_q) \mathbf{R}^{(q)}, & \text{otherwise} \end{cases} \quad (2.440)$$

(\mathbf{I} being the unit tensor), which is valid in any point including the region occupied by p th inclusion ($p \neq q$).

Another problem, addressed in (Buryachenko and Pagano, 2003), consists in evaluating the tensor defined by

$$\mathbf{T}_{pq}(\mathbf{X}_p - \mathbf{X}_q) = \langle \mathbf{T}_q(\mathbf{x} - \mathbf{X}_q) \rangle_{(p)} = \frac{1}{v_p} \iiint_{v_p} \mathbf{T}_q(\mathbf{x} - \mathbf{X}_q) d\mathbf{x}, \quad (2.441)$$

where \mathbf{T}_q is given by eqn (2.439). The most straightforward way here is to integrate (2.441) numerically using the known analytical expression of \mathbf{T}_q (2.440). An alternate, however, much more elegant and "power-saving" analytical way consists in utilizing the theory developed for many-inclusion problem. In the case of identical spherical inclusions, the tensor \mathbf{T}_{pq} has been found by Willis and Acton (1976), among others. Here, we derive it in the case of arbitrarily sized, shaped, positioned and orientated spheroidal inclusions.

First, we note that due to conditions $\mathbf{L}^{(p)} = \mathbf{L}^{(0)}$ ($p = 1, 2, \dots, N$) and $\beta_p = 0$ ($p \neq q$) assumed above, no disturbance fields are expected around the inclusions others than q th one. It follows from (2.378) and (2.379) that in this case all the unknowns $\mathbf{A}_t^{(p)} = 0$ for $p \neq q$, $t = 1, 2, \dots$. The inclusion-related coefficients $\mathbf{D}_t^{(p)}$ are, however, nonzero in a general case: so, the eqns (2.385) and (2.400) give us

$$\mathbf{D}_t^{(p)} = \mathbf{a}_t^{(p)} = \eta_{1t}^{(q)(p)} \mathbf{A}_1^{(q)} \quad (2.442)$$

provided $\nu_p = \nu_0$ and $\mathbf{A}_k^{(q)} = 0$ for $k > 1$. In other words, in the case $\mathbf{L}^{(p)} = \mathbf{L}^{(0)}$ the solution \mathbf{u}_p can be thought as a local expansion in a vicinity of the point \mathbf{X}_p of the disturbance field \mathbf{u} (2.389) caused by the inclusion centered at \mathbf{X}_q .

Now, we combine the eqns (2.439) and (2.441) to write

$$\mathbf{T}_{pq}(\mathbf{X}_p - \mathbf{X}_q) \beta_q = \frac{1}{v_q} \langle \sigma \rangle_{(p)}. \quad (2.443)$$

Averaging of stress inside the inclusion is done already: applying the eqn (2.427) and then (2.439) to (2.443) results in

$$\mathbf{T}_{pq}(\mathbf{X}_p - \mathbf{X}_q) \beta_q = \frac{1}{v_q} \mathbf{L}^{(0)} \mathbf{P}^{(p)} \eta_{11}^{(q)(p)} \mathbf{A}_1^{(q)}. \quad (2.444)$$

The vector $\mathbf{A}_1^{(q)}$, in turn, is related linearly to β_q . Taking account of eqn (2.431) gives the final formula:

$$\mathbf{T}_{pq}(\mathbf{X}_p - \mathbf{X}_q) = \frac{1}{v_q} \mathbf{L}^{(0)} \mathbf{P}^{(p)} \eta_{11}^{(q)(p)} \mathbf{R}^{(q)}, \quad (2.445)$$

where the constant matrices $\mathbf{P}^{(p)}$ and $\mathbf{R}^{(q)}$ are given by the eqns (2.426) and (2.432), respectively. In (2.445), $\eta_{11}^{(q)(p)}$ is the only distance $\mathbf{X}_{qp} = \mathbf{X}_p - \mathbf{X}_q$ and orientation $\boldsymbol{\Omega}_{qp}$ dependent term which can be evaluated either by utilizing the re-expansion formulae or, alternatively, with aid of the numerical technique developed in the framework of present work

In the next section the above developed theory will be applied to evaluate the effective thermoelastic properties of random structure composites reinforced by the clusters of deterministic structure typical for the clay nanocomposites (see Buryachenko, Kushch and Roy (2005) for details).

2.5 Effective thermoelastic properties of random structure composites reinforced by the clusters of deterministic structure (application to clay nanocomposites)

2.5.1 Introduction

A considerable number of methods are known in the linear theory of statistically homogeneous composites; appropriate, but by no means exhaustive, references are provided by the reviews of Christensen (1979) Willis (1981), Mura (1987), Nemat-Nasser and Hori (1993), Buryachenko (2001), Torquato (2002), Milton (2003). It appears today that variants of self consistent (or effective medium) method (Kröner, 1958) the mean field method (Mori and Tanaka, 1973; Benveniste, 1987) are the most popular and widely used methods. The notion of an effective field in which each particle is located is a basic concept of such powerful methods in micromechanics as the methods of self-consistent fields and effective fields (see for references Buryachenko, 2001). The “quasi-crystalline” approximation by Lax (1952) is often used for truncation of the hierarchy of integral equations equations involved leading to neglect of direct multiparticle interactions of inclusions. The last deficiency was overcome recently by the multiparticle effective field method (MEFM), put forward and developed by one of the authors (references may be found in the survey by Buryachenko, 2001) The MEFM is based on the theory of functions of random variables and Green’s functions. Within this method a hierarchy of statistical moment equations for conditional averages of the stresses in the inclusions is derived. The hierarchy is established by introducing the notion of an effective field. In this way the interaction of different inclusions is taken directly into account.

Significantly less research has been performed for *statistically inhomogeneous* composites. In such a case, the ergodicity fails and ensemble and averages do not coincide. The degenerate case of this materials is a random matrix composite bounded in some directions as well as the composites medium for that the inclusions are located in a region bounded in some directions although unrestricted Ness of the domain of inclusion locations does not preclude statistical inhomogeneity. For example, any laminated composite materials with randomly reinforced by aligned fibers in each ply, is a statistically inhomogeneous material.

A particular case of composite materials containing particle-rich and particle-poor regions is the clustered materials where such regions have a concrete shape and random locations that does not assumes the loss of statistical homogeneity of the composite structure. We will analyze in this paper a special sort of clustered materials which are polymeric composites reinforced with clay crystals of nanometer scale recently attracted tremendous attention in the material society. A general comprehensive review of the various types of nanocomposites was given by Komarneni (1992). A particular class of nanocomposites is clay nanocomposites (see e.g Giannelis, 1996; Luo and Daniel, 2003; Fornes and Paul, 2003; Wang and Pyrz, 2004a,b; Sheng *et al.*, 2004 where additional references can be found). In general, layered silicate-reinforced presenting many challenges for mechanics are conditionally divided into three types (see Giannelis *et al.*, 1999; Carrado, 2003): conventional composites where the layered silicate is presented as the original aggregate state of the clay particles (tactoids) with no intercalation of the matrix material into the

layered silicate; intercalated nanocomposites (modeled in this paper) where the matrix material is inserted in the form of thin (a few nm) layers into the space between the parallel silicate layers of extremely small thickness ($\sim 1\text{nm}$); completely exfoliated or delaminated nanocomposites where the individual silicate platelets of 1nm thickness are randomly dispersed in a continuous polymer matrix (see e.g. Usuki *et al.*, 1993). Although, of course, it is possible that some portion of nanocomposites forms the exfoliation morphology and the other remains the intercalation morphology (see Koo *et al.*, 2003). Layered silicate based polymer nanocomposites have gained significant technological interest because of the recent commercialization of nylon 6 and polypropylene based materials (see e.g. Krishnamoorti and Yurekli, 2001; Kiersnowski and Piglowski, 2004). Generally, exfoliated nanocomposites demonstrate better properties than intercalated ones at the same nanoplate concentration. Completely exfoliated nanocomposites were intensively analyzed in the framework of conventional micromechanics by the Mori and Tanaka (1973) method (MTM, see Hui and Shia, 1998; Masenelly-Varlot *et al.*, 2002; Wang and Pyrz, 2004), by Halpin-Tsai (see Halpin and Cardos, 1976) equation (Brune and Bicerano, 2002), by the generalized Takayanagi's model method taking the interphase properties into account (see Ji, 2002). However, exfoliation of layered minerals is seriously hampered by the fact that sheet-like materials exhibit a strong tendency to agglomeration due to their big contact surfaces. So, the ratios surface to volume increase much steeper with respect to the aspect ratios for sheets compared to rods (see e.g. Fisher, 2003). Single clay layers were proposed to be an ideal reinforcing agent due to their extremely small aspect ratio ($\alpha = 0.001 - 0.01$), the nanometer filler thickness being comparable to the scale of the polymer chain structure, as well as to their high stiffness ($200 - 400\text{GPa}$). A doubling of the tensile modulus and strength is achieved, and the heat distortion temperature increases by 100°C for nylon-layered silicate nanocomposites containing as little as 2% vol. nanoplates. Polymer/clay nanocomposites Most notable are also the enhancements of other unexpected physical properties including barrier, flammability resistance, ablation performance, atomic oxygen resistance, and impact strength (see for references Lincoln *et al.*, 2001; Ray and Okamoto, 2003; Sheng *et al.*, 2004), which occur with only a few percent addition of nanoplates leading to reduced price in term of filler concentration and retention of polymeric processability. There are already existing applications of such nanocomposites, and many appealing expectations regarding their potential. A small aspect ratio of nanoplates provides a ultra-large interfacial area between the constituents ($\sim 750\text{m}^2$ per gram of silicate material) and a small distance between the nanoelements approaching molecular dimensions such that for a system comprising of 1nm thick plates, the distance between plates (considered as discs with a diameter $1\mu\text{m}$) approaches 10nm at only 7 vol. % of plates (see Vaia and Krishnamoorti, 2002; Vaia and Lincoln, 2002). Due to the high surface area and small inter-layer distances, the silicate platelets can, in principle, change the properties of polymer matrix due to the changing of polymer morphology and chain conformation. So Vaia and Giannelis (2001) emphasized that the presence of many chains at interfaces means that much of the polymer is really 'interphase-like' instead of having bulk-like properties that modify the thermodynamics of polymer chain conformations and kinetics of chain motion. Thus, many mechanical, physical, and chemical factors could potentially formate the properties of nanocomposites, and the better understanding of their relative contributions is needed. A fundamental question is whether we consider the properties of each phase the same as in the absent of another phases and, therefore pure mechanical interaction between the phases is assumed, or whether one has to account

for physical and chemical effects the filler has on the matrix. In principle, comparison of observed experimental and predicted modeling behaviors allows for answering on this question that the nanocomposite properties are due to changes in the polymer matrix induced by the nanoelements or not. A question of a correct choice of a micromechanical model applicable to nanocomposites presents many challenges for mechanics and will be considered in this paper from the point of view of allowing for the clustering effect in the clay nanocomposites.

Even though the different fractal descriptors are used for the identification of clustered structures, it is not sufficient to predict the overall properties of composites due to a few reasons. The first one is that these parameters do not complete enough for the characterization of the micromorphology of fillers simple because one can present other morphology with the same descriptors. More informative characteristics of the random configurations use statistical second-order quantities which examine the association fillers relative to other particle in an immediate local neighborhood of the reference filler. Other one that is that the prediction of mechanical properties requires one or another micromechanical model. Bruce and Bicerano (2002), as well as Sheng *et al.* (2004) (see also Kornmann, 2001) have emphasized that the notions of the matrix and inclusions widely used in conventional micromechanics can no longer be directly applied to nanoclay composites due to the hierarchical structure of clusters which, nevertheless, can be treated as a sort of equivalent (on effective) inhomogeneities embedded, in turn, in the bulk matrix material. Description of the composite cluster structure as well as a micromechanical modeling are significantly simplified in the case of clusters of a deterministic structure. In the most part such the clusters (called then the clusters of periodic structure) can be described as “cutted-out” from the infinite periodic media. A popular micromechanical modeling can be conditionally described by two limiting kinds of approaches both of them are based on the concept of effective properties of clusters. In the first case the effective properties of a cluster are estimated for the infinite periodic media (as well as for the infinite statistically homogeneous media) from which a cluster was mentally “cutted-out”. The effective properties of the layered clusters were estimated by Halpin-Tsai equation (see Halpin and Kardos, 1976; Brune and Bicerano, 2002) and by Mori and Tanaka (1993) method (MTM, see Wang and Pyrz, 2004b). Among the related approaches concerned with the conventional clustered random structure composites, it might be well to point out the analysis of clustered fiber composites by Bhattacharyya and Lagoudas (2000) by the MTM (see also analysis of nanofiber composites by Shi *et al.*, 2004). In the second sort of approaches based on the “cutted-out” of a cluster, the effective elastic properties of a cluster extracted from the composite is estimated through the equalization of the strain energy function at the set of inclusions combining the cluster to the potential energy stored in a homogeneous area with effective properties and the sizes of the cluster. It should be mentioned that the choice of the area referred as a cluster and “cutted-out” from the composite for the forthcoming analysis by one or another micromechanical method is not unique and defined by a subjective partiality of a researcher. So, in both papers by Luo and Daniel (2003) and by Sheng *et al.* (2004), the silicate aligned clusters in nanocomposites of random structure were modeled in the framework of laminated theory (see e.g. Cristensen, 1979) as the laminated structures containing n silicate plates with the thickness d_s separated by the matrix layer of the thickness d . However, Luo and Daniel (2003) estimated the effective properties of a cluster bounded by two matrix layers $d/2$ in thick that with necessity leads to an invariance of the cluster effective moduli on the

layer number n . Sheng *et al.* (2004) (see also Brune and Bicerano, 2002) have proposed an alternative cluster bounded by two silicate plates that yields the dependence of the cluster effective moduli on n simply because the volume concentration of silica in such a cluster is not a constant $d/(d + d_s)$ as in the model by Luo and Daniel (2003) but varies from $2d/(2d + d_s)$ at $n = 2$ till $d/(d + d_s)$ at $n = \infty$.

The modeling and simulation of random nano- and micro-structures are becoming more and more ambitious due to the advances in modern computer software and hardware (see Buryachenko, 2004). In so doing, the combination of computational micromechanics with analytical micromechanics seems to be very promising because it allows for exploring the most powerful features of the both mentioned groups of methods. The so-called numerical MEFM presents a universally rigorous scheme of both analyses of the microstructures and prediction of macroscopic properties and the statistical distributions of the local stress fields. One of the main advantages of the MEFM is in an efficient calculation of the general integral equations, which allows for hierarchical improvement of the method. Numerical solutions can be used to construct concentration factors for single and a finite number of interacting clustered inclusions in the infinite matrix, which then can be incorporated into the general framework of analytical micromechanics (such as e.g. the MEFM). In this light, the method of solution of a finite number of interacting spheroidal inclusions developed one from the authors (see Kushch, 1996, 1997, 1998a,b) and based on the multipole expansion technique is best suited for incorporation into the numerical MEFM. The basic idea of method consists in expansion the displacement vector into a series over the set of vectorial functions satisfying the governing equations of elastic equilibrium. The re-expansion formulae derived for these functions provide exact satisfaction of the interfacial boundary conditions. Incorporation of the multipole expansion technique into the MEFM in this paper will make possible to abandon from the majority of simplified assumptions exploring at the analysis of random structure composites reinforced by the clusters of deterministic structure.

However, the mechanical and thermal properties of nanoelements have not often been measured due to the difficulties of creating homogeneous and uniform samples subjected to homogeneous loading. As a result, it is desirable to develop the model forming the mechanical properties of nanoelements over their unique topology that may overcome the limitations of atomistic simulation concerning the wide range of length scale (10^{-9} - 10^{-6} m). Unlike many other fields in science and engineering, the evolution of NT to its current level significantly depends on the contributions from modeling and simulation (see e.g. Thostenson, *et al.* 2001; Qian, *et al.* 2002; Zhang, *et al.* 2002; Friesecke and James, 2000; Odegard, *et al.* 2003). Computational approaches, based on the molecular dynamic (MD) approach, are currently limited to nanoscale and cannot deal with the micro-length scales which should be analyzed by a continuum mechanics approach. These studies rely on fitting of atomistic simulation results to determine the important elastic parameters such as elastic moduli that implicitly assumes a local nature of constitutive law of continuum mechanics at the nanoscale based, in turn, on the assumption that a field scale (internal stress inhomogeneity) infinitely exceeds a material scale (molecular inhomogeneity) (see the papers mentioned above). In the case of comparable scales of a molecular scale of analyzed structures and the scale of inhomogeneity of internal stresses, that with necessity yields nonlocal character of the constitutive law in the area of coupling of the mentioned scales, this popular basic assumption acting as a bridge between nano- and micromechanics can be considered as an approximation of the real nonlocal constitutive law (see e.g.

Buryachenko, 2001). The most challenging issue of nanotechnology (see Ghoneim, 2003; Buryachenko, 2004) is how mechanics can contribute to our understanding of the bridging mechanism between the coupled scales, which is described by the nonlocal constitutive equations involving the parameters of a relevant effective nonlocal operator with the nanostructure. However, a creation of such the bridging mechanism is beyond the scope of the current work and will be concerned with the forthcoming publications. In this paper only continuum mechanics approach will be explored with known thermoelastic properties of constituent phases.

The present analysis should be make it clear that micromechanical modeling based on continuum mechanics must be used with caution for nanocomposites. The goal of this paper is to better understand the origin of the reinforcing efficiency of clustered nanocomposites. Due to their relative simplicity and instantaneosity, the micromechanical model proposed provides the ability to evaluate the key factors controlling the effective elastic behavior, and to explore large design spaces. The model accounting for the existence of both exfoliation and intercalation explains the reduction of the reinforcement efficiency of clay nano plates as a result of the incomplete exfoliation (or clustering). Detailed parametric analyses demonstrate the influence on the effective elastic moduli and stress concentrator factors of such the key factors as: a shape of nanoelements, interlayer distance, and the number of nanoelements in the stacks of deterministic structure.

2.5.2 Preliminaries

Basic equations

Let a linear elastic body occupy an open bounded domain $w \subset R^3$ with a smooth boundary Γ and with a characteristic function W . The domain w contains a homogeneous matrix $v^{(0)}$ and a statistically homogeneous set $X = (\Omega_i)$ of clusters Ω_i with characteristic functions V_i and bounded by the closed smooth surfaces Γ_i ($i = 1, 2, \dots$). It is assumed that the clusters can be grouped into components (phases) $\Omega^{(k)}$ ($k = 1, 2, \dots, N$) with identical mechanical and geometrical properties (such as the shape, size, orientation, and microstructure of clusters). At first no restrictions are imposed on the elastic symmetry of the phases or on the geometry of the clusters. The local strain tensor $\boldsymbol{\varepsilon}$ is related to the displacements \mathbf{u} via the linearized strain–displacement equation

$$\boldsymbol{\varepsilon} = \frac{1}{2}[\nabla \otimes \mathbf{u} + (\nabla \otimes \mathbf{u})^\top]. \quad (2.446)$$

Here \otimes denotes tensor product, and $(\cdot)^\top$ denotes matrix transposition. The stress tensor, $\boldsymbol{\sigma}$, satisfies the equilibrium equation (no body force acting):

$$\nabla \cdot \boldsymbol{\sigma} = \mathbf{0}. \quad (2.447)$$

Stresses and strains are related to each other via the constitutive equations

$$\boldsymbol{\sigma}(\mathbf{x}) = \mathbf{L}(\mathbf{x})\boldsymbol{\varepsilon}(\mathbf{x}) + \boldsymbol{\alpha}(\mathbf{x}) \text{ or } \boldsymbol{\varepsilon}(\mathbf{x}) = \mathbf{M}(\mathbf{x})\boldsymbol{\sigma}(\mathbf{x}) + \boldsymbol{\beta}(\mathbf{x}), \quad (2.448)$$

where $\mathbf{L}(\mathbf{x})$ and $\mathbf{M}(\mathbf{x}) \equiv \mathbf{L}(\mathbf{x})^{-1}$ are the known phase stiffness and compliance fourth-order tensors, and the common notation for contracted products has been employed: $\mathbf{L}\boldsymbol{\varepsilon} = L_{ijkl}\varepsilon_{kl}$. $\boldsymbol{\beta}(\mathbf{x})$ and $\boldsymbol{\alpha}(\mathbf{x}) \equiv -\mathbf{L}(\mathbf{x})\boldsymbol{\beta}(\mathbf{x})$ are second-order tensors of local eigenstrains

and eigenstresses. In particular, for isotropic constituents the local stiffness tensor $\mathbf{L}(\mathbf{x})$ is given in terms of the local bulk modulus $k(\mathbf{x})$ and the local shear modulus $\mu(\mathbf{x})$, and the local eigenstrain $\boldsymbol{\beta}(\mathbf{x})$ is given in terms of the bulk component $\beta_0(\mathbf{x})$ by the relations:

$$\mathbf{L}(\mathbf{x}) = (3k, 2\mu) \equiv 3k(\mathbf{x})\mathbf{N}^1 + 2\mu(\mathbf{x})\mathbf{N}^2, \quad \boldsymbol{\beta}(\mathbf{x}) = \beta_0(\mathbf{x})\boldsymbol{\delta}, \quad (2.449)$$

$\mathbf{N}_1 = \boldsymbol{\delta} \otimes \boldsymbol{\delta}/d$, $\mathbf{N}_2 = \mathbf{I} - \mathbf{N}_1$; $\boldsymbol{\delta}$ and \mathbf{I} are the unit second-order and fourth-order tensors. By virtue of the isotropic elastic moduli (2.449), we arrive at the Navier equation

$$\nabla \cdot \boldsymbol{\sigma} = (1 - 2\nu) \Delta \mathbf{u} + \nabla (\nabla \cdot \mathbf{u}) = \mathbf{0}, \quad (2.450)$$

where $\nu = (3k - 2\mu)/(6k + 2\mu)$ is a Poisson ratio. All tensors \mathbf{f} ($\mathbf{f} = \mathbf{L}, \mathbf{M}, \boldsymbol{\alpha}, \boldsymbol{\beta}$) of material properties are decomposed as $\mathbf{f} \equiv \mathbf{f}^{(0)} + \mathbf{f}_1(\mathbf{x}) = \mathbf{f}^{(0)} + \mathbf{f}_1^{(m)}(\mathbf{x})$. Here and in the following, the upper index $^{(m)}$ indicates the components and the lower index i indicates the individual cluster; $v^{(0)} = w \setminus v$, $v \equiv \cup \Omega^{(k)} \equiv \cup \Omega_i$, $V(\mathbf{x}) = \sum V^{(k)} = \sum V_i(\mathbf{x})$, and $V^{(k)}(\mathbf{x})$ is a characteristic function of $\Omega^{(k)}$ equals 1 at $\mathbf{x} \in \Omega^{(k)}$ and 0 otherwise, ($m = 0, k; k = 1, 2, \dots, N; i = 1, 2, \dots$).

It is assumed that each cluster of the component k has a deterministic identical structure meaning that in the local coordinate system $\mathbf{e}_l^{(k)}$ ($l = 1, 2, 3$) connected with the each cluster $\Omega_i \subset \Omega^{(k)}$ the geometrical and mechanical properties of inclusions embedded in this cluster are identical. In this local coordinate system $\mathbf{e}_l^{(k)}$ the inclusions $v_j \subset \Omega^{(k)}$ ($j = 1, \dots, n^{\Omega^{(k)}} k = 1, \dots, N$) with characteristic functions V_j^v and mechanical properties $\mathbf{f}_j^{v(k)}(\mathbf{z})$ ($\mathbf{f} = \mathbf{L}, \mathbf{M}, \boldsymbol{\alpha}, \boldsymbol{\beta}$) have the centers \mathbf{z}_j .

We assume that the phases (the inclusions and matrix) are perfectly bonded, so that the displacements and the traction components are continuous across the interphase boundaries, i.e.

$$[[\boldsymbol{\sigma}\mathbf{n}]] = \mathbf{0}, \quad [[\mathbf{u}]] = \mathbf{0} \quad (2.451)$$

on the interface boundary Γ^{int} where \mathbf{n} is the normal vector on Γ^{int} and $[[(\cdot)]]$ is a jump operator. The traction

$$\mathbf{t}(\mathbf{x}) = \boldsymbol{\sigma}(\mathbf{x})\mathbf{n}(\mathbf{x}) = [\mathbf{L}(\mathbf{x})\boldsymbol{\varepsilon}(\mathbf{x}) + \boldsymbol{\alpha}(\mathbf{x})]\mathbf{n}(\mathbf{x}) \quad (2.452)$$

acting on any plane with the normal $\mathbf{n}(\mathbf{x})$ through the point \mathbf{x} can be represented in terms of displacements $\mathbf{t}(\mathbf{x}) = \hat{\mathbf{t}}(\mathbf{n}, \nabla)\mathbf{u}(\mathbf{x}) + \boldsymbol{\alpha}(\mathbf{x})\mathbf{n}$, where $\hat{t}_{ik}(\mathbf{n}, \nabla) = L_{ijkl}n_j(\mathbf{x})\partial/\partial x_l$. is the so-called "stress operator." The boundary conditions at the interface boundary will be considered together with one from the homogeneous boundary conditions on Γ with the unit outward normal \mathbf{n}^Γ

$$\mathbf{u}(\mathbf{x}) = \boldsymbol{\varepsilon}^\Gamma \mathbf{x}, \quad \boldsymbol{\varepsilon}^\Gamma(\mathbf{x}) \equiv \text{const.}, \quad \mathbf{x} \in \Gamma, \quad (2.453)$$

$$\mathbf{t}^\Gamma(\mathbf{x}) \equiv \boldsymbol{\sigma}^\Gamma(\mathbf{x})\mathbf{n}^\Gamma(\mathbf{x}), \quad \boldsymbol{\sigma}^\Gamma(\mathbf{x}) = \text{const.}, \quad \mathbf{x} \in \Gamma. \quad (2.454)$$

where $\boldsymbol{\varepsilon}^\Gamma(\mathbf{x}) = \frac{1}{2}[\nabla \otimes \mathbf{u}^\Gamma(\mathbf{x}) + (\nabla \otimes \mathbf{u}^\Gamma(\mathbf{x}))^\top]$, $\mathbf{x} \in \Gamma$. We will consider the interior problem when the body occupies the interior domain with respect to Γ .

Statistical description of the composite microstructure

It is assumed that the representative mesodomain w contains N sorts of statistically large number of clusters $\Omega_i \subset \Omega^{(k)}$ ($i = 1, 2, \dots; k = 1, 2, \dots, N$) with characteristic functions

$V_i(\mathbf{x})$ described by the statistically homogeneous random field. All the random quantities under discussion are statistically homogeneous and, hence, the ensemble averaging could be replaced by volume averaging

$$\langle(\cdot)\rangle = \bar{w}^{-1} \int (\cdot) W(\mathbf{x}) d\mathbf{x}, \quad \langle(\cdot)\rangle^{(k)} = [\bar{\Omega}^{(k)}]^{-1} \int (\cdot) V^{(k)}(\mathbf{x}) d\mathbf{x}, \quad (2.455)$$

where $\sum V^{(k)} = \sum V_i \equiv V$, $k = 1, 2, \dots, N$; $i = 1, 2, \dots$. $V^{(k)}$ is the characteristic functions of $\Omega^{(k)}$. The bar appearing above the region represents its measure, e.g. $\bar{\Omega}_1 \equiv \text{mes } \Omega_1$. The average over component $\Omega^{(k)}$ agrees with the ensemble average over an individual cluster $\Omega_i \in \Omega^{(k)}$ ($i = 1, 2, \dots$): $\langle(\cdot)\rangle_i = \langle(\cdot)\rangle^{(k)}$; the notation $\langle(\cdot)\rangle_i(\mathbf{x})$ at $\mathbf{x} \in \Omega_i \subset \Omega^k$ means the average over an ensemble realization of surrounding clusters (but not over the volume Ω_i of a particular cluster, in contrast to $\langle(\cdot)\rangle_{(i)}$).

For the description of the random structure of a composite material let us introduce a conditional probability density $\varphi(\Omega_i, \mathbf{x}_i | \Omega_1, \mathbf{x}_1, \dots, \Omega_n, \mathbf{x}_n)$, which is a probability density to find the i -th cluster with the center \mathbf{x}_i in the domain Ω_i with fixed clusters $\Omega_1, \dots, \Omega_n$ with the centers $\mathbf{x}_1, \dots, \mathbf{x}_n$. The notation

$\varphi(\Omega_i, \mathbf{x}_i | \Omega_1, \mathbf{x}_1, \dots, \Omega_n, \mathbf{x}_n)$ denotes the case $\mathbf{x}_i \neq \mathbf{x}_1, \dots, \mathbf{x}_n$. Of course, $\varphi(\Omega_i, \mathbf{x}_i | \Omega_1, \mathbf{x}_1, \dots, \Omega_n, \mathbf{x}_n) = 0$ for values of \mathbf{x}_i lying inside the "included volumes" $\cup \Omega_{im}^0$ ($m = 1, \dots, n$), where $\Omega_{im}^0 \supset \Omega_m$ with characteristic functions Ω_{0m} (since inclusions cannot overlap), and $\varphi(\Omega_i, \mathbf{x}_i | \Omega_1, \mathbf{x}_1, \dots, \Omega_n, \mathbf{x}_n) \rightarrow \varphi(\Omega_i, \mathbf{x}_i)$ at $|\mathbf{x}_i - \mathbf{x}_m| \rightarrow \infty$, $m = 1, \dots, n$ (since no long-range order is assumed). For the sake of simplicity of forthcoming calculations we will assume the hypothesis

$$\varphi(v_q, \mathbf{x}_q | v_i, \mathbf{x}_i) = h_2(\rho), \quad \rho \equiv |(\mathbf{a}_i^0)^{-1}(\mathbf{x}_j - \mathbf{x}_i)| \quad (2.456)$$

where $(\mathbf{a}_i^0)^{-1}$ identifies a matrix of affine transformation which transfers Ω_{ij}^0 being the ellipsoidal "included volume" ("correlation hole") into a unit sphere. In so doing, the shape of "correlation hole" Ω_{ij}^0 does not depend on the inclusion Ω_j : $\Omega_{ij}^0 = \Omega_i^0$. For spherical inclusions the relation (2.455) is realized for a statistical isotropy of the composite structure. Only if the pair distribution function $g(\mathbf{x}_i - \mathbf{x}_m) \equiv \varphi(\Omega_i, \mathbf{x}_i | \Omega_m, \mathbf{x}_m) / n^{(k)}$ depends on $|\mathbf{x}_m - \mathbf{x}_i|$ it is called the radial distribution function. $\varphi(\Omega_i)$ is a number density $n^{(k)}$ of clusters of the kind $\Omega^{(k)} \ni \Omega_i$ and $c^{(k)}$ is the concentration, i.e. volume fraction, of the clusters $\Omega^{(k)}$: $c^{(k)} = \langle V^{(k)}(\mathbf{x}) \rangle = \bar{\Omega}_i n^{(k)}$ ($k = 1, 2, \dots, N$; $i = 1, 2, \dots$), $c^{(0)} = 1 - \langle V \rangle$. Hereinafter we will use the notations $\langle(\cdot)\rangle(\mathbf{x})$ and $\langle(\cdot) | \Omega_1, \mathbf{x}_1; \dots; \Omega_n, \mathbf{x}_n \rangle(\mathbf{x})$ for the average and for the conditional average taken for the ensemble of a statistically homogeneous field $X = (\Omega_i)$ at the point \mathbf{x} , on the condition that there are clusters at the points $\mathbf{x}_1, \dots, \mathbf{x}_n$ and $\mathbf{x}_1 \neq \dots \neq \mathbf{x}_n$. Similarly, $V(\mathbf{x} | \Omega_1, \mathbf{x}_1; \dots; \Omega_n, \mathbf{x}_n)$ is a random characteristic function of clusters $\mathbf{x} \in v$ under the condition that $\Omega_1 \neq \dots \neq \Omega_n$. The notations $\langle(\cdot) | \Omega_1, \mathbf{x}_1; \dots; \Omega_n, \mathbf{x}_n \rangle(\mathbf{x})$ and $V(\mathbf{x} | \Omega_1, \mathbf{x}_1; \dots; \Omega_n, \mathbf{x}_n)$ are used for the case $\mathbf{x} \notin \Omega_1, \dots, \Omega_n$. The notation for the conditional probability density $\varphi(\Omega_i, \mathbf{x}_i | \Omega_1, \mathbf{x}_1, \dots, \Omega_n, \mathbf{x}_n; \mathbf{x}_0)$ is considered under the condition that the inclusions $\Omega_1, \dots, \Omega_n$ are located at the points $\mathbf{x}_1, \dots, \mathbf{x}_n$, whereas the matrix position is denoted by \mathbf{x}_0 .

Effective fields and statistical averages

A general integral equation describing the stress field in random structure composites is known (see for references e.g. Buryachenko, 2001)

$$\boldsymbol{\sigma}(\mathbf{x}) = \langle \boldsymbol{\sigma} \rangle(\mathbf{x}) + \int \boldsymbol{\Gamma}(\mathbf{x} - \mathbf{y}) \{ \boldsymbol{\eta}(\mathbf{y}) - \langle \boldsymbol{\eta} \rangle(\mathbf{y}) \} d\mathbf{y}. \quad (2.457)$$

where we define the tensor $\boldsymbol{\eta}(\mathbf{y}) = \mathbf{M}_1(\mathbf{y})\boldsymbol{\sigma}(\mathbf{y}) + \boldsymbol{\beta}_1(\mathbf{y})$ called the strain polarization tensor which is simply a notational convenience. The kernel, $\boldsymbol{\Gamma}(\mathbf{x}-\mathbf{y}) \equiv -\mathbf{L}^{(0)} [\mathbf{I}\delta(\mathbf{x}-\mathbf{y}) + \mathbf{U}(\mathbf{x}-\mathbf{y})\mathbf{L}^{(0)}]$ called the Green stress tensor is defined by the second derivative \mathbf{U} of the infinite-homogeneous-body Green's function \mathbf{G} of the Navier' equation with an elastic modulus tensor $\mathbf{L}^{(0)}$: $\nabla\{\mathbf{L}^{(0)}\frac{1}{2}[\nabla \otimes \mathbf{G}(\mathbf{x}) + (\nabla \otimes \mathbf{G}(\mathbf{x}))^\top]\} = -\boldsymbol{\delta}\delta(\mathbf{x})$, vanishing at infinity ($|\mathbf{x}| \rightarrow \infty$), $\delta(\mathbf{x})$ is the Dirac delta function.

Let the clusters $\Omega_1, \dots, \Omega_n$ be fixed and we define two sorts of effective fields $\bar{\boldsymbol{\sigma}}_i(\mathbf{x})$ and $\tilde{\boldsymbol{\sigma}}_{1,\dots,n}(\mathbf{x})$ ($i = 1, \dots, n$; $\mathbf{x} \in \Omega_1, \dots, \Omega_n$) by the use of the rearrangement of Eq. (2.457) in the following form [see Buryachenko (2001) for the earliest references of related manipulations]

$$\boldsymbol{\sigma}(\mathbf{x}) = \bar{\boldsymbol{\sigma}}_i(\mathbf{x}) + \int \boldsymbol{\Gamma}(\mathbf{x}-\mathbf{y})V_i(\mathbf{y})\boldsymbol{\eta}(\mathbf{y})d\mathbf{y}, \quad (2.458)$$

$$\bar{\boldsymbol{\sigma}}_i(\mathbf{x}) = \tilde{\boldsymbol{\sigma}}_{1,\dots,n}(\mathbf{x}) + \sum_{j \neq i} \int \boldsymbol{\Gamma}(\mathbf{x}-\mathbf{y})V_j(\mathbf{y})\boldsymbol{\eta}(\mathbf{y})d\mathbf{y}, \quad (2.459)$$

$$\begin{aligned} \tilde{\boldsymbol{\sigma}}_{1,\dots,n}(\mathbf{x}) &= \langle \boldsymbol{\sigma} \rangle(\mathbf{x}) \\ &+ \int \boldsymbol{\Gamma}(\mathbf{x}-\mathbf{y})\{\boldsymbol{\eta}(\mathbf{y})V(\mathbf{y}); \Omega_1, \mathbf{x}_1; \dots; \Omega_n, \mathbf{x}_n\} - \langle \boldsymbol{\eta} \rangle(\mathbf{y})\}d\mathbf{y}, \end{aligned} \quad (2.460)$$

for $\mathbf{x} \in \Omega_i$, $i = 1, 2, \dots, n$. Then, considering some conditional statistical averages of the general integral equation (2.457) leads to an infinite system of integral equations ($n = 1, 2, \dots$)

$$\begin{aligned} \langle \boldsymbol{\sigma} | \Omega_1, \mathbf{x}_1; \dots; \Omega_n, \mathbf{x}_n \rangle(\mathbf{x}) &- \sum_{i=1}^n \int \boldsymbol{\Gamma}(\mathbf{x}-\mathbf{y})\langle V_i(\mathbf{y})\boldsymbol{\eta} | \Omega_1, \mathbf{x}_1; \dots; \Omega_n, \mathbf{x}_n \rangle(\mathbf{y})d\mathbf{y} \\ &= \langle \boldsymbol{\sigma} \rangle(\mathbf{x}) + \int \boldsymbol{\Gamma}(\mathbf{x}-\mathbf{y})\{\langle \boldsymbol{\eta} | \Omega_1, \mathbf{x}_1; \dots; \Omega_n, \mathbf{x}_n \rangle(\mathbf{y}) - \langle \boldsymbol{\eta} \rangle(\mathbf{y})\}d\mathbf{y}, \end{aligned} \quad (2.461)$$

where $\mathbf{x} \in \Omega_1, \dots, \Omega_n$ in the n-th line of the system.

The definitions of the effective fields $\bar{\boldsymbol{\sigma}}_i(\mathbf{x})$, $\tilde{\boldsymbol{\sigma}}_{1,2,\dots,n}(\mathbf{x})$ as well as their statistical averages $\langle \bar{\boldsymbol{\sigma}}_i \rangle(\mathbf{x})$, $\langle \tilde{\boldsymbol{\sigma}}_{1,2,\dots,n} \rangle(\mathbf{x})$ are nothing more than notation convenience for different terms of the infinite systems (2.461).

2.5.3 Approximate and closure effective field hypotheses

In order to simplify the exact system (2.458) we now apply the main hypothesis of many micromechanical methods, the approximation called the effective field hypothesis:

H1) *Each cluster Ω_i has an ellipsoidal form and is located in the field (2.459)*

$$\bar{\boldsymbol{\sigma}}_i(\mathbf{y}) \equiv \bar{\boldsymbol{\sigma}}(\mathbf{x}_i) \quad (\mathbf{y} \in \Omega_i) \quad (2.462)$$

which is homogeneous over the cluster Ω_i , and the perturbation introduced by the cluster Ω_i at the point $\mathbf{y} \notin \Omega_i$ is defined by the relation

$$\int \boldsymbol{\Gamma}(\mathbf{y}-\mathbf{x})V_i(\mathbf{x})\boldsymbol{\eta}(\mathbf{x})d\mathbf{x} = \bar{\Omega}_i\mathbf{T}_i(\mathbf{y}-\mathbf{x}_i)\boldsymbol{\eta}_i. \quad (2.463)$$

Hereafter $\boldsymbol{\eta}_i \equiv \langle \boldsymbol{\eta}(\mathbf{x})V_i(\mathbf{x}) \rangle_{(i)}$ is an average over the volume of the cluster Ω_i (but not over the ensemble), $\langle (\cdot) \rangle_i \equiv \langle \langle (\cdot) \rangle_{(i)} \rangle$, and the tensors

$$\begin{aligned}\bar{\Omega}_i \mathbf{T}_i(\mathbf{y} - \mathbf{x}_i) &= \begin{cases} \int \Gamma(\mathbf{y} - \mathbf{x}) V_i(\mathbf{x}) d\mathbf{x} \equiv \mathbf{Q}_i & \text{for } \mathbf{y} \in \Omega_i \\ \int \Gamma(\mathbf{y} - \mathbf{x}) V_i(\mathbf{x}) d\mathbf{x} \equiv \mathbf{0} & \text{otherwise} \end{cases}, \\ \mathbf{T}_{ij}(\mathbf{x}_i - \mathbf{x}_j) &= \langle \mathbf{T}_i(\mathbf{z} - \mathbf{x}_i) \rangle_j\end{aligned}\quad (2.464)$$

($\mathbf{z} \in \Omega_j \neq \Omega_i$) have analytical representations for spherical inclusions in an isotropic matrix (see for reference Buryachenko, 2001). The tensor \mathbf{Q}_i is associated with the well-known Eshelby tensor by $\mathbf{S}_i = \mathbf{I} - \mathbf{M}^{(0)} \mathbf{Q}_i$.

For the termination of the hierarchy of statistical moment equations (2.461) we will use the closure effective field hypothesis:

H2) For a sufficiently large n , we complete the system (2.461) by the assumption $\langle \tilde{\boldsymbol{\sigma}}_{1,\dots,j,\dots,n+1}(\mathbf{x}) \rangle_i = \langle \tilde{\boldsymbol{\sigma}}_{1,\dots,n}(\mathbf{x}) \rangle_i$, where the right-hand-side of the equality does not contain the index $j \neq i$ ($i = 1, \dots, n$; $j = 1, \dots, n+1$; $\mathbf{x} \in \Omega_i$).

The fundamental differences of the hypothesis **H2** and “quasi-crystalline” approximation by Lax (1952)

$$\langle \bar{\boldsymbol{\sigma}}_i(\mathbf{x}) | \Omega_i, \mathbf{x}_i; \Omega_j, \mathbf{x}_j \rangle = \langle \bar{\boldsymbol{\sigma}}_i \rangle, \quad \mathbf{x} \in \Omega_i \quad (2.465)$$

as well as of the assumptions (2.462) and (2.463) were discussed by Buryachenko (2001).

According to hypothesis **H1** and in view of the linearity of the problem there exist constant fourth and second-rank tensors $\mathbf{B}_i(\mathbf{x})$, $\mathbf{R}_i(\mathbf{x})$ and $\mathbf{C}_i(\mathbf{x})$, $\mathbf{F}_i(\mathbf{x})$, such that

$$\boldsymbol{\sigma}(\mathbf{x}) = \mathbf{B}_i(\mathbf{x}) \bar{\boldsymbol{\sigma}}(\mathbf{x}_i) + \mathbf{C}_i(\mathbf{x}), \quad \bar{\Omega}_i \boldsymbol{\eta}(\mathbf{x}) = \mathbf{R}_i(\mathbf{x}) \bar{\boldsymbol{\sigma}}(\mathbf{x}_i) + \mathbf{F}_i(\mathbf{x}), \quad \mathbf{x} \in \Omega_i, \quad (2.466)$$

where $\Omega_i \subset \Omega^{(i)}$ and $\mathbf{R}_i(\mathbf{x}) = \bar{\Omega}_i \mathbf{M}_1^{(i)}(\mathbf{x}) \mathbf{B}_i(\mathbf{x})$, $\mathbf{F}_i(\mathbf{x}) = \bar{\Omega}_i [\mathbf{M}_1^{(i)}(\mathbf{x}) \mathbf{C}_i(\mathbf{x}) + \boldsymbol{\beta}_1(\mathbf{x})]$. According to Eshelby’s (1957) theorem there are the following relations between the averaged tensors (2.466) $\mathbf{R}_i = \bar{\Omega}_i \mathbf{Q}_i^{-1} (\mathbf{I} - \mathbf{B}_i)$, $\mathbf{F}_i = -\bar{\Omega}_i \mathbf{Q}_i^{-1} \mathbf{C}_i$, where the notation of a material tensor \mathbf{f}_i without argument \mathbf{x} stands their average over the volume of the cluster Ω_i : $\mathbf{f}_i \equiv \langle \mathbf{f}(\mathbf{x}) \rangle_{(i)}$ (\mathbf{f} stands for $\mathbf{B}, \mathbf{C}, \mathbf{R}, \mathbf{F}$). In parallel with the notation of the average material tensor \mathbf{f}_i over the cluster Ω_i we will also use the notation $\underline{\mathbf{f}}^{(i)}$ underlining that the average is carried out over i th sort of clusters $\Omega^{(i)}$ also these averages coincide for $\Omega_i \subset \Omega^{(i)}$. It should be mentioned that the field $\bar{\boldsymbol{\sigma}}(\mathbf{x}_i)$ can vary with the location of the center \mathbf{x}_i of the cluster considered, but the field $\bar{\boldsymbol{\sigma}}(\mathbf{y})$ ($\mathbf{y} \in \Omega_i$) is homogeneous over the cluster Ω_i . Because of this the application of Eshelby’s theorem is correct.

It should be mentioned that for clustered materials being considered $\mathbf{R}_k(\mathbf{x})$, $\mathbf{F}_k(\mathbf{x}) \equiv \mathbf{0}$ for the matrix’s part of the cluster $\mathbf{x} \in \Omega^{(k)} \setminus \cup_j v_j$ ($j = 1, \dots, n^{\Omega(k)}$; $k = 1, \dots, N$). Therefore,

$$\mathbf{R}^{(k)} = \sum_{j=1}^{n^{\Omega(k)}} \int_{v_j} \mathbf{M}_{j1}^{v(k)}(\mathbf{x}) \mathbf{B}_j^{v(k)}(\mathbf{x}) d\mathbf{x}, \quad (2.467)$$

$$\mathbf{F}^{(k)} = \sum_{j=1}^{n^{\Omega(k)}} \int_{v_j} \left[\mathbf{M}_{j1}^{v(k)}(\mathbf{x}) \mathbf{C}_j^{v(k)}(\mathbf{x}) + \boldsymbol{\beta}_{j1}^{v(k)} \right] d\mathbf{x}, \quad (2.468)$$

where $\mathbf{f}^{(k)}(\mathbf{x}) = \mathbf{f}_j^{v(k)}(\mathbf{x})$ at $\mathbf{x} \in v_i \subset \Omega^{(k)}$. As can be seen from Eq. (2.467) and (2.468) the concentrator tensors $\mathbf{R}^{(k)}$ and $\mathbf{F}^{(k)}$ do not depend explicitly on the shape and the size of the cluster Ω_k but only on the geometrical and mechanical properties of inclusions v_j constituent the cluster Ω_k . This dependence becomes apparent thought the tensors

$\mathbf{B}_k(\mathbf{x})$ and $\mathbf{C}_k(\mathbf{x})$ describing the thermoelastic solution (considered in Section 6) for $n^{v(k)}$ interacting inclusions v_j ($j = 1, \dots, n^{\Omega(k)}$) inside infinite matrix subjected to the remote homogeneous loading $\bar{\boldsymbol{\sigma}}(\mathbf{x}_k)$. Therefore the tensors $\mathbf{B}_j^{v(k)}(\mathbf{x})$ and $\mathbf{C}_j^{v(k)}(\mathbf{x})$ depend on the mechanical and geometrical parameters of all inclusions v_j ($j = 1, \dots, n^{\Omega(k)}$) in the cluster Ω_k being considered.

For the particular case of the homogeneous ellipsoidal domain Ω_k with $\mathbf{M}_1(\mathbf{x}) = \mathbf{M}_1^{(k)} \equiv \text{const}$, $\boldsymbol{\beta}_1(\mathbf{x}) = \boldsymbol{\beta}_1^{(k)} \equiv \text{const}$, we have

$$\mathbf{R}_k = \bar{\Omega}_k \mathbf{M}_1^{(k)} (\mathbf{I} + \mathbf{Q}_k \mathbf{M}_1^{(k)})^{-1}, \quad \mathbf{F}_k = \bar{\Omega}_k (\mathbf{I} + \mathbf{M}_1^{(k)} \mathbf{Q}_k)^{-1} \boldsymbol{\beta}_1^{(k)}. \quad (2.469)$$

By comparison of relation (2.466) with (2.468), (2.469) we see that the average thermoelastic response (i.e. the tensors \mathbf{B} , \mathbf{C} , \mathbf{R} , \mathbf{F}) of any cluster is the same as that of some fictitious ellipsoidal homogeneous inclusion with thermoelastic parameters

$$\mathbf{M}_1^{f(k)} = \mathbf{R} (\mathbf{I} \bar{\Omega}_k - \mathbf{Q}_k \mathbf{R}_k)^{-1}, \quad \boldsymbol{\beta}_1^{f(k)} = \bar{\Omega}_k^{-1} (\mathbf{M}_1^{f(k)} \mathbf{Q}_k + \mathbf{I}) \mathbf{F}_k. \quad (2.470)$$

The parameters (2.470) of fictitious ellipsoidal inclusions are simply a notational convenience and explicitely depend on the volume $\bar{\Omega}_k$ of the cluster. No restrictions are imposed on the microtopology of the cluster as well as on the inhomogeneity of the stress state in the cluster. They were introduced only as a tribute to tradition (see Introduction) and can be used just for estimations of the tensors \mathbf{R}_k and \mathbf{F}_k by the use of the attached Eshelby' solution (2.469), although the tensors \mathbf{R}_k and \mathbf{F}_k used for introduction of the fictitious properties (2.470) must be previously evaluated by Eqs. (2.467) and (2.468) from the thermoelastic solution for a single cluster in the infinite matrix (see Section 6). As it will be demonstrated, the dependence of effective properties \mathbf{M}^* and $\boldsymbol{\beta}^*$ on the internal structure and mechanical properties of clusters take place only through the tensors \mathbf{R}_k and \mathbf{F}_k .

Using hypothesis **H1**, the system (2.459) for k fixed clusters with fixed values $\tilde{\boldsymbol{\sigma}}_{1,\dots,k}(\mathbf{x})$ ($\mathbf{x} \in \Omega_i$, $i = 1, \dots, k$) on the right-hand side of the equations becomes algebraic when the solution (2.466) for one inclusion in the field $\bar{\boldsymbol{\sigma}}(\mathbf{x}_i)$ ($i = 1, \dots, k$) is applied

$$\mathbf{R}_i \bar{\boldsymbol{\sigma}}(\mathbf{x}_i) + \mathbf{F}_i = \sum_{j=1}^k \mathbf{Z}_{ij} \left\{ \mathbf{R}_j \tilde{\boldsymbol{\sigma}}_{1,\dots,k}(\mathbf{x}_j) + \mathbf{F}_j \right\}, \quad (2.471)$$

where the matrix \mathbf{Z}^{-1} has the elements $(\mathbf{Z}^{-1})_{ij}$

$$(\mathbf{Z}^{-1})_{ij} = \mathbf{I} \delta_{ij} - (1 - \delta_{ij}) \mathbf{R}_j \mathbf{T}_{ij}(\mathbf{x}_i - \mathbf{x}_j), \quad (i, j = 1, \dots, n). \quad (2.472)$$

Averaging (2.461) over the volume of the considered inclusion v_i and using the hypothesis **H1** (2.463) lead to

$$\begin{aligned} & \langle \boldsymbol{\eta} | \Omega_1, \mathbf{x}_1; \dots; \Omega_n, \mathbf{x}_n \rangle(\mathbf{x}) - \mathbf{R}_i \sum_{j \neq i}^n \mathbf{T}_{ij}(\mathbf{x}_i - \mathbf{x}_j) \langle V_i(\mathbf{y}) \boldsymbol{\eta} | \Omega_1, \mathbf{x}_1; \dots; \Omega_n, \mathbf{x}_n \rangle_j \\ & = \boldsymbol{\eta}_i^0(\mathbf{x}_i) + \mathbf{R}_i \int \mathbf{T}_{iq}(\mathbf{x}_i - \mathbf{x}_q) \langle \boldsymbol{\eta} |; \Omega_1, \mathbf{x}_1; \dots; \Omega_n, \mathbf{x}_n \rangle_q - \mathbf{T}_i(\mathbf{x}_i - \mathbf{x}_q) \langle \boldsymbol{\eta} \rangle d\mathbf{x}_q, \end{aligned} \quad (2.473)$$

($n = 1, 2, \dots$; $i, j = 1, \dots, n$), where $\boldsymbol{\eta}_i^0 = \mathbf{R}_i \langle \boldsymbol{\sigma} \rangle + \mathbf{F}_i$.

2.5.4 Effective thermoelastic properties of clustered composites

General case of multicomponent clusters

In the framework of the hypothesis **H1**, substitution of the solution (2.466), and (2.471) (at $k = 2$) for binary interacting inclusions into the first equation of the system (2.473) at $n = 1$, and averaging the result obtained over the cluster Ω_i leads to the linear equation with respect to $\langle \bar{\sigma} \rangle_i$

$$\langle \bar{\sigma} \rangle_i = \mathbf{R}_i^{-1} \sum_{j=1}^N \{ \mathbf{Y}_{ij} \mathbf{R}_j \langle \sigma \rangle + (\mathbf{Y}_{ij} - \mathbf{I} \delta_{ij}) \mathbf{F}_j \} \quad (2.474)$$

from which the effective properties can be found

$$\mathbf{M}^* = \mathbf{M}^{(0)} + \sum_{i,j=1}^N \mathbf{Y}_{ij} \mathbf{R}_j n^{(i)}, \quad (2.475)$$

$$\boldsymbol{\beta}^* = \boldsymbol{\beta}^{(0)} + \sum_{i,j=1}^N \mathbf{Y}_{ij} \mathbf{F}_j n^{(i)}, \quad (2.476)$$

where the matrix \mathbf{Y}^{-1} with the following elements ($i, j = 1, 2, \dots, N$)

$$(\mathbf{Y}^{-1})_{ij} = \delta_{ij} \left[\mathbf{I} - \sum_{q=1}^N \int \mathcal{T}_{iq}(\mathbf{x}_i - \mathbf{x}_q) d\mathbf{x}_q \right] - \int \mathcal{F}_{ij}(\mathbf{x}_i - \mathbf{x}_j) d\mathbf{x}_j, \quad (2.477)$$

$$\mathcal{T}_{iq}(\mathbf{x}_i, \mathbf{x}_q) = \mathbf{R}_i \mathbf{T}_{iq}(\mathbf{x}_i - \mathbf{x}_q) \mathbf{Z}_{qi} \varphi(v_q, \mathbf{x}_q |; v_i, \mathbf{x}_i), \quad (2.478)$$

$$\mathcal{F}_{iq}(\mathbf{x}_i, \mathbf{x}_q) = \mathbf{R}_i \left[\mathbf{T}_{iq}(\mathbf{x}_i - \mathbf{x}_q) \mathbf{Z}_{qq} \varphi(v_q, \mathbf{x}_q |; v_i, \mathbf{x}_i) - \mathbf{T}_i(\mathbf{x}_i - \mathbf{x}_q) n^{(q)}(\mathbf{x}_q) \right] \quad (2.479)$$

determines the action of the surrounding inclusions on the isolated one and is defined simply by the solution of the problem for purely mechanical loading (with $\boldsymbol{\beta} \equiv 0$). Thus, the effective thermoelastic properties \mathbf{M}^* (2.478) and $\boldsymbol{\beta}^*$ (2.479) as well as the stress concentrator factor of the effective field (2.476) are defined by the average thermoelastic response inside the infinite matrix of the individual clusters describing by the tensor \mathbf{R}_i (2.467) and \mathbf{F}_i (2.468) rather than detailed stress distribution inside these clusters.

Particular case of one sort of clusters

A special particular case of one sort of clusters ($N = 1$) significantly simplifies the representations for the effective properties (2.475) and (2.476), and, moreover, makes possible to establish a unique relation between the effective parameters \mathbf{M}^* and $\boldsymbol{\beta}^*$ which is similar to the exact classical formula by Levin (1967) (see also Rosen and Hashin, 1970) for two phases composites and based only on the additional assumption **H1**). Indeed, the system (2.473) has principally the same structure as the system for the pure elastic problem (with $\mathbf{F} \equiv \mathbf{0}$). Therefore, we can apply the traditional analysis procedure of purely elastic composites and represent $\langle \boldsymbol{\eta} \rangle^{(1)}$ as a linear function of the external field $\boldsymbol{\eta}^0$

$$\langle \boldsymbol{\eta} \rangle^{(1)} = \mathbf{Y} \boldsymbol{\eta}^0 \quad (2.480)$$

and therefore

$$\mathbf{R} \langle \bar{\sigma} \rangle^{(1)} + \mathbf{F} = \mathbf{Y} (\mathbf{R} \boldsymbol{\sigma}^0 + \mathbf{F}). \quad (2.481)$$

The comparison of (2.473) with (2.480) leads to the fact that \mathbf{Y} only depends on the tensors \mathbf{R} , \mathbf{T}_{ij} and \mathbf{T}_j . The tensor \mathbf{Y} is determined by the purely elastic action (with $\mathbf{F} \equiv \mathbf{0}$) of the surrounding inclusions on the separated one. The actual form of the tensor \mathbf{Y} , used in the analysis as an approximation, depends on additional assumptions for closing of the infinite system (2.473). In particular, for purely elastic composites (with $\beta_1 \equiv \mathbf{0}$) with fictitious homogeneous inclusions (2.469), (2.470) such relations are represented in Appendix A for commonly applied methods of micromechanics, i.e. effective medium method by Kröner (1958), differential method, the MTM, and MEFM.

The local stresses inside the cluster are found by

$$\langle \boldsymbol{\sigma} \rangle_i(\mathbf{x}) = \mathbf{C}(\mathbf{x}) + \mathbf{B}(\mathbf{x})\mathbf{R}^{-1} [\mathbf{Y}(\mathbf{R}\boldsymbol{\sigma}^0 + \mathbf{F}) - \mathbf{F}], \quad (2.482)$$

where $\langle \boldsymbol{\sigma} \rangle_i(\mathbf{x})$ means the statistical average of the local stress state at $\mathbf{x} \in \Omega_i \subset \Omega^1$ over an ensemble realization of surrounding clusters (but not over the volume Ω_i of a particular cluster, in contrast to $\langle \boldsymbol{\sigma} \rangle^{(1)}$).

Estimation of effective thermoelastic properties can be found from Eq. (2.482)

$$\mathbf{M}^* = \mathbf{M}^{(0)} + \mathbf{Y}\mathbf{R}n^{(1)}, \quad (2.483)$$

$$\boldsymbol{\beta}^* = \boldsymbol{\beta}^{(0)} + \mathbf{Y}\mathbf{F}n^{(1)}. \quad (2.484)$$

Elimination of the tensor \mathbf{Y} from Eqs. (2.483) and (2.484) leads to the unique representation of $\boldsymbol{\beta}^*$ through \mathbf{M}^*

$$\boldsymbol{\beta}^* = \boldsymbol{\beta}^{(0)} + (\mathbf{M}^* - \mathbf{M}^{(0)})\mathbf{R}^{-1}\mathbf{F}, \quad (2.485)$$

which is similar to the classical exact relation for two-phase composites

$$\boldsymbol{\beta}^* = \boldsymbol{\beta}^{(0)} + (\mathbf{M}^* - \mathbf{M}^{(0)})(\mathbf{M}^{(1)} - \mathbf{M}^{(0)})^{-1}(\boldsymbol{\beta}^{(1)} - \boldsymbol{\beta}^{(0)}), \quad (2.486)$$

(see Levin, 1967; Rosen and Hashin (1970)). It is not surprising that the exact relations (2.486) is derived from the approximate one (2.485) since the additional assumption **H1** does not expand the class of the considered materials and homogenization methods. The representation (2.486) is formally invariant with respect to the replacement $v^{(1)} \leftrightarrow v^{(0)}$, although this can not be said about the relation (2.485), obtained for matrix clustered structure composites with ellipsoidal inclusions.

Our main objective is it to prove the general relation (2.485) which is valid in the framework of hypothesis **H1** only. No restrictions are imposed on the concrete statistically homogeneous microstructure of the whole composite material with a single sort of clusters being analyzed as well as on the microtopology of clusters or on the inhomogeneity of the stress state in the clusters.

2.5.5 Application to nanocilicate composites

For simplicity, the internal structure of an intercalated clay particle is idealized as a multi-layer stack containing $n^{\Omega(1)} \equiv n$ single silicate plate with uniform inter-layer spacing d , as depicted in Fig.2.36a. Exfoliated clay nanolayers will be considered as alligned oblate spheroids with a small aspect ratio ($\alpha = b/a \ll 1$, typically on the order of 0.01) described by the equation

$$\frac{x_1^2}{a^2} + \frac{x_2^2}{a^2} + \frac{x_3^2}{b^2} = 1 \quad (2.487)$$

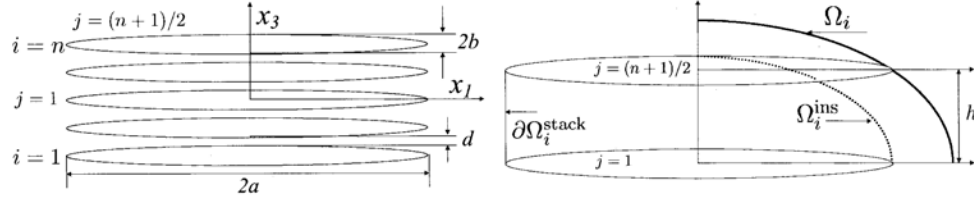


Figure 2.36: Schematic representation of a cluster. a) A stack of oblate spheroids, b) Definition of the correlation hole Ω_i^0

in the local coordinate system connected with the spheroid semi-axes which in turn are parallel to the global coordinate system. Intercalated clusters can vary in thickness and inter-layer spacing d depending on the degree of intercalation. Usually the plate thickness observed was roughly 1nm, the inter-layer spacing ranged from 2 to over 5 nm, and the number of plates per stack varied from 1 to 50. It is assumed that all stacks are randomly located, aligned and identical i.e. has the same geometrical structures (a, b, d, n) and elastic properties of nanoplates (see Fig.2.36a). The volume concentration of inclusions (oblate spheroids) v_i in the composite material is $c = \frac{4}{3}\pi a^2 b n^{(1)} n^{\Omega(1)}$.

The stack containing n ellipsoids (2.487) is inscribed in the surface $\partial\Omega_i$ called a cluster surface described by the equations

$$\partial\Omega_i = \begin{cases} x_1^2/a^2 + x_2^2/a^2 + (x_3 - h)^2/b^2 = 1, & \text{if } h \leq x_3 \leq h + b, \\ x_1^2/a^2 + x_2^2/a^2 = 1, & \text{if } |x_3| \leq h, \\ x_1^2/a^2 + x_2^2/a^2 + (x_3 + h)^2/b^2 = 1, & \text{if } -h - b \leq x_3 \leq -h, \end{cases} \quad (2.488)$$

where $h = (2a + b)(n - 1)/2$ (see Fig.2.36b). We can inscribe into the domain Ω_i the spheroid Ω_i^{ins} of maximum possible volume bounded by the surface

$$x_1^2/a^2 + x_2^2/a^2 + x_3^2/c^2 = 1 \quad (2.489)$$

with semi-axes a and $\bar{b} = h + b$. We will assume that the correlation hole Ω_i^0 (see Eq. (2.456)) is a spheroid of minimum possible volume

$$x_1^2/a_\Omega^2 + x_2^2/a_\Omega^2 + x_3^2/b_\Omega^2 = 1 \quad (2.490)$$

with the same aspect ratio as the spheroid Ω_i^{ins} : $\alpha^\Omega = a_\Omega/b_\Omega = a/\bar{b}$. A simple geometrical analysis leads to the boundaries of the semi-axes of the spheroid Ω_i^0 : $a\sqrt{a^2 + h^2}/\rho_1 \leq a_\Omega \leq a\sqrt{a^2 + b^2}/\rho_2$, $c\sqrt{a^2 + h^2}/\rho_1 \leq c_\Omega \leq c\sqrt{a^2 + b^2}/\rho_2$, where $\rho_k^2 = \bar{b}^2/(1 - \epsilon^2 \cos^2 \phi_k)$ ($k = 1, 2$) is a polar representation of a cross-section $(\partial\Omega_i^{\text{ins}} \cap \{x_2 = 0\})$ with an eccentricity $\epsilon = \sqrt{1 - \min(a, \bar{b})^2/\max(a, \bar{b})^2}$, and $\phi_1 = \arctg(h/a)$, $\phi_2 = \arctg(\bar{b}/a)$.

It should be mentioned that in the case of exploring of the one particle approximation of the MEFM being explored in this paper for obtaining of numerical results in Section 7, the estimations of the effective properties obtained depend only on the shape of the correlation hole Ω_i^0 rather than on its size. In such a case the tensor \mathbf{Y} defining the effective properties (2.475) and (2.476) and determined by purely elastic action (with $\boldsymbol{\beta} \equiv \mathbf{0}$) of the surrounding clusters on the separate one, is represented by Eq. (A.8).

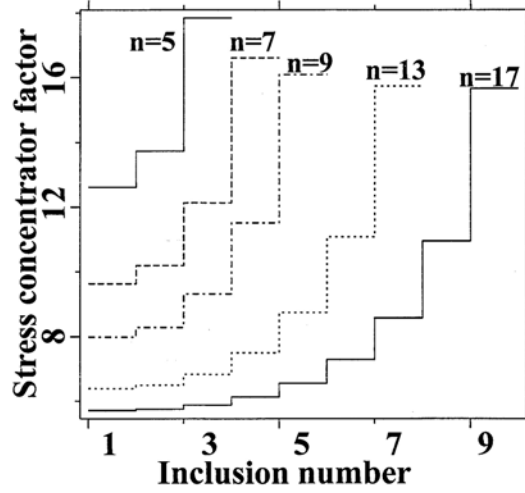


Figure 2.37: Average stress concentrator factor $\langle \sigma_{11} \rangle_{(j)} / \langle \sigma_{11} \rangle$ the different spheroids $j = 1, \dots, (n + 1)/2$ in the clusters containing n inclusions

2.5.6 Numerical results

This section attempts to quantitatively investigate the performance of the present approach to the estimation of effective elastic properties of nanocomposites. The results are directly compared with solutions obtained from simplified assumptions (such as Mori-Tanaka approach) and they are presented in order to place the advantages and limitations of the refined approach in evidence.

Let us consider a nanocomposite made from the Epox 862 reinforced by the oblate spheroidal nanoplates. The matrix is described by isotropic elastic properties with Young's modulus $E^{(0)} = 3.01 \text{ GPa}$, Poisson's ratio $\nu^{(0)} = 0.41$ (see Tandon *et al.*, 2002). Experimental research and molecular dynamic simulation indicated that nanoplates can be effectively considered in the framework of continuum mechanics as the homogeneous oblate spheroidal isotropic homogeneous inclusions with a small aspect ratio ($\alpha \leq 0.01$) with the axis of symmetry coinciding with the axis Ox_3 . In the parametric analysis we will consider a nanocomposite reinforced by the isotropic nano-inclusions with the properties $E^{(1)} = 300 \text{ GPa}$, $\nu^{(1)} = 0.4$ (see Sheng *et al.*, 2004) arranged into the randomly located aligned clusters containing n inclusions with $a = 1$ (see Fig.2.36a). Numerical analysis of a finite number of inclusions (see Section 6) is performed in all cases for number of harmonics $n^p = 11$ that provide a relevant accuracy of obtained solutions (estimation of the accuracy is presented in Kushch, 1996, 1998a).

At first, we will analyze the average stress concentrator factors

$\langle \sigma_{11} \rangle_{(i)} / \langle \sigma_{11} \rangle$, $\langle \sigma_{33} \rangle_{(i)} / \langle \sigma_{33} \rangle$ ($i = 1, \dots, n$, $\alpha = 0.01$ and $d = 4b$, $a = 1$) at the inclusions of one isolated cluster Ω_k in the infinite matrix subjected to the homogeneous loading $\langle \sigma_{ij} \rangle = \delta_{1i} \delta_{1j}$ and $\langle \sigma_{ij} \rangle = \delta_{3i} \delta_{3j}$, respectively.

In Figs.2.37 and 2.38 it can be seen that the stress concentrator factor $\langle \sigma_{11} \rangle_{(i)} / \langle \sigma_{11} \rangle$ ($i = 1, \dots, n$) significantly (almost in three times) decrease from the outer spheroid to

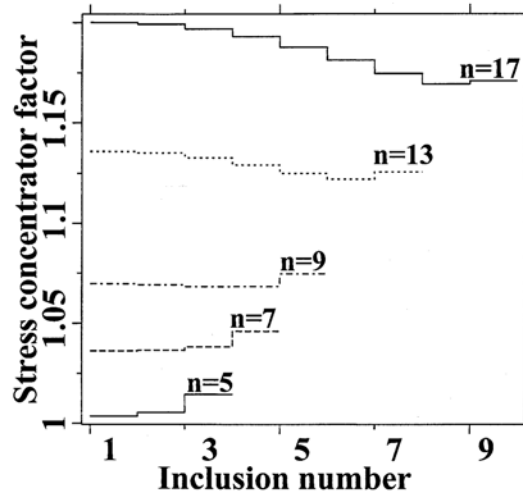


Figure 2.38: Average stress concentrator factor $\langle \sigma_{33} \rangle_{(j)} / \langle \sigma_{33} \rangle$ in the different spheroids $j = 1, \dots, (n + 1)/2$ in the clusters containing n inclusions

the central spheroid of the cluster. Hereafter one depicts the stress concentrator factors of inclusions v_i ($i = (n + 1)/2, \dots, n$) numbered by the subscript $j = 1, \dots, (n + 1)/2$ ($j = i - (n - 1)/2$, see Fig. 1a). This decreasing of stress concentrator factor growths with the extension of an inclusion number in the cluster. So, variation of $\langle \sigma_{11} \rangle_{(i)} / \langle \sigma_{11} \rangle$ inside the stack reaches 2.7 times at $n = 17$ while for $n = 5$ the stress concentrator factors is varying just on 40%. If the number of the spheroids is much enough (more than 13) then the average stress concentrator factors in three external spheroids differ between the clusters with 13 and 17 spheroids just on 1% (see Fig.2).

Such a behavior is qualitative confirmed by 2D finite element analysis by Sheng *et al.* (2004) of three rectangular inclusions in the infinite matrix. The large stress in the outer inclusions counteracts to the stress concentrator at the internal inclusions of the cluster (shielding effect). Only a small amount of load is transferred to the middle silicate layer, due to the low shear modulus of the galleries. In so doing, a variation of stress concentrator factor $\langle \sigma_{33} \rangle_{(i)} / \langle \sigma_{33} \rangle$ in the different inclusions in a cluster is small enough and slightly increase from outer inclusions to the internal inclusions of the cluster only for a large number of inclusions in the stack. This effect is distinctive for both the functionally graded and clustered materials of random structure composites reinforced by the spherical inclusions when the local effective stiffness increase from the cluster boundary to the cluster center that with necessity yield the increasing of stress concentrator factor in the cluster center (see for details Buryachenko, 2001).

In Fig.2.39 the influence of the inter-layer spacing $d = 2, 3, 5, 9b$ is analyzed at the fixed values of all remaining ones ($n = 9, \alpha = 0.01$). As can be seen $\langle \sigma_{11} \rangle_{(i)} / \langle \sigma_{11} \rangle$ increase, as it is expected, with extension of d . However, in the range of the inter-layer spacing of principal practical interest $d = 2 \div 9b$ the average stress concentrator factors at the spheroids in the cluster significantly below of the limiting stress concentrator factor $\langle \sigma_{11} \rangle_{(i)} / \langle \sigma_{11} \rangle = 38.9$ for an isolated inclusion in the infinite matrix at $d \rightarrow \infty$. It should be mentioned

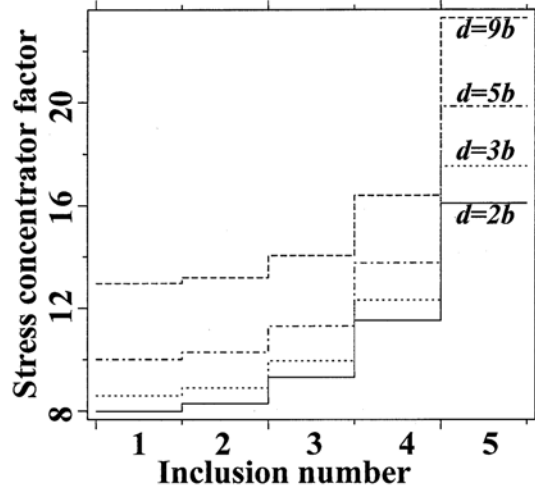


Figure 2.39: Average stress concentrator factor $\langle \sigma_{11} \rangle_{(j)} / \langle \sigma_{11} \rangle$ in the different spheroids $j = 1, \dots, (n + 1)/2$ in the clusters with different inter-layer spacing. inclusions.

that analogous stress concentrator factor for the isolated spheroid with $\alpha = 0.001$ is $\langle \sigma_{11} \rangle_{(i)} / \langle \sigma_{11} \rangle = 85.4$ in excess of the value $\langle \sigma_{11} \rangle_{(i)} / \langle \sigma_{11} \rangle = 38.9$ ($\alpha = 0.01$) by a factor 2.2. Thus, an oblate silicate spheroid with $\alpha = 0.01$ can not be approximated by an infinite layer ($\alpha \ll 1$) in contrast with the the another limiting case when prolate spheroidal nanofiber with $\alpha = 100$ can be recognized as an infinite cylinder (see Buryachenko and Roy, 2005).

We now turn our attention to the analysis of effective elastic moduli of composites reinforced by randomly located identical aligned ($\alpha = 0.01$, $d = 4b$, $a = 1$) with different number of the oblate spheroids in the clusters $n = 1, 2, 5, 13, 17$. As can be seen in Figs.2.40 and 2.41, increasing of the inclusion number in the clusters leads to decreasing of the effective Young moduli E_3^* and E_1^* in both the transversal symmetry direction Ox_3 and the longitudinal direction Ox_1 . Thus, exfoliation is favored over intercalation as far as composite modulus enhancement is concern. The reason of such a behavior is explained by decreasing of the average stress concentrator factors $\mathbf{B}_i^{v(1)}$ (2.466) ($i = 1, \dots, N$) at the individual inclusions in a single cluster in the infinite matrix with a rise in the inclusion number in a cluster (see Figs. 2.37 and 2.38). In so doing, influence of surrounding clusters on the chosen one Ω_k in the composite material describing by the effective field $\langle \bar{\sigma} \rangle_k$ (2.474) does not culminate in elimination of the slackening effect of the stress concentrator factors in an individual cluster.

It should be mentioned that the case $n = 1$ corresponds to the Mori-Tanaka approach (see Mori and Tanaka, 1993; Benveniste, 1987; Wang and Pyrz, 2004a; as well as the comprehensive review by Buryachenko, 2001). This approach was applied by Hui and Shia (1998) and by Shia and Hui *et al.* (1998) to the analyses of unidirectional nanocomposites with dispersed and parallel flake-like inclusions at the simplified assumption of complete exfoliation and full dispersion of nanoplates. In so doing a disagreement of the prediction of effective moduli and experimental data was attributed by Shia and Hui *et al.* (1998)

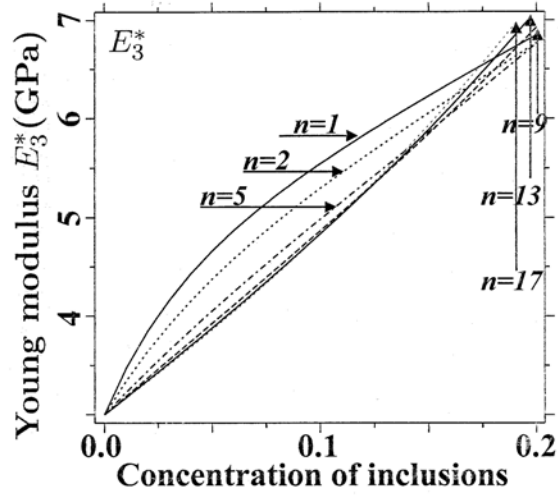


Figure 2.40: Effective elastic modulus $E_3^*(c)$ for the different inclusion number $n = 1, 2, 5, 13, 17$ in the clusters.

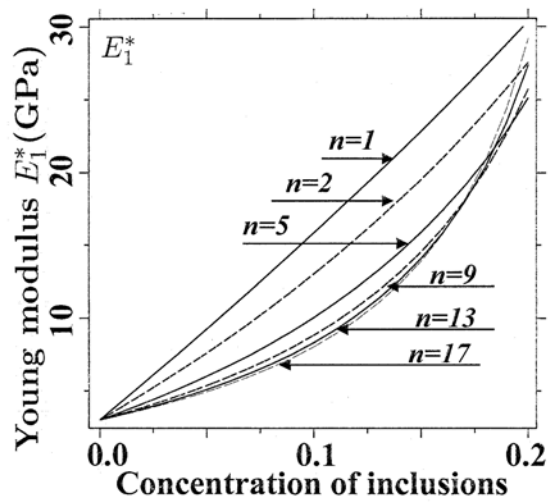


Figure 2.41: Effective elastic modulus $E_1^*(c)$ for the different inclusion number $n = 1, 2, 5, 13, 17$ in the clusters.

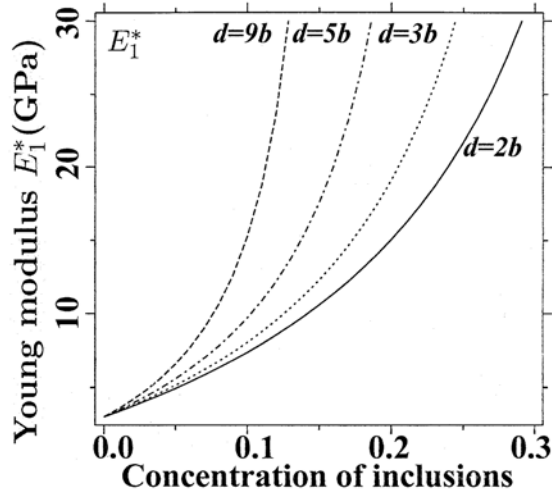


Figure 2.42: Effective elastic modulus $E_1^*(c)$ for the different inter-layer spacing $d = 2, 3, 5, 9b(n = 9)$.

to debonding between clay nanolayers and the matrix. However, we can conclude now, from Figs.2.40 and 2.41, that the reduction of effective moduli of nanocomposites with the clusterisation does not uniquely depend with debonding and can be explained by pure elastic sheilding effect of diminution of stress concentrator factors at the internal nanoinclusions in the clusters (see Figs. from 2.37 to 2.39). As can be seen in Figs.2.40 and 2.41, the effective elastic moduli are not sensitive to the inclusion number of spheroids inside the clusters if $n \geq 9$. Because of this, we will investigate the inter-layer space $d = 2, 3, 5, 9b$ on the effective Young moduli E_1^* (see Fig.2.42) and E_3^* (see Fig.2.43) at the fixed $\alpha = 0.01$ and $n = 9$. As one would expect, increasing of the inter-layer spacing slacking the interaction of the spheroids inside the cluster according to Fig.2.39 leads to a rice of the effective Young moduli. In so doing, E_1^* and E_3^* rice in 2.1 and 1.3 times, respectively, at $c = 0.1$. Moreover, an accelerated growth of E_1^* at $n = 9$ and $c \geq 0.05$ fells even more significant than the increasing of E_1^* for a single spheroid in the clusters (see Fig.2.41) that is explained by some sort of sheilding effect in the composite material at $n = 1$.

Thus, we come to a practically important conclusion that the clustering of stiff oblate spheroidal inclusions leads to the weakening of the reinforcement effect of nanocomposites and, therefore, the completely expholiated nanocomposites offer maximum stiffness among nanocomposites with clustered aligned structure. This result has a qualitative confirmation by numerical simulation by Sheng *et al.* (2004) who described this effect in $2D$ finite element analysis of periodic structure composites with a quasirandom location of a number of clusters containing the aligned three rectangular inclusions in the large unite cell. Furthermore, a well known experimental data (see e.g. Kornmann *et al.*, 2002) also point to the decreasing of effective elastic properties with the grough of clustering with the maximum of effective stiffness of nanocomposites corresponding to the completely exfoliated structures.

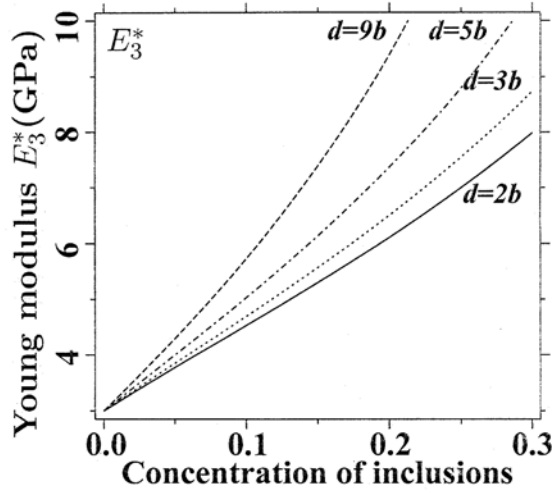


Figure 2.43: Effective elastic modulus $E_3^*(c)$ for the different inter-layer spacing $d = 2, 3, 5, 9b(n = 9)$.

Kornmann *et al.* (2002) explained this behavior at the intuitive level of justification: as the interlamellar spacing is increased, the effective particle volume fraction is also increased. The corresponding reduction of particle stiffness is much weaker effect that increased the volume fraction. Now, this intuitive explanation can be replaced by rigorous justification confirmed by Figs.2.37 and 2.41.

However, the mentioned behavior of decreasing of the effective stiffness with the increasing of the number of nanoplates in the clusters is drastically changing with the variation of the inclusion shape. So, the one of the most critical technological problem is a significant growth of the effective viscosity of suspensions at the clustering of spherical inclusions. For a fixed filler content, the viscosity of a system with agglomerates of spherical inclusions is always higher than that of the "well-dispersed" sample (see for references e.g. Lipatov, 1995). In Figs.2.44 and 2.45 the functional dependences $E_1^* \sim c$ and $E_3^* \sim c$ are presented for the spherical inclusions in the clusters ($a = 1$, $\alpha = 1$, $d = 0.04a$, $n = 1, 2, 5, 9, 13, 17$). As can be seen, both the effective Young's E_1^* and E_3^* at the fixed c increase with the increasing of n . However, the dependence $E_1^* \sim c$ varies very slightly with the variation of n (just on 0.9% at $c = 0.2$) as opposite to the dependence $E_3^* \sim c$ varying in 1.9 times at $c = 0.2$.

Now we will analyze in more details the influence of the inclusion shape in the composite materials reinforced by the clusters with $n = 9$ which are large enough for generating of maximum cluster effect. In Figs.2.46 and 2.47 an influence of an aspect ratio $\alpha = b/a$ varying from 0.001 til 10 is investigated with the fixed $d = 0.04a$, $a \equiv 1$, $n = 9$. It is interesting that the behavior of the dependences $E_1^* \sim c$ for the fixed α and $E_1^* \sim \alpha$ at the fixed c are both monotonic. In so doing the dependence $E_3^* \sim c$ for the fixed α is monotonically growing as the functions $E_1^* \sim c$ for the fixed α while the variation of dependences $E_3^* \sim \alpha$ at the fixed c is not monotonic and achieves its minimum for the investigated values of α at $\alpha = 0.1$. Nonmonotonic behavior of functions $E_3^* \sim \alpha$ at the fixed c for the

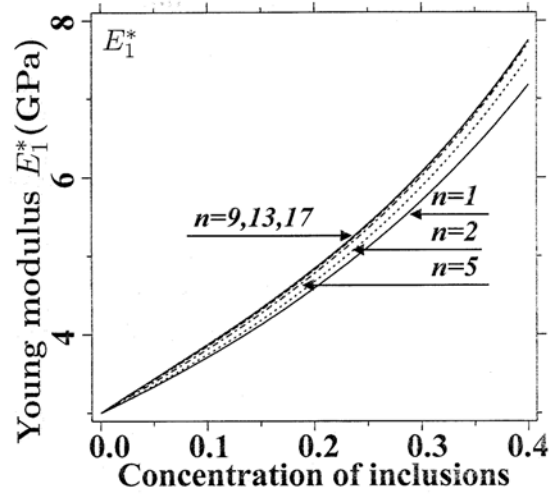


Figure 2.44: Effective elastic modulus E_1^* vs c for the different inclusion number $n = 1, 2, 5, 13, 17$ in the clusters.

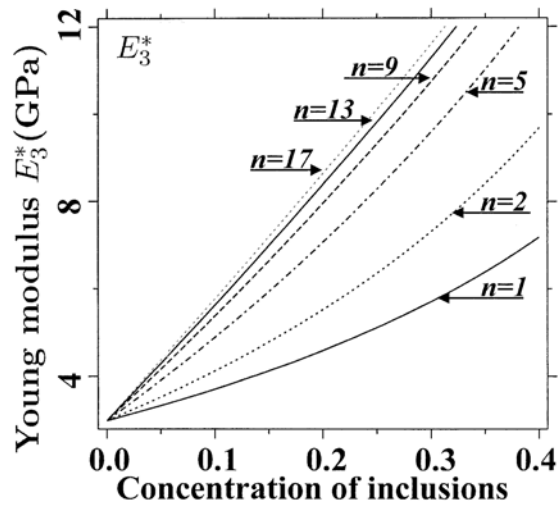


Figure 2.45: Effective elastic modulus E_3^* vs volume concentration of inclusions c for the different inclusion number $n = 1, 2, 5, 13, 17$ in the clusters.

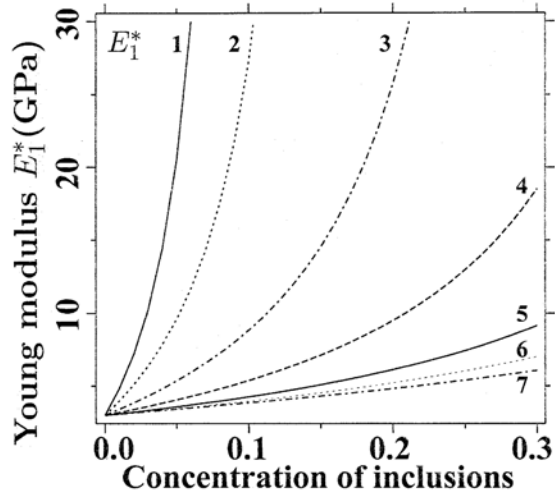


Figure 2.46: Effective elastic modulus E_1^* vs c for $\alpha = 0.001$ (curve 1); 0.003 (2); 0.01 (3); 0.03 (4), 0.1 (5), 0.3 (6), 1.0(7).

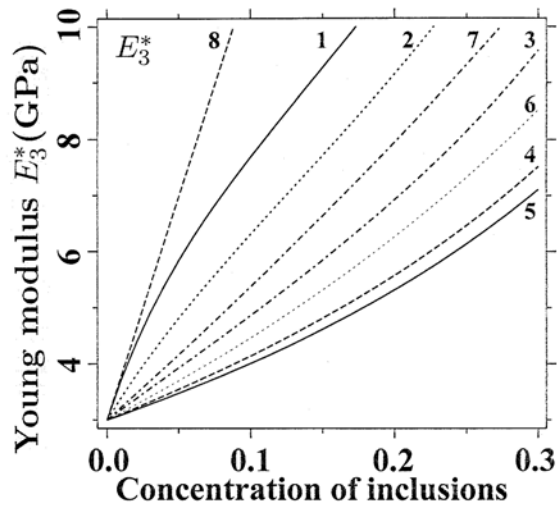


Figure 2.47: Effective elastic modulus E_3^* vs $c^{(1)}$ for $\alpha = 0.001$ (curve 1); 0.003 (2); 0.01 (3); 0.03 (4), 0.1 (5), 0.3 (6), 1.0(7).

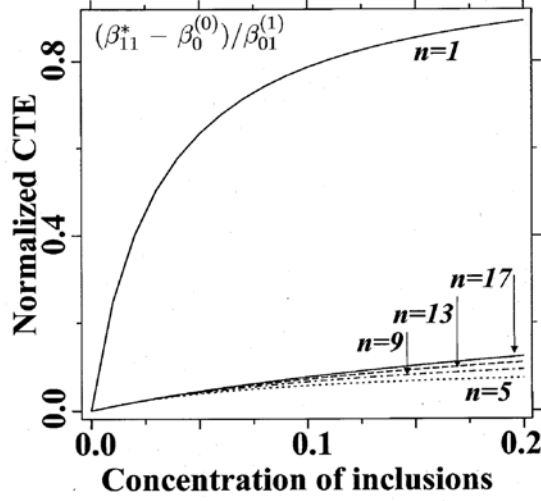


Figure 2.48: Normalized CTE $(\beta_{11}^* - \beta_0^{(0)})/\beta_{01}^{(1)}$ vs $c^{(1)}$ for the different inclusion number $n = 1, 5, 9, 13, 17$ in the clusters.

analyzed clustered material correlates well with the analogous dependences $E_3^* \sim \alpha$ at the fixed c for completely exfoliated system corresponding to MTM estimations achieving its minimum for investigated values of α at $\alpha = 0.3$.

We are coming now to the estimation of an effective coefficient of thermal expansion (CTE) β^* (2.476). The normalized CTE $(\beta_{11}^* - \beta_0^{(0)})/\beta_{01}^{(1)}$ and $(\beta_{33}^* - \beta_0^{(0)})/\beta_{01}^{(1)}$ are presented in Figs.2.48 and 2.49, respectively, as the functions of the volume concentration of nanoinclusions $c^{(1)}$ for an isotropic CTE of both constituents $\beta^{(0)} = \beta_0^{(0)} \delta$, $\beta^{(1)} = \beta_0^{(1)} \delta$, and $\beta_1^{(1)} = \beta_{01}^{(1)} \delta$. Nonmonotonical behavior of the value $(\beta_{33}^* - \beta_0^{(0)})/\beta_{01}^{(1)} \sim c^{(1)}$ for the completely exfoliated nanocomposites ($n = 1$) is explained by the Poisson's effect. Indeed, even for the small concentration of isotropic nanoplates with positive CTE, the residual strains $\langle \varepsilon_{33} \rangle$ at $\langle \sigma \rangle \equiv \mathbf{0}$ are governed by the shrinkage of oblate stiff nanoelements in the Ox_1 -direction leading to the negative deformation of the matrix in a perpendicular direction. With the growth of nanoelement concentration, the mentioned effect is compensated by the shrinkage of nanoelements in the transversal direction yielding the decrease of the effective CTE in this direction. For the clustered nanocomposites ($n > 1$), the weak dependencies of β^* vs $c^{(1)}$ are explained by the shielding effect analogous to the pure elastic case (see Figs. from 2.36 to 2.38).

Thus, based on the MEFM, a micromechanical model has been developed to predict the effective moduli and stress concentrator factors of random structure nanocomposites reinforced by the aligned silicate nanoplate clusters of deterministic structure. The model accounts for the existence of both the exfoliated and intercolated nanoplates, and is able to analyze the effect of the aspect ratio of nanoelements, interlayer distances, and the number of nanoelements in the clusters on the effective thermoelastic properties. The proposed analytical-numerical method is efficient from a computational standpoint and

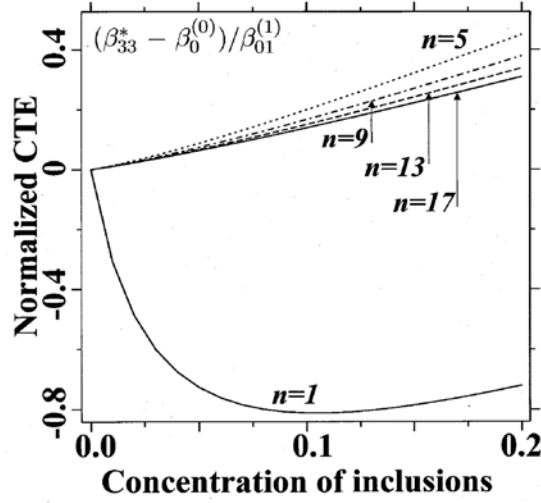


Figure 2.49: Normalized CTE $(\beta_{33}^* - \beta_0^{(0)})/\beta_{01}^{(1)}$ vs $c^{(1)}$ for the different inclusion number $n = 1, 5, 9, 13, 17$ in the clusters.

provides high-accuracy analysis of a wide class of random structure composites reinforced by the clusters of an arbitrary deterministic structure when interaction of clusters is estimated in the frameworks of the different most popular methods of micromechanics such as the MEFM, MTM, self-consistent method, and the differential method. Numerical results were obtained for a special sort of clusters modeling intercalated silicate nanoplates as a stack of identical parallel oblate spheroids. In so doing interaction of oblate spheroidal nanoelements inside the cluster is evaluated by the accurate numerical method based on the the multipole expansion technique wich is best suited for forthcoming incorporation into the numerical version of the MEFM proposed in the present paper and make possible to abandon from the majority of simplified assumptions exploring at the analysis of random structure composites reinforced by the clusters of deterministic structure.

References

- Abramovitz, M., Stegun, I.A. (1964). *Handbook for mathematical functions*. NBS Applied Mathematics Series, vol. 55. Flammarion, Paris.
- Bateman, G., Erdelyi, A., 1953. *Higher Transcendental Functions*, vol.2. McGraw Hill, New York.
- Benveniste, Y. (1987) A new approach to application of Mori-Tanaka's theory in composite materials. *Mech. Mater.* **6**, 147–157.
- Bhattacharyya, A., Lagoudas, D. C. (2000) Effective elastic moduli of two-phase transversely isotropic composites with aligned clustered fibers. *Acta Mechanica*, **145**, 65–93.
- Brune, D. A., Bicerano, J. (2002) Micromechanics of nanocomposites: comparison of tensile and compressive elastic moduli, and prediction of effects of incomplete exfoliation and imperfect alignment on modulus. *Polymer*, **43**, 369–387.
- Buryachenko, V.A. (2001) Multiparticle effective field and related methods in micromechanics of composite materials. *Appl. Mech. Rev.*, **54**(1), 1–47.
- Buryachenko, V. A. (2004) Foreword to special issue on recent advances in micromechanics of composite materials. *Int. J. Multiscale Computational Engineering* **2**, vii-viii.
- Buryachenko, V.A., Kushch, V.I. (2005) Effective transverse elastic moduli of composites at non-dilute concentration of a random field of aligned fibers. *ZAMP*, in press.
- V.A.Buryachenko, V.I.Kushch, A.Roy (2005) Effective thermoelastic properties of random structure composites reinforced by the clusters of deterministic structure (application to clay nanocomposites) *J. Mech. Phys. Solids* - submitted
- Buryachenko, V.A. and Pagano, N.J., 2005. The multiscale analysis of multiple interacting inclusions problem: Finite number of interacting inclusions. *Math. Mech. of Solids* **10**, 25-62.
- Buryachenko, V.A., Parton, V.Z. (1992) Multi-partical differential methods in the statics of composites. *Priklad. Mekh. Tekhn. Fiz.* (3), 148–156. (In Russian. Engl. Transl. *J. Appl. Mech. Tech. Phys.* **33**, 455–464.)
- Buryachenko, V. A. and Roy. A. (2005) Effective elastic moduli of nanocomposites with prescribed random orientation of nanofibers. *Composites B*. (In press).
- Bystroem, Johan (2003) Influence of the inclusions distribution on the effective properties of heterogeneous media. *Composites: Part B*, **34**, 587–592.
- Carrado, K. (2003) *Polymer-clay nanocomposites*. Advance Polymer Materials, (Eds. G. O. Shonaike, S. A. Advani), CRC Press, Boca Raton, London. NY, pp. 349–437.
- Christensen, R. M. (1979) *Mechanics of Composite Materials*. Wiley Interscience, NY.
- Dong, C.Y., Lo, S.H., Cheung, Y.K. Numerical solution for elastic half-plane inclusion problems by different integral equation approaches *Engineering Analysis with Boundary Elements* **28** (2004) 123–130.
- Dvorak, G.J. and Benveniste, Y., 1992. On transformation strains and uniform fields in multiphase elastic media. *Proc. Roy. Soc. London A* **437**, 291–310.
- Erdelyi, A. et al. (1954) *Tables of integral transforms*. McGraw-Hill, NY
- Erdogan, F., Gupta, G.D. and Ratwani, M., 1974. Interaction between a circular inclusion and an arbitrary oriented crack. *ASME Journal of Applied Mechanics* **41**, 1007–1013.
- Eshelby, J.D., 1957 The determination of the elastic field of an ellipsoidal inclusion, and related problems. *Proc. R. Soc. London A* **241**, 376–396.
- Fischer, H. (2003) Polymer nanocomposites: from fundamental research to specific applications. *Materials Science and Engineering*, **23**, 763–772

- Fornes T. D., Paul D. R. (2003) Modeling properties of nylon 6/clay nanocomposites using composite theories *Polymer* **44**, 4993—5013
- Friesecke G. and James R. D. (2000) A scheme for the passage from atomic to continuum theory for thin films, nanotubes and nanorods. *J. Mech. Phys. Solids*. **48**, 1519–1540.
- Giannelis, E. P. (1996) Polymer layered silicate nanocomposites. *Adv. Mater.* **8**, 29—35.
- Giannelis, E. P., Krishnamoorti, R., Manias, E. (1999) Polymer-silicate nanocomposites: Model systems for confined polymers and polymer brushes. *Adv. Polymer Sci.*, **138**, 107–147.
- Ghoneim, N. M., Busso, E. P., Kioussis, N., Huang, H. (2003) Multiscale modeling of nanomechanics and micromechanics: an overview. *Philosophical Magazine* **83**, 3475–3528.
- Golovchan ,V.T., Guz, A.N., Kohanenko, Yu., Kushch, V.I., 1993. *Mechanics of composites* (in 12 v.) V.1. Statics of materials. Naukova dumka, Kiev.
- Gupta, D.P. (1960) Stresses in a semi-infinite plate with a circular hole due to a distributed load on the straight boundary. *J. Technol.*, **5**, #1, 7–13.
- Halpin, J. C., Kardos, J. L. (1976) The Halpin-Tsai equations: a review. *Polym. Eng. Sci.*, **16**, 344–352.
- Hobson, E.W. (1931) *The Theory of Spherical and Ellipsoidal Harmonics*. Cambridge University Press, Massachusetts.
- Horii, H. and Nemat-Nasser, S., 1985. Elastic field of interacting inhomogeneities. *International Journal of Solids and Structures* **21**, 731–745.
- Hui, C. Y., Shia, D. (1998) Simple formulas for the effective moduli of unidirectional aligned composites. *Polym. Eng. Sci.* **38**, 774—782.
- Ivanov, E.A. (1968). *Diffraction of electromagnetic fields on two bodies*. Nauka i Technika, Minsk.
- Jeffery, G.B. (1920). Plane stress and plane strain in bipolar coordinates. *Proc. R. Soc. London A* **221**, 265–293.
- Ji, X. L., Jing, J. K., Jiang, W., Jiang, B. Z. (2002) Tensile modulus of polymer nanocomposites. *Polym. Eng. Sci.*, **42**, 983–993.
- Kaloerov, S.A. and Goryanskaya, E.S. (1995). Two-dimensional stress state of multiply-connected anisotropic solid with holes and cracks. *Theoretical and Applied Mechanics* **25** 45–56.
- Kantorovich, L.V. and Krylov, V.I. (1964) *Approximate Methods of Higher Analysis*. Wiley, New York.
- Kiersnowski A., Piglowski J. (2004) Polymer-layered silicate nanocomposites based on poly(ϵ -caprolactone) *European Polymer J.* **40**, 1199–1207.
- Komarneni, S. (1992) Nanocomposites. *J. Mater Chem.* **2**, 1219—1230.
- Koo C. M., Kim S. O., and Chung I. J. (2003) Study on morphology evolution, orientational behavior, and anisotropic phase formation of highly filled polymer-layered silicate nanocomposites. *Macromolecules*, **36**, 2748–2757.
- Kooi, C.B. and Verruijt, A. (2001). Interaction of circular holes in an infinite elastic medium. *Tunneling and Underground Space Technology* **16**, 59–62.
- Kornmann, X. (2001) *Synthesis and characterisation of thermosetlayered silicate nanocomposites*. PhD thesis, Lulea University of Technology, Division of Polymer Engineering, Sweden.
- Kornmann, X., Thomann, R., Mülhaupt R., Finter, J., Berglund L. (2002) Synthesis of amine-cured, epoxy-layered silicate nanocomposites: the influence of the silicate surface

modification on the properties. *J. Appl. Polym. Science* **86**, 2643–2652.

Kosmodamiansky A.S. (1972). *Stress distribution in the isotropic multiply-connected solids*. University Publ., Donetsk.

Krishnamoorti R., Yurekli K. (2001) Rheology of polymer layered silicate nanocomposites Current Opinion *Colloid & Interface Science* **6**, 464-470.

Kröner, E. (1958) Berechnung der elastischen Konstanten des Vielkristalls aus den Konstanten des Einkristalls. *Z. Physik.* **151**, 504–518.

Kushch, V. (1996) Elastic equilibrium of a medium containing finite number of aligned spheroidal inclusions *Int. J. Solids Struct.* **33**, 1175-1189.

Kushch, V.I. (1997) Microstresses and effective elastic moduli of a solid reinforced by periodically distributed spheroidal inclusions. *Int. J. Solids Structures* **34**, 1353-1366.

Kushch, V.I. (1998a) Elastic equilibrium of a medium containing a finite number of arbitrarily oriented spheroidal inclusions. *Int. J. Solids Structures* **35**, 1187–1198.

Kushch, V.I. (1998b) *The stress state and effective thermoelastic properties of piece-homogeneous solids with spheroidal interfaces*. Dr. Sci. thesis. Institute of Mechanics of the National Academy of Sciences, Kiev, Ukraine.

Kushch, V.I., Sangani, A.S., Spelt, P.D.M. and Koch, D.L. (2002) Finite Weber number motion of bubbles through a nearly inviscid liquid. *J. Fluid Mechanics* **460**, 241–280

Kushch, V.I., Shmegeera, S.V. and Buryachenko, V.A. (2005). Interacting elliptic inclusions by the method of complex potentials. *International Journal of Solids and Structures*, in press.

Kushch, V.I. and Shmegeera, S.V. (2005). Elastic equilibrium of a half plane containing a finite array of elliptic inclusions. *International Journal of Solids and Structures*, in press.

Lax, M. (1952) Multiple scattering of waves II. The effective fields dense systems. *Phys. Rev.* **85**, 621–629.

Levin, V.M. (1967) Thermal expansion coefficient of heterogeneous materials. *Izv. AN SSSR, Mekh. Tverd. Tela* (2), 88–94. (In Russian. Engl. Transl. *Mech. Solids* **2**(2), 58–61.)

Lincoln, D. M., Vaia, R. A., Wang, Z.-G., Hsiao, B. S. (2001) Secondary structure and elevated temperature crystallite morphology of nylon-6/layered silicate nanocomposites. *Polymer* **42**, 1621–1631.

Lipatov Y. S. (1995) *Polymer Reinforcement*. ChemTec Publishing.

Lu, S-Y. and Kim, S., 1990. Effective thermal conductivity of composites containing spheroidal inclusions. *AIChE Journal* **36**, 927–938.

Luo, J.-J. and Daniel, I. M. (2003) Characterization and modeling of mechanical behavior of polymer/clay nanocomposites. *Composites Science and Technology* **63**, 1607—1616.

Masenny-Varlot, K., Reynaud, E., Vigier, G., Varlet, J. (2002) Mechanical properties of clay-reinforced polyamide. *J. Polym. Sci. Part. B: Polyme. Phys.* **40**, 272–283.

Meisner, M.J. and Kouris, D.A., 1995. Interaction of two elliptic inclusions. *International Journal of Solids and Structures* **32**, 451–466.

Milton, G. W. (2003) *The Theory of Composites*. Appl. Comput. Math., v. 6, Cambridge University Press.

Mori, T., Tanaka, K. (1973) Average stress in matrix and average elastic energy of materials with misfitting inclusions. *Acta Metall.* **21**, 571–574.

Mura, T. (1982) *Micromechanics of defects in solids*.- Martinus Nijhoff: The Hague, Netherlands.

Muskhelishvili, N.I. (1953) *Some basic problems of the mathematical theory of elasticity*. Groningen, P. Noordhoff, 1953.

- Nemat-Nasser, S. and Hori, M. (1993) *Micromechanics: Overall Properties of Heterogeneous Materials*. Elsevier, North-Holland.
- Noda, N.-A. and Matsumo, T., 1998. Singular integral equation method for interaction between elliptic inclusions. *ASME Journal of Applied Mechanics* **65**, 310–319.
- Norris, A.N., Callegari, A.J., Sheng, P.A. (1985) A generalized differential effective medium theory. *J. Mech. Phys. Solids*. **33**, 525–543.
- Podil'chuk, Yu.N., 1984. *The boundary value problems of statics of elastic solid*. Naukova Dumka, Kiev.
- Ponte Castañeda, P. and Willis, J. R. (1995) The effect of spatial distribution on the effective behavior of composite materials and cracked media. *J. Mech. Phys. Solids*, **43**, 1919–1951.
- Ray, S. S. and Okamoto, M. (2003) Polymer/layered silicate nanocomposites: a review from preparation to processing. *Prog. Polyme. Sci.* **28**, 1539–1641.
- Ru, C.Q., 2000. Eshelby's problem for two-dimensional piezoelectric inclusions of arbitrary shape *Proc. R. Soc. London A* **456**, 1051–1068.
- Qian D., Wagner G. J., Liu W.K., Yu M.-F., Ruoff R. S. (2002) Mechanics of carbon nanotubes. *Applied Mechanical Review*, **55**, 495–533.
- Rosen, B.W., Hashin, Z. (1970) Effective thermal expansion coefficient and specific heats of composite materials. *Int. J. Engng. Sci.* **8**, 157–173.
- Savin, G. N. (1961) *Stress Concentration Around Holes*. Pergamon Press, NY.
- Sheng, N., Boyce, M.C., Parks, D. M., Rutledge, G. C., Abes, J. I. and Cohen, R. E., 2004. Multiscale micromechanical modeling of polymer/clay nanocomposites and the effective clay particle. *Polymer* **45**, 487–506.
- Shi, D.-L., Feng, X.-Q., Huang, Y. Y., Hwang K.-C., Gao, H. (2004) The effect of nanotube waviness and agglomeration on the nanotube-reinforced composites. *Trans. ASME. J. Engng. Materials Technology* **126**, 250–257.
- Shia, D., Hui, C. Y., Burnside, S. D., Giannelis, E. P. (1998) An interface model for the prediction of Young's modulus of layered silicate-elastomer nanocomposites. *Polym Composite*, **19**, 608–617.
- Stevenson, A.C., 1942. On the equilibrium of plates. *Philosophical Magazine*, Ser.7 **33**, 639–661.
- Tandon, G.P., Kim, R.Y. and Rice, B.P., 2002. Influence of vapor-grown carbon nanocomposites on thermomechanical properties of graphite-epoxy composites. *Proc. American Society for Composites 17th Technical Conference*. Purdue University, West Lafayette, Indiana, Paper 2039.
- Thostenson E.T., Ren Z.F., Chou T.-W. (2001) Advances in the science and technology of carbon nanotubes and their composites: a review. *Composites Science and Technology* **61**, 1899–1912.
- Torquato, S. (2002) *Random Heterogeneous Materials: Microstructure and Macroscopic Properties*. Springer-Verlag, 2002.
- Tsuchida E., Saito Y., Nakahara I., Kodama M. (1987) Stresses in a semi-infinite elastic body containing a prolate spheroidal cavity subjected to an axisymmetrical pressure//*Bulletin of the JSME* **25** 891-897.
- Ulitko, A.F. (1979) *The method of vectorial eigenfunctions in spatial elasticity problems*. Naukova dumka, Kiev.
- Ustinov, Yu. A. (1965) Stress concentration in a halfplane and plane with circular holes under tensile load. *Izv. AN USSR, Ser. Mech.*, **1**.

Usuki, A., Kojima, Y., Kawasumi, M., Okada, A., Fukushima, Y., Kurauchi, T., et al. (1993) Synthesis of Nylon 6-clay hybrid. *J. Mater. Res.* **8**, 1179–1184.

Vaia, R. A., Giannelis, E. P. (2001) Polymer nanocomposites: status and opportunities. *MRS Bulletin*, **26**(5), 394–401.

Vaia, R. A., Krishnamoorti, R. (2002) *Polymer Nanocomposites: Introduction. Polymer Nanocomposites. Synthesis, Characterization, and Modeling.* (Eds. R. A. Vaia, R. Krishnamoorti), ACS, Washington.

Vaia, R. A., Lincoln, D. (2002) *Mesoscopic Structure of polymer-inorganic nanocomposites. Polymer Nanocomposites. Synthesis, Characterization, and Modeling.* (Eds. R. A. Vaia, R. Krishnamoorti), ACS, Washington.

Verruijt, A. (1998) Deformations of an elastic half plane with a circular cavity. *Int. J. Solids Structures* **35**, 2795–2804.

Wang J., Pyrz R. (2004a) Prediction of the overall moduli of layered silicate-reinforced nanocomposites—part I: basic theory and formulas. *Composites Science and Technology* **64**, 925–934

Wang J., Pyrz R. (2004b) Prediction of the overall moduli of layered silicate-reinforced nanocomposites—part II: analyses. *Composites Science and Technology* **64**, 935–944.

Willis, J. R. (1981), Variational and related methods for the overall properties of composites. *Advances in Applied Mechanics*, **21**, 1–78.

Willis, J.R. and Acton, J.R., 1976. The overall elastic moduli of a dilute suspension of spheres. *Quarterly J. Mech. Appl. Math.* **29**, 163–177.

Zhang P., Huang Y., Philippe H. G., Hwang K. (2002) On the continuum modeling of carbon nanotubes. *Acta Mechanica Sinica*, **18**, 528–536.

Appendix A: The evaluation of the tensor \mathbf{Y} (2.480)

Effective medium method

The additional closing hypothesis of the effective medium method is described as follows: Each inclusion in the composite behaves as an isolated one in a homogeneous medium whose properties coincide with the effective properties. Formally this means

$$\mathbf{H2} : \quad \mathbf{Y} \equiv \mathbf{I}, \quad \mathbf{M}^* = \mathbf{M}^{(0)} + \mathbf{R}(\mathbf{M}^*)n^{(1)}, \quad (\text{A.1})$$

where the tensor $\mathbf{R}(\mathbf{M}^*)$ is calculated by the use of the formulae (2.472) with $\mathbf{M}^{(0)}$, $\mathbf{M}^{(q)}$, and $\bar{\Omega}_k$ being replaced by \mathbf{M}^* , $\mathbf{M}^{f(q)}$, and \bar{v}_q , respectively.

The so-called differential scheme of constructing effective elastic moduli also belongs to the class of the effective medium methods (see e.g. Norris *et. al.*, 1985). This scheme is considered as a process of consecutive additions of infinitesimal values of the inclusion phase in a uniform medium with a modulus equal to the effective modulus of the medium with the previous additions of inclusions to the matrix, which yields the closed-form equation

$$\mathbf{H2} : \quad \mathbf{Y} \equiv \mathbf{I}, \quad \frac{d\mathbf{M}^*}{dc^{(1)}} = \frac{1}{(1 - c^{(1)})\bar{v}_1} \mathbf{R}(\mathbf{M}^*). \quad (\text{A.2})$$

Buryachenko and Parton (1992) proposed a differential version of the MEFM, in which at each step of the differential scheme (A.2) a problem of n interacting inclusions inside some effective medium is solved.

Mori–Tanaka method

According to the closing hypothesis of the Mori–Tanaka (1973) method each inclusion in the composite is considered as an isolated one, located inside an infinite matrix and loaded by the effective field $\langle \bar{\boldsymbol{\sigma}} \rangle_i \equiv \langle \boldsymbol{\sigma} \rangle^{(0)}$. Then from the equation $c^{(1)}\mathbf{B}\langle \boldsymbol{\sigma} \rangle^0 + c^{(0)}\langle \boldsymbol{\sigma} \rangle^0 = \boldsymbol{\sigma}^0$ we obtain

$$\mathbf{H2} : \quad \mathbf{Y}^{-1} = \mathbf{I} + (\mathbf{B} - \mathbf{I})c^{(1)}. \quad (\text{A.3})$$

The MEFM

The final representation of the tensor \mathbf{Y} is significantly simplified at the “quasi–crystalline” approximation by Lax (1952) expressed as

$$\mathbf{H2} : \quad \mathbf{Z}_{ij} = \mathbf{I}\delta_{ij}, \quad (\text{A.4})$$

which leads to the one particle approximation of MEFM (see for references Buryachenko, 2001)

$$\mathbf{Y}^{-1} = \mathbf{I} - \mathbf{R} \int [\mathbf{T}_{iq}(\mathbf{x}_i - \mathbf{x}_q)\varphi(\Omega_q, \mathbf{x}_q; \Omega_i, \mathbf{x}_i) - \mathbf{T}_i(\mathbf{x}_i - \mathbf{x}_q)n^{(1)}] d\mathbf{x}_q. \quad (\text{A.5})$$

Under a point approximation of the inclusions (exact for infinitely spaced heterogeneities) we have

$$\mathbf{T}_{iq}(\mathbf{x}_i - \mathbf{x}_q) = \mathbf{T}_i(\mathbf{x}_i - \mathbf{x}_q) = \boldsymbol{\Gamma}(\mathbf{x}_i - \mathbf{x}_q), \quad (\text{A.6})$$

and from (A.5) one receives

$$\mathbf{Y}^{-1} = \mathbf{I} - \mathbf{R} \int \boldsymbol{\Gamma}(\mathbf{x}_i - \mathbf{x}_q) [\varphi(\Omega_q, \mathbf{x}_q; \Omega_i, \mathbf{x}_i) - n^{(1)}] d\mathbf{x}_q. \quad (\text{A.7})$$

The representation (A.7) is follow from the results obtained by the use of the variational method by Ponte Castañeda and Willis (1995) (see also for references Buryachenko, 2001), who considered in detail the case of multicomponent composites and the effect of the spatial distribution of the homogeneous inclusions. Only in particular cases, in which the shape of the correlation hole v_i^0 is homothetic to the inclusion shape v_i the formulae (A.3) and (A.6) coincide. Under the simplest conditional probability density (2.456), Eq. (A.7) is simplified

$$\mathbf{Y}^{-1} = \mathbf{I} - \mathbf{R}\mathbf{Q}_i^0 n^{\Omega(1)}, \quad (\text{A.8})$$

where \mathbf{Q}_i^0 is defined by Eq. (2.464) for the domain Ω_i^0 defined in Subsection 2.2 and constructed in Section 5.

In the case of two particle approximation of the MEFM, a representation of the tensor \mathbf{Y} (2.477) is simplified for one sort of clusters

$$\begin{aligned} \mathbf{Y}^{-1} &= \mathbf{I} - \mathbf{R} \int \mathbf{T}_{iq}(\mathbf{x}_i - \mathbf{x}_q)\mathbf{Z}_{qi}\varphi(\Omega_q, \mathbf{x}_q; \Omega_i, \mathbf{x}_i)d\mathbf{x}_q \\ &= \mathbf{I} - \mathbf{R} \int [\mathbf{T}_{iq}(\mathbf{x}_i - \mathbf{x}_q)\mathbf{Z}_{qq}\varphi(\Omega_q, \mathbf{x}_q; \Omega_i, \mathbf{x}_i) - \mathbf{T}_i(\mathbf{x}_i - \mathbf{x}_q)n^{(1)}] d\mathbf{x}_q. \end{aligned} \quad (\text{A.9})$$